KOMEX

KURILE OKHOTSK SEA MARINE EXPERIMENT

CRUISE REPORTS: KOMEX I and II

RV PROFESSOR GAGARINSKY CRUISE 22
RV AKADEMIK M. A. LAVRENTYEV CRUISE 28

VLADIVOSTOK - PUSAN - OKHOTSK SEA - PUSAN - VLADIVOSTOK
7 JULY - 12 SEPTEMBER 1998

Edited by Nicole Biebow and Edna Hütten

The KOMEX I and II marine expeditions were initialized on responsibility of
the P. P. Shirshov Institute of Oceanology, Moscow,
the Pacific Oceanological Institute (POI), Vladivostok,
and the GEOMAR Research Center for Marine Geosciences, Kiel

GEOMAR
Forschungszentrum
für marine Geowissenschaften
der Christian-Albrechts-Universität
zu Kiel

KIEL 1999

GEOMAR REPORT 82

GEOMAR
Research Center
for Marine Geosciences
Christian Albrechts University
in Kiel

Redaktion dieses Reports:
Nicole Biebow und Edna Hütten

GEOMAR REPORT
ISSN 0936 - 5788

GEOMAR
Forschungszentrum
für marine Geowissenschaften
Wischhofstr. 1-3
D - 24148 Kiel
Tel. (0431) 600-2555, 600-2505

Editors of this issue:
Nicole Biebow and Edna Hütten

GEOMAR REPORT
ISSN 0936 - 5788

GEOMAR
Research Center
for Marine Geosciences
Wischhofstr. 1-3
D - 24148 Kiel
Tel. (49) 431 / 600-2555, 600-2505

Table of contents

APPENDICES

Preface: KOMEX: *K*urile *O*khotsk Sea *M*arine *EX*periment

N. Biebow and E. Suess

Bound by the Asian continent to the northwest and north and the Kurile-Kamchatka-Island Arc to the east and southeast, the Sea of Okhotsk is the second largest marginal sea of the Pacific Ocean. It is characterized by its complicated tectonic structure, its high methane production rate and seeping activity, its distinct seasonal character of climate and oceanography and its high level of primary productivity. Therefore it represents a climate-forcing and ecologically highly sensitive system which offers a unique opportunity to carry out multi-disciplinary geoscientific research. The tectonics, environment, and ecology of the Sea of Okhotsk and the adjacent Kurile Island Arc are thus of high priority to understand the global climate change.

The joint German- Russian project KOMEX (***K***urile ***O***khotsk Sea ***M***arine ***EX***periment) funded for the initial phase by the German Federal Ministry of Education, Science and Technology (BMBF) and the Russian Ministry of Science and Technology, addresses the following distinct features of the Sea of Okhotsk through cooperation of various Russian-German working groups:

The Sea of Okhotsk is characterized by the highest potential marine methane production rate in the northern hemisphere; its seasonal ice-cover regulates the gas exchange with the atmosphere in an extraordinary way.

- The shelf areas around Sakhalin, Magadan west of Kamchatka, the Kurile Island Arc and the Kurile-Kamchatka subduction zone belong to an area with exceptionally active methane and fluid vents. Here depositionally bound, fermentatively formed and subduction-induced fluid vents generate enormous reservoirs of CH_4, CO_2 and other dissolved trace components. They are in direct contact with the bottom water and in shelf areas with the atmosphere. The influence of submarine fluid vents on ecology, sedimentology, water chemistry and atmospheric trace gases is still unknown and one of the central questions of the KOMEX project.
- The margins of the Sea of Okhotsk contain gas hydrates. Fluctuations of deep-sea temperatures and sea level have an impact on the stability of gas hydrates on the shelf and slope areas. Methane is released in great quantities, which as a greenhouse gas contributes to the atmospheric warming in an accelerating feedback.
- The Kurile Island Arc is a 1200 km long subduction system and one of the most active volcanic regions on Earth. As the eastern boundary of the Sea of Okhotsk, this subduction zone has not only a significant influence on its geodynamic evolution but it also plays an important role in mass transfer and material cycling in this area. Since the

discovery of fluid venting in accretionary wedges in subduction systems, the origin and evolution of fluids is of central interest. The question wether the fluids are recycled back to the ocean and/or influence the geochemical signature of the island arc magma is of major interest as well. For understanding and assessing the marine biogeochemical cycle it is of crucial importance to know and quantify not only the sedimentological but also the magmatic components. Additionally the input of volatiles and readily volatile elements into the atmosphere by volcanic eruptions is of importance and influences the global climate significantly. The Kurile Island Arc is an excellent area to study the influence of an active subduction system on the hydrosphere's and atmosphere's geochemical cycle, because it includes magmatic, hydrographic and atmospheric sources and sinks.

The Sea of Okhotsk covers an area equal the size of the North Sea and the Baltic Sea combined. To the east, the Sea of Okhotsk is bordered by the Kamchatka Penisula and the Kurile Island Arc. The water exchange through numerous straits into the open Pacific has a considerable impact on the circulation and intermediate-water formation in the western Pacific. Therefore, this exchange affects the oceanography and climate of the entire northwestern Pacific region. Additionally, the Sea of Okhotsk plays a crucial role as an interglacial high production zone which counteracts the natural atmospheric CO_2 increase during the late Quaternary melting periods and the succeeding interglacials. Several aspects of the influence of environmental parameters on the ocean-climate system in high latitudes can be studied in the Sea of Okhotsk:

- The Amur River is the only large Sibirian river which does not drain into the Arctic Ocean. Thus, a direct link between land covered with ice and the Pacific Ocean has existed during ice ages. This allows the reconstruction of terrestrial-marine interactions under glacial and interglacial conditions.

- From December to April each year the Sea of Okhotsk is largely ice-covered. During this period cold water flows into the Pacific Ocean. During glacial periods in contrast, the Sea of Okhotsk was completely ice-covered. Thus, the climatic change from glacial to interglacial periods has important effects on the production of cold water masses in the NW-Pacific which can be reconstructed from sediment records.

- The Sea of Okhotsk is characterized by an extremely high primary productivity, which has a seasonal character and is dominated by silicious plankton. Bathymetry and water depth of the Sea of Okhotsk are highly variable. Therefore, several types of sediment facies ranging from pelagic muds to organic-rich slope sediments are deposited. This variety of biogenic sediment facies presents an excellent opportunity to study paleoceanographical time slices with different resolutions. Meltwater influence, ice cover,

river input, and glacial-interglacial changes are controlling mechanisms for bioproduction, especially for the carbon and silica cycles.

The Kuriles form a characteristic island arc in the northwestern Pacific under which the oldest parts of the Pacific plate are subducted. Currently it is unclear, if the marginal sea was formed as a typical backarc basin with an opening at the northern border of the Kurile Basin or if it is an independent microplate.

- The plate tectonic character, the Sea of Okhotsk's age and the structure of the geologic margins and underlying basement are major topics of the geophysical and geological investigations as well as

- the investigation of the Kurile Island Arc magmatic rocks to characterize the plate-tectonic situation by their geochemical signature.

Those manifold objectives of the KOMEX project in this key area of the system earth can only be achieved by a multidisciplinary approach. Therefore, Russian-German working groups include geologists, geochemists, geophysicists, sedimentologists, paleontologists, paleo-ceanographers, volcanologists, biogeochemists and oceanographers. A successful base has been laid for the project in several pilot studies between 1992-1997. Interdisciplinary cooperation was established in July/August 1992 during the first joint expedition aboard *RV Akademik Nesmeyanov* which included scientists of the Pacific Oceanological Institute (POI, Vladivostok), the National Research Institute of Marine Fisheries and Oceanography (VNIRO, Moscow) and GEOMAR. This was followed by a short ice-expedition during the winter months to sample gases under the ice cover of the Sea of Okhotsk north of Sakhalin. The workshop on the Russian-German Cooperation in the Sea of Okhotsk-Kurile Island Arc was held in Moscow in November 1993 to compile the scientific results from the working area, especially from former studies of Russian partners and to define the common research topics and scientific objectives. Results of this workshop were integrated into the mature project.
In September/October 1994 the EC (INTAS)-funded expedition POSETIV (Paramushir-Okhotsk Sea Expedition to Investigate Venting) was carried out by the Pacific Oceanological Institute (Vladivostok), the Institute for Geophysics and Geology (Yuzhno-Sakhalinsk) and the P.P. Shirshov Institute (Moscow) with the participation of the Depts. of Marine Geology of the Netherlands Institute of Sea Research (NIOZ). In August 1995, another joint expedition, GERDA (Geophyical Researches in the Derugin Basin Area), took place. GEOMAR, the P.P. Shirshov Institute of Oceanology and the Pacific Oceanological Institute participated as well as Tokyo University. The program was mainly financed by GEOMAR and Tokyo University. Finally, in August/September 1996 another BMBF-financed expedition, GREGORY (German-Russian Expedition for Geological/Geophyical Okhotsk Sea Research) took place with the

participation of the Far Eastern Geological Institute and the Pacific Oceanological Institute (Vladivostok), the P.P. Shirshov Institute (Moscow) and GEOMAR. Important insights into the working area have been obtained thanks to these findings, data sets, and sample collections, and to the initiation of a Russian-German cooperation based on mutual trust and understanding. These conditions and experiences are the basis for a close cooperation which has been cultivated and will now be continued under the project KOMEX.

Due to distinct logistical demands of the different working groups, two expeditions with research vessels of the Pacific Oceanological Institute based in Vladivostok, will take place each year. The first cruise on board *RV Professor Gagarinsky* will focus on tectonic and structural objectives as well as on the detection and mapping of possible seafloor seepage areas. These investigations will provide the basic data for the second cruise aboard *RV Akademik Lavrentyev* with more marine-geological, geochemical and oceanographic objectives. During this cruise, seeping areas will be studied in detail by video-controlled systems. Besides water and plankton sampling as well as geological sampling for vent-geology, paleoceanology and volcanology programmes will be carried out.

Accordingly, the first joint KOMEX cruise in 1998 aboard *RV Professor Gagarinsky* took place from July 7th to August 10th 1998 followed by the second joint KOMEX cruise aboard *RV Akademik Lavrentyev* which departed from Vladivostok on August 7th and returned on September 12th 1998. The following report provides the results of these expeditions in two parts; including details of the participating institutions, the working groups and initial interpretations of the main findings.

PART I:

RV PROFESSOR GAGARINSKY CRUISE 22

CRUISE REPORT KOMEX I:

INESSA

INVESTIGATION OF EASTERN SAKHALIN SEEPAGE AREAS

VLADIVOSTOK - PUSAN - SEA OF OKHOTSK - PUSAN - VLADIVOSTOK

JULY 7 - AUGUST 10, 1998

1. Introduction and Background

B.V. Baranov, B.Ya. Karp, H.K. Wong, and S. Lammers

1.1 Tectonics

From the tectonic and geodynamic point of view, the Okhotsk Sea is a region of great interest. This sea occupies the bulk of the separate Okhotsk plate which is squeezed between four major plates: the North American, Eurasian, Pacific and Amurian plates (Fig. 1.1).

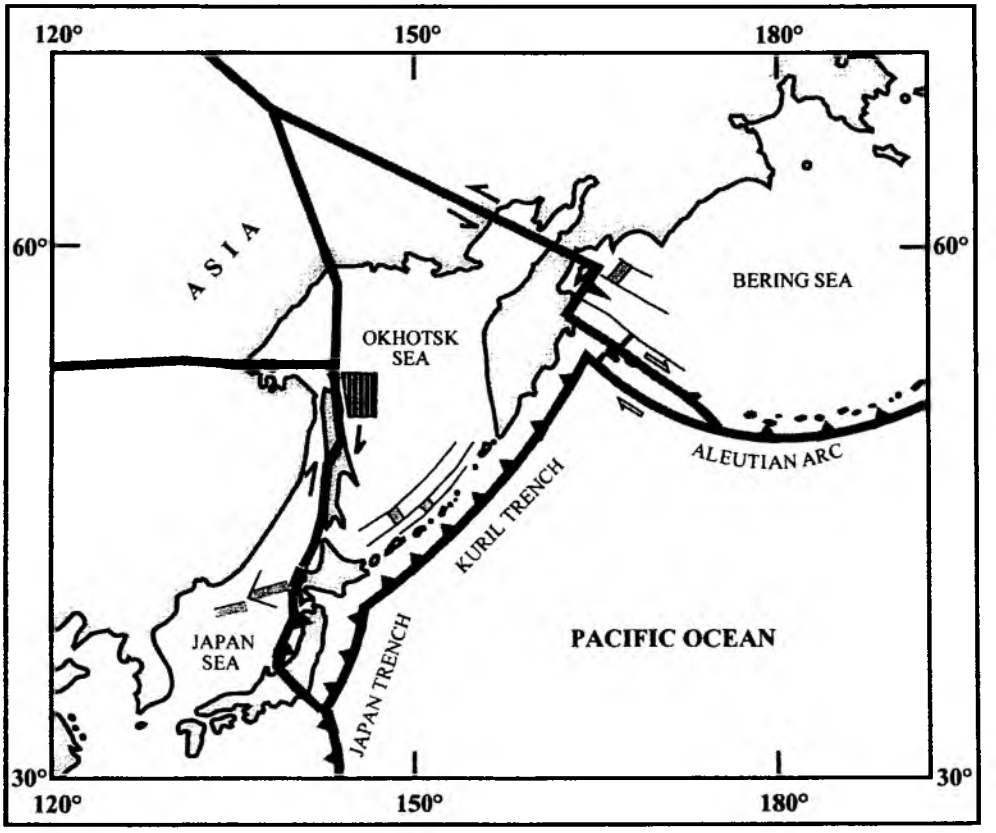

Fig. 1.1: *Location of the INESSA study area (shaded) and recent plate geometry of the northwestern Pacific. The Okhotsk plate corresponds to the Okhotsk Sea and parts of the adjacent land areas. Dark gray lines with teeth indicate subduction zones with arrows marking the strike-slip boundaries. Light gray lines show inactive spreading axes in backarc areas (as suggested for the Okhotsk Sea). Thick black lines indicate recent extensional axes in the western Bering Sea.*

Therefore, the geodynamics of the Okhotsk plate are closely connected with the character of relative movements between these plates and the Okhotsk Sea can be regarded as a key region for a better understanding of the geodynamics of northwestern Asia as a whole.

During the past three years, two cruises have been carried out in the Okhotsk Sea: Cruise 16 of the *RV Professor Gagarinsky* (1995) in the eastern Derugin Basin (Gerda Report, 1995) and Cruise 27 of the *RV Akademik M. A. Lavrentyev* (1996) in the central sea and on the

northwestern slope of the Kurile Basin (Nürnberg et al., 1996). These cruises were organized within the framework of the German-Russian scientific cooperation between GEOMAR (Kiel), POI (Vladivostok) and IORAS (Moscow) and represented the pilot and initial phase of the KOMEX project.

The data obtained in these two cruises provide evidence to support the Okhotsk Rift System and Kurile Basin opening model which have been developed recently (Baranov et al., 1995). According to this model, a large extensional province appeared in this area starting from Paleogene time as a result of the clockwise rotation of the Okhotsk plate. It was also suggested that the western Okhotsk plate could have been influenced by the existence of the Sakhalin Shear Zone (Dozorova et al., 1998).

The Sakhalin Shear Zone represents the recent transform boundary between the Okhotsk and Amurian plates. It stretches for a distance of about 2,000 km from northernmost Sakhalin Island to the eastern Japan Sea (Savostin et al., 1983; Jolivet et al., 1991) (Fig. 1.1). This boundary on Sakhalin Island corresponds to the strike-slip fault systems trending mainly in the N-S direction (Zanyukov, 1972; Rozhdestvenskiy, 1982, 1986; Savostin et al., 1983; Fournier et al., 1994). Both transpressional and transtensional structures occur along this boundary because of the complexity of these fault systems as detailed structural investigations and focal mechanism solutions indicate (Savostin et al., 1983; Fournier et al., 1994).

It is suggested that along this boundary the relative motion between the Okhotsk and Amurian plates appears in a broad zone because shallow earthquakes occur not only on Sakhalin Island but also offshore. Evidence for recent tectonic activity was obtained during the GERDA cruise (1995) in the eastern Derugin Basin located about 150-200 km away from the eastern coast of Sakhalin Island. The tectonic pattern of this area represents a rather complex system of normal faults and conjugated strike-slips (Dozorova et al., 1998). Some authors (Ginsburg et al., 1993) suggested recent tectonic activity on the Sakhalin continental slope, but the fault kinematics of this area are still uncertain.

Recent faults in the eastern offshore area of Sakhalin may serve as conduits for gas penetration to the sea floor. Two seepage areas located off northern Sakhalin were known and investigated before (Ginsburg et al., 1993) and a third one was found on the GREGORY cruise (1996) near southern Sakhalin (Nürnberg et al., 1996). It is well known that gas seeps are widespread on the inner slopes of trenches (subduction zones) and are connected with the existing fault pattern and the stress regime as was shown during submersible investigations of the Japan and Nankai Trenches (Kaiko-Tokai meeting, 1998). The offshore eastern Sakhalin region is related to another type of plate boundary, viz. a transform boundary, and detailed mapping of these seeps can be very useful in understanding the tectonic regime of this zone.

1.2 Methane and carbon dioxide in surface waters

An important objective of cruise 22 of the *RV Professor Gagarinsky* is the quantification of the sources and sinks of CH_4 and CO_2, geochemical end-members in both the production and decomposition of organic matter as well as the most important atmospheric trace gases. This task includes geochemical investigations of the cycling within the water column as well as the estimation of the transport rates between the sea and the atmosphere, which are primarily driven by the saturation gradients between the surface water and the atmospheric partial pressures of the gases.

As CH_4 and CO_2 are major components in diagenetic processes, sediments are their primary reservoirs in the marine environment and global efforts are being made to quantify the re-entry of carbon and other associated elements from these reservoirs into the oceans, usually summarized under the term "venting" or "seepage". The most promising places to investigate in this respect are tectonically active plate boundaries in regions where sedimentary organic matter accumulates, preferably along continental margins and shelves.

Areas of active venting may be recognized geophysically (e.g., by the occurrence of gas pockets, gas flares, pockmark-like structures, and deformations of BSR's) or geochemically (e.g., by anomalously high ambient methane concentrations).

The Sea of Okhotsk is one of the most promising marginal seas for a quantification of the rates and oscillations of carbon exchange between lithosphere, hydrosphere and atmosphere since it features a large variety of organic carbon reservoirs, e.g. as gas hydrates, oil and gas, and hydrothermal vents. Other significant environmental effects to be investigated are the supply of freshwater from the Amur River and seasonal climatic variations.

The air-sea measurements were chosen to accompany the geophysical surveys on the first KOMEX cruise - INESSA - with the *RV Professor Gagarinsky*, as profiling at a constant speed of 5 knots provides excellent conditions to perform continuous gas analyses of the surface waters. Also, for the first time since 1992, an area off NE Sakhalin between 52.5°-53.3°N and 143°-144.5°W could now be surveyed again. This area was previously found to be a net source of atmospheric methane (Lammers et al., 1995).

1.3 Objectives

The INESSA (INvestigation of the East Sakhalin Seepage Area) area of cruise 22 of the *RV Professor Gagarinsky* is located on the eastern slope off northern Sakhalin Island. The geophysical surveys in this cruise have the following main objectives:

- to elaborate on the tectonic pattern of the Sakhalin continental slope near seepage areas and to compare it with structures observed on Sakhalin Island itself;
- to obtain regional seismic cross-sections for seismic facies and sequence analyses and studies on sea level fluctuations;
- to investigate the known areas of gas seeps as well as to find new seepage areas; and

- to prepare recommendations for the forthcoming geological cruise on the *RV Akademik Lavrentyev* on the choice of the best sites for TV observations, coring and water sampling.

2. INSTRUMENTS AND METHODS

By B. Ya. Karp, S. Lammers, T. Lüdmann, H. K. Wong, A. Sudakov, and S. M. Nikolaev

2.1 Geophysical survey

A basic tool for the interpretation of seismic data is the concept of seismic stratigraphy. Reflections from the subsurface generated at sedimentary or structural interfaces with a significant change in acoustic impedance can be classified according to their external geometries, termination patterns (onlap, offlap etc.) and internal reflection configurations. Each succession of relatively conformable reflectors bounded at its top and base by unconformities or their correlative conformities is interpreted to correspond to a depositional sequence. Such a sequence is chronostratigraphically significant because it is deposited during a given interval of geologic time defined by ages of the sequence boundaries. Differences in internal reflection configuration, amplitude, continuity and frequency content between sequences suggest changes in the seismic facies, and these are attributed to changes in the depo-environment. Thus, seismo-stratigraphic interpretations provide an important tool for the reconstruction of the tectonic regime and the paleo-environment of an area.

The equipment used during the 1998 cruise of the *RV Professor Gagarinsky* includes

- a seismic reflection system consisting of a two-GI-gun array, an 8 channel mini-streamer, a multi-channel digital data acquisition system, an air gun trigger unit, a pressurized air distribution board and a linescan recorder. A single-channel digital data acquisition system permits real-time data monitoring (quality control) on screen and profile hard-copy printout on a line printer. Each of the S.S.I. GI-guns deployed has a maximum volume of 2.5 *l* (45 + 105 cu. in.). The two-gun array was pressurized nominally at 150 bar, towed behind the ship and triggered at 10.8 second intervals (every 25m at 4.5 knots) along prescribed profiles with pulses generated by a master clock. Each active channel of the GECO PRAKLA 8-channel mini-streamer has a length of 12.5 m.

  The operational characteristics of the multi-channel seismic reflection system are summarized in Tab. 2.1.

Table 2.1: Operational characteristics of the multi-channel seismic reflection system.

Source	
Type	2 × GI 45/105
Pressure	150 bar nominal
Firing interval	10.8 sec
Source depth	
Streamer	
First channel offset	150 m
No. of channels	8
Length of active section	12.5 m
Length of inactive section between active sections	12.5 m
Streamer depth	ca. 10 m
Recording	
Recording length	8 sec
Sampling frequency	1000 Hz
Bandpass analog filter	18-250 Hz

On the one hand, signals from the eight channels are separately digitized via a PC-based A/D converter board, multiplexed, and written onto high capacity EXABYTE tapes. Back in the home laboratory, the data will be demultiplexed and transformed to the standard SEGY format. They will then be processed using the *iXL* seismic processing software package. The processing steps include sorting, digital filtering, NMO-correction, stacking, deconvolution and migration. On the other hand, the incoming analog signals from the different channels of the streamer are summed, amplified, bandpass filtered (15-350 Hz), and written onto a DAT-tape for archiving, displayed online on an EPC 4800 graphic recorder, as well as directed to the single-channel digital data acquisition system for monitoring and data storage.

- a single channel seismic reflection system made up of a 3 *l* air gun, a streamer, an amplifier-filter system, and a single-channel digital data acquisition system based on a commercial sound card (Sound Blaster Pro) which writes the analog signal on the harddisk of a 386-PC (see Tab. 2.1 for characteristics). Simultaneously, 620 traces were displayed on the computer monitor. Backups were made offline on magneto-optical disks. On/off switching of the seismic recording on harddisk, on-screen seismic signal display and the adjustment of the dynamic range of the seismic signal were controlled by software developed for this purpose.

Table 2: Specification of the single-channel data acquisition system.

Length of trace	4 sec.
Start delay	optional from 0 to 2 sec in 1 sec steps
Sampling rate	optional from 0.05 ms to 2 ms; here: 2 ms
Data format	8 bits sign

- a 2-12 kHz echosounder system consisting of a towed, four element transducer, a transmitter with a power output of 10 kW at 0.75 % duty cycle, a receiver, a digital data acquisition system and a linescan recorder. The output frequency of the system is adjustable between 2-12 kHz, and the pulse width may be varied within the range of 1-32 cycles of the frequency selected. In addition, the functions of gain, time-varied gain with adjustable delay, AGC, bandpass filtering, key programming and swell compensation are integrated;
- an analog sidescan sonar system for shallow water applications which consists of a towed transducer with depressor, a transceiver, a 4-channel DAT-recorder and an analog monitoring system. The towed, variable beam transducers have a horizontal beam width of 1° and a pulse width of 0.1 ms at an output frequency of 100 kHz. The beams can be tilted down either 0°, 10° or 20° below the horizontal and the vertical beam width is adjustable to a value of 20° or 40°;
- a Russian, surface-towed, MBM-1™ marine proton magnetometer for magnetic total intensity measurements. This magnetometer has a measuring range of 20,000-100,000 nT and an accuracy of 2-4 nT over its entire measuring range. The magnetometer sensor was towed by a non-magnetic cable at a distance of 250 m behind the ship. The magnetic data were written on an analogue recorder for visual display and stored on an IBM PC-386 at a sampling rate of 10 seconds;
- a Russian shipboard gravity meter consisting of four highly-damped, spring-type GMN™ marine gravimeters mounted on GMS-2™ gyrostabilized platforms installed in a special laboratory on board. The gravimeters achieved an accuracy of 0.8 mgal. In order to reduce cross-coupling errors, a straight-line model of two gravimeters was used. The gravity data were written on an analogue recorder for visual inspection and stored on an IBM PC-386 at a sampling rate of 4 seconds. Gravity observations were started at the pier in Vladivostok at a gravity base station three days before the beginning of the cruise;
- a Russian GEL-3™ wide-beam echo-sounder for bathymetric measurements. This echo-sounder has a measuring range of up to 10 km water depth and operates at a frequency of 12.4 kHz. The water depths were recorded on an analogue echograph which was then sampled manually every 5 minutes; and

- a shipboard global positioning system.

2.2 Gas survey

Saturations of dissolved methane and carbon dioxide in the surface waters were measured using a flow-through system that maintains equilibrium between continuously pumped surface seawater and air. CH_4 and CO_2 concentrations could be sequentially measured in an equilibrated gas phase as well as in air and, by taking temperature differences into account, the saturation of both species relative to their partial pressures in the ambient atmosphere could be calculated (for further details of the system see Rehder, 1996).

Sequences of air, equilibrated air, and two different gas standards were sequentially introduced into a two-channel gas-chromatograph (SRI 8610C) and detected by flame- ionisation-detection (FID). A catalytic reduction to CH_4 (by means of a H_2-fed Ni-catalyst at 380° C) made the CO_2 detectable by flame-ionisation. From the multiple gas analyses, standard deviations were found to be less than 1.2% for methane and less than 0.6% for carbon dioxide.

The system was adjusted to record the water values at intervals of 8 minutes, i.e., with a resolution of 0.67 nm at an average speed of 5 knots. The GC analyses were accompanied by sensor recordings of the salinity, temperature, and pH of the supplied seawater. Both data acquisition and system control were performed by the SRI-PeakSimple software installed on a laptop computer.

3. RESULTS

3.1 Seismic stratigraphy of the different physiographic provinces

By B. Ya. Karp, H. K. Wong, T. Lüdmann, and V. N. Karnaukh

3.1.1 Basinal province

The sedimentary column of the basinal province of the Derugin Basin ranges in thickness from 0.6 to >2.3 s TWT depending on the topography of the acoustic basement. This basement is characterized either by finely stratified reflectors, or an envelope of diffraction hyperbolas, or opaque reflectors (lacking any further penetration). Asymmetric blocks and relatively symmetric highs can be recognized.

The basinal province of the Derugin Basin studied can be divided into three areas, each having its own distinct seismo-stratigraphic characteristics (Fig. 3.1). The first (area I) lies in the south. Its sedimentary section comprises four seismic units: two well-stratified sequences and two semi-transparent sequences (profile 3, Figs. 3.2 and 3.3). The upper well-stratified sequence consists of subparallel seismic reflections. The total sequence thickness is 0.3-0.6 s, increasing progressively to the south. A flat-lying high amplitude reflector running subparallel to the seafloor occurs near its lower boundary (BSR). The upper semi-transparent sequence has only occasional, low amplitude, discontinuous reflectors. The sequence thickness is 0.24-0.35 s. A second BSR is found within this sequence. The lower well-stratified sequence is distinguishable from its upper counterpart in that subparallel reflections are grouped into several subsequences separated by transparent layers. In all, four subsequences bounded by minor unconformities are present. In places, the reflection pattern of this sequence suggests regional subsidence. The sequence thickness varies from 0.6 to 1.4 s. The lower semi-transparent sequence, with a thickness of 0.2-0.3 s TWT, exhibits the same seismic facies characteristics as its upper counterpart. Numerous small erosional channels dissect the seafloor in the southern part of this area (profile 3, Fig. 3.3) according to our new (this cruise) and old (GERDA expedition) seismic data.

The sedimentary section of area II is characterized by the presence of a medium amplitude, acoustically turbid sequence (B2) lacking any significant internal structures and bounded above by a distinct erosional truncation (profile 40, Fig. 3.4). This sequence is overlain by a thin, well-stratified, onlapping sediment fill of the youngest sequence B1. Underlying the turbid facies B2 is likewise a well-stratified sequence B3. Its upper part is laterally discontinuous and occurs as a basinal fill, while its lower part is represented by well-stratified, high amplitude reflectors exhibiting antiforms that are progressively more distinct with depth. The next stratigraphically older sequence (B4) is semi-transparent with only occasional, more-or-less conformal internal reflections reminiscent of hemi-pelagic sedimentation. It is underlain by sequence B5, the facies of which is very similar to that of the lower section of B3. The oldest

sequence penetrated (B6) is characterized by strong, intermittent reflectors that are often hyperbolic.

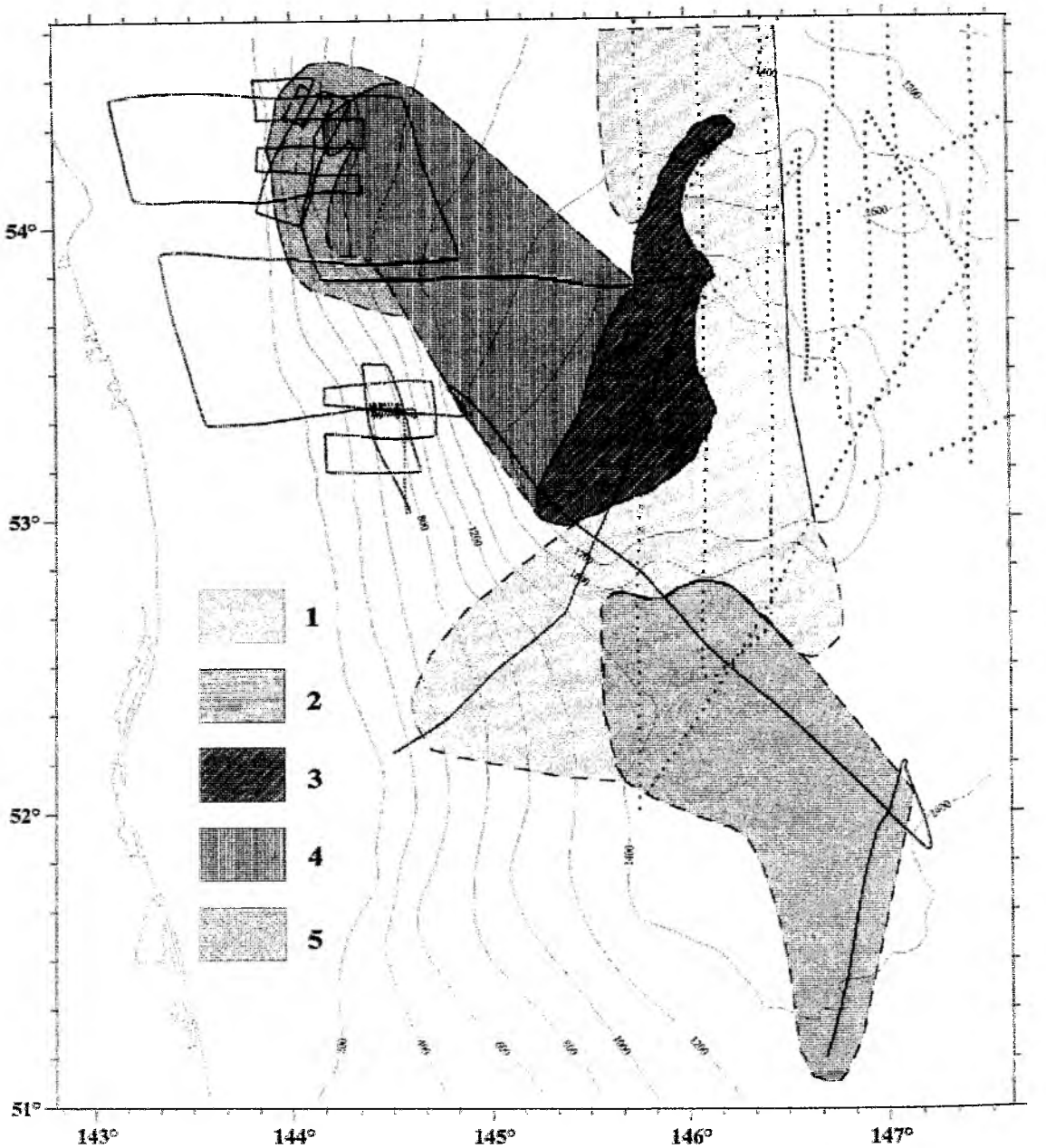

Fig. 3.1: Map of the location of areas with different seismo-stratigraphic characteristics. 1=area I; 2=area I with erosional channels incised into the seafloor; 3=area II; 4=area III; 5=young, lenticular sedimentary body; see text for explanation. Thick continuous lines give the location of profiles, present study (INESSA cruise); dotted lines that of the GERDA cruise. Thin continuous lines are isobaths in meters.

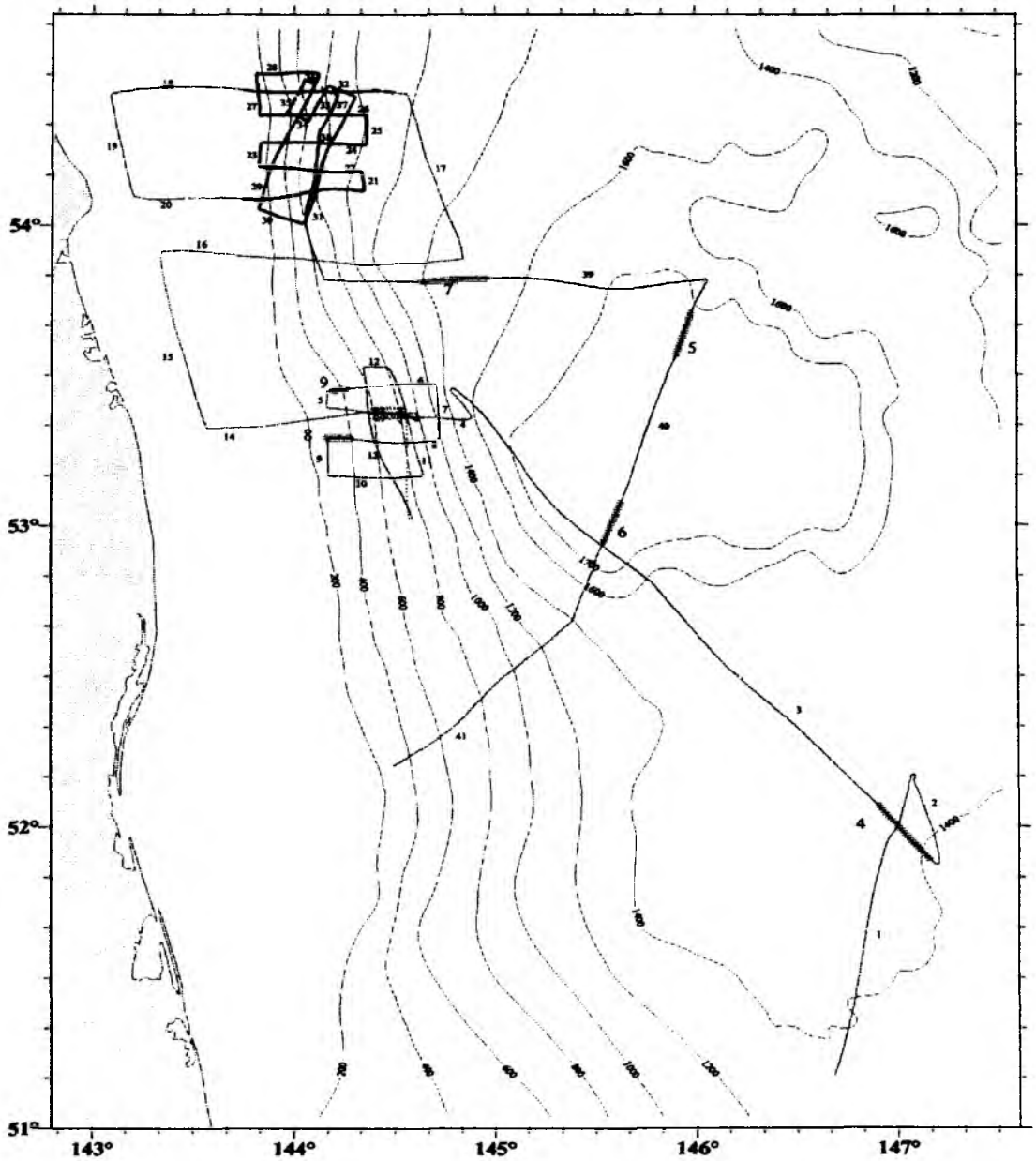

Fig. 3.2: Location of the selected profiles shown in Figs. 3.3-3.8 (large numbers). Small numbers are profile numbers.

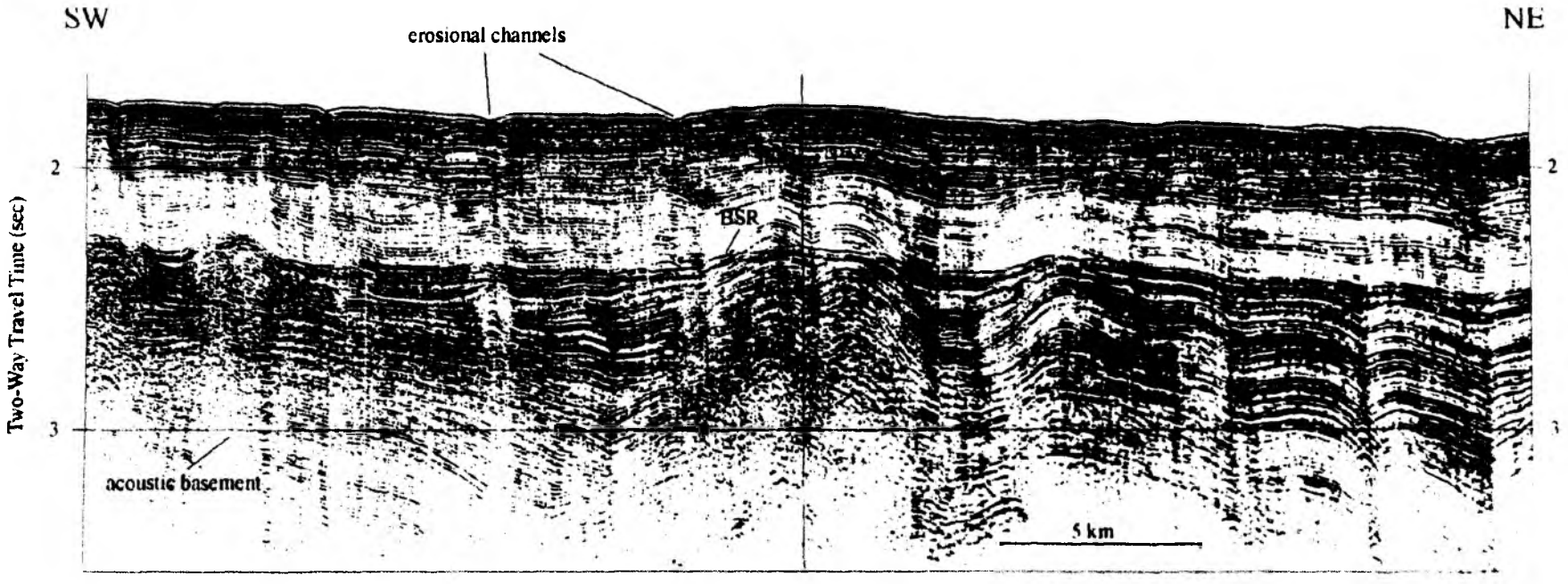

Fig. 3.3: Reflection seismic profile 3 within area I of the basinal province of the Derugin Basin, showing a succession of two well-stratified and two semi-transparent sequences. Note that the seafloor is incised by numerous erosional channels. See Fig. 3.2 for profile location.

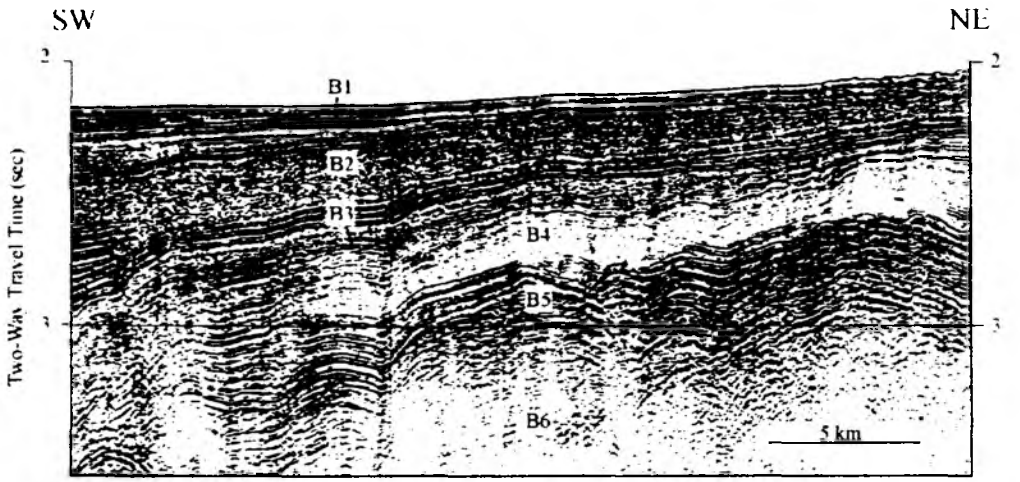

Fig. 3.4: *Part of reflection seismic profile 40 within the basinal province of the Derugin Basin showing the 6 seismic sequences recognized (B1-B6). See Fig. 3.2 for profile location.*

Area II lies in the western part of the deep Derugin Basin with a tongue-like extension onto the northern slope. In general, the turbid facies increases in thickness from 0.1 to 0.6 s to the south. In the western basin, however, it fills an acoustic basement depression adjacent to the continental slope, with a thickness exceeding 2.1 s TWT, at which depth the acoustic basement was not yet reached. Here, high amplitude reflectors conformal to the top of the underlying stratified sequence appear. The reflection pattern of this stratified sequence suggests syn-deformational subsidence. On seismic cross-sections, the lateral transition between the turbid sequence of area II and the well-stratified sequence of area I is very abrupt (profile 40, Fig. 3.5).

Area III differs from II in that the turbid sequence thickens considerably and that the underlying well-stratified sequence disappears, whereby the total sediment thickness increases (profile 39, Fig. 3.6). It occupies the northwestern lower slope and the western basin floor of the Derugin Basin, covering a depth range of about 700-1700 m (Fig. 3.1).

Although a slightly different seismic stratigraphic subdivision of the basinal deposits is used here, the sequence stratigraphy just described is directly comparable to that of the GERDA investigations (Karp et al., 1995; Baranov et al., in press).

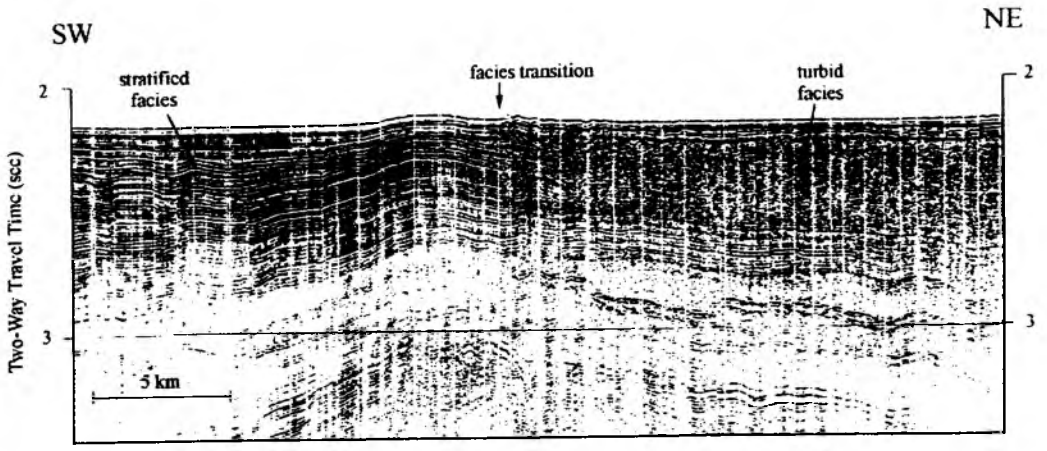

Fig. 3.5: Part of reflection seismic profile 40 on the southwestern slope of the Derugin Basin showing the transition between the turbid facies and the well-straified facies. See Fig. 3.2 for profile location.

3.1.2 Western slope of the Derugin Basin

The well-stratified sedimentary unit SL to which the turbid facies also grades in the southern seepage area consists of a series of parallel reflectors of differing amplitudes and frequency contents. It is, however, very difficult to subdivide into sequences despite its thickness of >1 sec TWT. This is because unconformities which function as sequence boundaries are here difficult to recognize (profile 8, Fig. 3.7).

Firstly, the occurrence of gas in the sediments results in phenomena such as acoustic masking and velocity pull-down (or pull-up) with apparent bending and interruption of the stratal interfaces. Secondly, the BSR's are subparallel to the seafloor and therefore intersect the strata only at an oblique angle, making true, low angle unconformities difficult to discern. Lastly, landwards at about 350 m water depth, the seafloor descends in a series of steps (e.g., profile 8) each of which marks an en echelon normal fault with a small throw (3.5 kHz echosounder profile 6, Fig. 3.8). These normal faults produce reflections and diffractions that are oblique and dissect the prominent stratal horizons into short, offset segments. Again, unconformities would be hard to recognize under these conditions.

At the northern seepage area, the youngest sequence constitutes a lenticular sedimentary body that occupies that upper basinal slope (Fig. 3.1). This lens does not continue into the southern seepage area.

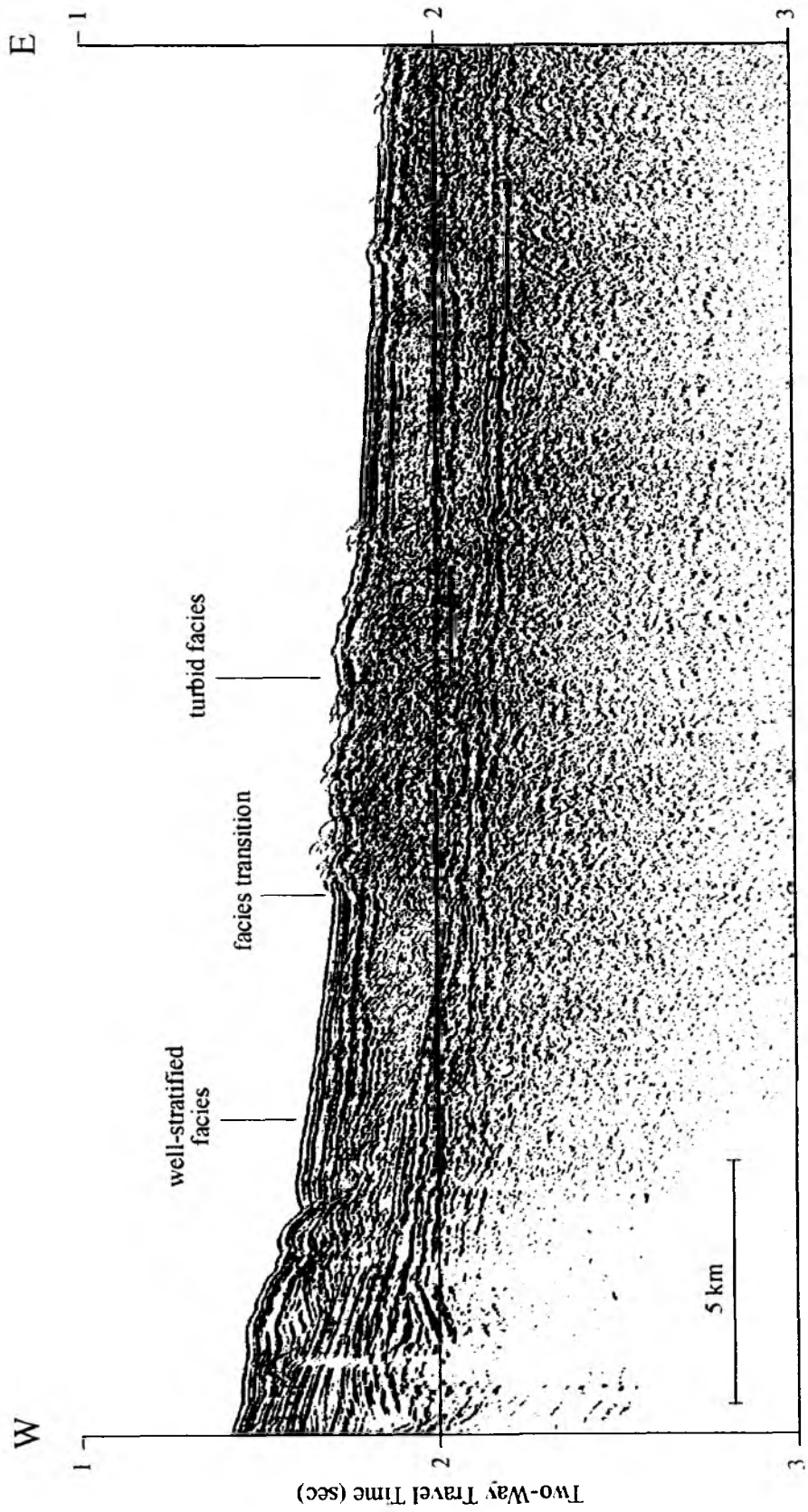

Fig. 3.6: *Part of reflection seismic profile 39 on the southwestern slope of the Derugin Basin showing the transition between the turbid facies and the well-stratified facies. See Fig. 3.2 for profile location.*

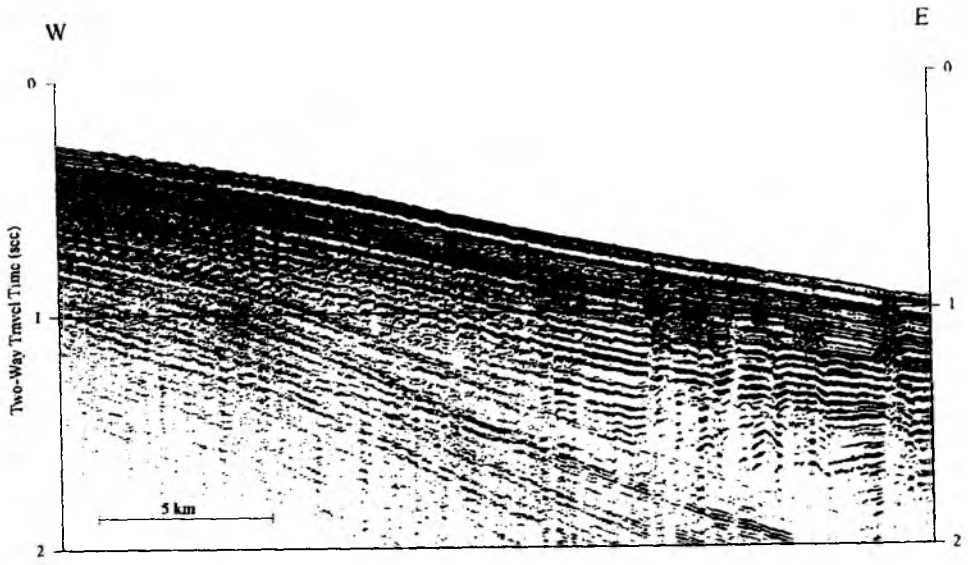

Fig. 3.7: *Part of reflection seismic profile 8 showing the well-stratified sedimentary unit SL on the basin slope within the southern seepage area. Note that the occurence of gas in the sediments leads to velocity pull-down, velocity pull-up and acoustic masking. See Fig. 3.2 for profile location.*

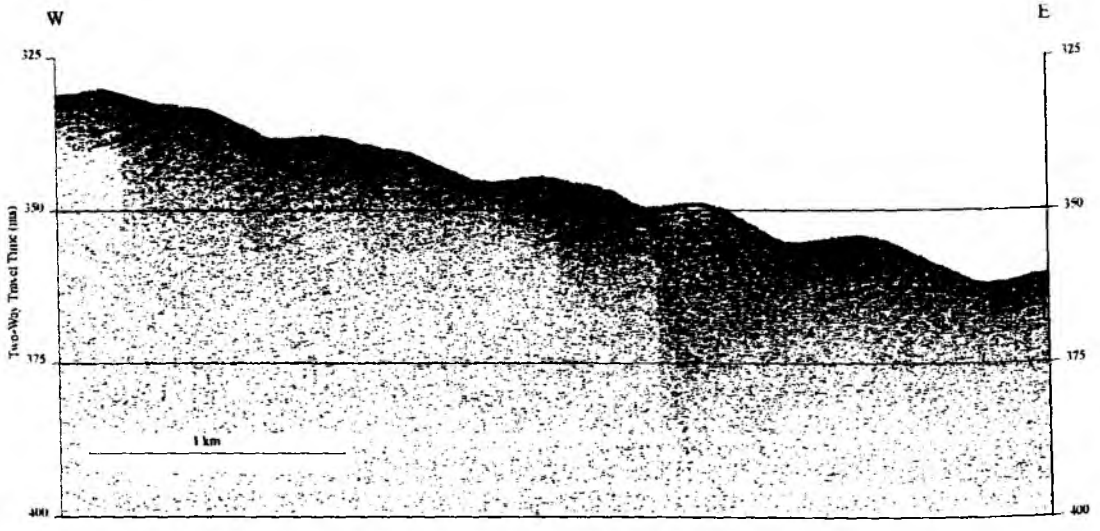

Fig. 3.8: *Part of echosounder profile 6 showing the stepwise descent of the seafloor along en echelon normal faults with small throws. See Fig. 3.2 for profile location.*

3.2 Gravity and magnetics

By S.M. Nikolaev and T. Kolpashikova

Gravity and magnetic measurements were carried out simultaneously with the seismic reflection survey. Magnetic anomalies can be calculated after the regional magnetic field and its temporal variations are subtracted from the measured field values, a process that will take place at the home laboratory in Vladivostok. Also, the gravity anomaly field will be calculated after the gravity observations at the base station in Vladivostok are completed.

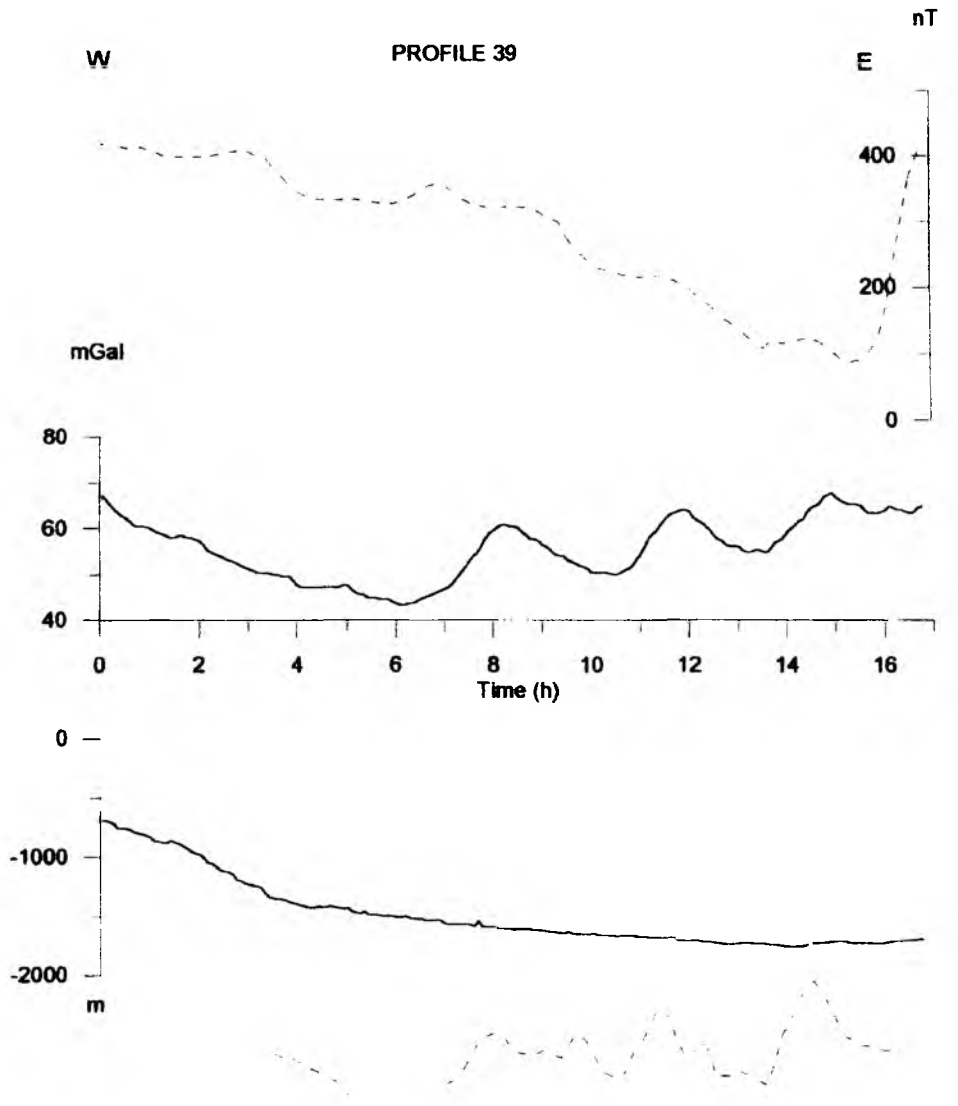

Fig. 3.9: *Relative values of the gravity (solid line) and magnetic (dashed line) fields along profile 39 (top). Bathymetry (solid line) and acoustic basement (dashed line) profiles (bottom). See Fig. 3.2 for profile location.*

Gravity and magnetic measurements were carried out during this cruise in the region with a thick sedimentary section, which has resulted in a sufficient decrease in anomalies connected with density and magnetic heterogeneities in the lower crustal layers. Thus, along most of the profiles, a gradual increase in geophysical fields from the deep basin in the direction of the shelf

can be observed. The increase in geophysical fields which is mainly connected with progressive shallowing is complicated by a number of minor local geophysical anomalies. They apparently are caused by crustal blocks bounded by faults or by changes in physical properties of the sediments due to gas venting along these faults.

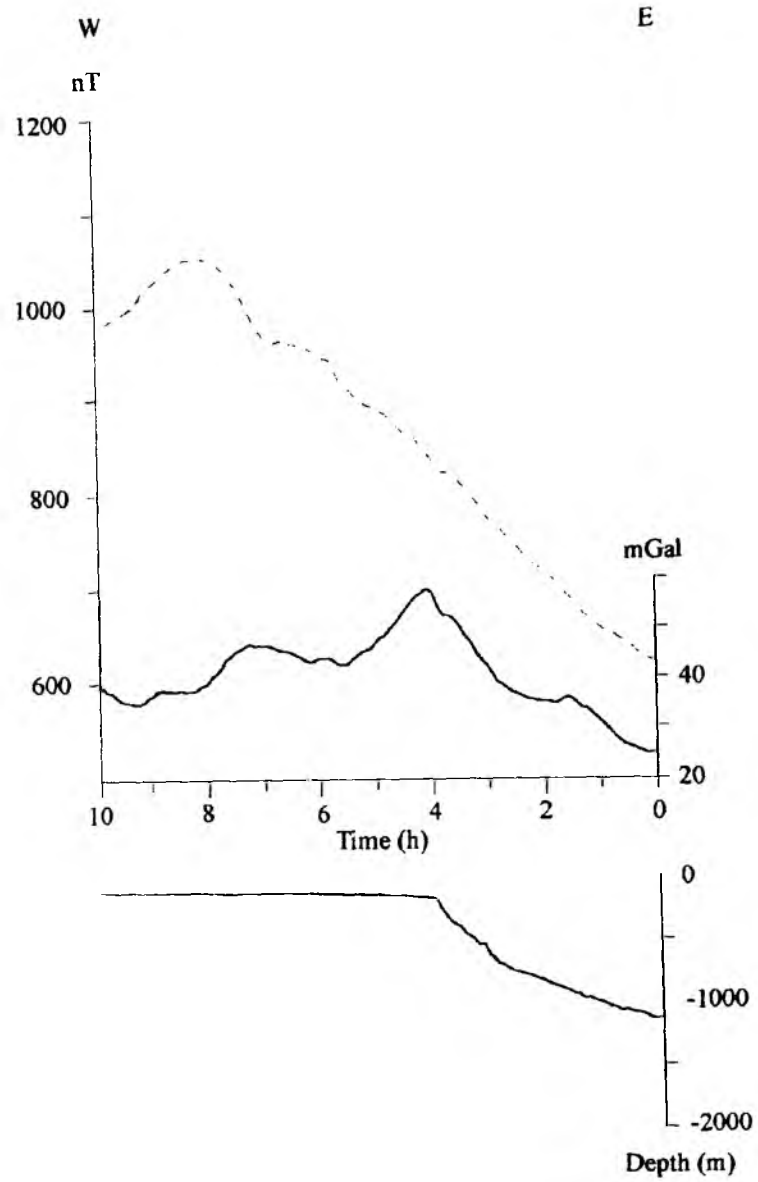

Fig. 3.10: *Relative values of the gravity (solid line) and magnetic (dashed line) fields along profile 18 (top). Bathymetry (solid line, bottom). See Fig. 3.2 for profile location.*

Two geophysical profiles with the most representative local anomalies are shown in Figs. 10 and 11. On the profile 39 (Fig. 3.9), the acoustic basement was determined and basement highs are found to coincide with large positive local gravity anomalies and weak magnetic anomalies. The latter are caused by a decrease in the thickness of the upper sedimentary layer. On the shelf

where the upper sedimentary layer is thicker, the basement high within the continental slope is marked by a positive local gravity anomaly which is not manifested in the magnetic field.

The acoustic basement trough at the end of profile 39 is poorly exhibited in the gravity field but it is represented by an abrupt increase in the magnetic field. It points to changes in the magnetic and density characteristics of the sediments here. On this profile within the continental slope, only a small local magnetic anomaly is observed. This anomaly reflects a crustal block separated by faults which are distinctly expressed in the bottom morphology. We suggest that this anomaly is caused by a change in magnetic properties of the sediment due to gas venting along the faults.

The nature of the large positive gravity anomaly with a maximum over the shelfbreak (located in the middle part of profile 18, Fig. 3.10) is extremely interesting. The increase in gravity field from the slope towards the shelf is caused by a decrease in water depth. The abrupt decrease in gravity is associated with the fact that the basement trough is sediment-filled. An abrupt change in the sign of the gravity gradient and the absence of magnetic anomalies justify such an interpretation.

The data obtained in this cruise allow the conclusion that the magnetic and gravity anomalies in the study area have different origins. The former are caused mainly by the influence of the lower crustal layers with high density and the latter characterize primarily the changes in sediment thickness.

3.3 Bathymetry

By B. V. Baranov and K. A. Dozorova

Bathymetric investigations conducted during the INESSA cruise were concentrated on mapping the major morphological features of the eastern Sakhalin slope and that of the seepage areas. The study area is shown in Fig. 3.11.

The total length of the bathymetric profiles was 1,969 km (including 1,878 km of seismic profiles). During transit to the study area, additional data on the morphology of the Polevoy Ridge and the southern slope of Derugin Basin were obtained.

The network of tracks included four E-W regional profiles crossing the study area from the Sakhalin shelf to the Derugin Basin (4, 14, 16 and 18; Fig. 3.12), three long profiles connecting the study areas of the GERDA cruise in 1995 and the present cruise (39, 40 and 41), and two sets of profiles representing surveys in the northern (N) and southern (S) seepage areas (Fig. 3.13).

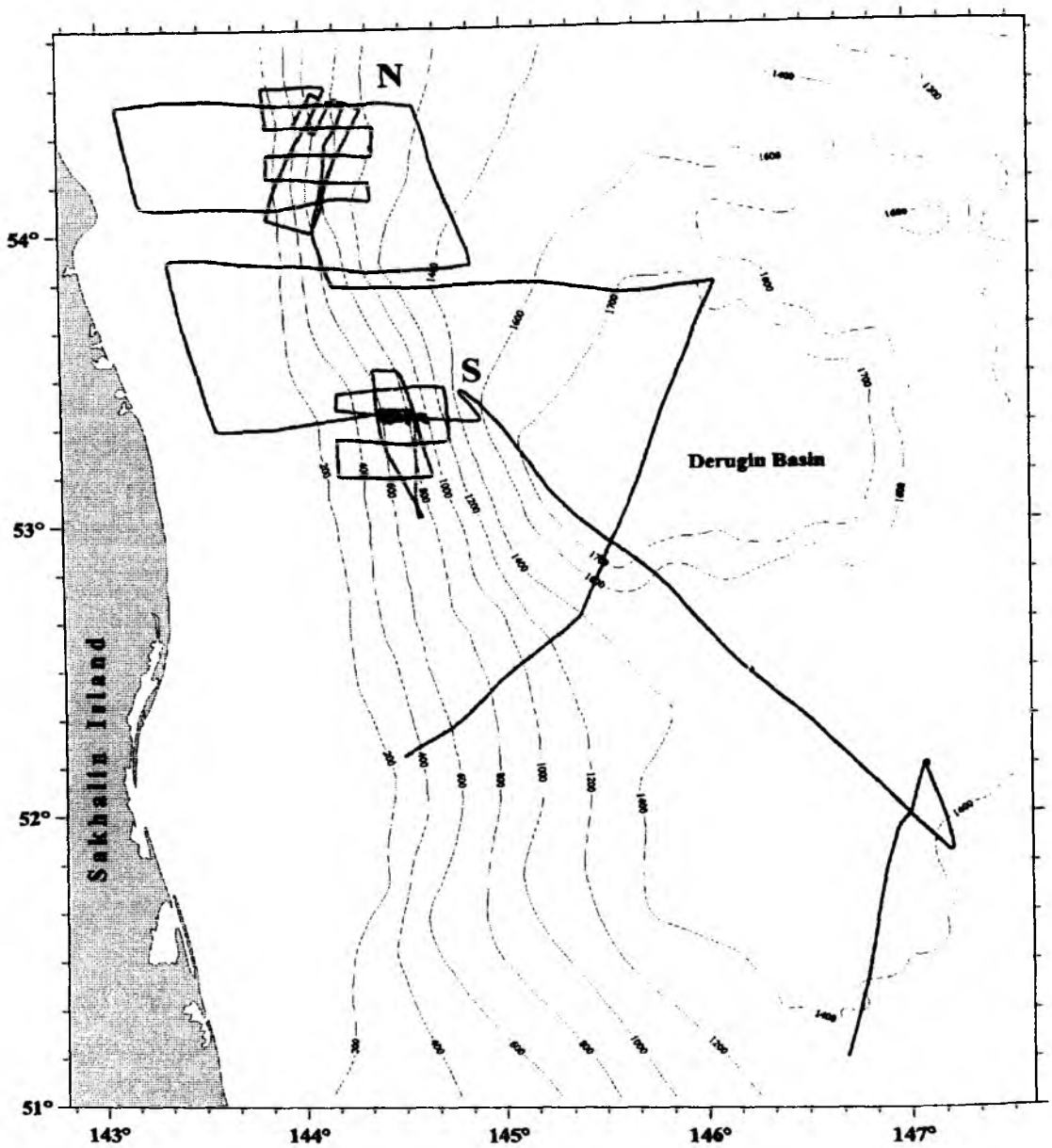

Fig. 3.11: General bathymetry and track locations within the study area. N=northern seepage area, S=southern seepage area. Contour interval is 200m.

Both of these seepage areas were covered by E-W, N-S and NNE-SSW profiles with lengths of 20-60 nm some 5-10 nm apart organized in a semi-regular network. In addition, a small region within the southern seepage area was covered by a dense net of echosounder profiles with a spacing of 0.5-1 nm. The same coverage was used during a previous cruise of the *RV Andropov* for the northern seepage area (Ginsburg et al., 1993).

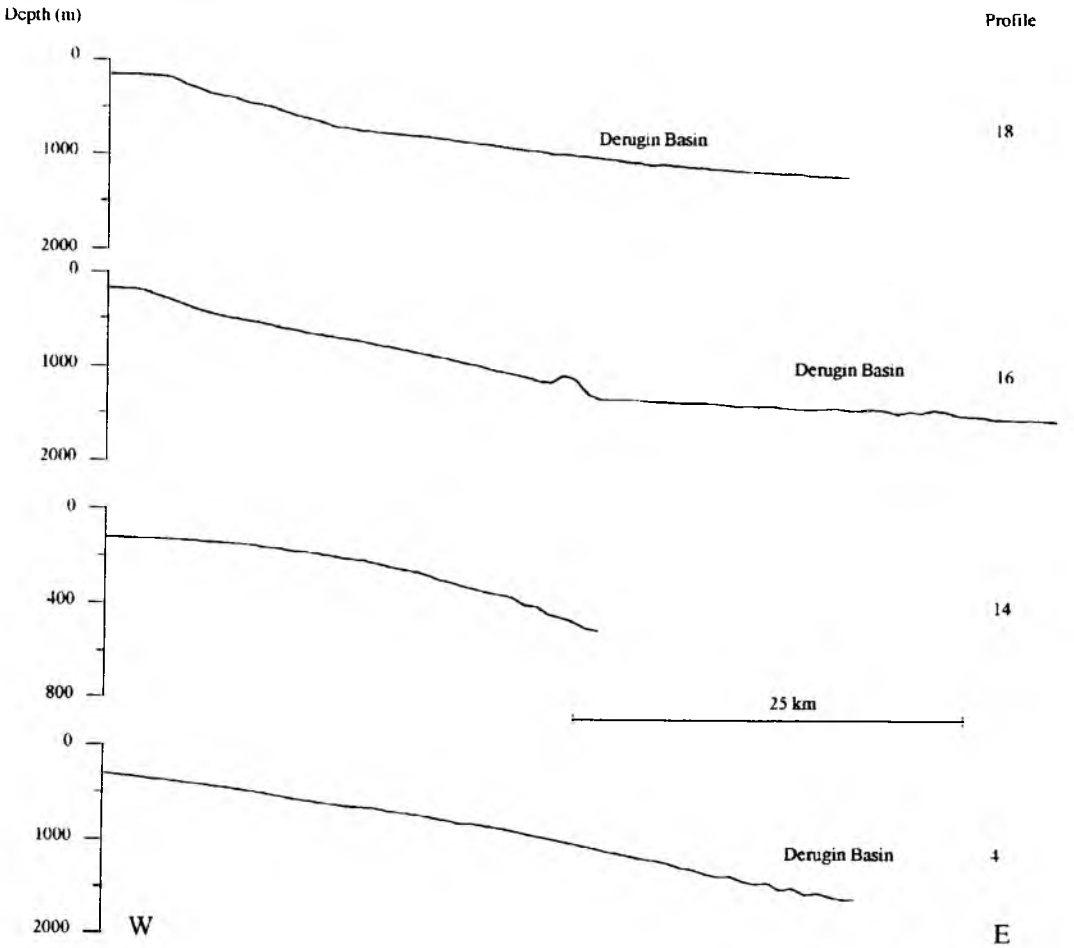

Fig. 3.12: Bathymetric profiles across the Sakhalin slope showing the morphology of the southern (profiles 4 and 14) and northern (profiles 16 and 18) areas.

3.3.1 The east Sakhalin continental slope

During the INESSA expedition, the continental slope was covered by profiles at a spacing of 90 nm between 53°N and 54.5°N (Fig. 3.11). Within this study area, as can be seen on the GEBCO bathymetric map, the slope has a near-meridional strike (NNW, 350°). However, on separate minor transects, the slope is found to stretch in a zigzag manner in the NNE (10°) direction in general.

Regional profiles (4, 14, 16 and 18) shown in Fig. 3.12 demonstrate the structure of this slope. Clearly, the slope morphology is in general extremely simple and changes only slightly from south to north. In the northern part of the study area, the shelfbreak is very distinct and can be traced at depths between 170-180m (profiles 16 and 18). In the south, the shelfbreak is less distinct and two steps are evident: the first is located at 200-210m and the second at 130-135m. Landwards of the shelfbreak lies the shelf which is represented by a eastward sloping plain within the depth range of 180-50m. On profile 15 which transects the shelf in a N-S direction,

sandwaves are observed. Their morphology suggests that the currents along Sakhalin are oriented from north to south.

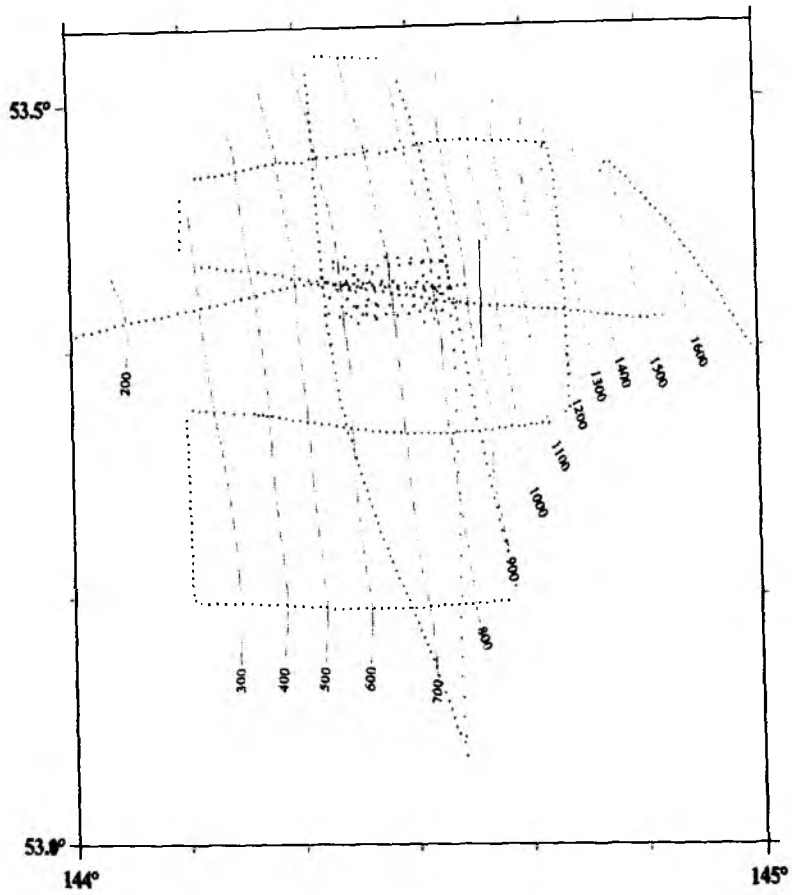

Fig. 3.13: Bathymetry of the southern area. Contour interval is 100m. Dotted lines show tracks, rectangle indicates detailed area shown in Fig. 3.8.

The continental slope in the southern part of the study area is in general more gentle (1.5°) compared to the north (2.5°). As a result, the shelf width is approximately equal to the slope width in the southern area but exceeds it by a factor of two in the north. The slope morphologies also differ. In the southern part of the area, it has a convex profile and an additional gentle step within the depth range from 500-600 to 700-800m. In contrast, the slope of the northern area has a concave profile with an upper slope gradient of 4-5° and a depth range reaching from the shelfbreak to 400-500m.

Our bathymetric survey shows that the transition from the continental slope off Sakhalin to the Derugin Basin floor may be smooth but may also consist of several steps. On profile 16 (Fig. 3.12), the seafloor gradient changes twice, viz. at the depth intervals of 1150-1300m and 1400-1480m respectively. Farther seawards lies the abyssal plain. A second example is given by profile 4 (Fig. 3.12) in which a series of highs of up to 50m above the surrounding seafloor

exist between the slope and the basin. Another difference between the southern and northern areas lies in their minor morphological peculiarities.

3.3.2 Morphological features of the slope in the southern and northern vent areas

Southern area:

The morphology of the slope was investigated on the basis of the track network in the 840-560m depth range (Fig. 3.13). It can be divided into two parts: a lower (840-660m) and an upper slope (660-560m). The structure of the lower slope is simpler; it has a slightly convex form, suggesting that it is accumulative in nature. The surface of the lower slope is locally complicated by small grooves and mounds. The characteristics of their distribution will be discussed later along with a description of the seeps (see 4.4).

The morphology of the upper slope is characterized by the existence of numerous relief steps. These steps are distributed within the depth interval of 380-750m. The largest are located in the upper part of this interval. Farther along the slope they become progressively smaller and finally disappear. 3.5 kHz echo-sounder profiles (Figs. 3.14 and 3.15) show that these steps are associated with normal fault scarps. However, a final analysis can only be made after the seismic profiles are processed and studied in conjunction with the echosounder profiles.

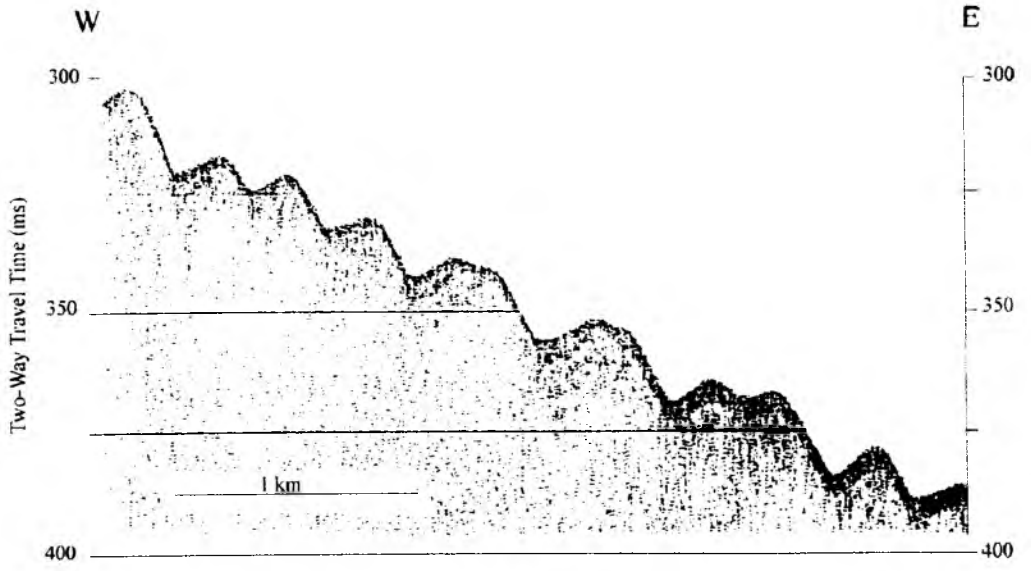

Fig. 3.14: *3.5 kHz echosounder record showing step-like morphology of the upper slope (southern area). Part of profile 14.*

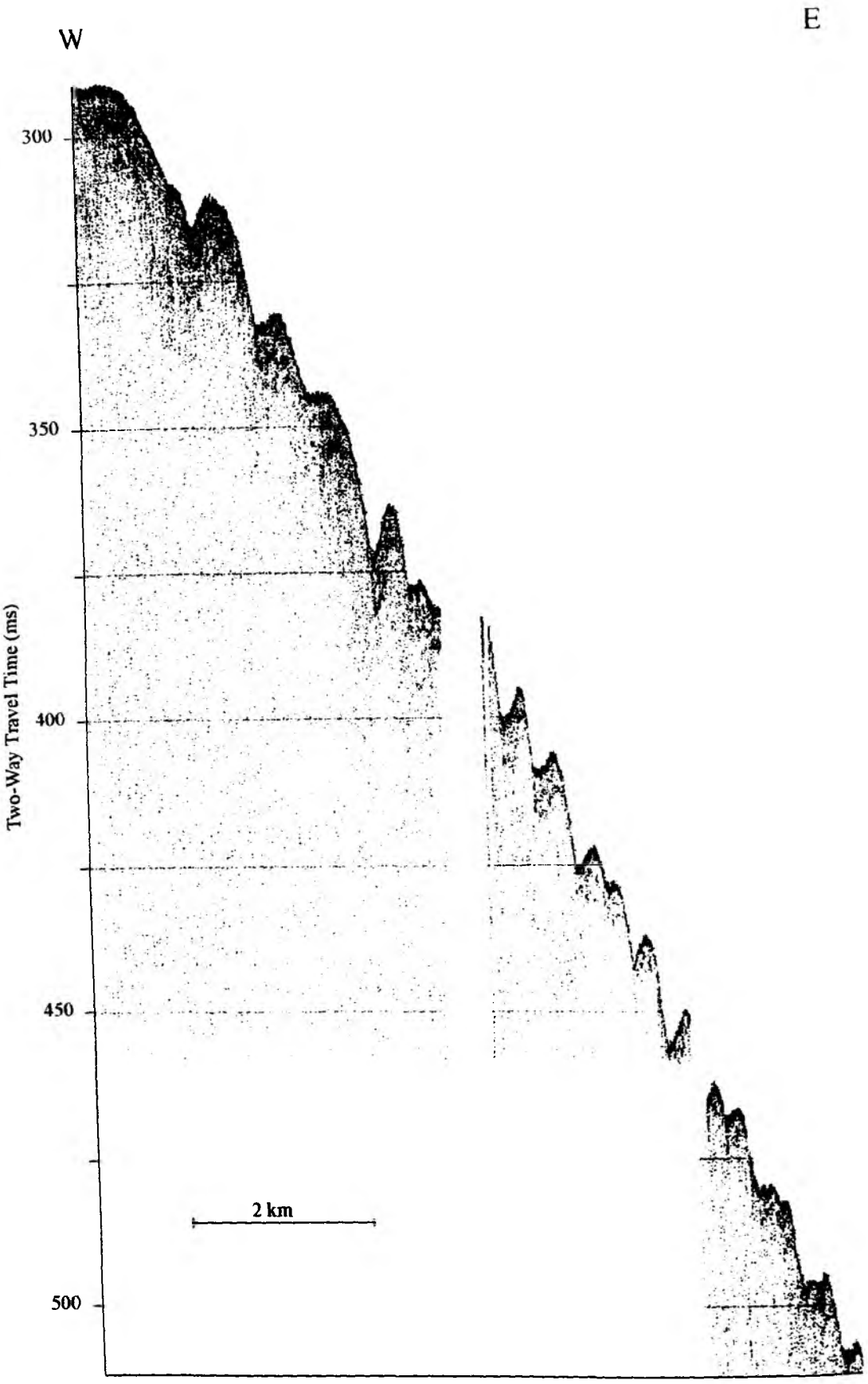

Fig. 3.15: *3.5 kHz echosounder record showing step-like morphology of the upper slope (southern area). Part of profile 10.*

Northern area (Fig. 3.16):

Data obtained from the northern area show that the slope morphology here is different from that to the south. The zone from the shelfbreak down to a water depth of 900-950m was studied in the northern area. Between the shelfbreak and 680m depth, the seafloor is steeper than at greater depths. Sometimes it has a step-like structure, but the morphology of the steps here contrasts sharply with that in the southern area. Firstly, the gradient is gentler and secondly their steep sides face upslope while their gentle sides face downslope.

The 3.5 kHz echosounder records permit a determination of the displacement character on these steps (Fig. 3.17). On profile 16 which lies in the north (according to its relief), the step-like structures can be observed at depths of 430-540m. It can be clearly seen that the steps are made up of deformed sediments. Structures reminiscent of drag folds are also present. Deformations have also been observed within the upper sedimentary column on other profiles crossing the northern area.

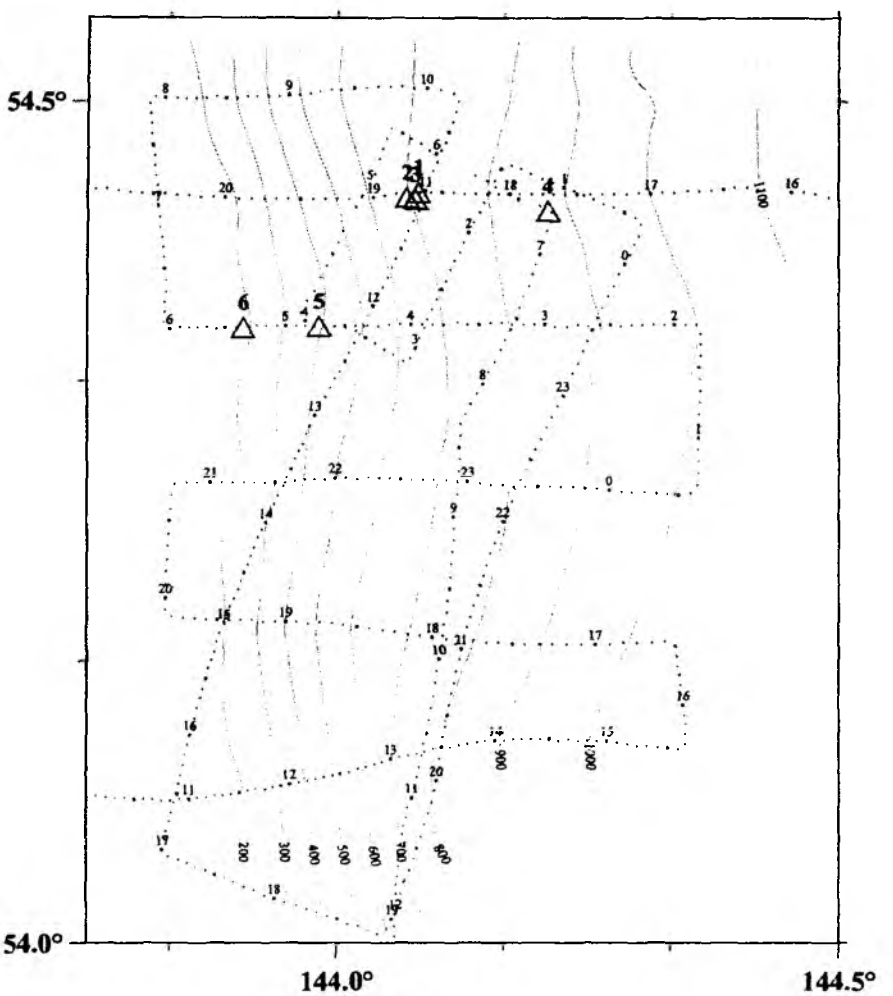

Fig. 3.16: *Bathymetric map of the northern area. Dotted lines indicate tracks, numbers give the time (UTC). Triangles mark seeps with numbering after Ginsburg et al. (1993).*

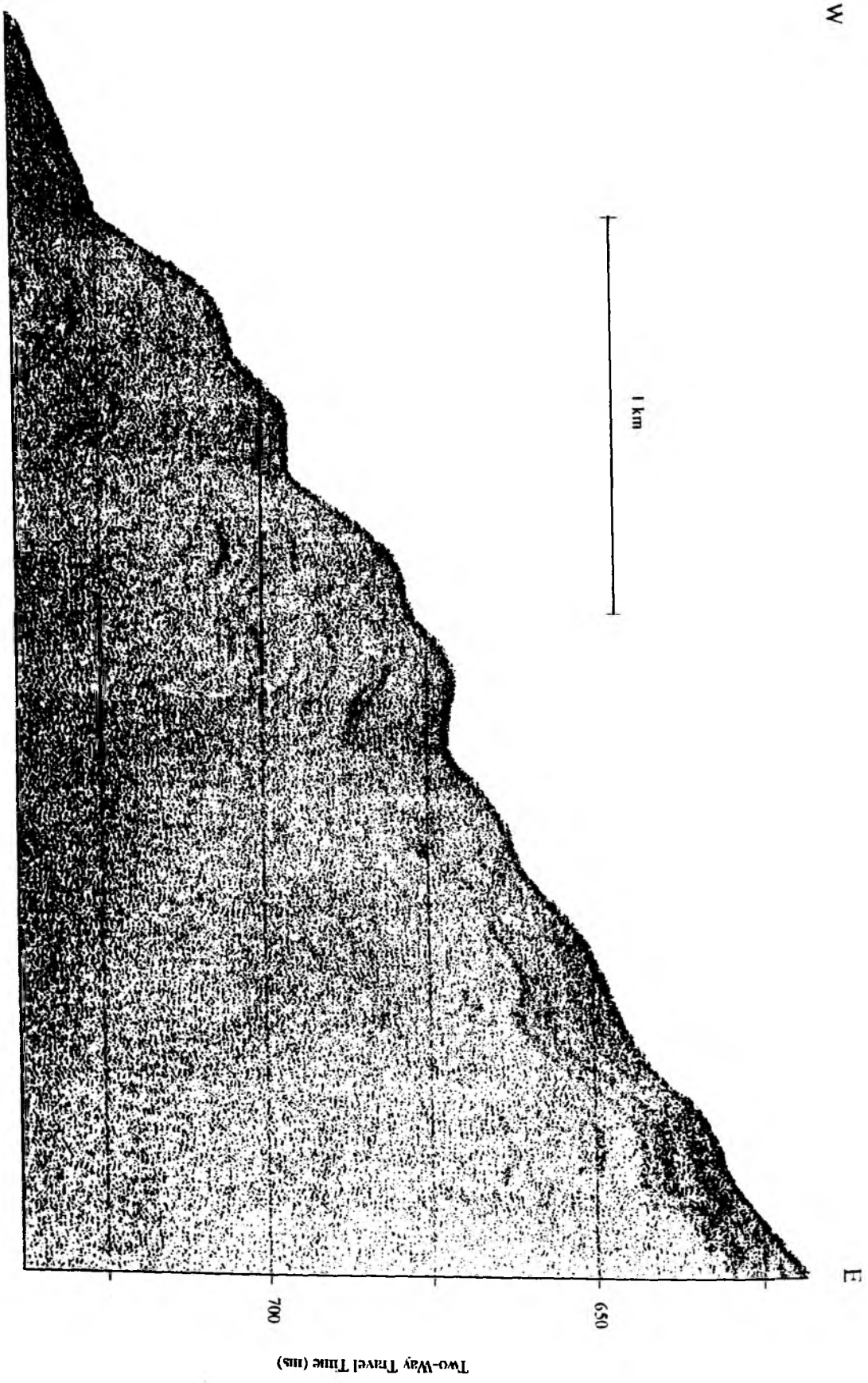

Fig. 3.17: Compressional structures on the slope of the northern area. Part of profile 16, 3.5 kHz record.

4. DISCUSSIONS

4.1 Tectonic structure of the INESSA area

By B. V. Baranov, B. Ya. Karp, H. K. Wong, T. Lüdmann, and K. A. Dozorova

Gnibidenko and Svarichevsky (1984) and Ginsburg et al. (1993) published their concepts on the systems of ancient and recent faults on the eastern Sakhalin slope. For example, they suggested the existence of a large, north-south striking rupture zone separating Sakhalin Island from the Derugin Basin. However, the tectonic nature of this zone remains obscure. Two fault systems oriented NNW and NNE have also been recognized in this region.

Tectonic data obtained during the INESSA expedition permit the formulation of a new approach to this question. The most interesting data were collected from the northern seepage area. All seismic profiles from this area show numerous stratal offsets. According to the displacement character of the reflectors, these offsets can be interpreted to mark reverse faults and thrusts (Fig. 4.1). Some of them appear to dip towards the continental slope while others dip towards the Derugin Basin. More detailed determination of the dip azimuths as well as the nature of the faults will be possible only after processing of the seismic data.

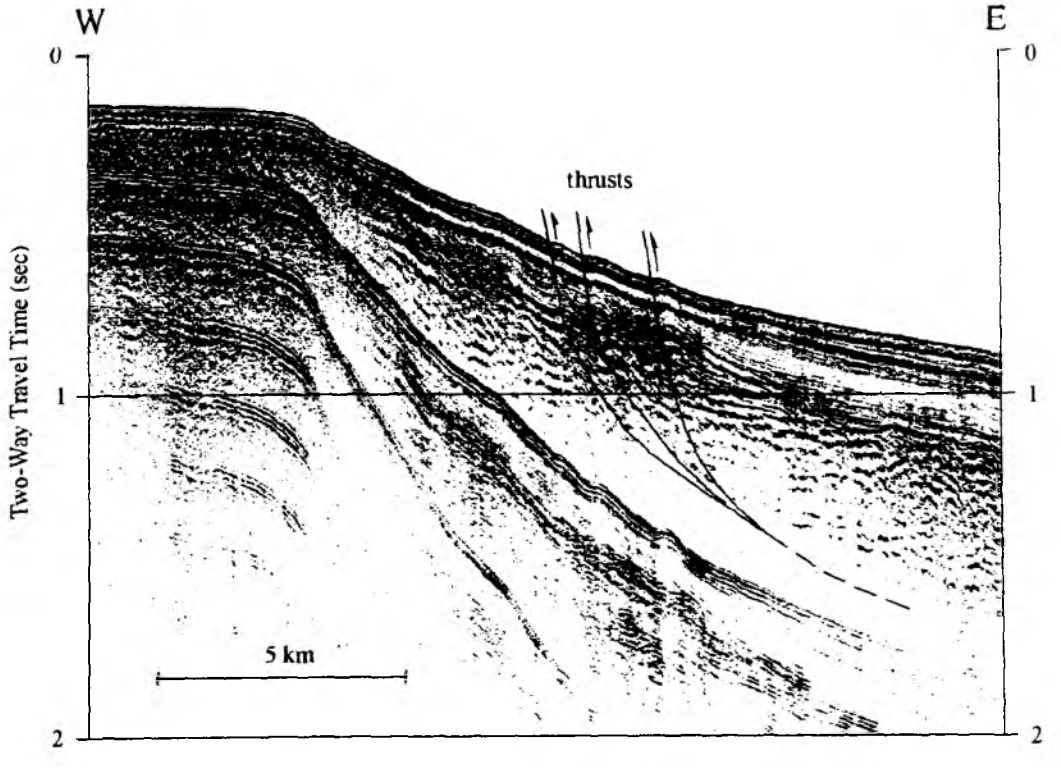

Fig. 4.1: *Part of seismic profile 28 showing thrusts on the slope of the northern area.*

In the northern area and on two profiles to the south, the main faults can be well-correlated across profiles so that their strikes (in the NW and NNW directions) can be inferred. Near the

northern seeps, these faults are concentrated in two zones (Fig. 4.2): upslope where the bottom gradient is particularly steep beginning at 700m water depth, and downslope starting from 800m depth. The abundance of these faults decreases to the south. They are widespread in the northern part of the area, but cease to exist south of about 54°22'N.

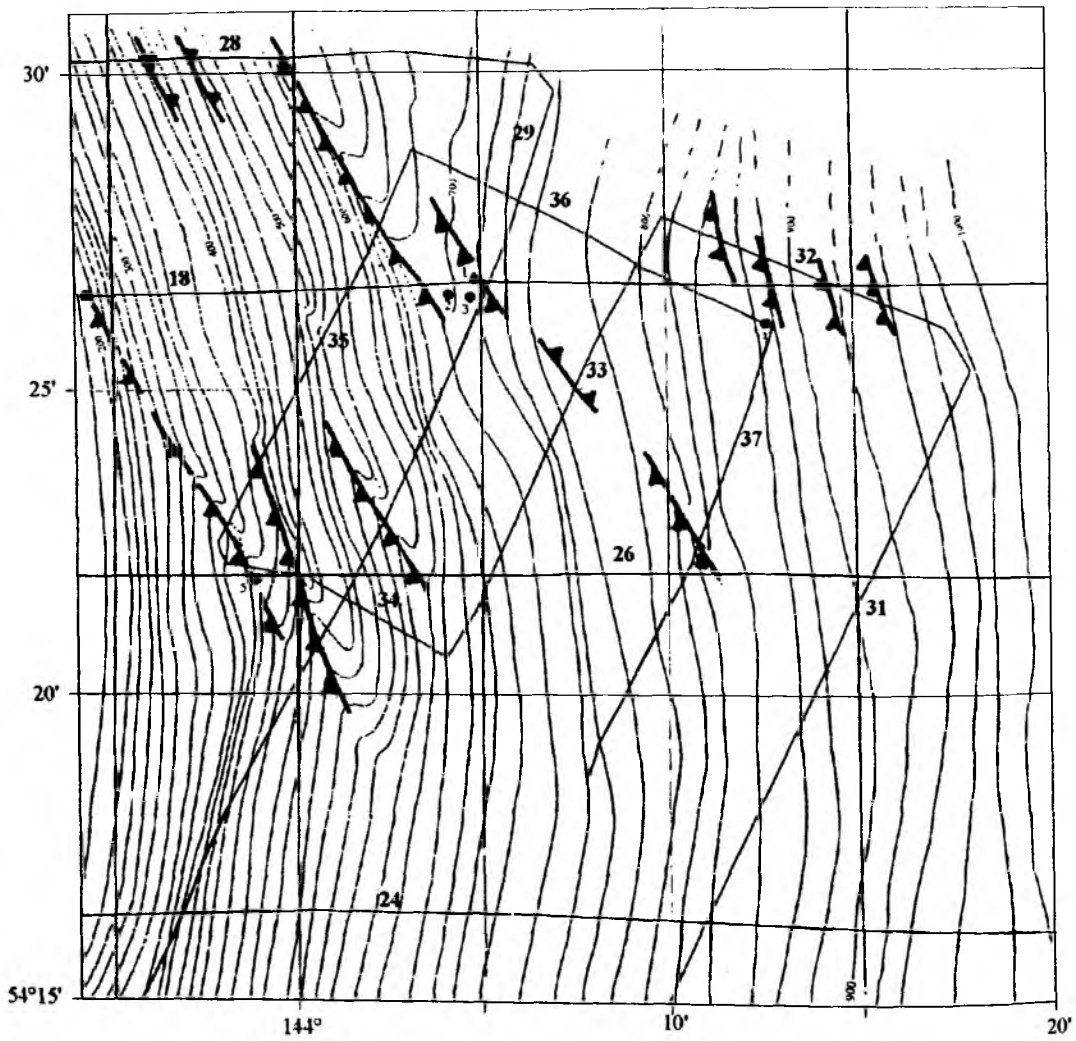

Fig. 4.2: Map showing the distribution of thrust zones. Dots show seep locations.

It should be noted that at this latitude, there is a change in the strike of the slope above the 600m isobath. To the north the slope strikes north-northwest; to the south it changes to north-northeast. The former corresponds to the strike of the reverse faults and one may assume that the latter gives the strike of the second fault system which is possibly strike-slip. We will return to this question again later. It suffices to note that the gradual disappearance of reverse faults towards the southeast implies that an orthogonal system of faults exists here and that these faults must in such a case be strike-slip. Faults within this reverse fault system form typical steps on the upper part of the slope and gentle scarps on its lower part.

The tectonic style of the southern seepage area is not very obvious. It should be noted that reverse faults that are widespread in the northern area are absent on seismic profiles from the south. Nevertheless, step-like relief on the upper slope is better manifested here. However, it is not possible to draw any conclusions on the type of displacements responsible for this morphology from the seismic profiles or from the 3.5 kHz echosounder records. On the echograms, such features look very similar to a series of normal fault scarps (see Figs. 3.14 and 3.15) although similarities to a system of reverse fault steps are present on some profiles.

The tectonic style of the eastern Sakhalin continental slope changes significantly from north to south. In the north, it is governed by a system of NNW- to NW-striking thrusts and reverse faults which governs the slope morphology. We can assume the existence of NNE-oriented strike-slips here. In the south, the faults are less well seismically expressed. They may show vertical displacements but are not correlatable with each other. Thus, one may conclude that the main displacements here are represented by strike-slips.

4.2 Seismo-stratigraphy and paleo-depo-environment

By H. K. Wong, B. Ya. Karp, B. V. Baranov, and T. Lüdmann

4.2.1 Basinal province

We suggest that sequence B1 is of Holocene age, and that the erosional unconformity between B1 and B2 marks the end of glaciation in this area. The turbid facies B2 is interpreted to represent glacial deposits. Similar seismic facies have been reported in other high latitude areas and have been attributed to sediments of the same origin (Anderson and Molnia, 1989; Menzies, 1995; Syvitski et al., 1997). The abundance of ice-rafted debris (glacial erratics) in bottom samples reported from the Derugin Basin (Gorbarenko et al., 1990; Vogt et al., 1997) lends further support to this interpretation. Deep sea drilling in the northwestern Pacific near the Meiji Guyot (site 192, leg 145) has presented strong evidence for a sudden increase in the vigor of deepsea circulation, in sedimentation rate, and in the component of fine-grained terrrestrial debris at the inception of glaciation (Rea et al., 1993). This change in sedimentation was dated at 2.6 ma before present. For lack of better information, we assume that the lower boundary of sequence B2 is of a similar age, so that B2 itself is formed in the Upper Pleistocene.

In the past, it was generally believed that Siberia was too dry to support the development of a large ice cap (CLIMAP Project Members, 1981; Biryukov et al., 1998; Velichko et al., 1993). Thus, the Sea of Okhotsk would have only experienced minor glaciations during the Pleistocene. Recent evidence, including computer model simulations, however, suggests that a Pleistocene highland ice sheet probably developed over the North Pacific Rim and spilled over into the Sea of Okhotsk (Hughes, 1995; Grosswald, in press; Grosswald and Hughes, 1998). During the stadials, ice could have advanced as grounded ice over the northern shelf, and

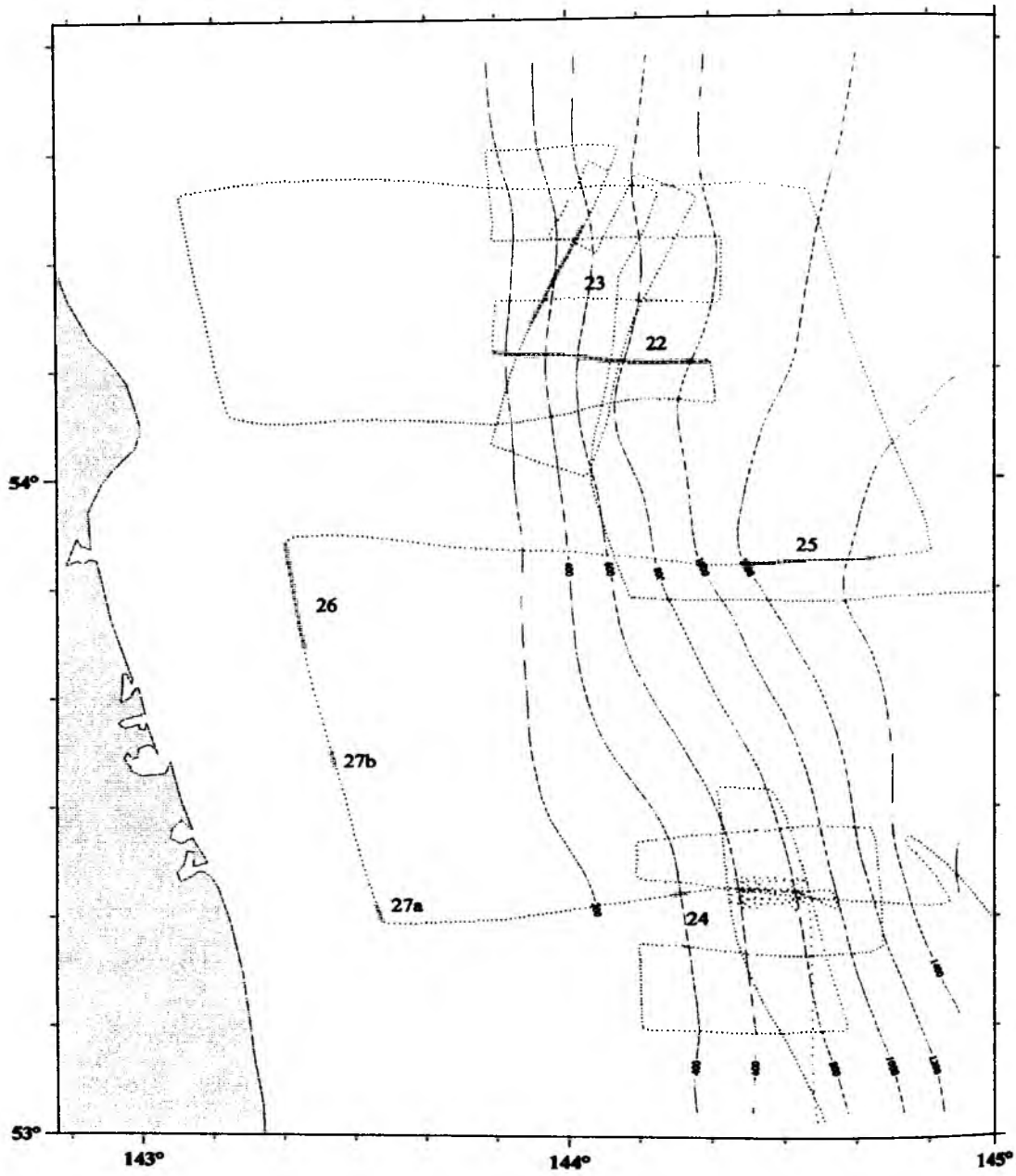

Fig. 4.3: Location of the selected profiles shown in Figs. 4.4-4.10.

continued as floating ice southwards, ending as a calving ice front along the Kurile Islands which acted as a pinning point. During interstadials, the ice front probably retreated to the northern shelf of the Okhotsk Sea. If this scenario is assumed to be qualitatively true, then a large amount of glacial sediments must have been transported over and deposited in our study areas, although the depositional pattern would be difficult to predict because the location of the ice front and its changes through time as well as the accompanying changes in the drainage systems, especially that of the Amur, cannot be readily reconstructed. However, the tongue-like extension of area II northwards onto the basinal slope suggests that ice advance from Sakhalin Island into the Derugin Basin must have played an important role in shaping the glacial sediment distribution pattern.

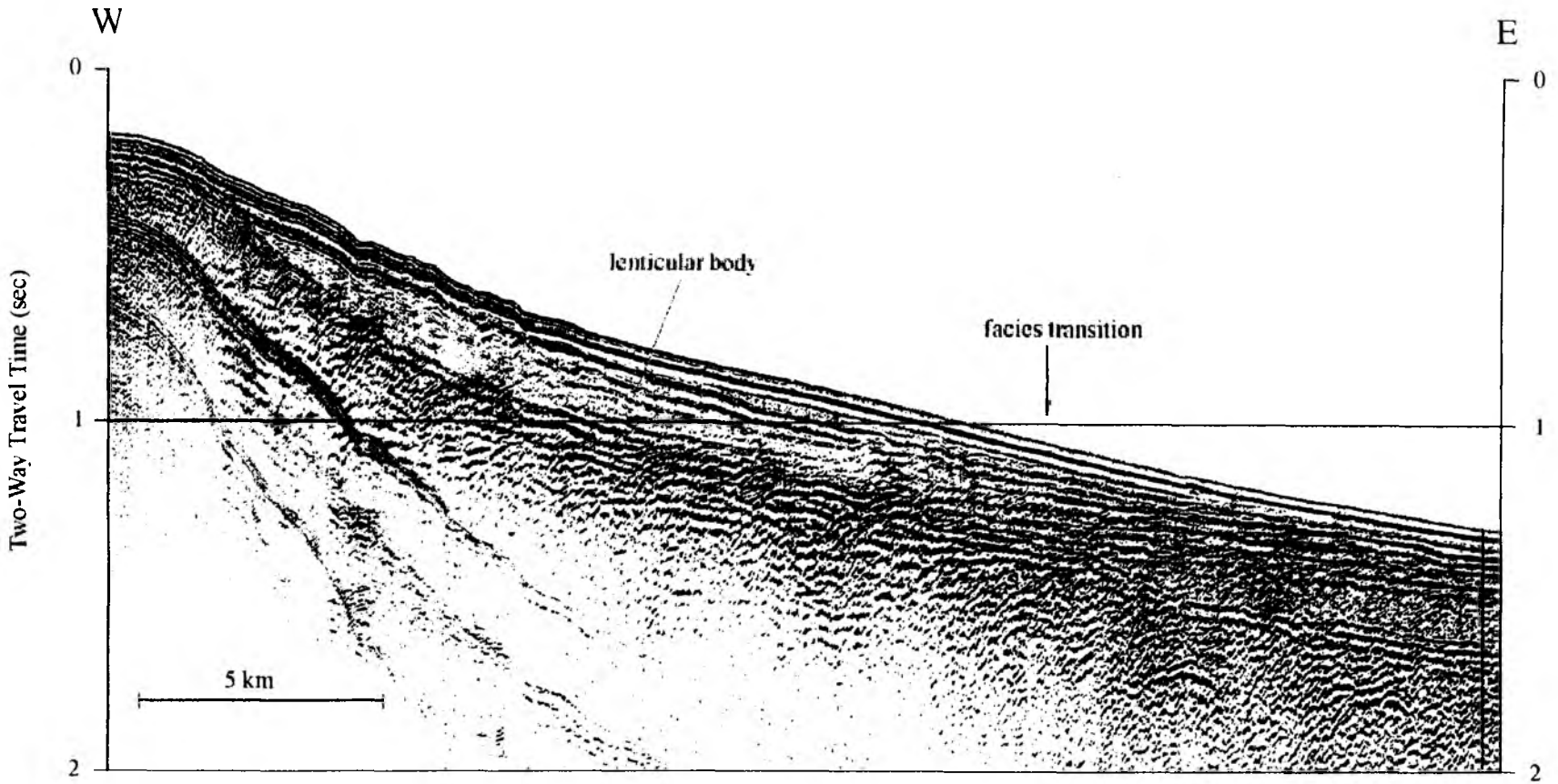

Fig. 4.4: *Reflection seismic profile 22 within the northern seepage area showing a lenticular, semi-transparent sedimentary body comprising two subsequences. See text for explanation. Note that the turbid facies grades abruptly to a well-stratified facies. See Fig. 4.3 for lacation.*

The turbid internal configuration of sequence B2 precludes its interpretation as glacial-marine sediments. Thus, our data provide evidence for grounded ice within the Derugin Basin, including its deepest parts, during the Upper Pleistocene. Progressive thickening of sequence B2 in the southerly direction is consistent with a southward advance of the ice front. Prior to this time, however, the high amplitude, stratified reflections of B3 suggest that glacial-marine conditions must have prevailed. That is, the spillover of the Siberian ice cap into the Sea of Okhotsk must have started as a floating ice sheet in the Derugin area in the Lower Pleistocene and became grounded only later in the Upper Pleistocene.

The sequences B4 to B6 are pre-Pleistocene in age. Gnibidenko and Khvedchuk (1982) reported that the maximum thickness of the Plio-Quaternary section within the Derugin Basin is about 1 km. In contrast, the profile I-I' of Zhuravlev (1984) implies that the corresponding thickness (thickness of their Pomyzskoe seismic unit) may exceed 1.2 km. Our profiles suggest that, if our age assignments are approximately correct, the maximum Quaternary thickness would reach about 1 km.

Using a core located at about 54.1°N, 146.3°E within the deep basin floor of the Derugin Basin, Gorbarenko et al. (1990) determined that the Holocene section consists of diatomaceous ooze, fine silt and pelite and is <1m in thickness. Our data suggest that the Holocene at the intersection of profiles 39 and 40 about 45 km away is beyond the resolution of our air gun seismic system, which is estimated to be about 15m.

4.2.2 Western slope of the Derugin Basin

As has already been mentioned, the turbid facies of the basinal province generally terminates abruptly at a sharp, steep boundary on or near the western and southwestern slope, giving way to well-stratified sediments. These boundaries mark not only a sudden lateral change in seismic facies, but often also in the dip of the strata. Such changes may be accompanied by different stratal offsets or offsets in opposite directions at different depths. These characteristics are typical for strike-slip faults (Christie-Blick and Biddle, 1985; Harding et al., 1983), the occurrences of which we infer from our data. Because the strike-slip faults (transpressive in the northern seepage area and transtensional in the southern seepage area) form an en echelon system (see 1.1), the depths at which the facies transitions occur vary. On the western slope, they range between 700m in the northern seepage area (NSA, profile 22, Figs. 4.3 and 4.4) and 1,500m in the southern seepage area (SSA, profiles 8 and 10). On the southwestern slope, they are at about 1,600m (profile 40, Fig. 3.5).

At the NSA, the spatial distribution of the stratified unit SL is limited. Here, Vogt et al. (1997) reported from 4 cores a 1-4.5m thick biogenic horizon underlain by terrigenous sediments that extend to the core bottom. On our profiles, the thick Holocene sequence consists of an upper

subsequence conformal to the seafloor and a lower, stratified to semi-transparent, truncated subsequence that terminates toplap updip (Fig. 4.4).

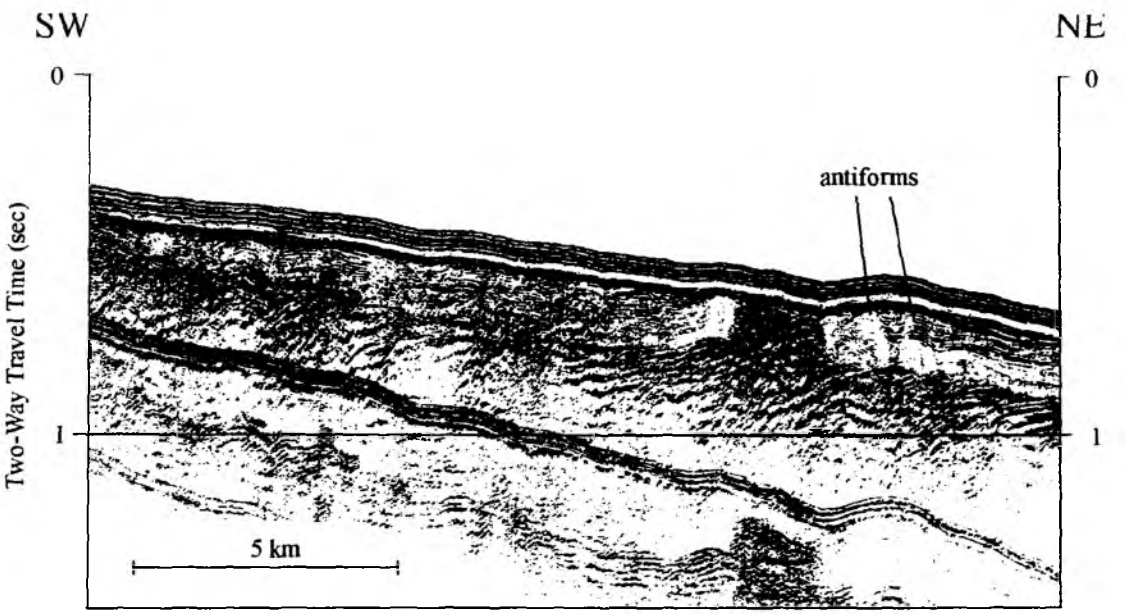

Fig. 4.5: Part of reflection seismic profile 29 from the upper slope of the Derugin Basin within the northern seepage area showing antiforms in the Holocene section. See Fig. 4.3 for profile location.

It is underlain by a stratified, partly discontinuous, high amplitude Pleistocene sequence which is in turn succeeded by a chaotic unit with intermittent reflections. On the upper slope, the Holocene section becomes more transparent although compressional features such as antiforms with their axes striking NW-SE are sometimes discernible (profile 29, Fig. 4.5). The base of the Holocene is a marked erosional unconformity. All in all, the upper slope here is dominated by this lenticular, compressionally deformed, semi-transparent, Holocene sedimentary body which we interpret to represent fluvial deposits of the River Amur.

Generally, it is believed that during the Holocene, fluvial sediments from the River Amur are transported east of Sakhalin southwards. Part of these sediments fill the Derugin Basin, while the remainder are subsequently deposited at a site to the south to form a large sedimentary apron east of central Sakhalin. The large reflectances (high amplitudes), the lack of echo prolongation and the limited penetration on 3.5 kHz echosounder profiles suggest that sediments on the western slope of the Derugin Basin are coarse and compacted (profile 14, Fig. 4.6).

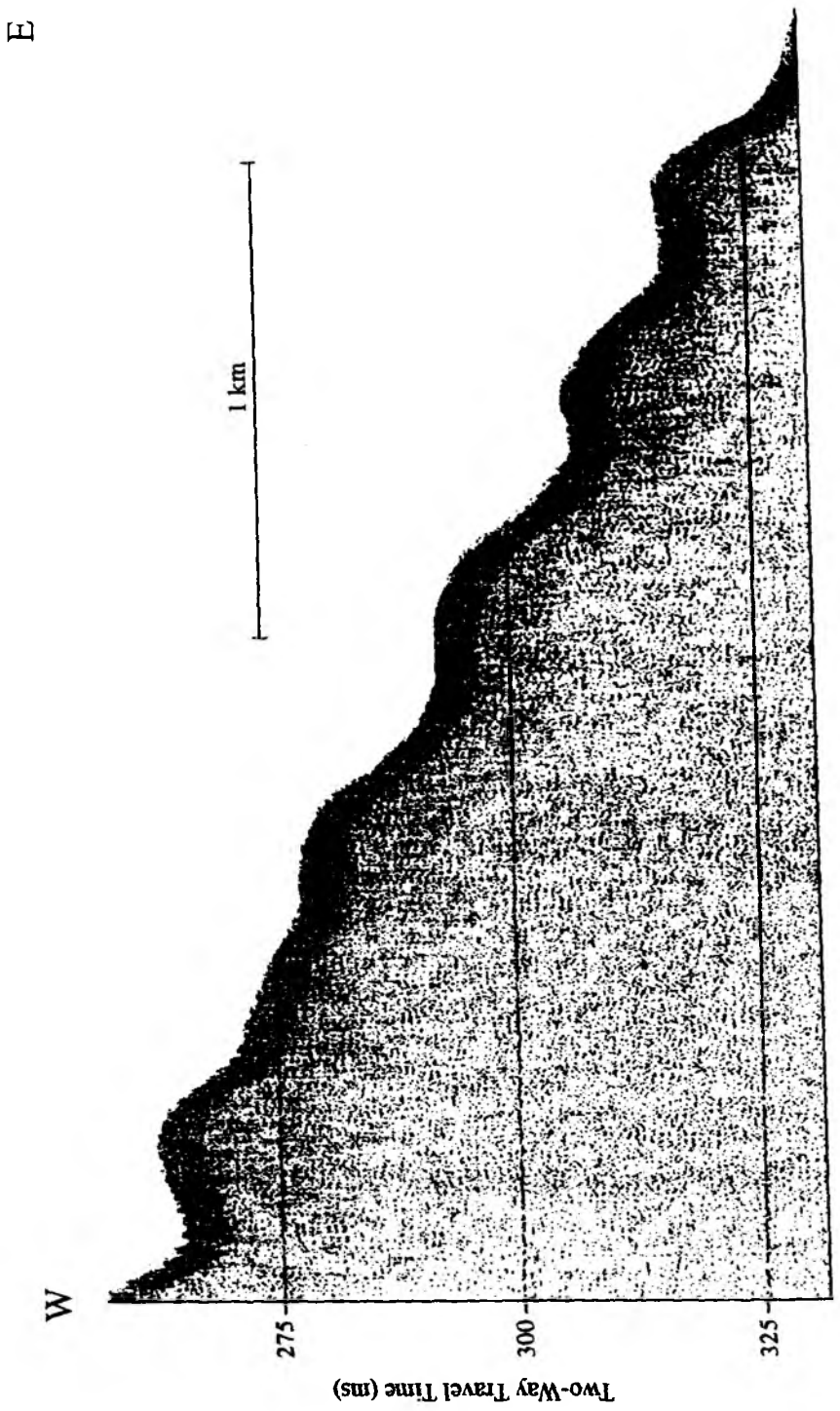

Fig. 4.6: *Part of echosounder profile 14 showing a high reflectance seafloor characterized by a lack of echo prolongation and limited penetration. See Fig. 4.3 for profile location.*

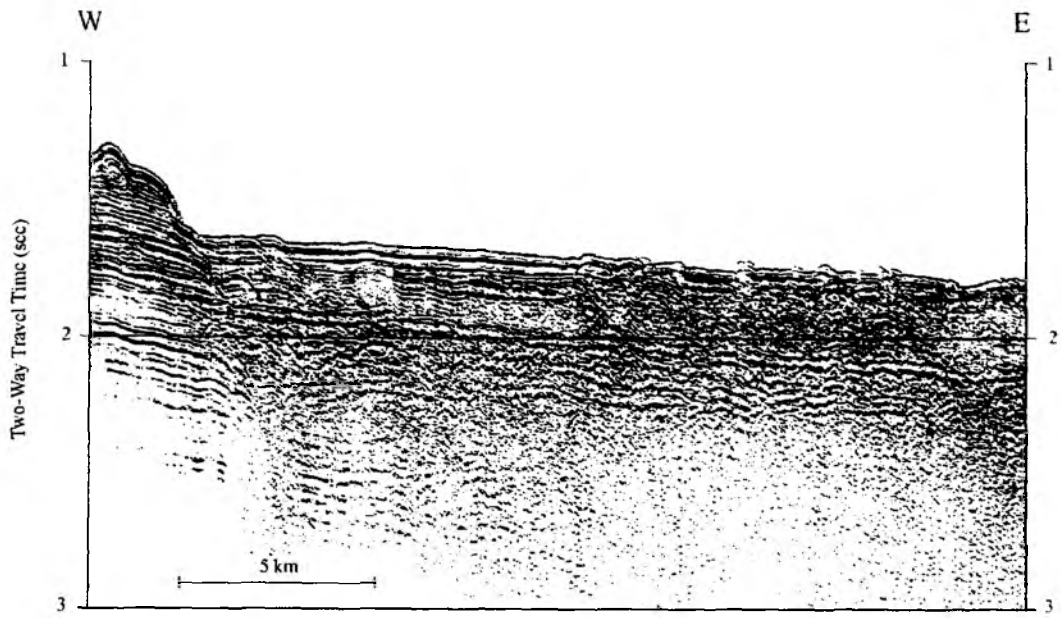

Fig. 4.7: Part of reflection seismic profile 16 with oblique reflectors interpreted as dipping strata dissected by steeper thrusts or overthrusts. See Fig. 4.3 for profile location.

Either the fine fraction is winnowed out, or it is deposited largely in the apron. Evidence for the former can be found in the correlation of the locations of the gas vents in the SSA with those of the methane anomalies in the surface waters. The southwestward displacement of the methane anomaly maximum with respect to the vents (see 4.3) suggests that there are significant currents flowing up the western flanks of the Derugin Basin from a northeasterly direction. This direction is also consistent with the NW-SE orientation of stripes of high and low backscattering strength mapped on sidescan profiles in this area. These currents may be responsible for the winnowing. If, however, only the coarse fraction is deposited on the western slope and the fine fraction is confined largely to the sedimentary apron, then the amount of sediments carried into the Sea of Okhotsk by the River Amur must be exceedingly large (52×10^6 t/a; Milliman and Meade, 1983).

Within the turbid facies at the western part of the NSA (profiles 16, 18, 20; Fig. 4.7) are correlatable, northwesterly dipping, partly continuous reflectors which probably represent dipping strata dissected by steeper thrusts or overthrusts. The fault trace of these thrusts can be reconstructed at locations where two or more of the prominent, flat-lying stratal interfaces at different depths are offset.

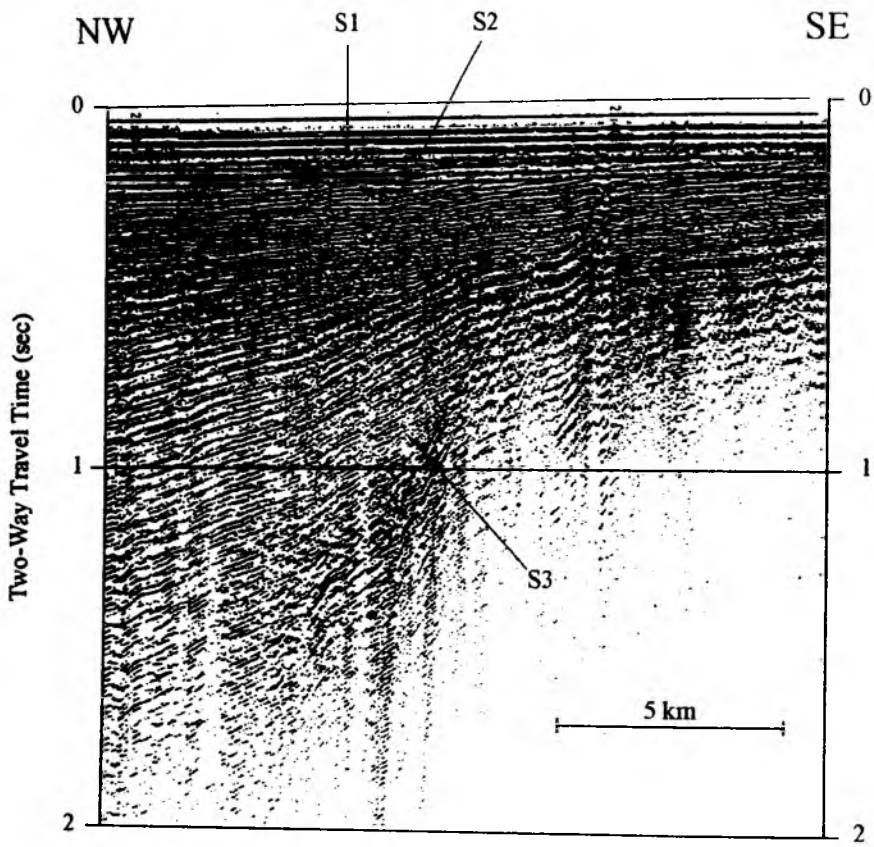

Fig. 4.8: Part of reflection seismic profile 15 which crosses the southern part of the East Shmidt Trough showing the upper basinal sequences S1 to S3. See Fig. 4.3 for profile location.

4.2.3 East Sakhalin shelf

The East Sakhalin shelf within our study area is dominated by the East Sakhalin Basin, which is separated into two subbasins by the Schmidt anticlinal zone (Gnibidenko and Khvedchuk, 1982). The western subbasin (the Piltun-Chaivinsk Trough) has a Neogene thickness (to the top of the metamorphosed Upper Cretaceous basement) of 5-9 km (Alperovich and Chernyavsky, 1973), while the corresponding value for the eastern subbasin (the East Schmidt Trough) is >7 km (Margulis et al., 1979).

Profile 15 subparallel to the Sakhalin shelf crosses the two subbasins of the East Sakhalin Basin. It shows that the Schmidt anticline is bounded by steep faults and that the basinal sediments penetrated can be divided into 3 sequences (Fig. 4.8). The lowermost sequence S3 comprises subparallel, large amplitude reflectors of low frequency and high continuity. The middle sequence S2 is a basinal fill which onlaps S3 in the south and downlaps it in the north. It probably represents fluvial-glacial sediments of the Pleistocene. The uppermost sequence S1 consists most likely of Holocene fluvial deposits derived from the River Amur. Both sequences S1 and S2 diverge and therefore thicken to the north, suggesting an increase in distance to the

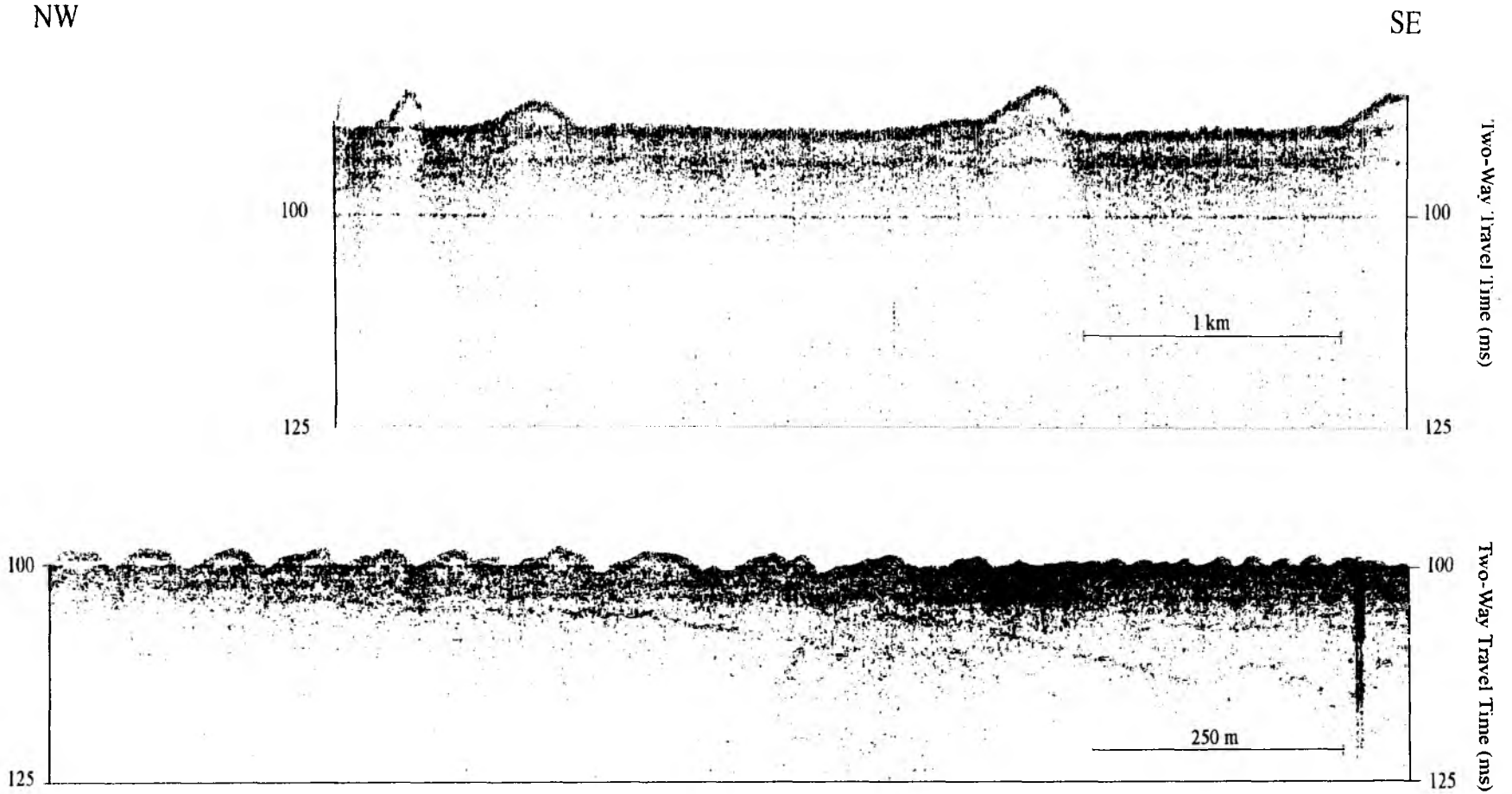

Fig. 4.9: *Part of echosounder profile 15 showing possible asymmetric sand ridges 2-4m in amplitude and several hundred meters in width. See Fig. 4.3 for profile location.*

Fig. 4.10: *Part of echosounder profile 15 showing a sandwave field. See Fig. 4.3 for profile location.*

sediment source as one moves south. The maximum of the shelf sequences penetrated is about 2 sec TWT.

3.5 kHz echosounder data obtained along profile 15 shows large sand ridges (?) with an asymmetric cross-section, 2-4 m in amplitude and several hundred meters in width (Fig. 4.9). They are possibly tidal in origin (the long axis of the tidal ellipse here is oriented north-south and the tidal current is of the order of 5 cm/s, Talley and Nagata, 1995) in which case they would be oriented parallel to the flow of the Amur (see Berné et al., 1997; Gensous et al., 1993; Nio and Yang, 1991). The sand ridges are succeeded by a distinct sandwave field (Fig. 4.10). These observations imply that the hydrodynamic regime plays a very important role in shaping the present-day bottom morphology on the inner northern East Sakhalin shelf.
In general, the inner East Sakhalin shelf is characterized by a thick, divergent, well- stratified sedimentary section that progrades seawards. This section is capped by a distinct erosional unconformity (glacial erosional surface) which is overlain by a Holocene sequence conformal to the seafloor. The shelf usually grades to the slope province across a well defined shelfbreak, although a ramp margin geometry has also been observed. This may be a result of tectonic influence.

4.3 Saturations of methane and carbon dioxide in the surface waters off Sakhalin

By S. Lammers

4.3.1 Preliminary results

During 15 days of continuous analyses, roughly 5400 GC measurements of CH_4 and CO_2 were performed, 50 % of which are surface water values and 25 % air values. About 250 MBytes of GC and sensor data require post-processing, synchronization with the recorded GPS data, and summarizing before reliable conclusions can be drawn. It must also be taken into account that a correlation between surface measurements and vent activity remains uncertain, unless information from CTD and gas surveys of the deeper water column is available. Here, a first overview on the observations on methane is given, since this information is of higher importance for the planning of the subsequent vent surveys with the *RV Akademik Lavrentyev*.

At first sight, supersaturation of methane in surface waters dominated in all survey areas off Sakhalin, only seldom was methane in equilibrium with air (i.e., 100 % saturation). Fig. 4.11 illustrates the maxima of CH_4 saturations observed in the southern survey area (between 144-145°W and 53-53.6°N) with more than 450 % saturation relative to the ambient atmosphere. The average value in this area was roughly 170 %. The data shown refer to a constant in-situ temperature (17° C) and salinity (30‰) and are thus subject to modification after post-processing.

Fig. 4.11: Methane saturation maxima observed in the southern seepage area (between 144-145°W and 53-53.6°N) with more than 450% saturation relative to the ambient atmosphere against an average value in this area of roughly 170%. These saturation values are calculated relative to a constant in-situ temperature (17°C) and salinity (30‰).

Towards the north, the surface hydrography was increasingly affected by the Amur freshwater discharge, as local salinity minima as low as 23 ‰ (ambient: about 28 ‰) were recorded. Variation of salinities by almost 4 ‰ within 20 nm might be attributed to a fanning of freshwater flows north and northeast of Sakhalin.

In the northern survey area, CH_4 supersaturation was also abundant, although less intense compared to the southern area. Maxima between 370 % and 230 % were observed, ambient values being 120-150 %. A correlation with salinity was not evident.

Tab. 4.1: Compilation of significant maxima of the CH_4 saturation with associated values of salinity and temperature. Saturations are calculated for 17°C water temperature and 30 ‰ salinity.

CH_4 (ppm)	Sat. (%)	Sal. (ppt)	Temp. (°C)	Date	Time (UTC)	Filename
6.98	370	28.2	14.8	24.07.1998	03:19:56	cha#40.chr
6.51	350	28.1	14.8	24.07.1998	04:17:39	cha#52.chr
6.34	340	28.1	15.4	24.07.1998	06:57:43	cha#92.chr
6.20	330	24.2	15.2	24.07.1998	18:41:49	cha#268.chr
4.27	230	22.2	16.7	24.07.1998	23:37:52	cha#342.chr
7.04	380	25.2	15.0	26.07.1998	06:15:29	cha#92.chr
6.97	370	31.0	17.4	29.07.1998	02:43:20	cha#24.chr
4.55	240	31.3	11.3	30.07.1998	17:47:21	cha#258.chr
6.40	340	31.3	9.0	30.07.1998	20:35:18	cha#300.chr

4.3.2 Discussion and outlook

From the first overview on the raw data from the INESSA gas survey, it is already evident that most parts of the areas investigated are net sources with respect to atmospheric methane. The largest supersaturations in the southern survey area appear to be isolated from surface currents and may thus be the surficial image of an intensive venting located at about 700m water depth at the major fault zone of this area (cf. chapter 4.1, 4.4). The horizontal distance between the surface maximum and the presumed vent is roughly 5 nm in a NE-SW direction which parallels the prevailing water current. If this assumption is correct, it would be a remarkable height of the water column penetrated by a vent plume. Whether sources of methane other than venting (e.g., hydrographic features, *in situ* methanogenesis etc.) contribute to the overall supersaturation in this region needs to be clarified by the subsequent hydrographic surveys with the *RV Akademik Lavrentyev*.

As primarily intended, the data of the INESSA gas survey will permit an integration of the air-sea fluxes of methane and carbon dioxide over the study area. A major drawback in doing this is that data coverage is restricted to the region east of Sakhalin due to a severe delay of the cruise. The reliability of GPS recordings requires improvement on future expeditions. All in all, the combination of geophysical and surface gas surveys allows us to maximize both data resolution and ship time usage.

4.4 Areas of Gas Seepage

By B. V. Baranov, B. Ya. Karp and H. K. Wong

4.4.1 Mapping of the seeps

The seeps are found in two areas - a southern and a northern area located at latitudes of 53°25'N and 54°26' N respectively. Ten vent sites were known before our cruise: 6 sites in the southern seepage area and 4 in the northern. Two additional sites were found during the present cruise.

A detailed bathymetric map was prepared for the southern seepage area (Fig. 4.12). Here, the seeps are located in two zones, namely at the depth ranges of 700-800m and 500-600m respectively. The morphology of these zones is quite different.

The morphology of the upper slope has already been described (see 3.3.2). The lower slope is characterized by the existence of grooves and mounds. Our profiles show that the active seeps correlate with them. Unfortunately, our data are insufficient for an accurate determination of the strike of these (relief) structural elements; but we presume that they are oriented in the west-northwesterly direction as indicated by the contour deviations of Fig. 4.12. Mounds are seen distinctly on 3.5 kHz echosounder records (Fig. 4.13) and thus can serve as indicators during the search for new seeps.

Four sites of known seeps and two new sites were found during the cruise in the northern seepage area. The coordinates of the new sites are: (1) 54°21.959'N, 143°58.911'E, depth 390m; (2) 54°26.21'N, 143°54.24'E, depth 194m. A detailed bathymetric map of this field has been compiled earlier (Ginsburg et al., 1993), but regional profiles carried out during the present cruise yield new information on the morphology of this region. As the track spacing was rather large, we prepared the map manually (Fig. 4.14).

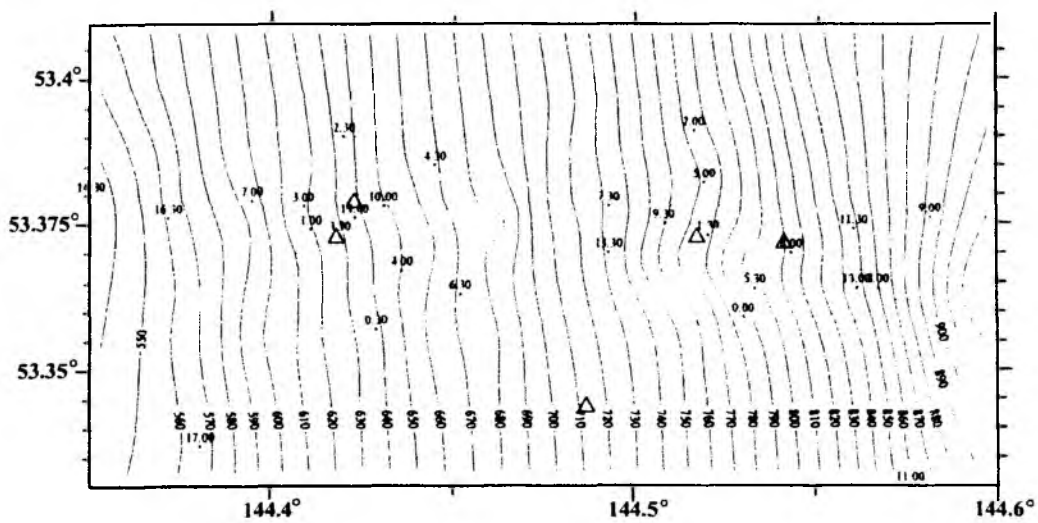

Fig. 4.12: *Bathymetric map of the southern seepage area. Contour interval is 10m. Triangles indicate seep location. Dotted lines show tracks.*

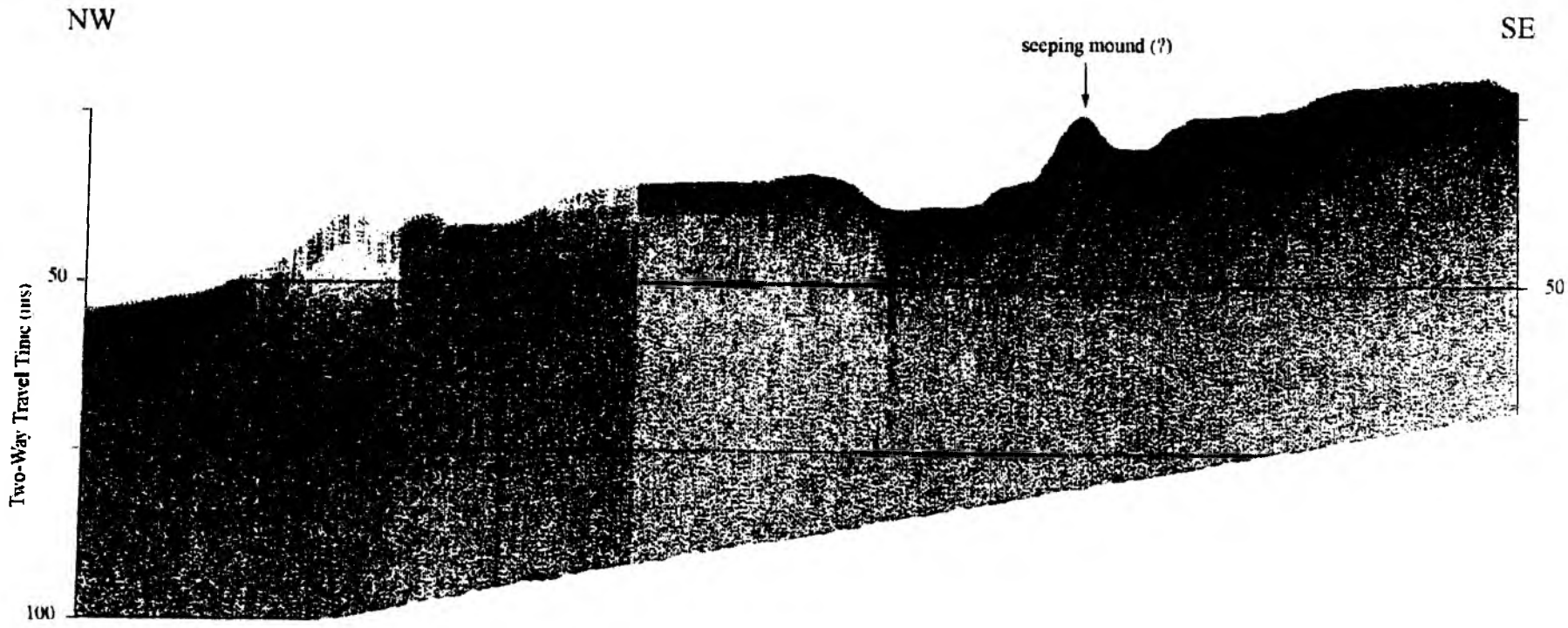

Fig. 4.13: Example of mound associated with a presumed seep. Part of profile 13, 3.5 kHz record.

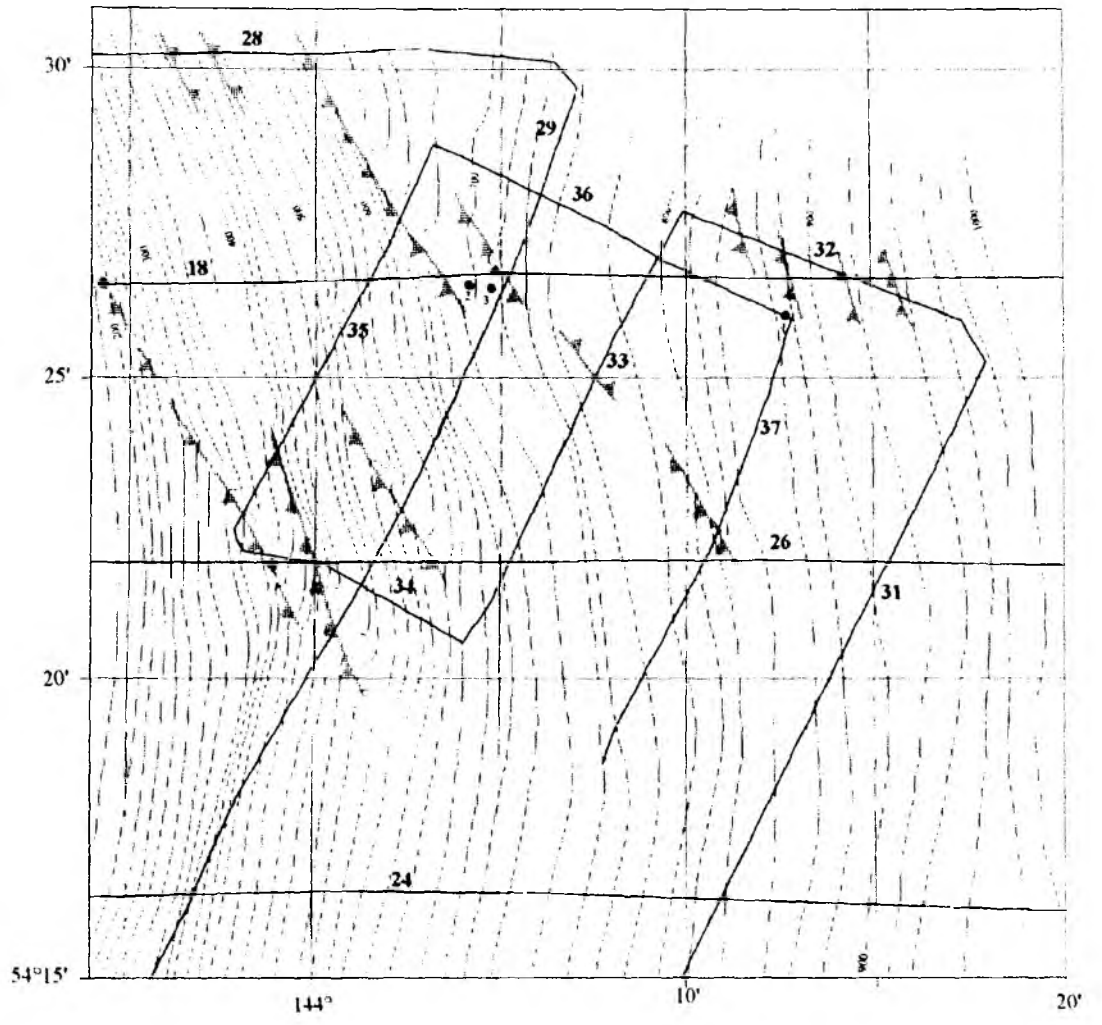

Fig. 4.14: Bathymetric map of the northern seepage area. Dots show seep locations.

It can be seen here that the seeps are well correlated with certain relief elements, namely with steps which are characteristic of the northern part of the slope.

3.5 kHz echosounder records demonstrate clearly that seep sites are morphologically quite different from the surrounding areas. Firstly, they represent symmetrical mounds of about 10 m in height. In addition, reverse fault scarps dominate in the north while asymmetric normal fault scarps exist in the south. Secondly, the upper sedimentary layers of each of these mounds curve up on echo-sounder records which point strongly to gas saturation in the sediments (Figs. 4.15 and 4.16). This fact should be regarded as a powerful prospecting indicator and should be used in the search for active vents.

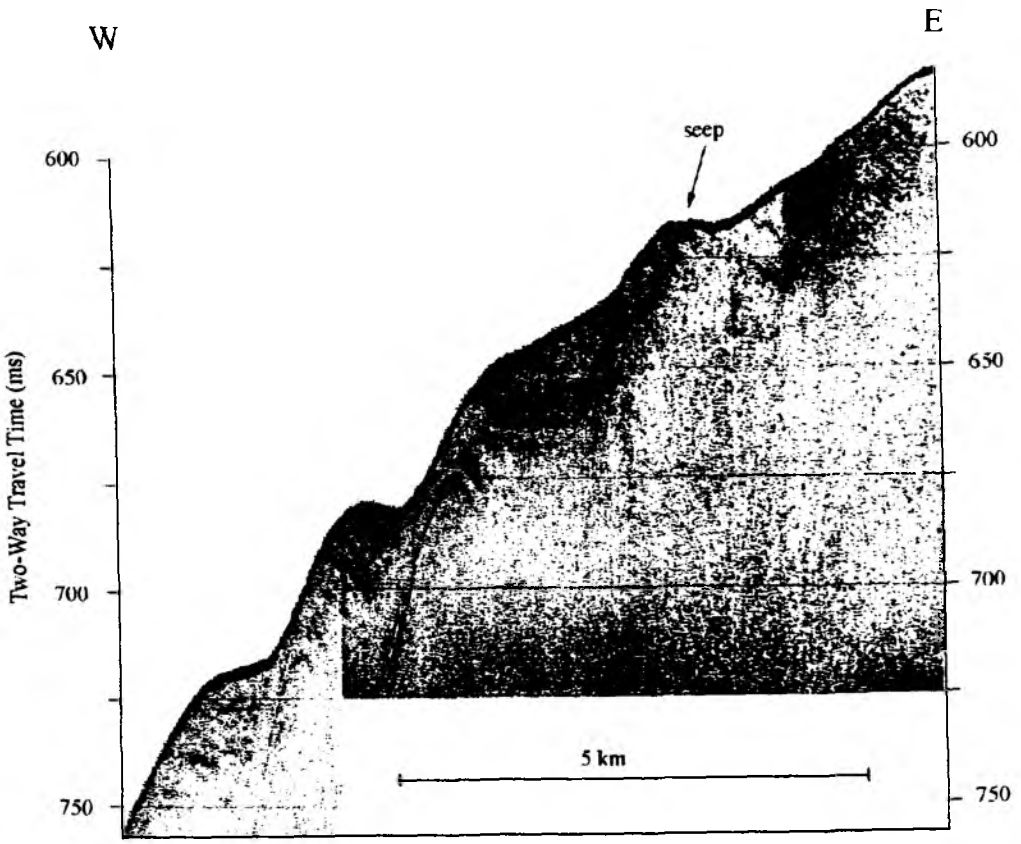

Fig. 4.15: Example of mound with seep on the Sakhalin slope. Part of profile 29, 3.5 kHz record.

Bathymetric investigations carried out during the INESSA cruise show that there are significant morphological differences between the northern and the southern seepage areas. These differences can be observed in the general structure, the form of the slope, as well as in the structure and character of its separate elements. Two explanations for these differences may be offered: the first is tectonic and the second in terms of the sedimentation regime. We will discuss the first possibility in chapter 5.2 while the second has been discussed in the section of this report on seismo-stratigraphy and sedimentation regime.

4.4.2 Botton simulating reflectors and the gas hydrate zone

High amplitude BSR's (bottom simulating reflector) which approximately follow the bottom relief are observed over extensive parts of the study area suggesting the widespread occurrence of gas hydrated-cemented sediments (Fig. 4.17; Hyndman and Davis, 1992; Hyndman and Spencer, 1992; Lee et al., 1994). Along profile 1 at water depths around 1,400m, the shallow BSR occurs at about 200 ms subbottom. It marks the upper boundary of the gas hydrate zone in which sediments cemented by gas hydrates are found. At depths shallower than this boundary, the hydrates are unstable and gas coexists in combination with pore water (Mienert and Posewang, 1997). A second, characteristically strong BSR cutting across the well-defined stratifications near the upper boundary of the middle sequence is found at greater depths (ca. 530 ms subbottom; see 3.1). It marks the lower boundary of the gas hydrate stability field. Its

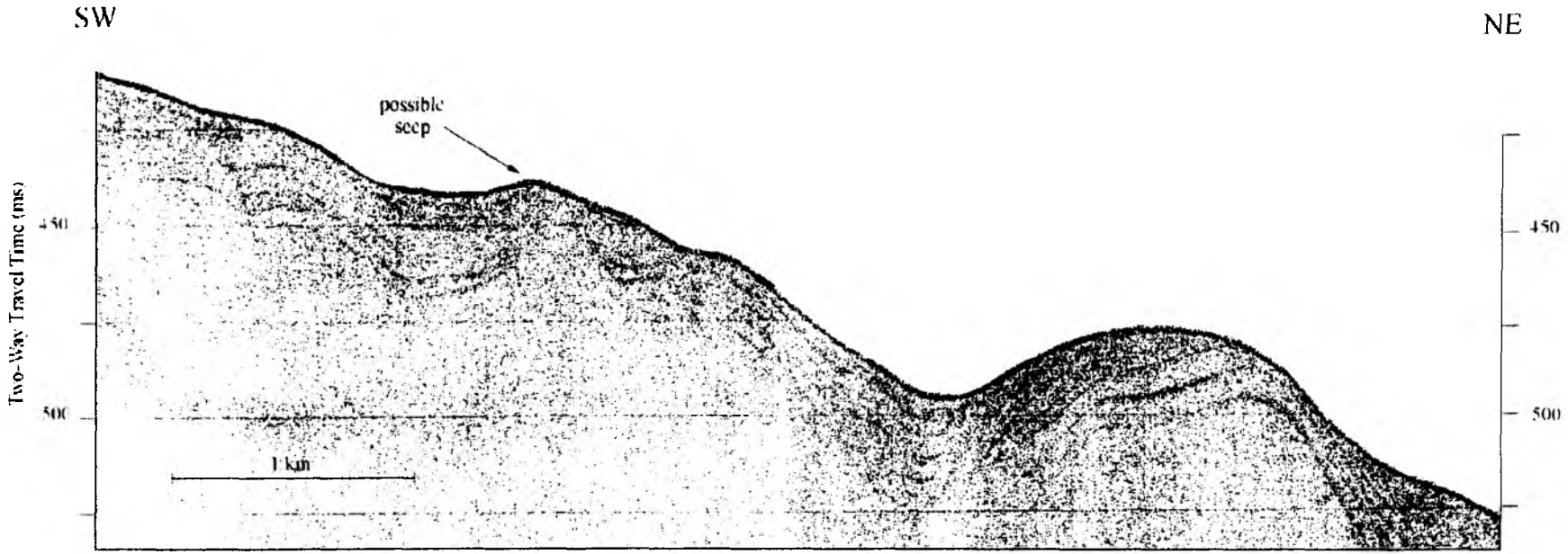

Fig. 4.16: Example of a possible seep with associated mound. Part of profile 26, 3.5 kHz record.

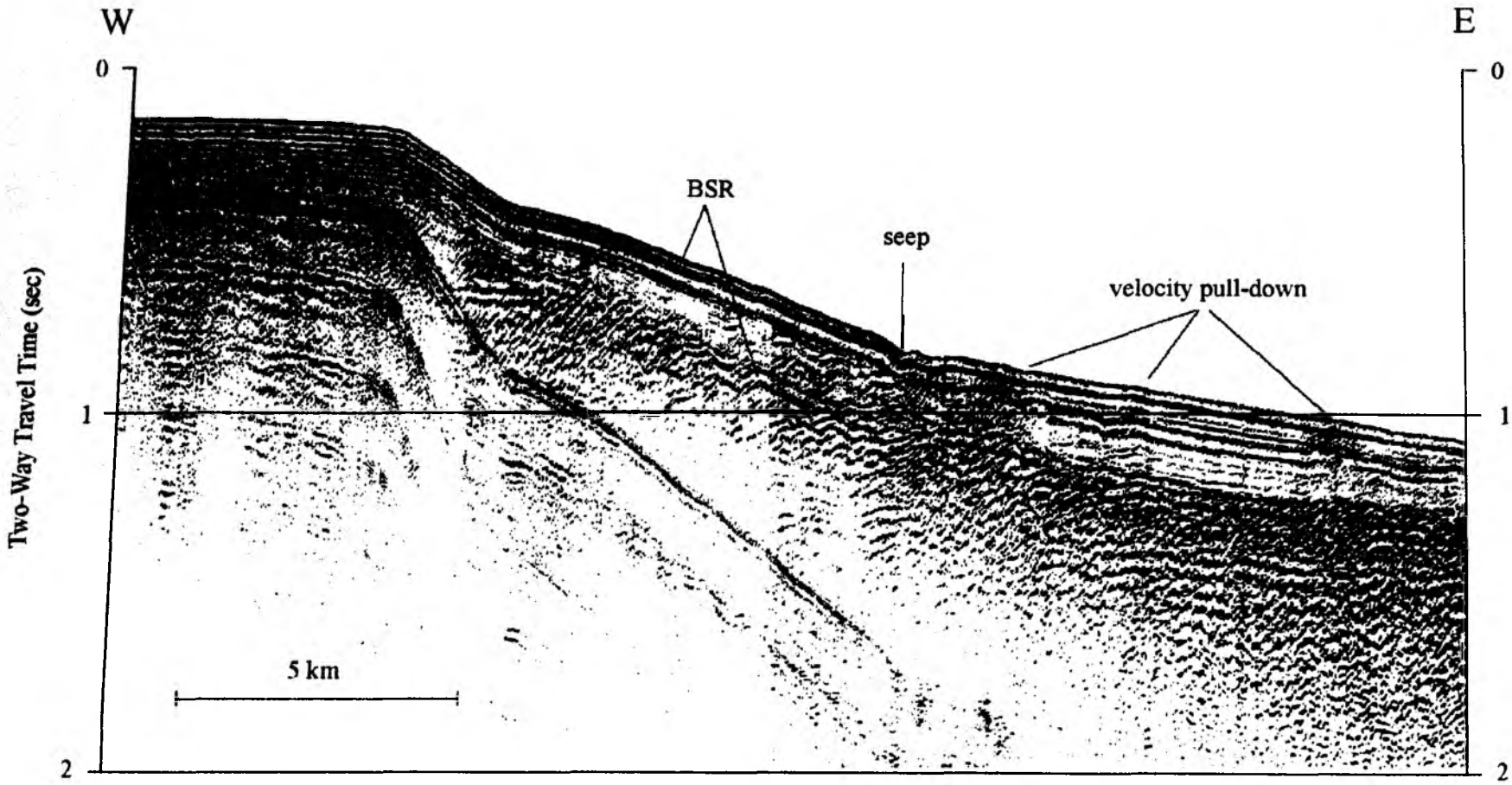

Fig. 4.17: Seismic profile showing a cross-section of seeps. Part of profile 18.

position is a function of the water depth (hydrostatic pressure), the thermal gradient (temperature) and the gas composition. Between these two BSR's, gas hydrate can coexist with gas. The average thickness of the gas hydrate zone along this profile is about 330 ms. Assuming a mean velocity of 1,780m/s (Mienert and Posewang, 1997), this corresponds to a thickness of 290m, a value which is comparable to that of 285m reported from the northern Norwegian Sea. We note that the surface geothermal gradient in the Norwegian Sea is considerably lower (5.5°C/100m) than that measured in the eastern Derugin Basin (8°C/100m; GERDA, 1995), but the water depth (1,000m) and the bottom temperature (at 65°N) are also both lower. At shallower water depths, the thickness of the gas hydrate stability zone is reduced (200m in thickness at 300m depth along profile 14).

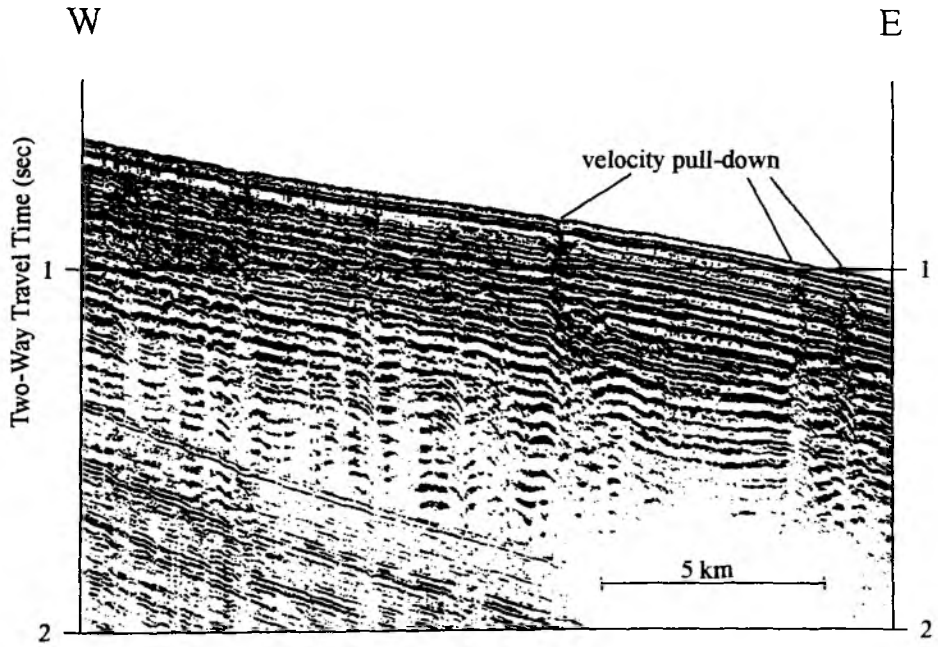

Fig. 4.18: Velocity pull-down structure. Part of profile 10, southern area.

The sedimentary column of the study area, especially that of the southern seepage area, is repeatedly interrupted by vertically oriented regions of acoustic turbidity in which some of the reflectors are masked and in general the reflection amplitudes are reduced. Typical are also apparent deformations and interruptions of the (mostly flat-lying) horizons. These include velocity pull-down (gas has a lower seismic velocity; Fig. 4.18) and increased amplitudes (enhanced acoustic impedance contrasts), but velocity pull-up is also common (mean velocity of gas hydrate may be higher than that of the surrounding sediment). These regions may mark channels along which gas rises through the sediments. Isolated troughs at the seafloor may represent pockmarks, places where gas has reached the bottom and sediments have been locally removed by the rapidly escaping gas. However, not all of these "pockmarks" are underlain by turbid zones and not all turbid zones are accompanied by "pockmarks".

Adjacent to the southern seepage area where the shelf is characterized by a ramp margin without a distinct shelfbreak, the lower BSR ascends from its normal depth towards the seafloor. The points of ascent lie within the water depth range of 450-550m. The 6 gas seeps with their accompanying plumes at the seafloor all occur near to but seawards of the points of ascent. Because these points can be correlated to thrusts, a causal relationship between thrust tectonics (and hence the partial destruction of the integrity of the gas hydrate zone with its consequent pressure release) and gas seepage is strongly suggested.

5. Conclusions

INESSA scientific party

KOMEX is a multidisciplinary project and encompasses a number of objectives related to a study of the Okhotsk Sea geosystem, in particular its structure and evolution. The INESSA expedition is directed at two of these objectives: (1) an investigation of the tectonic structure of the Okhotsk Sea, and (2) a study of the sedimentation history and paleo-environment. In addition, special attention is paid to the problem of a possible causal relationship between tectonic pattern and seep distribution. It is well known that such a relationship exists in subduction zones. Therefore, finding and formulating a similar relationship here and, based on this, making specific recommendations for the following geological and geochemical KOMEX cruise on the *RV Akademik Lavrentyev* was one of the important tasks of the present cruise.

5.1 Tectonics

The tectonic regime of the continental slope off Sakhalin Island, at least in the northern INESSA study area, is controlled by a system of thrusts and reverse faults oriented in a NW-SE direction. Faults exist on the entire continental slope from the shelf down to a depth of approximately 1,000m. These faults are active because they continue through the sedimentary column to reach the seafloor where they form scarps or step-like relief on the slope.

The area around Sakhalin Island is seismically active. All earthquakes here are shallow with focal depths of as a rule not more than 30 km. The general trend of the seismicity is north-south. The epicentres of the earthquake with moderate magnitudes (M>5) occur on both flanks of this island, though to the south the majority of them are concentrated along the western coast. The eastern boundary of seismicity lies in the Okhotsk Sea and includes the system of reverse faults investigated during this cruise.

It is reasonable to assume that the tectonic pattern offshore Sakhalin corresponds to that of Sakhalin Island. As is already known, the main structure of the Sakhalin Island is the Central Sakhalin Fault (Fig. 5.1). It extends for a distance of 600 km and disappears in the north under Quaternary sediments and in the south in the La Peruse Strait between Sakhalin and Hokkaido. The Central Sakhalin Fault strikes almost north-south, being slightly distorted near 142° and 143°E. It consists of a series of almost linear segments. The longest among them are oriented in the northwesterly direction (340-0°) and are displaced relative to each other by shorter segments represented by right-lateral strike-slips striking from N10°E to N45°E. The ratio of the long to the short segments determines fault stretching in general. These faults extend from the southern part of the island in a north-northeastern direction to the northern edge of Terpeniya Bay and consist of many right-lateral strike-slips in between. Farther to the north its strike changes to north-northwest because there are not

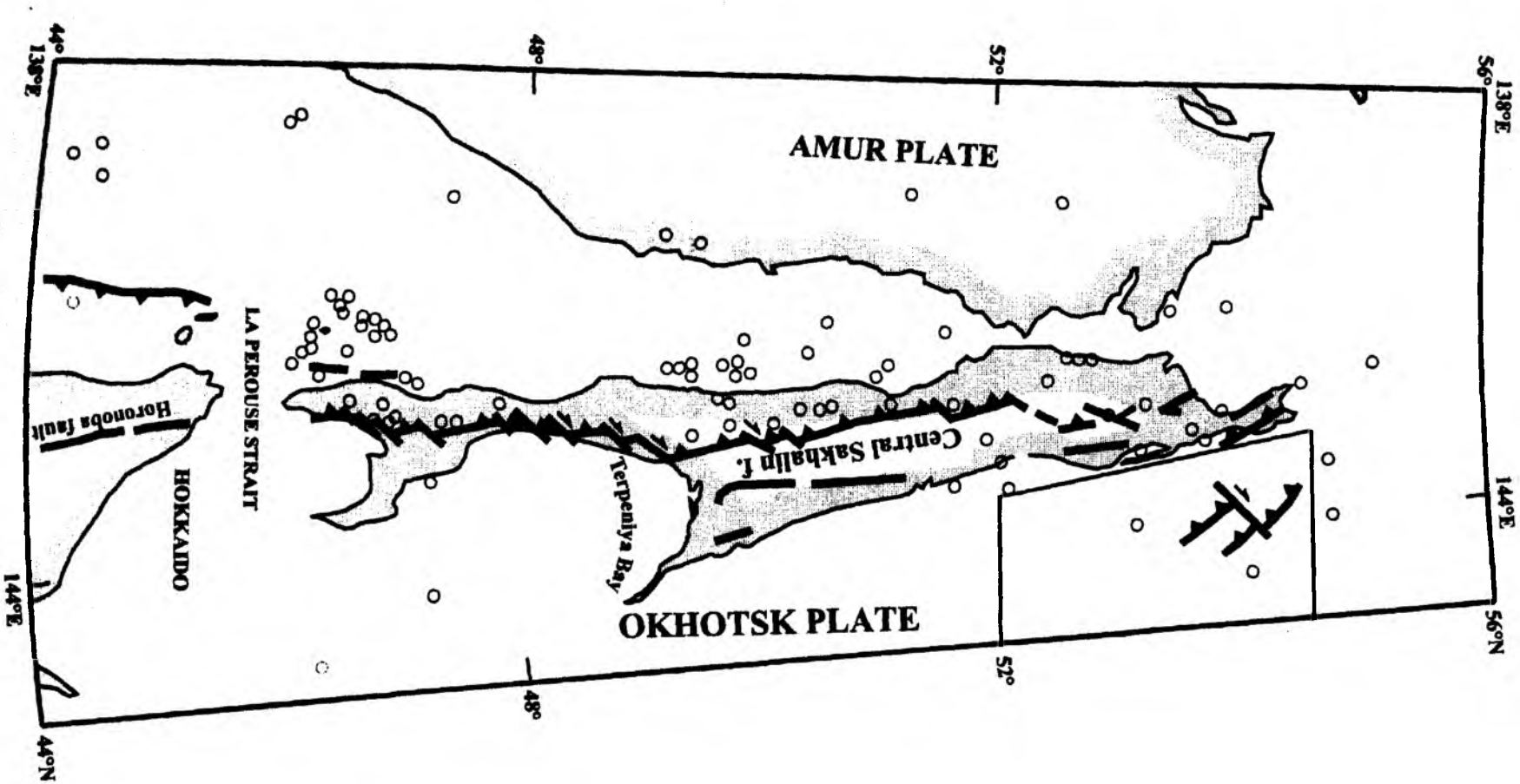

Fig. 5.1: Tectonic structure of Sakhalin Island and the INESSA area (dashed line). Lines with teeth mark reverse faults, lines with arrow indicate strike-slips. Dotted line shows eastern boundary of the Sakhalin seismic belt. Thin lines give contours of gravity anomalies.

many strike-slips in this segment. Detailed structural investigations carried out on the short as well as on the long fault segments demonstrate that the former are almost pure dextral strike-slips and the latter are thrusts with a strike-slip component (Fournier et al., 1994). This structural pattern corresponds to the orientation of faults mapped during the INESSA cruise.

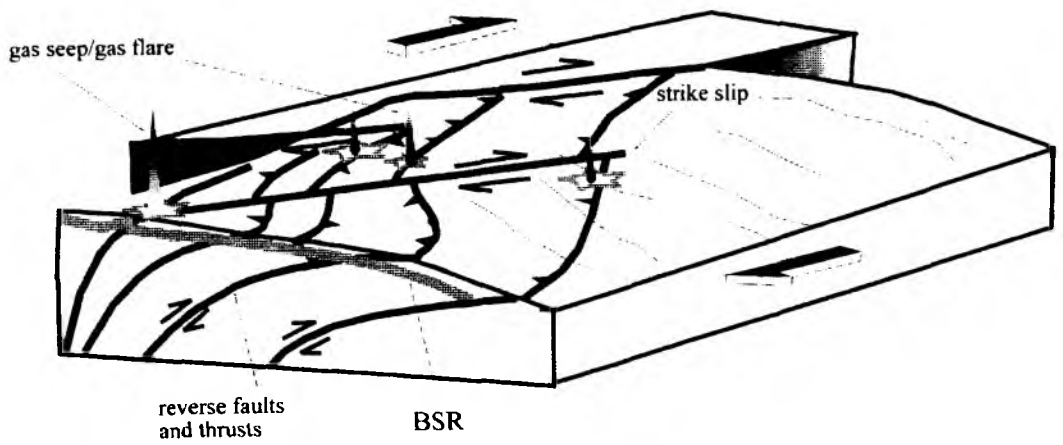

Fig. 5.2: Cartoon of the offshore structure and seep locations in the Sakhalin Shear Zone.

5.2 Seep distribution

The character of seep distribution on the eastern Sakhalin margin suggests that gas seeps correlate with certain tectonic zones and are directly controlled by the tectonic regime. It is obvious that for the northern area, all known seeps are located near reverse faults generated under conditions of NE-SW compression. The structural pattern existing here is similar to the tectonic regime in subduction zones, especially in those with a thick sedimentary cover (Oregon type) where gas conduits are represented by reverse faults and thrusts (Fig. 5.2).

6. REFERENCES

Alperovich, I.M. & G.A. Chernyavsky, 1973. Report of the „Hecauteus" Expedition-1 in the Okhotsk Sea, 1966. Oceanogr. Mag., 19, 57-59.

Anderson, J.B. & B.F. Molnia, 1989. Glacial-Marine Sedimentation. Short Course in Geology, 9, Amer. Geophys. Un., Washington, D.C., 127 pp.

Baranov, B.V., K.A. Dozorova & A.S. Svarichevsky, 1995. Cenozoic kinematics of the Okhotsk plate: opening of the back-arc basin and Okhotsk rift system. Abstracts of the International Lithosphere Program Workshop, Miyagi, Japan.

Baranov, B.V., B.Ya. Karp, T. Dickmann, K.A. Dozorova & V.N. Karnaukh, in press. Tectonics of the central Ionian Rift, eastern Derugin Basin (Okhotsk Sea). Tectonics.

Berné, S., T. Marsset, G. Lericolais, J.F. Bourillet, M. de Batist, J.Y. Reynaud & B. Tessier, 1997. Origin of some offshore sand bodies around France. Geo-Eco-Marina, 2, 57-76.

Biryukov, V.Y., M.A. Faustova, P.A. Kaplin, Y.A. Pavlidis, E.A. Romanova & A.A. Velichko, 1998. The paleogeography of Arctic shelf and coastal zone of Eurasia at the time of the last glaciation (18,000 yr. B.P.). Palaeogeography, Palaeoclimatology, Palaeoecology, 68, 117-125.

Christie-Blick, N. & K. T. Biddle, 1985. Deformation and basin formation along strike-slip faults. In: K. T. Biddle & N. Christie-Blick (eds.), Strike-Slip Deformation, Basin Formation, and Sedimentation. Soc. Econ. Paleontol. Mineral., Spec. Publ. 37, 1-34.

CLIMAP Project Members, 1981. Seasonal Reconstructions of the Earth's Surface at the Last Glacial Maximum. Boulder, Geological Society of America.

Dozorova, K.A., B.V. Baranov, B.Ya. Karp & V.A. Karnaukh, 1998. Sakhalin Shear Zone and origin of the Derugin Basin (Okhotsk Sea). Abstracts of the 6th Zonenshain Conference, Moscow.

Fournier M., L. Jolivet, Ph. Huchon, K.F. Sergeyev & L.S. Oscorbin, 1994. Neogene strike-slip faulting in Sakhalin and Japan Sea opening. Journ. Geoph. Res., 99, 2701-2725.

Gensous, B., D. Williamson & M. Tesson, 1993. Late-Quaternary transgressive and highstand deposits of a deltaic shelf (Rhône delta, France). Spec. Publs. Int. Ass. Sediment., 18, 197-211.

GERDA, 1995. Report of R/V Professor Gagarinskiy Cruise 16 „GERDA": Geophysical Research in the Derugin Basin Area (the Okhotsk Sea), 36 pp.

Ginsburg, G.D., V.A. Soloviev, R.E. Cranston, T.D. Lorenson & K.A. Kvenvolden, 1993. Gas hydrates from continental slope, offshore Sakhalin Island, Okhotsk Sea. Geo-Marine Letters, 13, 41-48.

Gnibidenko, H.S. & I.I. Khvedchuk, 1982. The tectonics of the Okhotsk Sea. Mar. Geol. 50, 155-198.

Gnibidenko, H.S. & A.S. Svarichevsky, 1984. Tectonics of the Okhotsk deep-sea basin. In: R.L. Carlson & K. Kobayashi (eds.), Geodynamics of the Backarc Regions, Tectonophys., 102, 225-244.

Gorbarenko, S.A., N.N. Kovalyukh, L.Yu. Odinokova, V.F. Rybakov, T.N. Tokarchuk & V.V. Shapovalov, 1990. Upper Quaternary sediments of the Sea of Okhotsk and the reconstruction of paleoceanologic conditions. Geol. of Pac. Ocean., 6(2), 309-330.

Grosswald, M.G., in press. Late Weichselian ice sheets in Arctic and Pacific Siberia. Quaternary International.

Grosswald, M.G. & T.J. Hughes, 1998. Evidence for Quaternary glaciation of the Sea of Okhotsk. In: S. Horie (ed.), International Project on Paleolimnology and Late Cenozoic Climate (IPPCCE) Newsletter No. 11, 3-25.

Harding, T.P., R.F. Gregory & L.H. Stephens, 1983. Convergent wrench fault and positive flower structure, Ardmore Basin, Oklahoma. In: A.W. Bally (ed.), Seismic Expression of Structural Styles. Amer. Assoc. Petr. Geol., Studies Geol., 15(3), 4.2-13-4.2-17.

Hughes, T.J., 1995. A search for marine ice sheets in Pleistocene Beringia. In: Simakov, K.V. (ed.), Proceedings of the International Conf. on Arctic Margins, Magadan, Russia, Sept. 1994, 81-94.

Hyndman, R.D. & E.E. Davis, 1992. A mechanism for the formation of methane hydrate and seafloor bottom-simulating reflectors by rapid fluid expulsion. Journ. Geophys. Res., 97(B5), 7025-7041.

Hyndman, R.D. & G.D. Spencer, 1992. A seismic study of methane hydrate marine bttom simulating reflectors. Journ. Geophys. Res., 97(B5), 6683-6698.

Jolivet L., P. Huchon, J.P. Brun, N. Chamot-Rooke, X. Le Pichon & J.C. Thomas, 1991. Arc deformation and marginal basin opening: Japan Sea as a case study. Journ. Geophys. Res., 96, 4367-4384.

Kaiko-Tokai project, 1998. Tectonics of subduction in the Nankai Trough. International Symposium on Japan - France Kaiko - Tokai Project, Abtract Vol., 82 pp.

Karp, B., V. Karnaukh & T. Dickmann, 1995. Seismics. In: Report of R/V Professor Gagarinskiy Cruise 16 „GERDA": Geophysical Research in the Derugin Basin Area (the Okhotsk Sea), 24-31.

Lammers, S., E. Suess, M.N. Mansurov &, V. Anikiev, 1995. Variations of atmospheric methane supply from the Sea of Okhotsk induced by seasonal ice cover. Global Biogeochem. Cycles, 9(3), 351-358.

Lee, M.W., D.R. Hutchinson, W.F. Agena, W.P. Dillon, J.J. Miller & B.A. Swift, 1994. Seismic character of gas hydrates on the southeastern U. S. continental margin. Mar. Geophys. Res., 16, 163-184.

Rea, D.K., I.A. Basov, T.R. Janecek, A. Palmer-Julson et al., 1993. Proc. ODP, Init. Repts., 145, College Station, TX (Ocean Drilling Program) 1040 pp.

Margulis, L.S., V.B. Mudretzov, B.G. Sapojnikov, G.P. Fedotov & I.I. Khvedchuk, 1979. Geology of the northwest part of the Okhotsk Sea. Sov. Geol., 7, 61-71 (in Russian).

Menzies, J., (ed.), 1995. Past Glacial Environments: Sediments, Forms and Techniques. Glacial Environments Ser., Vol. 2, Butterworth-Heinemann, Oxford, 598 pp.

Mienert, J. & Posewang, J., 1997. Flach- und Tiefwassergashydrate in Sedimenten polarer Kontinentalränder des Nordatlantiks. Geowissenschaften, 15(9), 287-291.

Milliman, J.D. & R.H. Meade, 1983. World-wide delivery of river sediments to the oceans. J. Geol., 91(1), 1-21.

Nio, S.D. & C.S. Yang, 1991. Sea-level fluctuations and the geometric variability of tide-dominated sandbodies. In: K.T. Biddle & W. Schlager (eds.), The Record of Sea-Level Fluctuations. Sediment. Geol., 70, 161-193.

Nürnberg, D., Baranov, B.V., Karp, B.Ya. (eds.), 1997. RV Akademik Lavrentyev cruise 27 - cruise report Gregory, Geomar Report, 60, 69 pp.

Rea, D.K., I.A. Basov & Janecek, T.R., 1993. Cenozoic paleoceanography of the North Pacific Ocean; Results of ODP Leg 145, the North Pacific transects. Eos Transactions, 74, 173.

Rehder, G., 1996. Quellen und Senken marinen Methans zwischen Schelf und offenem Ozean. Diss. Univ. Kiel.

Rozhdestvenskiy, S.S., 1982. The role of wrench faults in the structure of Sakhalin. Geotectonics, 16, 323-332 (in Russian).

Rozhdestvenskiy, S.S., 1986. Evolution of the Sakhalin fold system. Tectonophysics, 127, 331-339.

Savostin, L.A., L.P. Zonenshain & B.V. Baranov, 1983. Geology and plate tectonics of the Sea of Okhotsk, In: Hilde T.W.C. and Uyeda S. (eds.), Geodynamics of the Western Pacific-Indonesian Region. Geodynamic Series AGU, 11, 189-222.

Syvitski, J., A.K. Cooper & M.S. Stoker, (eds.), 1997. COLDSEIS (Seismic Facies of Glacigenic Deposits). Spec. Issue, Mar. Geol., 143, 1-262.

Talley, L.D. & Y. Nagata (eds.), 1995. The Okhotsk Sea and Oyashio Region. North Pacific Marine Science Organisation (Report of Working Group 1). Pices Scientific Rept. No. 2, 227 pp.

Velichko, A.A., (ed.), 1993. Climate and Landscape Evolution in Northern Eurasia, the Late Pleistocene and Holocene. Moskva, „Nauka" (in Russian).

Vogt, C., J. Grützner, S. Gorbarenko, A. Astakhov & D. Nürnberg, 1997. Sedimentation at the northeastern slope of Sakhalin. In: Cruise Report of the R/V Akademik M.A. Lavrentyev Cruise 27 „Gregory": German-Russian Expedition for Geological/ Geophysical Okhotsk Sea Research. GEOMAR Report, 60, 41-43.

Zanyukov V.N., 1972. The central Sakhalin fault and its role in the tectonic evolution of the island. Papers of the Acad. Sci. USSR (in Russian).
Zhuravlev, A.V., 1984. Comparison between the Derugin and Tinro basins of the Okhotsk Sea. Geology of the Pacific, 4, 21-27 (in Russian).

Appendices

Appendix 1

List of profiles KOMEX 98, cruise 22 of the RV Professor Gagarinsky, Sea of Okhotsk, July 98

Profile No.	Start				End				Course	Duration	Distance	
	Date (d.mm.yy)	Time (hh:min)	Latitude (N)	Longitude (E)	Date (d.mm.yy)	Time (hh:min)	Latitude (N)	Longitude (E)	(°)	(hh:min)	nm	km
1	20.07.98	12:30	51°12.86	146°42.16	21.07.98	00:20	52°09.24	147°03.87	13	11:50	57.6	106.7
2	21.07.98	01:05	52°08.50	147°05.27	21.07.98	04:25	51°52.88	147°12.41	162	03:20	16.6	30.7
3	21.07.98	04:39	51°52.59	147°10.97	22.07.98	07:16	53°22.46	144°56.18	316	26:37	121.0	224.0
4	22.07.98	10:33	53°21.15	144°52.01	22.07.98	15:44	53°23.56	144°10.42	274	05:11	25.2	46.7
5	22.07.98	15:52	53°23.59	144°09.76	22.07.98	16:24	53°26.57	144°09.77	360	00:32	3.0	5.6
6	22.07.98	16:34	53°26.99	144°10.52	22.07.98	20:31	53°28.17	144°42.08	86	03:57	18.5	34.2
7	22.07.98	20:50	53°27.07	144°42.64	22.07.98	22:56	53°17.44	144°43.66	174	02:06	10	18.5
8	22.07.98	23:15	53°16.91	144°41.88	23.07.98	03:37	53°17.63	144°10.36	270	04:22	19.2	35.6
9	23.07.98	03:43	53°17.36	144°10.04	23.07.98	05:39	53°09.96	144°10.44	178	01:56	7.0	12.9
10	23.07.98	05:47	53°09.78	144°11.35	23.07.98	09:04	53°09.80	144°38.00	90	03:17	16.2	30.0
11	23.07.98	09:15	53°10.46	144°38.62	23.07.98	13:24	53°31.19	144°28.90	345	04:11	21.8	40.0
12	23.07.98	13:37	53°31.72	144°27.65	23 07.98	14:23	53°31.87	144°21.51	270	00:46	3.6	6.6
13	23.07.98	14:31	53°31.39	144°20.98	23.07.98	20:22	53°06.90	144°31.75	164	05:51	24.9	46.0
14	24.07.98	08:54	53°22.56	144°35.58	24.07.98	16:13	53°19.50	143°34.34	266	07.19	37.1	68.7
15	24.07.98	16:18	53°19.79	143°33.86	24.07.98	22:05	53°54.12	143°20.27	348	05:47	35.0	64.8
16	24.07.98	22:18	53°54.82	143°21.95	25.07.98	08:25	53°53.30	144°50.06	92	10:07	51.9	96.1
17	25.07.98	08:31	53°53.66	144°50.39	25.07.98	15:16	54°25.95	144°33.81	341	06:45	33.3	61.7
18	25.07.98	15:22	54°26.31	144°33.11	26.07.98	01:55	54°26.21	143°05.63	272	10:33	50.6	93.7
19	26.07.98	02:02	54°25.81	143°05.31	26.07.98	05:52	54°05.96	143°12.18	167	03:50	20.4	37.8
20	26.07.98	05:55	54°05.66	143°12.46	26.07.98	15:35	54°06.89	144°20.36	92	09:40	39.9	73.9
21	26.07.98	15:41	54°07.17	144°20.85	26.07.98	16:29	54°10.49	144°20.22	355	00:48	3.1	5.7
22	26.07.98	16:36	54°10.49	144°19.45	26.07..98	19:50	54°11.57	143°50.00	272	03:14	17.1	31.7
23	26.07.98	19:55	54°11.88	143°49.73	26.07.98	20:45	54°16.32	143°50.38	5	00:50	4.0	7.4
24	26.07.98	20:49	54°16.35	143°50.83	27.07.98	00:37	54°16.14	144°21.42	92	03:48	17.5	32.4
25	27.07.98	00:42	54°16.56	144°21.56	27.07.98	01:46	54°21.58	144°21.71	360	01:04	5.0	9.3
26	27.07.98	01:50	54°22.01	144°21.29	27.07.98	06:00	54°21.87	143°50.93	270	04:10	17.5	32.4
27	27.07.98	06:05	54°22.10	143°49.61	27.07.98	07:51	54°29.99	143°48.68	358	01:46	8.0	14.8
28	27.07.98	07:56	54°30.60	143°49.12	27.07.98	10:06	54°30.44	144°06.24	90	02:10	9.9	18.3

Profile No.	Start				End				Course	Duration	Distance	
	Date (d.mm.yy)	Time (hh:min)	Latitude (N)	Longitude (E)	Date (d.mm.yy)	Time (hh:min)	Latitude (N)	Longitude (E)	(°)	(hh:min)	nm	km
29	27.07.98	10:17	54°29.82	144°07.15	27.07.98	16:58	54°03.39	143°49.59	202	06:41	28.8	53.3
30	27.07.98	17:06	54°03.06	143°50.06	27.07.98	18:50	54°00.33	144°02.44	112	01:44	7.7	14.3
31	27.07.98	18:56	54°00.58	144°03.13	28.07.98	00:16	54°15.28	144°18.05	20	05:20	16.5	30.6
32	28.07.98	00:27	54°25.93	144°17.48	28.07.98	01:25	54°27.72	144°10.30	291	00:58	4.5	8.3
33	28.07.98	01:30	54°27.57	144°09.76	28.07.98	03:05	54°20.79	144°04.37	201	01:35	7.8	14.4
34	28.07.98	03:11	54°20.76	144°03.76	28.07.98	04:02	54°22.26	143°57.83	300	00:51	3.6	6.7
35*	28.07.98	04:06	54°22.53	143°57.95	28.07.98	05:23	54°28.97	144°03.18	28	01:17	6.7	12.4
36*	28.07.98	05:29	54°28.91	144°03.78	28.07.98	06:39	54°26.10	144°12.65	115	01:10	6.0	11.1
37*	28.07.98	06:43	54°25.75	144°12.79	28.07.98	08:20	54°18.46	144°07.36	202	01:37	8.7	16.1
38*	28.07.98	08:20	54°18.46	144°07.36	28.07.98	14:51	53°49.32	144°09.00	180	06:31	29.0	53.7
39	28.07.98	14:57	53°49.18	144°09.49	29.07.98	07:45	53°49.17	146°02.92	90	16:48	67.3	124.6
40	29.07.98	07:53	53°48.68	146°03.43	30.07.98	00:24	52°41.05	145°23.02	200	16:31	72.1	133.5
41	30.07.98	00:27	52°41.01	145°22.98	30.07.98	09:16	52°12.33	144°29.94	228	08:49	43.4	80.4
42	31.07.98	08:17	50°05.09	147°30.59	31.07.98	21:00	49°09.01	146°34.88	213	12:43	66.7	123.5
									Total	**212:51**	**1041.2**	**1969.1**
									Total: airgun profiles	**202:16**	**990.8**	**1877.8**

* no airgun profiles

Appendix 2

List of participants

1. Dr. Boris Karp	Co-Chief Scientist, seismics (POI, FED RAS)
2. Prof. How Kin Wong	Co-Chief Scientist, mar. geophysics (IfBM, UniHH)
3. Dr. Nicole Biebow	Marine geology (GEOMAR)
4. Dr. Boris Baranov	Tectonics (IO, RAS)
5. Mrs. Karina Dozorova	Tectonics (IO, RAS)
6. Mr. Martin Jovanovic	Seismics (IfBM, UniHH)
7. Dr. Viktor Karnaukh	Seismics (POI, FED RAS)
8. Mrs. Tatyana Kolpashchikova	Gravity (POI, FED RAS)
9. Dr. Sergei Nikolaev	Gravity (POI, FED RAS)
10. Dr. Stefan Lammers	Geochemistry (GEOMAR)
11. Dr. Thomas L¸dmann	Seismics (IfBM, UniHH)
12. Mr. Matthias Lurati	Seismics (IfBM, UniHHU)
13. Ms. Alke-Marit Paulsen	Seismics (IfBM, UniHH)
14. Mr. Anatoly Sudakov	Seismics (POI, FED RAS)
15. Mr. Nikolay Tsovbun	Magnetics (POI, FED RAS)

GEOMAR:	Research Center for Marine Geosciences, Christian-Albrechts-University, Kiel
IfBM, UniHH:	Institute of Biogeochemistry and Marine Chemistry, Hamburg University, Hamburg
IO RAS:	P. P. Shirshov Institute of Oceanology, Russian Academy of Sciences, Moscow
POI FED RAS:	Pacific Oceanology Institute, Far Eastern Division of the Russian Academy of Sciences, Vladivostok

PART II:

RV AKADEMIK M.A. LAVRENTYEV CRUISE 28

CRUISE REPORT KOMEX II:

VLADIVOSTOK - PUSAN - SEA OF OKHOTSK - PUSAN - VLADIVOSTOK

AUGUST 3 - SEPTEMBER 12, 1998

1. INTRODUCTION

R. Kulinich, E. Suess, and N. Biebow

The 28th expedition of as part of the KOMEX-program was organized to continue and develop investigations which were begun during the 22nd expedition of *RV Professor Gagarinsky* from July 7th to August 10th and are described in part I of this Report. The objectives of the *Lavrentyev*-expedition comprise and contribute to four research topics:

1. Detailed investigations of gas and fluid vent fields of the north-eastern shelf and the upper slope of Sakhalin Island and their contribution to air-sea exchange of trace gases;
2. Detailed investigations of carbonate-barite mineralization in the Derugin Basin to clarify their source and tectonic origin;
3. Coring program for paleoceanological investigations along a meridional and a latitudinal transect crossing the Sea of Okhotsk;
4. Dredging of volcanic rocks to assess the volatile elements in Kurile Basin magmas and of basement rocks to gain information on the basement structure.

1. Results of several previous expeditions are the basis for the detailed study of gas and fluid venting, in particular of methane, which emanates from the sea floor into the water column near northeastern Sakhalin Island. Fluid venting is known to be widespread on the inner slopes of trenches and there results from dewatering related to the stress regime of subduction tectonics and fracture zones (Kulm et al., 1986; Suess et al. 1997; von Huene et al. 1998; and Kaiko-Tokai Meeting; Tokyo, Japan,1998). However, the gas emissions off Sakhalin are situated in a different geodynamic regime and hence the problem of their origin, spatial extent, and eventually the quantification of rates of fluid discharge are the subject of particular investigations during the KOMEX-Project and are addressed during this expedition. Although the dominant gas being emitted is methane, carbon dioxide also plays a part in the total gas budget and helium serves as important tracer for vent fluids (Winckler et al., 1997).

   Helium along with tritium and oxygen isotopes will be measured on seawater samples collected during the Lavrentyev-expedition to gain information on the various sources of fluid input into the Sea of Okhotsk.

   The first submarine gas emissions on the north-eastern shelf and slope off Sakhalin were found in 1988 during the cruise of *RV Morskoy Geofizik* which was organized by the Pacific Oceanological Institute, Far Eastern Branch of the Russian Academy of Sciences (Obshirov et al., 1989). In 1991, in the same area new gas vents were found as well as gas hydrates in surface sediments (Ginsburg et al., 1993). In 1992, a systematic survey of methane in the shelf and upper slope off Sakhalin as well as in Amur Bay from board the *RV Akademik Nesmeyanov* resulted in the first estimate of methane exchange between the sea

surface and the atmosphere (Lammers et al., 1995). In particular, the role of seasonal ice cover in methane release which results from submarine emissions was pointed out by this investigation. Based on these past findings, work has begun during the current *RV Akademik Lavrentyev* and *RV Professor Gagarinsky* expeditions to establish a methane monitoring program at selected sites in the Sea of Okhotsk.

In 1996, that same region was investigated during the joint German-Russian 27th expedition of *RV Akademik Lavrentyev*. The methane distribution in sediments and in the water column as well as tectonic objectives were then studied. During the Gagarinsky-expedition which immediately preceded the Lavrentyev-expedition gas emission sites were mapped and seismic reflection surveys carried out to better understand the region's tectonics. This information was exchanged during a joint port call in Pusan on the 5th/6th of August and two areas, the "Southern" and "Northern Sector", were selected for work during the Lavrentyev-expedition.

2. Interest in seafloor mineralization in the Derugin Basin was started by a single find of barite-calcite formations dredged in the early-1980s (Astakhova et al. 1987; Astakhova 1993). Subsequently, barite and calcite were again collected in the Derugin Basin during the 23rd expedition of *RV Akademik Nesmeyanov* in 1993. Several associations of different morphologies were found in a sediment core. There was convincing evidence from fabric and carbon isotopes of the associated calcite that the samples were authigenic; i.e. formed in place. It was proposed that in the Derugin Basin a vent complex exists or existed for the last several thousand years from which methane- and barium-containing fluids emanated from one or several vent systems (Derkachev and Bohrmann, in prep.). To verify this hypothesis it will be necessary to show that the barite occurence was not a single find and to ascertain which geochemical and tectonic processes are responsible for the formation of carbonate-barite mineralization. Therefore, the search for carbonate-barite formations in the region of their initial discovery became a major task of the expedition. Sea floor observations, pore water analyses, and trace gas measurements in the bottom water column seem the most suitable strategy to address this task.

3. The Sea of Okhotsk, being the largest marginal sea, exerts a significant influence on the environment of a vast region of the earth, including the adjacent continent as well as the whole northern part of the Pacific Ocean. Being also one of the most productive regions of the world's ocean, the Sea of Okhotsk is likely to play a significant role in the balance of atmospheric carbon dioxide by acting as a major sink through fixing carbon in its surface waters via primary production and transporting it into deep oceanic waters of the North Pacific. In a high latitude basin surrounded by land, where climate changes are expressed more strongly than in the open ocean and where high sedimentation rates are expected, the Sea of Okhotsk is a unique location for studying high-resolution climate change. For that

reason, a major paleoceanological program on Pleistocene climate became part of this expedition.

Two transects were chosen for this investigation based on the surface circulation. One stretches in meridional direction from the continental slope of south-eastern Sakhalin to the Kurile Basin and covers a large range of water depths. This would yield information on the change of paleoenvironment of the water column and would allow to assess the role of this region in the balance of atmospheric carbon dioxide and hence past global climate change. In addition, this transect allows to address the influence which the warm waters of high salt content of the Soya Current exert on the change of paleoceanology of the Sea of Okhotsk and its water exchange with the Pacific Ocean.

The second transect is oriented in latitudinal direction and crosses the central region which is characterized by different hydrographic regimes. The western part of the transect is situated within the influence of the continental slope off Sakhalin. This region is affected by the Amur River run-off and receives high rates of sediment supply. The eastern part of the transect, near the Kamchatka Peninsula, is influenced by the Kamchatka Current which enters the Sea of Okhotsk from this side of the North Pacific Ocean. The central part of the transect is the region with the lowest sedimentation rates.

4. The Sea of Okhotsk has a complex and heterogenous basement structure (Geodekyan et al., 1976; Sergeev et al., 1987; Gnibidenko, 1979; Bogdanov, 1988; Frolova et al., 1989; Vasiliev et al., 1990; Avdeiko et al., 1992; Lelikov, 1992; Baranov et al., 1995). The bedrock complex includes metamorphic rocks presumably of Paleozoic age, Middle and Upper Mesozoic granitoids, Cenozoic volcanic rocks, and Mesozoic to Cenozoic sedimentary rocks.

   The collection dredged from the Academy of Sciences Rise during the 27th Lavrentyev-expedition included volcanic, plutonic and sedimentary rocks (Nürnberg et al., 1997). The volcanic rocks show a large variety of composition and secondary alteration and are represented by a series of rocks from basalts to dacites. Plutonic rocks included biotite and biotite-amphibole granite, granodiorite and tonalite. These granitoids are similar in composition to rocks of Cretaceous radiometric age (121-75 Ma) previously dredged in the area.

   The basement structure of the Kurile Basin has been studied insufficiently. The most reliable data are based on sediments, whereas the composition of the acoustic basement is practically unknown. It is believed to be composed of volcano-sedimentary and siliceous units (Bogdanov, 1988). The higher than usual heat flow and the presence of diapiric structures in the sediments suggest very recent volcanic and tectonic processes taking place. The small Pleistocene submarine volcano, about 1000 m high and about 6.5 km in diameter, which was found at the eastern part of the Kurile Basin during the past Lavrentyev-expedition, confirmed this assumption. Basaltic andesites containing olivine, clinopyroxene,

orthopyroxene, hornblende and plagioclase, recovered from this submarine edifice have the basic geochemical affinities of high-K calc-alkaline island-arc magmas, with high Sr and Ba, but low Ti, Cr and Ni contents. Rare earth patterns are similar to island-arc volcanics of the back-arc area of the Kurile Island Arc. The basaltic andesite yielded K-Ar ages from 0.932-0.042 to 1.632-0.051 million years. The island-arc signature of these rocks tentatively suggests the presence of continental crust type basement beneath the eastern part of the Kurile Basin (Tararin et al., in press).

Therefore one of the objective is to obtain volcanological and geochemical investigations to trace the origin and pre-eruptive evolution of magmatic volatiles (H_2O, SO_2, CO_2, Cl, F, B) in the region of the Kurile Island Arc. Interaction and dependencies between crustal and mantle sources, petrogenetic processes as well as the type and amount of volatiles in the eruptive products will be studied by applying geochemical and petrological methods. In order to accomplish both objectives, suspected volcanic and basement structures in the Kurile Basin will be dredged.

2. CRUISE NARRATIVE

E. Suess and R. Kulinich

2.1 Weekly progress reports

The research vessel *Akademik M.A.Lavrentyev* departed from Vladivostok on August 3rd, 1998 with 17 scientists and 39 crew members on board. Modifications on a deck of the ship had been performed to accomodate a self-contained mobile deep-sea winch system with a 20 mm conducting cable for work at sea. It is planned to use the conducting cable for OFOS deployments and coring primarily during the first half of the cruise and for dredging, after appropriately securing the electrical termination, during the second half of the cruise. The vessel arrived at Pusan on August 5th, 1998. On the following day, the German scientists as well as their scientific equipment arrived and were transferred on board. On the same day *RV Professor Gagarinsky* arrived at Pusan after completion of work in the Sea of Okhotsk. During 5th/6th of August the results of geophysical investigations carried out on this vessel were exchanged with the scientists preparing to sail on board *RV Akademik Lavrentyev*. The data obtained during that cruise are described in part I of this report. On August 8th,*RV Akademik Lavrentyev* left Pusan and made its way to the Sea of Okhotsk. The complete cruise track is shown in Fig. 2.1

Transit to the first area of investigation lasted 4 days. This period was used for preparing and testing of equipment and laboratories for the upcoming work; the exellent weather favoured the preparations and tests. On August 12th the vessel approached the South Sakhalin slope where previously a gas plume had been reported from echosounding records (Nürnberg et al., 1997). The echosounding survey, conducted as the first station during the expedtion, identified the same anomalous reflection observed previously, but showed it to be a morphological feature and not related to gas venting. This interpretation was confirmed by the absence of any appreciable methane concentrations in the water column. Therefore, an OFOS survey was not carried out and the vessel proceeded to work at the adjacent paleoceanography station. Here the sampling program consisting of deployment of the multinet, the CTD, the multicorer and two types of gravity coring equipment was successfully completed by the morning of August 13th. All deployments and surveys are listed in the List of Stations, which is appended to this report amd will be referred to in the Cruise Narative. This station was positioned at the beginning of the N-S paleoceanographic transect (Fig. 2.2), the southern extension of which into the western Kurile Basin will be completed at the end of the cruise. After that the vessel proceeded to the north-eastern shelf and slope area of Sakhalin where active methane vent fields are known. On the way, water and sediment sampling for paleoceanologic objectives was carried out at station LV-28-4 using the same equipment as before. During the first two weeks of the expedition,.

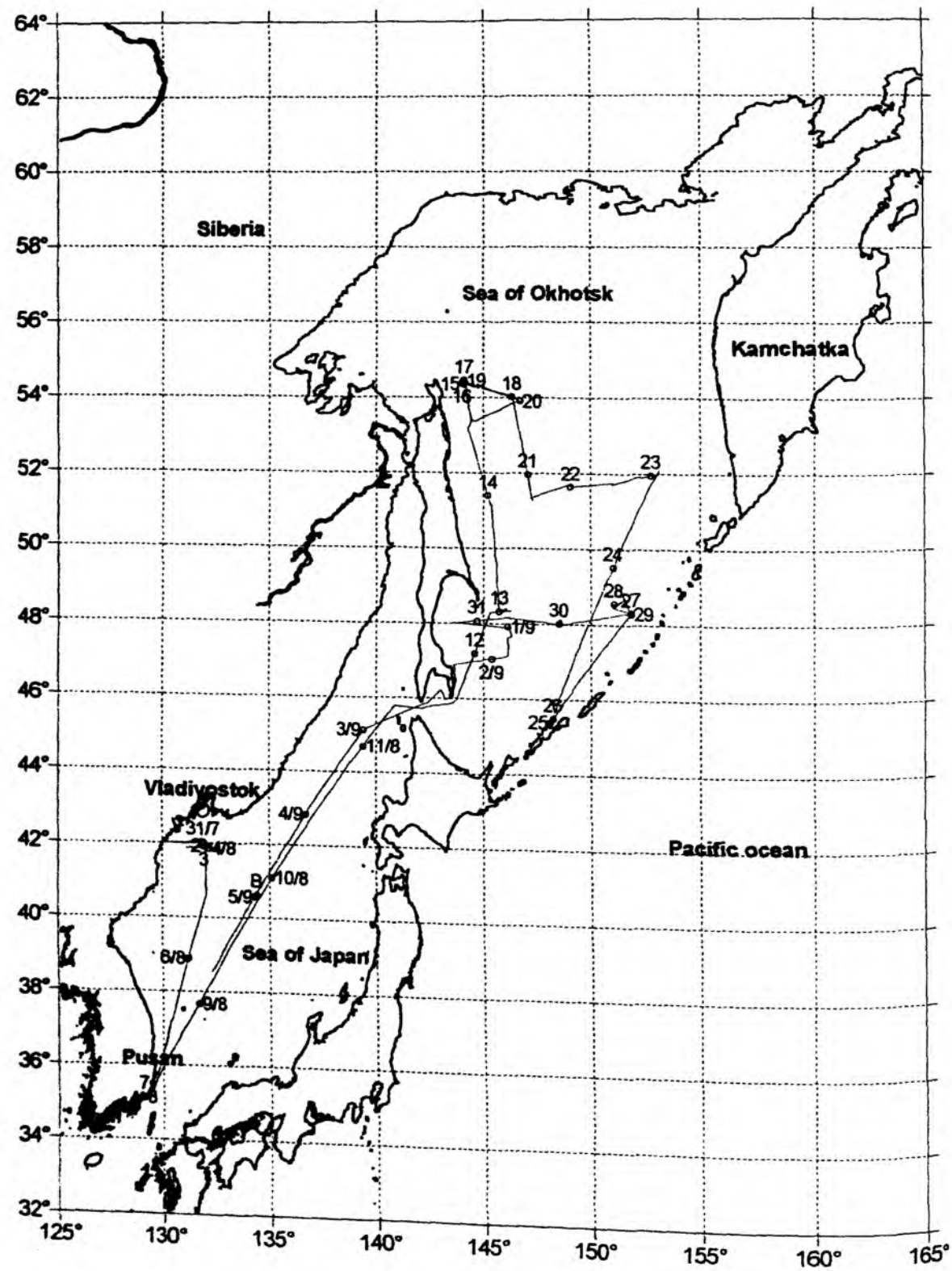

Fig. 2.1: Ship's track of RV Akademik Lavrentyev in the 28th cruise, August-September 1998. B - Sea bath position in the Sea of Japan.

besides transit, the set of geologic and hydrographic equipment was fully operational and successfully deployed with the arrival in the area of gas vent fields

The following week of August 15th-23rd, was devoted to the detailed investigation of the gas vent areas concentrated on the shelf edge and upper continental slope off Sakhalin Island as well as an area of suspected barite mineralization in the Derugin Basin (Fig. 2.2). During this work the full complement of methods and technical facilities available on board the vessel were used, namely: echosounding, OFOS, Multicorer, Multinet, gravity corers, CTD-rosette and acoustic imaging of water column features by the ship's 20-kHz hydroacoustic equipment. Favorable weather allowed to complete the program as planned and to obtain significant results. Detailed work on a large number of stations (see: Appendix 1) was carried out, and high-resolution bathymetric surveys were completed in the areas of OFOS-deployments at the North Sakhalin slope and the Derugin Basin.

Poor weather during August 15th/16th forced the program to be divided into two parts and required transit twice between the North Sakhalin slope and the Derugin Basin. All equipment operated to satisfaction including the MobiWinch and the OFOS-system. All science stations were occupied and completed as planned, the communication and cooperation between the Russian and German teams and the vessel's crew were excellent. Highlights during that past week were the hydrochemical surveys of several gas plumes and sampling of water for methane, mapping and documentation with the OFOS of an active vent field on the shelf-slope break; recovery of 100 kg of carbonate concretions, chimneys, cemented burrows, and large numbers of bivalve shells, presumably of vent fauna. Several glendonites (pseudomorphs of calcite after ikaite, a rare hydrated calcium carbonate mineral) were found at the gas vent field site, and biologists recovered by trawl dead vent organisms and numerous other biological specimens, presumably vent biota. Coring vent sediments for pore water was successful, but no gas hydrates were observed nor sampled.

A quite significant discovery was made of a sub-sea barite landscape in the Derugin Basin, where hundreds of chimneys, edifices and blocks up to several metres high were seen along 2.5 miles of the OFOS track in 1550 m depth (Station LV-28-31-1). More than 1 ton of barite chimney fragments were dredged and 6 m of barite-turbidite-sediment were cored from a small basin in the area of the chimney structures. Up to 2000 nl/l of methane were measured in the deep water which fills the barite basin. The sediment between the barite edifices was populated by vent fauna, but no sulfide-, oxide-, silicate-precipitates were found; some inorganic carbonates were present. The very BIG question remains: is the barite landscape formed by a giant cold seep or is the result of hydrothermal activity related to crustal stretching ? The water samples taken for helium analyses from the depths of the barite basin should provide a partial answer soon.

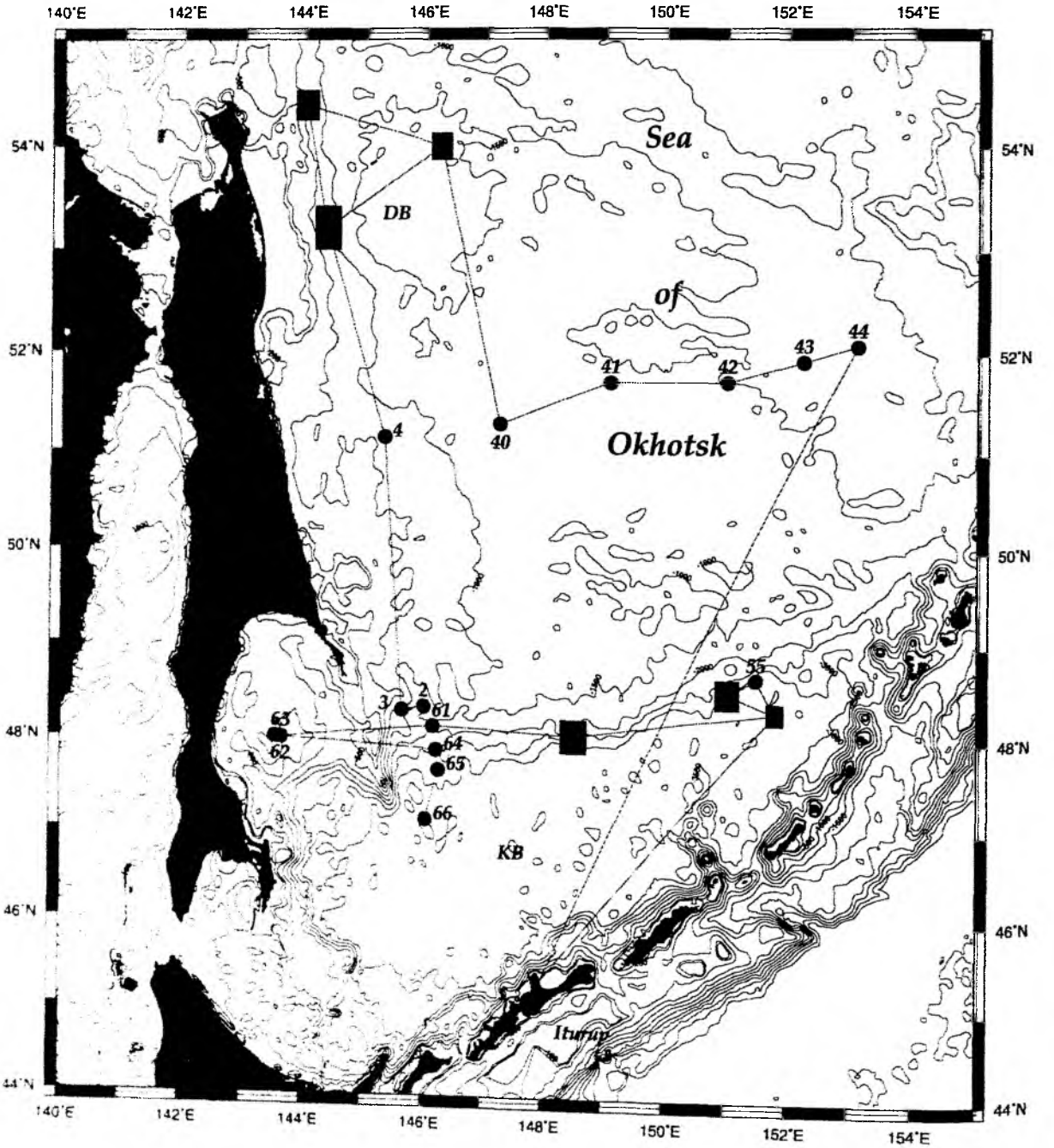

Fig. 2.2: Map of working areas (shaded polygons) and stations (dots) during the 28-th Cruise of RV Akademik M.A. Lavrentyev, August-September 1998.

The paleoceanology program also went well beyond expectations. The east-west transect (Fig. 2.2) completed on August 23rd yielded more than 150 m of sediment from 9 stations with 2 deployments of gravity coring equipment each (see: Appendix 1). The MUC- and MUN-deployments went equally well. It is clear that the excellent performance of the MobiWinch and the ship's handling of the heavy equipment were important factors in securing success. The initial results of the magnetic susceptibility records from all cores of the E-W transect across the Sea of Ochotsk will allow a very detailed age model to be constructed. This model is based on the occurrence of ash layers of known age, of cycle stratigraphy, and biostratigraphic markers. All cores penetrated well beyond isotope stage 5 and 6; several as far back as stage 9. The older sections contain a number of hitherto unknown ash layers which should provide excellent age levels, once properly dated. It appears that the sedimentation rates in the center of the Sea of Ochotsk are lowest and increase towards both the Kamchatka Peninsula in the east and Sakhalin Island in the west. In spite of the sampling and coring success, the difficulties of the vessel in keeping station poses a problem for both the exact correlation of statigraphic units in the sediment cores for paleoceanographic studies as well as for sampling the very small features of gas venting areas or fluid escape. There is a discrepancy evident in the different lengths of sediment cores retrieved by the different gravity coring systems used by the Russian and German teams, respectively. Currently it is unclear whether one system compresses or the other lengthens the cores, or if the distance between coring sites caused by drift is so large that "real" differences in sediment accumulation might be the cause.

The week from 24th-30th of August was largely devoted to the dredging program in the Kurile Basin (Fig. 2.2). The transit to that area provided the opportunity, on the evening of 24th August, for the "Bergfest", a party to celebrate the half-way-point of the cruise. Most of the following day fresh water was taking on at Prostor Bay of Iturup Island.

The vessel left Prostor Bay at 10.00 am on 26th of August and arrived a day later at the first dredging location, a small seamount which rises 1000m high above the floor of the Kurile Basin. Over the following 2 days 6 dredge hauls were taken (one dredge lost) and we recovered fresh volcanic material twice, in part vesicular basalt but also in part hydrothermally altered material. The samples contained palagonite and a complex mixture of basaltic, sedimentary and hydrothermal material, and nontronite, chalcedony, and metal sulfides were clearly identified in this mixture.

A suspected volcanic structure near the northern wall of the basin was the second dredge target; here we obtained no useful rock material because of thick sediments and numerous drop stones; we abandoned the site after 4 dredges. Eventually, we dredged the 3rd target, a steep slope with suspected exposures of basement rocks underlying the Sea of Okhotsk; but only sediment was obtained here and one dredge came up empty on the 30th of August.

During work in the Kurile Basin, the typhoon REX had been building in the Pacific off Japan and although mostly stationary, moved slowly northward and threatened to intersect our

The paleoceanology program also went well beyond expectations. The east-west transect (Fig. 2.2) completed on August 23rd yielded more than 150 m of sediment from 9 stations with 2 deployments of gravity coring equipment each (see: Appendix 1). The MUC- and MUN-deployments went equally well. It is clear that the excellent performance of the MobiWinch and the ship's handling of the heavy equipment were important factors in securing success. The initial results of the magnetic susceptibility records from all cores of the E-W transect across the Sea of Ochotsk will allow a very detailed age model to be constructed. This model is based on the occurrence of ash layers of known age, of cycle stratigraphy, and biostratigraphic markers. All cores penetrated well beyond isotope stage 5 and 6; several as far back as stage 9. The older sections contain a number of hitherto unknown ash layers which should provide excellent age levels, once properly dated. It appears that the sedimentation rates in the center of the Sea of Ochotsk are lowest and increase towards both the Kamchatka Peninsula in the east and Sakhalin Island in the west. In spite of the sampling and coring success, the difficulties of the vessel in keeping station poses a problem for both the exact correlation of statigraphic units in the sediment cores for paleoceanographic studies as well as for sampling the very small features of gas venting areas or fluid escape. There is a discrepancy evident in the different lengths of sediment cores retrieved by the different gravity coring systems used by the Russian and German teams, respectively. Currently it is unclear whether one system compresses or the other lengthens the cores, or if the distance between coring sites caused by drift is so large that "real" differences in sediment accumulation might be the cause.

The week from 24th-30th of August was largely devoted to the dredging program in the Kurile Basin (Fig. 2.2). The transit to that area provided the opportunity, on the evening of 24th August, for the "Bergfest", a party to celebrate the half-way-point of the cruise. Most of the following day fresh water was taking on at Prostor Bay of Iturup Island.

The vessel left Prostor Bay at 10.00 am on 26th of August and arrived a day later at the first dredging location, a small seamount which rises 1000m high above the floor of the Kurile Basin. Over the following 2 days 6 dredge hauls were taken (one dredge lost) and we recovered fresh volcanic material twice, in part vesicular basalt but also in part hydrothermally altered material. The samples contained palagonite and a complex mixture of basaltic, sedimentary and hydrothermal material, and nontronite, chalcedony, and metal sulfides were clearly identified in this mixture.

A suspected volcanic structure near the northern wall of the basin was the second dredge target; here we obtained no useful rock material because of thick sediments and numerous drop stones; we abandoned the site after 4 dredges. Eventually, we dredged the 3rd target, a steep slope with suspected exposures of basement rocks underlying the Sea of Okhotsk; but only sediment was obtained here and one dredge came up empty on the 30th of August.

During work in the Kurile Basin, the typhoon REX had been building in the Pacific off Japan and although mostly stationary, moved slowly northward and threatened to intersect our

eventual passage towards Pusan. We therefore decided to cut short the moderately successful dredging program and steamed west and began work on the final segment of the N-S paleoceanographic transect. Here we arrived for the last week's work in the morning of 31st August, but soon after completing the CTD- and MUN-deployments encountered a mechanical problem with the block while retrieving the MUC. The bearing had been worn out and major repair was required by the vessel's engineers. In order to use the ship time during repairs, we steamed towards Terpeniya Bay and completed sampling at the "Methane monitoring station" before returning to the paleoceanographic transect the following morning. September 1st turned out not to be our day because of mounting mechanical problems. The ship's mechanics and engineers twice repaired the bearing on the block. Each time we were able to retrieve one more core for paleoceanologic work, but each time the bearing failed. Eventually the friction caused by the main bolt of the block which was out of alignment added over 2 tons of extra pull on the winch. This load was too excessive to continue coring with heavy equipment. In order to protect the conducting cable from damage by running it over a block of smaller diameter and preventing loss of equipment or endangering personnel in case of complete failure, we decided to terminate the geological program short of completing the last 2 stations. During the night of September 1st/2nd the hydrographic winch also developed problems while running the CTD. Fortunately, the winch could be repaired after several hours and we completed the CTD- and mulitnet-deployments at the remaining paleoceanographic stations of the N-S transect. Because of the excellent results obtained by the 20 kHz hydroacoustic system in detecting gas plumes, we added a survey for gas vents along the 100 m depth contour from the southern end of Terpeniya Bay and into Aniva Bay before steaming through La Peruse Strait on the following morning. Hence the scientific program during the 28th voyage of *RV Akademik M.A. Lavrentyev* was completed at 03:00 on September 3rd and the vessel proceded towards Pusan. Passage through the Sea of Japan was used to demobilise heavy equipment, complete work on samples, and run final analyses during the following 2 days. This was completed in the late afternoon of September 5th and concluded with a "sea bath" at 40°37.9 N and 134°20.7 E which was enjoyed immensely by all. The temperature at this spot was 20°C and the water depth 3212m. During the evening of that day, the Russian team invited all for a concluding party of a most successful expedition, when numerous new results and abundant samples were collected. The vessel steamed towards Pusan, where we arrived at anchorage at midnight of September 6th. The following morning, pilot was taken aboard and we proceeded into the Port of Pusan and tied up at the pier at 10.00 am local time.

2.2 Observations and recommendations

With the very successful conclusion of the first field season of the KOMEX-program with back-to-back expeditions, there was valuable experience gained along with significant results in working together. The intent was to not duplicate efforts and to bring to the program the best expertise, infrastructure, and equipment that each partner had available. This experience should be assessed and utilized in order to optimize the scientific work by the teams from Russia and Germany and to improve the performance of the vessel and equipment. The following points need attention in preparing and running future expeditions in the KOMEX-program:

- MobiWinch: Overall excellent performance; dredging and coring should be done with deep sea wire and not with cable; the conducting cable should be used only for OFOS, TV-grab and other equipment requiring electrical power; consider obtaining 2 separate cable drums;
- OFOS-deployment:Yielded the most new scientific information by documenting vent sites; quality of video-camera on OFOS and positioning and navigation by vessel need to be more accurate;
- 20 kHz hydro-acoustic system: Yielded the most unexpected and valuable data for plume imaging; system needs to be more fully used in sampling strategy of vent sites; if possible the sounding depth should be enlarged to 2000m.
- Coring equipment: Worked very successfully but handling on deck is dangerous; more deck space for long cores should be available; see also: Comparison between SL-R and SL-G gravity coring systems;
- Dredging: TV-grab sampling should be added to dredging;
- Single beam echosounder: Works well, but survey strategy should be improved; in the more distant future, swath mapping by multibeam systems should seriously be considered;
- 3.5 kHz hydro-acoustic system: The towed system did not work to satisfaction and has limited depth range; installing a permanent system on the vessel needs consideration;
- Hydrowinch: The 2000m conducting cable is too short; the limitation prevented to obtain samples in Kurile Basin to verify hydrothermalism/active volcanism; 5000 m cable is needed;
- Methane analyses: Discrete sample analyses should be supplemented by simultaneous and continuous measurements in surface waters by equilibrator; discrete sample throughput should be much larger;
- Endurance of vessel: Maximum fresh water supply for 3 weeks limits scientific work; endurance needs to be improved considerably (60 days);
- Station-keeping capability: The vessel's ability to keep station and course at slow speed is currently a problem for planned OFOS-, TV-grab and/or VESP (=vent sampler)-

deployments; station-keeping needs improvement up to several hours; repair of bow thruster needs consideration;

- Cold room: Use of ship's cold storage facility was excellent for pore water squeezing; AWI container did not work but would have been a bad alternative because of poor accessibility on fore-deck;
- Ship-shore communication: Telex communication worked for minimum needs; satellite-link or alternatives, perhaps including e-mail, seem important for the future work.

3. INSTRUMENTATION AND METHODS

3.1 Bathymetry, profiling, and positioning

A. Svarichevsky, A. Salyuk, and T. Emelyanova

The main purpose of the bathymetric survey during the expedition was to map the seafloor morphology in detail especially in the area of gas vents during the search for new gas vents and define their position for precise sampling. Therefore, the tasks of the bathymetry work on board were:

1. Echosounding surveys in the areas under study and along all the ship tracks;
2. Echosounding surveys to search for new and verify the known gas sources.

Bathymetric mapping was carried out with the echosounding system designed by Elac Corporation (Kiel, Germany) especially adapted for the Holming Corporation (Finland). The echosounding system has a fixed transducer providing a radiated energy of 200 W and/or 2 kW. The duration of the impulses are 1, 3 and 10 ms, the main frequency is 12 kHz, the beam width is 100x100. The reflection signal received is formed by an array of receivers as separate analogous beam of 9.20x4.30 width. The depth values are written on an analogue line-scan recorder and stored by a digital system on hard disk (PC 486). The analog recorder has a delay of 1 m to 9999 m. Water depths were registered in 10 sec intervals during survey programs and in 1 min interval during long transits. The sound velocity for sea water was considered to be 1500 m/s and constant. Variations due to sea water temperature and ambient pressure were not taken into consideration.

The locations for the observations during the cruise were determined by GPS navigation. The receiving set GPS 120 designed by GARMIN was used to determine the ship's location. All navigation data were stored on PC 486. A computer network was developed to provide all laboratories with bathymetric and navigation data in addition to the usual echosounder, the ship's experimental hydroacoustic system «SARGAN-EM-UDM». This system is described in chapter 3.5.

The echosounding survey preceded the geological work with the OFOS-system. Surveys were carried out in 7 areas and profiles were taken between stations as well (Fig.2.2). Aditionally, in areas where station work was planned echosounding was done along parallel profiles (Tab. 3.1). On the basis of the data obtained, the bathymetric maps were compiled using the «Surfer-6» program.

Tab. 3.1: Locations of the studied areas defined by the follow coordinates:

1.North-East Sakhalin shelf and slope

The northern part:

1. 54°28.5 N	**3.** 54°22.5 N
144°00.0 E	144°05.0 E
2. 54°28.5 N	**4.** 54°22.5 N
144°07.0 E	144°12.5 E

The southern part:

1. 54° 22.9 N	**2.** 54°20.7 N
144°.57.6 E	144°01.5 E

2. Derugin Basin:

1. 54°01.5 N	**3.** 53°59.0 N
146°16.0 E	144°18.0 E
2. 54°01.5 N	**4.** 53°59.0 N
144°18.0 E	144°16.0 E

3. Kurile Basin

Northern wall:

1. 48°33.0 N	**5.** 48°28.0 N
150°59.0 E	150°59.0 E
2. 48°33.0 N	**6.** 48°28.0 N
151°03.5 E	151°03.5 E
3. 48°05.0 N	**7.** 48°00.0 N
148°27.6 E	148°38.0 E
4. 48°08.5 N	**8.** 47°58.6 N
148°33.2 E	148°31.9 E

Sea mount:	48°.31.0 N
2377.06 m	151°.81.9 E

3.2 Ocean floor observation system (OFOS)

J. Greinert, H. Sahling, and F. Kulescha

Introduction:

The towed video-/camera-sled OFOS (Ocean Floor Observation System) is one of the most reliable tools to discover the ocean floor and map hydrothermal vents and cold seeps. Chemoautotrophic organisms and authigenic precipitates are the main manifestations of fluid flow at the sea floor. Therefore the optical observation with a camera sled provides information on the distribution and extension of potential vent sites and on the topography. Without this information other tools cannot be deployed successfully in the target area.

The slides taken during the OFOS profiles are used to estimate the influence of seepage on the observed megafauna. The megafauna visible on the photos can be identified by comparing the fauna with the organisms recovered from the biological trawl. Quantitative characterization of the communities based on statistical analysis of the phototransects (establishing of dominant groups, calculation of relative abundance, patches, clusters etc.) will lead to an estimation of

biomass. Drawing conclusions from the fluid dependence of characteristic symbiontic animals makes a detailed estimation of the venting area possible. Based on this, a rough calculation of mass fluxes can be achieved. In addition to biological observations, geological features like scarps, outcrops or authigenic crusts and chimneys and investigations of their distribution and size provided clues as to how the fluid venting mechanism works and to the possible linkage to tectonic settings.

Technical aspects:

The GPI Kiel is the owner of the OFOS-sled which was built by *Preussag*. For the on-line observations, OFOS is equipped with a monochrome videocamera (*OSPREY OE 1323*), four lamps (24V, 150 W) and two deep-sea batteries (12V, 230 Ah) providing energy for about 15 hours. A sector of about 12 m^2 is visible. The observations are recorded continuously on videotapes.

The sled is manually adjusted by a winch operator at ca. 1 kn ship's speed and towed 2 to 4 meters above the seafloor. A bottom contact-alert for determining the OFOS's distance from the bottom is provided by a weight on a 3 m-rope visible by camera. Pictures with a stillcamera (*Benthos 372-A*) and the *Benthos flash system (383-RH/380-RH*, 600 Ws) were taken by remote control from board ship or automatically every 10 to 45 seconds. The stillcamera was charged with a 800-slides film (*Kodak Ektachrome*, 200 ASA). To control the photographic quality some films were developed during the cruise, but the greater part will be developed in a professional laboratory at home.

The automatically taken interval shots help to investigate the observed structures statistically. For scaling the pictures two parallel laser beams (*GTG Lasersystem*, 5 mW, 660 nm) make a 50 cm space scale on the seafloor. Every slide shows the time of taking as well as the day of the month. All data are registered and synchronised by time (UTC) as a ruling parameter.

To determine the exact position of OFOS is essential for the mapping of vents and associated structures. Aboard ship, position and depth are recorded by GPS and a 12 kHz-echosounder every 10 seconds. It is difficult to define the respective position of OFOS when deployed, therefore all data available have to be used to calculate in relation to the ship's position: wire length, wire deviation, drift etc. Depending on water depth, currents, ship's speed, and course, the TV-sled trails 200-300 m behind the ship when at a water depth of around 600 m. Distances given on maps and in tables following the OFOS data should therefore be taken with caution as a deviation up to 0.2 nm has to be reckoned with for the above-mentioned reasons. The positions of vent sites and other noteworthy occurences along the OFOS tracks are more reliable as these distances are relatively accurate.

3.3 Recovery of Sea floor samples

3.3.1 Recovery of deep-sea sediments

A Botsul, A. Derkachev, S. Gorbarenko, A. Kaiser, D. Nürnberg, H. Oehmke, Y. Terekhov, R. Tiedemann, and R. Werner

Seafloor sediments were recovered with the Standard Multicorer (MUC), the GEOMAR gravity corer (GC), the POI gravity corer, and the POI Hydrocorer. The multicorer usually gains the undisturbed uppermost sediment column and therefore, covers the gap the gravity corer, which recovers long sediment cores, but often lacks sediment surfaces, would leave otherwise.

During cruise 28 of *RV Akademik Lavrentyev*, 18 multicorer (MUC) deployments were run. Only two runs failed to retrieve sediments. 15 GEOMAR gravity cores (GC) were taken, in total recovering ca. 96 m. Four cores came up empty. 11 POI gravity corers were recovered successfully (ca. 59 m), one was empty. In addition, 2 POI hydrocorers (HYC) were run which successfully recovered 3 m of seafloor sediments.

Multicorer:

The multicorer is a pyramidal metal cage with a fixed frame in its center. The frame consists of an apparatus possessing 8 plastic tubes (length 61 cm, diameter 10 cm, open at both sides), and a release mechamism. Additional weights increase the total load of the MUC. Each tube is equipped with two lids which are fixed in an open position with springs when lowering the device to the seafloor. When reaching the sediment surface, the frame containing the tubes is pushed into the sediment. When the corer is pulled up, the springs are deactivated and the lids tightly close on both ends of the sediment-filled tubes. On average, the sediment recovery is ca. 30-40 cm with each tube. Furthermore, the bottom water directly overlying the sediment/water interface is trapped in the tubes as well.

Gravity corer:

The GEOMAR gravity corer (GC) applied by the German group consists of a long steel tube (length 5.75 m, diameter 0.18 m), which includes a removeable plastic liner of the same length (diameter 0.125 m). At the lower end, a core catcher prevents the sediment from sliding out of the tube. At the upper end, the tube is fixed to a large weight (1500 kg), which pushes the gravity corer deeply into the sediment. The maximum sediment recovery of ca. 6 m can be extended by connecting additional tubes. Depending on the type of sediment, cores of up to 15 m length were retrieved during this cruise. Aboard ship, the plastic liners are pulled out of the steel tube and sliced into 1-meter segments.

The POI gravity corer run by the Russian geologists has a 8.35 m long steel tube (inner diameter 0.145 m). The 700 kg-weight is directly attached to the upper part of the tube. In contrast to the plastic liners used by the GEOMAR corer, a thin polyethylene sleeve is inserted

into the core. After coring, the sleeve taking up the sediment is pulled out and cut into sections of 1-1.3 m length.

Hydrocorer:

The POI hydrocorer has a 6 m long tube with a diameter of 12.6 cm. In it there is a hydrostatic head which creates a pumping effect during the penetration of the device into the sediment. Two split halves of a steel tube inserted into the corer allow a quick removal of the sediment core on deck.

3.3.2 Rocks and Dredging

Ye. Lelikov, I.A. Tararin, E.P. Terechov, R. Werner, and J. Geldmacher

Dredging was carried out to collect samples from volcanoes and basement outcrops. Cylindrical dredges 50 cm in diameter with a steel wire were operated by a stern winch and the A-frame. A RIKADENKI multi pen recorder was used to detect bottom contact and bites of the dredge.

The dredging sites were set in areas where steep scarps with possible bedrock outcrops were identified by the detailed bathymetry and seismic reflection profiling obtained during *R V Akademik Lavrentyev* cruise 27 and by echosounding survey during cruise 28. The dredge was trailed along the sea floor from the lower slope towards its upper part of rises, ravines and submarine volcanoes. The location of dredging was determined by the GPS system aboard the ship at the moment of the first contact of the dredge with the sea floor. The depth of the dredging sites was determined by the echosound recordings.

Taking into account the widespread ice-rafted debris in the Okhotsk Sea, detailed analysis of the obtained material was carried out to identify bedrocks. The criteria used for evaluation include but are not restricted to

a) the shape of the samples (angular vs. well-rounded),

b) the existence of fresh surfaces formed by tearing away from the bedrock outcrops,

c) homogeneity of the dredged material.

3.3.3 Biological specimens

S. V. Galkin, H. Sahling, and D. N. Zasko

Introduction:

Even if the taxonomic composition of common fauna in the Sea of Okhotsk has already been studied thoroughly, the influence of seeping processes on the biological communities is not known. Gas seepage in the Sea of Okhotsk was first described at the Paramushir gas-hydrate site (Zonenshain et al., 1987). In general, the seepage of reduced chemical compounds has the potential of fuelling a complex trophic food web based on chemoautotrophic microorganisms. These microorganisms can occur either as free living bacteria or symbiontic species leading to different community structures. Chemosynthesis can be regarded as primary production and dominates the biomass and flux of organic matter at the sites but the spatial scale of this process

is not known. Characteristic macrofauna sometimes is the only visual manifestation of recent venting, e.g. at the Paramushir seeps the benthic community is dominated by the symbiont-bearing bivalve *Conchocele bisecta*. This bivalve harbors sulphur and methane oxidizing bacteria (Galchenko et al., 1988) indicating a continuous flow of methane.
This expedition is the first attempt to discover seeps and associated fauna in the western part of the Sea of Okhotsk.

The main objectives of biological investigation at the vents are:

1. Discovery and mapping of seep communities inhabited by specific fauna by the video/camera-sled OFOS (Ocean Floor Observation System, see: Chapter 3.2).
2. Determination of the taxonomic composition, diversity and abundance of benthic fauna (incl. meiofauna) by deploying trawl (TWL) and multiple corer (MUC).
3. Estimation of the degree of taxonomical and ecological isolation of benthic fauna compared to the background community.
4. Investigation of the trophic strategy of dominant animals, looking for evidence of their fluid dependence, determination of sulfur- or methane-based chemoautotrophy by analysis of stable nitrogen and carbon isotopes, light- and transmissionelectronmicroscopy.
5. Investigation of the relationship of characteristic fauna to known vent and seep habitates by molecularbiological techniques.
6. Geochemical characterization of the seep habitat.
7. Determination of specific organisms which might be used for bioindication of certain geochemical processes.
8. Estimation of the organic carbon pool and flux.

Methods:

Recovery of sea floor samples.

For collecting benthic animals a small biological bottom trawl has been used. The steel frame (120 cm x 30 cm) was equipped with a triple-layered net (outer: 45 mm double 3,1 x 2 capron net; middle: 7 mm knotty net; inner: at termination 1 m long sieve net, cell 1,0 mm) 3 m long. The trawl was towed onto the ship's heck by wire and drawn over the sea floor for 10 - 20 min. Some organisms could be collected from the MUC cores (see below), the geological dredge (DR) and the gravity corers (dead mollusks shells) as well.

Sample preservation:

All samples were sieved immediately after recovery (re-suspending the light fraction) through a 1,0 mm sieve. The animals were extracted in the lab and sorted into taxonomic groups. After the determination of the wet weight of selected specimens with beam-scales these species were fixed. Specimens for taxonomic identification, anatomical and histological study were fixed in 70% ethanol or 4% buffered formaldehyd (stored in 70% ethanol). Soft tissues for stable

isotope analyses were dried at 50 - 60 °C or frozen at -25 °C. Parts of the tissue for transmission electron and light microscopy were fixed in 5% glutaraldehyd or 4% paraformaldehyd, respectively. For molecularbiological analyses symbiont-bearing tissues of selected animals were frozen at -25 °C separately from symbiont-free tissues.

3.4 Sediment processing aboard the ship

A. Botsul, N. Biebow, A. Derkachev, S. Gorbarenko, A. Kaiser, D. Nürnberg, H. Oehmke, Y. Terekhov, R. Tiedemann, and R. Werner

GEOMAR approach:

D. Nürnberg, R. Tiedemann, N. Biebow, and A. Kaiser

Up to 7 multicorer tubes were cut into 1 cm-slices and stored immediately after coring. Bottom water and fluff layers at the water/sediment-interface were sampled separately for pH and gas analyses (see: chapter 3.5). At nearly each station, tubes were sampled for stable isotope and coarse fraction analyses, organo-geochemical (TOC, biomarker), inorganic-geochemical analyses (GEOMAR), the determination of biogenic silica (GEOMAR), and micropaleontology (AWI) (Appendix 3.1). One tube was utilized by Russian scientists (paleoceanography).

Each 1-meter liner segment of the GEOMAR gravity corer was cut into work and archive halves. Prior to sedimentological description (Appendix 3.2), the magnetic susceptibility was continuously measured. The photographic documentation will be performed at the home laboratory. The lithology was documented accordingly. For X-ray photography, 25x10x0.5 cm sediment slices were prepared and stored in plastic lids. Subsamples were routinely taken for smear slide investigations (Appendix 3.3). Further sampling for the determination of the water content, physical properties, stable isotopes, coarse grain fraction, geochemistry, and micropaleontology will be done at home (Fig. 3.1).

Especially for the Russian collegues, 10 ml syringes taken every 5 to 10 cm will be provided. In return, the German group received 10 ml syringe samples from the Russian gravity corer every 10 cm. After processing, the cores were stored on the ship's deck.

Smear slides were prepared for each lithological unit (Appendix 3.3) and partly investigated under the microscope. Biogenic and terrigenous sediment components were distinguished. A rough quantification of grain size fractions (sand >63 µm, silt 2 µm - 63 µm, clay <2 µm) and single components was derived by scanning the smear slides and classifying them into 4 classes of occurrence: rare, common, abundant and rich. This method provides preliminary knowledge on the lithological sediment composition (Appendix 3.2).

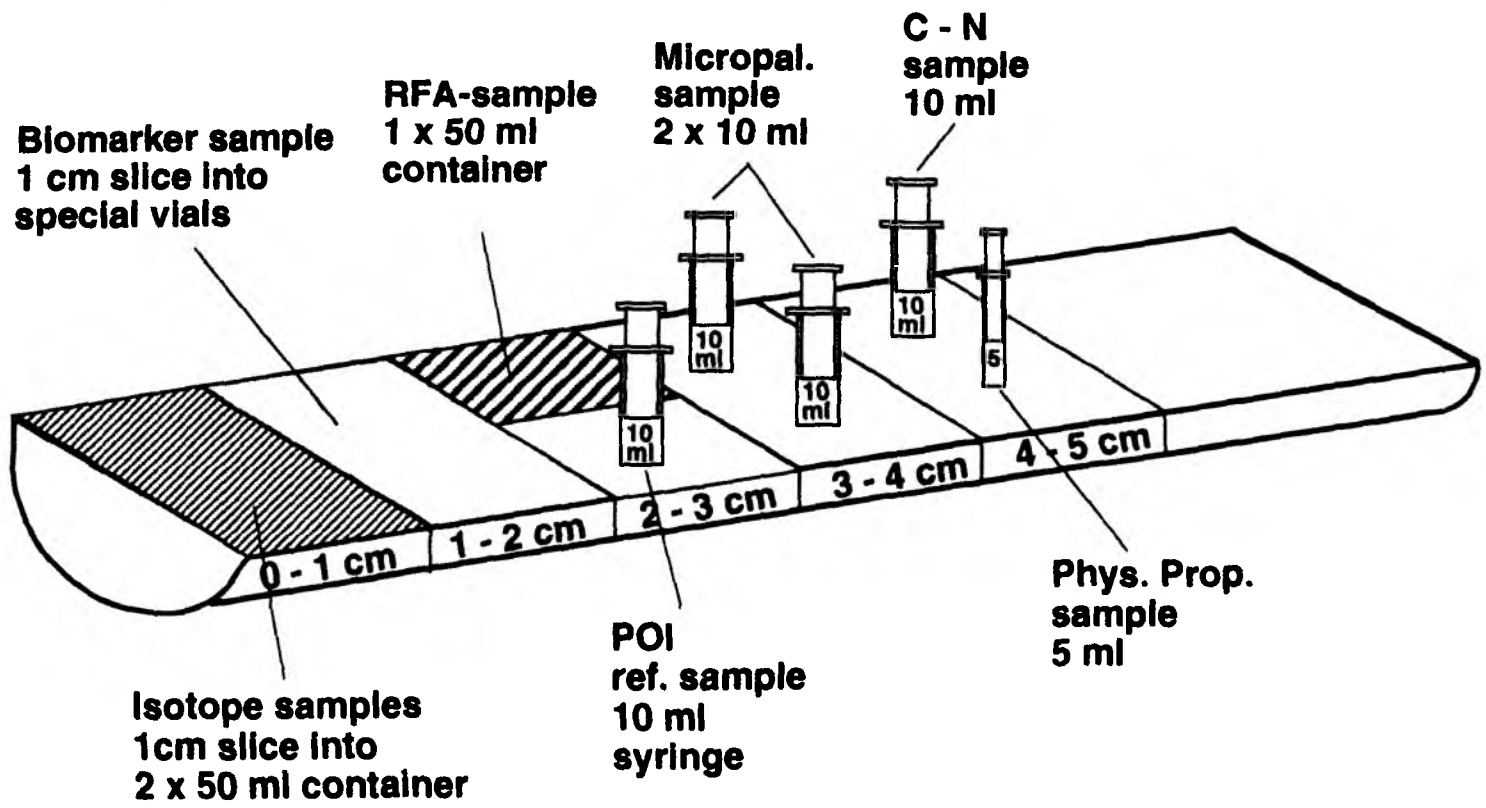

Fig. 3.1: Sampling plan of GEOMAR gravity cores.

POI approach

S. Gorbarenko and A. Derkachev

During the cruise, the following steps of sediment sampling and processing were performed:

1. Sampling for the analysis of gas components and pore water chemistry.
2. Measuring water content and magnetic susceptibility were carried out every 3 cm by a microwave meter (MWM-8) and a magnetic susceptibility meter (IMV-2), which was in direct contact with the sediment covered by a polyethylene foil. Data were directly stored on a computer. The devices were designed by the Western Company, Kaliningrad (Russia).
3. Samples were taken every 20-50 cm to measure the sediment humidity and density following the weight method.
4. Visual description, sampling, preparation and the preliminary study of smear slides with the microscope POLAM L-211.
5. Samples for micropaleontological studies and oxygen and carbon isotopic analyses (0-9 cm through 10 cm), granulometric (10 cm) and geochemical (5-10 cm) measurements were taken.
6. Removal of the clay fraction and classification into the grain size fractions 0.05-0.1 mm, 0.1.-0.25 mm, and fractions larger than 0.25 mm for mineralogical analyses.
7. Separation and microscopic study of authigenic minerals, calcite nodules and calcite-barite crusts.
8. In-line vent sampling for gasgeochemical analyses of pore water (pH, Eh, methane), and gas hydrates.

Physical properties of the sediments

A. Botsul and S. Gorbarenko

The analysis of sedimentary physical properties was mainly performed to establish a lithostratigraphy of the Quaternary sediments. In addition, the physical properties are necessary to calculate sediment accumulation rates. Since it is difficult to preserve the sediment's natural humidity, humidity measurements were directly carried out aboard the ship, immediately after cutting the core (Appendix Table 3.4).

Two methods were used: First, the standard weight method and, second, humidity measurements with a microwave moisture meter (MWM-8, Western Company, Kaliningrad). The standard method includes the sampling of 50 cm^3 of non-disturbed sediment, subsequent drying at 105°C temperature, and weighing before and after drying. Based on these data, the density of the natural sediment (D), the density of the mineral base (D_p), the mineralogical density (D_t), the volume humidity (W_v), and the weight humidity (W_w) were calculated applying the following equations:

$D=P_O/V$;

$D_p=P/V$;

$W_V=(P_O-P)/V*g*100\%$;

$W_W=(P_O-P)/P_O*100\%$,

where P_O and P is the sediment sample weight before and after drying (g); V - sample volume (cm^3); g - pore water density (g/cm^3) (1,00).

Magnetic susceptibility

R. Tiedemann and S. Gorbarenko

Records of magnetic susceptibility mainly reflect the content of ferrimagnetic minerals in the sediments. During the cruise, measurements of magnetic susceptibility were obtained with two different methods, the compatibility of which was already shown by Nürnberg et al. (1996):

1. Whole core segments (1m length) retrieved with the GEOMAR gravity corer were measured with a Bartington loop sensor (MS2C) in conjunction with a control unit (MS2). The sensor generates an alternating (f = 565 Hz) magnetic field of low intensity; any material brought into the sensor changes the oscillator frequency. This frequency information is returned to the control unit where it is converted into a value of magnetic susceptibility. Magnetic susceptibility was measured in SI units ($*10^{-5}$) in 2 cm intervals along the cores. Artificial minima of magnetic susceptibility usually occurring at both ends of each core section were identified and removed from the data set.

2. Cores collected with the POI-gravity corer were measured with a sensor directly at the sediment surface (IMV-2). Magnetic susceptibility and humidity values were obtained every 3 cm along the cores. The magnetic susceptibility was measured in cgs-mode.

Micropaleontology

A. Nimmergut and R. Tiedemann

In order to specify stratigraphic control points in selected sediment cores, the last occurrence of distinct radiolarian species was identified. Approximately 5 ml sediment were extracted from distinct horizons, subsequently disaggregated and sieved through a 500 µm and a 40 µm sieve. The residue was embedded into Canada balsam on glas slides for light microscopy. Slides were roughly scanned for appearance and/or non-appearance of the radiolarian *Lychnocarnoma nipponika sakaii*.

3.5 Water column sampling and pore water sampling and their composition

A. Salyuk, G. Winckler, V. Sosnin, G. Pavlova, Y. Shul'ga, A. Obzhirov, B. Domeyer, J. Geldmacher, J. Greinert, A. Kaiser, B. Li, and A. Nimmergut

CTD-Rosette

G. Winckler, A. Salyuk, and V. Sosnin

Water column studies were carried out using a CTD (Conductivity-Temperature-Depth) and associated rosette water sampling system. The instrumentation package included a Seabird 911 plus CTD with temperature, conductivity and pressure sensors. The instrument also logged data from a 25 cm transmissiometer, a Datasonics altimeter and an oxygen sensor.

The rosette system was a Sea-Bird 32 twelve-position rosette with 10L-Niskin-type water samplers.

Downcasts proceeded continuously at 1m/sec until the bottom-trigger alarm sounded. The first water sample was generally collected at this depth, the others collected on the upcast. Due to lacking length of the one-way induction cable (ca. 2250 m) used for the deployment of the rosette system, some CTD casts in the Kurile Basin (#55-1) and on the N-S Transect (#61, #64, #65, #66) were limited to the upper 2250 m and, unfortunately, the lower water column could not be investigated.

Separate data files were collected and processed for each cast. Processing was performed using modular processing routines provided by the software package SEASOFT (Version 4.214.). Raw CTD data were converted by being averaged to 1 dbar intervals.

A total of 24 CTD stations were sampled in all areas and are tabulated in Tab. 3.2. Water samples were collected for methane, higher hydrocarbons, oxygen concentration, alkalinity and pH, carbon isotopes, nutrients, earth alkali elements, oxygen isotopes, tritium and helium isotope analyses; nutrient concentration analyses were performed on board through an autoanalyzer system and oxygen titrated using the Winkler method. The data are tabulated and discussed below, isotope results will follow from post-cruise laboratory analyses.

Table 3.2: CTD Statistics

Station	C_xH	O_2	TA	pH	nut	$\delta^{13}C$ Geo	$\delta^{13}C$ Pal	E A	$\delta^{18}O$	$^3He/^4He$	^3H IUP	^3H POI
North/South Transect												
2-1 CTD	x	x	x	x	x	x			x	x	x	
3-1 CTD	x	x			x	x	x	x	x	x	x	
North Sakhalin Shelf and slope												
5-1 CTD	x	x			x	x			x	x	x	
6-1 CTD	x	x			x	x			x			
8-1 CTD	x	x			x	x	x	x	x	x	x	
11-1 CTD	x	x	x	x	x	x			x	x	x	
14-1 CTD	x	x			x	x	x	x	x	x	x	
20-1 CTD	x	x	x	x	x	x			x	x	x	x
					x							
Derugin Basin												
28-1 CTD	x	x	x	x	x	x	x	x	x	x	x	
29-1 CTD	x	x			x	x	x	x	x	x	x	x
39-1 CTD	x	x	x	x	x	x			x	x	x	x
East/West Transect												
4-2 CTD	x	x			x	x	x	x	x	x	x	
40-1 CTD	x	x	x	x	x	x	x	x	x	x	x	x
41-1 CTD	x	x	x	x	x	x	x	x	x	x	x	x
42-2 CTD	x	x	x	x	x	x	x	x	x	x	x	x
43-1 CTD	x	x	x	x	x	x	x	x	x	x	x	x
44-5 CTD	(x)	x	x	x	x	x	x	x	x	x	x	x
Kurile Basin												
55-1 CTD	(x)	x			x	x	x		x	x	x	x
Methane Stations												
62-1 CTD	(x)	x			x	x			x	x	x	
63-1 CTD	(x)	x			x	x			x	x	x	x
North/South Transect												
61-1 CTD	(x)	x			x	x	x	x	x	x	x	
64-1 CTD	(x)	x			x	x	x	x	x	x	x	x
65-1 CTD	(x)	x			x	x	x	x	x	x	x	x
66-2 CTD	(x)	x			x	x	x	x	x	x	x	x

Carbonate System

G. Pavlova and Y. Shul'ga

Data collection and analysis:

Carbonate chemistry data in seawater for 13 CTD stations (CTD and chemical sampling were carried out concurrently) and in porewater for 6 MUC and 7 SL stations are presented here. Station locations and corresponding sampling depths are listed in Table 3.2.

We can characterize the CO_2 system by measuring any two of the four basic carbonate parameters: the partial pressure of carbon dioxide (pCO_2), total inorganic carbon (TCO_2), total alkalinity (TA) and pH. The other parameters may be calculated using thermodynamic relations.

pH and TA were measured on this cruise. These parameters are the most important ones for studying sediment porewater. We can run TA using a small volume unit of porewater (about 1 ml) and measure pH in the sediments directly.

Total alkalinity is defined as the sum of all bases that can accept a proton at the carbonic end-point (Dickson, 1981). It is defined by

$$TA = [HCO_3^-] + 2[CO_3^{2-}] + [B(OH)_4^-] + [OH^-] - [H^+] + \text{bases}, \qquad (1)$$

where $[OH^-]$ includes the OH^- bound to Mg^{2+} and $[H^+]$ includes the $[H^+]$ to SO_4^{2-} and F^-. TA also includes minor concentration of other bases that can accept a proton

$$\text{Bases} = [SiO(OH)_3^-] + [HPO_4^{2-}] + 2[PO_4^{3-}] + [NH_3] \qquad (2)$$

For seawater in the open ocean (aerobic conditions, pH 7.5-8.2), the carbonic and boric acid systems have considerable influence only on the TA value (Gieskes, 1974). But for marginal sea and especially for sediment porewater the contribution of other bases to eq. (1) may be considerable, too, and must be taken into account. It may do using concentrations of weak acids together with thermodynamic information about their dissociation constants.

Samples for ***total alkalinity in the seawater*** were taken into the 250 ml borosilicate glass flasks in the manner of Dickson (1994a), poisoned with 50 µl of saturated mercuric chloride solution to prevent any biological activity and analyzed by direct titration in an open cell of 25 ml of seawater with 0.02N HCl (Ivanenkov and Lyakhin, 1978). The acid was standardized daily with Na_2CO_3 solution prepared from pre-weighted crystals dried at 280°C and dissolved in deionized water free of CO_2. To remove carbon dioxide during titration the samples and standards were flushed with a continuous stream of pure nitrogen. The mixture of methylene blue and methyl red was used as an indicator and titration was completed when the green color of the solution turned to light-pink and left quite stable (pH at the end point is equal to 5.4-5.5). The Brinkman/Dosimat 665 motor-driven piston burette reproducible to ±0.001ml in the

delivered volumes was applied for analysis. Concentrations were converted from volumetric to weight with the help of seawater densities calculated at the temperature of total alkalinity titration. Based on the analysis of seawater replicates, analytical precision ±2.6 μM/kg (n=10) for total alkalinity was achieved in this study.

Hydrogen ion activity (pH) in seawater was determined by direct potentiometry (Bates, 1973). Seawater was drawn according to the procedure described by Chipman and Guenther (1994) and measurements were conducted immediately after sampling at 25±0.1°C with glass (OP-0718) and saturated calomel (OP-0830P) electrodes manufactured by Radelkis (Hungary). A closed flowing electrochemical cell was used to avoid exchange of CO_2 with the atmosphere, changes in liquid-junction potential of the reference electrode and stress on the glass electrode. The e.m.f. was registrated on the Radelkis OP-208 digital pH-meter characterized by high input impedance (>10^{13} Ω) and sensitivity ±0.1 mV. Electrodes were standardized in the SWS-scale (Dickson, 1994) and a tris-seawater buffer with $pH_{SWS}(25)$=8.0893 prepared following the prescription of Millero (1994) was used as a standard before and after each set of measurements. Control for the Nerst behavior (slope) of the electrode pair was realized with the help of Russian NBS standards with pH 6.86 (phosphate buffer) and 4.01 (phtalate buffer) at 25°C. Based on the analysis of seawater replicates, the analytical precision of ±0.0044 (n=20) for $pH_{SWS}(25)$ was achieved.

Samples for ***total alkalinity in the sediment porewater*** were analyzed by direct titration in an open cell of 1 ml of porewater with 0.02N HCl using the same procedure as with seawater titration. The Brinkman/Dosimat 665 motor-driven piston burette reproducible to ±0.001ml in the delivered volumes was applied for analysis. Concentrations were converted from volume to weight with help of porewater densities calculated with the temperature during total alkalinity titration. Based on analysis in porewater replicates, an analytical precision of ±0.014mM/kg (n=8) for total alkalinity in porewater was achieved in this study.

Samples for ***calcium (Ca) in the sediment porewater*** were taken in plastic flasks, preserved with hydrochloric acid to create pH = 2 and analyzed by complexometric titration of 1 ml of porewater (Tsunogai, 1968). EGTA is used as a titrant and GHA [glyoxal- bic (2 hydroxyanil)], a sensitive and selective reagent for calcium, is used as metal indicator at pH 11.7. Calcium is extracted into a small volume of organic solvent (n- Butanol) as its GHA-complex, and the calcium is titrated with EGTA. The end point is sharp, and occurs when the red colour of the organic layer vanishes. The EGTA was standardized daily with standard calcium solution prepared from 1.0309 g pure calcium carbonate dissolved in hydrochloric acid and diluted to 1 litre after the addition of 13.114 g magnesium sulphate ($MgSO_4$* $7H_2O$), 0.0243 g strontium chloride ($SrCl_2$* $2H_2O$) and 27.47 g sodium chloride. The solution was 10.30 mM in calcium, 53.20 mM in magnesium, 0.091 mM in strontium and 470 mM in

sodium, as in seawater. The Brinkman/Dosimat 665 motor-driven piston burette reproducible to ±0.001ml in the delivered volumes was applied for analysis. Concentrations were converted from volumetric to weight with help of porewater densities calculated at the temperature of calcium titration. Based on analysis in porewater replicates analytical precision of ±0.007mM/kg (n=8) for calcium in porewater was achieved in this study.

pH measurements in sediments were conducted immediately after sampling at 25±0.1°C with glass (ESL-63-07) and Ag/AgCl (EVL-1M3) electrodes manufactured in Russia in the open electrochemical cell. The electro-motive force (EMF) was registrated on the Radelkis OP-208 digital pH-meter characterized by sensitivity ±0.1 mV. Electrodes were standardized in the SWS-scale (Dickson, 1994) and tris-seawater buffer with $pH_{SWS}(25)=8.0893$ prepared after Millero (1994) was used as a standard before and after each set of measurements. Control for the Nerst behavior (slope) of the electrode pair was realized with the help of Russian NBS standards with pH 6.86 (phosphate buffer) and 4.01 (phtalate buffer) at 25°C.

Laboratory set for the ***direct measurements of oxidation-reduction potential (Eh)*** consists of an electrochemical cell and pH-meter (OP-208). Smooth platinum redox-metric electrode (platinum wire), Ti-silicate glass (EO-021) and Fe-silicate glass (EO-035) electrodes, developed at the Research Institute of Chemistry of Glass, St. Petersburg University, served as electrode-indicators. EMF was measured by pH-meter OP-208 with an accuracy of 0.1mv. A temperature of samples was measured with a mercury thermometer with an accuracy of 0.1°C. The temperature of 25°C of the measuring cell was supported by a U-8 thermostat. For better contact, a sediment sample at the electrode-sediment boundary was deluted with seawater (sw) in the proportion $V_{sediment}/V_{sw}=10:1$. Solutions of iron (Fe^{2+}, Fe^{3+}, $C=10^{-3}$ mol/l m) with EDTA (ethylendiaminetetracetic acid) were used as mediators for reduced sediments of the Okhotsk Sea. The mediator interacts with the redox system of the sediments very quickly and promotes the fast establishing of equilibrium potential on the electrodes. The amount of the mediator introduced into the sediments must not alter the redox conditions of the sample. It was found that the volume of the mediator must provide a redox-buffer 50-100 times less than the redox-buffer of the samples: $\beta x V_{sed}/C_{med} x V_{med} \geq 50\text{-}100$, where β is an oxidation volume. The volume of the added mediator (V_{med}) is calculated from the above-mentioned formula. Eh of the mediator solution must be optimally close to the Eh of the sediments. Ratio Fe^{3+}/Fe^{2+} in the mediator is 1:10.

The oxidation volume (β) was determined potentiometrically by Pt-electrode. As a redox system, the system $Fe(CN)_6^{3-,4-}$ with a concentration of $C=10^{-3}$ mol/l and a ratio of 10:1 was used to determine β of the sediment sample. The values of β were calculated by the formula deduced from Nernst's equation:

$\beta = C_{ox}xV_oxC_{red}xV_o(1-A) / (C_{ox}xV_o - C_{red}xV_oxA)xV_{sed}$,

where V_o is the volume of the $Fe(CN)_6^{3-}$ and $Fe(CN)_6^{4-}$ mixed solution;

V_{sed} is the volume of sediment added;

C_{ox} is the concentration of $Fe(CN)_6^{3-}$, mol/l;

C_{red} is the concentration of $Fe(CN)_6^{4-}$, mol/l;

A - antilog $(E_2 - E_1) / \theta$, $\theta = 59.16$ mv;

E_1 is the potential of the solution free from sediment;

E_2 is the potential of the solution containing sediment.

The duration of β measurements is 10-30 minutes.

After β was determined, 30 ml of sediment were taken into the cell and diluted with seawater (3 ml) and stirred; 2 ml of mediator solution were added and stirred again. The cell containing the sediment was controlled thermostatically at 25°C; 30 min later sediment Eh was recorded with an accuracy of 1 mv according to the readings of Pt, Ti and Fe electrodes.

Various *carbonate parameters in situ*, pH, pCO_2, TCO_2, H_2CO_3, Lc and La (abbreviations are listed in Tab. 3.3) in seawater and porewater were calculated from the combination of total alkalinity and $pH_{SWS}(25)$ after Skirrow (1975) and Millero (1979). Equilibrium constants for CO_2 solubility, for carbonic, boric, phosphoric, silicic acids and for ammonium (SWS-scale), and the solubility products of calcite and aragonite in seawater as a function of temperature and salinity at 1 atm total pressure and equations for calculating the effect of pressure on the thermodynamic constants recommended by Millero (1995) were used for calculations. The total amounts of such conservative constituents as borate and calcium (for seawater) were determined from the salinity rations of Culkin (1965) and Millero (1979), respectively. Calcium for porewater was analyzed by complexometric titration with EGTA (Tsunogai, 1968). Apparent oxygen utilization (AOU), defined as the difference between the solubility of oxygen at a potential temperature, salinity and the observed oxygen concentration, was calculated after Weiss (1970).

<u>CH_4 and higher hydro carbons</u>

A. Obzhirov

Special soft bottles are used to take water from the Niskin bottles without air contact. Gas is extracted from the water by a specific vacuum installation designed by POI (Obshirov, 1993), and subsequently analyzed by gas chromatography aboard ship.

Methane and heavy hydrocarbons (ethane, propane, butane and their homollogues) are analyzed by a flame-ionization detector. Oxygen, nitrogen and carbon dioxide are analyzed by a catharometer. Sensitivity of the hydrocarbon analysis is 0.000001 %, of other gases ca. 0.01%. The calculation of gas concentrations is controlled by gas standards (Certificate Scotty

II, No. 016801, Alltech Associations, Inc; 10 and 1000 ppm of methane and 500 pm of carbon dioxide).

Table 3.3: *Symbols, units for measurement, and abbreviations.*

AOU	apparent oxygen utilization, µM/kg
H_2CO_3	dissolved H_2CO_3, mM/kg
CO_3	carbonate ion concentration, mM/kg
H	depth, m
La	aragonite saturation degree
Lc	calcite saturation degree
NTA	normalized total alkalinity, mM/kg (=TA*35/S)
$NTCO_2$	normalized total inorganic carbon, mM/kg (=TCO_2*35/S)
O_2	oxygen concentration, µM/l
pCO_2	partial pressure of carbon dioxide, µatm
$pH_{SWS}(25)$	pH at 25 °C temperature and one atmosphere total pressure
pH(p,t)	pH at in situ temperature and pressure
S	salinity, psu
TA	total alkalinity, mM/kg
TCO_2	total inorganic carbon, mM/kg
T	temperature, °C

Nutrients and chloride

B. Domeyer

To detect anomalies in the major ion composition in pore fluids such as caused by gas hydrate destabilisation or injection of fresh water at vent sites, chloride was measured by conventional Ag-Cl-precipitation (Winkler-Method) using commercial $AgNO_3$ standardized titrants against IAPSO seawater. The method was adjusted for small sample volumes (0.1000 ml) in order to conserve pore waters. Precise bottom water chloride concentrations were needed from the sites where suspected vents were cored. For this purpose Cl was measured in 15 hydrocast samples (14-1 CTD; 20-1 CTD; 39-1 CTD) from the Sakhalin slope and the Derugin Basin spanning water depths from ≈*300* to ≈*1550m* (Fig. 3.2). Precision and accuracy was determined against CTD-derived chlorosities and found to be ±0.2% and ±0.04g/l, respectively.

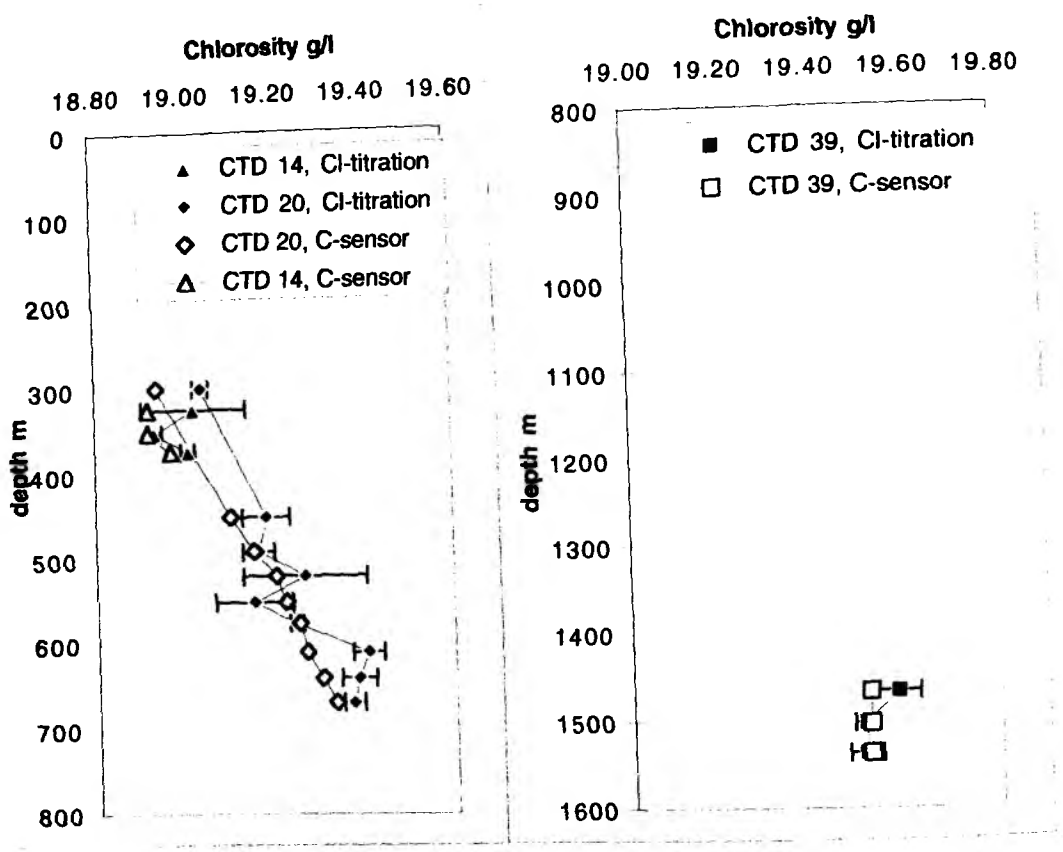

Fig. 3.2: Chloride contents in 15 hydrocast samples from the Sakhalin slope and the Derugin Basin.

Pore water sampling and analysis

B. Domeyer, J. Geldmacher, J. Greinert, A. Kaiser, and H. Sahling

Sediment samples were taken from the cores listed in Table 3.4. The sediment samples were squeezed at 4°C room temperature using a polypropylene squeezer pressurized by argon;the samples were filtered on line through 0,2µm cellulose acetate membrane filters.

The analytical techniques used on board to measure the various dissolved constiuents are listed in Table 3.5. Concentrations of dissolved nitrate, phosphate, ammonia were determined using an autoanalyzer working with standard photometric procedures. Silicat and H_2S were measured using standard photometric hand methods. Chloride was determined by Mohr titration.The number of samples taken from each core and the types of analyses performed on board are shown in Table 3.4.

pH electrodes were used for the determination of pH in the sediment; they were calibrated using buffers prepared in artifical seawater (Dickson, 1993). BIS and 2- Aminopyridine were used as buffers in the neutral pH range (pH 7 to 9). Subsamples from selected porewaters were taken for alkalinity measurements.

Table 3.4 : Number of samples taken from each core and types of analyses performed

Station	PO_4	NO_2	NO_3	NH_4	H_2S	Cl	pH sediment in Situ	pH sws (25)	TA mg-eq/kg	Number of samples
North/south transect										
2-2 MUC	x	x	x	x	x		x		x	19
2-4 SL-R	x	x	x	x	x		x		x	21
North Sakhalin Shelf and slope										
15-2 MUC	x	x	x	x	x	x	x			9
17-2 SL-G	x	x	x	x	x	x	x	x	x	15
20-2 SL-G	x	x	x	x	x	x	x	x	x	47
20-3 HYC	x	x	x	x	x	x	x	x	x	26
21-1 SL-R	x	x	x	x	x	x	x	x	x	14
30-3 MUC (3 Cores)	x	x	x	x	x	x	x	x	x	38
30-4 (2 Cores)	x	x	x	x	x	x	x	x	x	32
Derugin Basin										
24-1 SL-G	x	x	x	x	x	x	x			1
25-1 HYC	x	x	x	x	x	x	x	x	x	24
34-1 MUC	x	x	x	x	x	x	x		x	30
37-1 SL-R	x	x	x	x	x	x	x	x	x	40
East/West Transect										
44-2 MUC	x	x	x	x	x		x		x	17
44-3 SL-R	x	x	x	x	x		x	x	x	23

In addition to pore water sampling, sediment samples were taken for porosity and for methane analysis.

Table 3.5: *Techniques used for pore water analysis*

Constituent	Method	Reference
Ammonium	Autoanalyzer	Grasshof et al. (1983)
Phosphate	Autoanalyzer	Grasshof et al. (1983)
Nitrate	Autoanalyzer	Grasshof et al. (1983)
Nitrite	Autoanalyzer	Grasshof et al. (1983)
Silicate	Hand methode	Grasshof et al. (1983)
Hydrogen sulphide	spectrophotometry	Grasshof et al. (1983)
Chloride	Mohr ($AgNO_3$) titration	Gieskes et al (1991)

Acoustic imaging

B. Li

The ship's experimental system «SARGAN-EM-UDM» was used to search for gas vents. This system includes the updated hydroacoustic fish-prospecting echosounder «SARGAN-EM» with an acoustic transmitter-receiver and the autonomous gauge system UDM. The UDM block contains a PC, a two-channel multifrequency amplifier with a specific processor and the necessary mathematical supply. The recording and accumulation of acoustic data is realized as specific files by the gauge system UDM.

Technical characteristics of the hydroacoustic echo sounder «SARGAN-EM» are as follows:

	Low frequency	High frequency
Generator power P, W	1000	500
Radiation level SL, dB//μPa/1 m	220	230
Amplification factor G, dB//V	90	83
Frequency, kHz	20	135
Beam width, degree	10	4
Receiver sensibility VR, dB//V/μPa	-100	-100
Duration of sound impulse, ms	3	1

The UDM system allows echosounding signals to be received by two independent channels, to be amplified, detected and transformed into an analogous-digital signal. The UDM allows to enter, record and reflect the echosounding and navigational information with the help of an IBM PC P-166. Color echograms are displayed on a computer monitor immediately after the signal is received. The time and coordinates are recorded every 5 minutes.

The technical data of the UDM system are as follows:

Width of working frequence, kHz	12 ÷ 200
Frequence band, kHz	1
Maxima amplification, dB	≥ 100
Time adjustment of amlification:	
mode of time changing	linear
Interval of amplification changing, dB	40
Input resistance (for each channel), KΩ	3

Multi Plankton Sampler

A. Nimmergut

To sample the water column vertically, a Multi Plankton Sampler constructed by Hydro-Bios Apperatebau GMBH, Kiel, was applied. Five nets, each 2.5 m long, with a mesh size of 55 mm are connected to the underwater instrument. This has an 50 x 50 cm opening for inflow at its top and is fitted with an engine for opening and closing the nets as well as a depth-measuring device. Both are connected with the board instrument where the actual depth is shown and from which the nets can be opened and closed while the net is brought up the water column.

The net ends lead to sampling buckets of 10,10 cm in diameter and net windows with a mesh size of 41mm. These contain the sampled material of the depth intervals chosen and can be taken off for preserving the samples which are finally poisoned with ethanol at a ratio of 1:1.

The Plankton Net samples are taken for the investigation of radiolarians. The objective is the documentation of the vertical and biogeographical distribution of radiolarians in the water column. Therefore the mixed surface layer, the dicothermal layer, the layer below the dicotherme, and two deeper layers are sampled. The upper three of these layers are met at approximately 0-50 m, 50-130 m and 130-200 m depth respectively according to vertical temperature profiles given by CTD measurements. Where it was possible, samples were taken down to 1000 m depth at the intervals 200-500 m and 500-1000 m depth. Where the sea floor was shallower, sample intervals from 200-300 m and 300-500 m depth were chosen.

The application of flow meters situated within the nets makes quantitative studies possible. The differences between the flow meter values (the flow meter rotation values are proportional to the water volume flown through the net) after (F = final value) and before (S = start value) one deployment multiplied by the opening diameter of the under water instrument (0.25 m^2) (A) and the impeller (0.3 m) (P) defines the water volume in m^3 flown through each net (Appendix 7).

$(F-S) \times P \times A = m^3$

$(F-S) \times 0.3 \times 0.25 = m^3$

$(F-S) \times 0.75 = m^3$

In this equation the differences due to mesh size and blocking of the meshes with biological material is not taken into account.

Further on the results from the plankton samples will be compared with results from the investigation of the surface sediment assemblages at the various sites.

4. RESULTS

4.1 Hydrography of the Sea of Okhotsk

G. Winckler, V. Sosnin, and A. Salyuk

The results of this section are relevant to the following three chapters, all of which depend on general knowledge about the hydrography of the Sea of Okhotsk. The question of vent distribution on the shelf and the slope is governed by the dynamics of the shelf circulation (chapter 4.2), the Derugin Basin objectives are concerned with the deep water exchange or even with the stagnation of the deep part of the basin (chapter 4.3). The palaeoceanographic objectives obviously are highly dependent on detailed knowledge of the current hydrographic situation (chapter 4.4).

General Hydrography of the Sea of Okhotsk

Monsoon-like atmospheric circulation and the geographical vicinity near the Siberian cold pole determine the climate of the Okhotsk Sea. The monsoon character of atmospheric circulation is the result of the interaction of the main atmosphere centers: in winter, the Asian anticyclone and the Aleutian minimum dominate the climate; in summer, the North Pacific (Hawaiian) maximum and the center of low pressure above Asia rule the climate. There are significant differences between climatic conditions of the northern and southern parts of the sea. Northwestern and northern regions of the sea have a harsh continental climate, whereas in the southern part of the sea the climate is much milder, effected by the proximity to the Pacific ocean.

The winter monsoon is the main reason for harsh winters with a dominance of northern winds, therefore half of the year the sea is covered with ice. The maximum coverage is reached in March. During winter, most parts of the Okhotsk Sea are covered with ice. During mild winters, the southeast part of the sea is almost free from ice; however, such winters occur only 2 - 3 times a decade. At the East Sakhalin coast the process of ice formation begins in the middle/at the end of November; the ice coverage is kept up to the end of May/beginning of June. During the first half of summer, a high pressure area builds up above the not yet warmed Sea of Okhotsk, therefore even during the summer the southern regions of the sea remain very cool. During the second half of summer cyclonic activity predominates the climate. Often cloudy weather with fog and rain prevails at this time of year.

These conditions of atmospheric circulation form thermal and salinity regimes as well as the general circulation of the sea. A subarctic water structure with an extremely thin heated surface layer is characteristic for the Okhotsk Sea. The cold subsurface layer has a temperature close to the freezing point of sea water (- 1.8 °C). This layer is a remnant of the mixed upper winter layer whose temperature and thickness is determined by the conditions of the previous winter season. The warm intermediate layer has a lower absolute value and lies in a greater depth in

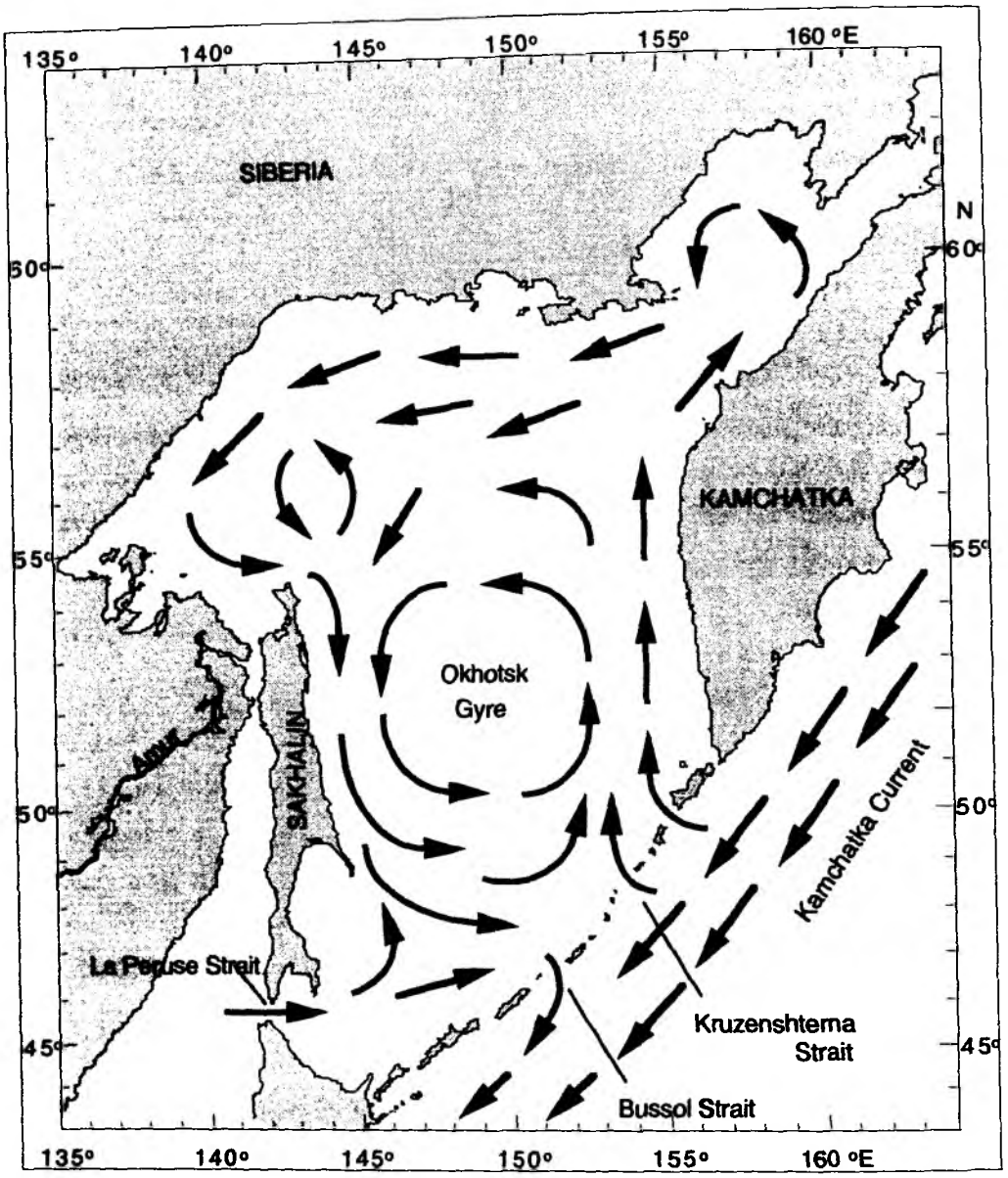

Fig 4.1: Mean currents in the Sea of Okhotsk

comparison with the ocean (2.6°C and 600 m correspondingly). Beneath the maximum, the temperature monotonously decreases with depth. This constitutes the typical temperature distribution for the summer season.

Positive values for the fresh water balance are characteristic for the sea since precipitation prevails over evaporation. The input of fresh water decreases the salinity in the upper layer. Thus, the typical surface salinity is of the order of 32.0 - 32.5 PSU and monotonously increases to the bottom to 34.5 PSU. River runoff plays an important role in the fresh water budget. Its maximum is connected with the Amur input. The freshened brown-green traces of its waters move from the Amur Inlet through the Sakhalin Gulf along the northeast and east coast of Sakhalin Island.

The general circulation of the sea has a cyclonic character (Fig. 4.1). The mean current velocity does not exceed 0.4 - 1.0 knots. The water exchange with the Japan Sea is carried out through the Tartar Strait and La Peruse Strait. Pacific waters enter the sea through the northern straits and returns to the ocean through the southern straits of the Kurile Islands. There is a steady cyclonic circulation especially well noticeable in winter time on satellite photos which monitor the ice drift. One of the stable cyclonic eddies is just above the Derugin Basin.

The current along the East Sakhalin coast is of special interest. It constitutes a link in the circuit of general circulation of the sea, which joins the drain of Amur river at the northern edge of the island. The current speed here is near 1-1.5 knots. According to our indirect data (magnitude of the ship's drift, angle of cable deviation and velocity of winds), the Northern Sakhalin Shelf area shows a southward stream with a velocity of not less than 1.5-2.0 knots.

Tidal phenomena play a special role in the formation and short-period variability of the water structure in the straits and on the shelf. Tidal currents exceed the mean currents and have a reverse character. The average velocity of tidal currents is 0.4-3.0 knots, but considerably increases in straits and in regions with an abrupt change in bottom relief. Maximum tidal currents can be found in the Gulf of Shelikhova and in the Shantar region where it reaches 8 knots. Rather impressive velocities are observed in the Kuril straits, too. The maximum tidal velocity of 11 knots is measured in the strait of Nadezda.

Tides on the East Sakhalin coast have diurnal and incorrect diurnal character. The maximum magnitudes of these tides occur in June-July and in December-January, but the minimum magnitudes occur in March/April and September.

Southern Sakhalin Shelf

Stations 2-1 and 3-2 , both located on the slope of the southern Sakhalin shelf, reflect exemplarily the different dynamic conditions in the region. Hydrographic data are shown in Fig. 4.2. Station 2-1 is an example of active interaction of different water masses and intense mixing of the upper layer. Obviously, the large warm intrusion, which is observed in the cold subsurface layer and several small intrusions in deeper layers reflect the interaction of the Sakhalin current with one of the cyclonic eddies in the southern Sea of Okhotsk.

Station 3-2 reflects a different situation although the distance between Station 2-1 and 3-2 is only 30 km and the water depth is comparable: as shown by the temperature profile, only little features of vertical mixing are observed here. Station 3-2 presents a typical subarctic thermohaline vertical structure.

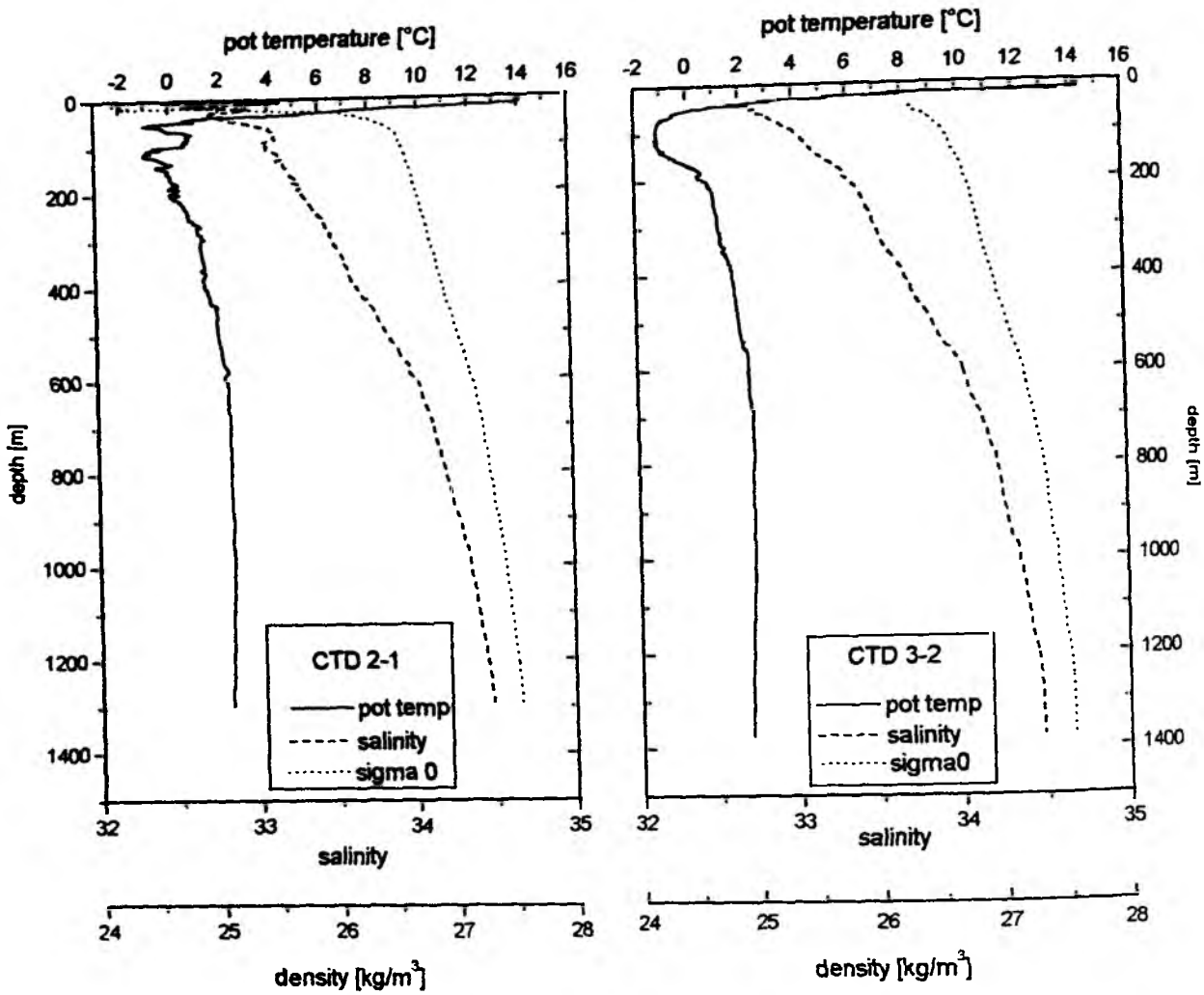

Fig. 4.2: Comparison of the hydrographic data derived from CTD-stations 2-1 and 3-2.

Northern Sakhalin Shelf

Stations 5, 6 and 8 represent a transect across the northern Sakhalin Shelf (Appendix 4, Fig. A4.2). CTD-data show the process of intense destruction and mixing of the subsurface cold layer across the shelf. Each station reflects a different stage of this process which is forced not only by the influence of the bottom relief but also by the local current features including tide. At station 5-1 we did not observe a cold subsurface layer. Instead, a well mixed near bottom layer with some intrusions appeared. The largest one is situated in a water depth of 250 m. It looks like a warm, salty intrusion on the background of the mixed layer. Temperature profiles of two other transect stations (CTD 6-1 and CTD 8-1) also show an intrusion at the same depth horizon but - compared to the profile - they appear as cold, fresh lenses in the warm intermediate layer. However, comparison of the three temperature profiles shows that the hydrographic characteristics of the feature are identical and that it is obviously the same intrusion. It is observed for several hours and has a spatial expansion of at least 15 miles. Its simultaneous existence on the shelf and slope stations allows us to draw some conclusions.

First, the mixed layer on the shelf was formed long before and the intrusion structure is a newer feature. The spatial expansion of the intrusion is at least 15 miles. Besides, the temporal variability of intrusions at 300 m and greater water depth suggest intensive intrusion processes which lead to the vertical mixing in this region.

As observed on the shelf-slope transect, the temperature and salinity distribution of the three stations in the northern part of the Sakhalin Shelf (CTD 11-1, 14-1, 20-1) also reflects the strong influence of the bottom depth (Appendix 4, Fig. A4.4). At the shallow stations (CTD 11-1, 14-1), a well-mixed near-bottom layer is observed due to tidal mixing on the shelf. At the slope station (CTD 20-1), the mixing under the cold subsurface layer is much less developed.

A remarkable feature of near shore tidal currents is that its orientation coincides with the direction of the coastal line. Hence, the velocity of mean currents is modulated by the tide and significantly increases at particular times. Taking into account the vertical inhomogenity of the current flow, it may lead to hydrodynamic instability, overturning and internal mixing. Obviously, the spatial expansion of such events depends on the scales of bottom relief inhomogenities on which the local increase of current velocity is possible. Besides, the vertical velocity shift can create favorable conditions for the split of a part of the gas plume and its horizontal transport.

Another interesting feature of the Sakhalin Shelf region is the highly variable fresh water fraction of the surface layer due to river runoff. Fig. 4.3 shows the salinity distribution of the upper 100 m for five CTD stations along the East Sakhalin coast from South to North. CTD 2-1, located in the southern shelf region, represents a typical background salinity distribution while the other four stations reflect the successive depletion of the salt concentration at the surface due to increasing influence of fresh Amur river runoff.

Derugin Basin

Three CTD stations 28-1, 29-1 and 39-1 were occupied in the Derugin Basin (Appendix 4, Fig. A4.6). The hydrographic data show that the Derugin Basin is the most stagnant zone of the Okhotsk Sea characterized by low mixing activity. It presents stable conditions typical for the subarctic. The characteristic curvature of the temperature profile below the cold layer at station 39-1 indicates its proximity to the center of the Derugin cyclonic eddy. The main feature of all profiles - absence of fine temperature structure - represents the minimum of vertical mixing for all CTD data of the cruise.

West-East Transect

The transect (CTD 4-1, CTD 40-1, 42-1, 43-1, 44-5) represents the whole spectrum of climate differences and dynamic conditions which influence the process of vertical water structure formation. Fig. 4.4 compares the hydrographic data of a station 40-1, located on the western

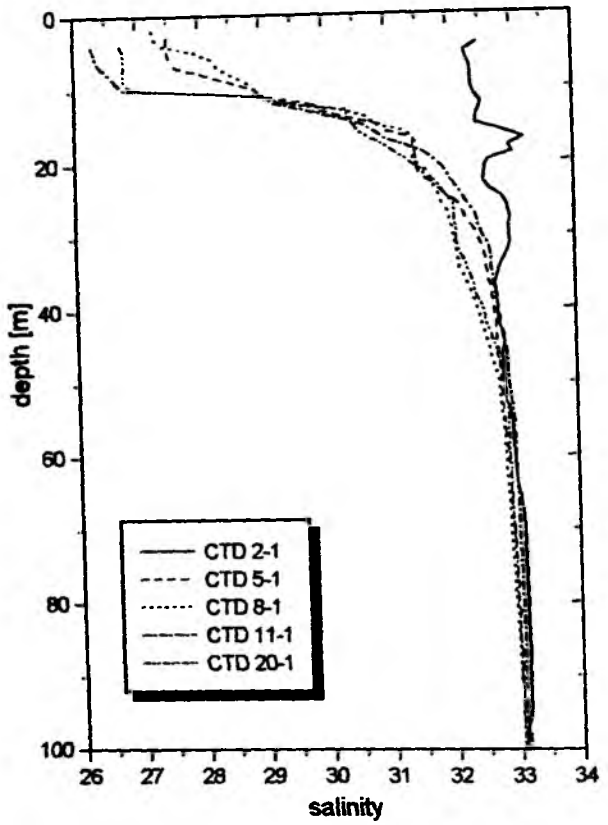

Fig. 4.3: Salinity distribution in the upper 100 m of five CTD stations situated along the East Sakhalin coast.

part of the transect, and station 44-5 on the eastern part of the transect and shows the high variability of the temperature minimum zone. The lowest temperatures in the subsurface cold layer were found in the western part of the sea and increased constantly towards the east from -0.92°C (St.40) till to 0.92°C (St.44). This is not only due to vertical mixing on the upper and lower boundaries of the cold layer but also to the mild conditions of the previous winter. The high value of internal mixing is typical for all transect stations. Multiple intrusions support the interleaving and leads to the mixing of the whole layer to the bottom (CTD 44-5). The cold subsurface layer at this station differs from the classical subarctic situation as there is no lower boundary of this layer. Instead of this, the near homogeneous layer characterizes this station as the one with the maximum intensity of vertical mixing.

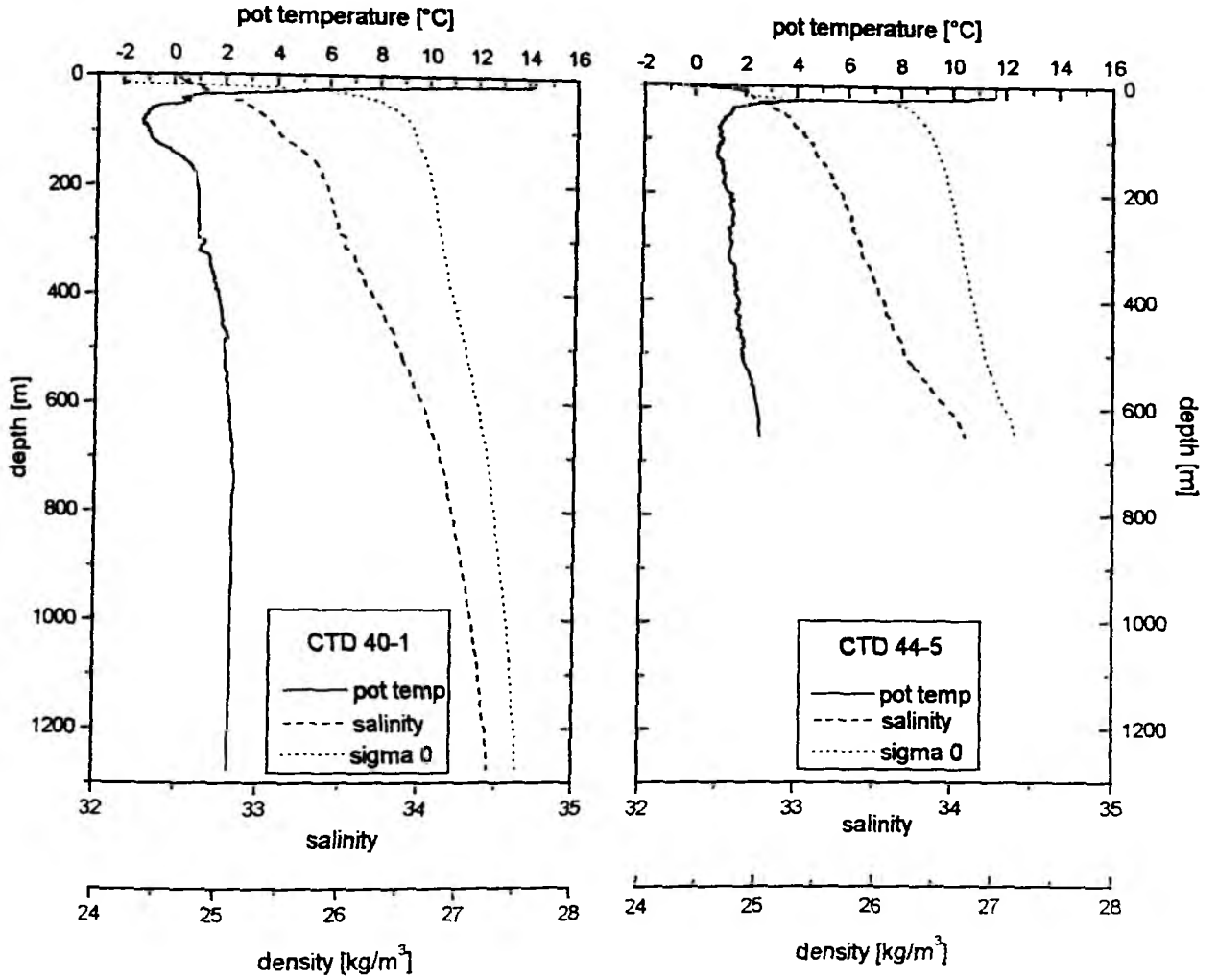

Fig. 4.4: Comparison of the hydrographic data derived from CTD-stations 40-1 and 44-5.

4.2 Fluid venting at the Sakhalin shelf and upper slope

4.2.1 Introduction

E. Suess

Submarine gas emissions off northern Sakhalin Island are persistent through time and confined to specific locations. They have been visited by research vessels repeatedly over the past decade. They are appropriately named "flares" (in Russian: "fakel") because their images on high frequency hydroacoustic recordings appear like torches in the otherwise featureless water column (Obzhirov et al., 1989; 1993). Indeed color-enhanced imaging of apparently linearly arranged gas emissions on the shelf-slope break, i.e. at 54°27'.000'N and 143°53.200'E conveys the impression of a wall of fire rather than the less dramatic one associated with the term plume (Figs.: 4.7-4.14).

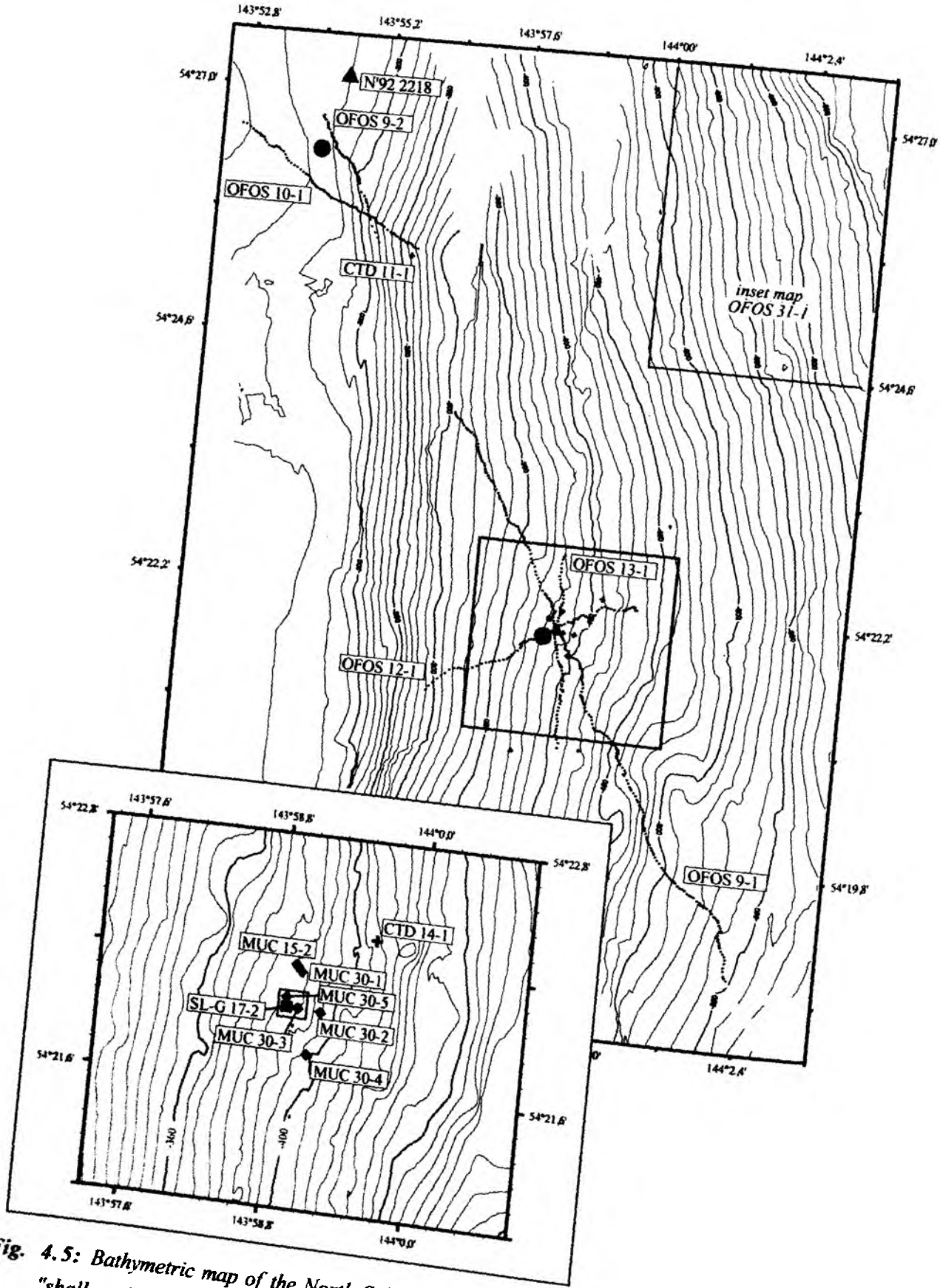

Fig. 4.5: *Bathymetric map of the North Sakhalin area at "Giselle flare" (inset map) and the "shallow slope flare" at the OFOS tracks 9-2 and 10-1.*

On the upper slope at water depths between 400-800m the plumes are fewer than at the shelf edge but appear more intense and better confined spatially. One of the tasks of *RV Akademik Lavrentyev* expedition was to map existing and locate new gas emission sites. The results of this survey are described in this chapter. Besides the high frequency and the fact that the entire shelf and slope waters show high, but regionally heterogenous, methane anomalies (sometimes exceeding background >10,000-fold), little is known about the geologic and tectonic control of these venting phenomena. The sediment and faunistic characteristics at these sites are suspected to be similar to those of cold vents (Suess et al., 1998) but have never been studied, nor is it known what the actual emission sites look like or ultimately what the rates, quantities, and composition of discharged fluids are.
Providing answers to these questions is a formidable task of KOMEX; several significant new results have been obtained during this voyage which are the subject of this chapter.

Strategy and background:
The use of OFOS, the Ocean Floor Observation System, is the first attempt ever to view the gas emission sites on the seafloor of the Sakhalin slope. Furthermore, coring sediments at "on-vent" sites and comparing their pore water and authigenic mineral compositions with those at "off-vent" sites represents another new task. Its results will contribute towards evaluating the geological, geochemical and biological importance of the gas vent fields for that region. The strategy includes biological sampling and characterization of vent-fauna as well as trace gas sampling, mostly of methane and helium. The trace gas results will be placed into the context of the shelf-slope hydrography and previously completed methane surveys. These surveys cover the water column vertically by CTD-casts and horizontally by the CH_4-CO_2-equilibrator system.
The general area of investigation at the "Northern Sector" (in Russian: "Severnaya") is shown in Fig 2.2 and a more detailed view provided in Figs. 4.5 and 4.6. Three areas with plume sites in this region were investigated in detail, the Kazansky-Flare (Sta. OFOS-9-2; CTD-11-1), the Giselle-Flare (Sta. OFOS-9-1; CTD-14-1) and the Obzhirov-Flare (Sta. OFOS-31-1; CTD-20-1).
The Kazansky-Flare is the first and one of the most persistent plumes at the shelf-slope break; it was noted by the hydroacoustic expert B.A. Kazansky and published in 1989 (Obzhirov et al., 1989). The site of the Giselle-Flare coincides with a morphological break in slope, thought to be a fault trace in the otherwise thickly covered upper slope sediments. Both sites are aligned along this suspected fault trace. The site of the Obzhirov-Flare is near where solid gas hydrates had been retrieved (Ginsburg et al., 1993). This area shows numerous plumes; neither is characterized nor mapped in detail.
The tracks OFOS-9-1 and OFOS-9-2 ran along the suspected fault-trace from about 500m to 190m crossing two of the plume sites. In both instances numerous bivalve colonies, mostly in life position but also abundant dead shell debris, were observed. This presumed vent fauna was more concentrated and confined spatially at the deeper sites, whereas the shallower site had a

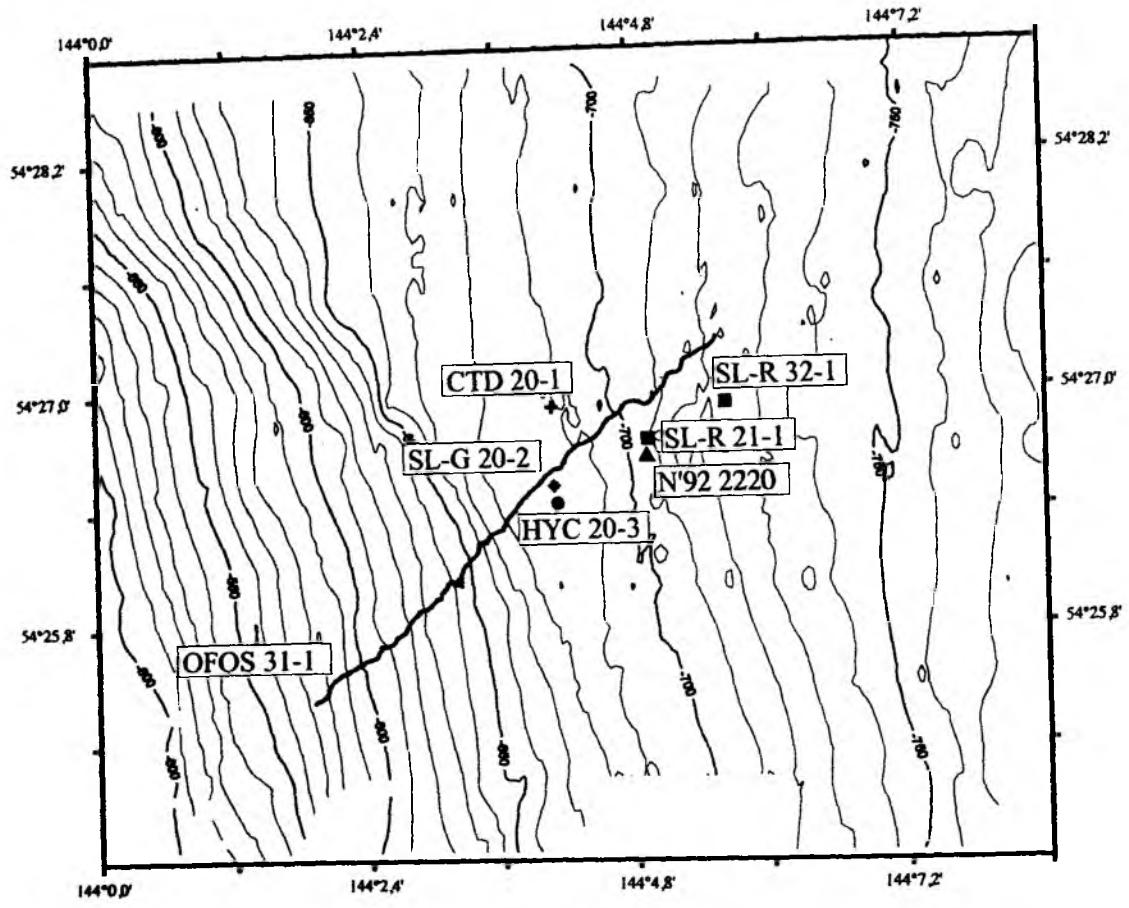

Fig. 4.6: *Staions at the North Sakhalin working area at the "Obzhirov flare" site. N'92 2220 marks a station of RV Akademik Nesmeyanov cruise in 1992.*

much more prolific benthic fauna but was less confined. The shallow fauna was assumed to not entirely represent vent fauna. Additional cross profiles (OFOS-10-1; OFOS-12-1; OFOS-13-1) were run to map the sites. The projected first and last sighting of vent fauna along these tracks allowed to define a "target box" of roughly 300 X 350m for detailed sampling. This box is indicated in Fig. 4.5.

Sampling of vent sites was also guided by the position of the plumes during the 20 kHz-survey (see: chapter 4.2.3: Acoustic features). Coring was attempted at two plume sites, CTD-casts were run at all 3 locations, and bottom trawls only at one site (Appendix 1). Coring the vent sites is difficult because of the small area into which the equipment has to be placed but also because hard grounds or coarse sediment often cause failure to retrieve material; 7 attempts for coring out of 12 were successful but only 3 penetrated sufficiently deeply to collect material for methane analyses and to obtain pore water profiles, the latter of which will be described here.

The sampling for gases was primarily for methane and helium, but also total dissolved carbon dioxide was evaluated. Each of the carbon gases has a characteristic isotope signature which is different from that of total dissolved carbon dioxide in seawater and hence serves as a tracer for carbon input from vent systems. A well-known effect of vent carbon input is the formation of

"isotopically light" carbonate concretions from methane oxidation which preserves evidence of vent activity in sediments even after the activity ceases (Bohrmann et al., 1998). The investigated area contains a large variety of such mineral assemblages from present or past gas venting systems which will be described in this chapter. One of the best tracers for venting activity is helium and its isotopes. The advantage of helium is that one isotope (^{3}He) is diagnostic of hydrothermal input related to mantle sources and the other (^{4}He) for cold vent input from sediment-dominated sources (Winckler et al., 1997).

4.2.2 Geological setting

R. Kulinich, Ye. Lelikov, and A. Svarichevsky

The area under study occupies the shelf edge and the upper slope and middle slope off north-eastern Sakhalin Island. The work was carried out between 54°19.200'N and 54°28.800'E defined by the results obtained during the *RV Professor Gagarinsky* expedition. The area was named Northern Sector or "Severnaya" (Fig. 2.1.5).

Bathymetry:

The bottom morphology has been studied in detail during the above-mentioned and many previous cruises. A description of the area is given in Part I of this report. During the *RV Akademik Lavrentyev* expedition echosoundings were continued both as a survey along specified profiles mostly preceeding station work and synchronous with station work. (Fig. 2.2). As a result, a more refined bottom relief map has been produced (Fig. 4.5). The current echosounding survey confirmed in general the rather simple topography of the area; however, in addition showed a clear division of the slope into a middle and upper part. A boundary lies approximately along the 300m isobath. The upper slope is steeper than the middle slope. Several low-amplitude linear deformations of the seafloor in north-westerly direction were confirmed; gas emission sites are grouped along these deformations.

General tectonics:

The tectonic and geodynamic regime of the region is reviewed comprehensively in Part I of this report. For this reason only the main geological and structural features of the area are given here. The shelf and slope of the eastern Sakhalin, as is the entire Sakhalin Island, are located along an active transform boundary between the Amur and Okhotsk Plates; this boundary is known as the Sakhalin Shear Zone (Savostin et al., 1983; Jolivet et al., 1991; Dozorova et al., 1998). Tectonic activity influences the eastern margin off Sakhalin, as is evident by recent seismic. It is likely that the slope off eastern Sakhalin is the morphological expression of the large NNW-trending fault zone which separates Sakhalin Island from the Derugin Basin. Numerous indications of small faults oriented mainly in NNW direction are evident both in the bottom relief and the seismic sections obtained during the *RV Professor Gagarinsky* expedition. Many of these are young reverse faults and thrusts. Their strike agrees generally with the

direction of the Sakhalin Fault and suggests a common origin. It has been pointed out that the vents known so far tend to be located at those fault zones (see Part I of the Report).

Sediments:
The eastern Sakhalin slope is overlain by a thick sedimentary cover which fills the East-Sakhalin Basin. The maximum sedimentary thickness of the individual basin parts reaches 8 km. In the east this basin is bounded by the Pogranichny Fault (Gnibidenko, 1979; Gnibidenko et al., 1982). The area under study is located in the immediate vicinity of the northern fault boundary within the Shmidt Rise, a horst-anticlinal feature. Here sediment thickness decreases to 1 km and less. Its composition includes two units. The lower unit comprises deformed terrigenous sediments of Neogene and Upper Paleogene age, the upper unit is represented by Pliocene-Quaternary deposits and shows intensive slope erosion.

Basement:
The sedimentary basement crops out at a few sites on the Shmidt Rise. It is represented by tectonic blocks of Paleozoic shales. It is not inconceivable that the basement also includes Mezozoic folded complexes (Geodekyan et al., 1976).

Deep structure:
The crust underneath the eastern Sakhalin shelf has continental crust affinities and is 32-33km thick. It includes a metabasaltic layer (V=6.6.-6.8km/c), a granite-metamorphic layer (V=5.8-6.0km/c), a volcano-sedimentary complex (V=4.6-5.0km/c), the lower terrigenous cover deformed (the Neogene, partially the Paleogene; V=3.5-4.5km/c), the upper cover of Pliocene-Quarternary age. With the slope the crust decreases to 28-29km in thickness, mainly due to the decreasing granite-metamorphic layer. Thus, the area under study is located in a transition zone, where the crust is reduced from its usual continental type to a stretched continental type (Gnibidenko, 1979). This transition is accompanied by tectonic instability and, as a result, fault generation which favours fluid and gas emanations.

4.2.3 Acoustic features

B. Li, V. Sosnin, A. Salyuk, E. Suess, and J. Greinert

The 20 kHz-hydroacoustic survey aboard *RV Akademik Lavrentyev* was one of the most reliable and amazingly successful tools in detecting gas plumes in the water column. The survey of regions with prospective gas emissions has shown rather well-defined and restricted locations generated by populations of acoustically contrasting patches over plumes in the water column. The spatial distribution of sites of gas emissions based on these plumes is summarized in a survey map (Appendix 2). The characteristics of plumes are based on the intensity of the return scatterings of sound, their spatial orientation and shapes. The acoustic manifestations of gas emissions differ considerably from each other (Fig. 4.7-4.9). The returning acoustic signals

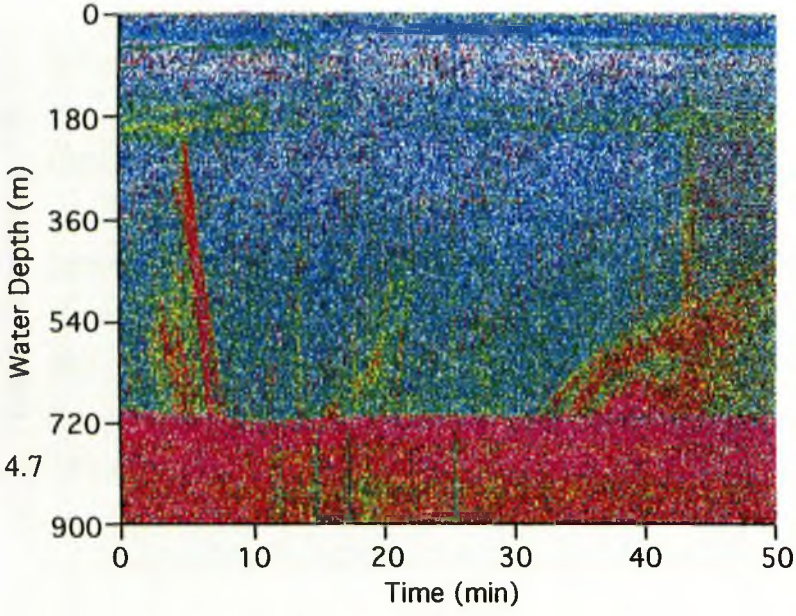

Fig. 4.7

Type of plumes:
***Fig. 4.7**: Ellipsoid shape.*
***Fig. 4.8**: Isolated shape.*
***Fig. 4.9**: "Hanging-cloud-on-mountain" shape.*

***Fig. 4.10**: Plume Tracking (see next page)*

***Fig 4.11**: Plume at upper slope site crossed by OFOS track 9-1 (Track Nr. 1 not shown on Fig. 4.10).*
***Fig 4.12 and 4.13**: Plume at gas hydrate site crossed twice; shown in Fig. 4.10 as Nr. 2 and Nr. 3).*
***Fig. 4.14**: Plume at gas hydrate site shown twice during turning of vessel, track Nr. 4 (Fig. 4.10).*

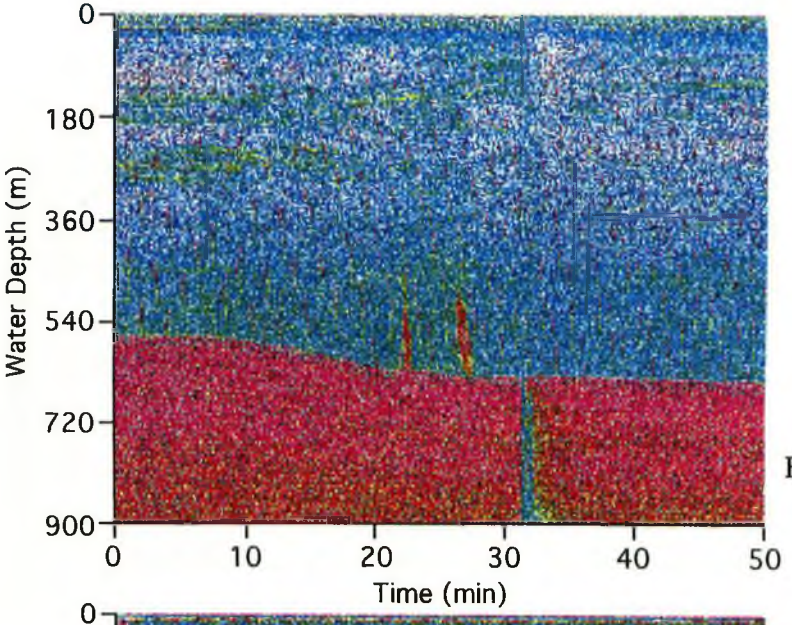
0
180
360
540
720
900
Water Depth (m)
0
10
20
30
40
50
Time (min)

Fig. 4.8

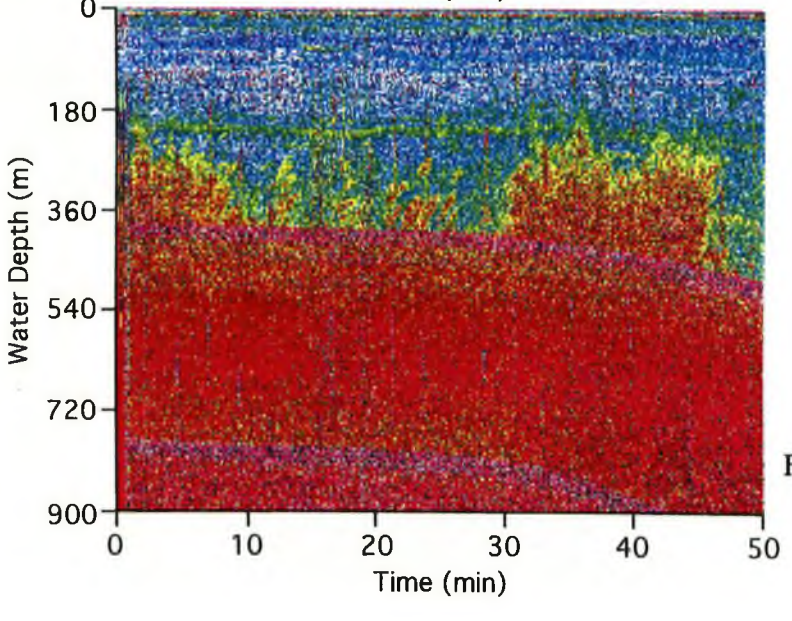
0
180
360
540
720
900
Water Depth (m)
0
10
20
30
40
50
Time (min)

Fig. 4.9

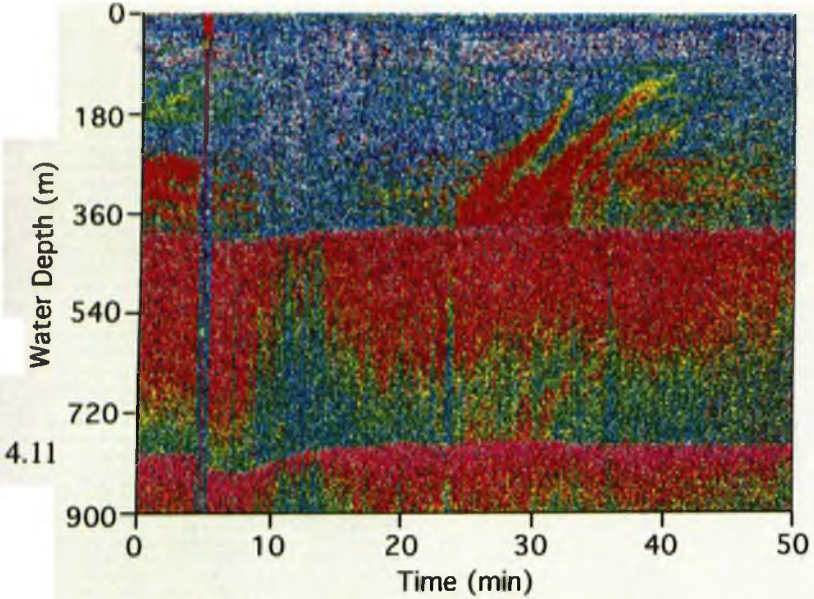

Fig. 4.11

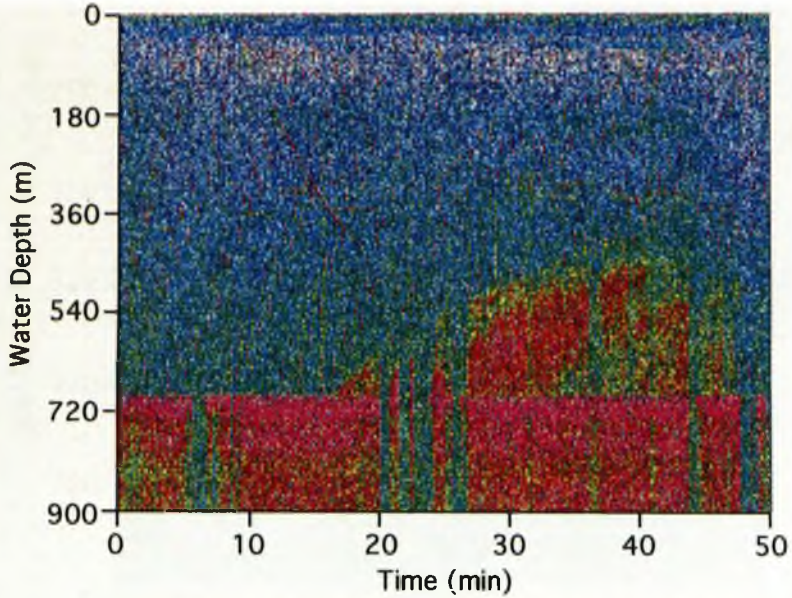

Fig. 4.12

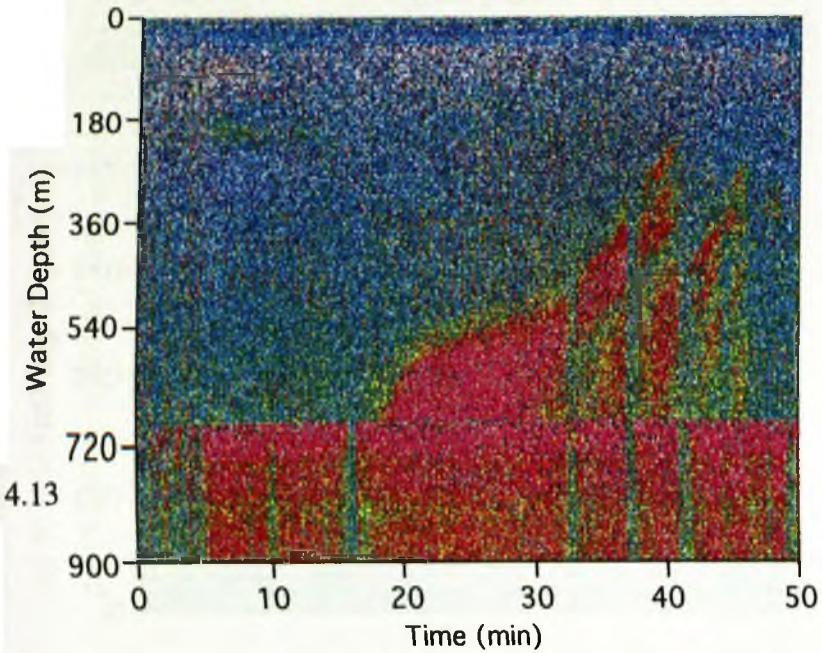

Fig. 4.13

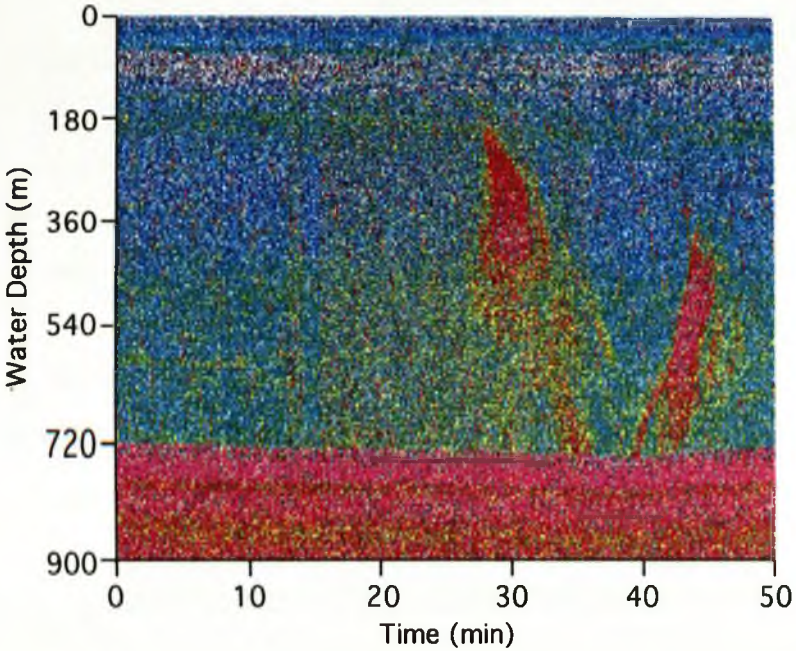

Fig. 4.14

vary in spatial expansion, intensity and acoustic profile. Up to 70 locations with features unique for gas emissions were found. Acoustic images of gas plumes generated by a sound frequency of 20 kHz at depths up to 1000 m are represented here. These acoustic images are transformed on a screen into colored optical images. These acoustic/optical images cannot be reproduced as sounds but can only be displayed on the screen.

The majority of these plumes are elongated narrow ellipsoids which are rooted in the seafloor, are oriented vertically, and are sharply distinguished acoustically from the surrounding environment (Fig. 4.7). The heights of the plumes are between 90 - 500m, the width up to 300m. Sometimes the plumes appear separated from the bottom and drift freely in the water but maintain their shape and spatial orientation (Fig. 4.8). Another type appears like a torch of fire shooting straight up from the seafloor. The height of these torches of fire reaches 400m with a width of up to 600m.

The third type of plumes could be described as clouds which are mainly found on the peaks of underwater ridges (Fig. 4.9). These clouds appear to accumulate over the summit of these ridges or hang above the peaks. Often these formations include horizontally oriented layers which connect two adjacent plumes.

Besides, there are entire fields of images caused by minor gas emissions; they appear like vegetation of brushes or grasslands. They are associated with all the above-mentioned images. These fields expand over a distance of 5-6 miles. Thus, the hydroacoustic measuring system SARGAN-IDM with an operational frequency of 20 kHz provides very valuable information on gas emissions and faciliated the positioning of the vessel to sample the apparent sources at the seafloor.

This capability for more accurate sampling of vent sites at the seafloor as well as methane distributions in the water column should be fully explored in the future. Here we show the success in sampling and video-imaging the seafloor from which gas plumes arise as well as their configuration in the water column. Figure 4.10 shows 4 segments of ship's tracks during which gas plumes were imaged. The track length corresponds to the distance the vessel travelled in 50 minutes and also corresponds to the full image usually displayed on the screen (Fig. 4.11-4.14).

On track 1 the plume at the 386m-site (Giselle-Flare) is shown; its core is at 54°22,070'N and 143°58,830'E, which falls in the center upper half of the target box derived from the OFOS surveys (Fig. 4.11). The top of the plume is deflected southward. The height above the bottom of the plume imaged is 200m. The plume appears to originate from at least 2 locations on the seafloor. At the speed of the vessel of 2 kn, the "footprint" of the plume is about 300m, which is larger than the 200m-clam-field traversed by OFOS at this site (see chapter 4.2.4).

Track 2 and 3 image the same gas plume (Obzhirov-Flare) twice during separate passes by the vessel over the site: the first in the attempt to place the CTD in the rising plume (station LV-28-20-1; Fig. 4.12) and the second during gravity coring (station LV-28-20-2; Fig. 4.13). The plume core is at 54°26.56'N and 144°04.100'E which falls onto the track of OFOS-31-1 but

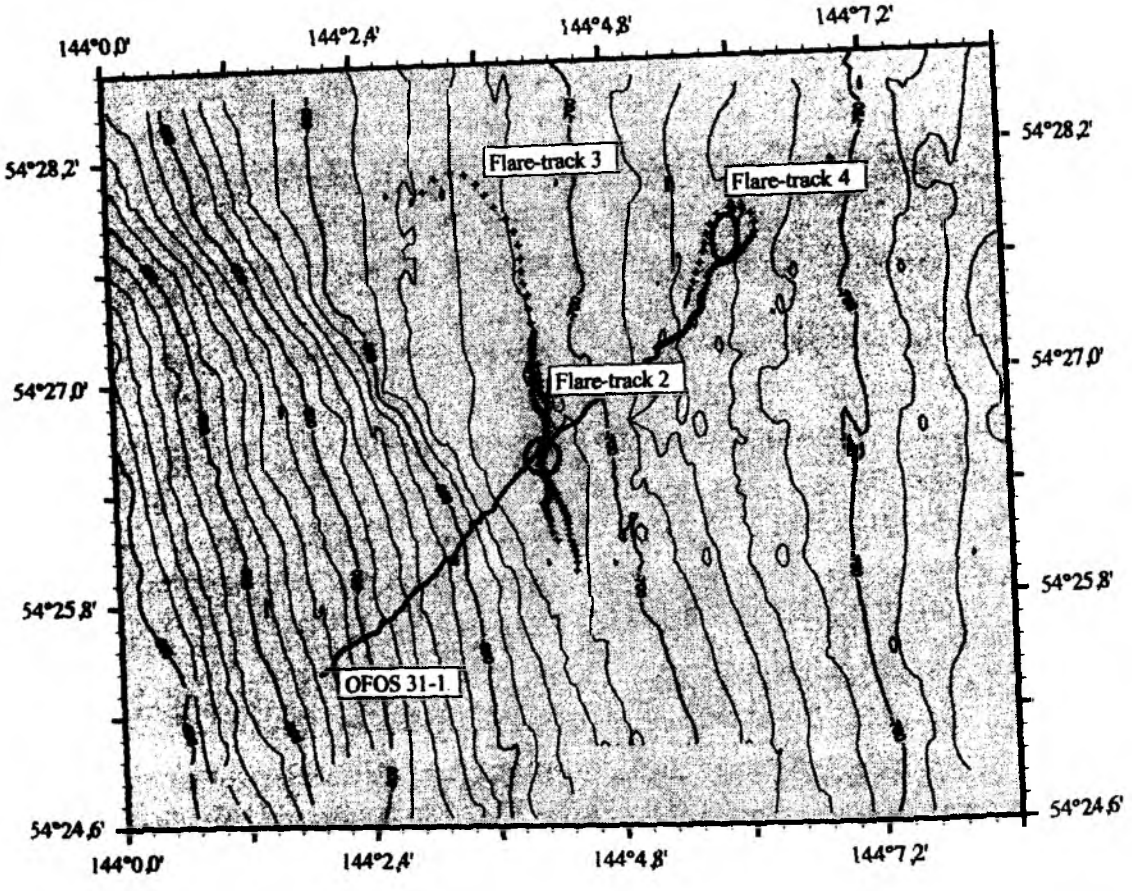

***Fig. 4.10**: Map of ship and OFOS tracks which recognized the "Obzhirov flare" site (open circle) as well as a new flair site in the northeast (open oval).*

well away from CTD-20-1. However, gravity cores SL-G-20-2 and HYC-20-3 were placed within about 100m of both the OFOS track as well as the projected origin of the plume at the seafloor. The footprint of the plume in both cases is about 500m. The shape of the plume as previously observed is deflected towards the south with increasing height from the seafloor.

The 4th track images a plume which had not been known before and was found at the end of the track of OFOS-31-1 when the vesel turned after taking aboard the equipment. The 20 kHz-image shows the top of the plume first (course 35°) and the base of the plume after turning (course 215°; Fig. 4.14). The tracks are well separated from each other so that the irregular three-dimensional shape of the plume may be constructed. The plume does not rise vertically nor does it have a circular diameter; instead it appears elongated. The shape is strongly affected by the dynamics of the water column.

In order to improve the knowledge on gas plume variability, we suggest to continue and enlarge the CTD-observations. We propose to provide the short-term monitoring of gas plume variability simultaneously with acoustic measurements in "free hunting regime", CTD observations, and current profiling on a daily cycle.

The evaluation of tidal influence on the plumes is of great importance, therefore tidal observations on moorings or by current profiling should be included at least. Current meter should be used simultaneously with CTD on the same multiwire cable.

4.2.4 OFOS observations

H. Sahling and J. Greinert

On the northern Sakhalin self and slope, 7 OFOS profiles where deployed in 4 different target areas, at the "Giselle Flare", the "Obshirov-Flare", the "Piltunsky-Flare", and the "Shallow Slope Flare". During all deployments indications of gas venting were found. The most spectacular manifestations of the existence of active vents were big clamfields consisting of thousands of shells formed by the Thyasirid bivalve *Conchocele* sp. (cf. *C. bisecta*) (see Plate 1). These visible shells are a reliable indicator for gas seepage even though no living clams could be identified on the video as its resolution is not high enough. However, about 120 slides from selected OFOS-profiles have been developed on board ship and provide additional information.

The "**Giselle-Flare**" at 385m water depth was rather intensely investigated: it was observed during three OFOS-profiles, sampled with gravity and multicorers as well as with a biological trawl (Fig. 4.15). Profiles were executed crossing the flare site 5 times recorded by the ship's 20 kHz-echosounder. Based on these observations, the expansion of the seepage area could be estimated and is plotted on Fig. 4.15. The OFOS tracks (9-1, 11-1 and 13-1) cross a field of thousands of clamshells spreading in different directions. We believe that the extension of the flare site-related clam fields on the seafloor agrees with that of the seepage area without much deviation. Only few spots within a confined area of approx. 300m in diameter are less densely covered with clams. But even outside the clustered fields single crawling clams could be observed, indicating that the influence of seeping is much more complex. Around the fields, ripple marks and bioturbation traces are visible as well as suspension feeders on stones etc. Along these two tracks geological features could not be observed which could provide more information on vent mechanisms. The seafloor is covered with soft sediment mostly.

The **"Shallow Slope Flare"** at the shelf and upper slope between 170 and 250m water depth were covered by two OFOS transects (OFOS 9-2 and 10-1; Fig. 4.5). OFOS 9-2 is the continuation of OFOS 9-1 which had to be interrupted after a short circuit on board. OFOS 10-1 constitutes the crossprofile to the previously covered track. The fauna observed is very diverse and abundant as can be expected in relatively shallow water depths. The developed slides show small openings and depressions of some cm in diameter. In the depressions and around the holes whitish material is visible, tentatively identified as bacterial mats. We suspect that these small patches are "mini flares" where seepage occurs. At least four "mini flares" within some 10m are visible on the slides. This agrees with the graphic recordings of the echosounder where

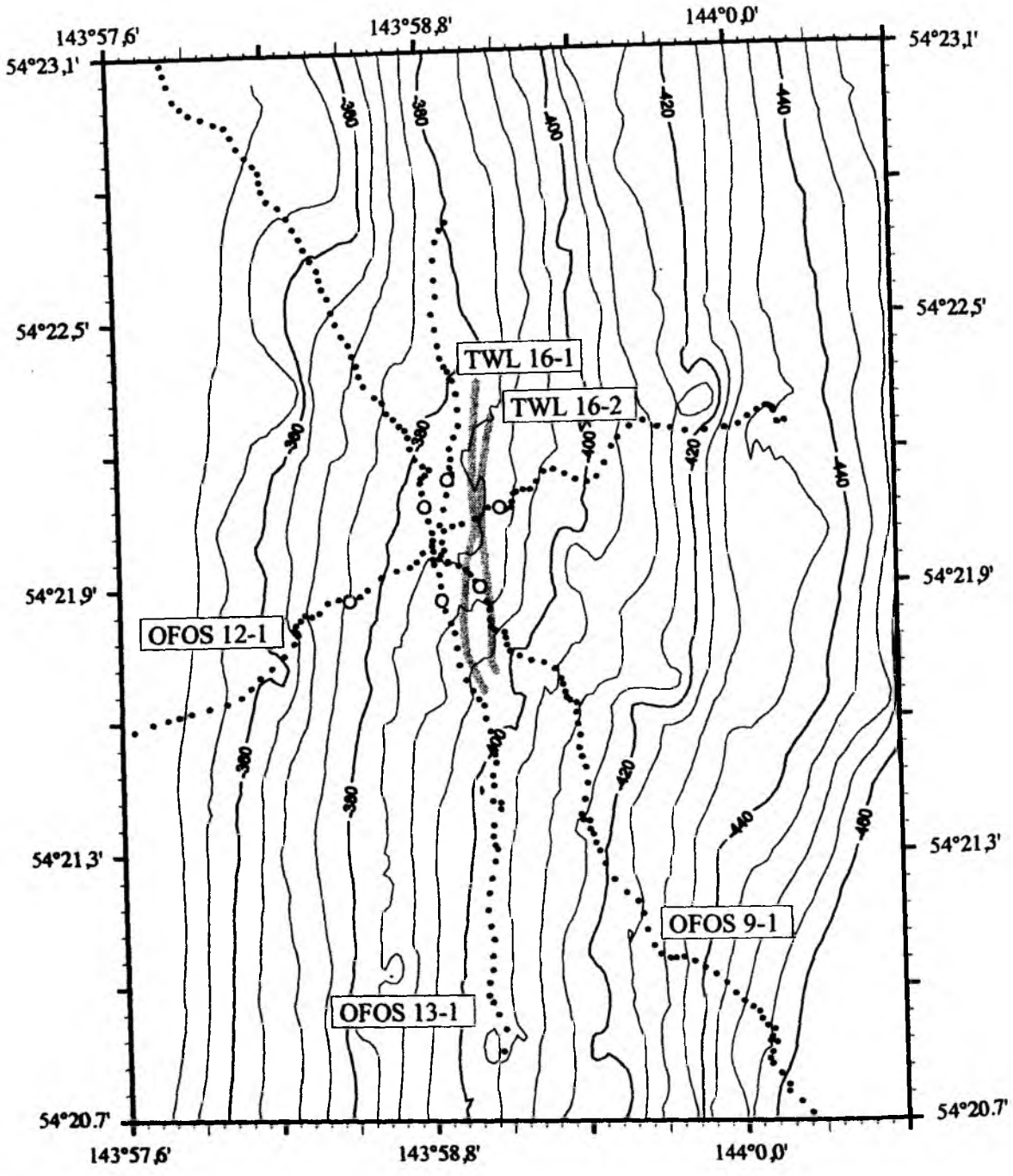

Fig. 4.15: *OFOS and trawl tracks carried out at the "Giselle flare" site. Open circles mark the boundary of the flare recognized by the 20kHz observations.*

not only single flares but broad plumes are visible. No animals characteristic for seeps could be observed. The fauna on the slope just beneath the shelf edge at around 180m is dominated by suspension feeding organisms. Near-bottom currents and a higher amount of hard substrate may be the reason for higher abundance of epibenthic animals at the upper slope compared to

the shelf. Similar to the "Giselle Flare", soft sediment covers the seafloor which does not yield further geological information for speculations about geologically induced venting mechanisms.

The seafloor at and around the "**Obshirov Flare**" was observed with OFOS 31-1 in an area where some flare sites have persisted over many years. Before reaching the target position, the slope between 570 and 670m water depth was investigated. Here, the sediment is smooth, soft and only slightly bioturbated. A first indicator of seepage occurred at the base of the slope, where a small plateau can be seen (Fig. 4.6). The slight turbidity of the water between OFOS and the bottom appeared together with more ripple marks and bioturbation traces on the seafloor surface and may well indicate a stronger nepheloid layer. Beginning the survey in the middle of the plateau at 690m and ending at about 710m, it could be seen that the surface is much rougher; sometimes stones with suspension feeding organisms were visible. Within a distance of about 300m, at least 3 very dense clusters of white and round-shaped organisms were observed and tentatively regarded as clams, but this needs to be confirmed by the slides which are not developed yet.

In the "**Piltunsky Flare**" area the observations of OFOS 33-1 were made at a water depth between 600 and 850m. Whether the ship's track crossed one of the flares indicated in Fig. 4.21 cannot be concluded as the sediment is generally soft, smooth and without any significant textures or geological features. In a slightly rough area of about 60 to 80m water depth, more gravel and patches of dull white-colored sediment could be observed together with white organisms, probably the bivalve *Conchocele*. The exact position of this track part is not well known but seems to be in a water depth around 750m.

Conclusions:

The benthic community observed and sampled at the northern Sakhalin slope flares could underline the fact that methane is the reduced chemical compound which fuels and dominates the chemical and biological habitat at the seeps. The Thyasirid bivalve *Conchocele* sp. is the most striking feature at the seeps. The only other symbiotrophic animals are some smaller bivalves and few pogonophorans.

Conchocele cf. *bisecta* is well known from the gas-venting area at Paramushir-Island. It harbours endosymbiontic bacteria able to oxidize methane and sulphide (Galchenko et al., 1988). These findings are in agreement with the observed chemical environment at the North Sakhalin slope flares. Even if no sediment could be recovered with living *Conchocele* sp., methane seems to be the dominant reduced chemical compound.

The methane-oxidizing endosymbionts investigated in detail are in terms of species number less commonly distributed among the symbiont-bearing macrofauna. Methane as the sole energy and carbon source is not very likely as methane can neither be fixed by the host (as sulphide can), nor can it be actively transported to the bacteria to secure a continuous supply of energy.

However, the reliance on methane as sole energy source or as a source of additional symbiotrophic nutrition indicates a very stable supply with methane and underlines the stability of the gas seepage at the north Sakhalin slope.
Very interesting is the finding of clamshells in the SL-R 21-1 which is probably a species of *Calyptogena*. This may indicate that the group of Vesicomyids has the potential of occurring at this site but might be absent because of a non-suitable chemical environment. All vesicomyids investigated so far harbor sulphur-oxidizing endosymbionts. Sulphide may have played a bigger role in the past history of the seep. Unfortunately, no direct indications of emanating fluids could be observed during the tracks at the North Sakhalin area on the video tapes. More detailed investigations along all the tracks will be made based on the developed slides.

4.2.5 Biological communities

S. V. Galkin, H. Sahling, and D.N. Zasko

The investigation area north Sakhalin Shelf and Slope combines four different target areas (Figs.: 4.5, 4.6, 4.10, 4.15, 4.21). The investigations concentrate on a well-defined flare site with the working title "Giselle-flare" or "380m flare site" recorded on the 20 kHz-echosounder. A very thorough investigation was undertaken, detailed visual observations during three OFOS profiles (OFOS 9-1, 12-1, 13-1) were combined with two trawl stations (16-1, 16-2) and four multicorer stations (30-2, 30-3, 30-4, 30-5).
At the second target, "gashydrate site" or "685m flare site", two gravity corers (21-1, 32-1) yielded bivalve shells; observations at an OFOS-profile (OFOS 31-1) were made as well.
The very shallow flares at a water depth of 200m were investigated only by two OFOS profiles (OFOS 9-2, 10-1), no samples were taken at this site or in the "Piltunski" area, where OFOS 33 was deployed.

Trawl samples

Substratum characteristics:

Both samples were taken at the seep field "Giselle flare" which had been observed by OFOS (9-1, 12-1, 13-1; see Fig. 4.15) in detail. The first trawl was deployed at St. 16-1 and stayed at the seafloor for 5 minutes only and yielded only ca. 10 l of sediment. Nevertheless the samples appeared to be taxonomically representative. The second trawl (St. 16-2, 20 minutes at seafloor) collected nearly 0.25 m^2 of grayish sediment (silty-pelite with sand) and a slight smell of hydrogen sulfide. The trawl contained various carbonate precipitates varying in form and size (up to 15-20 cm, 30-40 kg). Some precipitates contain pebbles and fragments of clam shells. A characteristic feature of this sample are several kg of shell fragments of the bivalve *Conchocele* sp. (cf. *C. bisecta*), two valves complete, one slightly damaged.

Faunal composition

Dominant animals in this sample are small Amphipoda (up to several thousand). Large Asteroidea and the crab *Chionoecetes opilio* are not abundant but dominate by weight. Rather frequent are gastropods (incl. large Buccinidae) and small bivalvia (4 species incl. symbiontic *Solemya* sp.). Other species are less abundant, but a conspicuously high diversity of polychaets and 20 to 30 specimens of pogonophora could be found.

Trophical specialization

The animals dominating by weight (Decapoda: Brachiura, Buccinidae, Asteroidea, Nephtiid polychaet's) are carnivores or scavengers. Deposit-feeders (mostly polychaet's, ophiuroids, holothurians, gastropods) are also well-represented. Suspension feeders are rare and not abundant. The feeding type of the amphipods, by number the most abundant species, remains uncertain.

There are three species which are probably symbiotrophic. The symbiont-bearing bivalve *Solemya* sp. is well-known from organic-rich and anoxic sediments, as well as pogonophoran tube worms.

The Thyasirid mollusk *Conchocele bisecta* dominates the Paramushir gas-hydrate seep community and shows important anatomical and physiological features connected with symbiotrophic nutrition. Experiments show that a considerable amount of organic carbon derived from methane and carbon dioxide is incorporated in mollusk tissues (Galchenko et al., 1988).

The presence of the above-mentioned species indicates recent bacterial chemosynthesis. It is worthwhile mentioning the high amounts of grayish mucus in the sediment. Similar mucus composed of free-living bacteria of the Beggiatoa-type has been observed in sediments from the Paramushir seep. The nature of the mucus at the Sakhalin vent site remains uncertain as remains the role of chemosynthetically derived organic matter in the nutrition of non-vent animals (e.g. Amphipoda).

Multicorer samples

Macrofaunal samples collected from several stations at one location (St. No. 30-2, 30-3, 30-4, 30-5) cannot be taken as quantitatively representative as animals were only picked by hand when the cores were sliced for geological and geochemical analyses. Only 1/2 of a core (MUC 30-4B) could be fixed quantitatively for meiofaunal investigations. The multicorers provided some additional information on microscale distribution of some animals, though. The MUC samples confirm that small Amphipoda seem to be most abundant and the common group (they occur in almost all tubes with up to 15(!) specimens in one tube which covers 78,52cm^2). Other animals seem to be rather irregularly distributed. The quantity of Pogonophora varied from 1 to 20 ind. per tube. It can be supposed that populations of these symbiotrophic organisms are

associated with local vents or sites rich in reduced compounds, reflecting the irregular microscale distribution within the field.

Gravity corers data

Conchocele shells could repeatedly be observed in the gravity core samples SL(R) 21-1 & SL(R) 32-1. In SL(R) 21-1, many shell fragments have been found in the horizons of 65-70 cm, 90-95 cm and 170-195 cm. In SL(R) 32-1, one complete *Conchocele* sp. at core depth 210 cm was recovered. The occurrence of a complete shell of *Calyptogena* sp. at 90-95 cm and one valve in 185-195 cm in the gravity core 21-1 seems out of character. It was the only recording at the Sakhalin vent site and furthermore was recovered in the Derugin Basin.

Conclusion

In the investigation area, ca. 35 species of bottom fauna have been recorded. Faunal composition and trophical orientation of dominant groups are common for the highly productive sedimented slopes of the Okhotsk Sea. Specific fauna associated with seeping is represented by the Thyasirid bivalve *Conchocele* sp. (cf. *Conchocele bisecta*), Solemyid bivalves (*Solemya* sp.) and perviate Pogonophora (2 spp. ?). The occurrence of these symbiotrophic animals suggests recent high activity of bacterial chemosynthesis in the area. The microdistribution of these individuals concluded from samples as well as from OFOS-observations seems to be patchy, which reflects the irregular input of reduced compounds.

4.2.6 Pore water composition

E. Suess, B. Domeyer, G. Pavlova, and Y. Shul'ga

Coring of sediments directly associated with gas emissions at the seafloor was one of the major tasks of this expedition and required considerable luck and special effort in surveying, navigation, and ship's equipment handling as well as a coordinated analytical program. In the two slope areas of gas venting of the "northern sector" (upper slope at 385m and middle slope at 685m) one gravity core each and one multicorer were retrieved from what we believe were the dead centres of the Giselle-Flare (Fig. 4.5 at 385m; MUC-30-3, SL-G-17-2) and the Boris-Li-Flare at 705m (Fig. 4.6; SL-R-21).

The upper slope site has one well-defined flare, the Giselle-Flare, which was extensively surveyed by OFOS; the middle slope site, the site where methane hydrates were found in 1981 has at least 3 well-defined flares, the "Obzhirov-Flare", the "Boris-Li-Flare" and a third as yet unnamed and apparently new flare, all three of which are aligned perpendicular to the tectonic fabric, whereby the new flare has an elongated foot print in that same direction (see section 4.2.3).

Surrounding these targets were 4 multicorers retrieved at the Giselle-Flare (Fig. 4.5, MUCs 30-1; 30-2; 30-4; 15-2) and the gravity cores near the Boris-Li-Flare (SL-G-30-2 and HYC-20-3).

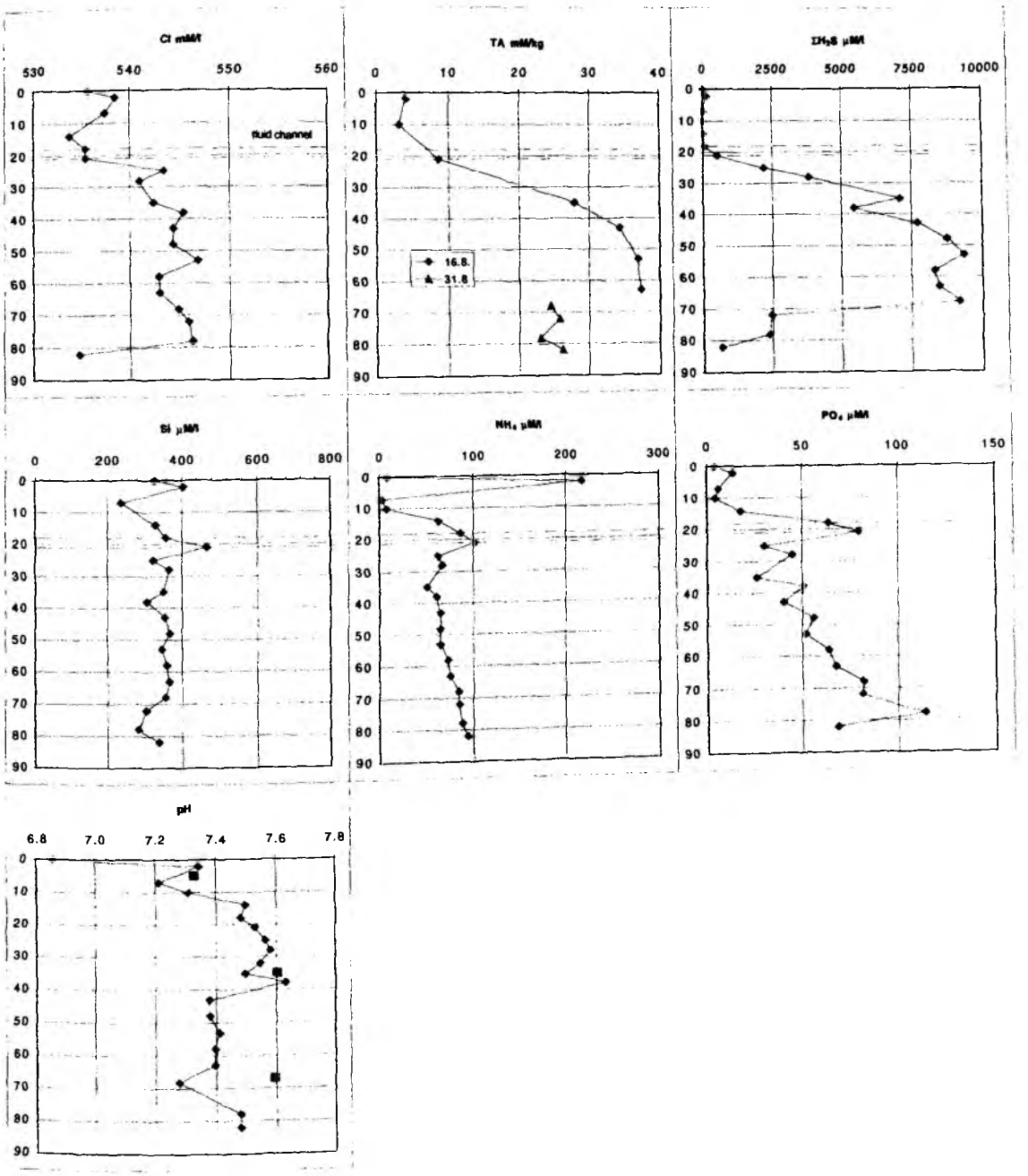

Fig.4.16: Pore water composition SL-G 17-2

The latter are situated less than 50m from the Obzhirov-Flare and may also be considered "on-vent".

The pore water composition from the gravity cores at these sites is shown in Figs. 4.16, 4.18. 4.19. Hereby the depth profiles of cores SL-G-20-2 and HYC-20-3 are stacked for a composite profile because the HYC-corer yielded the better near-surface sediment section and the SL-G-corer yielded the deeper sediment section. These are characterstics of the design of the coring equipment and are discussed in detail in section 4.3.4.

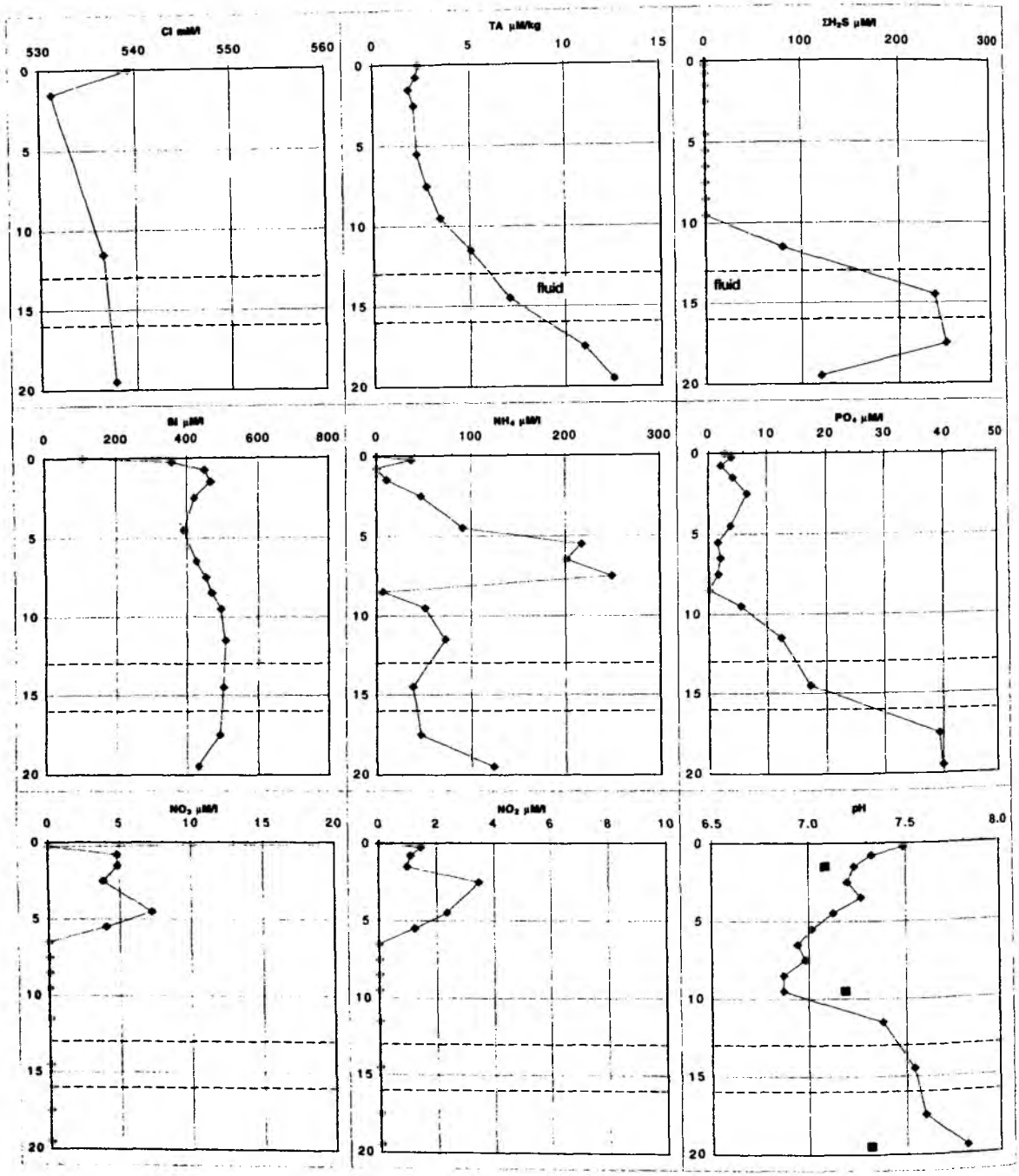

Fig. 4.17: *Pore water composition MUC 30-4C*

In addition, the carbonate parameters (Appendix 6) and the abbreviated core descriptions (Appendix 3.2) are shown. All cores contain abnormally high metabolite concentrations in their pore waters indicating enormous intensity of microbially-mediated material turnover. This is best documented by the extremely high H_2S-contents. Indeed, microbial activity fuelled by SO_4-reduction is so intense at sites that within the depth intervals cored, SO_4 appears to be completely exhausted. In core SL-G-17-2 the H_2S-content drops from almost 10 000 µmol/l at

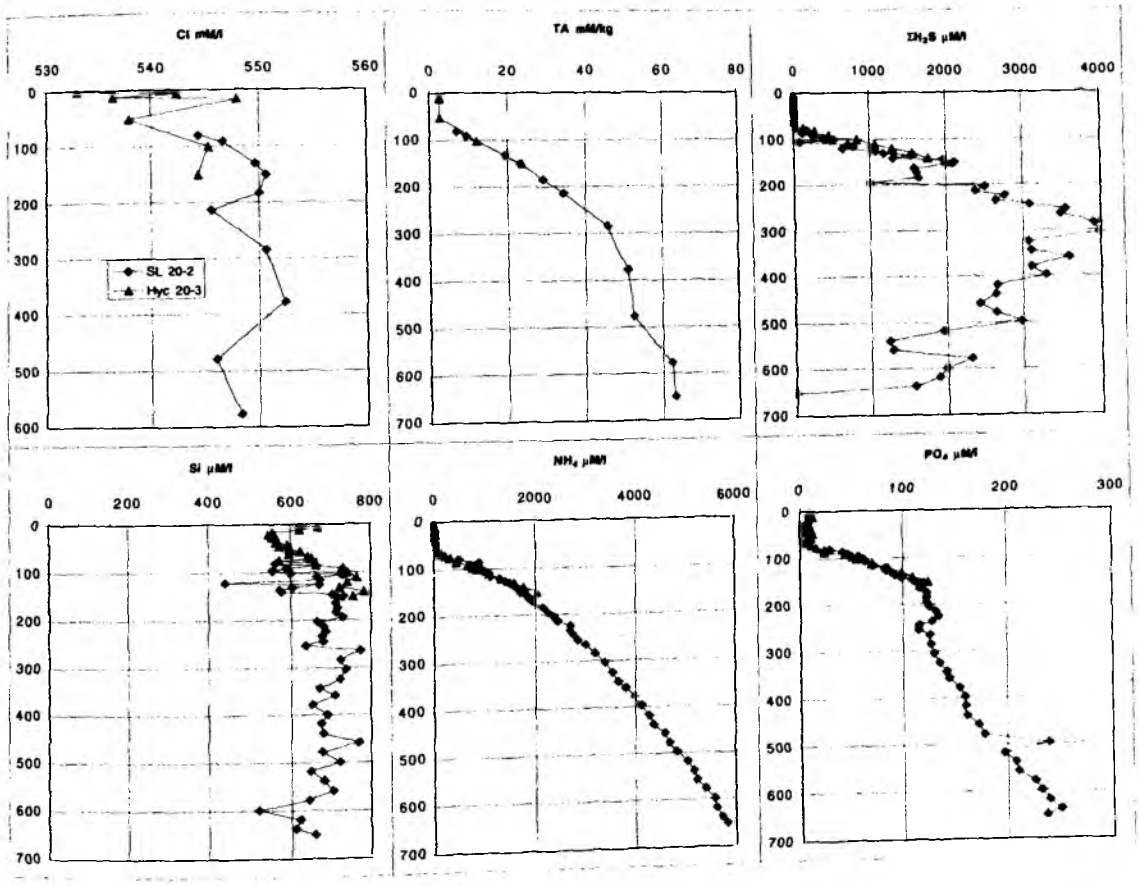

Fig. 4.18: Pore water composition SL-G 20-2 / 20-3

70 cmbsf to ‹ 500µmol/l at 82 cmbsf; in cores 20-2/20-3 the drop-off occurs at 660 cmbsf and in core 21-1 at 180 cmbsf. Shore-based SO_4-analyses should soon confirm this important information.

Almost identical to the H_2S-distribution pattern vary the depth-concentration patterns of total alkalinity (TA mM/kg) and PO_4 (µM/l). Dissolved Si (µM/l) is high and about constant throughout approaching amorphous silica saturation (1000 µM/l) in cores 20-2/20-3 and 21-1 but is distinctly lower (‹ 400 µM/l) in core 17-2.

The most significant characteristic which strongly supports methane oxidation as the dominant early diagenetic reaction is the dissolved NH_4- content; i.e. ‹ 100 µM/l, respectively, whereas core 20-2/20-3, the "not-so-dead-on-target" core, has › 6000 µM/l of dissolved ammonia.

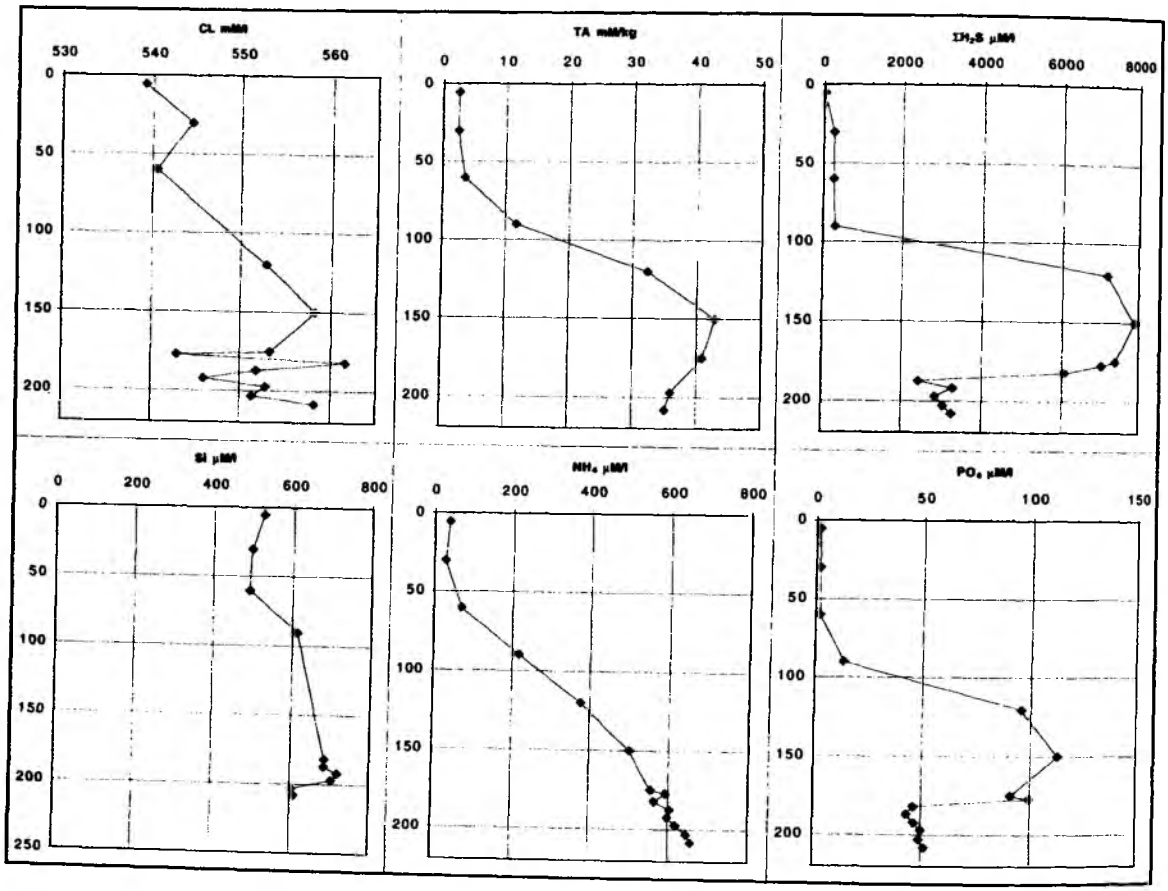

Fig. 4.19: Pore water composition SL-R 21-1

Such distribution is typical for vent cores (Suess and Whiticar, 1989) and results from almost exclusive methane oxidation reaction instead of the usual particulate sedimentary organic matter oxidation (POM).

Tentatively, the remineralization ratios (molar; on Redfield basis; Fig. 4.20) are: 106:1.6 for core 21-1, 106:0.2 for core 17-2 and 106:9.8 for cores 20-2/20-3. POM-dominated early diagenesis vs. CH_4-dominated diagenesis should at least have a remineralization ratio of 106:›10. Again, shore-based SO_4-analyses will enable a more accurate and most likely more convincing documentation that these vent cores indicate by enormously intense methane-oxidation. This contention will be supported by carbon isotope values of the dissolved inorganic carbon dioxide (DIC).

For this preliminary evaluation it suffices to note the high total CO_2 content (TCO_2 mM/kg) and the apparently astronomical supersaturation with respect to calcite and aragonite (max. ›60 times and ›40 times) calculated from the carbonate parameters (see Table in Appendix 6). The calculation at this time assumes normal seawater calcium (10 mM/kg) which surely is too high and will be determined by shore-based work later. The high supersaturation and presumed concurrent Ca-deficit results from authigenic calcium carbonate mineral formation in these vent cores. Concretions of many shapes and sizes were described notably in core 21-1 but also in

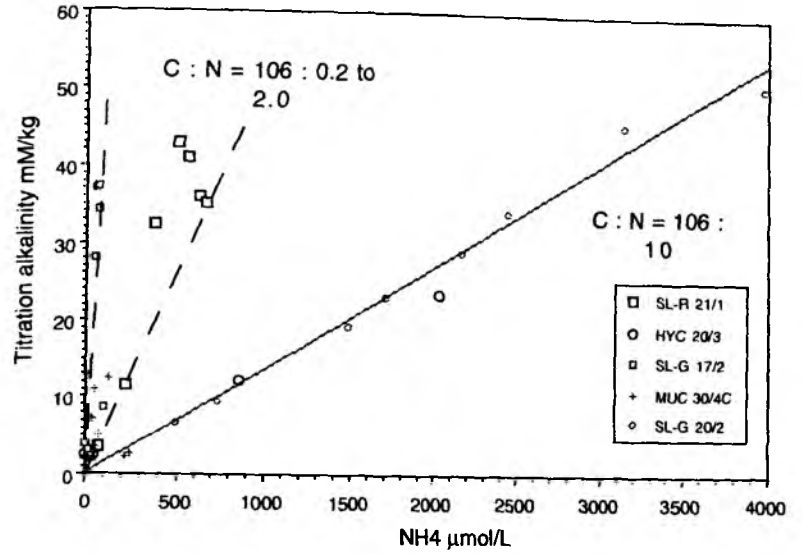

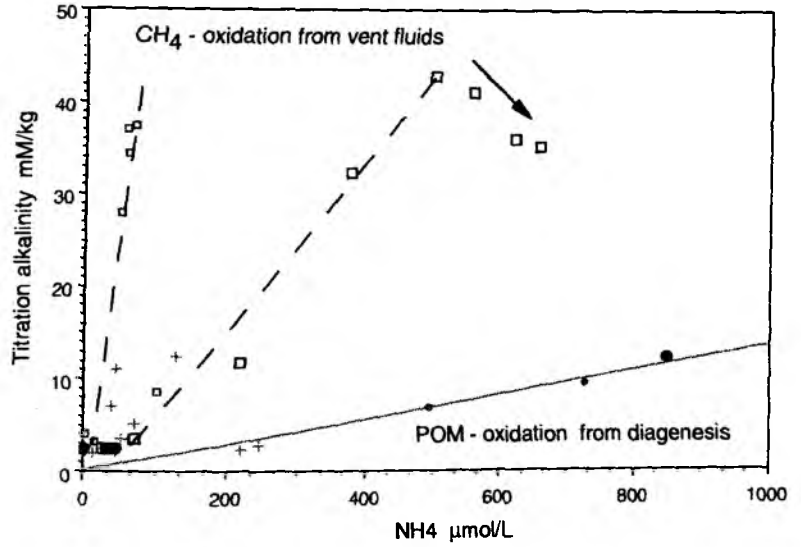

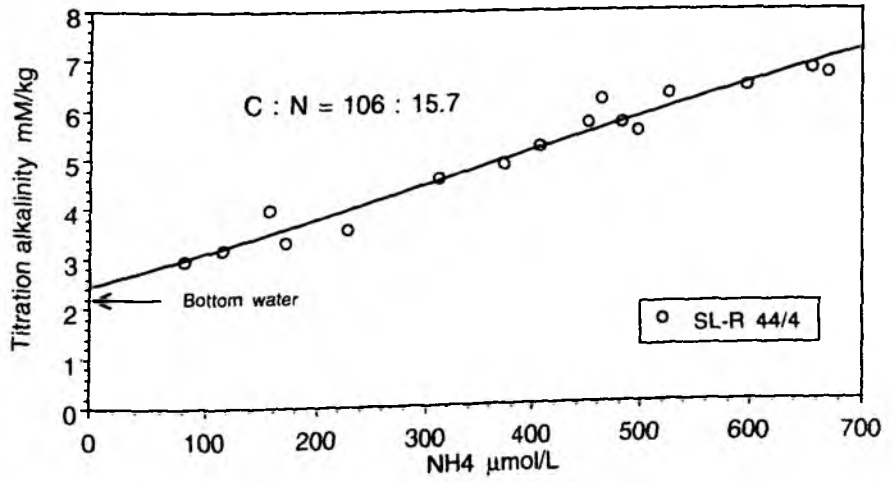

Fig. 4.20: *C and N remineralisation ratios.*

core 17-2. The core description (Appendix 3.2) further yields important information on fluid discharge and related reaction horizons at which methane consumption takes place. Fluid channels are suspected from the "watery fabric", the "gravelly texture", and the "sulfidic-troilite-lined" burrows and bivalve fragments observed in cores 17-2 at 16 - 21 cmbsf and 21-1 at >100 cmbsf. Coincident with these fluid channels and best developed in core 17-2 are maxima of SiO_2, NH_4, PO_4. These indicate a reaction zone in which most of the microbial turnover of methane must occur. Furthermore, the rather constant and low total alkalinity, the absence of H_2S and a significant break in interstitial Cl-content (Figs. 4.16; 4.18) strongly suggest that the vent fauna recirculates bottom water oxygen down to the level of the fluid channel (16 - 21 cmbsf) and somehow derives both CH_4 and H_2S for metabolic turnover. Such a scenario has been described and modelled for vents at the Aleutian subduction zone off Alaska (Wallmann et al., 1992). Thus the initial interpretation of the pore water data makes it abundantly clear that at least 2 active vents were cored, one underlying the Boris-Li-Flare and the other the Giselle-Flare, that methane-containing fluids ascend to within 20 cm of the seafloor, and that vent-biota appear to burrow down and tap this fluid and nutrient source and utilize it via aerobic methane and sulfide oxidation. Below the level of burrowing fauna, anaerobic microbially-mediated methane oxidation dominates early diagenesis, a result of which is the widespread formation of authigenic carbonate and possible other mineral assemblages.

4.2.7 Authigenic minerals and sediment fabrics

J. Greinert and A.N. Derkachev

Sediment cores in the North Sakhalin working area were taken at two different vent sites. Station SL-G 17-2 was positioned in the ***"Giselle-Flare"*** area in a water depth of 386m and recoverd 82 cm of well-sorted terrigenous sand with mud pebbles and olive-green-colored gravel. In 15 cm core depth, fragments of bivalve shells were found. To investigate the biological vent community two trawls (TWL 16-1 and 16-2) were undertaken and recovered abundant material of vent fauna and numerous carbonate concretions of different morphological types (about 30-40 kg) which can be summarized as follows:

1) Dark-gray-colored slabs like carbonate crusts up to 40 cm in size with a thickness of 1-2 cm.
2) Elongated tubular concretions, up to 3-4 cm in diameter and up to 20 cm in length. They are compact with a dark-gray color and a slightly rough surface. Many of the concretions show open channels of varying size. They represent carbonate cementation and probably biomineralization around worm burrows. Sometimes thin white rims (<1mm) could be observed inside the burrows which are of secondary origin.
3) Dendritic tubular concretions of dark-gray color.
4) Irregularly shaped carbonate cemented of gravel and pebble-size rock fragments.
5) Dark-gray-colored carbonate coatings on bivalve shells.

6) Gray-yellow-colored concretions of oval to elongated shape with a porous surface. Their configuration came from large aggregates of spherulitic clusters of large yellow crystals which are colorless in some segments. These crystals very likely show pseudomorphic replacements from ikaite to calcite, which are known as **glendonite**. Numerous small dendroid aggregates of white to yellow clusters (probably glendonite) were found in cavities and on the surface of these concretions.
7) Dense dark-gray concretions containing gray-yellow-colored glendonite crystals representing a carbonate cementation of the surrounding sediment pore space.

Many of the concretions have visibly been exposed to erosive conditions at the seafloor. Colored rims and crusts with epifauna are prove of this exposure.

At the second vent side near the ***"Obzhirov Flare"*** two cores were taken (HYC 20-3 and SL-R 21-1) in the immediate vicinity of vents in a water depth of around 678m. Here the sediments are represented by silty pelites to pelitic silts with a rather mottled, lense-like color distribution caused by diagenesis and intensive bioturbation activities. Throughout the core, dark-gray-colored hydrotroilite-dominated sediment parts in form of spots, lenses and thin layers could be observed. Some horizons with clam shell fragments were recognized in the cores at 125, 157, 175, 242 and 270 cm at station HYC 20-3 as well as 20, 70, 90, 147, 175-195 cm at station SL-R 21-1.
A mousse-like texture probably caused by methane seeping from the core during treatment could be recognized between 175-210 cm depth at SL-R 21-1 which differs from the relatively soft and water-saturated sediments of the remaining core.
Carbonate concretions were found in the same core at 175-195 and 200-210 cm below seafloor. They occurred either as coatings on shell fragments up to 10 cm thick, or as rough soft concretions of 3 to 4 cm in size as well as small tubular bodies. Increased methane concentrations are suspected in this part of the core because of its sediment texture coupled with a strong hydrogensulfide smell.

Conclusions :
The tubular concretions at the "***Giselle Flare***" are clearly the result of a micritic carbonate cementation of the sediment around worm tubes or primary ikkait crystals. The discovery of open burrows inside some of these tubular concretions suggests that the cementation of the surrounding sediment had taken place around the tube. The ocurrence of ikkait ($CaCO_3$ * 6 H_2O) and the recristallization to glendonit ($CaCO_3$) at a later point of time show that cold bottom water temperatures were present during the genesis of the ikkait.
Crust-like chunks indicate a carbonate precipitation at the boundary where HCO_3^- or

CO_3^{2-}-rich fluids seep into sediment horizons with higher amounts of Ca^{2+} and Mg^{2+} in the pore water. In contrast, irregular shaped chunks with rock fragments and drop stones are more likely the result of a diffuse cementation in surface-near sediment horizons.
Still unclear for all carbonates is the amount of the very likely methane-derived HCO_3^- or CO_3^{2-} incorporated in the authigenic carbonate minerals in contrast to released CO_2-species of degraded organic matter. Those questions can be answered by analyzing the carbon isotope value $\delta^{13}C$ which will be done at home.
The sediments at the ***"Obzhirov Flare"*** with hydrotroilite layers and the strong H_2S-smell show that a strong sulfate reduction occurs in relatively shallow sediment horizons. This very likely is induced by the high amounts of sedimented organic matter and ascending methane-rich fluids.

4.2.8 Trace gases and carbonate system

G. Winckler, A. Obzhirov, and G. Pavlova

Methane

Introduction:
First investigations of the gas distribution in the water column of the Okhotsk Sea were started in 1972 (Geodekyan et al., 1978). In 1984, the gasgeochmical laboratory of POI initiated annual expeditions to study the distribution of methane and heavy hydrocarbons and the potential use of gases as indicators for oil-gas prediction; during these expeditions the fault zones in the Sea of Okhotsk were to be mapped as well.
In the process, abnormal methane fields were found in the bottom water masses on the shelf and slope of the Sea of Okhotsk. In 1983, an echo-sounder registered a gas vent on a flank near Paramushir Island at a depth of about 800 m. This phenomenon has been studied during various expeditions (Zonenshain, 1987; Obzhirov, 1993; Gaedicke et al., 1997). During the observation period methane concentration of the vent increased from 200 nl/l to more than 1000 nl/l. Disintegrating gas hydrates are believed to be the source of the gas.
In 1988, a second gas vent was found on the shelf (150 - 180 m depth) and flank (700 - 800 m depth) of north-eastern Sakhalin Island (Obzhirov et al., 1989). In this vent region, the methane concentration of the bottom water reached 13500 nl/l. During the expeditions of 1989-1998, fresh gas vents were found in this and in other regions and the methane distribution in the water column was studied intensively (Obzhirov, 1993; Lammers et al., 1995). In the bottom sediments close to the gas vents, gas hydrates were found (Ginsburg et al., 1993) that pointed to gas hydrates as a source of emanating gas. The data of the previous expeditions have shown that there are a lot of gas emanations from the bottom sediments into the water column of the Sea of Okhotsk. But the nature of the gas distribution in vertical and horizontal directions has not sufficiently been researched yet. It is important to find out more about the seeping process and to estimate the scale of vertical and horizontal gas spreading in the water column.

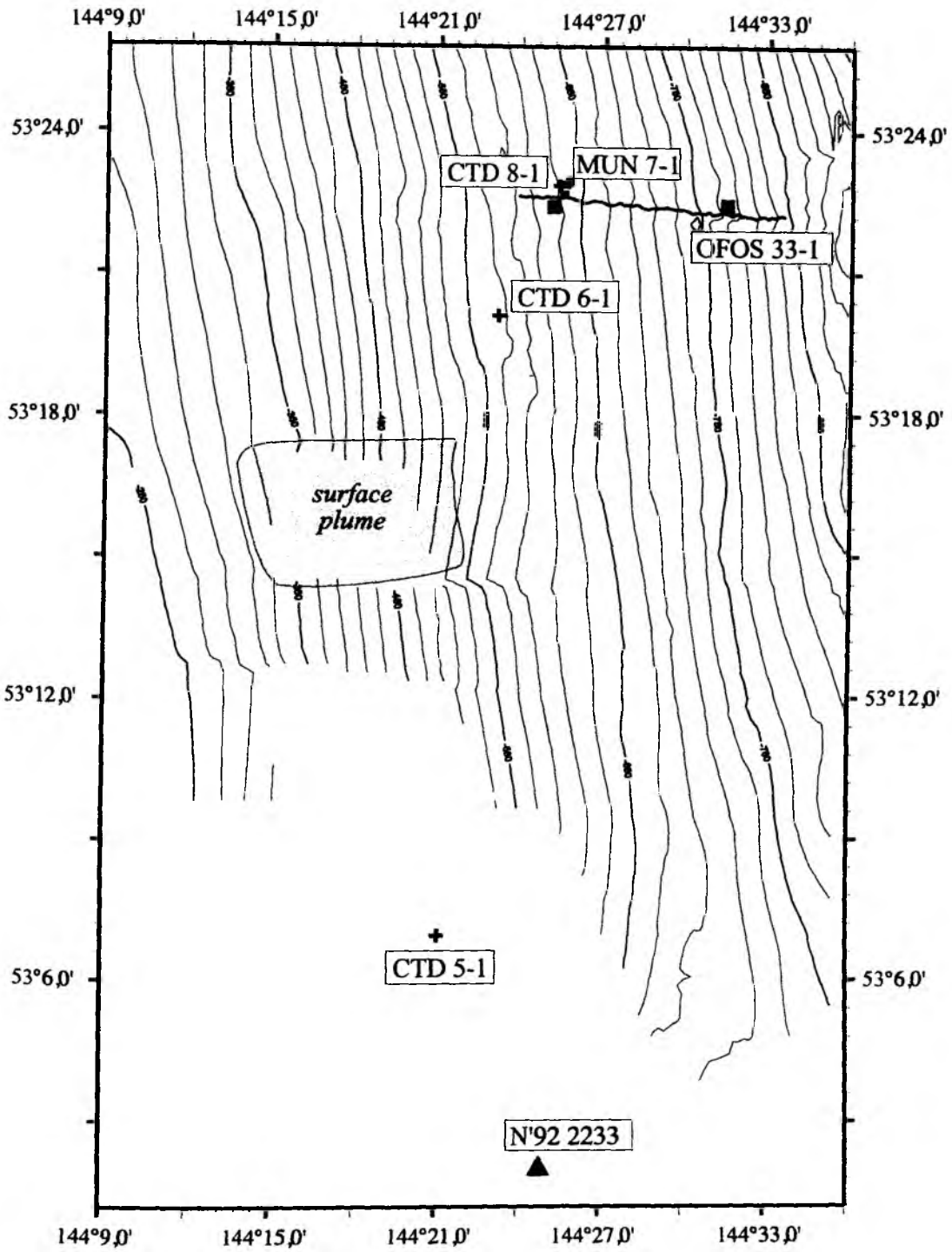

Fig. 4.21: *Map of the "Piltunsky flare" site area with stations undertaken during LV28. Gray area marks a methane anomaly at the surface observed during Gagarinsky cruise 22nd. The position of station 2233 from Nesmeyanov cruise in year 1992 is also plotted.*

These data can be used to solve problems such as the formation of biological and mineral associations, global climate change caused by an increase of methane and carbon dioxide

contents in the atmosphere, formation and disintegration of gas hydrates, detection of oil-gas deposits and activation of fracture zones.

Area 1:

The main goal of the gasgeochemical investigations at Stations 5-1, 6-1 and 8-1 was to study the distribution of methane in the water column in vertical and horizontal directions and to reveal its possible connection to the methane anomaly in surface waters discovered by S. Lammers during the cruise of *RV Professor Gagarinsky* . The investigations were carried out at 3 CTD stations LV28-5-1 (490m), LV28-6-1 (565m), LV28-8-1 (620m) (Fig. 4.21). The stations were situated along the profile crossing the surface methane anomaly from south to north. Station LV28-6-1 was located almost in the center of the surface methane anomaly, Station LV28-5-1 12.7 miles south of the previous station, Station LV28-8-1 3.5 miles north-east of Sta. LV28-5-1.

Methane anomalies were found in the water column at lower levels at all stations (LV28-5-1: 446 nl/l at 472m; LV28-6-1: 516 nl/l at 543m; LV28-8-1: 927 nl/l at 605m). Abnormal methane concentrations were observed at horizons 437m (Sta.5-1), 204m (Sta.6-1), 202m (Sta.8-1). In the surface layer (0-10m) methane concentrations did not exceed 69-57 nl/l at stations 5-1 and 6-1. Of special interest is Station 8-1 which shows a monotonous increase in the methane concentration to the bottom.

Carbon dioxide concentrations in the water column increase with depth: from 0.08-0.1ml/l at the surface, up to 0.85 ml/l at a depth of 605m. Low carbon dioxide concentrations (0.08-0.1 ml/l) were found in the surface water layer at 0-10m. The salinity of this layer was low (27.5‰), that is 5% less than at 50m depth. In the same depth interval the sharp changing of water temperature with increasing depth from 17°C to 1°C takes place. This decline is connected with the delivery of fresh Amur water to this area. The oxygen concentration in the water colum at the stations went down with increasing depth: 4.8-ml/l at the surface and 2.1 ml/l at a depth of 605m. Maximum oxygen concentrations were found at depths of 25-50m. The nitrogen amount varied between 11.4 and 13.0 ml/l. Its concentration decreased to 8.8-10.2 ml/l in the surface layer (0-10m).

Conclusion:

1. The methane concentrations in the upper layer (0-100m) do not exceed the background level (51-69 nl/l). Increasing methane concentrations from 104 nl/l at a depth of 25m to 128 nl/l at a depth of 50m are likely to be connected with the activation of methane-generating bacteria in the region of pycnocline and thermocline. Thus, from the data obtained at the 3 stations it may be deduced that abnormal methane concentrations do not penetrate from lower water horizons into the upper ones and into the atmosphere. Therefore, the surface methane anomaly observed by S. Lammers cannot be explained by the progress of methane from the bottom water to the surface water.

2. The surface methane anomaly is believed to be connected with short-period cycles of meteo- and hydrological variability. Warm surface water is likely to be transported by the west wind to the central region of the Sea of Okhotsk, and, as a result, an upwelling may come into existence in the transition zone between shelf and slope. Water saturated with methane may go up to the surface together with the upwelling. Methane concentrations in the bottom layer of the shelf slope (depth 315m) reached 910 nl/l (Obzhirov, 1993). If an upwelling effect exists, the bottom water masses are sure to transport abundant methane to the surface. Circumstantial evidence of this assumption could be the high methane concentration (360 nl/l) at a depth of 300 m at Station 8-1.
3. In this region a constant-in-time field of large methane amounts (300-900 nl/l) is observed in the depth interval from the bottom up to 200 m. The oil deposits (Odoptinskoe, etc.) are believed to be the source of the methane.

Area 2:

In this area gas was analyzed in the water columns of 3 CTD stations (LV28-11-1, LV28-14-1, LV28-20-1), in the bottom water of 3 MUC stations (LV28-15-2, LV28-30-2, LV28-30-4) and in the bottom sediments of 3 SL stations (LV28-17-2, LV28-20-3, LV28-21-1).

The main goal of the work was to reveal peculiarities of the gas distribution, especially of methane and carbon dioxide, gas spreading in vertical and horizontal directions in the water column and in the sediments.

An extremely high methane concentration (11076 nl/l) was found at station 20-1 at a water depth of 670m. At the next level (642m), the methane concentration decreased more than 100 times - to 67 nl/l. Low methane contents (67-85 nl/l) were observed at 3 horizons in the depth range of 642m to 578m. Then at the 4th level in the range from 553m to 452m, methane concentration increased up to 118-562 nl/l. Three horizons higher (300m-50m) the methane concentration dropped to 62-95 nl/l; at a depth of 8m, almost at the surface, it sharply increased to 309 nl/l.

A maximum carbon dioxide concentration (1.02 ml/l) was found at the lower horizon (670m) showing a methane anomaly. Its concentration decreased to 0.84 ml/l at the level of 642m where the amount of methane steeply decreased as well. At the next level (612m) the carbon dioxide content rose to 0.94 ml/l and then went down to 0.16 ml/l at the surface.

Station 14-1 was located 6.4 miles south-west from station LV28-20-1. The methane distribution within the water column of this station was quite different from that at the previous station. At the lower horizon (374m) the methane concentration amounted to 119 nl/l which exceeded the background concentration by 30-50%. Upwards from 324m to 203m the methane concentration went up to 208-139 nl/l. Then at 154-53m (surface horizons) it fell to 95-75 nl/l.

The carbon dioxide concentration found at this station was with some fluctuations decreasing from the lower level at 374m (0.74 ml/l) to the upper level at 53m (0.37 ml/l).

Station 11-1 was located 4 miles north-west from Station 14-1 and 8.4 miles south-west from station 20-1 on the shelf. At this station abnormal methane concentrations of 1812 and 1728 nl/l

were found at the lower levels (248 and 225 m correspondingly). Upwards, at horizons 201 and 152m, the methane concentration decreased to 237 and 101 nl/l correspondingly. At levels 100 and 51m, methane amounts were close to the background values 75 and 74 nl/l. At the level of 10m, methane concentration increased to 175 nl/l.

The carbon dioxide concentrations increased from the upper level of 10m (0.25 ml/l) to the level of 201m (0.73 ml/l). At the lower horizons where methane anomalies were found, carbon dioxide concentrations decreased to 0.64-0.70 ml/l.

The oxygen distribution in the water columns of these 3 stations showed standard values: 5-6 ml/l at the upper 10m level, 7.3 ml/l at 50-100m and then decreased to 2.1 ml/l at 642m (Sta. LV 28-20-1).

The nitrogen concentration fluctuated in the range from 10.7 to 15.6 ml/l in all water columns.

Conclusion:

On the basis of gasgeochemical data we have come to the following conclusions: The sediments of gas seeping areas are abnormally saturated with methane and carbon dioxide. Taking this into consideration, we can suggest that disintegrating gas hydrates are likely to be the source of methane and carbon dioxide.

Gas (methane) escapes from the sediment into the water as local fluid and travels through cracks connected with the Sakhalin North-Eastern Fault separating the Sakhalin shelf from the Derugin Basin. The activity of this process is likely to increase in comparison with 1988 when the gas vents were found in this region (Obzhirov et al., 1989). Evidence presented in support of this hypothesis can be found in the excessively high methane anomaly (153000nl/l) found in MUC 15-2 bottom water during this cruise. Previously, the highest methane concentration observed in the bottom water of this region reached 13500nl/l (Obzhirov, 1993). Methane distribution in the water column in vertical and horizontal directions is non-uniformly and shows sharp differences among concentrations. The methane content changed more than 100 times in vertical direction (from 11076nl/l at 670m to 67nl/l at 642m). At a distance of several hundred meters from a gas vent the methane concentration changes more than 10 times as it does in horizontal directions as well. All these facts point to complicated ways of gas (methane) motion in the water mass and interstratification of water layers with anomalous background methane concentrations.

1. In the upper water layers of stations LV 28-11-1 and LV 28-20-1 we found anomalous methane concentrations: 175 nl/l at 10m and 309 nl/l at 8m correspondingly. Methane concentrations of 60-70 nl/l can be counted as background values for this area. The methane anomalies observed are likely to be connected to methane seeping from the lower water levels saturated with methane emanating from gas vents. The process of gas travelling to the water surface remains to be studied. On the basis of the data about water stratification gained from various methane concentrations, it can be suggested that methane comes up to the surface water of upwelling zones and hydrologically unstable regions such as transition zones from the shelf to the slope with complex relief, tidal and other currents.

2. Carbon dioxide concentrations change at the horizons of methane anomalies. But these changes are unstable. Carbon dioxide shows both increases and decreases which probably depends on the specific features of microbiological oxidation and hydrological currents.

Carbonate system

Introduction:

The carbonate system regulates the pH of seawater (Skirrow, 1975) and thus, directly affects the form and migration of elements, as well as many geochemical and sedimentological processes taking place in the ocean. This system is of great interest because of the CO_2-effect on the climate. Once CO_2 is in solution, it can equilibrate with bicarbonate and carbonate ions. The carbonate ion concentration in the ocean controls the rate of precipitation and dissolution of $CaCO_3$. An unusual paragenesis of sulfide minerals, calcium carbonate and barite was found at cold vents (Suess, 1998). The study of the carbonate system at cold vent sediments, thus, is of great interest.

The investigations of the hydrochemical scientists' team aboard the *RV Akademik M.A. Lavrentyev* had the following objectives:

- to obtain carbonate data in seawater and to evaluate the distribution of carbonate parameters *in situ* in light of water structure and variations of hydrological characteristics;
- to obtain carbonate data of sediment pore water and to work out the approach for studying the carbonate system in sediments;
- to obtain the oxidation-reduction potential (Eh) data in sediments using different types of electrodes.

On board-measurements of $pH_{sws}(25)$ and total alkalinity are listed in Appendix 5. Calculated values of carbonate parameters *in situ* are indicated in Appendix 6.

Figure A4.4 (Appendix 4) display vertical profiles of measured and calculated hydrochemical parameters for Sta. 11-1 and Sta. 20-1 gathered at the North Sakhalin Shelf of the Okhotsk Sea. The main feature of the distribution of dissolved oxygen at Sta. 11-1 (Fig. A4.4) is a very high concentration (over 200 μM/l) for the entire water column, which reflects the rapid replenishment of water. Certainly the fast renewal of water leaves its imprint on the distribution of all parameters studied. The top 250-300m of Sta. 20-1 (Fig. A4.4) are characterized by high oxygen concentrations (over 200 μM/l), too. Beneath this depth the oxygen concentration decreases continuously down to the bottom and achieves the value of 66 μM/l .

Apparent oxygen utilization is a rough measure of oxygen consumed by oxidation since the water left its surface source. A negative AOU means supersaturation with respect to atmospheric oxygen, while a positive AOU means undersaturation. For both stations (Appendix 6, Table 6.1) the upper mixed-layer waters (about 10 m) are supersaturated with oxygen. Below this

depth to approximately 300m, the AOU increases rapidly with depth (because of the intensive oxidation process); then the growth rate is reduced.

For both stations, pH(p,t) (App. 6, Table 6.1; App. 4, Fig. A4.5) continuously decreases with depth and achieves the minimum value of 7.82 at the horizon of about 170m (St. 11-1) and 7.685 at about 575m (St. 20-1). Below the minimum value distribution pH(p,t) is uniform and average value is equal to 7.823 ± 0.005 (St.11-1) and 7.686 ± 0.002 (St. 20-1).

The CO_2 partial pressure (App. 6, Table 6.1; App. 4, Fig. A4.5) for the upper mixed layer is under saturation (278-302 µatm) for both stations and shows a layer of minimum values in layer 0-50m because of photosynthesis. Below the photic layer, organic debris is oxidized to carbon dioxide and therefore pCO_2 increases with depth and reaches 649 µatm at a depth of about 200m (St. 11-1) and 870 µatm at a depth of about 500m (St. 20-1). By way of comparison, a maximum pCO_2 value of over 1000 µatm was found in the intermediate and the deep waters in the North Pacific (Broecker et al., 1982). The pCO_2 distribution below 500m is uniform; the average value is equal to 885 ± 4 µatm. It coincides with the nutrients' uniform distribution. Average value is equal to 2.93 ± 0.05µM/l for PO_4 and 40.56 ± 0.25 µM/l for NO_3.

Total alkalinity variations (App. 6, Table 6.1; App. 4, Fig. A4.5) down to about 500m (St.20-1) mainly follow changes in salinity. Below 500m, NTA distribution is uniform and the average value is equal to 2.403 ± 0.001 mM/kg. For Sta. 11-1, NTA seawater is uniform practically for the entire water column below the upper mixed layer and the average value is equal to 2.379 ± 0.001 mM/kg. The normalized total inorganic carbon (App. 6, Table 6.1; App. 4, Fig. A4.5) is nearly constant below about 170m for Sta. 11-1 (2.338 ± 0.001 mM/kg) and 500m for Sta. 20-1 (2.386 ± 0.001 mM/kg).

Isotope tracers

Water samples for the analysis of the $^3He/^4He$ ratio, helium and neon concentration, tritium concentration and $^{18}O/^{16}O$ ratio were obtained from the water column. Isotope anaylses will be carried out on different mass spectrometric systems at the Institute for Environmental Physics (University of Heidelberg). In the North Sakhalin Shelf Area water samples were collected in order to study two different scientific objectives.

1.) Helium isotopes as vent tracer: Helium isotope analysis may be used to investigate the origin of vent fluids emitted from the seafloor. The background concentration and isotopic signature of helium in the water column is primarily determined by gas exchange with the atmosphere. An additional injection of helium from different sources (i.e. mantle-influenced and sediment-dominated regimes) into the water column results in supersaturations compared to the equilibrium concentrations and may be identified by their specific isotopic signature. Fluids derived from a crustal or sedimentary source show a radiogenic signature, stemming from alpha-decays of U and Th series elements. Consequently, ^4He anomalies in the water column

can serve as tracer for cold vent input as observed at the Cascadia Subduction zone and help to identify the source of methane emission.
Helium isotope data will be compared to the results of methane analysis. One of the main tasks is to find out if the methane anomalies (up to 11000 nl/l at CTD # 20-1) in the North Sakhalin Shelf Area are correlated with a vent-related ^{4}He anomaly.

2. Tracer Oceanography: Isotope analysis of different trace gases (^{3}He/^{4}He, Ne, ^{18}O/^{16}O, Tritium) will provide information on the regional water mass distribution. The tracer distribution will be related to the hydrographic parameters (salinity, temperature) in order to investigate characteristic circulation processes. In the North Sakhalin Shelf Area it is of special interest to investigate the origin and the influence of the fresh water component observed at the surface of most hydrographic profiles (see Figures, Appendix 4). Based on coupled tracer balances for ^{18}O and salinity, we will be able to obtain the regional and vertical distribution of fresh water components. Furthermore, ^{18}O data can be used to distinguish between different fresh water components, i.e. a continental source (river run-off) and marine sources (sea ice meltwater), and to evaluate their influence on the regional water mass distribution. Further information will be derived from ^{3}H data. The ^{3}H/^{3}He allows to describe the evolution of the vertical age structure of the water column which is displayed by the distribution of ^{3}H and its decay product, ^{3}He.

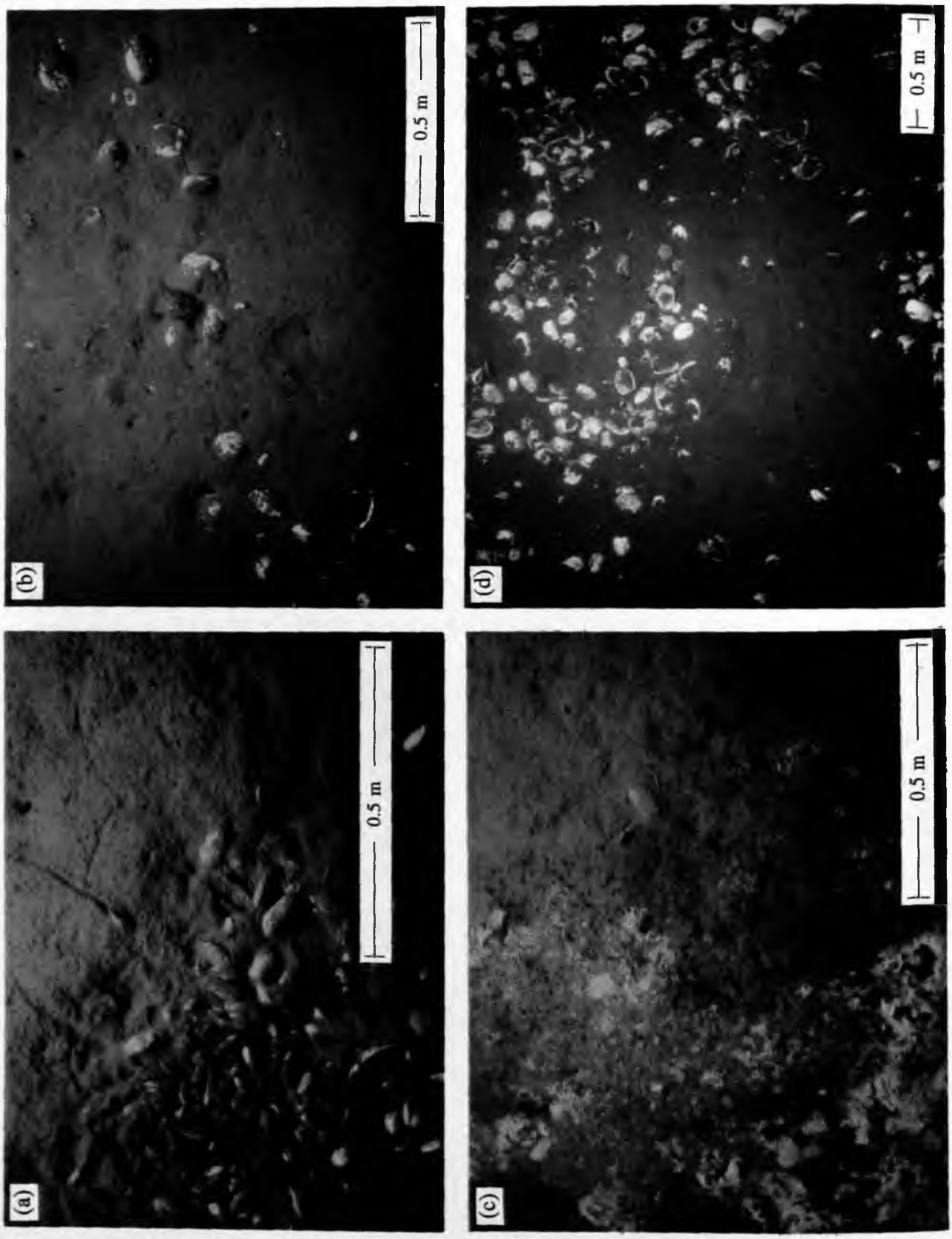

***Plate 1**: Visual indications of seepage at the continental slope off North Sakhalin. (a) Cluster of Calyptogena sp., Piltunsky Flare (OFOS 33; 10:38:41). (b) Living Conchocele sp., Obzhirov Flare (OFOS 31-1; 00:41:03). (c) Bacterial mats on anoxic sediment? Piltunsky Flare (OFOS 33; 10:40:22). (d) Shells of Conchocele sp., Giselle Flare (OFOS 9-1; 01:21:30).*

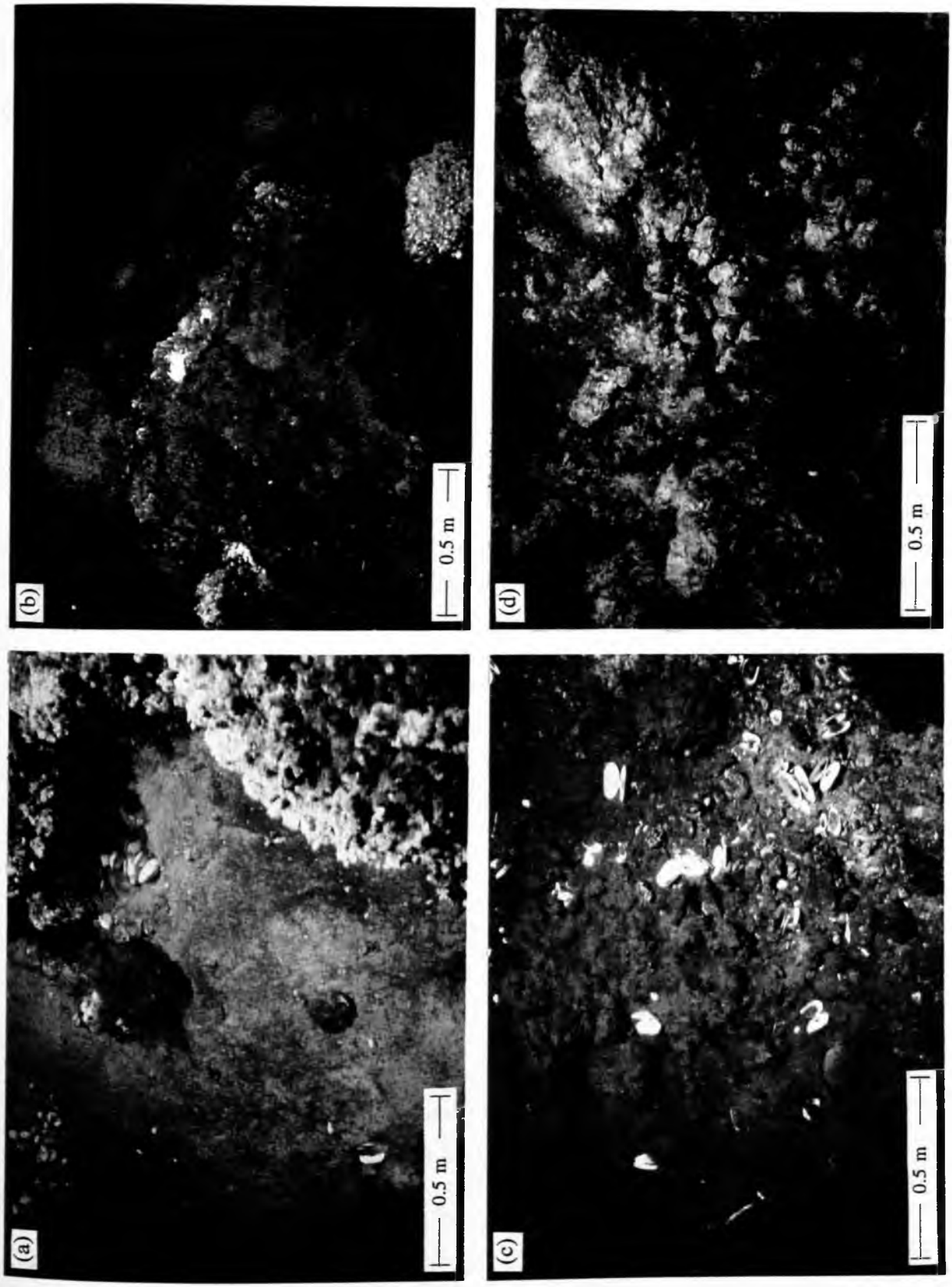

***Plate 2**: Visual indication of seepage in the Derugin Basin. Pictures taken during OFOS 23. (a) Living Calyptogena sp. and barite precipitates (20:27:45). (b) Barite chimney (20:30:32). (c) Calyptogena shells and shrimps (19:47:38). (d) Barite debris (19:16:10).*

4.3 Fluid venting and barite-cabonate-mineralization in the Derugin Basin

4.3.1 Introduction

E. Suess

Since the early 1980's, barite-carbonate mineral associations have been known from a structural high of the Derugin Basin (Astakhova et al. 1987; Astakhova, 1993). The porous, travertine-like fabric of some of the dredged lithologies appeared to have formed from fluids emanating at the seafloor. The light carbon isotope signature of the associated calcite ($\delta^{13}C$= -60 ‰ PDB) confirmed this origin and implied that methane may play a role as carbon source via oxidation. A hydrothermal origin was proposed, whereby it remained unclear if this implied geothermally-derived fluids; i.e. heated as the result of the regional geothermal gradient or hydrothermal fluids, in the strict sense, derived from seawater. Such fluids are heated and recirculated as a result of magmatic activity such as often related to crustal stretching. Subsequently, a very thorough sedimentological, mineralogical, petrographic and isotopic study on barite-calcite concretions, encrustations, burrow-fillings and bodies of many shapes and sizes which occured throughout a sediment core from the same area (Derkachev et al., in prep.) did support the earlier contention and additionally suggested that fluids might also rise through sedimentary portions of the structural high. These findings are the basis of the detailed investigation carried out during the *Lavrentyev*-expedition. Several important questions remained to be addressed: Is the venting process still active today or did the samples originate during past episodes of venting? If venting occured, and there seems to be no doubt about it, then what is the mechanism of ascent and where and what are the depth and source of the mineralizing fluids? How large is the area affected by fluid venting in the Derugin Basin and are there other mineral formations or gas emissions associated with the barite-calcite formations which might help answer the really big question: Cold seeps or hydrothermal vents?

Strategy and sampling:

The strategy during the *Lavrentyev*-expedition required an OFOS-survey, coring, dredging, bottom trawling, and water column sampling. A brief bathymetric survey covering an area of approx. 3 x 6 km around the sites of previous dredgings and coring of barite-calcite mineral formations showed a well-defined E-W trending (≈110°) ridge with a steep N-facing side dropping from 1500m at the summit down to >1650m in the basin. The S-facing flank appeared to slope more gently towards an area at 1550m of uneven morphology with hills, rises and depressions (Fig. 4.22).

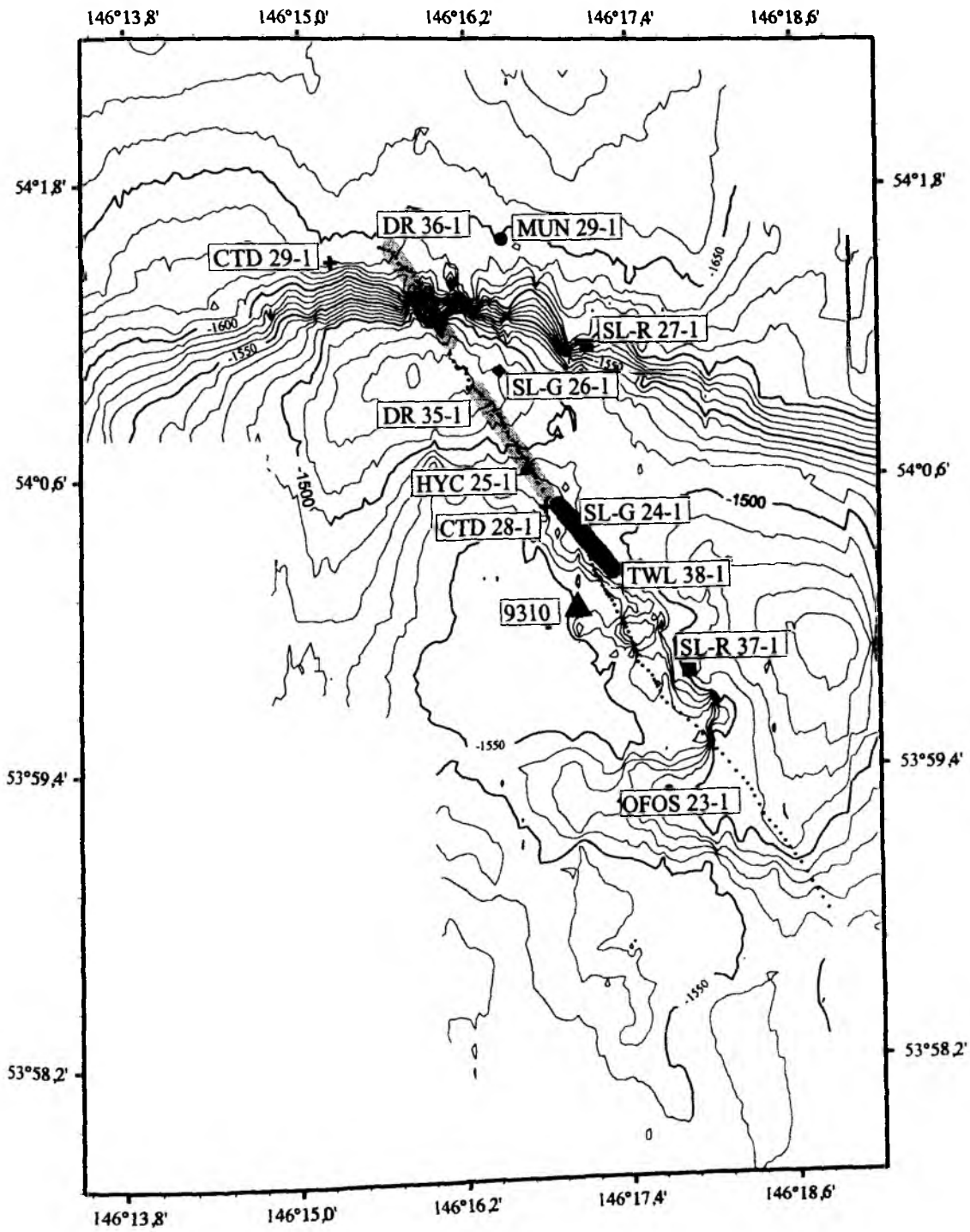

Fig. 4.22: Bathymetric map of the Derugin basin working area with undertaken core and CTD positions. Light gray lines mark the tracks of the dredge deployments, the dark gray line indicates the trawl track. Station 9310 shows the position of the gravity core recovered during 25th cruise of Akademik Nesmeyanov.

The OFOS-survey was run across this morphology between a rise and a depression and crossed over the crest of the ridge. Two cores only came up with sediment (SL-R-37-1 and HYC-25-1) from four attempts. Bottom trawl and dredges were successful. One dredge and the trawl were run up the gently sloping S-flank and the other dredge up the steep N-flank. Two of three CTD's were placed within 3 km of the ridge crest and the third CTD about 10 km away in a deeper part of the basin. Sampling was heavily concentrated in the near bottom water column, about 400m off the seafloor.

4.3.2 Geologic setting

R. Kulinich, A. Svarichevsky, and A. Derkachev

The Derugin Basin is located in the western part of the Sea of Okhotsk between the Sakhalin slope in the west, the Kashevarov Rise in the north-east and the Institute of Oceanology Rise in the south-east. In the south the Derugin basin is connected to the Makarov and Peter Shmidt Troughs, in the north it continues through the Iona Trough. As a geological structure, the Derugin Basin is an asymmetrical depression in the basement in which the abrupt western wall coincides with the eastern slope of Sakhalin Island. The eastern basin consists of a complex block construction with numerous horsts and grabens. Within one of such horsts the carbonate-barite mineralization was found.

Bathymetry:

The Derugin Basin is delineated by the 500m isobath. The bottom is the abyssal plain at an average depth of 1700m and a maximum depth of 1795m. The relief is heterogenous; the basin's western parts are the flat bathyal plains slightly elevated towards the walls. In the north-eastern part the relief is rougher and complicated by a series of small submarine mounts and hills.

Prior to this research, a detailed echosounding survey of the area had been done, on the basis of which the bottom topography map was compiled (Fig.4.22). The area is located within the not high plateau-like upland with a depth of 1500-1550m. In the north it is bounded by a sublatitudinal step, along which the floor drops off by 100-150m. In the north and east the elevated area is complicated by two isometric hills 30-40m high. Their nature remains unknown, but the carbonate-baritic formations taken during the dredging and trawling seemed to originate from the foot of these hills.

Sediments:

The sedimentary cover of the Derugin Basin is not constant.The maximum thickness was observed in the north-western part of the basin and reaches 2.5-3.0 km. The rest of the basin has a sedimentary thickness in the range of 1.5-2.0 km. The deeper sediment layers are approximately Eocene-Oligocene in age, the upper ones of Neogene-Quaternary age (Gnibidenko, 1982). The deeper sedimentary layers lie non-conformably on the basement, fill

depressions between rises and pinch out the slopes or folds. A complicated edifice underlies the sediment cover at the southern and eastern parts of the basin. The largest rises of the basement pierce that cover where diapiric structures were found. The area studied during the *Lavrentyev*-expedition is located in the northern part of the basin over a horst similar to the ones described above and is contained within the coordinates 53°59' - 54°01' N and 146°15' - 146°19' E (Fig. 4.22).

Basement:_

Composition and age of the basement of the Derugin Basin is not known for certain. It is likely to be similar to the basement of the neighboring rises. From the results obtained after the dredging of the structures and the basin's walls it has been proposed that the basement of the Derugin Basin is heterogenous. Its composition includes Late Paleozoic and Early Mezozoic rocks (silts, siliceous argillites, sandstones, hornfelses, altered effusive rocks) overlain by subaerial volcanic rocks of the calc-alkali series.

Deep structure:

The crust under the Derugin Basin may be of continental crust type. Its thickness decreases gradually from the west to the east from 29km at the boundary with the Sakhalin slope to 22km off the Kashevarov Rise. The crust includes all standard but reduced layers of the continental crusts.

4.3.3 OFOS observations

J. Greinert and H. Sahling

In the Derugin Basin the seafloor was observed during the OFOS-track 23-1 starting at a water depth of about 1530m (see Plate 2). During the track in NNW direction we crossed an approximately 50m-high horst at the beginning, followed by a flatter area of a graben and horst system, and climbed up to the ridge in 1470m water depth with a steep flank at the north (Fig. 4.23). During this track the most impressive features were pinnacle- or chimney-like build-ups, up to 10m in height and several meters in diameter. Often they showed a rounded shape with an irregular rough and porous white surface. Partly they were covered with separate smaller chimneys approximately 1m in height.

Along the whole track, chimneys standing even closer to each other could be seen with 15-100m of sediment and eroded blocks in between at the middle part of the southern and the upper part of the northern flank of the northern Ridge (Fig. 4.23). These findings were used for positioning the dredge stations DR 35-1 and 36-1. Based on samples recovered from these dredges and the later trawl TWL 38-1, the build-ups can be clearly identified as barite chimneys. The characteristic vent-fauna consisting of *Calyptogena* sp. and empty *Solemya* sp. shells was found along the whole track indicating active venting. Shells of *Calyptogena* were also observed on barite-chimneys, indicating seepage through these edifices.

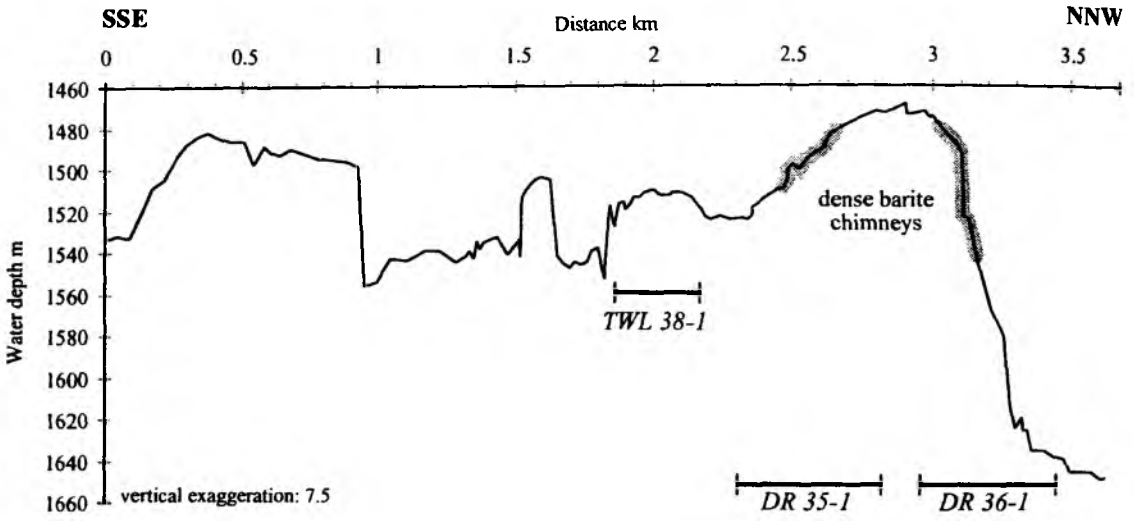

Fig.4.23: *Depth profile along OFOS-track 23-1 at the Derugin basin shows a horst and graben dominated relief. At the northermost ridge ares densely covered with barite chimneys are marked in gray.*

Conclusions:

The discovery of the massive chimney-like barite mineralization over the hole observed area at the Derugin Basin proves that probably strong venting has taken place over a long time and is still taking place. Further investigations based on slides taken by OFOS will provide more information on the distribution, shape and the detailed features of the chimneys as well as on the geological background.

The observed chemoautotrophic fauna *Calyptogena* sp. and *Solemya* sp. are well-known from seep areas and other reduced habitats. All vesicomyids and solemyids investigated so far harbor sulphur-oxidizing endosymbionts. The occurrence of the sulphur-based symbiotrophic bivalves *Calyptogena* and *Solemya* indicate a sulphide-rich fluid flow. Even though large methane anomalies near the bottom have been measured at CTD 28 and 29, there is no indication of the existence of methane oxidizing organisms like the clam *Conchocele* at the north Sakhalin Shelf.

4.3.4 Biological communities

S. V. Galkin, H. Sahling, and D. N. Zasko

Biological samples in the Derugin Basin have been collected at one trawl station (38-1), two dredge stations (35-1, 36-1) and one gravity corer station (37-1).

Description of samples

Substratum characteristics:

The trawl recovered around 0.5m^3, mostly (up to 3/4) washed barite (incl. large blocks >0,5m, few pebbles up to 25-30 cm) and (about 1/4) greenish-gray silty pelite sediment with a destinct H_2S smell.

Faunal composition and trophic specialization

The collected fauna is rather diverse (at least 20 species) but not abundant: apparently the bag collected a big amount of sediment and then was blocked by barites rather soon and stopped to catch. The dominating group of gastropodes (Provannidae ?) of 2 distinct spp. is represented mostly by empty shells but by small bivalves as well. The bivalves constitute the most diverse group: at least 4 specimens could be found in the recovered samples, including 2 symbiont-bearing forms: *Solemya* and *Calyptogena* sp. In contrast to the Sakhalin slope, suspension feeders are well represented. There are 2-3 species of Hexactinellid sponges, Hydroidea (2-3 spp), Madreporaria (ahermatypic corals, 2 spp) and presumably some bivalves. The occurrence of sessile suspension feeders correlate with the hard substratum found in the Derugin Basin (barite deposits and chimneys). It is worthwhile mentioning that "long red worms" were unusually frequent; they seemed very thin and consisted of a red tube without any apparent structure and were up to 10 cm long, tentatively identified as Protozoa (?) which often hide in barite cavities. Carnivores and scavengers are represented only by one small Pantopoda and a large galatheid *Munidopsis* sp.

Conclusion:

The specific vent fauna in the Derugin Basin is represented by the symbiont-bearing bivalves *Solemya* sp. and *Calyptogena* (2 spp.). Shells of *Calyptogena* sp. are well visible during the OFOS observations. One species of *Calyptogena* sp. 1 was recovered alive; the other (C. sp. 2 "elongated') only in form of dead shells. The occurrence of shells of *Calyptogena* sp. 1 in the gravity corer sample (37-1) at a horizon of 530 cm (see Chapter 4.3.6) suggests a steady existence of characteristic vent fauna in the region during the last 60.000 years.

4.3.5 Pore water profiles

E. Suess, G. Pavlova, B. Domeyer, H. Sahling, and J. Greinert

Two cores (SL-37-1 and HYC-25-1) of unusual barite-rich sediments were obtained from the Derugin Basin suspected vent site and intensively sampled for pore water analyses. Both show similar features in having quite low nutrient concentrations and erratic intervals with low chloride. Only the barite-turbidite-sand core (SL-R-37-1; Fig. 4.24) is discussed here in detail, but core HYC-25-1 is shown as well (Fig. 4.25).

It must be kept in mind that the major seawater ions, SO_4, Ca and Mg, will be determined in the shore-based laboratories and that therefore the interpretation is preliminary. The low titration

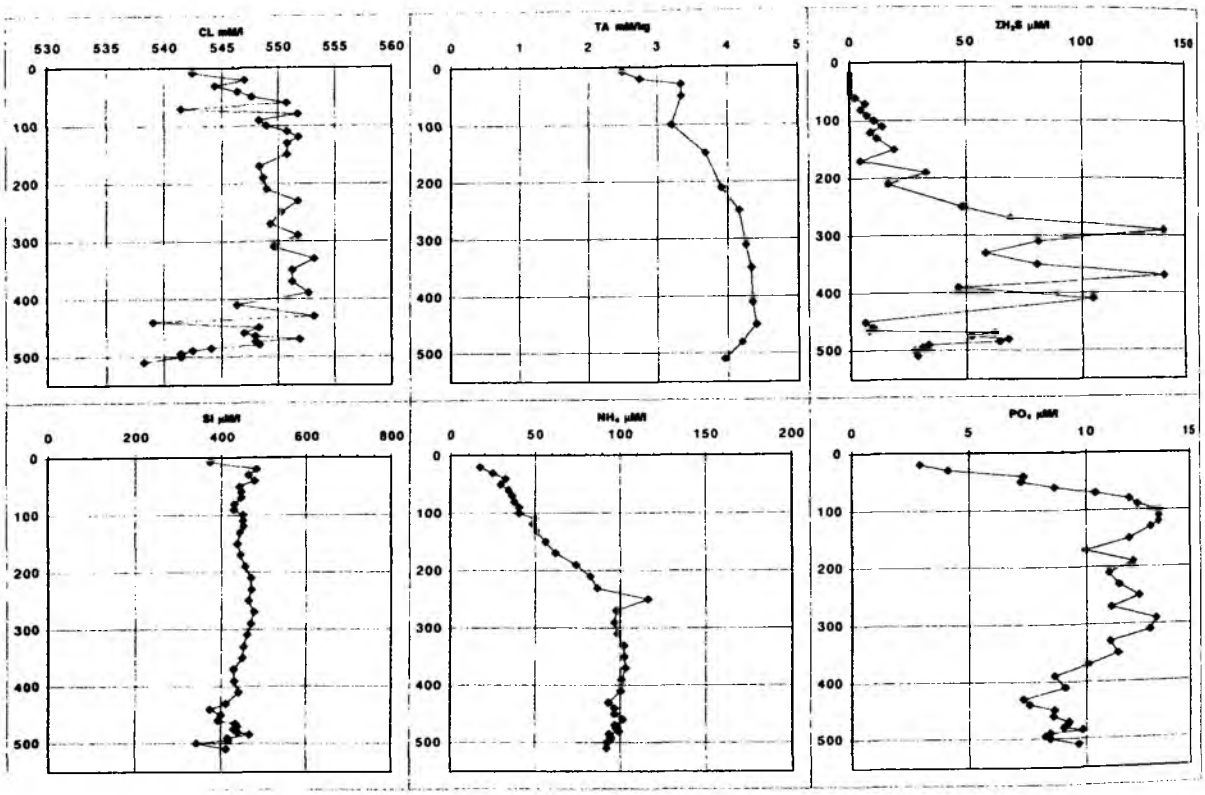

***Fig. 4.24**: Pore water composition SL-R 37-1*

alkalinity (Fig. 4.24) with only 4 mM/kg at 500 cmbsf showing only a slight increase is in agreement with low and almost constant SiO_2-concentration and the moderately high NH_4-contents. Around 200cmbsf, the hydrogen sulfide concentration increases significantly although remains low in general. All those features are typical for organic-poor sediment and low diagenetic activity. These distributions are to be expected from turbidite-type sediments. Unusual are the rather high dissolved PO_4-contents and the erratic Cl-distribution. The former are probably due to diagenetically remineralized organic phosphorus, but could also be derived from an inorganic phosphorus source, possibly related to venting. This interpretation, however, cannot be ascertained without mineralogic, petrographic, and geochemical analyses of the solid phases. The low erratic Cl-excussions at the surface, around 70 cmbsf, between 400-450 cmbsf, and in the lower-most core interval at 480-520 cmbsf appear to be significant. In Fig. 4.26 the analytical uncertainty is shown along with the bottom water Cl-content, expressed as chlorosities in g/l. It is clear that most values of the pore water approach but do not exceed the bottom water chloride and that deviations apparent are negative anomalies.

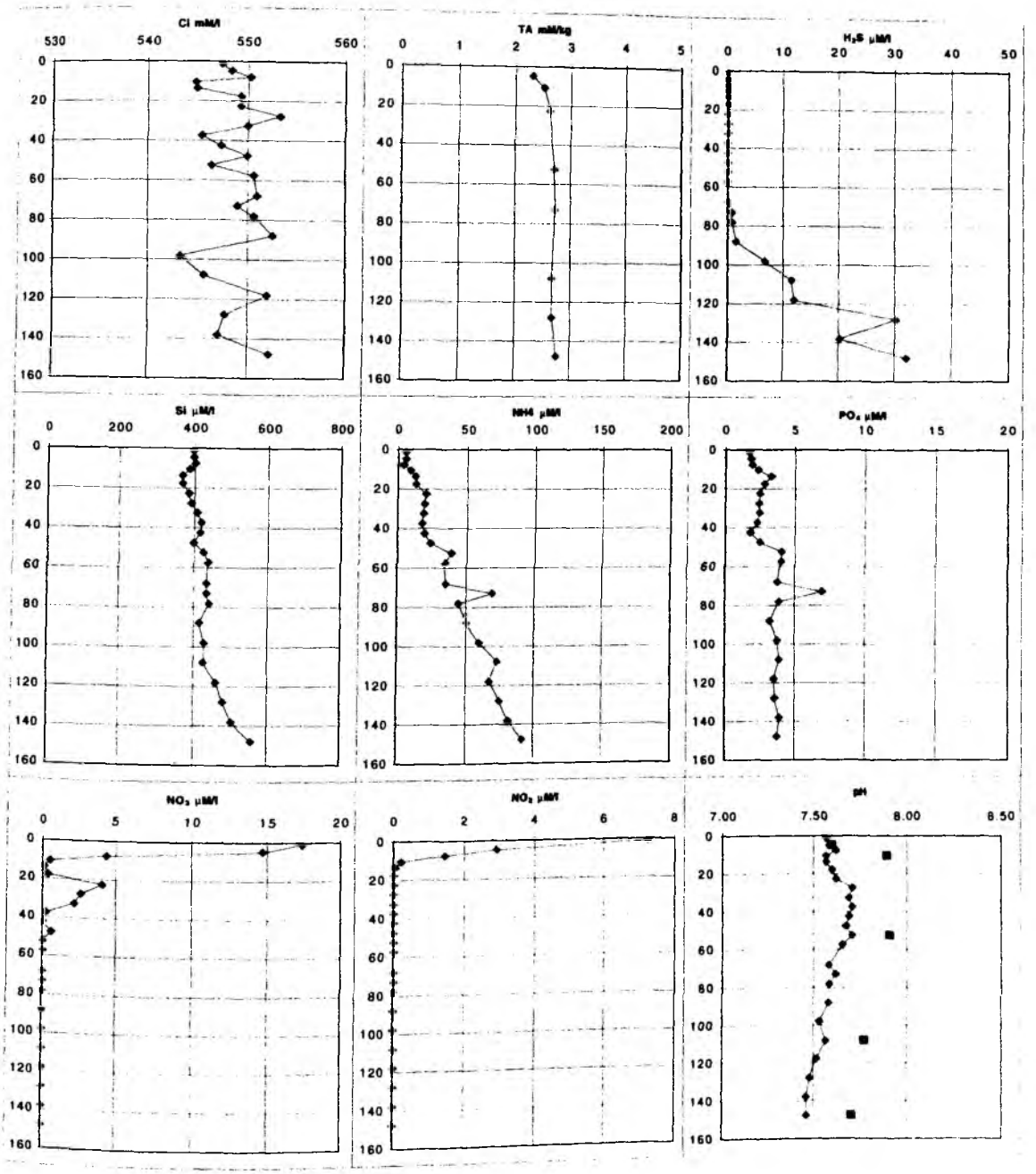

Fig. 4.25: Pore water composition HYC 25-1.

The core description (Fig. 4.27) shows that all 4 negative Cl-anomalies occur in very coarse intervals which consist of large porous barite fragments mixed with sand. There are at least 3 other coarse intervals that do not show negative Cl-anomalies. It is also worth noting that the lowermost, almost massive, barite rock interval shows the strongest Cl-anomalies. These are vaguely associated with low dissolved SiO_2-contents. The C:N remineralization ratio in the pore water perhaps suggests that methane oxidation may be the reason for apparently low N-org

content (Fig. 4.28). The C-isotope waters should give an indication of whether or not isotopically 'light' carbon from methane is present.

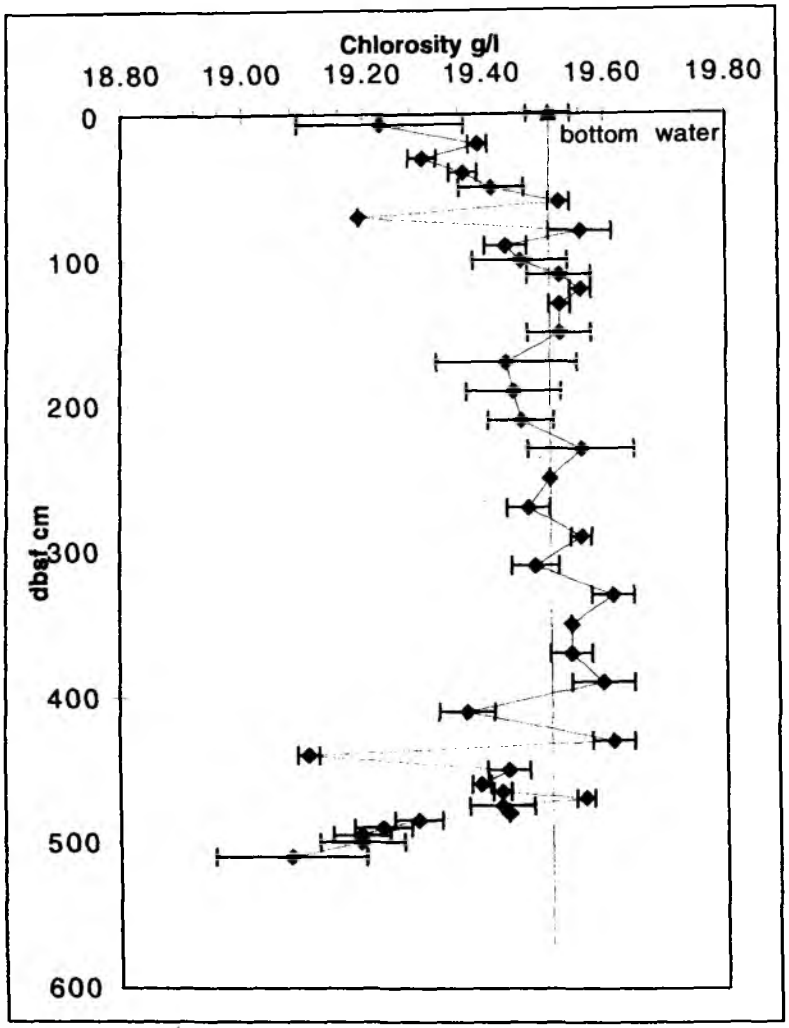

Fig. 4.26: Chloride anomalies in pore waters of core SL-R 37-1.

In summary, it is clear from the pore water composition that core SL-R-37-1 did not penetrate into an actively discharging barite vent or chimney but rather into a diagenetically unreactive organic-poor sediment. The erratic Cl-depletion in the coarse intervals could be due to relics of low Cl-fluids which are caught in the porous sediment-rock fabric. Trace elements, particularly Ba and isotopic analyses of Sr, Li and B as well as of H_2O should help answer this question. The answer is important in solving the big question of whether a giant sediment-hosted cold seep is responsible for the barite-calcite mineralization in the Derugin Basin or hydrothermal activity. As it stands now, the pore water results slightly favour the giant- cold-seep-hypothesis.

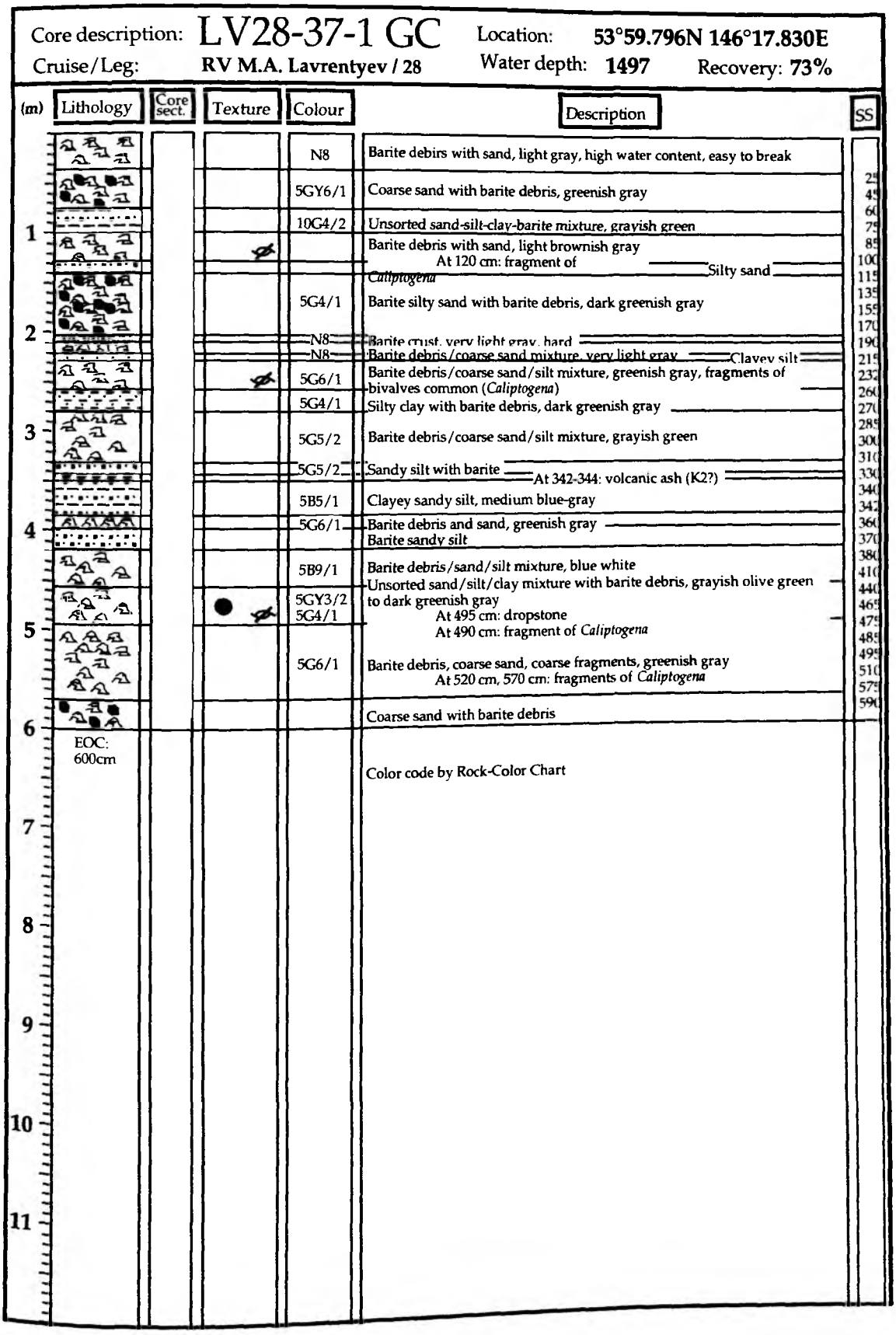

Fig. 4.27: Core description of core SL-R 37-1.

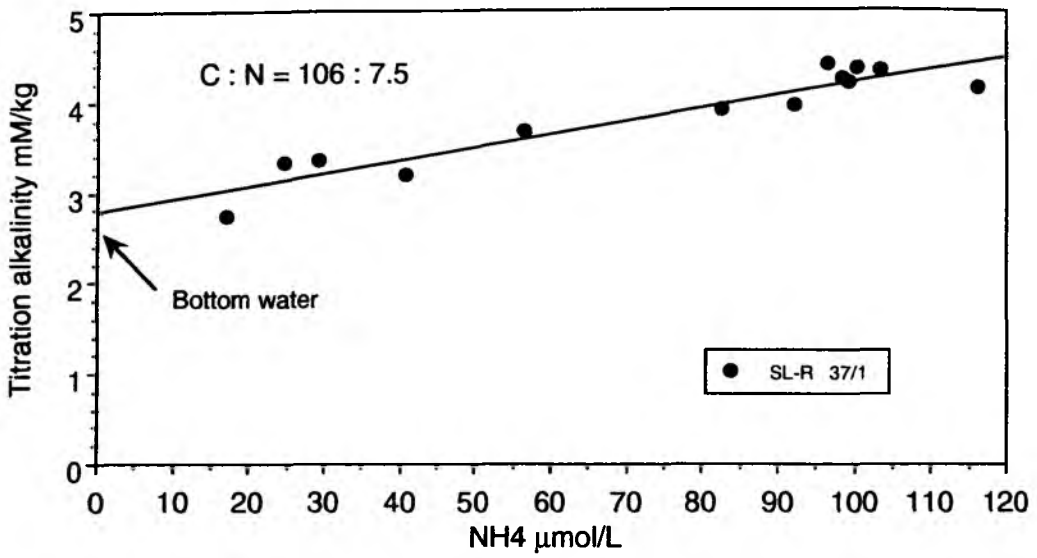

Fig. 4.28: *C:N remineralization ration in pore waters from core SL-R 37-1.*

4.3.6. Authigenic minerals and sedimentology

A. Derkachev, and J. Greinert

Authigenic travertine-like barites in the Derugin basin were first discovered during the 15th cruise of *RV Kallisto* in 1981 dredging the northern slope of a small rise in 1460 m water depth. The rise was dredged repeatedly approximately 3 km eastward from that point during the 23th cruise of *RV Pegas* in 1986 where similar precipitates were found. The results of these investigations are summarized by Astakhova et al. (1987; 1990), who interpreted the barites as hydrothermal in origin.

However, during the 25th cruise of *RV Akademik A. Nesmeyanov* in 1993 small barite - calcite preciptates were found in Holocene-Pleistocene sediments in core 9310 (54°0.07' N; 146°17.0' E) in 1507 m water depth. They were studied in detail by Derkachev et al. (in prep.) and show tube-like forms of cemented worm burrows of different size and intricately zoned composition. Similar precipitates could be recovered in gravity cores HYC 25-1, SL-G 26-1 and SL-R 37-1 as well as on the tracks of dredge DR 35-1 and trawl TWL 38-1 during this cruise. In addition to that, DR 36-1 and TWL 38-1 large quantities of travertine-like barite blocks were found which represent fragments of the huge barite chimneys which were discovered during OFOS-23-1. The recovery and observation of these barites constitute one of the most important successes of this cruise.

The sediments from station HYC 25-1 at the flat part of the upper rise consist of terrigenous silty clays of a dark grey colour with sand and gravel impurities enriched by diatoms in the upper 10 - 20 cm. Downwards they turn into slightly spotty, dark-gray, sticky, moderately dense clayey silt and silty clay with clay lumps up to 20 mm in size. On the sediment surface (0 - 5 cm) compacted clay fragments (15-30 mm) are criss-crossed by numerous biogenic burrows

with less than 1 mm in diameter. The composition of these fragments does not differ from the surrounding sediments. Tubular calcite precipitates were discovered in distinct zones of 25 - 30, 50 - 60, 70 - 80 and 125 - 135 cm depth similar to core 9310. Horizons with considerable amounts of barite or barite-calcite cemented forms were investigated between 50 - 100 cm in core HYC 25-1 and at 25 to 40 cm in an undisturbed sediment block recovered by dredge DR 35-1. Any regular distribution of these precipitates which could represent one homogeneous geological sediment body was not discovered. Most precipitates seem to be the result of pseudomorphosis and cementation of sediment pore space such as channels and worm tubes.

X-ray analyses and microscopic observations at station 9310 showed that the sediments containing carbonate concretions and tubular forms are carbonate-free. Minor impurities of calcite are marked in sediments adjacent to barite-calcite polytubular formations and concretions. On the other hand, barite is present in the entire sediment column, in the form of small authigenic crystals (0.01-0.1 mm) and large tubular fragments.

The authigenic carbonate - barite formations could be divided into different types:

A) irregular tubular calcitic, baritic - calcitic and baritic precipitates;

B) calcite concretions of various density;

C) baritic spherulites, separate barite crystals and their joints;

D) thin barite crusts.

On the basis of X-ray diffraction analysis and microscopic data for carbonate precipitates of station 9310 (Derkachev et al., in press), it seems very likely that they consist mainly of cryptocrystalline magnesian calcite (10-15 mol. % of Mg) which cements the intergranular pore space of a terrigenic matrix with biogenic compounds like diatoms, radiolaria and sponge spicules.

Tubular forms often show elongated forms of several cm in length and 3 to 6 mm in diameter. They are ramified with several lateral sprouts; sometimes those pieces build aggregates of closely accreted single tubular bodies cemented by calcite stretching in different directions. Their surfaces are rough and cavernous because of the irregular mineralization of the sediments. A description of the inner structure of the group of tubular bodies under investigation is mainly based on the results of station 9310. Examining cross sections of these tubular bodies it was found that 1) the concentrically - zonal structures show different types of mineralization; 2) the presence of a central channel with a diameter of < 1 mm (usually 0.5-0.8 mm), around which the formation of purely tubular bodies takes place; 3) tubular bodies are of an intricate structure and show numerous spurious secondary channels less than 0.1 mm in diameter, which cross the tubes by different angles and directions; 4) the internal channels show cementations of calcite, calcite - barite, barite or are uncemented; 5) concentric brown - grey halos around the inner channels which consist of organic mater ; 6) all tubular bodies contain a lot of clayey - detritic particles which testify their formation in the sediments.

Tubular forms with concentric - zonar structures are evidently one of the most frequently observed authigenic precipitates. Their walls consist of a 0.5 - 2 mm thick middle zone of carbonate-free sediment with microcristalline barite crystals sandwiched between two calcite-cemented ones. Inside the tubes faecal pellets can be observed which are the nucleuses for Mg-calcitic cementation.

Barytic tubular forms are detected in all parts of the cores. They differ from the above mentioned tubular forms by their lesser size of 0.3 - 10 mm in length, rarely up to 15 - 40 mm with 0.1 to 3 mm (usually 0.2-0.8 mm) in diameter. Their shape varies from spindle-like, thickening in the centre, to pear-shaped and bent - vermicular. The dense and dark-grey pieces with a dirty - green nuance show a rough surface due to the abundance of inclusions of terrigenic particles. At fractures a central channel is visible with accreted spherical brushes of a flap-type barite of yellowish-brown colour, sometimes ringed with a thin external calcite rim.

Calcite concretions of 15-20 mm up to 110 mm in size can be divided into soft oval but angular ones and dense, hard and well-rounded ones. In the fractured areas of the concretions numerous elongated channels (diameter less than 1 mm) cross the concretions in different directions. The channels are either empty or filled with brushes of calcite and blade-like barite crystals.

Barites can also be found as simple independent varieties like barite crusts, ovally-shaped spherolites and their aggregates (diameter 1-2 mm), pseudomorphic barites on foraminifera shells and other biogenic shells, single crystals as well as clusters. Dense barite crusts of a dark-gray color up to 1-2 mm thick were found only at station SL-G-26-1.
The travertine-like barite recovered from stations DR-36-1, TWL-38-1, DR-35-1 come in various forms: blocks of a diameter of 30-100 cm, big fragments, debris and sand-silty mixtures. The irregularly-shaped blocks are of a white to greyish-white color (rarely greenish-gray); they are strongly saturated with water and crumble easily. These blocks often showed a versicular structure and have a pore volume of approximately 60%. The cavities and channels found were covered by wafer-thin sheets of microcrystalline barites in places. Channel-like, irregular cavities which could be fluid-channels were found in some areas of the bigger blocks. As can be seen under the microscope, the barites consist of very fragile dendritic crystals and other crystals of a size of 0.01-0.2 mm which come in various forms (flipper-shaped, wing-shaped, wedge-shaped, lenticular) of a dull-white or pale yellow colour.

The core SL-R-37-1 was probably taken near the foot of one of the above-mentioned barite chimneys. In the 600 cm-core two layers of crumbled barite gruss containing big fragments as well as a sand-silt-clay sediment mixture were found at the top and base. At horizons 125, 209, 220, 255, 310, 480, 530, 540 cm, shell fragments of two different Calyptogena species were discovered. Furthermore, a volcanic ash layer (very likely K-2) approximately 26000 years old

was found at 342-344cm core depth. An insignificant enrichment of the investigated sediments with small calcite crystals was observed at horizons 120-125, 195-200, 420-425, 530-535cm. The entire core showed fragments of varying size of broken and eroded barite chimneys.

Discussion and conclusion:

More frequently, the carbonate and barite-carbonate precipitates consist of tubular bodies of the above-mentioned shapes. The study of the internal structure of these bodies proves the biogenic origin of the tubes. Those are mainly burrows of benthic organisms such as clams, pogonophora, polychaete, i.e. organism communities which are typical for acitve seepage zones (Embley et al., 1990; Kulm and Suess, 1990; McDonald et al., 1990; Paull et al, 1992; Roberts, Aharon, 1994; Barry et al., 1996; Suess et al., 1998). Some information about the sources and conditions for the carbonate and barite formations can be gained from the oxygen-, carbon- and sulfur-isotope data from authigenic precipitates of station 9310. The $\delta^{13}C$-data from -37.6 to -42.3 ‰ PDB indicate that methane is an important source for carbonate carbon, which is typical for carbonate precipitates at cold vents (Ritger et al., 1987; Lein et al., 1989; Kulm and Suess, 1990; Paull et al., 1992; Sample et al., 1993; Ginsburg and Soloviev, 1994; Roberts and Aharon, 1994; Bohrmann et al.,1998; Suess et al., 1998). Thus, it may be assumed that the carbonate crystallisation is mainly induced by the process of anaerobic microbiological methane oxidation of ascending fluids, probably mixed with dissolved carbon species of degraded organic matter. The rim-like carbonate cementation around the open burrows hints at a biomineralization-like process creating a rigid worm tube which can be used for the cristalization of pure barites. Isotope investigations on barites in core 9310 show $\delta^{34}S$ values from 24.9 to 80.1 ‰ CDT. Those isotope values indicate that residual sulfate at the upper part of the sulfate reduction zone was used for the mineralization of barite (Mizutani and Rafter, 1973; von Breymann et al., 1992; Torres et al., 1996 a,b) when dissolved Ba^{2+} in the ascending fluids pass this diagenetic zone or flow into the bottom water. A likely Ba-source for these barites seems to be biogenic-barite of silicieous plankton which grows in the Sea of Okhotsk in sufficient quantities and causes a high sediment accumulation (Koblenz-Mischke, 1965; Bogorov, 1974).

The age question of the tubular barites remains unanswered yet. Different morphological types have been spreading in the sediment through more than 20.000 years. Active fluid venting over a time interval of 20.000 yrs seems to be a likely origin for these barites.

Without geochemical analyses, the origin and source of the components for the genesis of the huge irregular barite blocks recovered at station DR 36-1 and TWL 38-1 are difficult to explain. The question is whether cold fluids of a deep sediment horizon situated below the sulfate reduction zone can provide barium of biogenic origin in such huge quantities to create the observed barite chimneys. Or are hydrothermal activities necessary for their growth as Lisitsin et al. (1990) have proposed in the Guaymas Basin in the Gulf of California.

4.3.7 Trace gases and carbonate system

G. Winckler, G. Pavlova, and A. Obzhirov

Methane

Gas samples for methane analysis were taken at three CTD stations (LV28-28-1, depth 1507m; 29-2, depth 1640m; 39-1, depth 1639m), one MUC station (LV28-34-1) and one SL station (LV28-37-1) (Table 3.2; Appendix 4). Previously, barites were found in bottom sediments of this region (Astakhova et al., 1993); gas investigations have not been carried out up to now. Therefore, one of the objectives of our expedition was the search for gas anomalies which could point to the presence of hydrothermalism. Station 988, where in 1985 gas samples of bottom water were analyzed (Obzhirov, 1993), was the station closest to the area under study. In 1985, abnormal methane concentrations were not observed.

The relief of the seafloor presents moderate heights and shallow basins. Strong methane anomalies were found in the lower horizon of stations LV28-28-1 (2429 nl/l) at a depth of 1493m and LV28-29-2 (1780 nl/l) at a depth of 1616m. The anomalies were constant within an interval of 200m above the seafloor. These stations were situated 1.1 mile apart from each other in the center of the barite mineralization area. At Sta. 39-1, which was located 8 miles south-east off Sta. 28-1, no abnormal methane concentrations were found. This points to a local methane source in this area.

High methane concentrations in the upper horizons found at 78m of Sta. 28-1 (267 nl/l), at 54m of Sta. 29-2 (124 nl/l) and at 50m of Sta. 39-1 (110 nl/l) attracted our interest. Carbon dioxide concentrations of the water column increased regularly from the surface to the bottom. But at Sta. 28-1 it decreased at a depth of 1493m (0.72 ml/l) in comparison with a depth of 1467m (0.81 ml/l). As already noted, a methane anomaly (2429 nl/l) was observed at the lower level at Sta. 28-1. At Sta. 39-1, the carbon dioxide concentration in the water column was slightly higher (1.01 ml/l) at a depth of 1596m than at Sta. 29-2.

Conclusion

A strong methane anomaly (up to 2429 nl/l) was found in the lower horizons over the field of barite mineralization. Methane dissipates 200 m over the seafloor and for a distance of 3-5 miles in horizontal direction. Organic matter in the sediments, producing methane under the effect of hydrothermal activity, is likely to be a source of methane. Barite mineralization is also connected with hydrothermal activity. Perhaps, in the bottom sediments of this region there are gas hydrates which disintegrate and release methane. A methane anomaly (267 nl/l) was found at Sta. 28-1 within the upper horizons. Perhaps, this is connected with methane penetration from the lower into the upper water layers.

Carbonate system

Figures A4.6 and A4.6 (appendix 4) display vertical profiles of measured and calculated hydrochemical parameters for Sta. 28-1 and Sta. 39-1, occupied at Derugin Basin.

Chemical sampling was carried out in detail only for the depth below about 1000m. Sampling for carbonate parameters at Sta. 39-1 was carried out for the near-bottom layer (1467-1596m) of the water column.

Seawater between 1000-1500m (Appendix 6, Table 6.1; Fig. A.4.6, A4.7) is homogenous not only in temperature (2.33 ± 0.01 ° C), dissolved oxygen (33 ± 2 μM/l) and AOU (298± 2 μM/kg), but also in pH(p,t) (7.629 ± 0.005), pCO_2 (960 ±7μatm), NTA (2.434 ± 0.003 mM/kg), $NTCO_2$ (2.426 ± 0.003 mM/kg), PO_4 (3.1 ± 0.1μM/l), NO_3 (43.0 ± 0.4 μM/l). An additional increase of NTA (10 μM/kg) and $NTCO_2$ (14μM/kg) near the bottom is the result of calcium carbonate dissolution in the undersaturated water.

Isotope tracers

Water samples for analyses of the $^3He/^4He$ ratio, helium and neon concentration, tritium concentration and $^{18}O/^{16}O$ ratio were obtained at three CTD stations in the Derugin Basin. In this investigation area the main objective is the use of the helium isotope data as geochemical tracer. During the investigations in the Derugin Basin carbonate-barite mineralization and strong methane anomalies both interpreted as venting indicators were found. However, it is still an open question which geochemical and/or tectonic process is responsible for the venting phenomenon. Helium isotope analyses may provide an answer to this question since different venting processes are characterized by different isotopic signatures: a hydrothermal origin of the vent fluids can be identified by enriched ^3He whereas a sedimentary source is expected to produce a radiogenic helium isotope signature, i.e. ^4He enrichment.

4.4 Paleoceanography and sedimentology of the Sea of Okhotsk

A Botsul, N. Biebow, A. Derkachev, S. Gorbarenko, A. Kaiser, D. Nürnberg, Y. Terekhov, R. Tiedemann, N. Nikolaeva and R. Werner

4.4.1 Introduction

From the paleoceanogaphic point of view, the Okhotsk Sea is still one of the poorly investigated marginal basins, although it is of extraordinary importance for the understanding of both regional paleoenvironmental changes and global changes in climate and oceanology. High sedimentation rates and the preservation of foraminiferal carbonate make the Sea of Okhotsk a unique location at high northern latitudes to obtain high resolution sediment records for reconstructing climatological changes in deep and surface water circulation that control paleoproductivity and deep water formation.

Recently, Talley (1991) has stressed the importance of the Okhotsk Sea water as a source for intermediate deep water formation in the Sea of Okhotsk. Elsewhere in the world ocean it has been shown that the intermediate deep waters were better ventilated during glaciation at the expense of the deep ocean. The modern circulation pattern tends to accumulate CO_2 in the deep Pacific. However, Zahn et al. (1991) suggest a young Pacific deep water mass produced in the marginal seas of the north Pacific to have contributed to the ventilation of the north Pacific at intermediate depth. Hence, one of the most pressing questions is if the process which generates Pacific Intermediate water in today's ocean was extended during glacial times into the Sea of Okhotsk. In order to study an assumed deep water formation in the Sea of Okhotsk, 4 coring sites have been selected at the northeastern slope of the Kurile basin forming a deep water transect between 1300 and 3200m water depth (Fig. 4.29). Unfortunately, only two sites were cored due to technical problems. However, it is expected that the cores LV28-2-4 and LV28-64-4 will provide some first information about a possible deep water formation.

Another important object of this cruise was to recover an East-West transect of 6 sites across the central Sea of Okhotsk in combination with a North-South transect off Sakhalin to reconstruct changes in paleoproductivity that are related to variations in the nutrient supply triggered by the influence of the Kamchatka Current and the Amur River. Today, one of the most significant environmental factors that can ultimately influence global climate is CO_2. The subarctic Pacific and the adjacent marginal seas like the Sea of Okhotsk show the largest biological production worldwide and are known to act primarily as a sink for CO_2. Processes of vertical ventilation and changes of the biological CO_2-pump transferring CO_2 from the atmosphere to the deep water reservoir are therefore of outstanding importance to understand climate change. During the cruise the successful recovery of high resolution sediment records along the North-South and the West-East transect promise important insights into the processes that have controlled

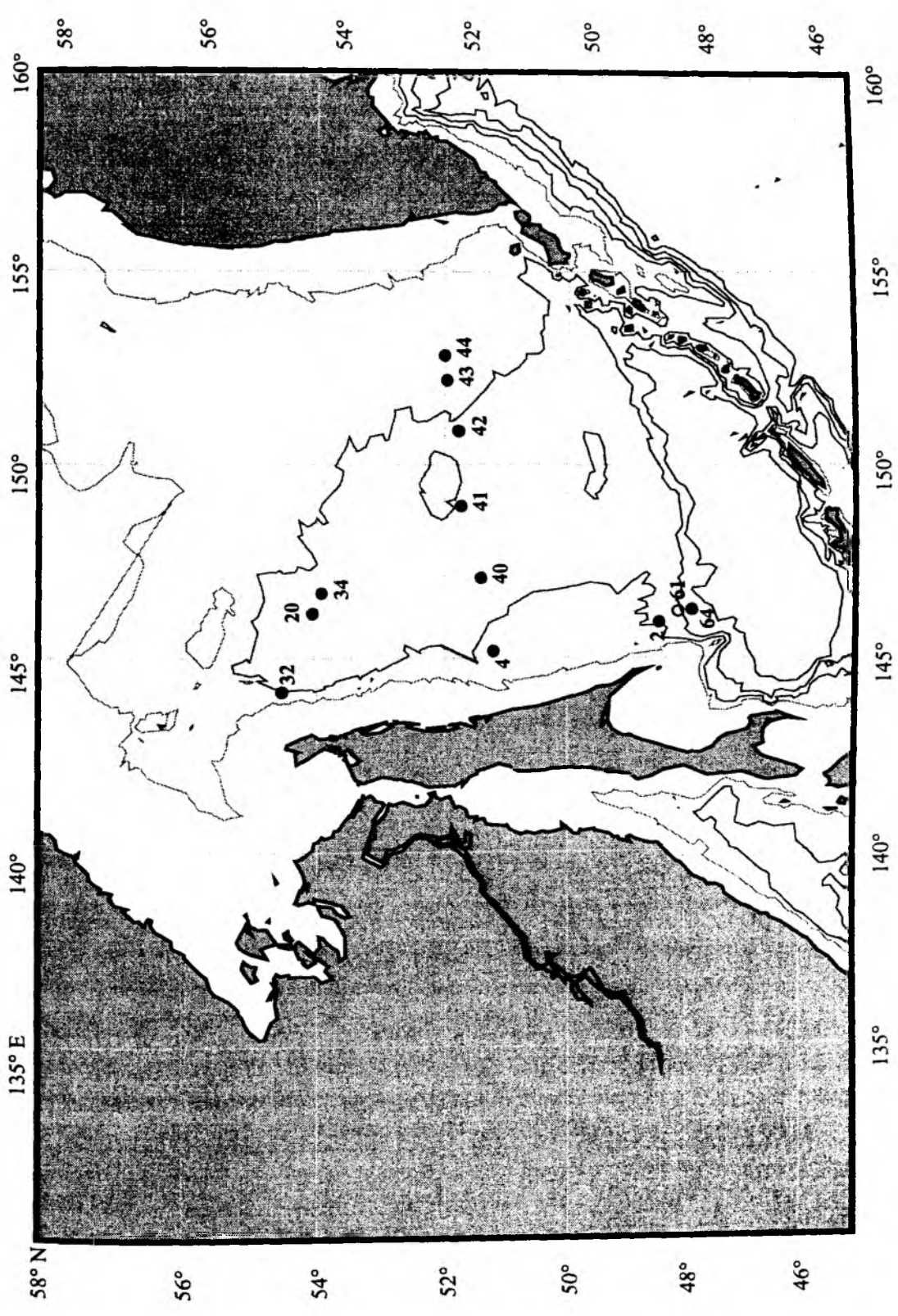

Fig. 4.29: Location map of paleoceanographic sites.

biological productivity during the last 300 kyr. An extreme high resolution record off Sakhalin with sedimentation rates of about 1 m/1000 years will provide detailed information about the Holocene variability in productivity.

Another goal is to examine the influence of vent fields that cause gas (methane) anomalies in bottom water masses and within sea floor deposits. Two cores were retrieved from the Derugin basin, which is stronly influenced by outgassing. One core originates from the center of a gas field; the other one was positioned outside the gas anomaly. A comparison between both sediment records is expected to provide information about the impact on paleoceanographic tracers that are used to characterize the chemical signature of deep water masses.

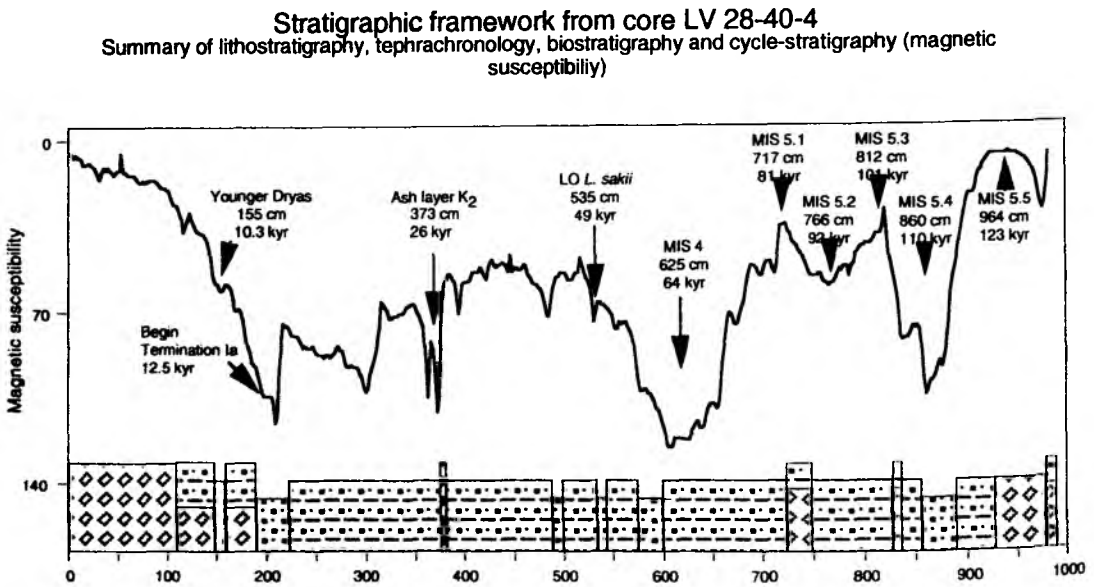

Fig. 4.30: *Stratigraphic framework of age control points that have been used to date our sediment records (e.g. core LV28-40-4). Ages result from lithostratigraphy, tephrachronology, biostratigraphy and cycle stratigraphy. Changes in sediment composition (bottom) are based on core description. MIS (number) indicates age of marine isotope stages.*

4.4.2 Stratigraphy

We combined results from tephrachronology, lithostratigraphy, biostratigraphy, and cyclic changes in magnetic susceptibility and developed a stratigraphic framework of age control points to date our sediment records (Fig. 4.30). In a first step, typical structures in the magnetic susceptibility curves and typical patterns of lithological changes are used to construct a detailed depth correlation beween sediment records (Fig. 4.31A&B, Fig. 4.32). This allows a quick

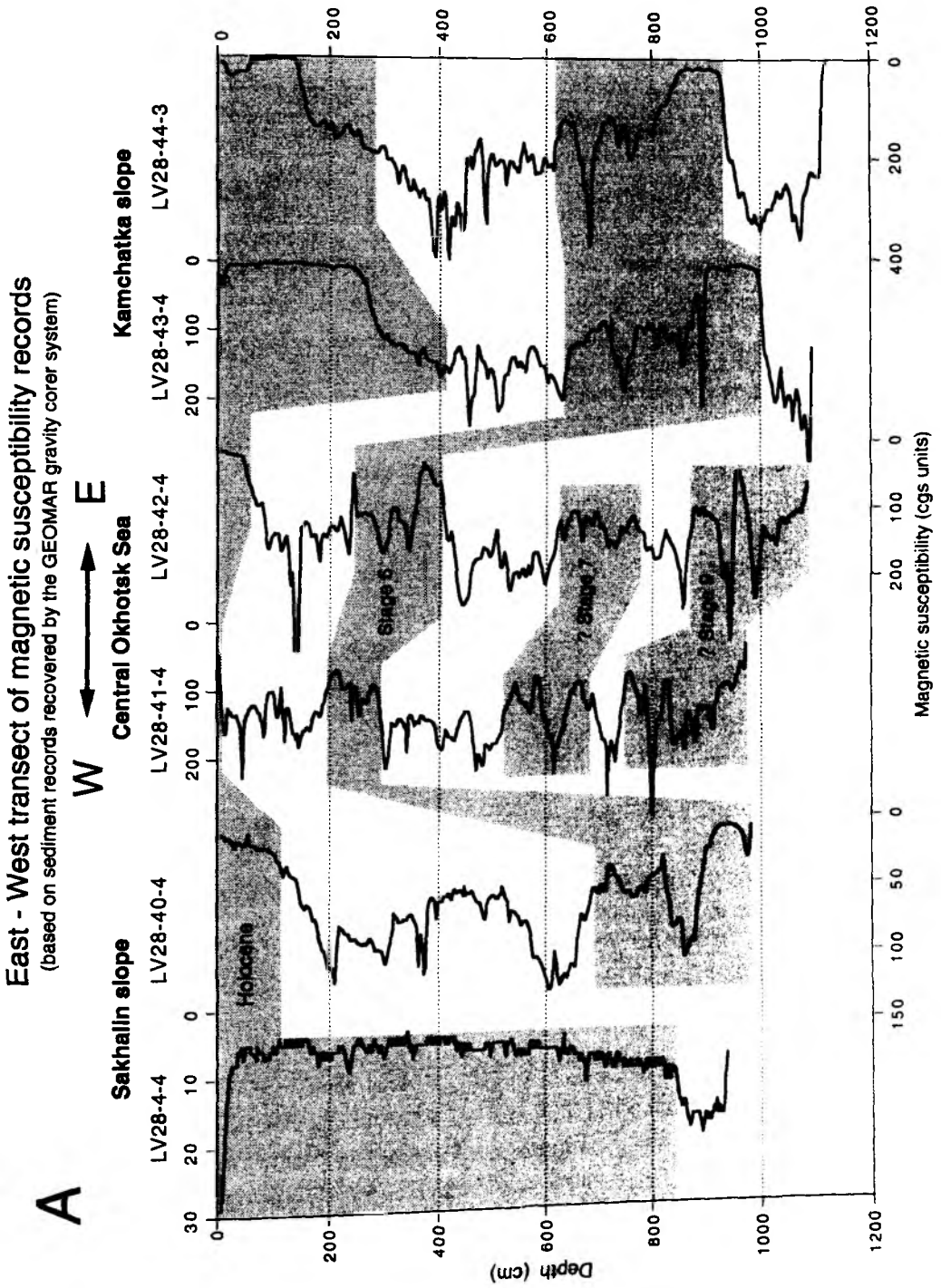

Fig. 4.31 A: East-West transect of magnetic susceptibility records and its correlation across the Sea of Okhotsk. A = GEOMAR sediment records, B = POI sediment records.

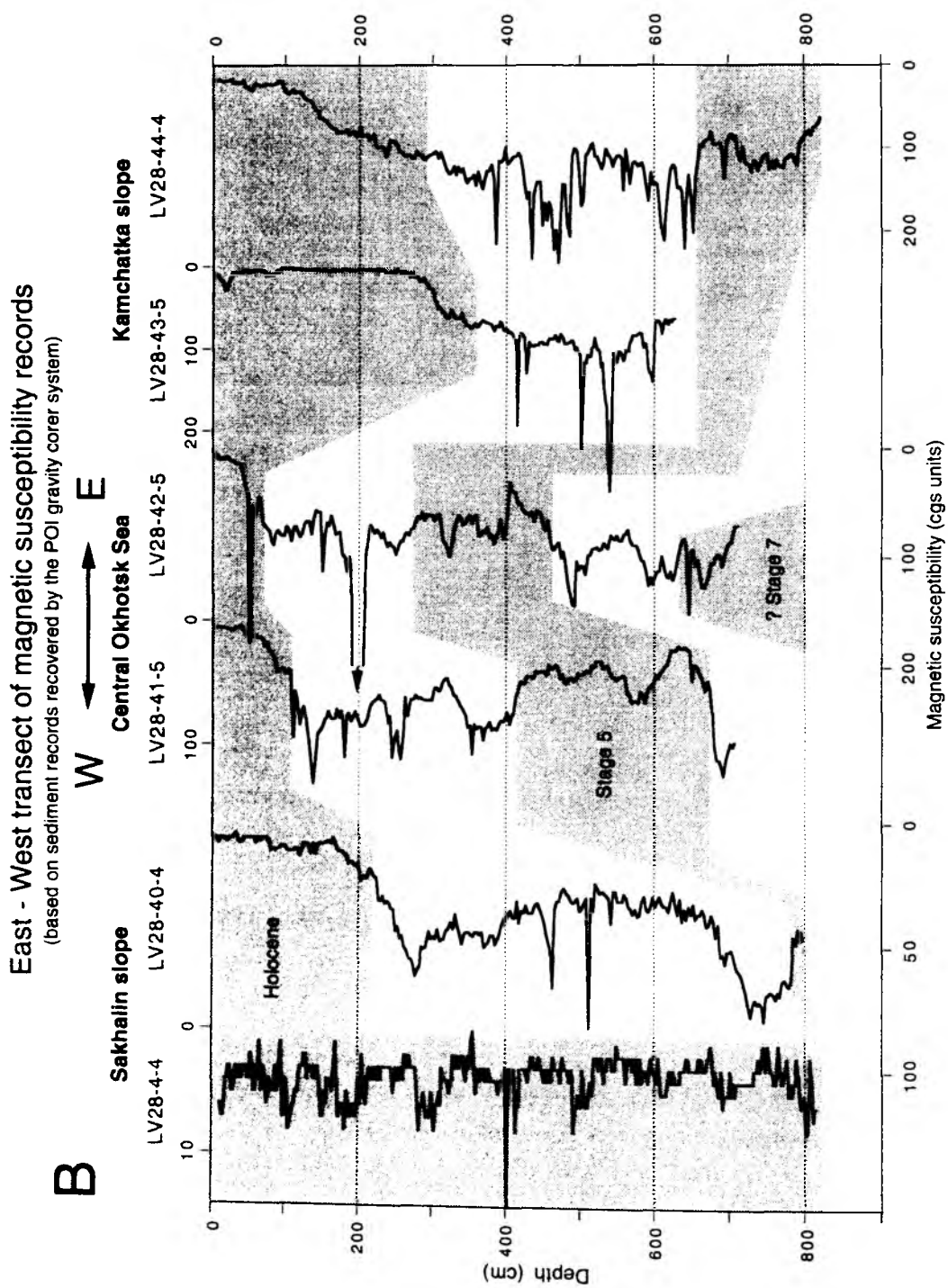

Fig. 4.31B: East-West transect of magnetic susceptibility records and its correlation across the Sea of Okhotsk. A = GEOMAR sediment records, B = POI sediment records.

transfer of age control points from dated reference records (LV28-40-4, LV28-42-4) to other records. Stratigraphic age control for the youngest part of the sediment records (oxygen isotope stage 1 and 2) is provided by identifying the Younger Dryas (10.3 kyr), the onset of Termination IA (12.5 kyr), and the ash layers K0 (8.3 kyr) and K2 (26 kyr). The ages are based on present results from Okhotsk Sea sediment records that include ^{14}C-dated oxygen isotope and magnetic susceptibility curves as well as ash layers (Gorbarenko, 1996; Nürnberg et al., 1997; Gorbarenko et al., 1998; Gorbarenko et al., in prep. and unpublished data). Marine isotope stages 3,4 and 5 (MIS 3-5) identified by magnetic suceptibility variability pattern were established in ^{14}C-dated oxygen isotope records (Gorbarenko, pers. comm., Gorbarenko, unpublished data of "A.K. Nesmeyanov" 25th expedition, 1991) Marine isotope stage 3 (MIS 3) is best identified by the last date of occurrence (49 kyr) of the radiolaria *Lychnocanoma nipponica sakaii* (Morley et al., 1982). The preceeding isotope stages 4 to 9 are identified by cyclic changes in the magnetic susceptibility record that result from 41-kyr and 23-kyr-rhythms in climate due to changes in axial tilt and orbital precession respectively. These glacial/interglacial changes are also characterized by distinct changes in lithology. This stratigraphic framework of age control points suggests that two sediment records (LV28-41-4, LV28-42-4) from the center of the Okhotsk Sea extend back into stage 9 (ca. 325 kyr.). So far, only sediment records reaching back into stage 6 have been available. Furthermore, these records exhibit five so far unknown ash-layers that occur within isotope stage 7 and 9. A more detailed description of the different stratigraphic approaches is given below:

Lithostratigraphy

Cores retrieved during the 1998 KOMEX cruise allow to establish a detailed lithostratigraphy, which is based on the successive deposition of clearly distinguishable lithological units being correlatable laterally over large areas of the Sea of Okhotsk. The results not only improve the lithostratigraphic results obtained during the 1996 GREGORY expedition (Nürnberg et al., 1996), but prolonged them further into the geological past (Fig. 4.32, Fig. 4.33).

Interglacial sediments

Wide parts of the Okhotsk Sea surface deposits commonly consist of a soft, brown diatomaceous ooze, which is mostly overlain by a ca. 1 cm thick brownish fluff layer. Grain sizes vary accordingly from silty sand to clayey silt depending on the water depth. Approximately 3-15cm below the surface, the brownish color changes to light olive-gray typical for diatomaceous oozes. Calcareous foraminifera and coccoliths are abundant. Concentrations of biogenic silica range up to 40% (unpubl. data). Diatom analyses performed by Zhuze (1962) revealed that the diatomaceous ooze belongs to the Holocene. Previous oxygen isotope investigations and AMS-radiocarbon datings on Core B34-90 from the southern slope of the Academy of Sciences Rise (Gorbarenko et al., 1998) further reveal that the base of the diatomaceous oozes ages to about 6 ky BP.

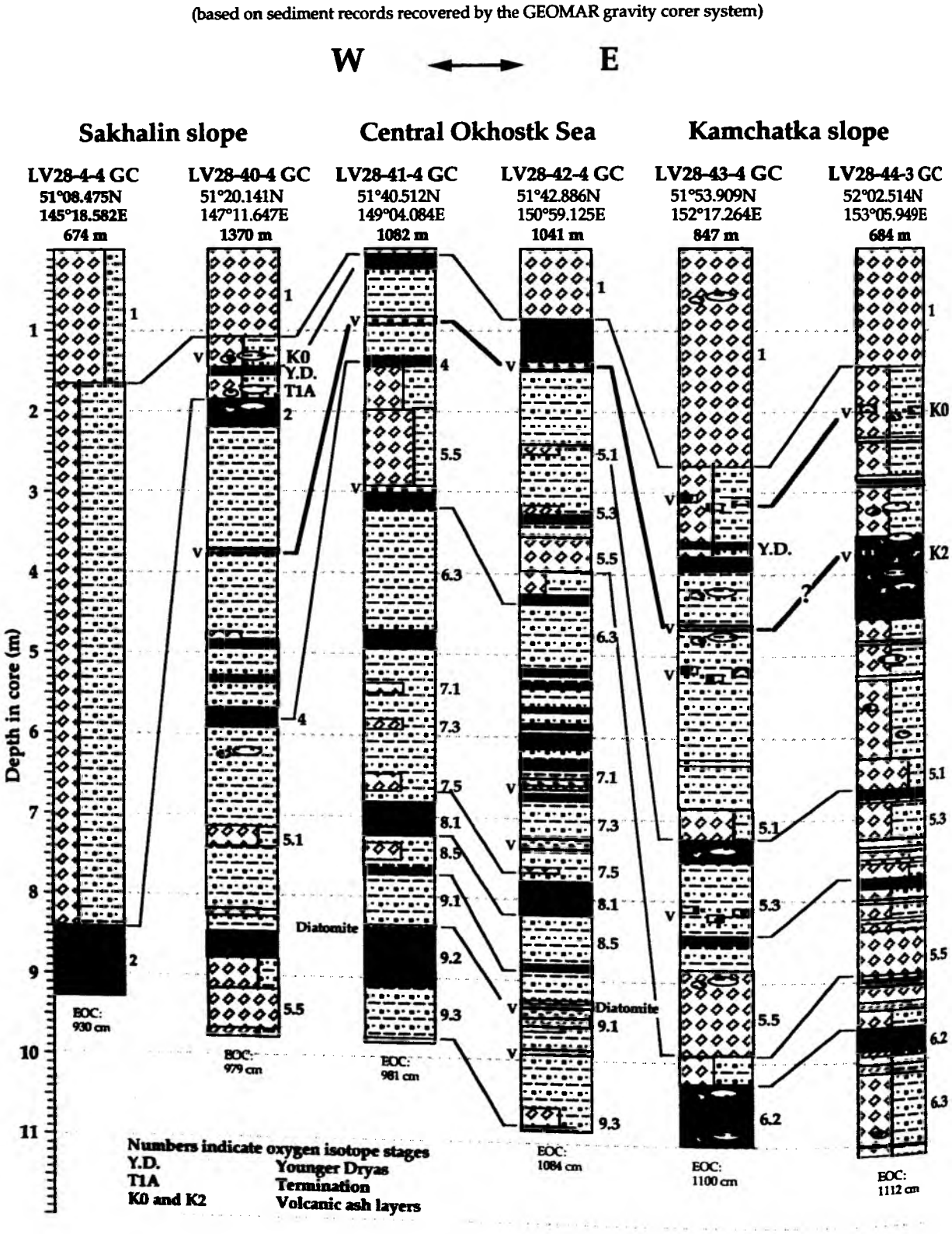

***Fig. 4.32:** Lithostratigraphic classification of central Okhotsk Sea sediment records (retrieved by GEOMAR) and core correlation based on lithology along an East-West transect.*

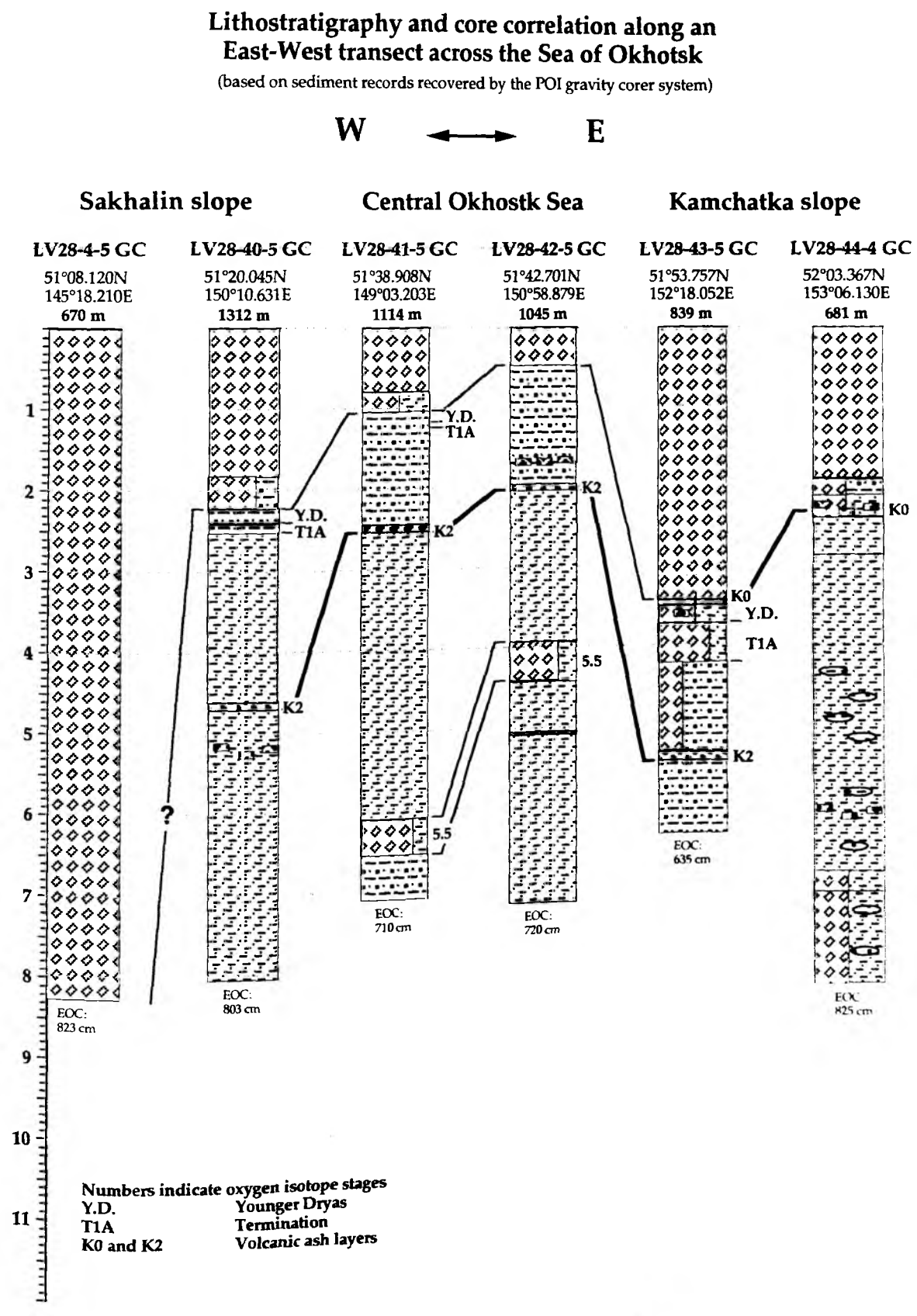

Fig. 4.33: Lithostratigraphic classification of central Okhotsk Sea sediment records (retrieved by POI) and core correlation based on lithology along an East-West transect.

Strongly bioturbated diatomaceous oozes with enhanced carbonate and total organic carbon concentrations exhibiting a pronounced decrease in the magnetic susceptibility records appear to be typical for interglacials. Oxygen isotope stages 5.5 and 9.1 show well-established pure diatomaceous oozes in cores LV28-40-4, LV28-42-4, LV28-43-4, and LV28-44-3, whereas interglacial substages 5.1, 5.3, 7.1, 7.3, 7.5, and 9.3 rather exhibit less diatomaceous and thus more olive-gray silty deposits. Nevertheless, due to both their olive color and the decreasing magnetic susceptibilities, these substages are clearly distinguishable from overlying and underlying successions in many cores investigated. It has to be considered, however, that the diatomaceous horizons did not simultaneously begin to form all over the Okhotsk Basin. Especially in the peripheric areas, it was formed later due to progressive environmental warming.

Glacial sediments

Glacial sediments consisting of dark-gray sandy to clayey silt and containing abundant dropstones of largely varying size (few mm to ca. 10cm) typically occur during glacial stages 2, 6 and 8. The dominating portion of detrital material causes high magnetic susceptibilities, partly enhanced by the significant influence of coarse ice-rafted dropstones. Calcareous shell fragments occur, but are rare. Opal concentrations decline below 10% (unpubl. data). Greenish diagenetic horizons are characteristic for the glacial deposits and may be related to the formation of authigenic clays (hydrotroillite).

Distinct variations in the coarse fraction (sand, pebbles), magnetic susceptibility values, and slightly varying carbonate and opal concentrations in these deposits suggest short but severe environmental changes even during glacial times. In fact, during glacial stages 6 and 8, the substages 6.3, 6.5, and 8.5 can be differentiated in cores LV28-41-4, LV28-42-4, and LV28-44-3.

Transitional sediments

The transition from peak glacial to peak interglacial climatic conditions is reflected in a "transitional type" of sediment characteristic for oxygen isotope stages 3, 4, and substages 5.2, 5.4, 6.3, 7.2, and 7.4 (best seen in cores LV28-41-4 and LV28-42-4). It is dominated by terrigenous components, although the diatom concentrations may gradually increase from cool (poor to weakly diatomaceous) to warm periods (diatomaceous), obtaining their maximum within the interglacial diatomaceous oozes. Accordingly, the magnetic susceptibility values exhibit a pronounced variability. Grain sizes vary between sandy silt and clayey sandy silt. The dark olive-gray to olive-gray (dependant on opal content) sediment is homogenous and includes reworked lenses of diatomaceous ooze due to strong bioturbation. Occasionally, small pebbles, sand layers, streaks and lenses occur. Foraminifers are common, and calcitic shell fragments can occasionally be observed even in deeper core segments.

The rapid change from relatively warm biogenic to cool terrigenous horizons also observed in the Bering Sea and the NW-Pacific (Bezrukov and Romankevich, 1960; Gorbarenko et al., in press.) is typically expressed in sharp lithological boundaries. Instead, the transition from cool to warm climates is gradually reflected in progressively increasing opal and carbonate concentrations from poor or weakly diatomaceous to strongly diatomaceous sediments. Especially, the transition from the Last Glacial Maximum (LGM) to the Holocene is represented as a two-step warming in cores LV28-40-4 and LV28-43-4. Glacial conditions successively improved (Termination 1A, ca. 12 ky B.P., Gorbarenko et al., in press), followed by a climatic rebound to glacial conditions (Younger Dryas at 10.300 yrs B.P.), and finally succeeded by the gradual climatic improvement of Termination 1B (ca. 9 ky B.P., Gorbarenko et al., in press), which culminated in Holocene optimum conditions.

Biostratigraphy

Two sediment records (LV28-40-4, LV28-43-4) were sampled in 10cm-intervals over the expected range of MIS 3 to determine the extinction of the radiolaria *Lychnocanoma nipponica sakaii* using the sediment fraction >40um. The last occurrence (LO) of *L. nipponica sakaii* occurred in core LV28-40-4 at 535±5 cm (Fig. 4.30) and in core LV28-43-4 between 540 and 560cm sediment depth. Morley et al. (1982) and Morley and Nigrini (1995) reported the last occurrence of *L. nipponica sakaii* in Pleistocene sediments from the northwest Pacific to have appeared between 46 and 54 kyr with most of the levels clustered around 49 kyr. This is corroborated by recently dated oxygen isotope records from the Okhotsk Sea (Gorarenko et al., in prep). At both Okhotsk Sea records, linear interpolation between the ages of mid-isotope stage 4 (64 kyr) and the ash layer K2 (26 kyr) also suggested an age of about 49 kyr. Thus, we used the LO of *L. nipponica sakaii* as a stratigraphic control point and transferred this age to the other sediment records by correlating the magnetic susceptibility records.

Tephrachronology

Mineralogical investigations previously carried out in the Sea of Okhotsk allow to identify several volcanic ashes within the sedimentary records, which may serve as stratigraphic time markers (Fig. 4.32, Fig. 4.33). Correlations with known material from the Kurile and Kamchatka Islands ground eruptions were carried out by Braytseva et al. (1996). Based on the results of radiocarbonic dating and oxygen isotope statigraphy (Gorbarenko et al., in press), reliable information on the stratigraphic position and the age of fresh volcanic ash layers was obtained. Two distinct ash layers being present in our cores were identified as ash layers K0 and K2, which are subsequently described in detail. At the base of core LV28-64-5 we found a thick ash layer which most probably relates to explosive volcanism on Hokkaido Island (Japan) ca. 32-35 kyr B.P. In addition, 5 new ashes previously unknown in the central Sea of Okhotsk were found in sediments of oxygen isotope stages 7 and 9 (LV28-41-4 and LV28-42-4). The

representative mineral composition of ashes found in sediment cores from the 1998 expedition is listed in Table 4.1.

Two prominent ash layers in the Sea of Okhotsk previously described (Tr and K3) were not found in our cores, unfortunately. The ash layer Tr resembles K0 and dates back to ca. 8300 yrs B.P. (Gorbarenko et al., in press.). The most probable source of Tr is the explosive eruption of the Tao-Rusyr volcano (Onekotan Island).
K3 is dated back to about 60000-65000 years (the upper part of isotope stage 4). Taking the latitudinal distribution pattern of K3 into account, the major eruption center is supposedly one of the volcanoes located in the middle part of the Kurile Island Arc (from Onekotan Island to Urup Island).

Volcanic ash layer K0

Ash layer K0 (average thickness 2cm) contains light-gray silt with admixtures of fine sand. It mainly consists of colorless volcanic glass of fluidal-porous appearance. Vesicular glass is only present in minor quantities. The reflection index (N) is 1.495-1.500. The ash layer is characterized by a clinopyroxene-orthopyroxene-magnetite association. The ratio of clinopyroxene to orthopyroxene (Cpx/Opx) varies from 0.96 to 2.14. The characteristic feature of K0 is the enhanced amount of brown-greenish hornblende. According to AMS ^{14}C-datings, K0 is dated 8300 years B.P. (Gorbarenko et al., 1998). The potential source of the pyroclastics is the explosive eruption (100 m^3) of the volcano "Kurile Lake" (Southern Kamchatka) (Braytseva et al., 1996).

The ash layer K0 was found at two sites: LV28-44 and LV28-43. It appears as fine, white-colored silt. The thickness of K0 varies considerably in the sediment records. Glasses commonly exhibit a fluidal texture and were observed at 345-349 cm and 306-315 cm in cores LV 28-43-5 and LV 28-43-4, respectively, and at 224-235 cm and presumably at 194-212 cm in cores LV 28-44-4 and LV 28-44-3, respectively. Due to the intensive bioturbation, the ash layer is strongly deformed, mainly consisting of single lenses from 2 mm to 2 cm in size. Numerous rounded lenses, oriented in different directions and filled with white volcanic ash (former tubes generated by burrowing organisms) were found in the underlying sediments 10-25 cm below the ash.

Volcanic ash layer K2

Ash layer K2, commonly 2-5 cm thick, is present in central parts of the Sea of Okhotsk. This layer contains gray silty-sandy ashes with a typical reddish tinge. Colorless volcanic glass of fragmentary-porous appearance, and - to a lesser degree - fluidal-porous appearance with numerous bubbles and cavities prevail. The reflection index (N) is 1.502-1.504. The content of crystalloclastics is below 10%. The ratio of clinopyroxene to ortopyroxene is highly variable

even within one layer, mainly due to size-variations of the pyroclastic material (differentiation process). The content of magnetite is approximately 38.4%. AMS ^{14}C-dating determines the age of the K2 layer as approximately 26000 years (Gorbarenko et al., in prep.). The most probable source for the pyroclastics are large explosive eruptions of the South Kamchatka volcanoes (e.g. Gorelaya Sopka, Opala, Ksudach, Kurile Lake).

K2 was found at the following sites: LV 28-2-4 (475-475.5 cm), LV 28-37-1 (342-344 cm), LV 28-40-4 (373-378 cm), LV 28-40-5 (462-464 cm), LV 28-41-4 (84-91 cm), LV 28-41-5 (242-247 cm), LV 28-42-4 (139-146 cm), LV 28-42-5 (194-204 cm), LV28-43-4 (465-468 cm), and LV28-43-5 (533-544 cm). The thickness of K2 increases from several mm (LV 28-2-4) in the western Sea of Okhotsk to ca. 11 cm (LV 28-43-5) towards Kamchatka. Size differentiation of pyroclastics is observed within the thickest layers. The light-gray silt of the lense-like fluidal texture present at the base is overlain by the reddish-gray ash layer with a clearly visible gradient from coarse-grained sand to sandy silt.

The investigated K2 ash layers are characterized by the predominance of pyroxene and magnetite (core LV28-41-5: 242-247 cm; core LV28-42-5: 194-196 cm; core LV28-43-5: 343-345 cm). Within all layers, orthopyroxene typically dominates over clinopyroxene. Practically all grains of pyroxene show a volcanic glass coating with short-prismatic idiomorphic crystals with smoothed face, and often crystal aggregates. Thin and long-axis prismatic apatite crystals with volcanic glass coatings are abundant. Magnetite also exhibits volcanic glass coatings.

Volcanic ash layer Spfa 1,2

At the base of core LV28-64-5 (1108-1113 cm) off southern Sakhalin, a thick, light-gray layer of sandy to silty volcanic ash appears. Its volcanic glass is composed of transparent thin-walled bubble fragments. The absence of crystalloclastics is most typical. Moreover, the content of heavy minerals (clinopyroxene, ortopyroxene, amphibole and magnetite) is very low (only a few singular grains). This type of volcanic glass is most probably related to the ash layer Spfa1 being present in the Sea of Japan and being generated by the explosive volcanism of the Shikotsu volcano on Hokkaido Island. The age is approximately 32-35 ka (Katsui, 1963; Minato et al., 1972).

Magnetic susceptibility

Fluctuations in magnetic susceptibility are indicative of changes in terrigenous sediment supply (magnetic minerals). In the Okhotsk Sea, according to the available ^{14}C-dated oxygen isotope records (Gorbarenko, 1991, Gorbarenko, unpublished data), high magnetic susceptibility values reflect an increased deposition of ice-rafted debris during glacials, whereas low values are associated with increased biogenic opal deposition during peak warm stages (eg. stage 5.5 or Holocene). Hence, fluctuations in magnetic susceptibility can be used to identify

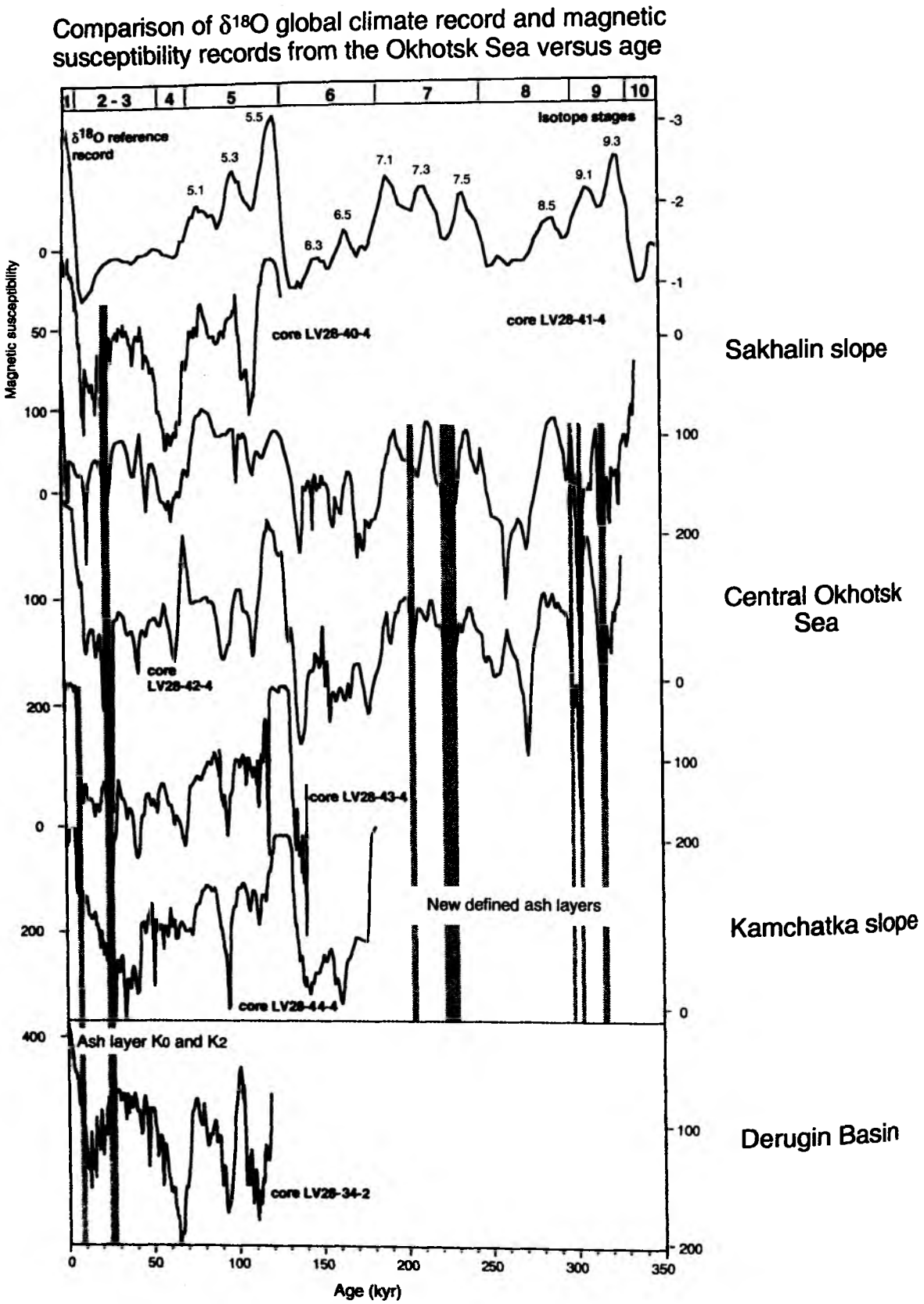

Fig. 4.34: *Preliminary age model of Okhotsk Sea sediment records. The oxygen isotope records (Bassinot et al., 1997) indicate cyclic changes that are also reflected in the magnetic susceptibility records. Oxygen isotope stages and substages are numbered. Shaded intervals mark ash layers.*

glacial/interglacial cycles as reflected in $\delta^{18}O$ global and regional climate records (Tiedemann and Haug, 1995; Gorbarenko et al., in press). The good correlation between Okhotsk Sea magnetic susceptibility and isotope records from stages 1-5 allows to use the $\delta^{18}O$ global climate record (Bassinot et al., 1997) to identify and date several substages within stages 4 to 9. This is demonstrated in Fig. 4.34. However, ash layers like K2 that are rich in magnetic minerals may change the basic climate signal by generating strong peaks in magnetic susceptibility (Fig. 4.31). Especially the basic structure in stage 9 (cores LV28-41 and LV28-42) is strongly influenced by the occurence of three ash layers. By deleting these intervals from the magnetic susceptibility record, two interstadials are recognized as suggested by the global climate record (event 9.1 and 9.3). Moreover, abrupt peaks in magnetic susceptibility values occasionally result also from larger dropstones (>3 cm in diameter), which are more common during glacials than during interglacials.

The onset of Termination Ia (12.5 kyr) and the Younger Dryas (10.3 kyr) are also easy to recognize in magnetic susceptibility records if the time resolution is high enough (Fig. 4.30). Available ^{14}C-dated magnetic susceptibility records from the central and western part of the Okhotsk Sea indicate that Termination Ia is associated with a strong drop in magnetic susceptibility values as observed in most of our records. The following climatic rebound of the Younger Dryas is marked by a short maximum that is caused by an increase in clay relative to biogenic opal. The subsequent decrease in magnetic susceptibility is marked by an increase in biogenic opal accumulation reaching maximum values during the last 6 kyr. This decrease in magnetic susceptibility is interupted by a small peak if ash layer K_0 (8.3 kyr) is present. A different pattern in magnetic susceptibility, however, may occur in the southeastern part of the Okhotsk Sea where nutrient-rich Pacific water of the Kamchatka Current triggers changes in the paleoproductivity. The expected magnetic susceptibility pattern might be analogous to records from the southern Bering Sea and the western periphery of the West Subarctic Pacific Gyre (Gorbarenko et al.,1996), where the increase in biogenic opal accumulation and the associated decrease in magnetic susceptibility starts close to the onset of Termination IA.

No detailed age model is developed for sediment profiles from sites LV28-4 at the upper slope off Sakhalin and no age model is provided for site LV28-64 at the northwestern slope of the Kurile Basin. At cores LV28-4-4 (-5), the magnetic susceptibility record is characterized by extremely low values and small amplitude fluctuations (Fig. 4.31). On the one hand, this may result from sulfate reduction. On the other hand, most of the sediment records consist of diamagnetic diatomaceous ooze. Hence, the persistingly high biogenic opal contents suggest a high resolution Holocene record (younger than 10kyr) with sedimentation rates higher than 1 m/kyr. At site LV28-64, the structure of the magnetic susceptibility curve shows no clear correlation to other records, except for the upper 250cm which may define the last 15 kyr. A considerable redeposition of sediment is indicated by two turbidites. The mineralogy of the ash

Table 4.1: Composition of heavy minerals in the Sea of Okhotsk (in %).

N st.	Depth, cm	Cpx	Opx	ΣHb	bgHb	bHb	gHb	OHb	Ilm	Br	Rt	Ep	Gar	Zi	Ap	Sph	Tou	An	Chl	Ol	Act	ΣMl	Ca	Py	Ba	Mgt	Cr	Leu	Sld
LV28-2-4	170-175	12.84	6.76	25.61	25.34	0.34	0.00	0.00	3.04	0.68	10.47	21.96	3.31	0.68	1.01	0.68	0.00	0.00	3.04	0.00	2.03	3.38	0.00	0.00	0.00	2.70	0.68	0.34	0.68
LV28-2-4	350-360	11.08	6.65	18.56	18.28	0.28	0.00	0.00	0.83	0.83	36.29	11.08	1.66	0.28	0.28	0.00	0.00	0.00	2.22	0.00	0.83	6.09	0.55	0.28	0.00	1.39	0.00	0.00	1.11
LV28-2-4	460-470	15.36	26.95	14.50	14.50	0.00	0.00	0.00	1.35	0.81	18.87	6.47	1.08	0.00	0.54	0.54	0.54	0.00	1.62	0.00	1.08	2.70	0.00	0.00	0.81	5.93	0.00	0.00	0.27
LV28-2-4*	470-475	15.41	46.51	5.23	4.94	0.29	0.00	0.00	1.74	1.45	5.81	3.49	0.58	0.00	0.29	0.00	0.00	0.00	0.87	0.00	0.58	0.87	0.00	0.00	0.29	16.28	0.00	0.29	0.00
LV28-4-5	0-10	10.31	4.47	24.74	24.05	0.34	0.00	0.34	3.44	2.06	17.18	15.12	2.41	1.03	1.37	0.00	0.00	0.00	1.72	0.00	1.03	1.03	0.34	5.50	0.00	6.87	0.34	0.34	0.34
LV28-4-5	660-670	7.45	5.88	22.75	22.75	0.00	0.00	0.00	2.75	2.35	16.08	16.08	1.96	0.39	1.57	1.18	0.00	0.00	1.57	0.00	0.78	9.41	0.00	7.45	0.00	1.57	0.00	0.00	0.78
LV28-16-1	0-10	15.34	1.70	25.85	25.28	0.57	0.00	0.00	8.24	0.00	6.53	19.60	5.68	2.27	0.85	1.99	0.00	0.00	1.99	0.00	1.99	2.84	0.28	0.00	0.00	3.69	0.28	0.85	0.00
LV28-17-1	0-10	12.10	5.19	23.34	23.05	0.29	0.00	0.00	9.51	0.00	7.49	20.46	5.19	2.02	1.44	2.02	0.86	0.29	2.31	0.00	1.73	2.59	0.29	0.00	0.00	2.88	0.00	0.00	0.29
LV28-17-1	45-50	7.49	4.79	26.05	25.75	0.30	0.00	0.00	11.68	0.00	4.19	20.36	6.89	2.99	1.20	1.50	0.00	0.00	1.80	0.00	1.50	1.50	0.30	0.00	0.00	7.78	0.00	0.00	0.00
LV28-20-3	0-5	13.02	3.85	28.11	28.11	0.00	0.00	0.00	4.44	0.59	17.16	15.68	0.89	0.30	0.59	0.59	0.00	0.59	3.85	0.00	1.48	4.73	0.30	0.00	0.00	2.96	0.30	0.59	0.00
LV28-20-3	35-40	14.11	3.90	27.93	27.63	0.00	0.00	0.30	3.00	0.30	14.11	23.12	1.80	0.60	0.00	0.00	0.00	0.00	1.80	0.00	1.80	6.61	0.30	0.00	0.00	0.60	0.00	0.00	0.00
LV28-20-3	135-140	14.02	3.35	24.39	24.09	0.00	0.00	0.30	3.05	0.00	18.90	15.55	0.30	0.30	0.61	0.91	0.00	0.00	1.52	0.00	0.91	13.41	0.61	0.00	0.00	1.83	0.00	0.30	0.00
LV28-20-3	190-195	11.80	3.24	31.56	31.27	0.29	0.00	0.00	2.06	0.00	19.76	15.63	2.06	1.18	0.88	0.59	0.00	0.00	2.06	0.00	1.47	6.78	0.00	0.00	0.00	0.88	0.00	0.00	0.00
LV28-20-3	280-290	10.12	3.47	25.72	23.70	0.29	1.45	0.29	3.18	0.00	26.88	12.14	1.45	1.16	0.58	1.16	0.00	0.00	3.18	0.00	0.29	9.25	0.29	0.00	0.00	0.87	0.00	0.00	0.29
LV28-21-1	0-10	11.30	6.38	26.67	25.80	0.87	0.00	0.00	2.61	0.00	15.36	17.68	2.03	0.87	1.45	0.58	0.00	0.00	2.90	0.00	2.03	5.22	0.29	0.29	0.00	4.35	0.00	0.00	0.00
LV28-21-1	25-30	8.88	4.44	31.36	30.77	0.00	0.59	0.00	2.96	0.30	16.57	18.05	0.89	1.48	1.48	0.00	0.00	0.00	1.48	0.00	0.89	9.17	0.30	0.00	0.00	1.78	0.00	0.00	0.00
LV28-21-1	90-95	9.37	6.34	26.89	25.98	0.91	0.00	0.00	3.93	0.00	16.62	18.43	1.51	0.91	1.81	0.30	0.00	0.00	2.42	0.00	1.81	8.76	0.30	0.00	0.00	0.60	0.00	0.00	0.00
LV28-21-1	150-160	8.02	2.78	27.78	27.16	0.62	0.00	0.00	2.78	0.00	22.84	15.12	0.93	0.62	0.00	1.23	0.00	0.00	4.32	0.00	0.93	11.73	0.00	0.00	0.00	0.62	0.00	0.00	0.31
LV28-21-1	170-180	13.94	3.94	31.82	31.82	0.00	0.00	0.00	0.91	0.00	16.06	16.06	1.82	0.61	0.91	0.91	0.00	0.00	3.03	0.00	0.30	8.48	0.30	0.00	0.00	0.91	0.00	0.00	0.00
LV28-21-1	190-200	10.95	9.17	27.22	26.04	0.59	0.30	0.30	2.96	0.00	9.76	20.71	2.66	0.30	1.78	0.30	0.00	0.00	1.78	0.00	2.07	4.14	0.00	3.55	0.00	2.66	0.00	0.00	0.00
LV28-25-1	30-40	5.08	2.54	4.13	4.13	0.00	0.00	0.00	2.22	0.00	2.54	0.00	0.00	0.32	0.00	0.00	0.00	0.00	0.00	0.00	0.00	0.32	0.00	0.32	82.54	0.00	0.00	0.00	0.00
LV28-25-1	110-120	10.81	6.31	6.31	5.71	0.30	0.00	0.30	1.20	0.00	6.01	3.30	0.30	0.00	0.00	0.30	0.00	0.00	0.60	0.00	0.30	1.20	0.00	13.51	48.35	1.50	0.00	0.00	0.00
LV28-25-1	150-160	5.41	5.71	6.31	6.01	0.30	0.00	0.00	1.50	0.00	1.50	2.70	0.30	0.00	0.00	0.00	0.00	0.00	0.30	0.00	0.00	0.00	0.00	42.04	33.33	0.90	0.00	0.00	0.00
LV28-34-2	33-34	20.88	20.00	15.00	14.71	0.00	0.00	0.29	3.24	0.29	17.94	6.76	0.29	0.00	0.59	0.29	0.29	0.00	1.18	1.18	0.29	1.76	0.00	1.47	2.35	6.18	0.00	0.00	0.00
LV28-34-2*	309-310	22.09	32.21	1.53	1.53	0.00	0.00	0.00	1.84	0.31	10.12	0.61	0.00	0.00	2.45	0.00	0.00	0.00	0.00	0.31	0.00	1.23	0.00	0.92	7.98	18.40	0.00	0.00	0.00
LV28-37-1*	342-344	11.99	22.71	0.32	0.32	0.00	0.00	0.00	1.26	0.00	7.57	0.32	0.00	0.00	0.00	0.00	0.00	0.00	0.00	0.00	0.00	0.63	0.00	4.42	38.17	12.62	0.00	0.00	0.00
LV28-40-5	200-210	13.50	7.98	26.99	24.23	0.61	0.61	1.53	6.44	0.00	11.96	17.79	2.15	0.61	0.61	0.92	0.00	0.00	1.23	0.00	0.61	3.37	0.31	0.00	0.00	5.52	0.00	0.00	0.00
LV28-40-5	420-430	21.41	12.23	15.60	15.29	0.31	0.00	0.00	3.98	0.00	15.60	12.54	1.53	0.00	0.31	0.00	0.00	0.31	2.14	0.00	1.22	3.98	0.31	0.00	0.00	8.87	0.00	0.00	0.00
LV28-40-5	760-770	15.28	6.67	20.83	19.17	0.83	0.00	0.83	2.22	0.00	9.72	17.22	1.67	1.39	1.11	0.83	0.56	0.00	2.22	0.00	2.50	8.33	0.28	0.00	0.00	9.17	0.00	0.00	0.00
LV28-41-5	15-25	18.60	10.67	24.39	22.56	0.91	0.30	0.61	3.66	0.00	12.80	6.40	2.13	0.30	0.30	0.00	0.00	0.61	0.30	0.30	0.91	3.35	0.91	0.30	0.00	14.02	0.00	0.00	0.00
LV28-41-5*	242-247	32.48	36.31	0.00	0.00	0.00	0.00	0.00	1.91	0.00	8.60	1.27	0.00	0.00	2.23	0.00	0.00	0.00	0.00	0.32	0.00	0.32	0.00	0.00	0.00	16.56	0.00	0.00	0.00
LV28-41-5	280-290	22.51	15.50	20.76	18.13	1.17	0.00	1.46	2.63	0.00	7.02	9.65	1.17	0.29	0.29	0.29	0.00	0.00	1.17	0.58	0.88	3.51	0.29	0.29	0.00	12.57	0.00	0.00	0.00

Table 4.1 cont: *Composition of heavy minerals in the Sea of Okhotsk (in %).*

N st.	Depth, cm	Cpx	Opx	∑Hb	bgHb	bHb	gHb	OHb	Ilm	Br	Rf	Ep	Gar	Zi	Ap	Sph	Tou	An	Chl	Ol	Act	∑Mi	Ca	Py	Ba	Mgt	Cr	Leu	Sid
LV28-41-5	550-560	12.39	9.67	23.87	23.26	0.00	0.00	0.60	4.53	0.00	12.69	15.11	1.51	0.30	2.42	0.00	0.00	0.00	2.72	0.00	1.81	4.23	0.30	0.00	0.00	8.16	0.00	0.00	0.00
LV28-42-5	0-15	24.23	18.10	12.88	12.27	0.31	0.00	0.31	2.15	0.31	10.12	12.88	1.53	0.00	0.92	0.31	0.00	0.00	2.45	0.00	1.84	1.53	0.61	0.00	0.00	9.82	0.00	0.00	0.31
LV28-42-5	172-178	21.86	18.86	14.07	12.28	0.90	0.30	0.60	2.10	0.30	11.08	11.98	0.60	0.00	1.20	0.30	0.30	0.00	1.80	0.30	0.30	1.20	0.00	0.00	0.00	13.77	0.00	0.00	0.00
LV28-42-5*	194-196	21.55	29.56	2.49	1.93	0.55	0.00	0.00	3.04	0.00	3.87	1.93	0.00	0.00	1.10	0.00	0.00	0.00	0.00	0.00	0.00	0.28	0.00	0.00	0.00	36.19	0.00	0.00	0.00
LV28-42-5	440-445	27.83	19.57	11.62	11.01	0.61	0.00	0.00	3.06	0.00	14.37	5.20	0.92	0.00	0.00	0.00	0.00	0.00	1.83	0.00	0.61	1.22	0.00	1.53	0.00	11.93	0.00	0.00	0.31
LV28-42-5	670-675	16.02	10.98	22.85	21.36	0.59	0.00	0.89	3.86	0.00	8.31	18.69	1.19	0.30	1.48	0.00	0.00	0.00	0.30	0.00	1.48	2.67	0.30	0.00	0.00	11.57	0.00	0.00	0.00
LV28-43-5	0-10	16.67	20.00	16.67	16.11	0.00	0.00	0.56	3.33	2.22	10.56	5.56	1.67	0.00	0.56	0.00	0.00	0.56	0.00	0.00	0.00	2.22	0.00	1.11	0.00	18.89	0.00	0.00	0.00
LV28-43-5	300-305	19.40	25.43	8.19	7.33	0.43	0.00	0.43	5.60	0.86	10.78	4.31	1.29	0.00	0.43	0.00	1.29	0.00	1.29	0.00	0.86	1.72	0.00	1.72	0.00	16.81	0.00	0.00	0.00
LV28-43-5*	343-345	18.21	28.66	8.36	7.76	0.00	0.00	0.60	5.37	0.60	16.72	2.99	0.00	0.00	1.19	0.00	0.00	0.00	0.00	0.00	0.60	2.39	0.00	0.00	0.00	14.93	0.00	0.00	0.00
LV28-43-5	400-405	21.85	14.77	34.77	31.08	1.54	0.31	1.85	1.23	0.00	9.23	4.31	0.00	0.00	1.23	0.00	0.00	0.00	0.62	0.00	0.00	1.85	0.00	0.00	0.00	10.15	0.00	0.00	0.00
LV28-43-5	590-595	26.95	24.55	9.58	9.28	0.00	0.00	0.30	2.99	0.00	11.98	2.10	1.50	0.00	0.90	0.00	0.30	0.00	0.60	0.00	1.20	2.69	0.30	0.00	0.00	14.37	0.00	0.00	0.00
LV28-44-4	0-15	25.95	22.52	10.31	9.16	0.38	0.00	0.76	5.34	0.00	11.83	6.87	1.91	0.00	0.00	0.00	0.00	0.38	1.53	0.00	0.76	1.15	0.00	1.15	0.00	10.31	0.00	0.00	0.00
LV28-44-4	142-150	22.63	17.74	22.63	20.80	0.00	0.00	1.83	1.22	0.61	11.62	3.06	1.53	0.31	0.00	0.00	0.31	0.00	2.14	0.00	1.22	3.36	0.00	0.61	0.00	11.01	0.00	0.00	0.00
LV28-44-4	255-260	19.50	12.69	40.25	37.15	0.00	0.00	3.10	2.17	0.00	7.74	1.55	0.93	0.31	0.93	0.00	0.00	0.00	1.24	0.00	0.00	1.86	0.00	0.00	0.00	10.84	0.00	0.00	0.00
LV28-44-4	675-680	25.22	18.40	9.50	8.31	0.59	0.00	0.59	2.37	0.00	15.73	3.86	0.89	0.00	0.30	0.00	0.00	0.00	2.97	0.00	0.59	1.78	0.00	0.00	0.00	18.40	0.00	0.00	0.00

Note to the table: Cpx - clinopyroxene, Opx - orthopyroxene, ∑Hb - sum of all hornblendes, bgHb - brown-green hornblende, bHb - brown hornblende, gHb - green hornblende, OHb - basaltic hornblende, Ilm - ilmenite, Br - iron oxides, Rf - rock fragments, Ep - epidote, Gar - garnet, Zi - zircon, Ap - apatite, Sph - sphene, Tou - tourmaline, An - sum of anatase, brukite, rutile, Chl - chlorite, Ol - olivine, Act - actinolite, ∑Mi - sum of different mica: colourless, green and brown, Ca - detrital carbonate grains, Py - pyrite, Ba - barite, Mgt - magnetite, Cr - Cr-spinel, Leu - leucoxene, Sid - siderite concretions.

* - ash interlayers.

layer that occurs at the base of the sediment profile allows no correlation to the known ash layers so far.

4.4.3 Sedimentology

Mineral composition of sediments in the Sea of Okhotsk

The investigation of the mineral composition in the sedimentary records of the E-W transect intends to decipher formation processes responsible for the different mineral associations with respect to the surrounding rock provinces ashore, volcanism, climate and the hydrodynamic conditions of the depositional environment. Especially, the analysis of the volcanoclastic sediment components allows to identify characteristic ash layers, which can be used for lithostratigraphic core correlation.

During the 1998 KOMEX cruise, 47 mineralogical analyses of the heavy mineral fraction (grain size 0.05-0.1 mm, specific weight >2.89 gr/cm^3) from both upper Pleistocene to Holocene deposits and volcanic ash layers were conducted.

In order to identify potential sources for the clastic material, the results of the mineralogical analysis were marked accordingly on a diagram showing the discriminant function values (Fig. 4.35). We applied the discriminant function equations which were previously calculated by generalizing the data on the mineralogical sediment composition in the world oceans (Derkachev & Nikolayeva, 1997) to specify distinct source areas and transport paths of heavy minerals.

The most pronounced mineral associations of the Sea of Okhotsk sediments (mean values on provinces) and, in addition, the most contrasting areas (e.g. the Gulf of Sakhalin influenced by Amur river supply and the volcanogenous-terrigenous complexes of the middle Kurile Islands) were marked on the discriminant functions diagram (Fig. 4.35).

The mineralogical composition off eastern and north-eastern Sakhalin Island (cores LV28-2-4, LV28-4-5, LV28-16-1, LV28-17-1, LV28-20-3, LV28-21-1) is represented by the epidote-hornblende association with an increased content of both the stable mineral group (especially garnet) and mica (Table 4.1). The formation of such mineral associations is most likely related to the weathering of granitic-metamorphic rocks in the source areas. In this respect, the Amur River plays an important role for the formation of the mineralogical sediment composition. Sea ice from the northwestern coastal areas, in addition, supplies considerable amounts of clastic material, which is clearly distinguishable on Fig. 4.35 (sites mentioned above and the Ayano-Okhotsk coast province). Both the enhanced (in comparison to the Amur mineral complex) content of pyroxene as well as the presence of pyroxene in association with epidote, chlorite, actinolite testify the weathering of weakly metamorphised volcanogenous rocks in the source

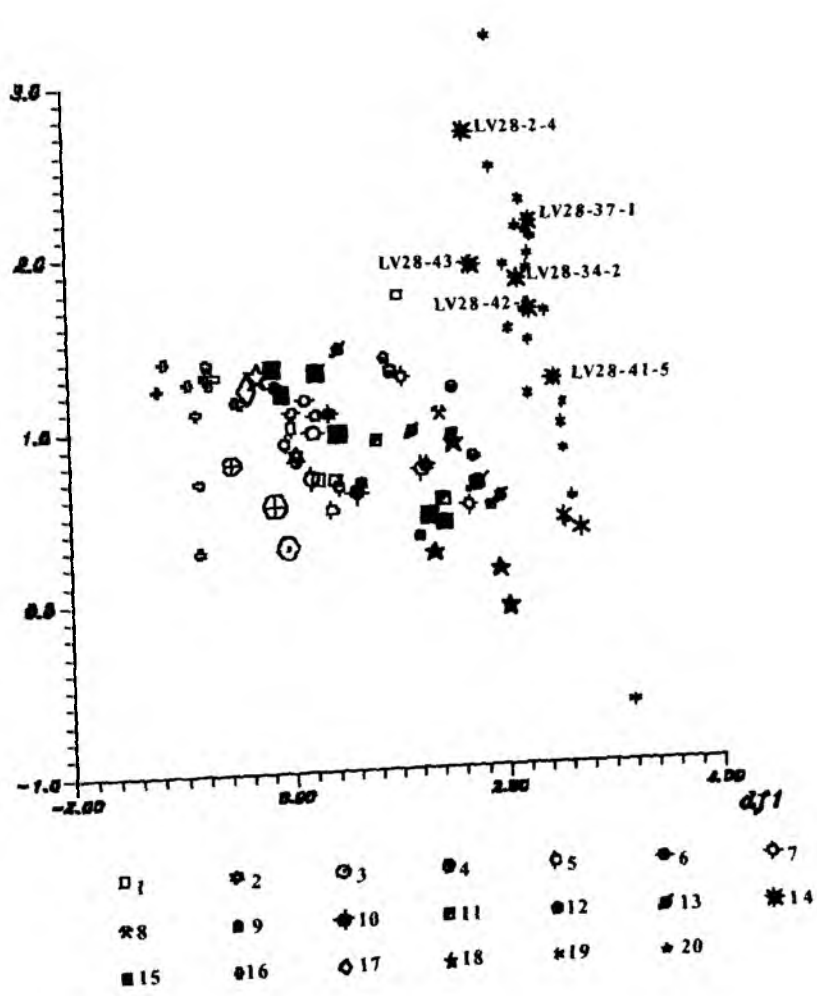

Fig. 4.35: *Mineral composition of the Sea of Okhotsk sediments on the plot of the discriminant functions values: 1-14 - the position of investigated stations on the discriminant functions plot: 1 - LV28-2-4; 2 - LV28-4-5; 3 - LV28-16-1; 4 - LV28-17-1; 5 - LV28-20-3; 6 - LV28-21-1; 7 - LV28-25-1; 8 - LV28-34-2; 9 - LV28-40-5; 10 - LV28-41-5; 11 - LV28-42-5; 12 - LV28-43-5; 13 - LV 28-44-4; 14 - ash layers. 15-20 - mean values of the mineral composition of different mineralogical provinces within the Sea of Okhotsk (Petelin, 1957): 15 - provinces of the northern part of the Sea of Okhotsk; 16 - province of Sakhalin Gulf; 17 - province of northern Sakhalin; 18 - province of southern Sakhalin; 19 - Kurile province; 20 - province of Kamchatka.*

Note to the figure:
The discriminant functions values were calculated in the following manner:

$$df1 = -5.678x_1 - 5.703x_2 - 5.738x_3 - 5.659x_4 - 5.705x_5 - 5.760x_6 - 5.743x_7 - 5.742x_8 + 571.785$$

$$df2 = -59.797x_1 - 59.714x_2 - 59.739x_3 - 59.717x_4 - 59.764x_5 - 59.825x_6 - 59.704x_7 - 59.674x_8 + 5976.46$$

where x_1 - sum of clinopyroxene and olivine, x_2 - orthopyroxene, x_3 - brown-green and green hornblendes, x_4 - brown and basaltic hornblendes, x_5 - sum of epidote, actinolite and chlorite, x_6 - sum of garnet, anastase, rutile, staurolite, anadalusite, korund, sillimanite, tourmaline and calcite, x_7 - sum of zircon, sphene, and apatite, x_8 - sum of alkaline pyroxene and alkaline amphibole. With the calculation using discriminant functions only minerals could be accounted for used in the equations: their sum was taken for 100%; ore and authigenic minerals, mica, rock fragments were not considered.

areas, outcrops of which are known from the north-western coast of the Sea of Okhotsk (Okhotsk-Chukotsk volcanic belt of Mezozoic to Cenozoic age).

Within central parts of the Sea of Okhotsk, with increasing distance from the source areas the clastic material partly loses its specific features and combines characteristica of various mineral associations and the Kamchatka volcanogenous material (cores LV28-40-5, Lv28-41-5). The content of unaltered fragments and crystals of both hornblende and pyroxene with volcanic glass coatings increases.

Off Kamchatka, the quantity of volcanogenous-terrigenous material being characteristic for the Kamchatka volcanogenous complex increases (mainly clinopyroxene, orthopyroxene, magnetite). The abundance of minerals which are typical for granitic-metamorphic rocks (hornblende, epidote, garnet) is connected with both the mineral transfer via sea ice from the northwestern coast of the Sea of Okhotsk and the erosion of the granitic-metamorphic complex of the Western-Kamchatka ridge.

The limited quantity of investigated samples prevents any statement about the downcore mineralogical variation and the corresponding paleoceanographic relationships during upper Pleistocene/Holocene times. However, in some cores from the eastern and central parts of the Sea of Okhotsk, the tendency to the enhanced presence of granitic-metamorphic rocks in upper Pleistocene sediments is apparent. This is visible at stations LV28-43-5 (400-405cm) and LV28-44-4 (255-260cm).

The volcanic ash layers (Fig. 4.35) differ specifically from the mineralogical composition of the pelagic and hemipelagic sediments. They are characterized by the magnetite-clinopyroxene-orthopyroxene association (often with apatite admixture), which is typical for mature island arcs (Magmatic Mountain Rocks, 1987; Derkachev & Nikolayeva, 1997).

Approximation of sedimentation rates

Sedimentation rates are an important parameter for all statements about changes in sediment deposition, especially for quantitative estimates of accumulation rates, and thus are fundamental for reconstructing paleoenvironmental changes in the Sea of Okhotsk. Our preliminary age model provides information about temporal and spatial changes in sedimentation rates for sites from the East-West transect across the central Sea of Okhotsk and for one site from the Derugin Basin (Fig. 4.36). Estimates of sedimentation rates are based on linear interpolation between age control points (see Chapter 4.3.2). As expected, the hemipelagic sediment records off Kamchatka and Sakhalin are characterized by high amplitude variations in sedimentation rates ranging from 3 to 35cm/kyr during the last 180 kyr. Slightly lower sedimentation rates of 4 - 17cm/kyr mark the Derugin Basin. In contrast, the pelagic sedimentation rates from the central

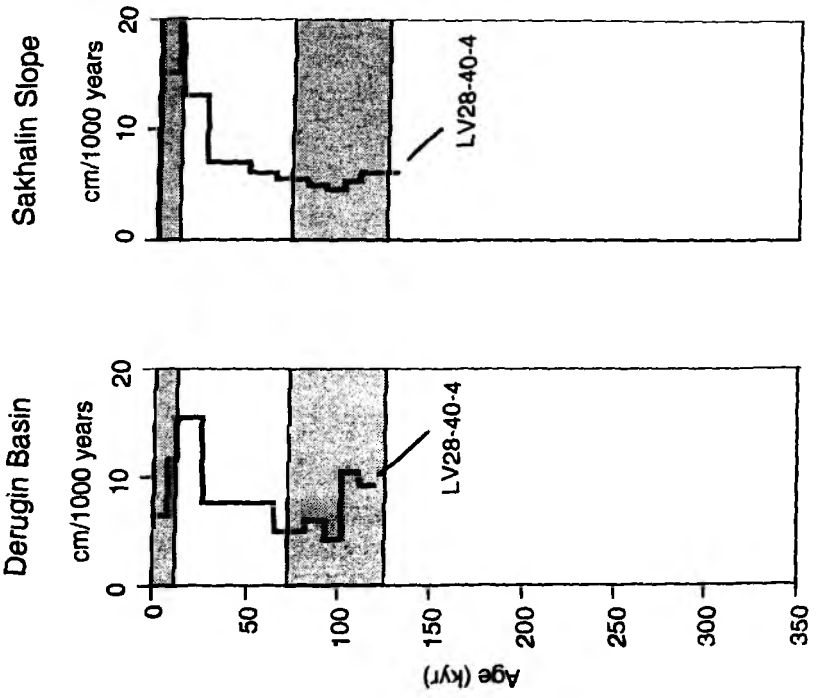

***Fig. 4.36**: Temporal and spatial variabilty of sedimentation rates along the West-East transect across the central Sea of Okhotsk and in the Derugin Basin. Shaded areas indicate warm stages.*

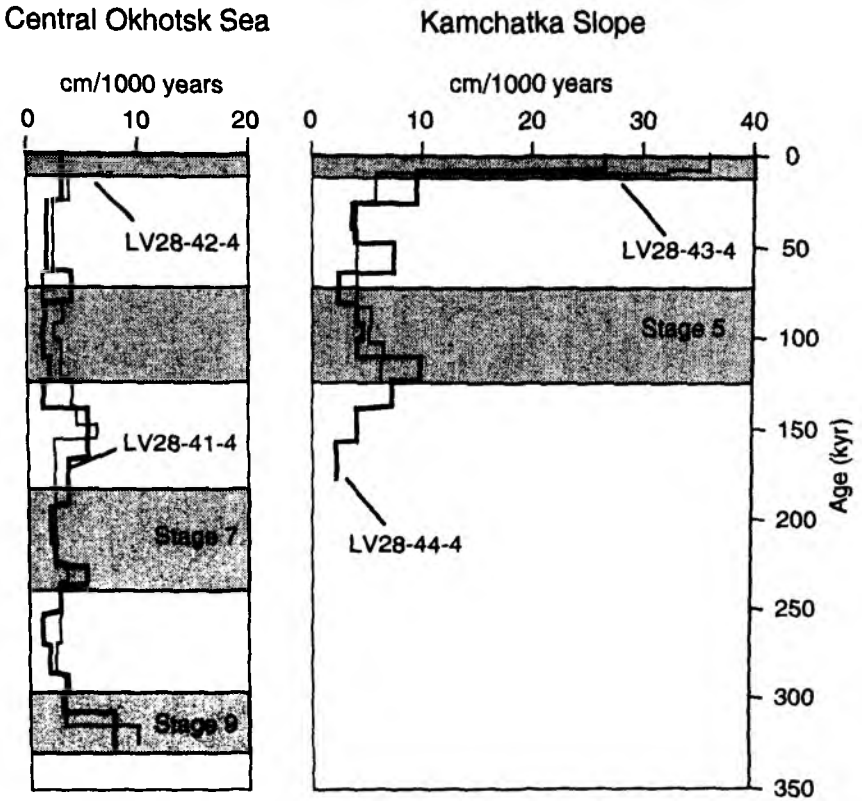
Central Okhotsk Sea
cm/1000 years
0
10
20
LV28-42-4
LV28-41-4
Stage 7
Stage 9
Kamchatka Slope
cm/1000 years
0
10
20
30
40
LV28-43-4
Stage 5
LV28-44-4
0
50
100
150
200
250
300
350
Age (kyr)

Sea of Okhotsk are distinctly lower and fluctuate only between 2 and 9cm/kyr over the last 320 kyr. Considering the last 200 kyr, the differences in sedimentation rates between the hemipelagic and pelagic records are more pronounced during peak warm stages including the glacial Terminations I and II, when maxima in sedimentation rates occur together with maxima in biogenic silica percentages. The hemipelagic sedimentation rates as well as the accumulation rates of biogenic silica are higher by factor 3 - 6 and clearly reflect the high productivity belts that are affected by the nutrient-rich Kamchatka Current, and off Sakhalin and in the Derugin Basin by the fluvial nutrient input of the Amur river. This suggests that the nutrient supply triggered by the influence of the Kamchatka Current and the Amur river is enhanced during interglacial times when ice cover is less pronounced. During the glacials, the most important feature is that the biogenic silica belt disappears and is displaced by deposition of large amounts of ice-rafted detritus and in addition by the supply of clay that originates from rivers (e.g. Amur) and exposed shelf areas. However, glacial sedimentation rates are in general lower (except for stage 6, central Sea of Okhotsk) as well as the differences between pelagic and hemipelagic sedimentation rates than during warm stages.

4.4.4 Comparison of POI- and Geomar-gravity coring systems

Magnetic susceptibility records offered an excellent opportunity to compare sediment profiles retrieved with the POI- and with the GEOMAR-gravity corer from equal sites because magnetic susceptibility was measured every second centimeter at POI and GEOMAR sediment records. In general, magnetic susceptibility records obtained from equal sites are in good agreement and allow a detailed visual correlation of distinct structures. This is demonstrated in Fig. 4.37 for sites LV28-34, LV28-40 and LV28-42. However, the correlation between identical time intervals indicate that the sediment profiles from GEOMAR cores are compressed or that the sediment profiles from POI cores are expanded. Estimated differences in the total sediment length from defined horizons to the top of the records are summarized in Table 4.2 for sites LV28-2, -40 to -43. In general, these estimates suggest that the POI sediment records are expanded by about 9.4 %, except for site LV28-41 (36.5 %). Holocene sediments (110 cm) were substracted from the POI core in calculations.

A detailed correlation of the sediment thickness between equal sediment sections indicates only small differences ranging between -20 and + 10cm (Fig. 4.37, section length in POI cores minus section length in GEOMAR cores). Because the ship's drifting (1-2 miles) prevented double-coring at identical positions, smaller differences are expected due to local variations in (*in situ*) sediment thickness. Larger deviations of -40 to + 36 cm (Fig. 4.37), however, occur above or below ash layers, although without revealing a characteristic pattern of positive or negative differences between equal sections of POI and GEOMAR records. From this, we may speculate that larger differences are restricted to intervals where abrupt changes in lithology are accompanied by distinct changes in physical properties, e.g. at ash layers that furthermore

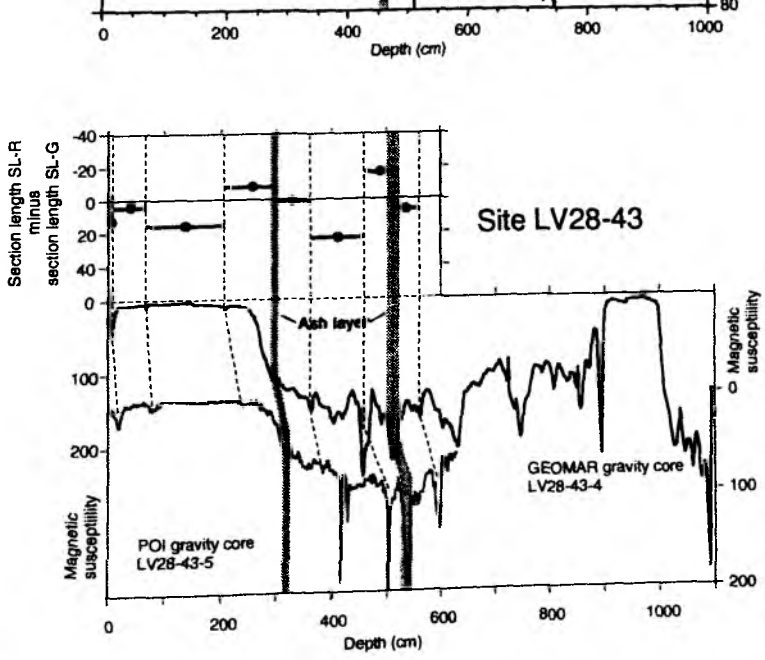

Fig. 4.37: Depth correlation and comparison of sediment thickness between sediment records from POI and GEOMAR gravity cores for sites LV28-40, -42, -43.

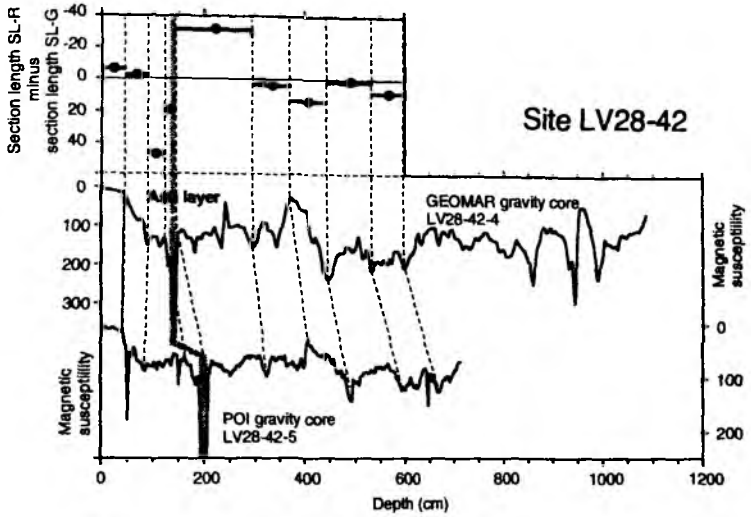
Section length SL-R minus section length SL-G
-40
-20
0
20
40
Site LV28-42
Ash layer
GEOMAR gravity core LV28-42-4
Magnetic susceptility
0
100
200
300
Magnetic susceptility
POI gravity core LV28-42-5
0
100
200
0
200
400
600
800
1000
1200
Depth (cm)

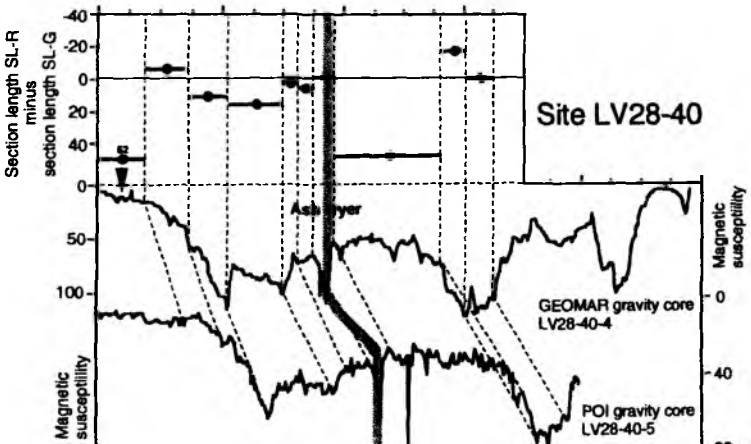
Section length SL-R minus section length SL-G
-40
-20
0
20
40
Site LV28-40
Ash layer
Magnetic susceptility
0
50
100
GEOMAR gravity core LV28-40-4
Magnetic susceptility
POI gravity core LV28-40-5
0
40

St.No	Ash K_0				Ash K_2				Boundary IS 3/4,L28-2; IS 3 base,L28-43				Boundary IS 4/5				IS,5,5 middle				MS min at IS 6-8			
	L SR	ΔL	Δ/L %	D_L SR	L SR	ΔL	Δ/L %	D_L SR	L SR	ΔL	Δ/L %	D_L SR	L SR	ΔL	Δ/L %	D_L SR	L SR	ΔL	Δ/L %	D_L SR	L SR	ΔL	Δ/L %	D_L SR
LV28-2					475	10	2.1	267.12	610	60	9.8	362.63												
LV28-40					462	85	18.5	205.4					780	13	16.6	382.31								
LV28-41					242	43	17.8	88.06									630	230	36.5	288.16				
LV28-42					194	60	30	93.31									425	40	9.4	204.01	590	60	10.2	297.3
LV28-43	345	45	13	107.71	533	8	1.7	207.14	600	40	7.1	244.67												

***Table 4.2**: Comparison of sediment thickness between POI and GEOMAR sediment records. Ash layers K_0 and K_2 and well defined events in magnetic susceptibility records (isotope stage boundaries) are used to estimate differences in core length (POI versus GEOMAR records) that occur between the top of the core and the outlined events.*

L = section length between core top and outlined events in POI cores (for ash layers, upper boundary is taken)

ΔL = total depth difference of identical levels between POI and GEOMAR cores in cm (note: difference is positive in all cores

ΔL,%- relative difference in %

D_L SR-integrated dry sediment masses in g/cm2 above of the outlined levels in POI cores

POI cores on average appear to be extended by 9.4 %. The large difference at site LV28-41 (36.5 %) is due to considerable sediment loss at the GEOMAR core (Holocene and stage 5.3) that occurred during the core handling on deck.

The upper 110 cm (Holocene) of the Russian core LV 28-41 was substracted from these core data for comparison with the German core.

often show a sharp bottom contact. Because neither coring systems has vacuum pumping effects during the coring process, it is reasonable to expect that the recovered sediment profiles generally become shorter compared to the *in situ* sediment sequence. This might be due to friction tension between the tube wall and the surrounding sediment during penetration. The larger tube-diameter of the POI coring system (147 mm) may also suppress compression effects during penetration more effectively than the GEOMAR coring system (115 mm). A stronger compression at GEOMAR records may result in a loss of time resolution and geological information. If the expected additional increase in dry densities and the associated decrease in sedimentation rates result in similar mass accumulation rates and thus balances the higher compression effect, then the GEOMAR coring system has the advantage of retrieving longer time intervals than the POI system. To address this question, high resolution records of dry bulk densities will be measured and compared after this cruise.

4.4.5 Conclusions and perspectives: Changes in the depositional environments

Central Okhotsk Sea (E-W- Transect) and Derugin Basin

Twelve sediment cores retrieved from 6 sites during the 28th cruise of *RV Akademik Lavrentyev* were taken along an E-W-profile within the central Okhotsk Sea covering an intermediate water transect of ca. 670m to 1370m (LV28-4, -40, -41, -42, -43, -44). An additional core was recovered from the Derugin Basin from ca. 1400m water depth. All lithostratigraphic units described in Chapter 4.3.2 (Lithostratigraphy) are present in these cores and could be traced laterally over wide areas. Figs. 4.32 and 4.33 exhibit the core correlation based on the lithology. This correlation is concluded from comparing the magnetic susceptibility records (Fig. 4.31).

Cores LV28-41-4 and -42-4 from the southern slope of the Institute of Oceanology Rise reach back presumably to oxygen isotope substage 9.3 (ca. 320 kyr) penetrating diatomaceous sediments at the base of the cores. These cores reveal the longest time sequence of normal pelagic sediment deposition that has ever been cored in the Sea of Okhotsk. They will serve as stratigraphic reference records. The records are marked by low sedimentation rates fluctuating between 2-10cm/kyr because changes in paleoproductivity are less extreme in contrast to the hemipelagic cores retrieved from the high productivity areas off Kamchatka and Sakhalin Island.

Based on smear slide investigations, the major differentiated sediment components show a typical pattern of variability through time (Fig. 4.38). Quartz mainly peaks during glacials (up to 40%) reflecting upper shelf erosion and thus an enhanced terrigenous flux to the deep basin. In contrast, the highest abundances of coccoliths and diatoms occur during the interglacials.

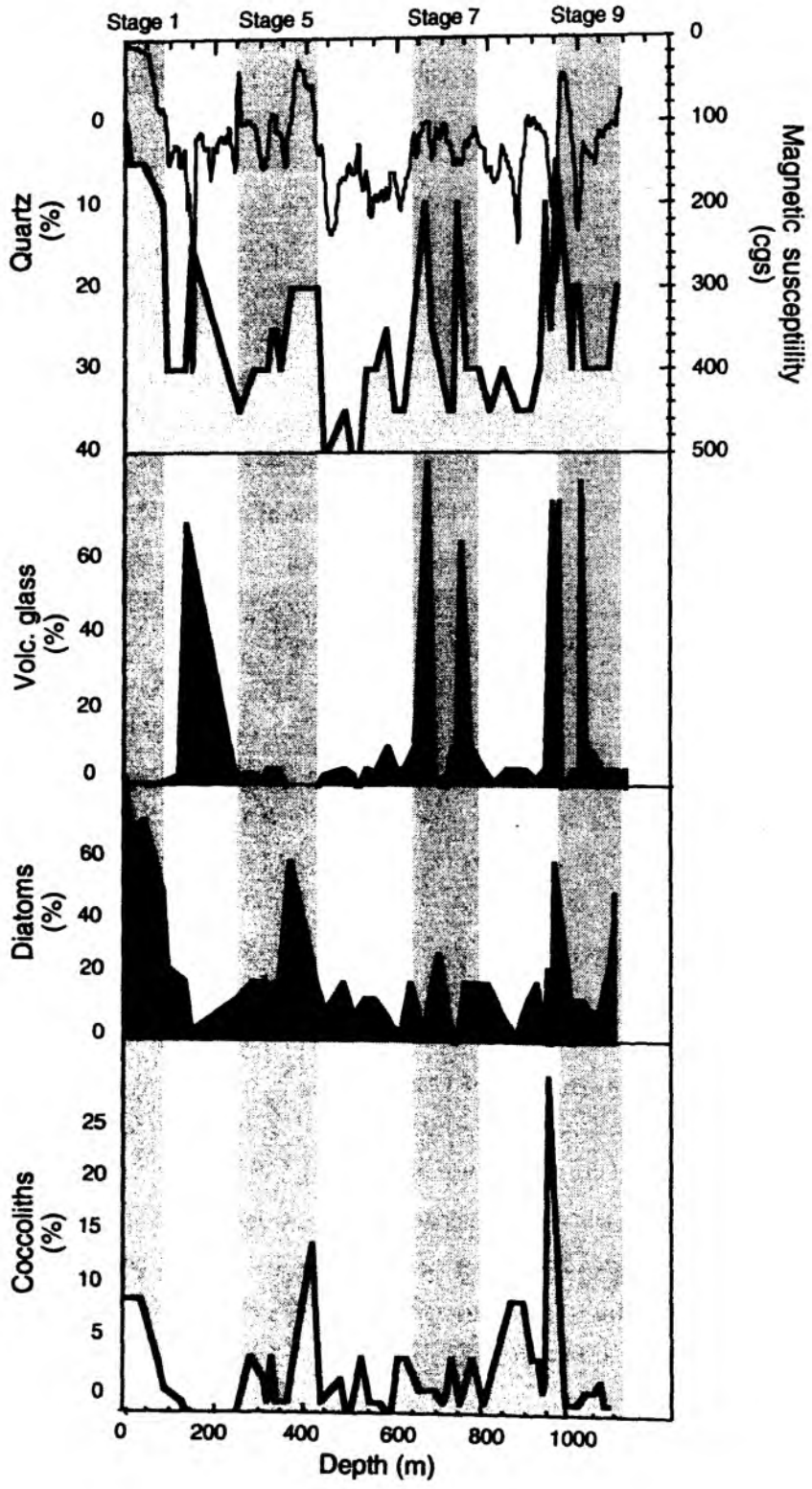

Fig. 4.38: *Preliminary results from smear slide analyses of core LV28-42-4 showing quartz, volcanic glass, diatom and coccolith contents in comparison to the magnetic susceptibility record. Shaded areas indicate interglacial stages.*

Distinct peaks of volcanic glass often occur together with enhanced quartz contents. These horizons accurately define volcanic ash layers even in lowermost parts of the core and serve as powerful stratigraphic time markers.

Favorable conditions for diatom productivity continued to occur during interstadials 8.5, 7.5, 7.3, 7.1, 5.5, 5.3, 5.1 and during Holocene times. The nearly similar appearance of the diatomaceous sediments favor similar environmental conditions which were subject to rapid changes through time. We suspect that during times of enhanced diatom production marine productivity was mainly initiated by high nutrient supply due to inflowing Pacific surface water masses (Kamchatka Current) favoring a stable water column with relatively warm surface waters comparable to the recent situation. The "Okhotsk Diochothermal Layer" most effectively prevents a vertical exchange of water masses during summer. Nutrients enriched in these surface waters can effectively be used up and therefore may contribute to the very high surface water productivity (Tally & Nagata, 1995). Largely ice-free conditions during most of the year may additionally have provided favorable environmental conditions for siliceous plankton growth.

The fact that Holocene and even stage 5-diatomaceous sediments are best established along the Kamchatka and Sakhalin continental slopes supports the idea that both the inflowing nutrient-rich Kamchatka Current and Amur river water mainly cause the enhanced surface productivity. Within the Okhotsk Sea central gyre, opal accumulation is distinctly lower (cores LV28-41, -42).

From the N-S-core-transect performed in 1996 (Nürnberg et al., 1996), it became evident that the Holocene diatomaceous ooze at the northernmost sites is less thick compared to the southern ones. This may partly be related to different sediment accumulation rates in both areas. It may, however, indicate a reduced plankton productivity due to less favorable conditions in the northern part of the Okhotsk Sea. Perennial sea ice coverage originating in the cold, shallow and low saline coastal waters in the north and subsequent drifting in a direction approximating the Okhotsk-Kurile current system may drastically reduce plankton growth. It may also indicate that the onset of surface productivity commenced earlier in the southern part contemporaneously with a progressively retreating ice cover from S to N and a stepwise northward intrusion of nutrient-rich Pacific surface waters. This assumption, however, needs to be proved by absolute age dating.

Most characteristic for the glacial sediments (e.g. stages 2-4, 6, and substages 5.2, 5.4, 9.2) is the shutdown in biogenic silica deposition and the depositional increase in ice-rated material. Enhanced occurrences of dropstones cover all size fractions (mainly small pebbles of ca. 0.5 cm, but also boulders up to 10cm). Since only single glacier systems existed onshore during

glacial times (e.g. Kamchatka mountain glacier) which were unlikely to have produced such enormous amounts of dropstones, sea ice is suggested to be the predominant transport agent for the coarse detrital material. Cliff fall and coastal adfreezing seem to be the most effective entrainment mechanisms for both angular and well-rounded dropstones of various sizes. Drifting ice subsequently distributed the pebbles basin-wide releasing its freight during ice-melt. The systematic investigation of ice-rafted detritus within the deep-sea sediments should allow to spatially and temporally reconstruct both the extension of glacial ice-coverage and varying transport directions.

The transition from pure glacial to interglacial environmental conditions is reflected in prevailing terrigenous sediment sequences being poorly to weakly diatomaceous. The increasing opal content, however, implies a rapid climatic improvement at the terminations. Since dropstones only rarely occur, the influence of sea ice on deep-sea sedimentation is much less established than during peak glacial times. We suspect that the retreating and deteriorating ice cover may reflect the changing surface water current system at that time.

In most cores investigated, the transitional weakly diatomaceous sediments gradually change to pure diatomaceous oozes during the beginning Holocene, implying the gradual onset of an extreme siliceous primary productivity. However, three cores from the lower Sakhalin and Kamchatka continental slopes (LV28-40-4 and LV28-43-4) and from the Derugin Basin (LV28-34-2) provide evidence for extremely rapid climatic short-term changes during the transition from glacial to interglacial conditions. In all three cores, Termination 1A (ca. 12 kyrs B.P.) and Termination 1B (ca. 9 kyrs B.P.), deposits reflecting the climatic improvement after the Last Glacial Maximum by enhanced diatom concentrations are sharply intercalated by glacial-type sediments belonging to the climatic short-term rebound of the Younger Dryas (10.300 yrs B.B.).

According to all indications, the retrieved high resolution sediment records from the E-W-transect and the Derugin Basin offer an excellent opportunity for future studies to reconstruct the climate history of paleoproductivity that is mainly triggered by the Kamchatka Current and the Amur river during times of low sea ice cover.

Northeastern slope of Sakhalin

During the 1998 KOMEX expedition, core LV28-32-1 (ca. 6m in length) was retrieved from the North Sakhalin continental slope from ca. 712m water depth. Despite the near continent, the surface and near-surface light olive-gray sediments contain high amounts of biogenics, in particular diatoms, mollusc and gastropod shells and carbonaceous shell fragments. Further downcore, diatom concentrations slightly decline and the near-surface diatomaceous ooze transfers to a diatomaceous sandy clayey silt. The portion of terrigenous material and ice-rafted

detritus gradually increases downcore. With increasing core depth, hydrogen sulfide odor is typical. Black streaks and mottles become abundant, and in the adjacant core LV27-2-4 from the 1996 GREGORY expedition authigenic pyrite is reported below 4.2m (Nürnberg et al., 1996). Thus, color, sediment composition and gas formation delineate the prevailing reducing conditions within the sediment. Adjacent cores recovered two years ago commonly show very low magnetic susceptibility values (Nürnberg et al., 1996), which may be caused by the early diagenetic alteration of the major magnetic minerals (Fe-oxides) favored by the specific redox-conditions.

Since we have no magnetic susceptibility record for core LV28-32-1, we can only speculate from the similarity to cores recovered during the 1996 GREGORY expedition that the diatomaceous silts and oozes near the northern Sakhalin continental slope are entirely of Holocene age. This points to an extreme bioproductivity during the Holocene, which is mainly driven by the distinctive Okhotsk Sea oceanography. The core location northeast off Sakhalin is influenced by the eastern part of the Okhotsk Gyre, which moves counterclockwise from the inflow of Pacific waters near Kamchatka across the northern shelf regions to the eastern coast of Sakhalin. It is still not well known how the surface waters of the Okhotsk Sea sustain their high nutrient content (Yang & Honjo, 1996). Admixtures of continental run-off probably provide a lot to the nutrient budget. And most important, the Amur River outflow which markedly influences the surface oceanography along Sakhalin continuously provides nutrients causing the long-lasting extreme bioproductivity.

Kurile Basin Deep Water transect (N-S-Transect)

Cores LV28-2-3 and LV28-2-4 are retrieved from the south-western slope of Sakhalin Island from ca. 1250m water depth and thus represent the northernmost cores of the Kurile Basin Deep-Water Transect. Detailed records of magnetic susceptibility and humidity (water content) of core LV28-2-4 can successfully be used for stratigraphical subdivision and core correlation (Fig. 4.39). Both the magnetic susceptibility and the humidity records strongly depend on the presence of biogenic components (preferentially the opal content) and generally mirror the downcore pattern of biogenic silica.

The humidity record (closed circles) coincides well with the manual humidity analyses (closed square), which confirms the validity of the moisture meter measurements. The general trend of the dry density records matches the magnetic susceptibility and humidity records and reflects major lithological changes and the position of ash layer K2 (Fig. 4.39).

On the basis of all available data (core description, tephrachronology and magnetic susceptibility records) the GEOMAR and POI cores at site LV28-2 (LV28-2-3 and LV28-2-4, respectively)

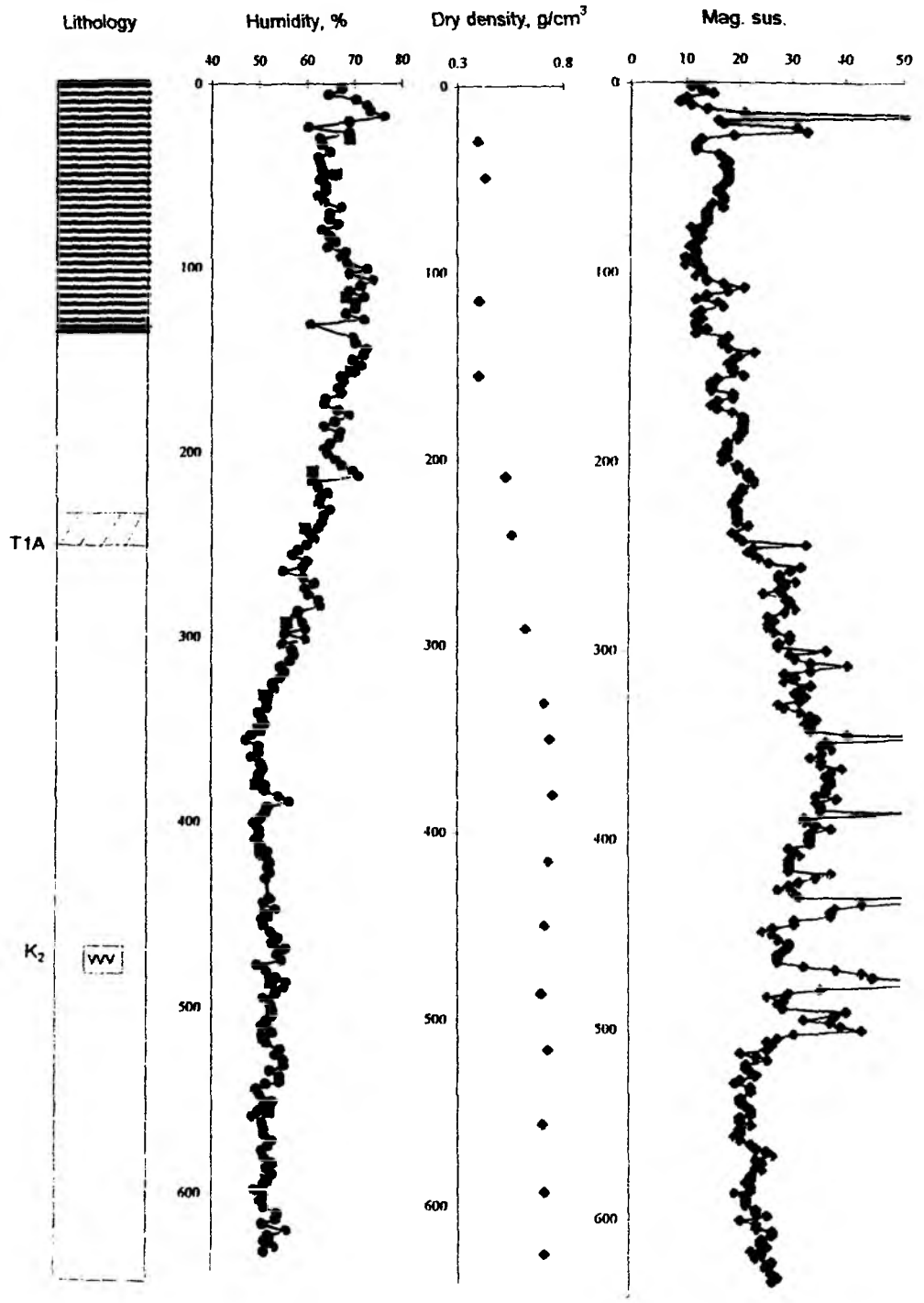

Fig. 4.39: Humidity, dry density and magnetic susceptibility records of core LV28-2-4 off South Sakhalin. The lithology is schematically indicated.

can be accurately correlated. According to the magnetic susceptibility pattern developed for the central Okhotsk Sea W-E-transect, the deep part of core LV28-2-3 (690-807cm) exhibiting low magnetic susceptibilities presumably belongs to MIS 5.1.

The overlying interval with high magnetic susceptibilities (690-560cm) in core LV28-2-3 belongs to MIS 4, and was thus formed during cold climatic conditions. Several pebbles occur within the upper part of this interval. The interval 560-470cm in core LV28-2-3 has moderate magnetic susceptibilities and can be correlated with the interval 620-510cm in core LV28-2-4 showing similar magnetic properties. The sediments below ash K2 (26 ka) possess moderate humidity and dry density and belong to MIS 3 with moderate climate condition.

The sediments from 470-250cm in core LV28-2-3 and from 510-250cm in core LV28-2-4 reaching up to Termination 1A have high magnetic susceptibilities, high dry densities, and the lowest water content observed and are typical glacial sediment (Fig. 4.39) and belong to MIS 2. Several spikes of the magnetic susceptibility record at this time reflect the occurrence of ice-rafted dropstones.

The onset of the climatic warming at Termination 1A is marked by both the appearance of greenish silt layers (251-235cm) with coccoliths and a sharp decrease of the magnetic susceptibility, dry density and humidity records (LV28-2-4). During the following Younger Dryas cooling, all physical parameters get stabilized and sediments slightly coarsen (sandy silt at 212-222 cm in core Lv28-2-3). The subsequent decrease of the magnetic susceptibility and dry density records and the rise of the humidity is related to the enhanced diatom accumulation (212cm and 200cm in cores LV28-2-3 and LV28-2-4, respectively). These lithological changes and variations in physical properties are most likely related to Termination 1B (9.5 ka). Very low magnetic susceptibility values in the upper 150cm and 130cm in cores LV28-2-3 and LV28-2-4, respectively, were similarly caused by the very intensive diatom accumulation during the last ca. 5-6 ka.

Magnetic susceptibility, humidity and dry density records of core LV28-2-4 indicate a strong variability of the Okhotsk Sea environment through MIS 1 to MIS 4. During the Last Glacial Maximum (MIS 2) and the beginning deglaciation (from 28-29 ka up to 12.5 ka) as well as during MIS 4, climate conditions were most severe. The prevailing terrigenous fraction with abundant coarse material and ice-rafted detritus suggests an extended sea ice cover, which distributes the coarse terrigenous material over the entire basin during summer melting (maybe not every summer). Small valley glaciers of northern and western Kamchatka presumably supplied additional terrigenous material via icebergs. Productivity during these times was low. The extended ice cover being present during most of the year may have restricted the solar radiation which is needed for the productivity cycle. Changes in both the vertical water

convection and nutrient supply to the photic layer may also have biassed productivity. During MIS 3, climate conditions were less severe as during MIS 2 and MIS 4 indicated by declining magnetic susceptibility and dry density values and an increasing water content. Nevertheless, productivity remained low.

4.5 Petrology and volcanology

I. Tararin, Ye. Lelikov, R. Werner, J. Geldmacher, E.P. Terekhov, and T.A. Emel'yanova

During *RV Akademik Lavrentyev* cruise 28, bedrock dredging and subsequent petrological studies were completed on 13 stations in 3 areas located on the northern slope of the Kurile Basin and at the submarine volcano in the eastern part of the Kurile Basin (Figs. 40 A-D, Appendix 1). Dredging sites were set where - according to seismic reflection data and echosounding survey - bedrock outcrops or the upper sedimentary unit occur. Additionally, dredging was carried out at two stations in the Derugin Basin.

4.5.1. Kurile Basin

Morphology and crustal structure:

The Kurile Basin is a marginal basin located at the convergent plate boundary between the Pacific plate and the Asian continent. It has a triangular shape, extends about 1100 km in W-E direction and is bordered by the Academy of Sciences Rise in the north and by the Kurile Island Arc in the south. The width of the Kurile Basin is ca. 200 km near Sakhalin Island but sharply decreases towards Shiashkotan Island. The seafloor morphology is dominated by a flat abyssal plain which slightly inclines SE and rises towards its margins. The average depth of the Kurile Basin is 3000m; its maximum depth amounts to 3374 m b.s.l. (below sea level).

The northern slopes of the basin show a relatively smooth surface which ascends towards the Academy of Sciences Rise. The slopes are cut by a number of valleys and canyons striking roughly perpendicularly to the rise. Prominent bathymetric highs being roughly conical and often slightly elongated subparallel to the basin margin rarely occur in the northern part. Only a few isolated bathymetric highs exist in the inner part of the basin.

The suboceanic crust of the Kurile Basin has a total thickness of 7-10 km (Belousov and Udintsev, 1981; Sergeev et al., 1987). The uppermost unit, a 3 - 4.5 km thick sedimentary sequence, comprises two layers: a stratified upper unit (Vp=1,5-2,3 km/c) up to 1 km thick and an "acoustic transparent" lower unit (Vp=2,2-4,5 km/c; Sergeev et al., 1987; Bogdanov, 1988) up to 3 km thick. The sedimentary sequence is underlain by the 3 - 4 km thick "basaltic" layer (Vp+6,4-6,8 km). Seismic reflection data indicate a unit with Vp=7,4 km/c below the "basaltic" layer (Snegovskoy, 1974; Belousov and Udintsev,1981; Sergeev et al., 1987). The upper mantle below the Kurile basin is characterized by seismic velocities up to 8 km/c. It is

noteworthy that the structure of the crust of the Kurile Basin significantly differs from the normal oceanic crust.

As a whole, magnetic anomalies strike parallel to the long axis of the Kurile Basin, W-E striking linear anomalies occur at its axial zone. The basin has intensive gravimetric Badgul anomalies similar to those of back-arc basins of marginal seas (Gnibidenko, 1979; Sergeev et al., 1987; Bogdanov, 1988). The Kurile Basin is characterized by high heat flow with average values 99±29mWm^2 (Sergeev et al., 1987; Bogdanov, 1988).

Data of the geological setting of the Kurile Basin are only available for the upper section of the sedimentary unit. The basement is poorly known. Bogdanov (1988) suggested that it consists mainly of basic volcanics, interbedded with predominantly sedimentary-volcanic and siliceous deposits. High heat flow and bathymetric highs protruding through the sedimentary strata indicate young volcanic activity. Therefore, we carried most of the dredging out on the submarine volcanic edifice in the eastern part of the Kurile Basin where a few fragments of Pleistocene island-arc volcanic rocks had been sampled for the first time during *RV Akademik Lavrentyev* cruise 27. Three dredges at this volcano (LV-28-45, 48 and 56; Fig. 4.0 D) yielded bedrocks from 2700-2450m water depth (Appendix 1).

The submarine volcano in the eastern part of the Kurile Basin:

The conical submarine volcanic edifice has a basal diameter of 5,5-6,5 km. Its base is located in 3200 m b.s.f.; the summit rises to 2370m water depth. According to seismic reflection data gained on *RV Akademik Lavrentyev* cruise 27, the volcano penetrates the sedimentary cover.

During *RV Akademik Lavrentyev* cruise 28, we recovered 7 dredges altogether from water depths of 3000 up to 2400 m. The dredging sites are shown in Figure 4.4 D.The dredges LV28-48 and LV28-56 from the upper and middle slopes of the volcano contained the most representative volcanic rocks. These samples comprise mostly angular blocks and fragments of pillow-like or breccious basalt and basaltic andesite lavas, ranging from some centimeter to more than 0,5 m in size. They are usually slightly weathered, sometimes with a thin (up to 3-4 cm) sedimentary and Mn-oxide coating. Some samples, however, show intense hydrothermal alteration. The surface of the boulders and blocks is very rough. Most of these probably came from large talus piles on the slopes of the volcano rather than from outcrops.

Petrographically, the basalt blocks are grey to dark grey, highly porphyric (up to 20-30%) and often vesicular in appearance (up to 20 vol.% vesicles) with rounded to oval-shaped vesicles commonly 1-2 mm in diameter (max. vesicle diameter ca. 3 mm). Phenocrysts are predominantly plagioclase and commonly form clusters. Individual crystals are usually 0,3-1 mm in size. Olivine, clinopyroxene, orthopyroxene and brown hornblende phenocrysts occur subordinately. Hornblende phenocrysts are typical for a more evolved chemical composition (e.g., basaltic andesite). The groundmass mainly consists of fresh tachylitic glass which contains numerous plagioclase microlites as well as clinopyroxene, orthopyroxene, hornblende and Fe-Ti oxides in varying amounts.

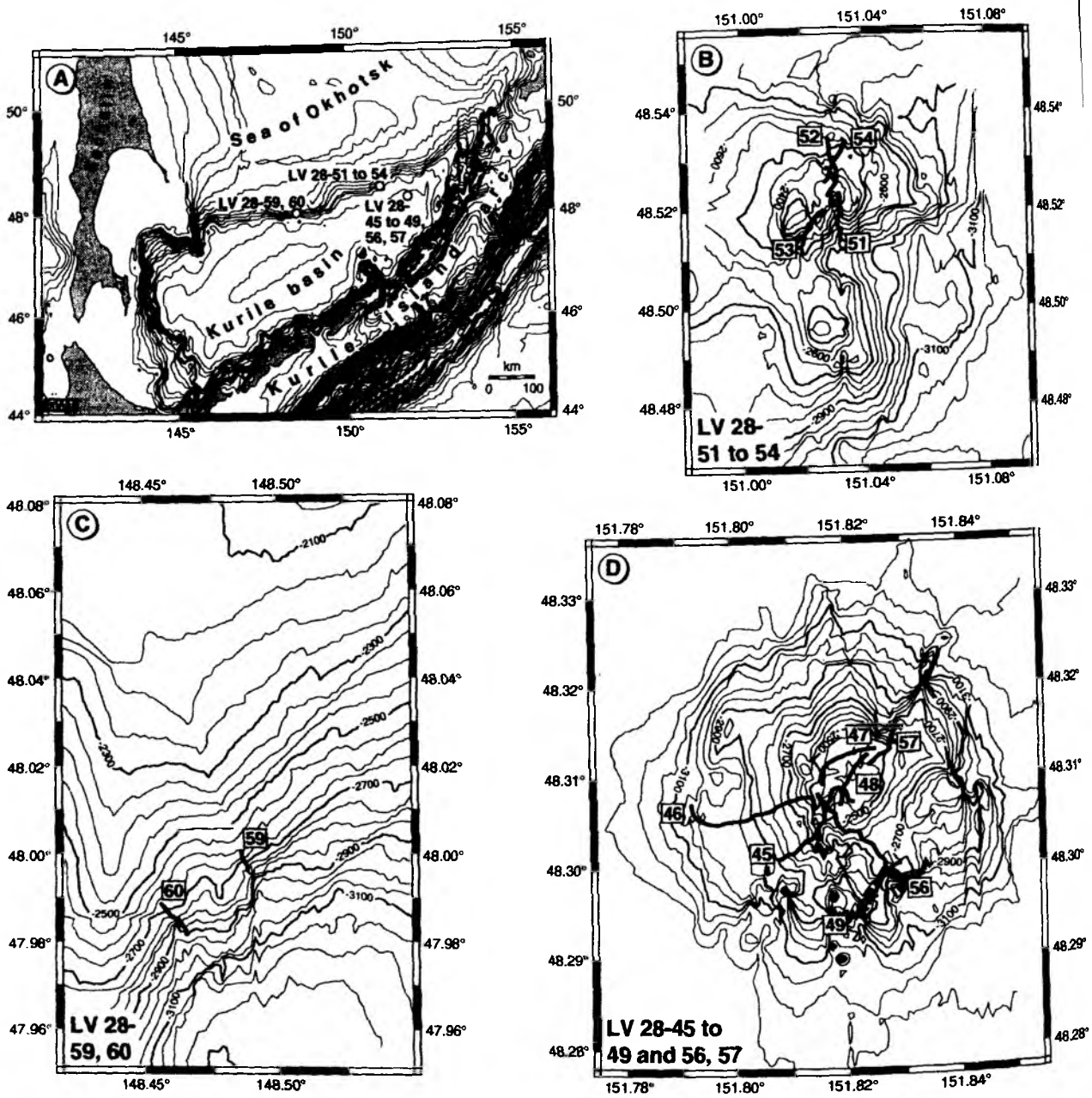

Fig. 4.40: A) Map showing sites dredged during RV "Akademik Lavrentyev" cruise 28 in the Kurile Basin. B-D) Detailed maps including dredge tracks of volcanic structures on the north-eastern slope of the Kurile basin (B), the central part of its northern slope (C) and the volcano in its eastern part (D).

A noteworthy feature of the lavas of the submarine volcano are common glomerophyric clusters of gabbronorite (Plag+Opx+Cpx), wehrlite (Ol+Cpx±Plag) and plagioclase-bearing clinopyroxenite which are considered to be most probably mantle xenoliths. They appear as round or oval-shaped spots with diameters of 1-4 cm, have well-defined rims, are yellow-green

Table 4.3: *Representative electron microprobe mineral analyses of Ol-Cpx-Opx-Hb-Pl basaltic andesite from the submarine volcano in the eastern part of the Kurile Basin (Sample LV27-18/1).*

	Olc	Oli	Opxc	Opxr	Cpxc	Cpxr	Hbc	Hbr	Plc	Plr
SiO_2	39.84	39.41	54.63	55.85	52.08	53.19	42.29	42.42	45.72	52.18
TiO_2	0.00	0.00	0.16	0.16	0.50	0.29	2.50	2.21	0.00	0.00
Al_2O_3	0.00	0.00	1.56	1.26	2.80	1.86	12.45	12.70	34.58	30.45
FeO	16.96	23.04	16.25	15.81	8.78	7.73	11.86	12.09	0.51	0.71
MnO	0.13	0.39	0.57	0.48	0.30	0.29	0.01	0.01	0.00	0.00
MgO	42.04	36.72	25.95	26.12	14.45	15.67	13.58	13.59	0.01	0.01
CaO	0.10	0.00	1.26	1.31	20.87	20.23	10.82	10.85	17.34	12.68
Na_2O	0.00	0.00	0.00	0.00	0.00	0.05	2.15	2.07	1.29	3.86
K_2O	0.00	0.00	0.00	0.00	0.00	0.00	0.10	0.11	0.00	0.00
Total	99.07	99.56	100.38	100.99	99.78	99.31	95.76	96.05	99.45	99.89
X_{Mg}	0.815	0.740	0.740	0.746	0.746	0.783	0.671	0.667	-	-
X_{An}	-	-	-	-	-	-	-	-	0.881	0.645
Wo	-	-	2.5	2.6	43.6	42.1	-	-	-	-
En	-	-	72.2	72.7	42.1	45.4	-	-	-	-
Fs	-	-	25.3	24.7	14.3	12.5	-	-	-	-

	Olr	Opxr	Cpxr	Hbr	Glass
SiO_2	38.47	55.14	49.78	44.41	64.04
TiO_2	0.00	0.27	0.60	1.91	0.68
$Al2O_3$	0.00	1.41	4.66	11.26	15.95
FeO	24.16	15.88	8.89	12.51	3.74
MnO	0.51	0.52	0.17	0.15	0.00
MgO	36.89	25.21	13.42	14.00	0.61
CaO	0.00	1.50	21.52	10.90	2.62
Na_2O	0.00	0.00	0.03	2.11	3.09
K_2O	0.00	0.00	0.00	0.30	4.79
Total	100.03	99.93	99.07	97.55	95.52
X_{Mg}	0.731	0.739	0.729	0.666	0.225
X_{An}	-	-	-	-	-
Wo	-	3.1	45.7	-	-
En	-	71.6	39.6	-	-
Fs	-	25.3	14.7	-	-

Notes: I - phenocryst, II - matrix microlite, c - core, r - rim of crystal. X_{Mg}=Mg/(Mg+Fe), X_{An}=Ca/(Ca+Na+K). Mineral compositions were determined with Camebax electron microprobe fitted with a Kevex energy dispersive detector at the Institute of Volcanology of the Russian Academy of Sciences.

and grey-green in hand-specimen, do not show any foliation and generally differ from the host-lava in colour, crystallinity, and vesicularity.

The vesicles in most of the fresh lavas are free from secondary minerals. Only a few vesicles in pillow rims are filled with green silica minerals, barite and pyrite, suggesting slight hydrothermal alteration. The surprisingly high vesicularity of many samples from this deep submarine volcano indicates an origin of the rocks from volatile-rich alkaline magmas.

Preliminary sample studies obtained from the submarine volcano during *RV Akademik Lavrentyev* cruise 28 suggest that these rocks are similar to those dredged at this volcano during *RV Akademik Lavrentyev* cruise 27 in 1996. Detailed petrographic descriptions of these

submarine volcanics have been given by Tararin et al. (in press). Following, we briefly summarize the principal petrographic and mineralogical features of the samples gained in 1996 for comparison. Representative microprobe analyses of the basalt minerals and glasses are given in Table 4.3.

The rocks have geochemical features typical for high-K and high-Al island-arc volcanics (Table 4.4). They are enriched in LILE and depleted in Zr, Ti, Nb and Y. The rare earth patterns are similar to those of island-arc lavas from the submarine volcanoes of the back-arc part of the Kurile Island Arc. K-Ar age dating of dredged basaltic andesites yielded ages of 0,932±0,042 and 1,632±0,051 Ma (Table 4.5).

***Table 4.4**: Major, trace and rare-earth elements analyses of basaltic andesite from the submarine volcano in the eastern part of the Kurile Basin.*

Sample	SiO_2	TiO_2	Al_2O_3	Fe_2O_3	FeO	MnO	MgO	CaO	Na_2O	K_2O	LOI	H_2O	Total
LV27-18/1	54.14	0.61	19.63	3.90	2.46	0.15	4.20	8.32	2.72	1.89	1.66	0.35	99.68
LV27-18/3	54.06	0.67	19.34	3.72	2.72	0.16	4.35	8.30	2.70	1.95	1.72	0.32	99.72

Sample	Rb	Sr	Ba	Nb	Zr	Y	La	Ce	Nd	Sm	Em	Tb	Yb
LV27-18/1	53	610	390	3.0	87	20	14	32	18	4.6	1.5	0.68	2.3
LV27-18/3	52	610	320	2.9	86	20	15	31	17	4.1	1.3	0.84	2.0

Sample	Lu	Cr	Ni	Co	V	Cu
LV27-18/1	0.40	36	24	15	165	60
LV27-18/3	0.34	37	29	19	180	63

Notes: Whole-rock analyses were carried out by wet chemical methods using standard techniques. Trace elements (Rb, Sr, Ba, Y, Nb, Zr) were determined by X-ray fluorescence techniques and REE concentrations by instrumental neutron activation analysis. Ni, Co, Cr, V, Cu were determined by quantitative spectroscopic methods.

Data from cruise 27 and previous studies have provided evidence for a continental crust basement of the eastern part of the Kurile Basin. The available data set suggests that the high-K and high-Al island arc basalts of the submarine volcano in the eastern part of Kurile Basin probably cannot be explained by simple crystal fractionation of a basaltic magma source. The data, however, are consistent with an origin of the island arc magmas by interaction of a primary basaltic liquid and continental crust - which would be in accordance with the andesitic temperature minima in quartz-pyroxene-feldspar eutectic. Obviously, the petrogenetic process proposed here is only a hypothesis. Future tests of this model will focus on quantitative modelling of geochemical and isotopic trends.

Submarine volcanic structures on the northeastern slope of the Kurile Basin:

A 6-7-km-long and 3.5-4 km wide submarine volcanic ridge extends in latitudinal direction on the NE-slope of the Kurile basin. The summit rises to 2320 m water depth. During cruise 28 we completed 4 dredging stations on the northern and southern slopes of the volcano (Fig. 4.4 B). The dredged material indicates that the volcanic ridge is covered by diatomaceous sediments and a lot of dropstones ranging in composition from granite to basalt. Only some small (up to 3-6

cm) angular basalt fragments recovered in dredge LV28-54-1 may possibly represent the volcanic bedrocks.

Table 4.5: *K-Ar ages of basaltic andesites dredged at the submarine volcano in the eastern part of the Kurile Basin during R/V "Akademik Lavrentyev" cruise 27.*

Sample	K, wet %	$40Ar_{rad.}$ 10^{-8} cm^3/g	$Ar_{contam.}$,%	K-Ar age, Ma
LV27-18/1	1.808±0.036	6.54±0.26	65.7	0.932±0.042
LV27-18/3	1.635±0.033	10.36±0.25	49.6	1.632±0.051

Note: K-Ar age dating was carried out at Research Institute of Natural Sciences Okayama University of Science by Tetsumaru Itaya.

The northern slope of the Kurile Basin:

Dredging in the central part of the northern slope of the Kurile Basin (Fig. 4.4 C) was carried out in order to receive new data on its geology and to sample Lower Miocene diatomaceous tuffs dredged previously during *RV Pervenetz* cruise 37 in 1981. Unfortunately, the dredges LV28-59 and 60 contained only clay sediments and dropstones.

4.5.2. Derugin Basin

According to the OFOS-survey, barite chimneys (up to 10-15 m high) were dredged in 1500 m water depth at two sites within an area of intensive hydrothermal activity in the Derugin Basin (DR LV28-35, 36). Dredging at these sites yielded numerous boulders and fragments (up to 100-150 kg) which are described in detail in chapter 4.3.6 of this report.

5. REFERENCES

Astakhova, N.V., 1992. Hydrothermal barite of the Okhotsk Sea. 29th International Geological Congress, Abstracts, 3, p. 759.

Astakhova, N.V., Narnov, G.A, and Yakusheva, I.N., 1990. Carbonate-barite mineralization in the Derugin depression (the Sea of Okhotsk). Tikhookeanskaya geologiya, 3, 37-42 (in Russian).

Astakhova, N.V., Lipkina, M.I., Mel'nichenko, Yu.I., 1987. Hydrothermal barite mineralization in Derugin Basin of the Sea of Okhotsk. Doklady Akademii Nauk SSSR, 295, 1, 212-215 (in Russian).

Avdeiko, G.A., Antonov, A.Yu., Volynetz, O.N. et al., 1992. Submarine volcanism and zonality of the Kuril Island Arc. Moscow, Nauka, 528 pp. (in Russian).

Baranov, V.B., Dozorova, K.A., Svarichevsky, A.S., 1995. Kurile Basin and Okhotsk Rift System: Kinetics of opening. Abstr. Third Internat. Conference on Asian Marine Geol. October 17-21, 1995. Cheju, Korea, 13-14.

Barry, J.P., Green, H.G., Orange, D.L., Baxter, C.H., Robison, B.H., Kochevar, R.E., Nybakken, J.W., Reed, D.L., McHugh, C.M., 1996. Biologic and geologic characterstics of cold seeps in Monterey Bay, California. Deep Sea Res. I, 43 (11-12), 1739-1762.

Bassinot, F.C. Labeyrie, L.D., Vincent, E., Quidelleur, X., Shackleton, N.J., Lancelot, Y., 1994. The astronomical theory of climate and the age of the Brunhes-Matuyama magnetic reversal. Earth and Planetary Science Letters, 126, 91-108.

Bates, R. G., 1973. Determination of pH: theory and practice. Wiley, N.Y., 386 pp.

Belousov, V.V., Udintsev, G.B. (eds.), 1981. Seafloor structure of the Okhotsk Sea. Moscow, Nauka, 176 pp. (in Russian).

Bezrukov, P.L., Romankevich, E.A., 1960. To stratigraphy and lithology of the sediments of the Northwestern Pacific. Doklady of the Russian Academy of Sciences, 130 (N2), 417-420.

Bogdanov, N.A., 1988. Tectonics of back-arc basins from marginal sea. Moscow, Nauka, 221 pp. (in Russian).

Bogorov, 1974. Plankton of the World Ocean. Moscow, Nauka (in Russian).

Bohrmann, G., Greinert, J., Suess, E., Torres, M., 1998. Authigenic carbonates from the Cascadia subduction zone and their relation to gas hydrate stability. Geology, July 1998, 26, (7), 647-650.

Braytseva, O.A., Melekestsev, I.V., Ponomareva, V.V., Kirianov, V.Yu., 1996. The caldera-forming eruption of Ksudach volcano about cal. AD 240, the greatest explosive event of our era in Kamchatka. Journal of Volcanology and Geothermal Research 70 (1-2), 49-66.

Broecker, W.S., Spencer, D.W., Craig, H., 1982. Hydrographic data, 1973-1974 in GEOSECS Pacific Expedition. Natl. Sci. Found, Washington, D.C., 3, 137 pp.

Chipman, D.W., Guenther, P., 1994. Water sampling for the parameters of the oceanic carbon dioxide system. In Dickson, A. G., Goyet, C. (eds.), Handbook of Methods for the Analysis of the Various Parameters of the Carbon System in Sea Water. DOE Publication, SOP-1, 6 pp.

Culkin, F., 1965. The major ion components of seawater. In Riley, J.P., Skirrow, G. (eds.), Chemical Oceanography. Academic Press, N.Y.

Derkachev, A.N., Bohrmann, G., in prep. Mineralogy of diagenetic calcite and barite formations in sediments from the Derugin Basin Sea of Okhotsk.

Derkachev, A.N., Nikolayeva, N.A., 1997. Mineralogical peculiarities of sediments: The recent sediment formation within marginal seas of the Asian East (statistical models). Vladivostok, Dal'nauka, 189-215 (in Russian).

Dickson, A. G., 1994. The measurements of sea water pH. Marine Chemistry, 44, 131-142.

Dickson, A.G., 1993. pH buffer for sea water media based on the total hydrogen ion concentration scale. Deep-Sea Res. I, 40, 107-118.

Dickson, A.G., 1981. An exact definition of total alkalinity and a procedure for the estimation of alkalinity and total CO_2 from titration data. Deep-Sea Res., 28, 609-623.

Dozorova, K.A., Baranov, B.V., Karp, B.Ya., Karnaukh, V.A., 1998. Sakhalin Shear Zone and the origin of the Derugin Basin (Okhotsk Sea). Abstracts of the 6th Zonenshain Conference, Moscow.

Embly, R.E., et al., 1990. Geological setting of chemosynthetic communities in the Monterey Fan Valley system. Deep Sea Res., 37 (11), 1651-1667.

Frolova, T.I., Perchuk, L.L., Burikokova, I.A., 1989. Magmatism and transformation of the crust from the active continental margins. Moscow, Nauka, 261 pp. (in Russian).

Gaedicke, C., Baranov, B.V., Obzhirov, A.I., Lelikov, Ye.P., Belykh, I.N., Basov, Ye.I., 1997. Seismic stratigraphy, BSR distribution, and venting of methane-rich fluids west off Paramushir and Onekotan Islands, northern Kurils. Marine Geology, 136, 259-276.

Galchenko, V.F., Lein, Yu.A., Ivanov, M.V., 1988. Quantitative estimation of primary chemosynthesis production in the rift zones of modern oceans. In Schidlowski, M. (chairperson), Terra Cognita, 8 (3), European union of Geosciences. Strasbourg, 223 pp.

Geodekyan, A.A., Udinsev, G.B. Baranov, B.V. et al., 1976. Bedrocks of the central Ochotsk Sea. Soviet Geology, 6, 12-31 (in Russian).

Gieskes, J.M., Garno, T, Brumsack, H., 1991. Chemical methods for interstitial water analysis aboard Joides Resolution. Ocean Drilling Program, Texas A&M University.

Ginsburg, G.D., Soloviev, V.A., 1994. Mud volcano gas hydrates in the Caspian Sea. Bulletin of the Geological Society of Denmark, 41, 95-100.

Ginsburg, G.D., Soloviev, V.A., Cranston, R.E., Lorenson, T.D., Kvenvolden, K.A., 1993. Gas hydrates from the continental slope, offshore Sakhalin Island, Okhotsk Sea. Geo.Mar. Lett., 13, 41-48.

Ginsburg, G.D., Soloviev, V.A., 1974. Submarine gas hydrates. St. Petersburg, 5-200 (in Russian).

Gnibidenko, G.S., 1979. Tectonics of the seafloor from the far east marginal seas. Moscow, Nauka, 163 pp. (in Russian).

Gnibidenko, H.S., Khvedchuk, I.I., 1982. The tectonics of the Okhotsk Sea. Mar. Geol., 50, 155-198.

Gorbarenko, S.A., 1996. Stable isotope and lithologic evidence of late-glacial and Holocene oceanography of the northwestern Pacific and its marginal seas. Quaternary Research, 46, 230-250.

Gorbarenko, S.A., Chekhovskaya, M.P., Southon, J.R., 1998. Detailed environmental changes in the Okhotsk Sea central part during the last glaciation-Holocene. Oceanology 38, 305-308.

Gorbarenko, S.A., Derkachev, A.N., Southon, J.R., Astakhov, A.C., Shapovalov, V.B., in prep. Lithostratigraphy and tephrochronology of the Okhotsk Sea sediments.

Ivanenkov, V.N., Lyakhin, Yu.I., 1978. Determination of total alkalinity in seawater. In Bordovsky, O. K., Ivanenkov, V. N. (eds.), Methods of hydrochemical investigations in the ocean. Nauka Publ. House, Moscow, 110-114 (in Russian).

Jolivet, L., Huchon, P., Brun, J.P. Chamot-Rooke, N., Le Pishon, X., Thomas, J.C., 1991. Arc deformation and marginal basin opening: Japan Sea - a case study. Journ. Geophys. Res., 96, 4367-4384.

Kaiko-Tokai Project, 1998. Tectonics of subduction in the Nankai Trough, International Symposium on Japan-France Kaiko-Tokia project. Abstract Vol., 82 pp.

Katsui, Y., 1963. Evolution and magnetic history of some Krakatau calderas in Hokkaido, Japan. Journ. Fac. Sci., Hokkaido Univ. Ser. IV, 11, 631-650.

Koblenz-Mishke, O.J., Volkovinsky, V.V., Kabanova, J.G., 1970. Plankton primary production of the world ocean. In Wooster, W. (ed.), Scientific exploration of the South Pacific. National Academy of Science, 183-193.

Kulm, L.D. et al., 1986. Oregon subduction zone: Venting, fauna, and carbonates. Science, 231, 561-566.

Kulm, L.D., Suess, E., 1990. Relationship between carbonate seposits and fluid venting: Oregon accretionary prism. J. Geophys. Res., 95, (B6), 8899-8915.

Lammers, S., Suess, E., Mansurov, M.N, Anikiev, V.V, 1995. Variations of atmospheric methane supply from the Sea of Okhotsk induced by the seasonal ice cover. Global Biochemical Cycle, 9(3), 351-358, September 1995.

Lein, A.Y., Galchenko, V.F., Pokrovskiy, B.G., et al., 1989. Marine carbonate concretions as a result of processes of microbe oxidizing of methane gas hydrate in the Sea of Okhotsk. Geochimiya, 10, 1396-1406 (in Russian).

Lelikov, E.P., 1992. Metamorphic complexes of the marginal seas of the Pacific. Vladivostok, Dal'nauka, 168 pp. (in Russian).

Lisitsin, A.P., Bogdanov, Yu.A., Gurvich, E.G., 1990. Hydrothermal formation of rifting systems in World Ocean. Moscow, Nauka, 5-255 (in Russian).

Magmatic Mountain Rocks, 1987, The evolution of magmatism in the Earth history. Moscow, Nauka, 5-438 (in Russian).

MacDonald, G., 1990. The role of methane chlatrates in past and future climates. Climate Change, 16, 247-281.

Millero, F. J., 1979. The thermodynamics of the carbonate system in seawater. Geochim. et Cosmochim. Acta, 43, 1651-1661.

Millero, F.J., 1995. Thermodynamics of the carbon dioxide system in the oceans. Geochim. et Cosmochim. Acta, 59, 661-677.

Minato, M., Hashimoto, S., Fujiwara, Y., Kumano, S., Okada, S., 1972. Stratigraphy of the Quaternary ash and pumiceous product in south-western Hokkaido, N. Japan. Journ. Fac. Sci., Hokkaido Univ. Ser. IV, 15, 679-736.

Mizutani, Y., Rafter, T.A., 1973. Isotopic behaviour of sulfate oxygen in the bacterial reduction of sulfate. Geochemical Journal, 6, 183-191.

Morley, J. J., Hays, J. D., Robertson, J. H., 1982. Stratigraphic framework for the late Pleistocene in the northwest Pacific Ocean. Deep-Sea Res., 29, 1485-1499.

Morley, J. J., Nigrini, C., 1995. Miocene to Pleistocene radiolarian biostratigraphy of north Pacific Sites 881, 885, 886, and 887. In Rea, D.K., Basov, I.A., Proceedings of ODP Scientific Results. 145, 55-91.

Nürnberg, D., Baranov, B.V., Karp, B.Y. (eds.), 1997. RV Akademik M.A. Lavrentyev cruise 27 - cruise report Gregory. Geomar Report, 60, 69 pp.

Nürnberg, D., Bijma, J., Hemleben, C., 1996. Assessing the reliability of magnesium in foraminiferal calcite as a proxy for water mass temperatures. Geochim. et Cosmochim. Acta, 60 (5), 803-814.

Obzhirov, A.I., 1993. Gas and geochemical fields of the benthic layer of seas and oceans. Moscow, Nauka, 131 pp.

Obzhirov, A.I., Kazanskiy, B.A., Melnischenko, Yu.I., 1989. Effects of sound dispersion in the near bottom water in marginal parts of the Okhotsk Sea (in Russian). Pac. Geol., 2, 119-121.

Paull, C.K., Chanton, J.P., Newmann, A.C., et al., 1992. Indicators of methane-derived carbonates and chemosynthetic organic carbon deposits: Examples from the Florida Escarpment. Palaios., 7, 361-375.

Ritger, S., Carson, B., Suess, E., 1987. Methane-derived authigenic carbonates formed by subduction-induced pore-water expulsion along the Oregon/Washington margin. Geological Society of America Bulletin, 98, 147-156.

Roberts, H.H., Aharon, P., 1994. Hydrocarbon-derived carbonate buildups of the northern Gulf of Mexico continental slope: A review of submersible investigations. Geo.-Mar. Letters, 14, 135-148.

Sample, J.C., Reid, M.R., Tobin, H.J., Moore, J., 1993. Carbonate deposits indicate channeled fluid flow along a zone of vertical faults at the deformation front of the Cascadia accretionary wedge (northwest US coast). Geology, 21, 507-510.

Savostin, L.A., Zonenshain, L.P., Baranov, B.V., 1983. Geology and plate tectonics of the Sea of Okhotsk. In Hilde, T.W.C. Uyeda, S. (eds.), Geodynamics of the Western Pacific-Indonesian Region. Geodynamic Series AGU, 189-222.

Sergeev, K.F., Zverev, S.M., Veitsman, P.S. et al. (eds.), 1987. Geologic-geophysical atlas of the Kurile-Kamchatka Island Arc. Leningrad, VSEGEI.

Skirrow, G., 1975. The dissolved gases - carbon dioxide. In Riley, J. P. Skirrow, G. (eds.), Chemical Oceanography. Academic Press, N.Y., 2, 1-192.

Snegovskoy, S.S., 1974. Seismic reflection study and tectonics of the southern part of the Okhotsk Sea and adjacent borders of the Pacific Ocean. Moscow, Nauka, 176 pp. (in Russian).

Suess, E., Bohrmann, G., von Huene, R., Linke, P., Wallmann, K., Lammers, S., Sahling, H., Winckler , G., Lutz, R.A., Orange, D., 1998. Fluid venting in the eastern Aleutian subduction zone. Journal of geophysical research, 103, no. B2, 2597-2614, Febuary 10.

Suess, E., Whiticar, M.J., 1989. Methane-derived CO_2 in pore fluids expelled from the Oregon subduction zone. Palaeogeogr. Palaeoclimatol. Palaeoceol., 71, 119-136.

Talley, L.D., Roemmich, D. (eds.), 1991. Deep-Sea Res. Part A: Oceanographic Research Papers, 38, suppl. no. 1A, New York, 654 pp.

Tally, L.B., Nagata, Y., 1995.The Okhotsk Sea and Oyashio Region. Inst. of Ocean Sci., Sidney, B.C., Canada, 227 pp.

Tararin, I.A., Lelikov, E.P., Itaya, T., in press. Pleistocene submarine volcanism of the eastern part of the Kurile Basin (Okhotsk Sea). Doklady Akademii Nauk SSSR (in Russian).

Tiedemann, R., Haug, G., 1995. Astronomical calibration of Site 882 cycle stratigraphy in the Northwest. Proc. ODP Sci. Res., 145, 283-293.

Torres, M.E., Brumsack, H.J., Bohrmann, G., Emeis, K.C., 1996a. Barite fronts in continental sediments: A new look at barium remobilization in the zone of sulfate reduction and formation of heavy barites in diagenetic fronts. Geochemical Geol., 127, 125-139.

Torres, M., Bohrmann, G., Suess, E., 1996. Authigenic barites and fluxes of barium associated with fluid seeps in the Peru subduction zone. Earth and Planet. Sci. Lett., 144, 469-481.

Tsunogai, S., Nishimura, M., Nakaya, S., 1968. Complexometric titration of calcium in the presence of larger amounts of magnesium,.Talanta, 15, 385-390.

Vasiliev, B.I., Putintsev, V.K., Makarovskii, B.A. et al., 1990. Bedrock complexes of the Okhotsk Sea submarine rises. In Bobykina, V.P., Vasiliev, B.I., Tomolev, G.M. (eds.), New data on geomorphology and geology of the West Pacific. Vladivostok, 5-16 (in Russian).

von Breymann, M.T., Brumsack, H., Emeis, K.C., 1992. Depositional and diagenetic behaviour of barium in the Japan Sea. Proceedings of the Ocean Drilling Program Scientific Results, 127/128, no. 1, 651-659.

von Huene, R., Klaeschen, D., Gutscher, M., Frühn, J., 1998. Mass and fluid flux during accretion at the Alaska margin. Geol. Soc. Am. Bull., 110, no. 4, 468-482.

Wallmann, K. Suess, E., Linke, P., Bohrmann, G., Sahling, H., Schlüter, M., Dählmann, A., Lammers, S., Greinert, J., von Mirbach, N., 1997. Quantifying fluid flow, solute mixing, and biogeochemical turnover at cold vents of the eastern Aleutian subduction zone. Geochim. et Cosmochim. Acta, 61 (24), 5209-5219.

Weiss, R. F., 1970. The solubility of nitrogen, oxygen and argon in water and seawater. Deep-Sea Res., 17, 721-735.

Winckler, G., Suess, E., Wallmann, K., de Lange, G.G., Westbrook, G.K., Bayer, R., 1997. Excess helium and argon of rediogenic origin in Mediterranean brine basins. Earth and Planetary Science Letters, 151, 225-231.

Yang, J., Honjo, S., 1996. Modelling the near-freezing dichothermal layer in the Sea of Okhotsk and its interannual variations. Journal of Geophysical Research, 101 (C7), 16421-16433.

Zahn, R., Peterson, T.F., Bornhold, B.D., Mix, A.C. , 1991. Water mass conversion in the glacial subarctic Pacific: Physical constraints and the benthic planktonic stable isotope record. Paleoceanography, 6, 543-560.

Zhuze A. P., 1962. Stratigraphy and paleontological investigations in the North-West Pacific. Academy of Sciences publishing House, 258 pp. (in Russian).

Zonenshayn, L.P., Murdmaa, I.O., Baranov, B.V., Koznetsov, A.P., Kurin, V.S., Barnsh, M.S., Valyashirv, G.M., Demiral, M., 1987. An underwater gas source in the Sea of Okhotsk. Oceanology, 27, 598.

Appendices

Appendix 1

List of Stations

LV 28: 28th expedition RV Akademik Lavrentyev

Date 1998 day month	Sta.-Nr.	Instrument	Begin (UTC)	at seafloor max. depth	off seafloor	End (UTC)	Duration hh:mm	Latitude °N Begin: at s/c /End: off s/c.	Longitude °E Begin: at s/c /End: off s/c.	Water depth m by ECH	Recovery	Remarks
North/South Transect												
12.08.	1-1	ECH	5:58			9:47	3:49	Survey 0 (see separate list)		194 / 1357		no acoustic anomalies, profile A
12.08.	2-1	CTD	11:00	11:15		12:58	1:58	48°20.176	146°01.628	1332	12 bottles	1=1500, 2=1250, 3=1000, 4=750, 5=500, 6=250, 7=200, 8=100, 9=50, 10=30, 11=25, 12=10 (depth m)
12.08.	2-2	MUC	13:00	13:46		14:36	1:36	48°21.737	146°03.071	1286	6 cores, 30 - 36 cm	
12.08.	2-3	SL-G	14:45	15:15		16:00	1:15	48°22.73	146°02.217	1285	807 cm	
12.08.	2-4	SL-R	16:15	16:45		17:15	1:00	48°22.73	146°02.217	1285	635 cm	
12.08.	3-1	CTD	20:17			21:00	0:43	48°18.255	145°39.62		none	cancelled because of drift
12.08.	3-2	CTD	21:50	22:32		23:10	1:20	48°18.39	145°40.97	1404	12 bottles	1=1350, 2=1325, 3=1310, 4=1290, 5=1270, 6=1250, 7=1000, 8=500, 9= 200, 10=73, 11=50, 12=10 (depth m)
13.08.	3-3	MUN	0:38	1:25		3:00	2:22	48°18.39	145°40.97	1404	5 nets, complete	
East/West Transect												
13.08.	4-1	MUN	17:33	18:18		18:55	1:22	51°08.964	145°20.497	676	5 nets, complete	
13.08.	4-2	CTD	19:10			20:00	0:50	51°09.16	145°19.09	678	12 bottles	1=680, 2=600, 3=500, 4=400, 5=300, 6=200, 7=100, 8=75, 9=50, 10=25, 11=10, 12=surface (depth m)
13.08.	4-3	MUC	20:03	20:21		20:45	0:42	51°08.897	145°18.91	675	8 cores, 37 - 46 cm	
13.08.	4-4	SL-G	21:00	21:17		21:33	0:33	51°08.475	145°18.582	674	930 cm	
13.08.	4-5	SL-R	21:50	22:06		22:26	0:35	51°08.12	145°18.21	670	850 cm	
North Sakhalin Shelf and Slope												
14.08.	5-1	CTD	10:32			11:25	0:53	53°06.94	144°21.06	490	11 bottles	1=471, 2=431, 3=401, 4=302, 5=201, 6=100, 8=50, 9=25, 10=11, 11= 5.5, 12= 2.9 (depth m), surface methane plume, RV Gagarinsky
14.08.	6-1	CTD	12:20			12:42	0:22	53°20.10	144°23.12	565	11 bottles	1=543, 2=500, 3=399, 4=303, 5=204 , 6=102, 8=51, 9=27, 10=11, 11=5, 12=1 (depth m); midway point between surface plume and vent site
14.08.	7-1	MUN	13:45	14:30		15:00	1:15	53°22.813	144°25.634	639	5 nets, complete	
14.08.	8-1	CTD	16:24			17:12	0:48	53°22.86	144°25.350	620	11 bottles	1=604, 2=552, 3=503, 4=470, 5=436, 6=401, 8=339, 9=299, 10=251, 11=150, 12=51 (depth m), gas vent field RV Gagarinsky; 53°22.74/144°25.48
14./15.08.	9-1	OFOS	22:35	23:08	3:25	3:41	5:06	54°18.695/54°24.194	144°02.267/143°56.867	557	2 video tapes, 550 photos	large clam field at gas vent site
15.08.	9-2	OFOS	5:05	5:13	6:01	6:08	1:03	54°25.593/54°26.630	143°55.193/143°54.066	227/178	1 video tape, 252 photos	cross profile
15.08.	10-1	OFOS	6:50	6:58	8:22	8:30	1:40	54°26.595/54°25.509	143°52.741/143°55.946	160/277	1 video tape, 538 photos	vent fauna at (1) 54°26.164/143°53.791 and at (2) 54°25.909/143°54.462
15.08.	11-1	CTD	9:04			9:40	0:36	54°25.45	143°55.78	261	12 bottles	1=247, 2=225, 3=201, 4=174, 5=152, 6=126, 7=100, 8=76, 9=51, 10=26, 11=10, 12=3 (depth m)
15.08.	12-1	OFOS	10:36	10:51	11:45	12:00	1:24	54°21.297/54°22.65	143°56.790/143°59.85	294/350	1 video tape, 201 photos	cross profile
15.08.	13-1	OFOS	12:46	13:00	13:56	14:15	1:29	54°20.91/54°22.977	143°59.6/143°59.22	404/400	1 video tape, 480 photos	cross profile
15.08.	14-1	CTD	15:33			15:54	0:21	54°22.33	143°59.60	385	12 bottles	1=373, 2=351, 3=324, 4=300, 5=270, 6=232, 7=203, 8=154, 9=105, 10=53, 11=26, 12=6 (depth m)
15.08.	14-2	MUN	16:25	16:50		17:35	1:10	54°20.792	143°58.281	440	5 nets, complete	
15.08.	14-3	ECH	18:59			19:41	0:42	Survey I (see separate list)		341/354		profiles B and C
15.08.	15-1	MUC	21:00	21:10		21:25	0:25	54°21.774	143°59.219	370	empty	
15.08.	15-2	MUC	23:41	23:57		0:14	0:35	54°22.173	143°58.940	378	2 cores, 20 and 5 cm	bacterial mat
16.08.	16-1	TWL	2:45	3:13	3:17	3:30	0:45	54°22.491/54°21.562	143°59.138/143°55.273	386/398	full	mostly sediment
16.08.	16-2	TWL	5:10	5:30	5:50	5:58	0:48	54°22.663/54°21.361	143°59.043/143°59.045	382/387	full	carbonate concretions, clam shells

LV 28: 28th expedition RV Akademik Lavrentyev

Date 1998 day month	Sta.-Nr.	Instrument	Begin (UTC)	at seafloor max. depth	off seafloor	End (UTC)	Duration hh:mm
16.08.	17-1	SL-R	7:45	7:55		8:04	0:19
16.08.	17-2	SL-G	8:44	8:50		9:05	0:21
16.08.	17-3	SL-G	10:07	10:21		10:30	
16.08.	18-1	ECH	11:28			13:51	2:23
16.08.	19-1	ECH	14:53			20:40	5:47
16.8./17.08.	20-1	CTD	23:35			0:20	0:45
17.08.	20-2	SL-G	1:16	1:24		1:37	0:21
17.08.	20-3	HYC	2:15	2:25		2:45	0:30
17.08.	21-1	SL-R	3:23	3:31		3:47	0:24
17.08.	22-1	ECH cont.	4:21			7:45	3:24

Derugin Basin

17.08.	22-2	ECH	14:34			18:11	3:37
17.08.	23-1	OFOS	18:48	19:26	21:30	22:10	3:22
	24-1	SL-G	22:36	22:58		23:28	0:51
17.08./18.08.	25-1	HYC	23:50	0:21		0:56	1:06
18.08.	26-1	SL-G	2:00	2:20		2:47	0:47
18.08.	27-1	SL-R	3:10	3:37		4:06	0:56
18.08.	28-1	CTD	4:37	5:25		6:23	1:46
18.08.	29-1	MUN	6:19	7:04		7:55	1:36
18.08.	29-2	CTD	8:25	8:40		9:02	0:37

North Sakhalin Shelf and Slope cont.

18.08.	30-1	MUC	17:26	17:58		18:10	0:44
18.08.	30-2	MUC	18:28	18:37		18:48	0:20
18.08.	30-3	MUC	19:11	19:21		19:33	0:22
18.08.	30-4	MUC	20:20	20:27		20:42	1:31
18.08.	30-5	MUC	21:57	22:09		22:22	2:02
18.08./19.08.	31-1	OFOS	23:12	23:31	1:24	1:44	2:32
19.08.	32-1	SL-R	2:06	2:19		2:54	0:48
19.08.	33-1	OFOS	8:17	8:28	11:35	11:54	3:37

Derugin Basin cont.

19.08.	34-1	MUC	20:41	21:14		21:45	1:04
19.08.	34-2	SL-G	22:10	22:32		22:57	0:47
20.08.	35-1	DR	1:38	2:27	3:08	3:27	1:51
20.08.	36-1	DR	4:43	5:20	5:38	6:08	1:25
20.08.	37-1	SL-R	6:55	7:15		7:47	0:52
20.08.	38-1	TWL	9:45	10:09	10:34	11:13	1:28
20.08.	39-1	CTD	12:31			13:08	0:37

East/West Transect cont.

Latitude °N Begin; at stc /End; off stc	Longitude °E Begin; at stc /End, off stc	Water depth m by ECH	Recovery	Remarks
54°21.782	143°59.780	392	empty	
54°21.967	143°58.893	386	62 cm	plus 3 samples (core catcher): top, middle, bottom
54°22.090	143°58.720	384	empty	
Survey I a (see separate list)				profiles D - H
Survey IIa (see separate list)				profiles I-Q, gas vent field at 54°28.532/144°04.068 (N2=Ginsburg et al.)
54°28.92	144°04.08	681	12 bottles	1=699, 2=640, 3=611, 4=578, 5=552, 6=521, 7=493, 8=451, 9=299, 10=151, 11=50, 12=8 (depth m)
54°28.611	144°04.093	686	575 cm	center of gas vent field
54°28.430	144°04.120	685	151 cm	hydrate site (N1=Ginsburg et al.)
54°28.751	144°04.940	702	208 cm	shell layers, very gaseous sediment at base
Survey IIb (see separate list)				profiles R-V
Survey IIc (see separate list)				profiles W-Z and AA
53.59 17/54°2.073	146°18.457/146°14.906	1483/1665	1 video tape, 519 photos	barite chimneys, burrows, vent fauna
54°00.414	146°16.852	1511	empty	
54°00.944	146°16.646	1491	148 cm	carbonate and barite concretions
54°01.038	146°16.452	1482	empty	
54°01.138	146°17.102	1545	empty	
54°00.460	146°16.790	1507	12 bottles	1=1492, 2=1466, 3=1435, 4=1400, 5=1370, 6=1333, 7=1300, 8=1250, 9=1200, 10=1000, 11=502, 12=76 (depth m)
54°1.578	146°16.469	1640	5 nets, complete	
54°1.493	146°15.220	1640	12 bottles	1=1615, 2=1600, 3=1566, 4=1531, 5=1490, 6=1450, 7=1411, 8=1371, 9=1331, 10=1252, 11=502, 12=53 (depth m)
54°22.120	143°58.993	384	empty	
54°21.957	143°59.174	392	mostly empty	core base contains methane and pogonophorans
54°21.955	143°58.960	386	4 cores, 21 - 23 cm	remove 4 barrels for better recovery, sand
54°21.749	143°59.091	398	4 cores, 21 cm each	4 barrels only, mud
54°22.014	143°58.877	382	2 cores, 18 cm	4 barrels only, mud
54°22.211/54°27.627	144°1.955/144°06.043	381	1 video tape, 380 photos	big clam field NNE of hydrate core site
54°26.932	144°5.634	712	599 cm	no evidence for hydrate, core archieved
53°22.693/53°22.126	144°23.856/144°34.386	598/868	1 video tape, 371 photos	1st WP: 53°22.650/144°25.080, missed 2nd WP: 53°22.44/144°31.44, 3 clam fields 3rd WP: 53°22.44/144°31.44, missed
53°51.914	146°44.961	1405	8 cores, 41 - 52 cm	station for paleoceanography, fluff layers
53°51.971	146°47.499	1431	969 cm	station for paleoceanography
54°0.413/54°0.988	146°16.534/146°18.449	1515/1486	full	sediment, barite & calc. burrows, extinct, vent fauna, barite chimney fragments
54°01.216/54°0.780	146°15.686/146°17.395	1490/1511	full	100s kg big chimney fragments, all barite; track from 54°01.297/146°15.875 to 54°00.940/146°16.323
53°59.796	146°17.830	1497	610 cm	barite layers at top and base
54°0.052/54°01.288	146°17.514/146°16.267	1522/1642	full	mostly barite fragments, benthic fauna
53°54.200	146°21.500	1639	12 bottles	1=1597, 2=1573, 3=1537, 4=1504, 5=1467, 6=1432, 7=1393, 8=1352, 9=1294, 10=1251, 11=501, 12=50 (depth m)

LV 28: 28th expedition RV Akademik Lavrentyev

Date 1998 day month	Sta.-Nr	Instrument	Begin (UTC)	at seafloor max. depth	off seafloor	End (UTC)	Duration hh:mm	Latitude °N Begin; at stc./End; off stc.	Longitude °E Begin; at stc./End; off stc.	Water depth m by ECH	Recovery	Remarks
21.08.	40-1	CTD	3:58		4:14	4:50	1:00	51°17.620	147°15.170	1315	12 bottles	1=1274, 2=1250, 3=1001, 4=751, 5=500, 6=250, 7=150, 8=86, 9=52, 10=24, 11=11, 12=2 (depth m)
21.08.	40-2	MUN	5:00		5:40	6:25	1:25	51°18.102	147°14.532	1315	5 nets, complete	
21.08.	40-3	MUC	7:43		8:14	8:45	1:02	51°20.087	147°13.090	1313	7 cores, 34 - 47 cm	
21.08.	40-4	SL-G	9:09		9:28	9:52	0:43	51°20.141	147°11.847	1370	979 cm	
21.08.	40-5	SL-R	10:08		10:29	10:53	0:45	51°20.045	147°10.831	1312	803 cm	
21.08.	41-1	CTD	17:48		18:15	18:40	0:54	51°42.910	149°05.000	1053	12 bottles	1=1041, 2=1000, 3=901, 4=750, 5=500, 6=250, 7=150, 8=100, 9=50, 10=25, 11=11, 12=1 (depth m)
21.08.	41-2	MUN	19:12		19:43	20:29	1:17	51°42.439	149°04.893	1036	5 nets, complete	
21.08.	41-3	MUC	20:50		21:14	21:42	0:52	51°41.478	149°04.427	1068	8 cores, 26 - 32 cm	
21.08.	41-4	SL-G	22:03		22:22	22:41	0:38	51°40.512	149°04.084	1092	981 cm	
21.08.	41-5	SL-R	22:57		23:21	23:48	0:51	51°38.908	149°03.203	1114	710 cm	
22.08.	42-1	MUN	6:46		7:19	8:20	1:34	51°44.997	151°00.969	1028	5 nets, complete	
22.08.	42-2	CTD	8:27		8:46	9:05	0:38	51°43.420	151°00.23	1015	12 bottles	1=1007, 2=950, 3=750, 4=501, 5=251, 6=150, 7=100, 8=76, 9=50, 10=26, 11=10, 12=3 (depth m)
22.08.	42-3	MUC	9:13		9:39	10:04	0:51	51°43.088	150°59.716	1036	8 cores, 25 - 32 cm	
22.08.	42-4	SL-G	10:33		10:56	11:16	0:43	51°42.886	150°59.125	1041	1084 cm	
22.08.	42-5	SL-R	11:51		12:09	12:36	0:45	51°42.701	150°58.879	1045	720 cm	
22.08.	43-1	CTD	17:35		17:46	18:05	0:30	51°55.860	152°14.850	831	12 bottles	1=819, 2=800,3= 750, 4=500, 5=250, 6=150, 7=100, 8=75, 9=49, 10=25, 11=11, 12=2 (depth m)
22.08.	43-2	MUN	18:17		18:34	19:00	0:43	51°55.464	152°15.325	844	5 nets, complete	
22.08.	43-3	MUC	19:20		19:44	20:06	0:46	51°54.461	152°16.600	842	8 cores, 28 - 32 cm	
22.08.	43-4	SL-G	20:34		20:51	21:16	0:42	51°53.909	152°17.264	847	1100 cm	
22.08.	43-5	SL-R	21:32		21:47	22:16	0:44	51°53.757	152°18.052	839	635 cm	
23.08.	44-1	MUN	1:09		1:25	1:57	0:48	51°59.970	153°05.124	700	5 nets, complete	
23.08.	44-2	MUC	2:24		2:40	3:00	0:36	52°01.152	153°05.872	694	8 cores, 26 - 32 cm	
23.08.	44-3	SL-G	3:26		3:35	3:49	0:24	52°02.514	153°05.949	684	1116cm	
23.08.	44-4	SL-R	4:10		4:20	4:33	0:23	52°03.367	153°06.130	681	825 cm	
23.08.	44-6	CTD	5:18		5:30	5:50	0:34	52°05.099	153°06.790	654	12 bottles	1=642, 2=600, 3=499, 4=376, 5=253, 6=151, 7=104, 8=76, 9=50, 10=25, 11=10, 12=2 (depth m)

Kurile Basin

26.08.	45-1	DR	19:48	21:42		23:02	3:18	48°18.141/48°18.421	151°46.684/151°49.317	2700/2450	full	few rocks, 9 boulders, many dropstones
27.08.	46-1	DR	0:12	1:26	2:04	2:33	2:21	48°18.483/48°18.583	151°48.897/151°48.781	2500/2522	empty	
27.08.	47-1	DR	2:50	3:26	4:30	5:05	2:15	48°18.790/48°18.570	151°49.465/151°48.654	2500/2470	half full	hung up, freed by reversing course; dropstones, sediment
27.08.	48-1	DR	5:48	6:54	7:38	8:03	2:05	48°18.409/48°18.814	151°49.079/151°49.520	2450/2400	full	one large volcanic boulder, many drop stones, much sediment, various (seamount?) rocks
27.08.	49-1	DR	9:54	10:25	12:42	13:10	3:16	48°17.852/48°17.690	151°49.017/151°49.238	2900/2980	full	mostly sediment and drop stones
27.08.	50-1	ECH	16:38			19:20	2:42	Survey III (see separate list)				Vulk. I A - D
27.08.	51-1	DR	21:07	21:58	22:50	23:11	2:04	48°31.002/48°31.002	151°01.873/151°01.843	2820/2300	almost empty	few small dropstones
28.08.	52-1	DR	0:08	1:10	2:21	3:25	3:17	48°32.050/48°31.150	151°01.690/151°01.690	2600/2350	full	one big rounded boulder covered partly with organic matter (sponge), sediment, drop stones
28.08.	53-1	DR	3:38	5:10	5:45	6:07	2:31	48°31.199/48°30.783	151°01.619/151°01.290	2360/2540	half full	dropstones, sponges and other organic matter, some Mn-Fe crusts
28.08.	54-1	DR	7:14	8:26	9:46	10:10	2:56	48°32.016/48°31.464	151°01.873/151°01.533	2600/1352	full	some small rocks, drop stones
28.08.	55-1	CTD	13:30		14:08	15:00	1:30	48°40.155	151°29.660	3104	12 bottles	1=2011, 2=1750, 3=1501, 4=1250, 5=1000, 6=752, 7=552, 8=376, 9=250, 10=153, 11=101, 12=51 (depth m); wire too short, stopped at 2055m (2/3 of water depth)
28.08.	55-2	MUN	15:10		15:43	16:30	1:20	48°41.957	151°29.000	2941	5 nets (complete)	
28.08.	56-1	DR	20:56	22:20	23:30	0:06	3:10	48°18.466/48°18.137	151°48.942/151°50.197	2500/2774	full	big fresh volcanic rock (30 kg), barite fragments, drop stones
29.08.	57-1	DR	1:25	2:27	3:44	4:11	2:46	48°18.792/48°18.807	151°49.593/151°49.833	2600	dredge lost	hung up, 2 pulls over 8 tons
29.08.	58-1	ECH	16:17			21:10	4:53	Survey IV (see separate list)				Vulk. II A - C

LV 28: 28th expedition RV Akademik Lavrentyev

Date 1998 day month	Sta.-Nr.	Instrument	Begin (UTC)	at seafloor max. depth	off seafloor	End (UTC)	Duration hh:mm	Latitude °N Begin: at sfc./End: off sfc.	Longitude °E Begin: at sfc./End: off sfc.	Water depth m by ECH	Recovery	Remarks
29.08.	59-1	DR	21:29	22:42	23:32	0:20	2:51	47°59.750/48°00.142	148°29.312/148°29.110	2700/2530	empty	
30.08.	60-1	DR	1:23	2:19	3:36	4:23	3:00	47°58.861/47°59.320	148°72.912/148°27.399	2800/2700	full	sediment, few small rocks
	North/South Transect cont.											
30.08.	61-1	CTD	13:08		13:50	14:34	1:26	48°08.310	146°10.640	1851	12 bottles	1=1780, 2=1750, 3=1500, 4=1250, 5=1000, 6=750, 7=503, 8=375, 9=252, 10=101, 11=50, 12=10 (depth m)
30.08.	61-2	MUN	14:44		15:14	16:05	1:21	48°09.771	146°10.540	1755	5 nets (complete)	
30.08.	61-3	MUC	16:28		17:00	18:04	1:36	48°10.318	146°11.280	1714	8 cores, 32 - 38 cm	block developed major problems during heaving; needs repair
	Methane Monitoring											
31.08.	62-1	CTD	3:48		3:56	4:04	0:16	47°59.650	143°39.470	75	7 bottles	Terpenia Bay; methane monitoring station: 1=75, 2=66, 3=51, 4=30, 5=20, 6=10, 7=15 (depth m)
31.08.	63-1	CTD	5:16		5:31	5:48	0:32	46°00.290	143°33.450	75	8 bottles	Terpenia Bay; methane monitoring station: 1=75, 2=71, 3=66, 4=60, 5=51, 6=26, 7=11, 8=2 (depth m)
	North/South Transect cont.											
31.08	64-1	CTD	16:33		17:15	18:05	1:32	47°52.980	146°13.590	2081	12 bottles	1=1914, 2=1749, 3=1497, 4=1250, 5=1001, 6=753, 7=500, 8=375, 9=252, 10=125, 11=50, 12=9 (depth m)
31.08	64-2	MUN	18:23		18:57	20:09	1:46	47°52.229	146°09.697	2582	5 nets (complete)	
31.08	64-3	MUC	20:28		21:15	22:00	1:32	47°54.203	146°07.110	2480	5 cores, 28 - 38 cm	
31.08	64-4	SL-G	22:24		22:50	23:58	1:34	47°54.427	146°05.708	2494	no recovery	cancelled midway because of serious mechanical problems with block despite repair
01.09.	64-5	SL-G	4:50		5:36	6:46	1:56	47°52.861	146°12.860	2601	1125 cm	
01.09	65-1	CTD	9:09			10:01	0:52	47°39.740	146°16.560	2976	12 bottles	station terminated early, wire to short and winch problems (one-way induction cable winch), bottles fired at shallow depths: 1=1167, 2=1000, 3=750, 4=502, 5=180, 6=139, 7=123, 8=99, 10=62, 11=49, 12=10 (depth m)
01.09	65-2	MUN	13:04		13:35	14:15	1:11	47°38.274	146°08.879	3154	5 nets (complete)	
01.09	66-1	MUN	18:10		18:42	19:45	1:35	47°08.060	146°06.760	3094	5 nets (complete)	
01.09	66-2	CTD	19:54		20:41	21:18	1:24	47°07.120	146°03.400	3040	12 bottles	wire too short, stopped at 2/3 of water column; 1=2250, 2=1999, 3=1750, 4=1499, 5=1250, 6=1000, 7=750, 8=501, 9=252, 10=176, 11=52, 12=10
	Methane Monitoring											
02.09	67-1	ECH	5:44			17:56	12:12	Survey V (see separate list)				Methane A - E
05.09	68-1	SBA	5:00				6:00	40°37.900	134°20.700	3312	complete	water temp. 20° tested by all

Latitude/Longitude:
OFOS on seafloor and off seafloor
CTD on seafloor at maximum depth
DR on seafloor and off seafloor
TWL on seafloor and off seafloor

Sampling equipment: CTD: Multisonde and hydrocasts
MUC: Multicorer
SL-R/G: Gravity corer
HYC: Hydrocorer
ECH: Echosounder
OFOS: TV-sled, Ocean Floor Observation System
MUN: Multinet
TWL: Trawl
DR: Dredge
SBA: Sea bath

Appendix 2

Hydroacoustic Anomalies

Total Table of Hydroacoustic anomalies in echosounding data in 28 cruise R/V "Akademik M.A. Lavrentiev" August-September 1998

Date UTC	Time UTC	Latitude grd	Longitude grd	Depth m	Height m	Device kHz	Remark
14.08.98	13.17	53.34867	144.40333	610	100	20	
	13.22	53.36050	144.40333	625	150	20	
	16.11	53.37716	144.41767	625	160	20	
	16.36	53.37950	144.41650	615	200	20	
	19.31	53.77493	144.26560		600	20	
15.08.98	01.09	54.36400	143.98506	380		20	
	04.06	54.44321	143.90080	175	25	12	bottom
	04.12	54.42768	143.90939	179	60	12	bottom
	04.29	54.43459	143.90913	186	50	12	bottom
	04.35	54.43828	143.90793	184	10	12	bottom
	04.42	54.44253	143.90315	179	20	12	bottom
	04.48	54.43103	143.90646	176	20	12	bottom
	06.01	54.44356	143.90251	179	25	12	bottom
	06.11	54.44683	143.90044	177		12	many
	06.17	54.44952	143.89954	176	150	12	
	06.25	54.45335	143.89525	174	50	12	many
	06.32	54.45703	143.89090	172		12	
	06.44	54.44963	143.87433	172	75	12	bottom, many
	06.50	54.44324	143.87822	159		12	
	06.53	54.44232	143.88135	160	40	12	bottom, many
	06.59	54.44118	143.88452	161		12	
	07.12	54.43761	143.89200	165	40	12	bottom, many
	07.22	54.43485	143.89906	170		12	bottom
15.08.98	04.00	54.42865	143.91795				many
	08.55	54.42411	143.92407	170		20	
	09.54	54.38335	143.90736				many
	10.28	54.35189	143.92935	150		20	
	07.43	54.43201	143.90675	177	210	12	bottom, many
	07.56	54.43035	143.91388	200		12	
	09.54	54.38335	143.90736	169	35	12	bottom, many
	09.56	54.37765	143.90338	165		12	bottom
	10.10	54.35262	143.89017	164	50	12	bottom, many
	10.15	54.33855	143.88133	163		12	bottom
	10.26	54.35003	143.92183	184	100	12	bottom, many
	10.38	54.35385	143.94734	298	50	12	bottom
	11.22	54.36710	143.98125	382	140	12	many
	11.26	54.36794	143.98413	385	130	12	
	11.23	54.36733	143.98150	375		20	
	12.26	54.34090	144.00093	458	110	12.20	bottom
	13.27	54.36603	143.98050	385		12.20	bottom
	13.33	54.36843	143.98154	383	385	12	
	13.35	54.36915	143.98183	383	115	12	bottom, many
	13.36	54.36921	143.98183	383		12	

	15.30	54.36943	143.98752	375	140	20	
	15.42	54.37300	143.98217	380	300	20	
	19.57	54.36786	143.98395	383	190	12	bottom, many
	20.00	54.36562	143.98346	428		12	
	20.53	54.36943	143.98152	382	170	12	bottom
	20.57	54.36625	143.98265	383		12	
	22.24	54.34090	144.00288	454	125	12	
	23.39	54.36541	143.97649	376	45	12	
	23.58	54.36925	143.98238	383	80	12	bottom, many
16.08.98	00.00	54.36987	143.98242	384		12	
	02.55	54.37012	143.98323	386	130	12	bottom, many
	03.00	54.36598	143.98235	384	384	12.20	
	03.48	54.36847	143.98602	390	100	20	
	04.20	54.36742	143.98161	383	110	12.20	bottom
	04.50	54.39700	143.98400	400	100	20	
	05.24	54.36953	143.98322	386	120	12	bottom, many
	05.30	54.36488	143.98399	387		12.20	
	06.28	54.33473	143.98198	400	100	20	
	07.37	54.36902	143.98322	385		12.20	many
	07.45	54.36589	143.98105	385	180	12	
	08.19	54.36667	143.98633	375	225	20.12	bottom
	08.21	54.37417	143.99683	380	75	20	
	08.43	54.36750	143.64933	380	350	20	
	08.38	54.36937	143.98413	386	175	12	bottom, many
	08.49	-	-	-	-	12	
	09.21	54.36650	143.98517	375	225	20	
	09.23	54.37300	143.99333	380	75	20	
	10.06	54.36859	143.98013	375	125	12.20	
	10.15	54.36700	143.98444	388	85	12.20	
	10.18	54.36681	143.98155			12	
	10.49	54.35435	143.97707	385	50	12	
	11.57	54.36658	143.99928	375	325	20	
	12.01	54.36663	143.98126	385	155	12	bottom
	13.20	54.34461	144.02069	503	500	12.20	
	13.34	54.34963	144.02477	485	170	12.20	bottom
	16.05	54.46665	144.09702	729	200	12	
	16.36	54.45846	144.06818	700	250	20	
	17.05	54.45302	144.00565	525	110	12	
	17.57	54.44975	144.03087	610	200	20	cloud
	17.58	54.44987	144.02689	610	120	20	cloud
	18.24	54.44579	144.03629	604	75	12	
	18.30				180	12	
	18.34	54.44667	144.08483	610	120	20	cloud
	18.36	54.44602	144.09529	610	150	20	
	18.42	54.44584	144.11859	700	200	20	
	19.18	54.44216	144.07607	689	230	12	many
	19.20	54.44205	144.06781	685		12.20	
	19.29	54.43965	144.03175	680	260	20	
	19.42	54.43305	144.07387	580	550	20	
	19.45	54.43333	144.08600	580	450	20	

	21.15	54.46850	144.14917	800	120	20	
	21.19	54.47450	144.15733	780	200	20	
	21.40	54.45050	144.09050	700	120	20	
	21.48	54.44418	144.07269	687	200	12.20	
	22.37	54.45138	144.05208	655	150	12	
	22.44	54.44367	144.06633	670	180	20	
	22.46	54.43850	144.07433	675	200	20	
	22.47	54.44130	144.06993	680	100	12.20	
	22.50	54.43809	144.07520			12	
	22.57	54.42780	144.08807	690	150	20	
	23.16	54.45129	144.05101	674	210	12	bottom
17.08.98	0.10	54.44432	144.06931	694	260	12	bottom, many
	0.14	54.44275	144.06813	695		12.20	bottom
	0.20	54.44123	144.06836	685	150	12	many
	0.25	54.43947	144.06918	684		12	
	0.46	54.44670	144.04907	661	300	12.20	
	01.17	54.44347	144.06859	685	320	12	bottom
	01.22	54.44245	144.06818	685		12.20	bottom
	01.30	54.44036	144.06985	683	320	12	bottom
	01.48	54.43968	144.06656	686	70	12	
	01.58	54.45930	144.07211	698	200	12.20	
	02.17	54.44439	144.06870	685		12	bottom, many
	02.19	54.44320	144.06854	985		12	bottom
	02.17	54.44300	144.06867	670	400	20	
	02.25	54.44065	144.06833	684	250	12	bottom, many
	02.28	54.43925	144.06895	685		12	bottom
	02.55	54.43919	144.08119	702	200	12	bottom
	02.58	54.44744	144.08237	703	310	12	bottom
	02.59	54.45167	144.08450	700	475	20	
	03.20	54.45015	144.08057	500	400	20	
	03.27	54.44706	144.08151	703	250	12	bottom
	05.00	54.41683	144.16817	810	250	20	
	05.08	54.40644	144.18843	840	200	20	
	05.32	54.39736	144.15106	782	100	12	cloud
	06.18	54.38950	144.16344	800	210	20	
	07.12	54.37533	144.08513	650	480	20	
	08.38	54.33266	144.46527	1080	610	20	
	08.46	54.32533	144.50626	1110	550	20	
	16.33	53.98109	146.28365	1561	225	12	bottom
	17.50	54.00500	146.26979	1479	150	12	many
	18.02	53.93347	146.30009	1494		12	
	19.05	53.99138	146.29980	1498	180	12	many
	19.13	53.99474	146.29385	1541		12	
	18.24	53.98494	146.30215	1514		12	many
	18.34	53.97583	146.31355	1556		12	
	20.19	54.01407	146.27458	1488		12	many
	20.25	54.01567	146.27205	1474	180	12	
	20.27	54.01607	146.27121	1473		12	many
	20.38	54.01925	146.26750	1487		12	

	20.47	54.02197	146.26439	1624	130	12	many
	20.54	54.02440	146.26279	1634	155	12	
	21.55	54.02449	146.26225	1637		12	many
	22.04	54.03375	146.25359	1662	170	12	
18.08.98	01.13	54.01677	146.28136	1503	125	12	cloud
	01.51	54.02021	146.25786	1490	340	12	bottom
	04.42	54.00811	146.27972	1333	100	12	
	05.26	54.00703	146.27850	1544	400	12	bottom, many
	05.27	54.00705	146.27817	1550		12	bottom
	06.52	54.02039	146.26573	1488	180	12	bottom
	07.15	54.01655	146.25537	1473	140	12	bottom
	10.56	54.06860	145.91740	1601	240	12	cloud
	12.18	54.14493	145.46281	1602	50	12	
	13.13	54.19054	145.15877		550	20	
	13.47	54.21617	144.97112	700	850	20	
	16.26	54.34330	144.12595	650		20	
	16.30	54.34626	144.10571			20	
19.08.98	0.35	54.44333	144.06883	620	40	20	
	01.40	54.45967	144.09867	710	500	20	cloud
	01.52	54.46285	144.09628	710	300	20	cloud
	06.49	53.62233	144.33200	660	200	20	
	06.54	53.60517	144.33783	660	200	20	
	07.17	53.52963	144.36192	625	300	20	
	09.08	53.37567	144.43317	625	450	20	cloud
	14.42	53.55675	145.27573			20	
	15.07	53.58704	145.40469			20	
		54.44637	144.08097	710		0	Obzhirov et all.,1989
		54.44307	144.06950	700		0	Ginsburg et all.,1993
		54.44210	144.07833	700		0	Soloviev et all.,1994
		54.43477	144.21020	865		0	
		53.37863	144.42317	640		0	
		53.37285	144.51735	760		0	
		53.37273	144.41817	620		0	
		53.37215	144.54067	700		0	
		53.34443	144.65905	1040		0	
		53.34390	144.48677	700		0	

Notes

bottom - flares on the bottom
many - flares in time interval with next row
cloud - flares on the water
publicated data - Obzhirov, A.I., Kazansky, B.A., Melnichenko, Yu.I. (1989): Effect of the sound scattering in the Okhotsk Sea water. - Pacific Geology, No 2: 119-121 (in Russian).

Ginsburg, G.D., Soloviev, V.A., Cranstone, R.E., Lorenson, T.D., and Kvenvolden, K.A., (1993): Gas Hydrates from continental slope, offshore Sakhaline Island, Okhotsk Sea. - Geo-Marine Letters, 13: 41-48.

Soloviev, B.A., Ginsburg, G.D., Duglas B.K., ... Obzirov A.I., Titaev, B.F. (1994): Gas Hydrates of the Sea of Okhotsk.-Otechestvennaya Geologiya, No 2: 10-17.

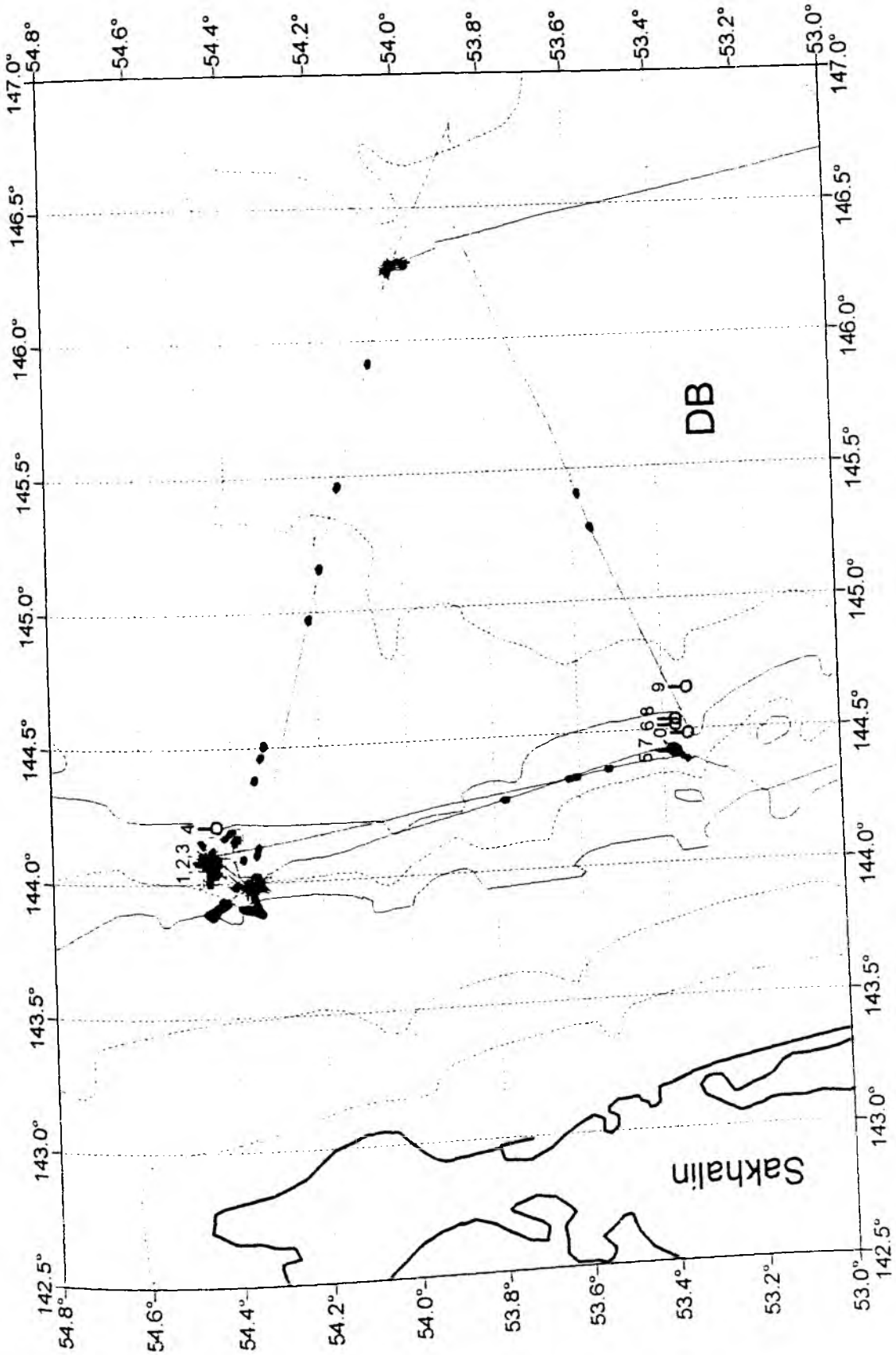

Fig. A2.1: Map of hydroacoustic anomalies in echosounding data recorded during the 28th cruise of RV Akademik M.A.Lavrentyev, August-September 1998

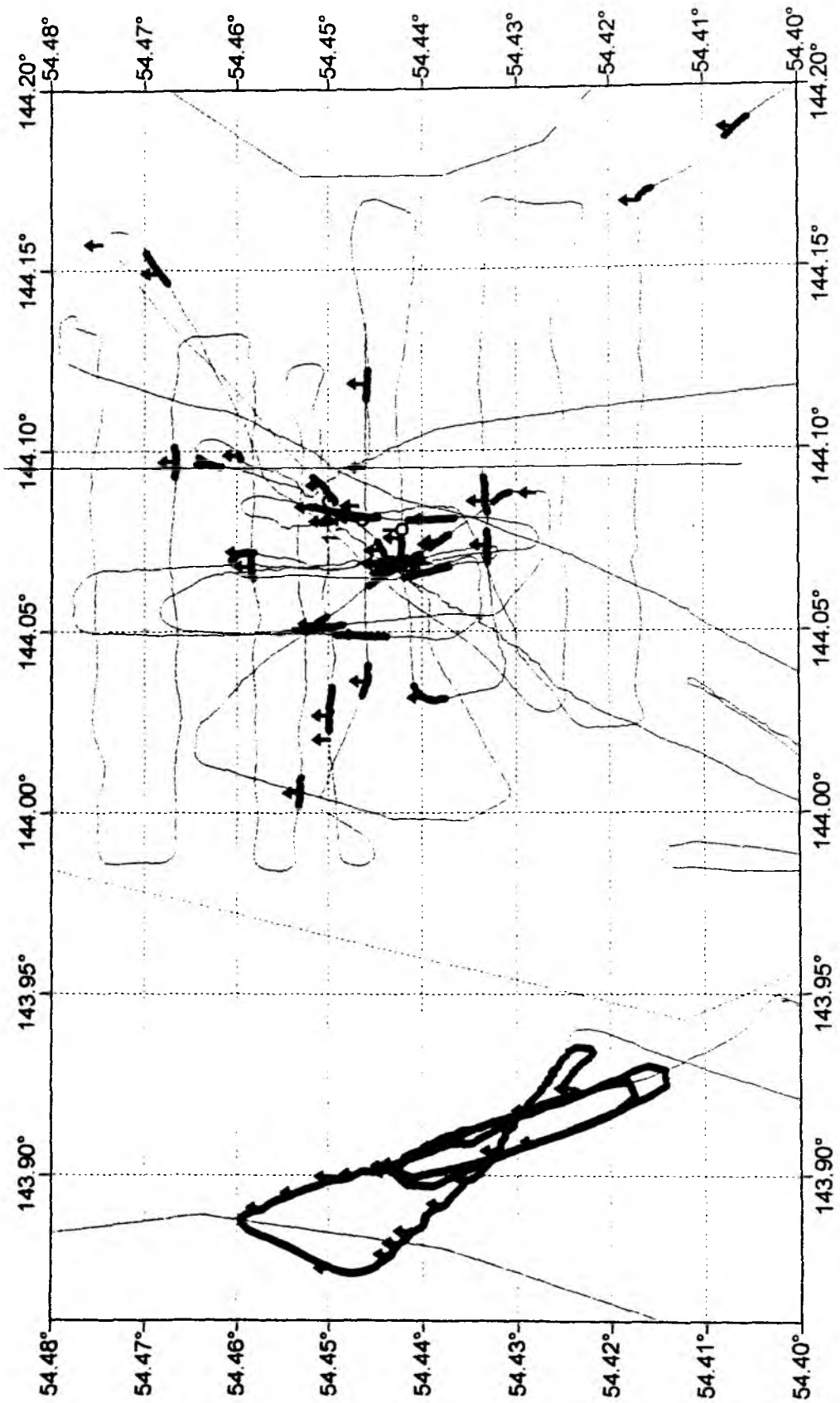

Fig. A2.2: Map of hydroacoustic anomalies in echosounding data recorded during the 28th cruise of RV Akademik M.A. Lavrentyev in the North Sakhalin shelf and slope area (northern part). Bold lines indicate long time spans of acoustic anomalies, arrows indicate single points of acoustic anomalies; numbers indicate anomalies known before; continuing anomalies of the type namd 'fields of fire' occur near the shelf/slope break.

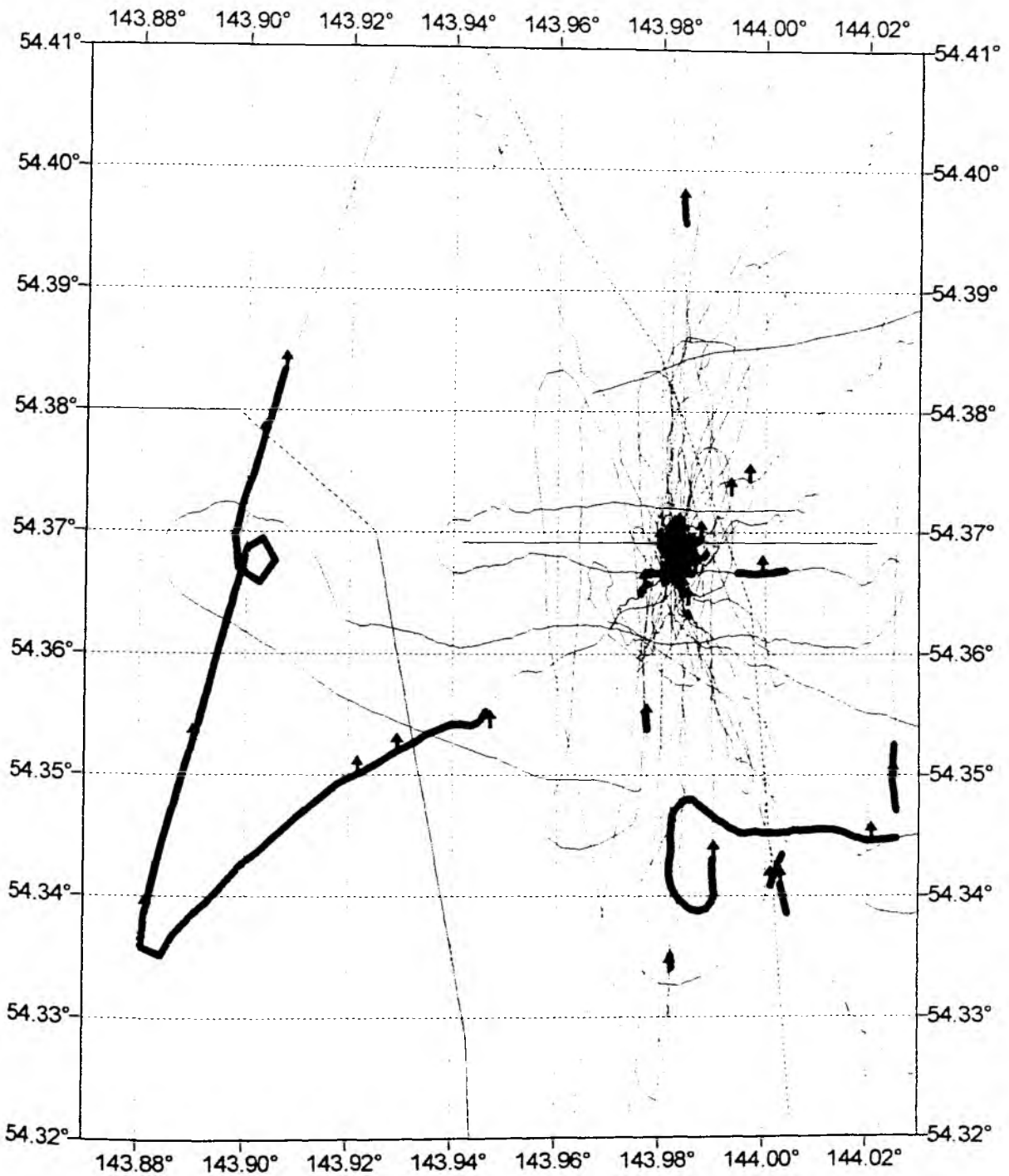

Fig. A2.3: Map of hydroacoustic anomalies in echosounding data recorded during he 28th cruise of RV Akademik M.A. Lavrentyev in the North Sakhalin shelf and slope area (southern part). Bold lines indicate time spans of acoustic anomalies; arrows indicate single points of acoustic anomalies; numbers indicate sites of hydroacoustic anomalies of the type named 'fields of fire' known before.

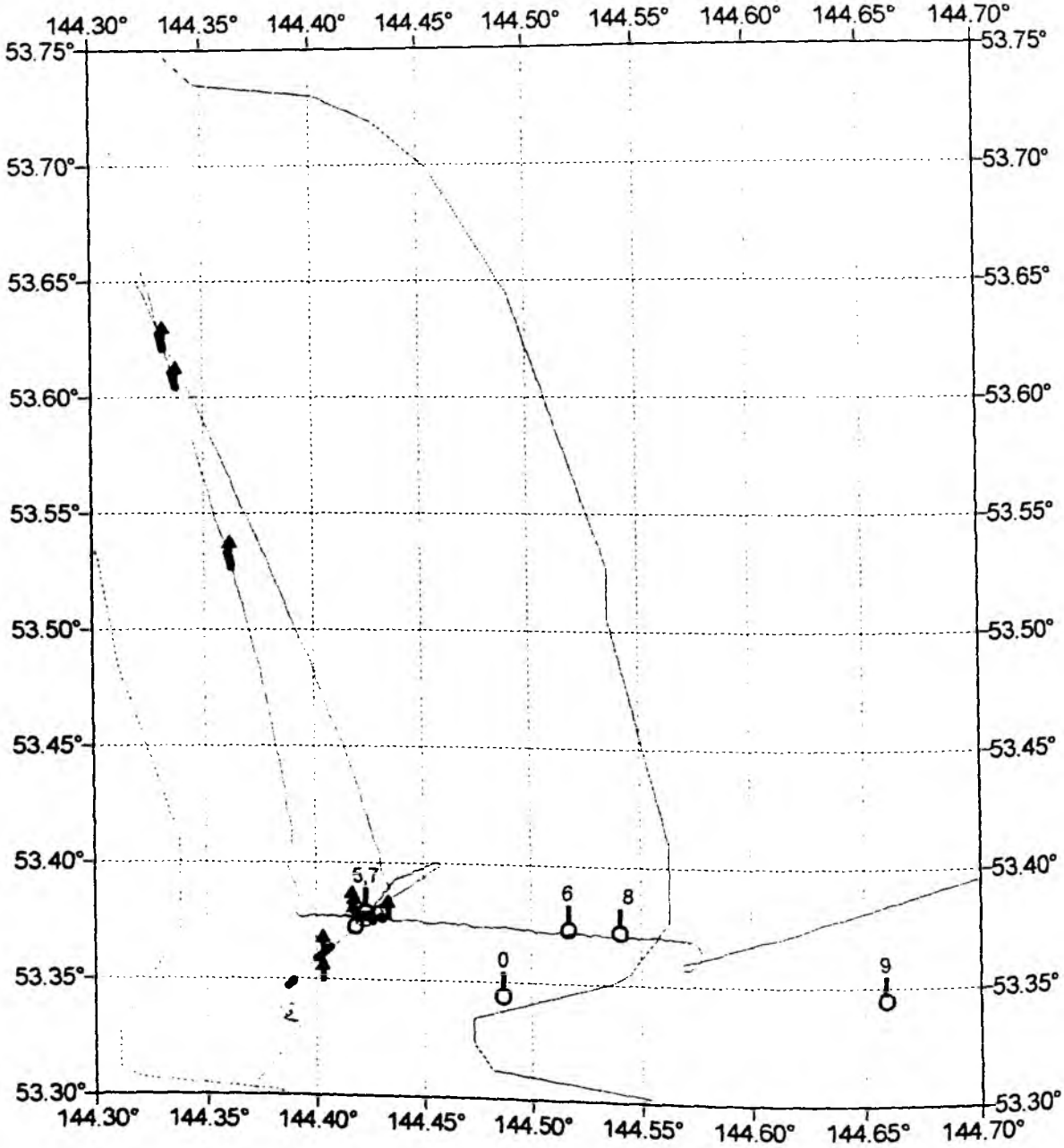

Fig. A2.4: Map of hydroacoustic anomalies in echosounding data recorded during he 28th cruise of RV Akademik M.A. Lavrentyev in the North Sakhalin shelf and slope area (southern part 2). Bold lines indicate time spans of acoustic anomalies; arrows indicate single points of acoustic anomalies; numbers indicate sites of hydroacoustic anomalies known before.

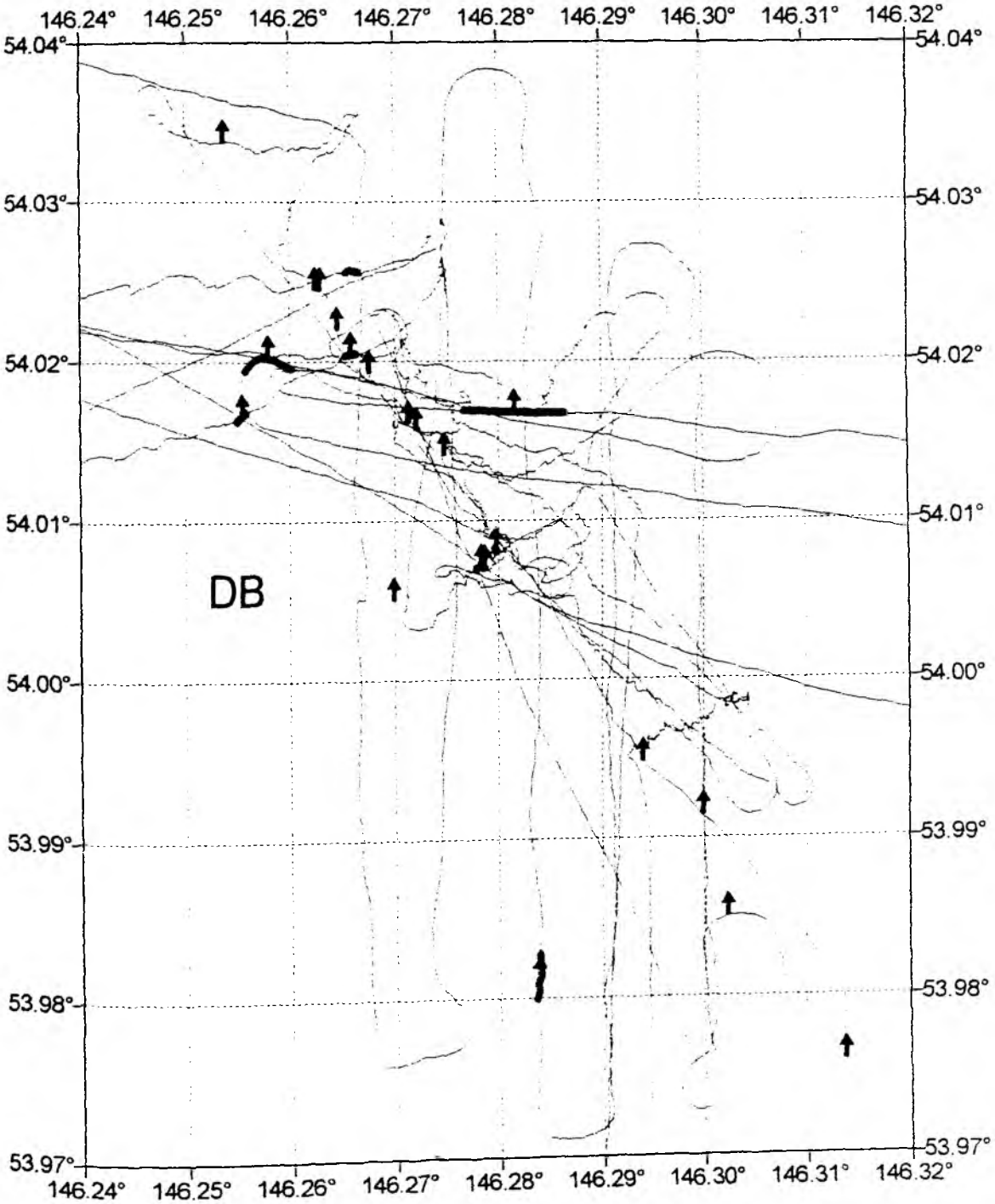

Fig. A2.5: Map of hydroacoustic anomalies in echosounding data recorded during he 28th cruise of RV Akademik M.A. Lavrentyev in the Derugin Basin. Bold lines indicate time spans of acoustic anomalies; arrows indicate single points of anomalies.

Appendix 3.1

Sampling Plan for Multicorer

Sampling plan for Multicorers:

Station:		Pore water	Radiolarians	Anorg. Geochemistry	Biomarker	Isotopes	Sediment	Physical properties	POI samples
LV28-2-2	Length of core	35 cm	30 cm /31 cm	32 cm	32 cm	36 cm	36 cm	36 cm	34 cm
48°21.737	Sample type	cm-slices	cm-slices	cm-slices	2 cm-slices	cm- slices	cm-slices	5cm³ syringes	1 cm slices
146°02.071	Sample	upper cm 0.5-,							
1286 m	interval	next 10 cm 1-, below 3- cm interval	whole core	whole core	whole core	whole core	whole core	whole core	whole core
	Amount of samples	21	61	32	17	36	36	36	34
LV28-4-3	Length of core	--	47 cm	37 cm	37 cm	47 cm	46 cm	46 cm	37
51°08.897	Sample type	--	cm-slices	cm-slices	2 cm-slices	2 cm-slices	cm-slices	5cm³ syringes	1 cm slices
145°18.91	Sample	--	whole core and				upper 5 cm in 1-	upper 5 cm in 1-	
675 m	interval		upper 2 cm from second core	whole core	whole core	5 cm interval	cm-, below 5 cm interval	cm-, below 5 cm interval	whole core
	Amount of samples	--	49	37	19	10	14	14	37
LV28-15-2	Length of core	6.5 cm	--	--	--	--	--	--	--
54°21.173	Sample type	cm-slices	--	--	--	--	--	--	--
143°58.940	Sample	upper cm 0.5-,	--	--	--	--	--	--	--
378 m	interval	below 1- cm interval and 2 samples from second core							
	Amount of samples	10	--	--	--	--	--	--	--
LV28-30-3	Length of core	23/21/21 cm	--	--	--	--	--	--	--
54°21.965	Sample type	cm-slices	--	--	--	--	--	--	--
143°58.980	Sample	upper cm 0.5-,	--	--	--	--	--	--	--
389 m	interval	next 10 cm 1-, below 3- cm interval							
	Amount of samples	41	--	--	--	--	--	--	--

Station:		Pore water	Radiolarians	Anorg. Geochemistry	Biomarker	Isotopes	Sediment	Physical properties	POI samples
LV28-34-1	Length of core	46 cm	42 cm	47 cm	46 cm	52 cm	48 cm	48 cm	41
53°51.914	Sample type	cm-slices	cm-slices	cm-slices	2 cm-slices	2 cm-slices	cm-slices	$5cm^3$ syringes	1 cm slices
146°44.961	Sample interval	upper cm 0.5-, next 10 cm 1-, below 3- cm interval	whole core and upper 2 cm from second core	whole core	whole core	5 cm interval	upper 5 cm in 1-cm-, below 5 cm interval	upper 5 cm in 1-cm-, below 5 cm interval	whole core
1405 m	Amount of samples	31	44	47	25	11	14	14	41
LV28-40-3	Length of core	--	36 cm	40 cm	42 cm	47 cm	41 cm	41 cm	34
51°20.087	Sample type	--	cm-slices	cm-slices	2 cm-slices	2 cm-slices	cm-slices	$5cm^3$ syringes	1 cm slices
147°13.090	Sample interval	--	whole core and upper 2 cm from second core	whole core	whole core	5 cm interval	upper 5 cm in 1-cm-, below 5 cm interval	upper 5 cm in 1-cm-, below 5 cm interval	whole core
1313 m	Amount of samples	--	38	40	22	10	13	13	34
LV28-41-3	Length of core	--	26 cm	26 cm	28 cm	32 cm	26 cm	26 cm	27
51°41.478	Sample type	--	cm-slices	cm-slices	2 cm-slices	2 cm-slices	cm-slices	$5cm^3$ syringes	1 cm slices
149°04.427	Sample interval	--	whole core and upper 2 cm from second core	whole core	whole core	5 cm interval	upper 5 cm in 1-cm-, below 5 cm interval	upper 5 cm in 1-cm-, below 5 cm interval	whole core
1068 m	Amount of samples	--	28	26	16	7	10	10	27
LV28-42-3	Length of core	--	28 cm	27 cm	28 cm	32 cm	31 cm	31 cm	25
51°43.089	Sample type	--	cm-slices	cm-slices	2 cm-slices	2 cm-slices	cm-slices	$5cm^3$ syringes	1 cm slices
150°59.716	Sample interval	--	whole core and upper 2 cm from second core	whole core	whole core	5 cm interval	upper 5 cm in 1-cm-, below 5 cm interval	upper 5 cm in 1-cm-, below 5 cm interval	whole core
1075 m	Amount of samples	--	30	27	16	7	11	11	25
LV28-43-3	Length of core	--	31 cm	31 cm	28 cm	32 cm	31 cm	31 cm	31
51°54.461	Sample type	--	cm-slices	cm-slices	2 cm-slices	2 cm-slices	cm-slices	$5cm^3$ syringes	1 cm slices
152°17.264	Sample interval	--	whole core and upper 2 cm from second core	whole core	whole core	5 cm interval	upper 5 cm in 1-cm-, below 5 cm interval	upper 5 cm in 1-cm-, below 5 cm interval	whole core
847 m									

Station:		Pore water	Radiolarians	Anorg. Geochemistry	Biomarker	Isotopes	Sedimentology	Physical properties	POI samples
	Amount of samples	--	33	31	16	7	11	11	31
LV28-44-2	Length of core	28 cm	30 cm	30 cm	32 cm	32 cm	31 cm	31 cm	29
52°01.152	Sample type	cm-slices	cm-slices	cm-slices	2 cm-slices	2 cm-slices	cm-slices	$5cm^3$ syringes	1 cm slices
153°05.872	Sample interval	upper cm 0.5-, next 10 cm 1-, below 3- cm interval	whole core and upper 2 cm from second core	whole core	whole core	5 cm interval	upper 5 cm in 1-cm-, below 5 cm interval	upper 5 cm in 1-cm-, below 5 cm interval	whole core
694 m	Amount of samples	18	32	30	18	7	11	11	29
LV28-61-3	Length of core	--	32 cm	32 cm	32 cm	37 cm	36 cm	36 cm	38
48°10.318	Sample type	--	cm-slices	cm-slices	2 cm-slices	2 cm-slices	cm-slices	$5cm^3$ syringes	1 cm slices
146°11.280	Sample interval	--	whole core and upper 2 cm from second core	whole core	whole core	5 cm interval	upper 5 cm in 1-cm-, below 5 cm interval	upper 5 cm in 1-cm-, below 5 cm interval	whole core
1720 m	Amount of samples	--	34	32	18	8	12	12	38
LV28-64-3	Length of core	--	30 cm	32 cm	36 cm	38 cm	--	38 cm	28
47°54.203	Sample type	--	cm-slices	cm-slices	2 cm-slices	2 cm-slices	--	$5cm^3$ syringes	1 cm slices
146°05.708	Sample interval	--	whole core and upper 2 cm from second core	whole core	whole core	whole core	--	2 cm slices whole core	whole core
2580 m	Amount of samples	--	32	32	20	21	--	21	28

Appendix 3.2

Core Description

Symbols used in graphical core descriptions

Lithology

- clay
- *silt*
- sand
- silty clay
- sandy silty clay
- sandy silt
- sandy silt with greenish diagenetic alteration
- diatomaceous ooze
- diatomaceous sediment
- weakly diatomaceous sediment
- barite debris with coarse sand
- coarse sand with barite debris
- volcanic ash, glass
- lenses of volcanic ash
- ss — smear slide

Texture

- sharp boundary
- weak boundary
- stratification
- gradational boundary
- lamination
- fining upwards
- fining downwards
- erosive surface
- degassing voids / fissures
- breccied texture
- slight bioturbation
- moderate bioturbation
- strong bioturbation
- lense (filled)
- dropstone
- sponge spicules
- wormtube
- plant fragments
- shell fragments
- authigenic carbonaceous concretions
- gradational color changes
- xxx — diagenetic horizont (often with authigenic clay minerals, dominantly smectite)

Colour code / Soil color chart

light olive-gray	5Y5/2
olive-gray	5Y4/2
dark olive-gray	5Y3/2
dark gray	5Y3/1
reddish	10Y5/3

Core description: **LV28-2-3 GC** Location: **48°22.730N 146°02.217E**

Cruise/Leg: **RV M.A. Lavrentyev / 28** Water depth: **1265** Recovery: **67%**

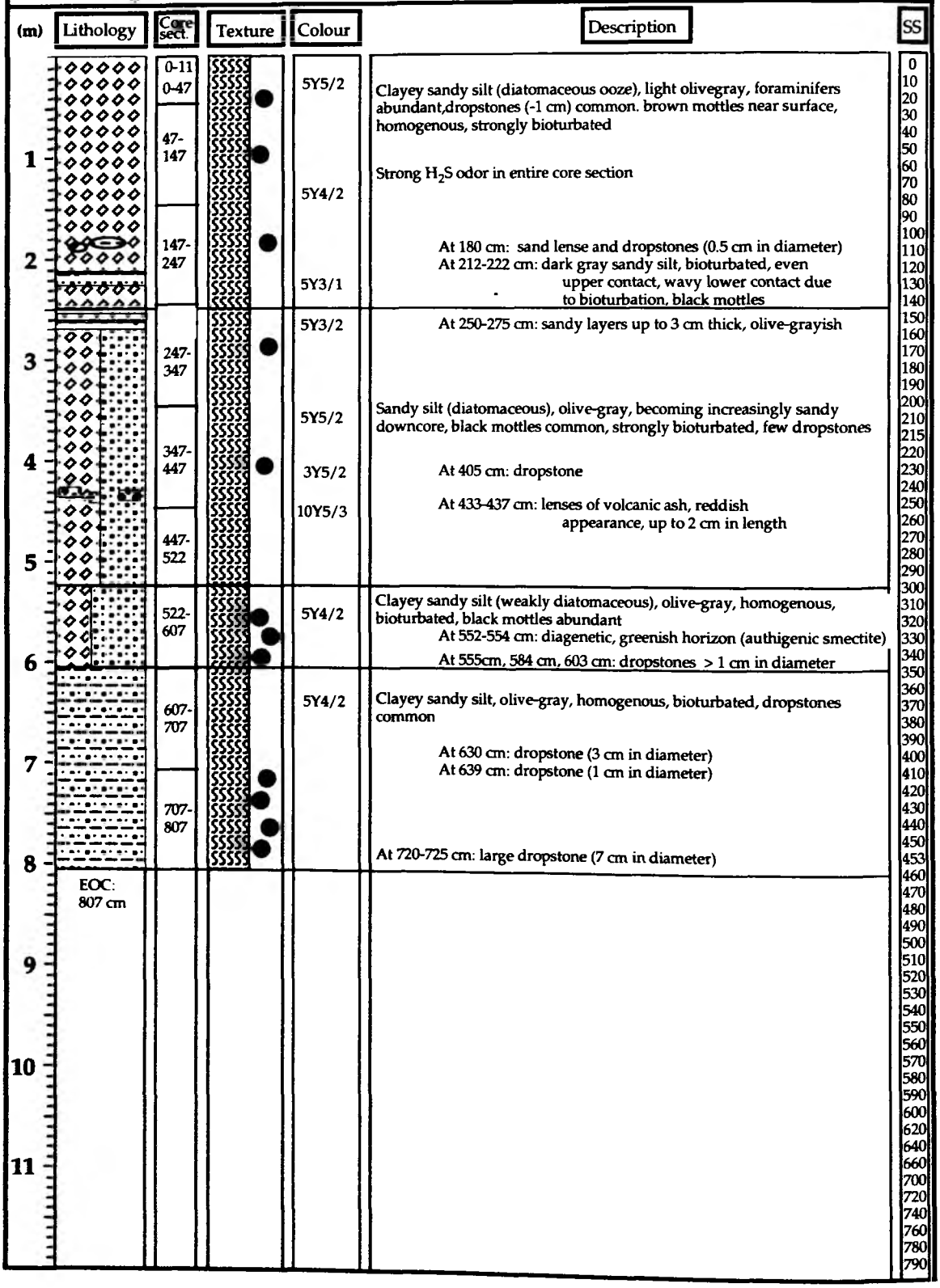

Core description: **LV28-2-4 GC** Location: **48°22.730N 146°02.217E**

Cruise/Leg: **RV M.A. Lavrentyev / 28** Water depth: **1265 m** Recovery: **76%**

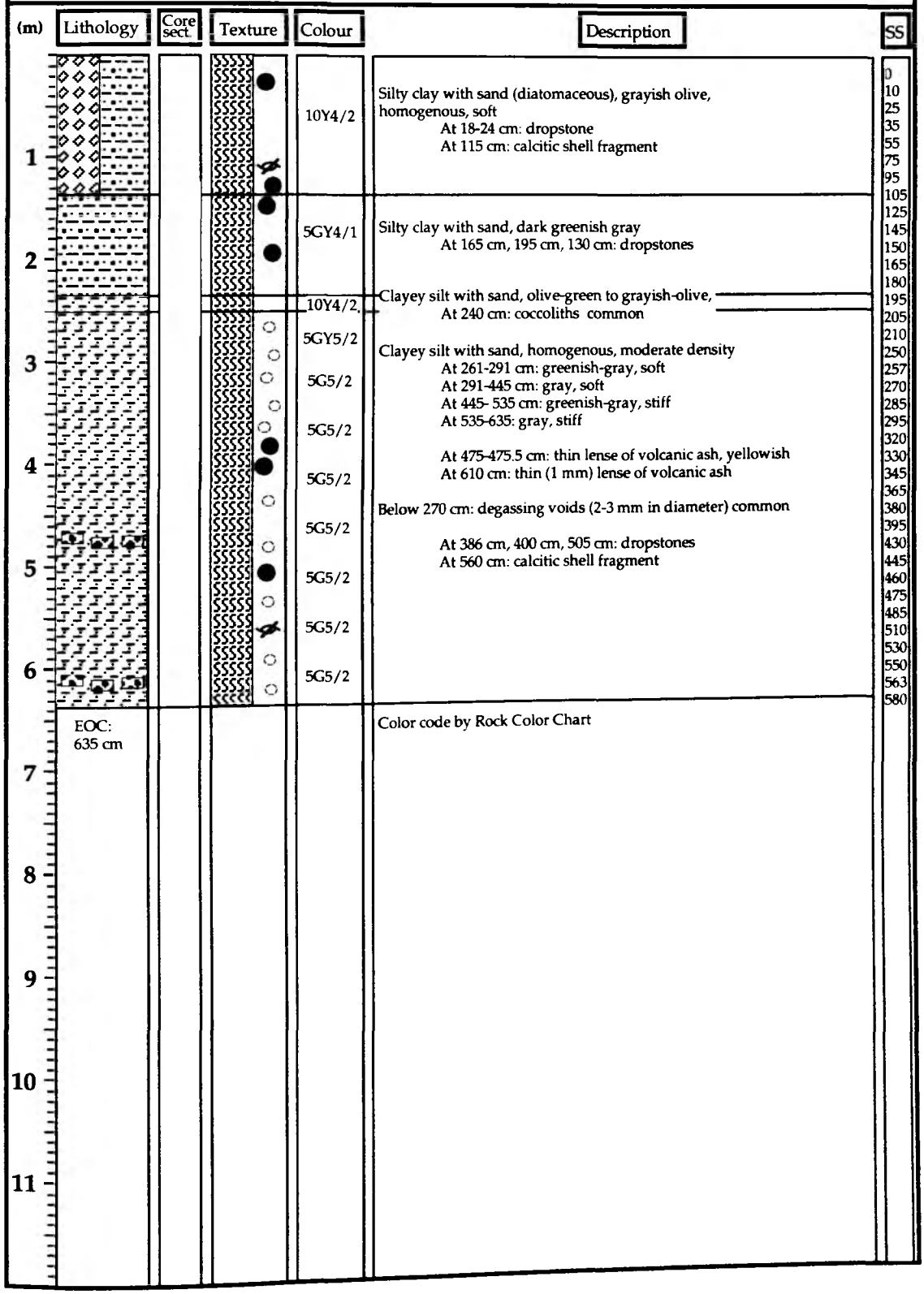

Core description: **LV28-4-4 GC**
Cruise/Leg: **RV M.A. Lavrentyev / 28**

Location: **51°08.475N 145°18.582E**
Water depth: **674 m** Recovery: **77%**

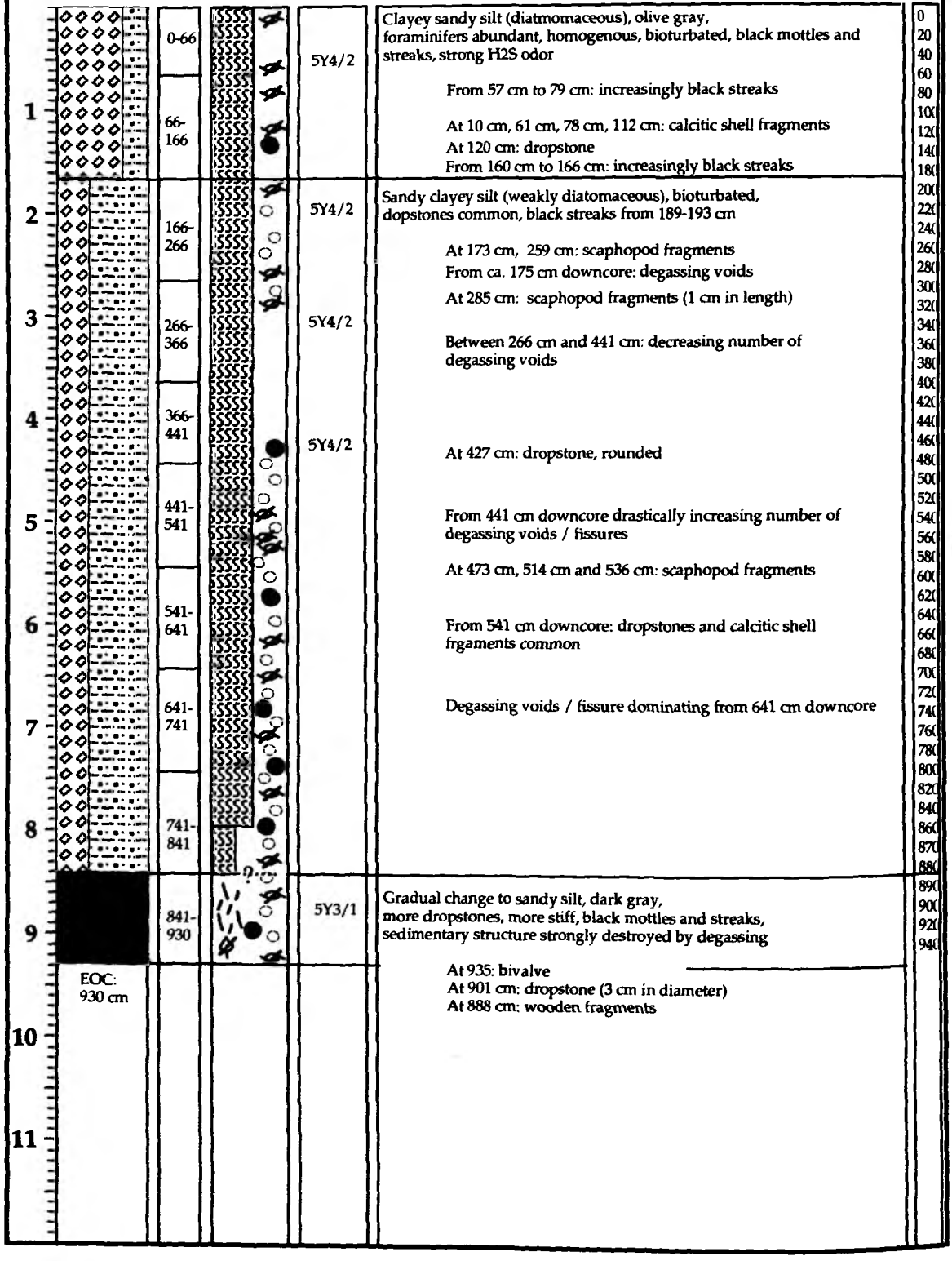

Core description: **LV28-4-5 GC** Location: **51°08.120N 145°18.210E**

Cruise/Leg: **RV M.A. Lavrentyev / 28** Water depth: **670 m** Recovery: **99%**

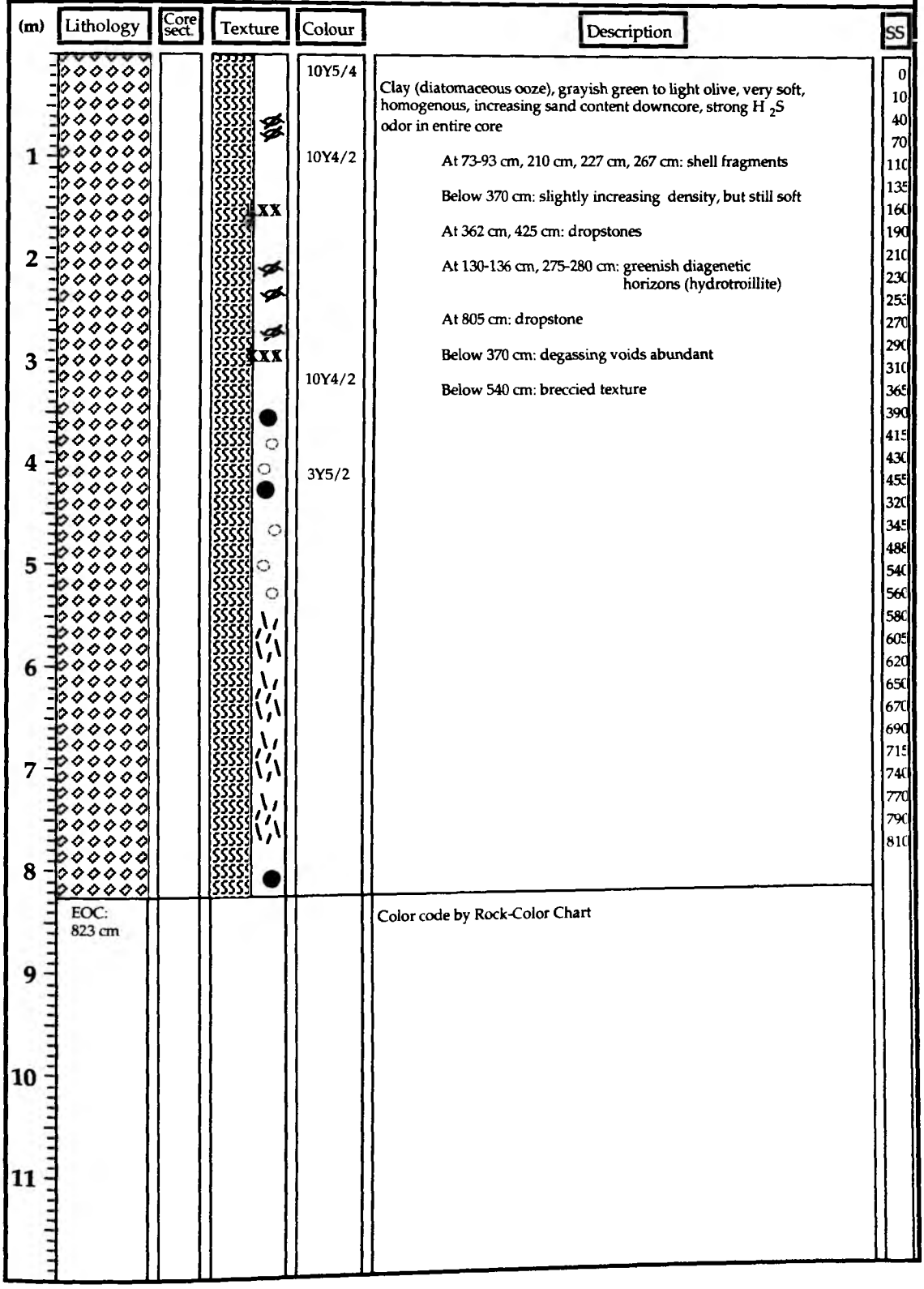

Core description: LV28-17-1 GC Location: 54°21.762N 143°58.760E

Cruise/Leg: RV M.A. Lavrentyev / 28 Water depth: 682 m Recovery: 6%

(m)	Lithology	Core sect.	Texture	Colour	Description	SS
				5Y3/2	Sand, olive-green, well-sorted, shell fragments and dropstones abundant At 15 cm: whole shell	
	EOC: 0.50 m				Color code by Rock-Color Chart	
1						
2						
3						
4						
5						
6						
7						
8						
9						
10						
11						

Core description: **LV28-20-2 GC** Location: **54°26.519N 144°04.093E**

Cruise/Leg: **RV M.A. Lavrentyev / 28** Water depth: **685 m** Recovery: **96%**

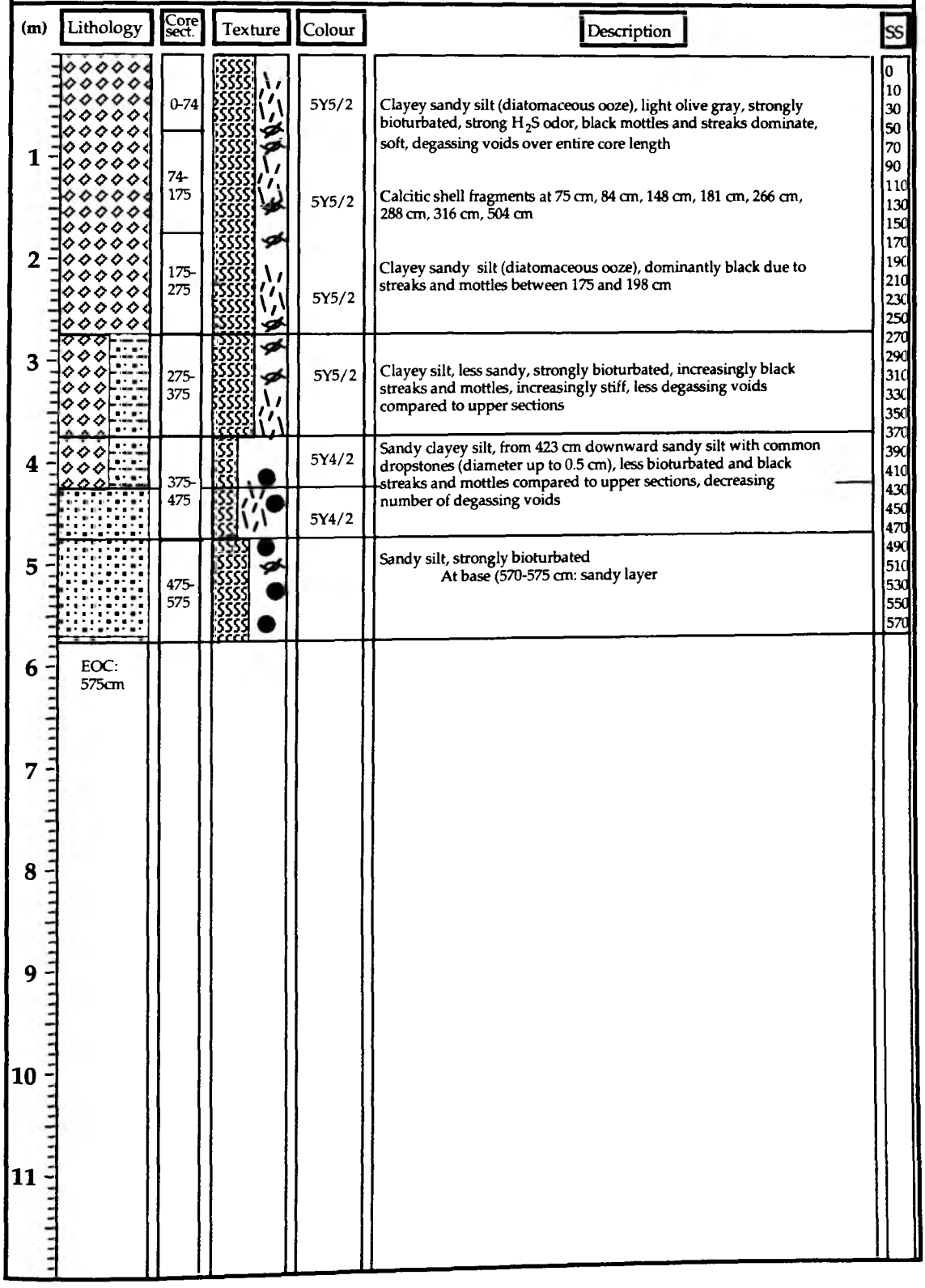

Core description: **LV28-20-3 HYC** Location: **54°26.430N 144°04.120E**

Cruise/Leg: **RV M.A. Lavrentyev / 28** Water depth: **685 m** Recovery: **50%**

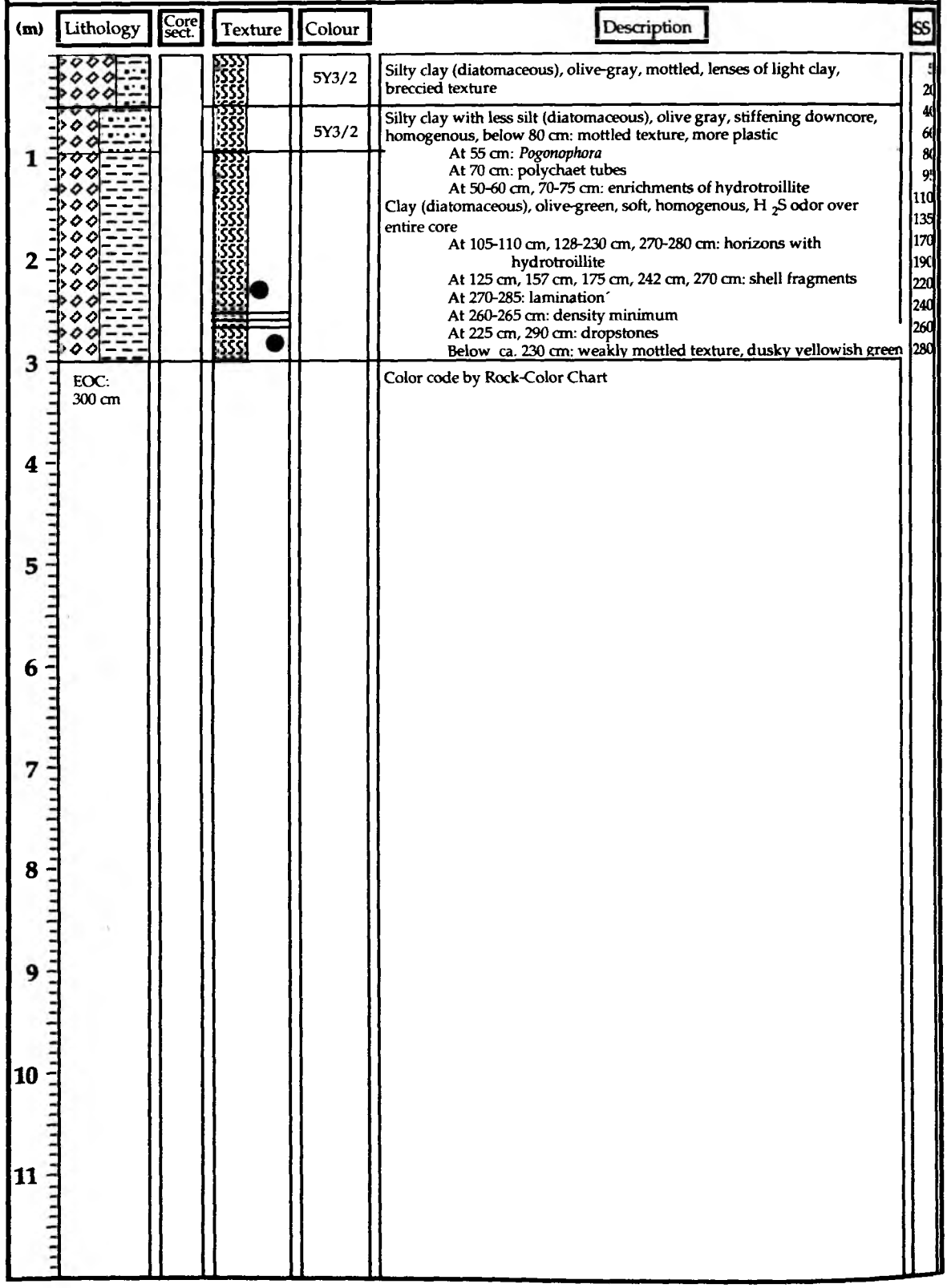

Silty clay (diatomaceous), olive-gray, mottled, lenses of light clay, breccied texture

Silty clay with less silt (diatomaceous), olive gray, stiffening downcore, homogenous, below 80 cm: mottled texture, more plastic

- At 55 cm: *Pogonophora*
- At 70 cm: polychaet tubes
- At 50-60 cm, 70-75 cm: enrichments of hydrotroillite

Clay (diatomaceous), olive-green, soft, homogenous, H_2S odor over entire core

- At 105-110 cm, 128-230 cm, 270-280 cm: horizons with hydrotroillite
- At 125 cm, 157 cm, 175 cm, 242 cm, 270 cm: shell fragments
- At 270-285: lamination´
- At 260-265 cm: density minimum
- At 225 cm, 290 cm: dropstones
- Below ca. 230 cm: weakly mottled texture, dusky yellowish green

Color code by Rock-Color Chart

SS: 5 20 40 60 80 95 110 135 170 190 220 240 260 280

Core description: **LV28-21-1 GC** Location: **54°26.751N 144°04.940E**

Cruise/Leg: **RV M.A. Lavrentyev / 28** Water depth: **702 m** Recovery: **25%**

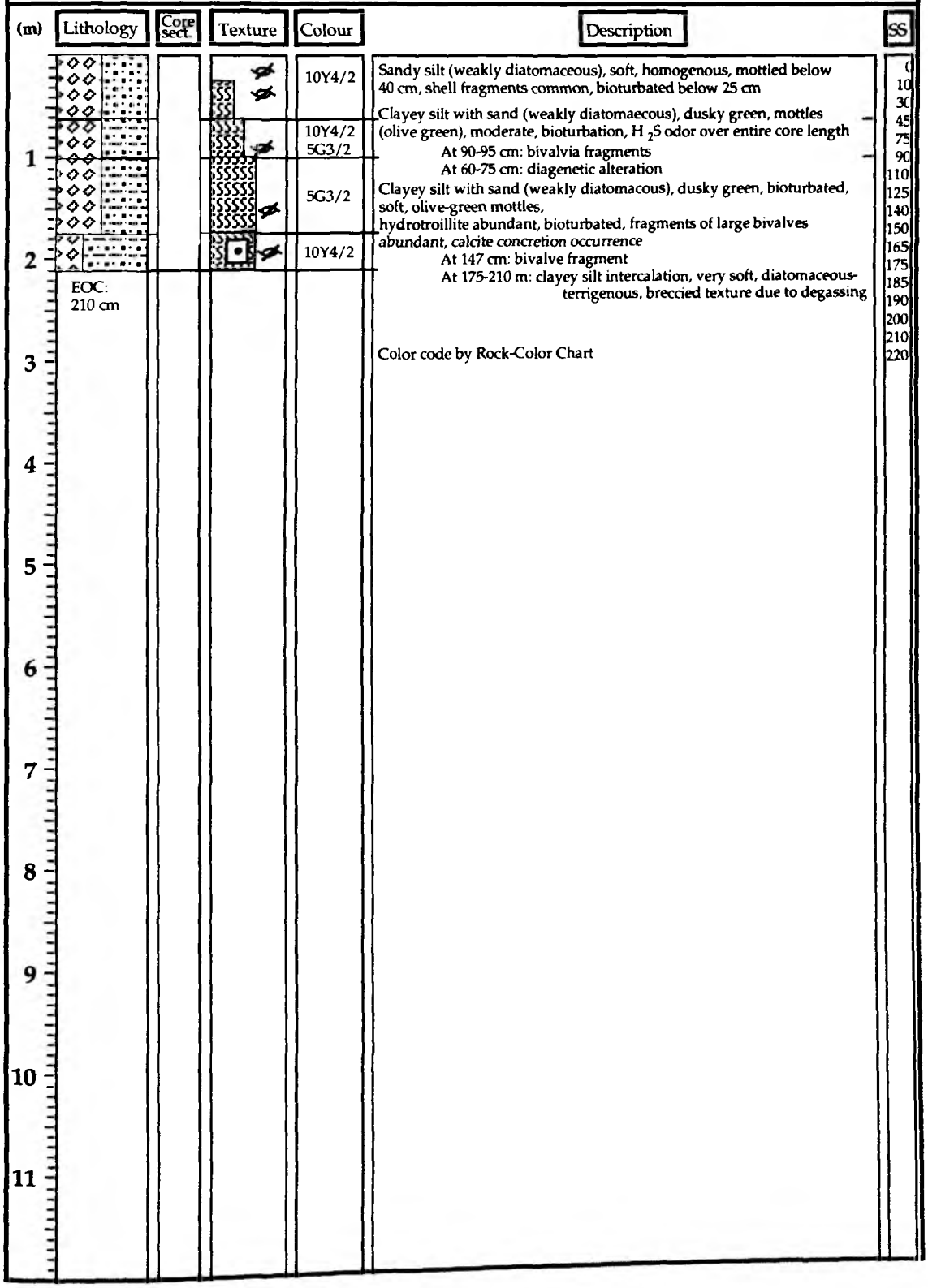

Core description: LV28-25-1 HYC Location: 54°00.844N 146°16.646E

Cruise/Leg: RV M.A. Lavrentyev / 28 Water depth: 1491 Recovery: 27%

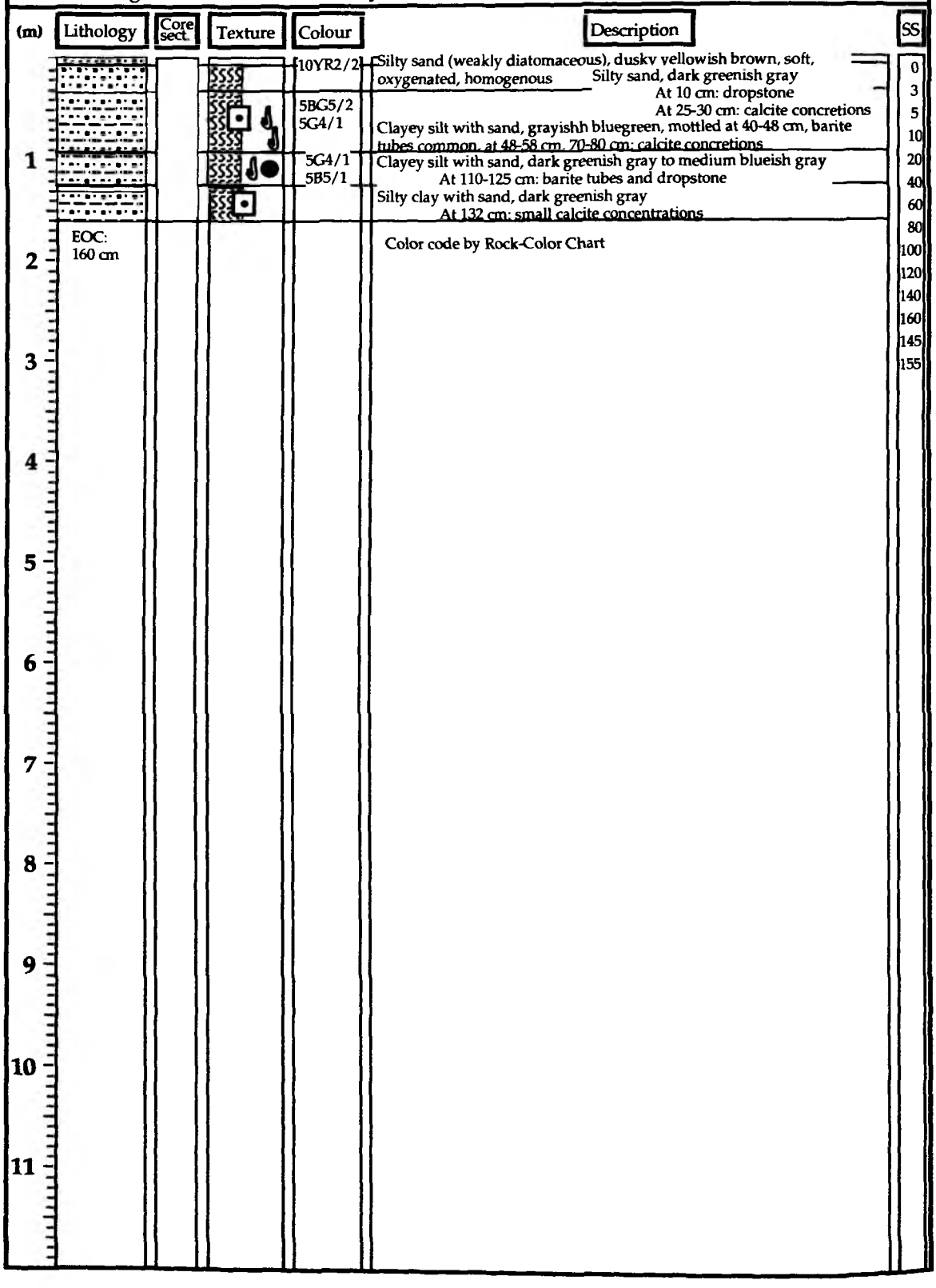

Core description: **LV28-32-1 GC** Location: **54°26.932N 144°5.634E**

Cruise/Leg: **RV M.A. Lavrentyev / 28** Water depth: **712 m** Recovery: **72%**

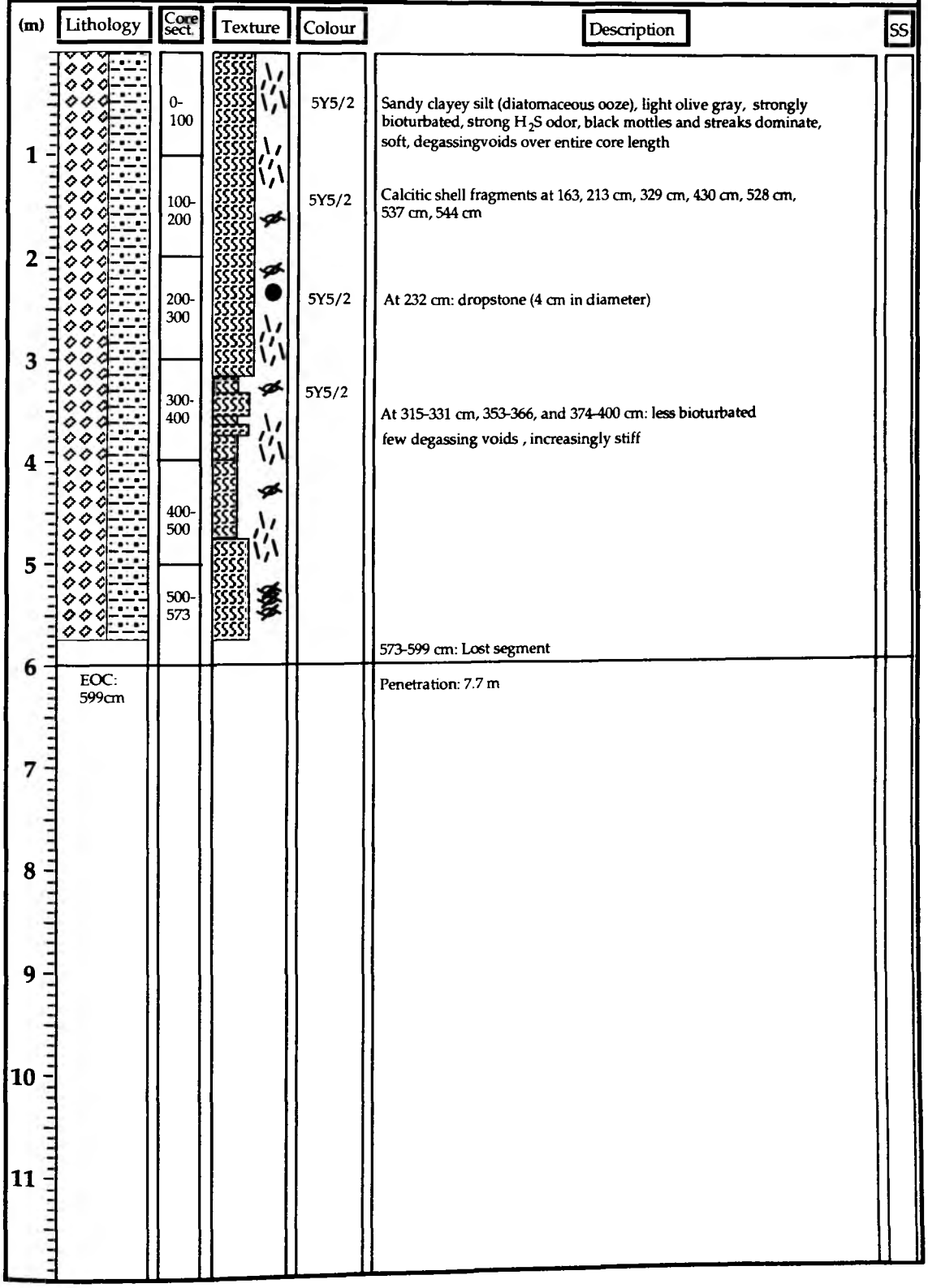

Core description: **LV28-34-2 GC** Location: **53°51.971N 146°47.499E**

Cruise/Leg: **RV M.A. Lavrentyev / 28** Water depth: **1431 m** Recovery: **81%**

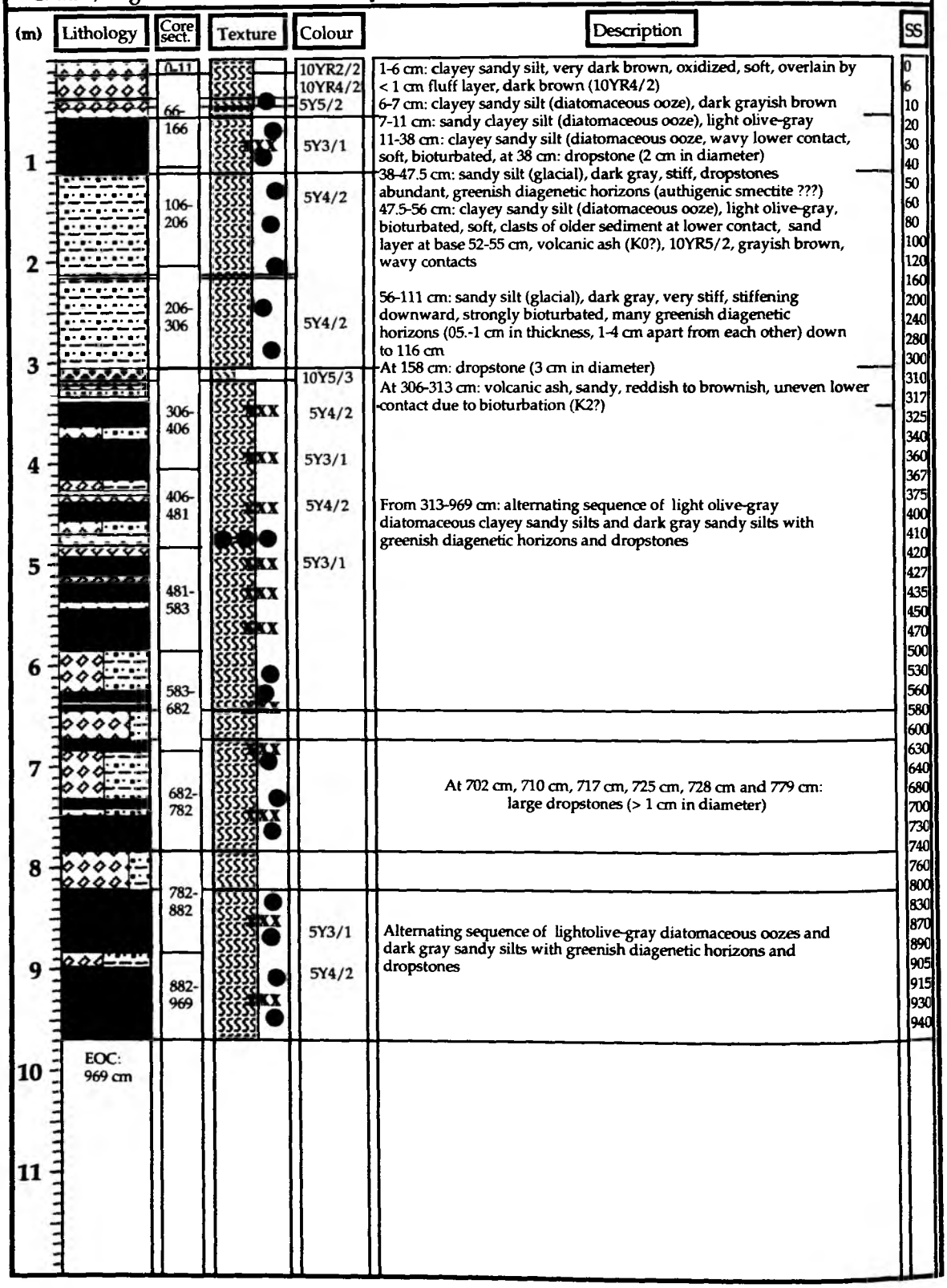

Core description: **LV28-37-1 GC** Location: **53°59.796N 146°17.830E**

Cruise/Leg: **RV M.A. Lavrentyev / 28** Water depth: **1497** Recovery: **73%**

(m)	Lithology	Core sect.	Texture	Colour	Description	SS
				N8	Barite debirs with sand, light gray, high water content, easy to break	2
				5GY6/1	Coarse sand with barite debris, greenish gray	4
				10G4/2	Unsorted sand-silt-clay-barite mixture, grayish green	6
1					Barite debris with sand, light brownish gray At 120 cm: fragment of *Caliptogena* — Silty sand	7 8 10
				5G4/1	Barite silty sand with barite debris, dark greenish gray	11 13
2				N8	Barite crust, very light gray, hard	15 17
				N8	Barite debris/coarse sand mixture, very light gray — Clayey silt	19 21
				5G6/1	Barite debris/coarse sand/silt mixture, greenish gray, fragments of bivalves common (*Caliptogena*)	23 26
				5G4/1	Silty clay with barite debris, dark greenish gray	27
3				5G5/2	Barite debris/coarse sand/silt mixture, grayish green	28 30
				5G5/2	Sandy silt with barite — At 342-344: volcanic ash (K2?)	31 33
				5B5/1	Clayey sandy silt, medium blue-gray	34 34
4				5G6/1	Barite debris and sand, greenish gray Barite sandy silt	36 37
				5B9/1	Barite debris/sand/silt mixture, blue white	38 41
				5GY3/2 5G4/1	Unsorted sand/silt/clay mixture with barite debris, grayish olive green to dark greenish gray At 495 cm: dropstone At 490 cm: fragment of *Caliptogena*	44 46 47
5				5G6/1	Barite debris, coarse sand, coarse fragments, greenish gray At 520 cm, 570 cm: fragments of *Caliptogena*	48 49 51 57
					Coarse sand with barite debris	59
6	EOC: 600cm				Color code by Rock-Color Chart	
7						
8						
9						
10						
11						

Core description: **LV28-40-4 GC** Location: **51°20.141N 147°11.647E**

Cruise/Leg: **RV M.A. Lavrentyev / 28** Water depth: **1370 m** Recovery: **82%**

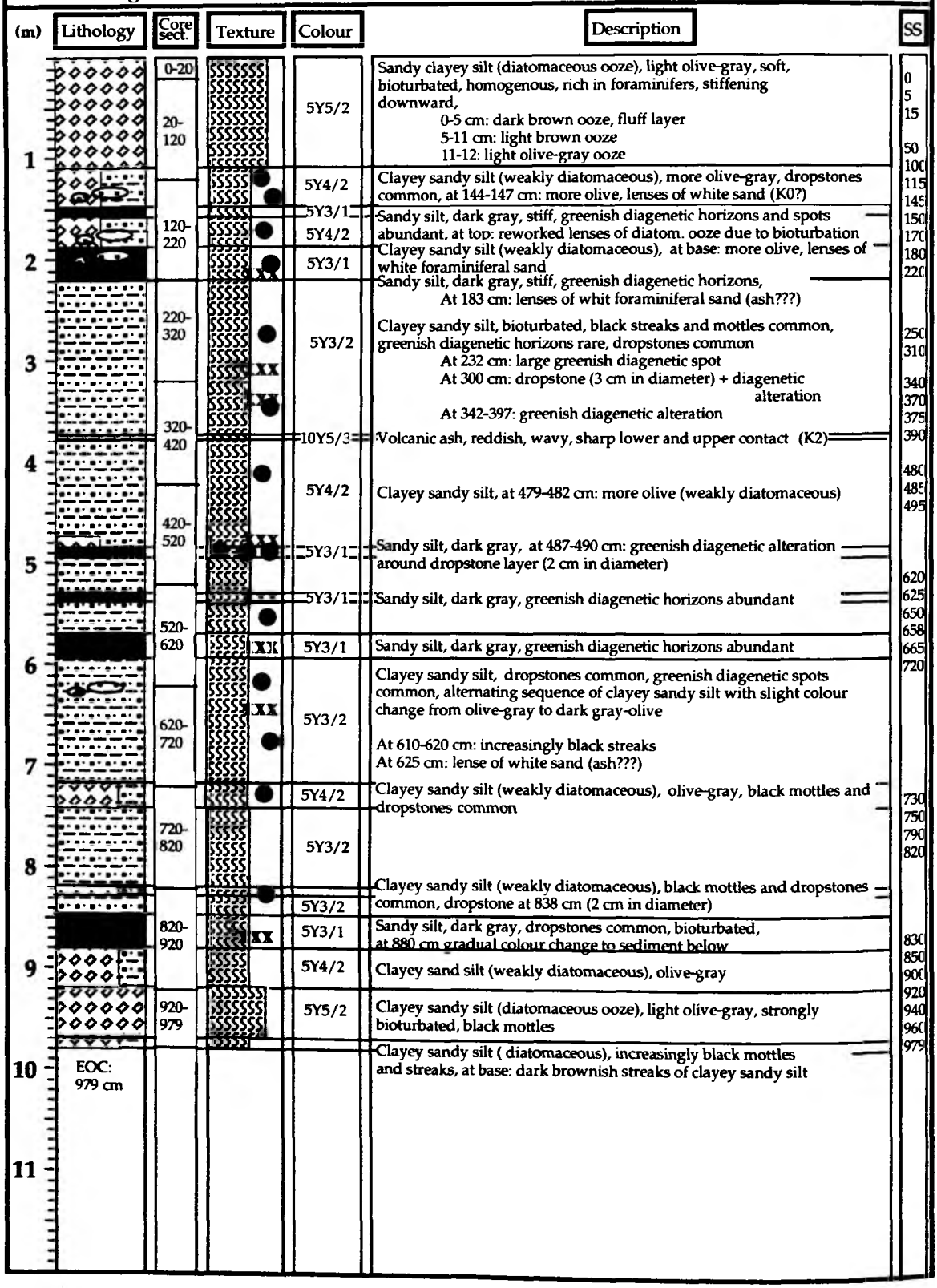

Core description: **LV28-40-5 GC** Location: **51°20.045N 150°10.631E**

Cruise/Leg: **RV M.A. Lavrentyev / 28** Water depth: **1312 m** Recovery: **96%**

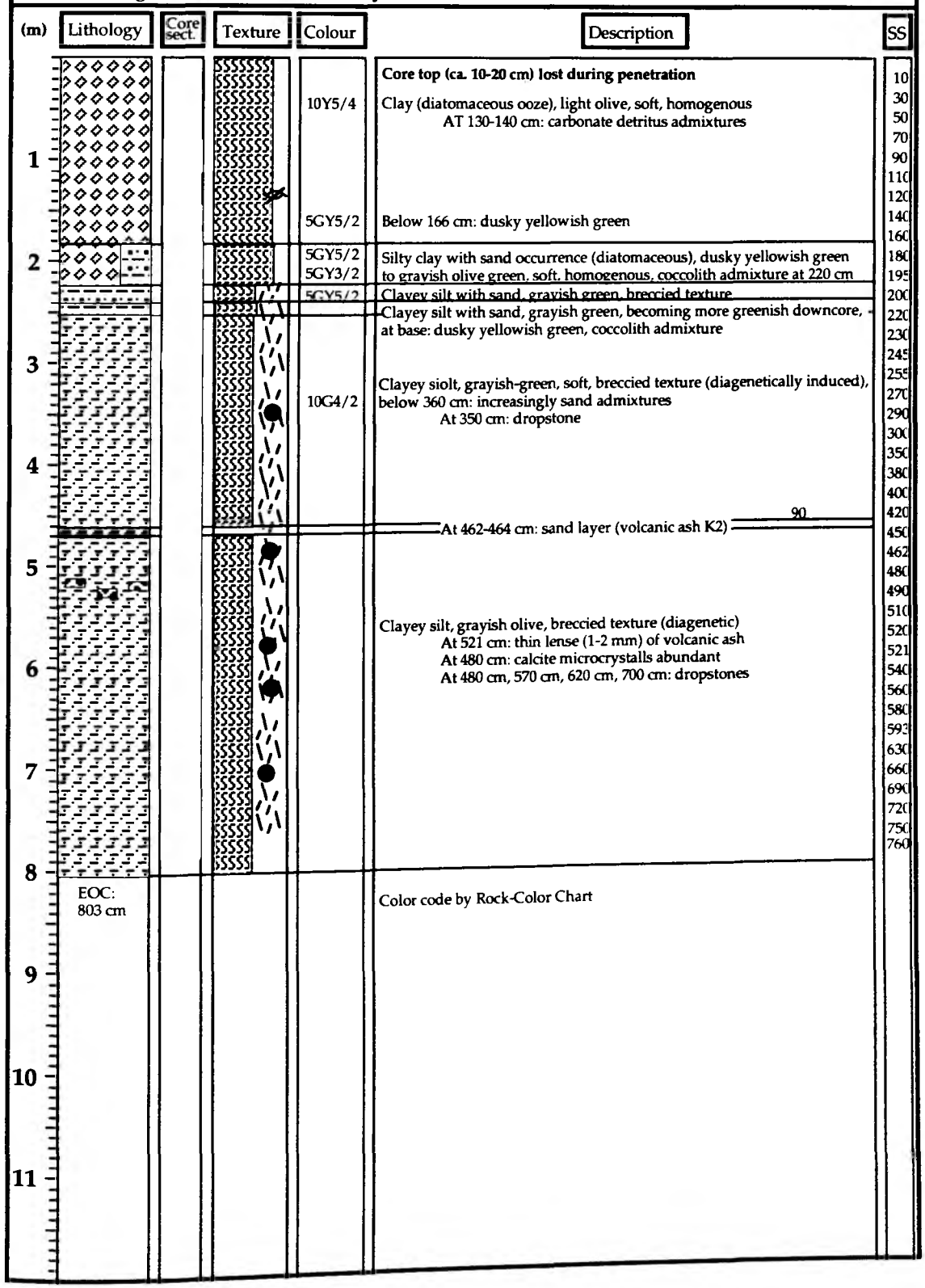

Core description: **LV28-41-4 GC** Location: **51°40.512N 149°04.084E**

Cruise/Leg: **RV M.A. Lavrentyev / 28** Water depth: **1082 m** Recovery: **82%**

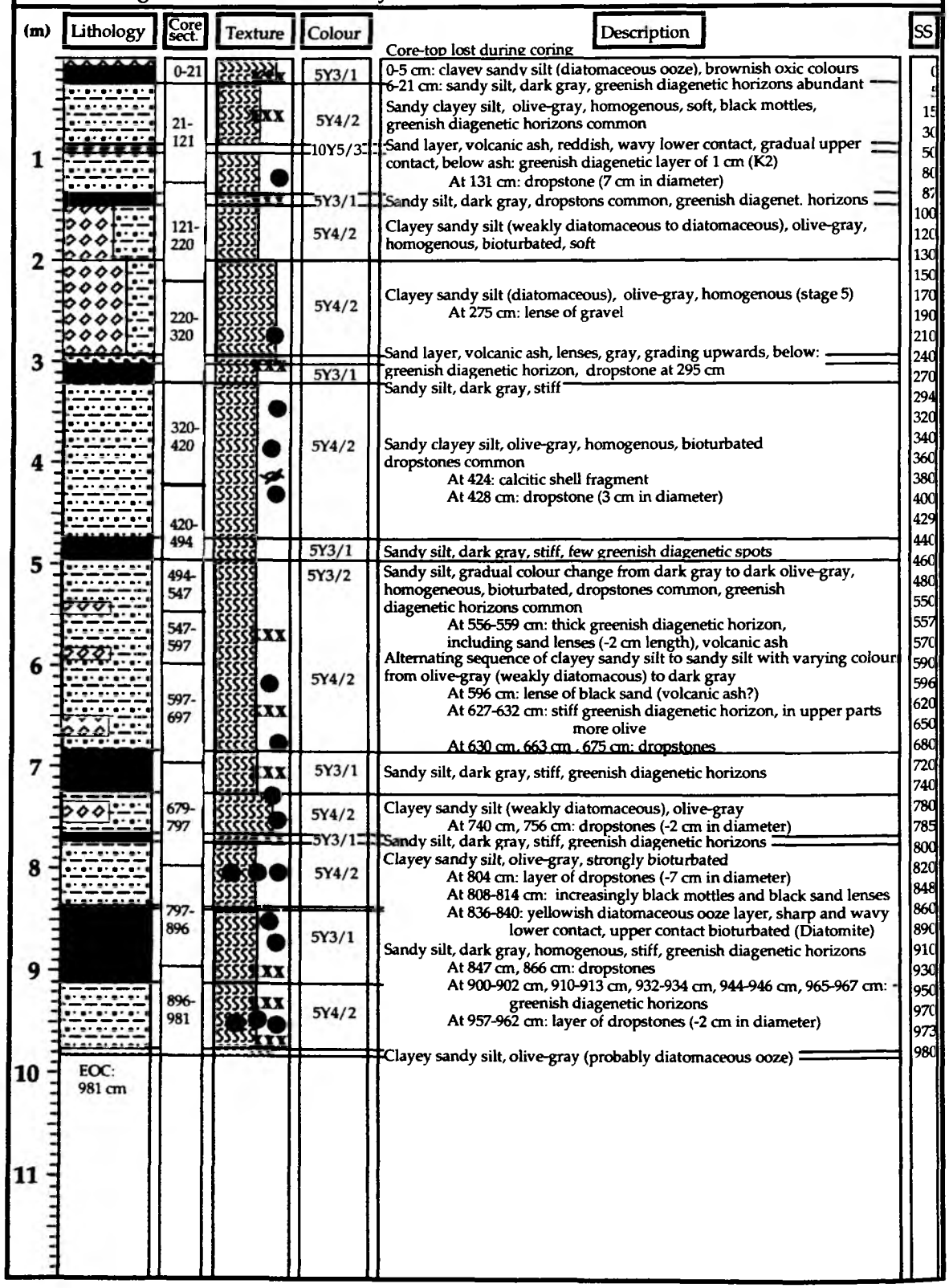

Core description: LV28-41-5 GC Location: 51°38.908N 149°03.203E

Cruise/Leg: RV M.A. Lavrentyev / 28 Water depth: 1114 m Recovery: 85%

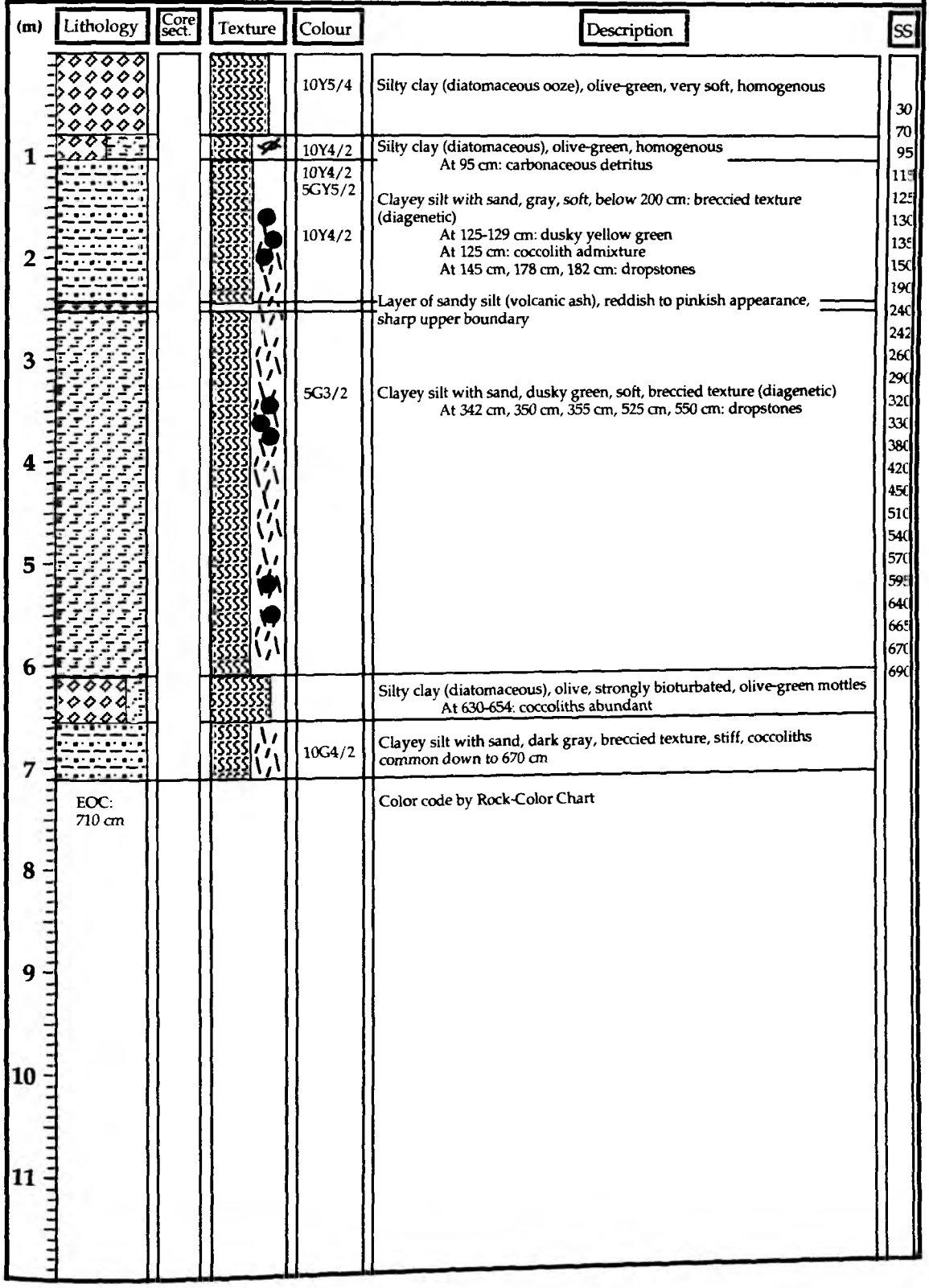

Core description: **LV28-42-4 GC** Location: **51°42.886N 150°59.125E**

Cruise/Leg: **RV M.A. Lavrentyev / 28** Water depth: **1041 m** Recovery: **90%**

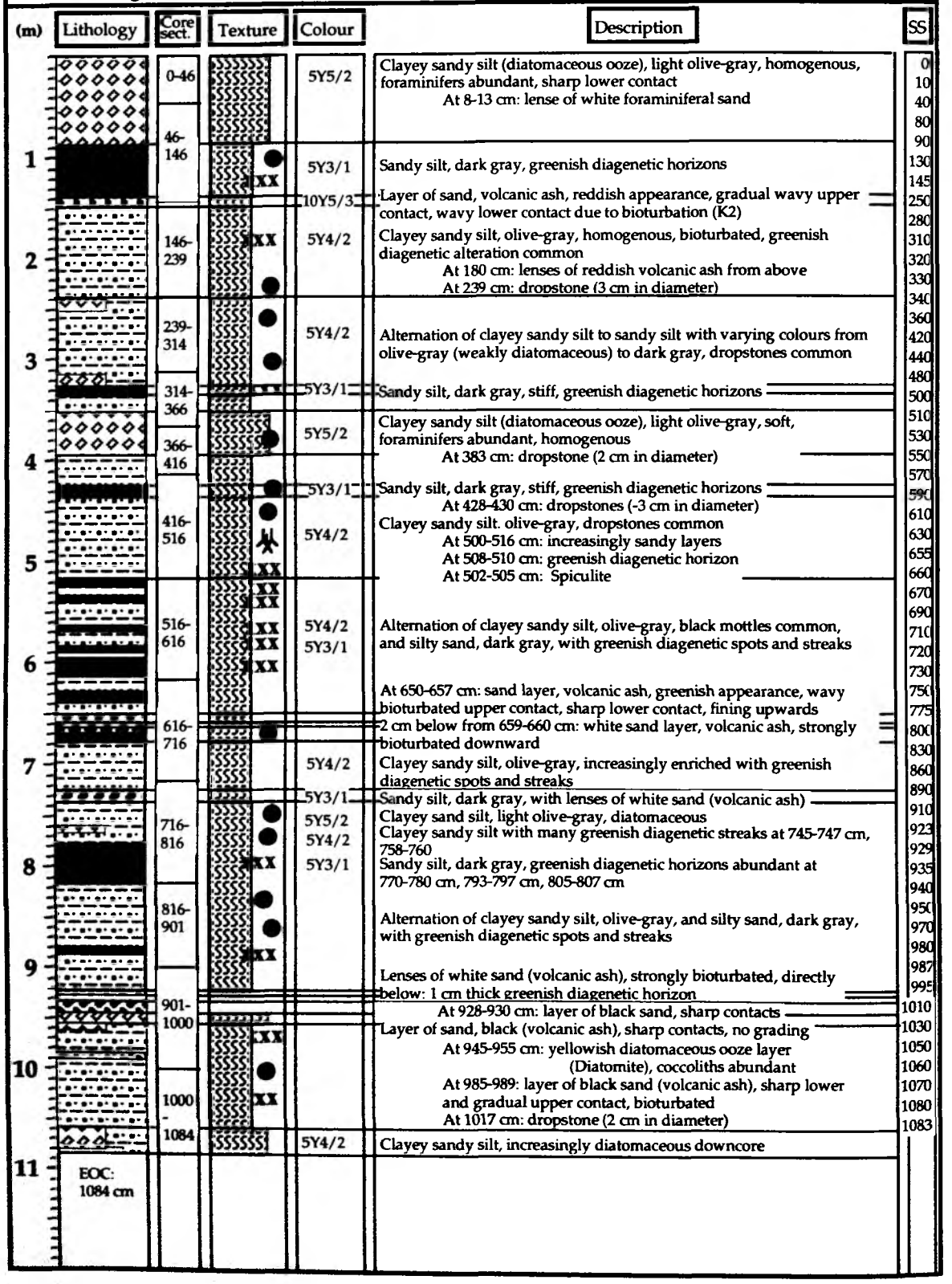

Core description: **LV28-42-5 GC** Location: **51°42.701N 150°58.879E**

Cruise/Leg: **RV M.A. Lavrentyev / 28** Water depth: **1045 m** Recovery: **86%**

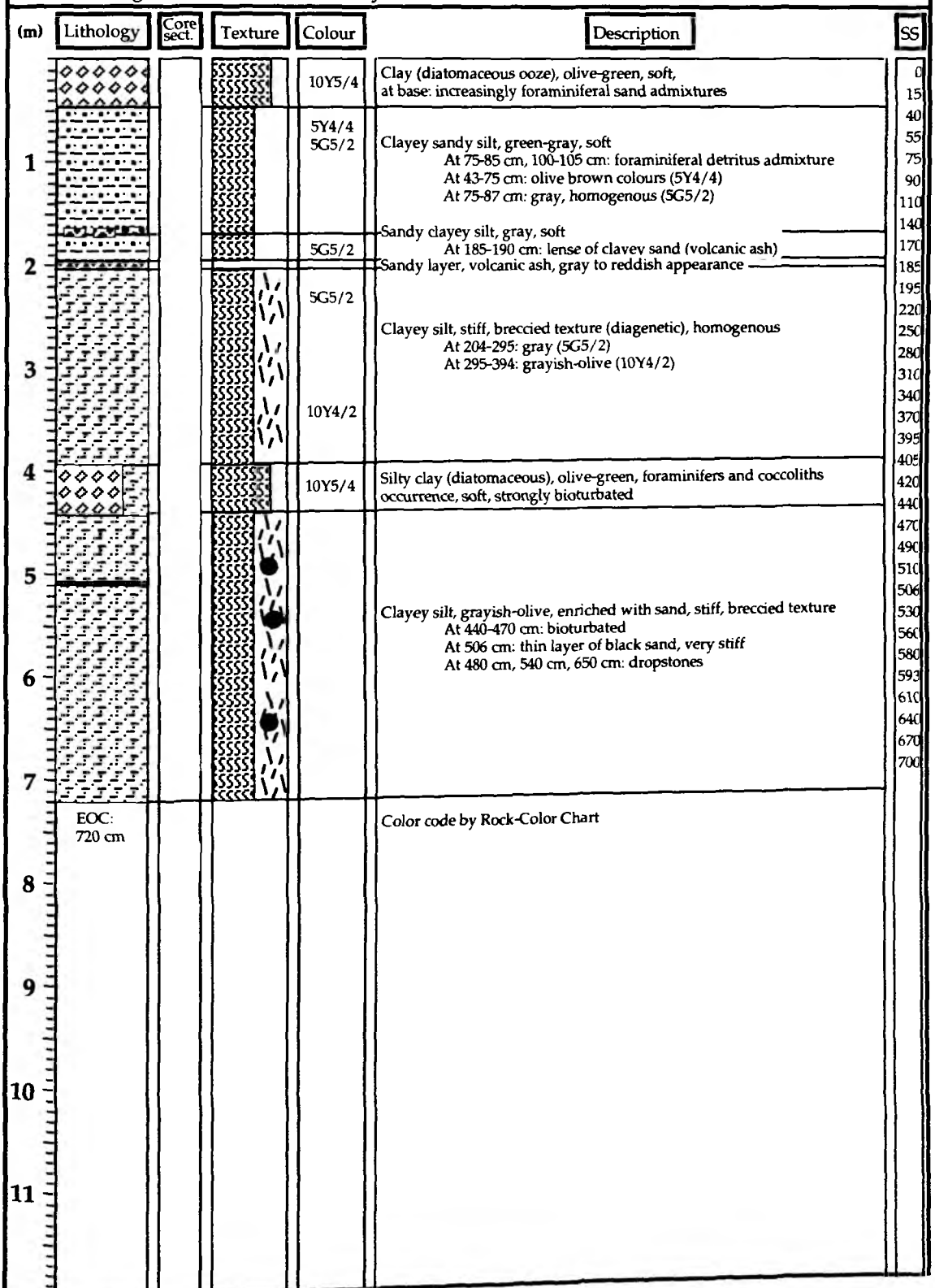

Core description: **LV28-43-4 GC** Location: **51°53.909N 152°17.264E**

Cruise/Leg: **RV M.A. Lavrentyev / 28** Water depth: **847 m** Recovery: **93%**

(m)	Lithology	Core sect.	Texture	Colour	Description	SS
		0-68		5Y5/2	Clayey sandy silt (diatomaceous ooze), light olive-gray, soft, foraminifers abundant, dropstones, common, bioturbated, homogenous	0 30 60 63 90
1		68-168			At 63 cm: lense of white foraminiferal sand From 258 cm downcore: gradually becoming mor olive-gray	
2		168-268				160 190 260 300
3		268-368		5Y4/2	Clayey sandy silt (weakly diatomaceous), olive-gray, foraminifers abundant, dropstones common At 306-315 cm: lenses of volcanic ash	309 350 365 370 380
				5Y3/1	Sandy silt, dark gray, homogenous, even and sharp upper contact	410
				5Y3/1	Sandy silt, dark gray, homogenous, dropstones abundant — Stage 2	450
4		368-468		5Y4/2	Clayey sandy silt, olive-gray, homogenous, black sand lenses and streaks abundant	467 470 480 520
					Volcanic ash, sandy, gray	526
5		468-543		5Y4/2	Clayey sandy silt, olive-gray, including lenses of bioturbated volcanic ash at top From 480-543 slight colour change to more olive, black mottles, streaks, and dropstones common, homogenous, lenses and layers of black sand abundant At 524-528 cm: lenses of white sand, glas shards (K2)	560 560 570 620 640
6		543-642			Alternation of clayey sandy silts showing gradual slight color changes from dark olive-gray to dark gray (depending on opal content?) At 629-632: gravel layer (0.5-1 cm in diameter)	660 680 700
7		642-742		5Y5/2	Clayey sandy silt (diatomaceous), light olive-gray, strongly bioturbated	720 740
			XXX	5Y3/2	Sandy clayey silt, dark olive-gray, lenses of black sand at 737 cm, 739 cm	750 780
8		742-842		5Y3/2 5Y3/1	Alternation of clayey sandy silts showing gradual slight color changes from dark olive-gray to dark gray (depending on opal content?), lenses and streaks of black sand over entire section At 810 cm, 825 cm: lenses of brownish sand (volcanic ash)	800 810 825 830 845
				5Y3/2	Sandy silt, dark olive-gray, greenish diagenetic spots	855
					At 875 cm: dropstone (2 cm in diameter)	865 880
9		842-942		5Y5/2	Clayey sandy silt (diatomaceous ooze), light olive-gray, homogenous, bioturbated, foraminifers abundant, top 15 cm intercalated by lenses of overlying sediment At 890 cm: large lense of black sand (5 cm in diameter)	885 890 895 896 900
10		942-1042		5Y4/2	Clayey sand silt (weakly diatomaceous), strongly bioturbated, black streaks and mottles abundant	940 960 980
		1042-1100	XXX XXX	5Y3/1	Sandy silt, dark gray, greenish diagenetic horizons abundant, bioturbated At 1028 cm: lense of black sand At 1064 cm: dropstones At 1072-1098 cm: brownish patches of clayey sandy silt	990 1010 1030 1040 1060 1098
11	EOC: 1100 cm					1100

Core description: **LV28-43-5 GC** Location: **51°53.757N 152°18.052E**

Cruise/Leg: **RV M.A. Lavrentyev / 28** Water depth: **839 m** Recovery: **76%**

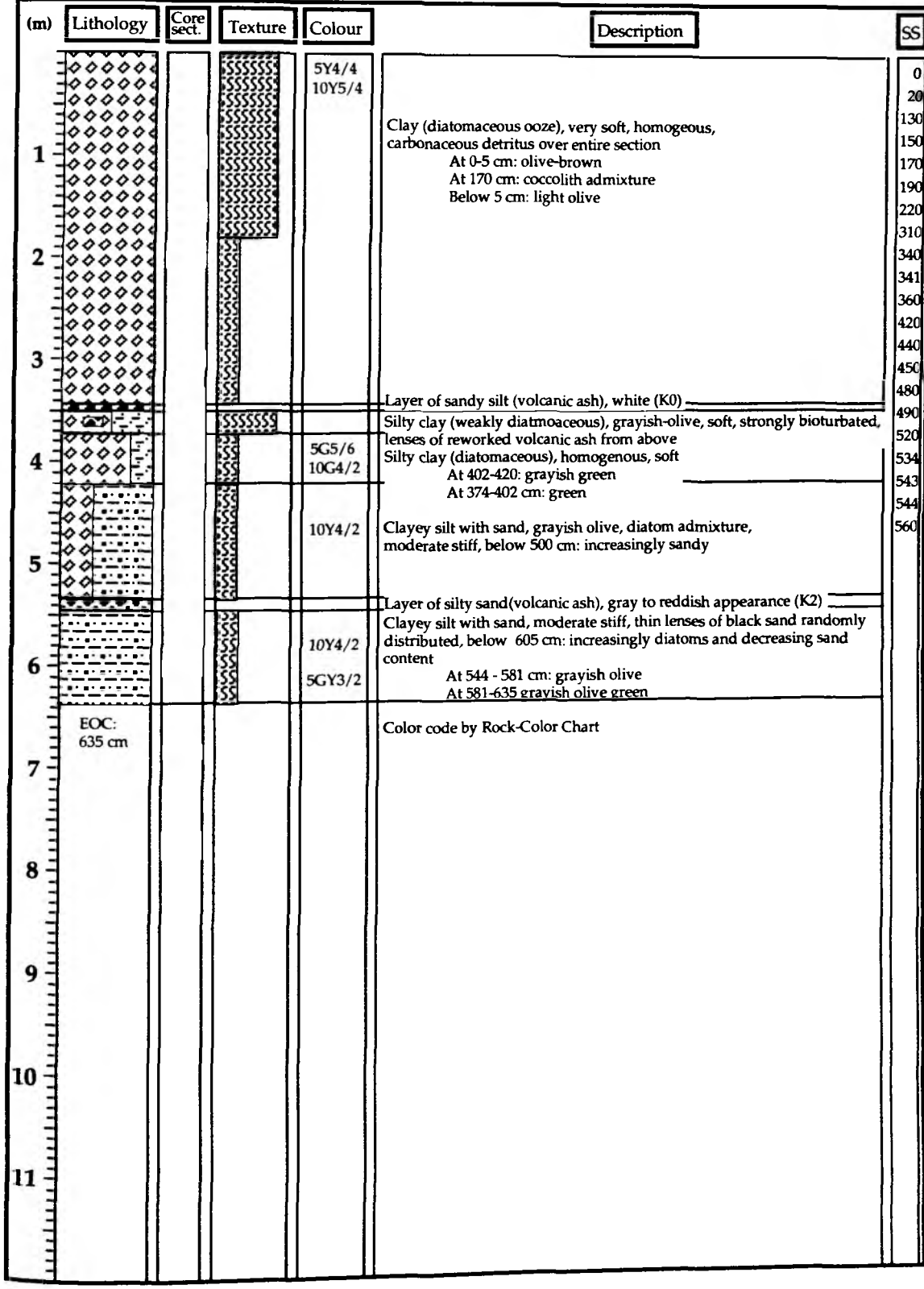

Core description: **LV28-44-3 GC** Location: **52°02.514´N 153°05.949´E**

Cruise/Leg: **RV M.A. Lavrentyev / 28** Water depth: **684 m** Recovery: **93%**

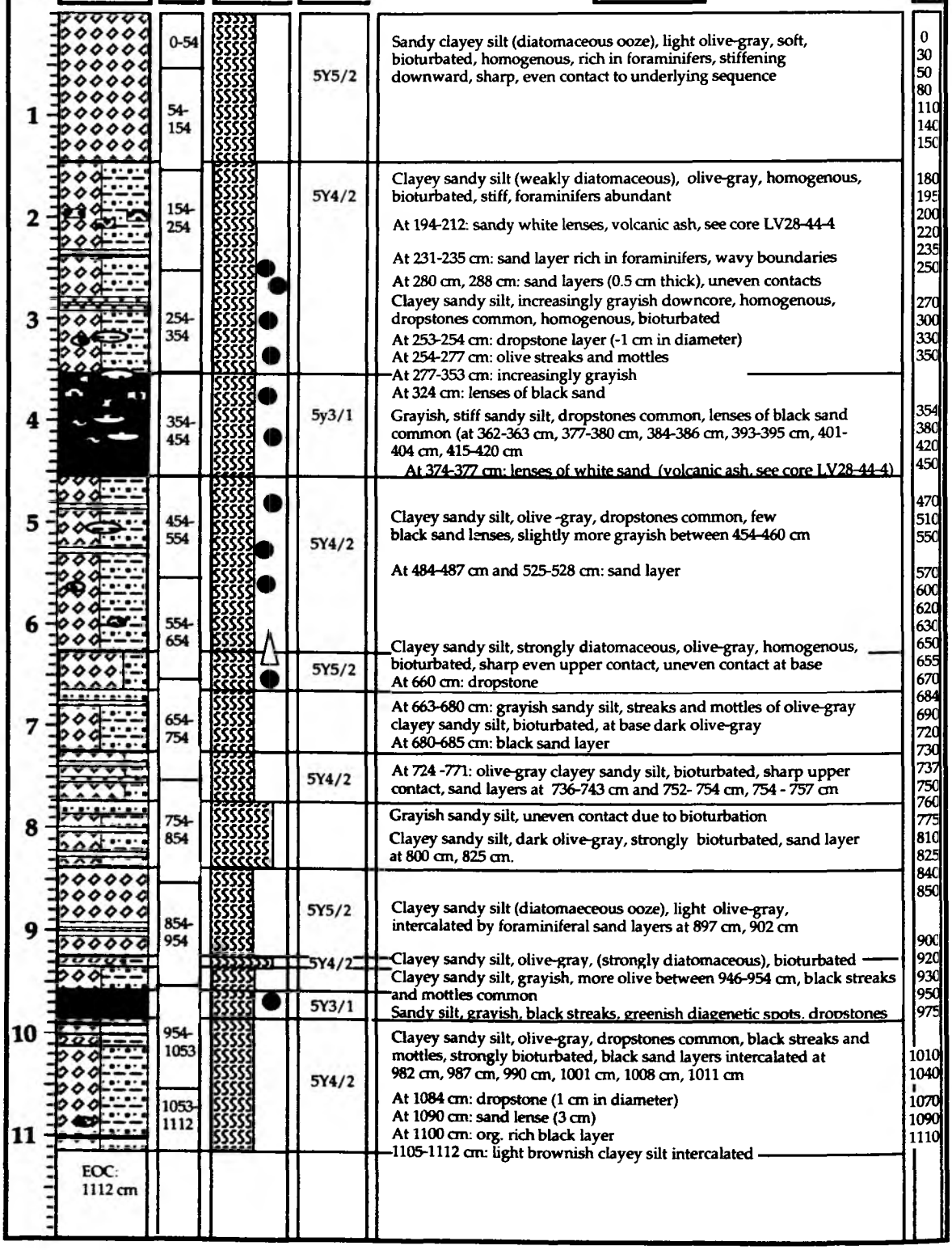

Core description: **LV28-44-4 GC** Location: **52°03.367N 153°06.130E**

Cruise/Leg: **RV M.A. Lavrentyev / 28** Water depth: **681 m** Recovery: **99%**

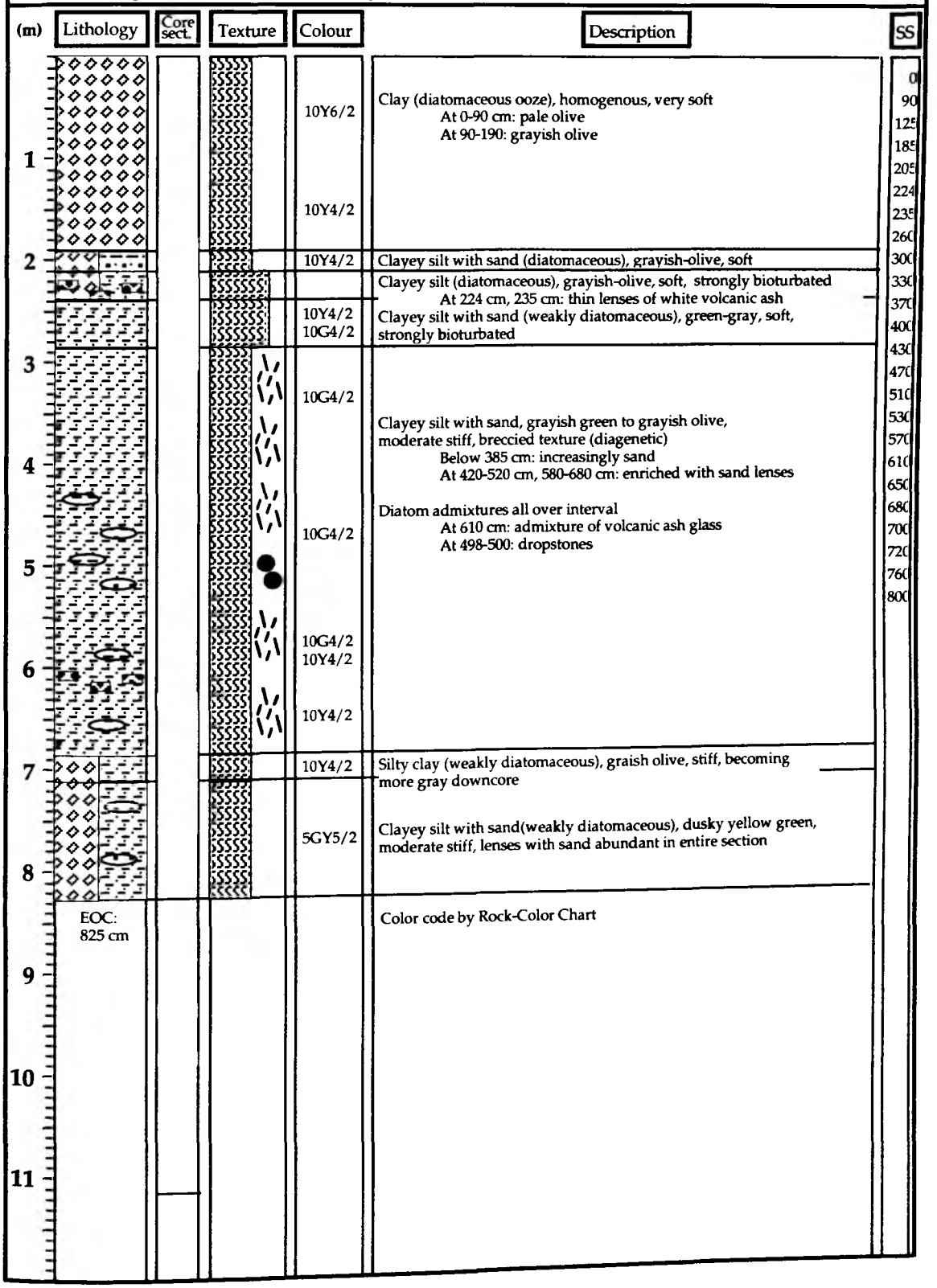

Core description: **LV28-64-5 GC** Location: **47°52.881N 146°12.860E**

Cruise/Leg: **RV M.A. Lavrentyev / 28** Water depth: **2520 m** Recovery: **94%**

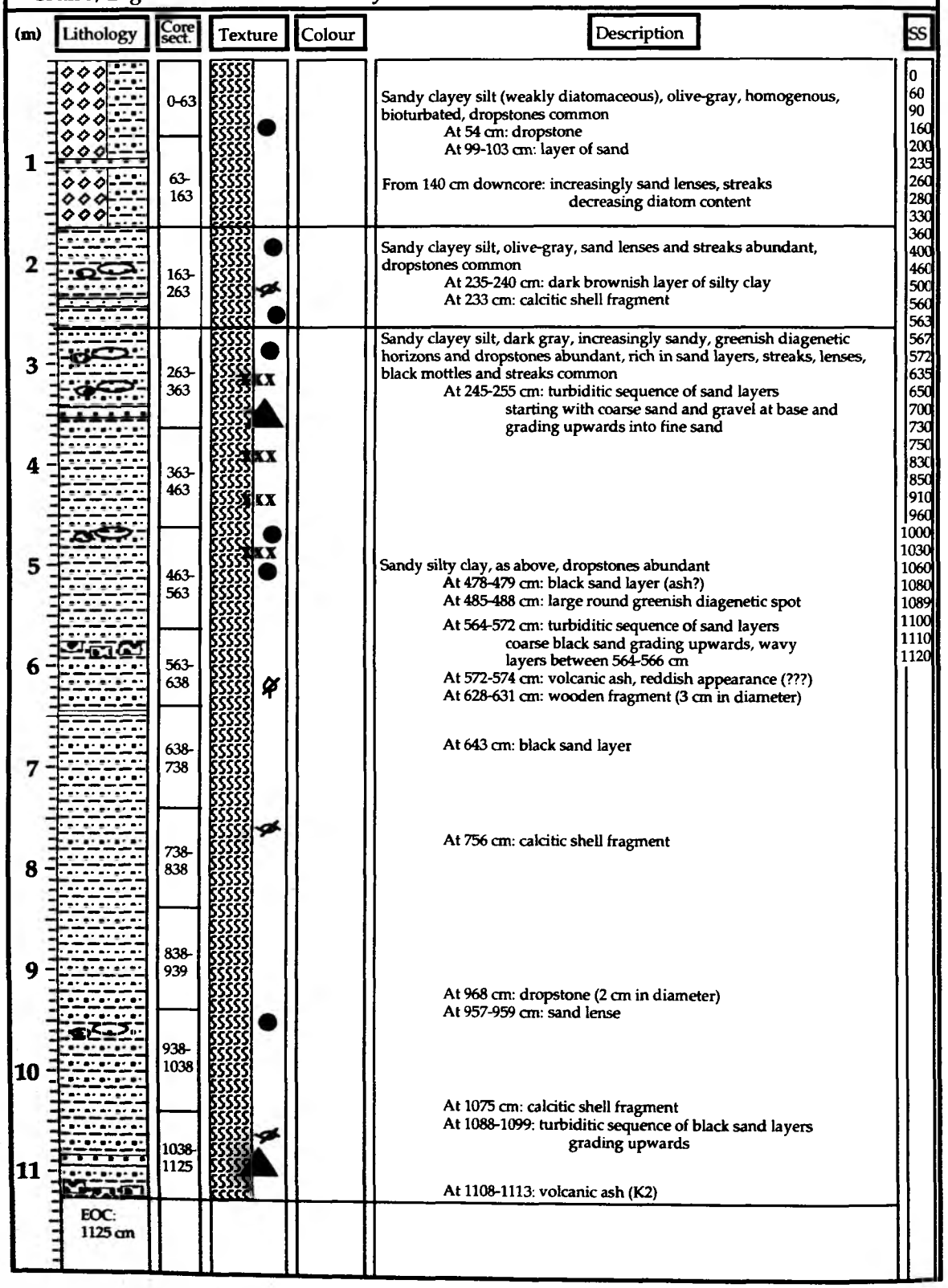

Appendix 3.3

Smear Slide Sampling

GEOMAR cores										
Station	2-3 SL	4-4 SL	20-2 SL	34-2 SL	40-4 SL	41-4 SL	42-4 SL	43-4 SL	44-3 SL	64-5 SL
Latitude	48 22.73	51 08.475	54 26.519	53 51.971	51 20.141	51 40.512	51 42.888	51 53.909	52 02.514	47 52.881
Longitude	146 02.217	145 18.582	144 04.093	148 47.499	147 11.647	149 04.084	150 59.125	152 17.264	153 05 949	146 12 860
Water depth (m)	1265	874	685	1431	1370	1082	1041	847	684	2601
Depth	0	0	0	0	0	0	0	0	0	0
in core (m)	10	20	10	5	5	5	10	30	30	60
	20	40	30	10	15	15	40	60	50	90
	30	60	50	20	50	30	80	63	80	160
	40	80	70	30	100	50	90	90	110	200
	50	100	90	40	115	80	130	160	140	235
	60	120	110	50	145	87	145	190	150	260
	70	140	130	60	150	100	250	260	160	260
	80	160	150	80	170	120	280	300	195	330
	90	200	170	100	180	130	310	309	200	360
	100	220	190	120	220	150	320	350	220	400
	110	240	210	160	250	170	330	365	235	460
	120	260	230	200	310	190	340	370	250	500
	130	280	250	240	340	210	360	380	270	560
	140	300	270	280	370	240	420	410	300	583
	150	320	290	300	375	270	440	450	330	587
	160	340	310	310	390	294	480	487	354	572
	170	360	330	317	430	320	500	470	380	600
	180	380	350	325	460	340	510	480	420	635
	190	400	370	340	485	360	530	520	450	650
	200	420	390	360	495	380	550	528	470	700
	210	440	410	367	620	400	570	560	510	730
	215	460	430	375	625	429	590	580	550	750
	220	480	450	400	650	440	610	590	570	830
	230	500	470	410	658	460	630	620	600	850
	240	520	490	420	665	480	655	640	620	910
	250	540	510	427	720	550	660	660	630	
	260	560	530	435	730	557	670	660	650	
	270	580	550	450	750	570	690	700	655	
	280	600	570	470	790	590	710	720	670	
	290	620		500	820	596	720	740	684	
	300	640		530	830	820	730	750	690	
	310	660		560	850	850	750	780	720	
	320	680		580	900	880	775	800	730	
	330	700		600	920	720	800	810	737	
	340	720		630	940	740	830	825	750	
	350	740		640	960	760	860	830	760	
	360	760		660	979	785	890	845	775	
	370	780		700		800	910	855	810	
	380	800		730		820	923	865	825	
	390	820		740		848	929	880	840	
	400	840		760		860	935	885	850	
	410	860		800		890	940	890	900	
	420	870		830		910	950	895	920	
	430	880		870		930	970	896	930	
	440	890		890		950	980	900	950	
	450	900		905		970	987	940	975	
	453	920		915		973	995	960	1010	
	460	940		930		980	1010	980	1040	
	470			940			1030	990	1070	
	480						1050	1010	1090	
	490						1060	1030	1110	
	500						1070	1040		
	510						1080	1060		
	520						1083	1098		
	530							1100		
	540									
	550									
	560									
	570									
	580									
	590									
	600									
	620									
	640									
	660									
	700									
	720									
	740									
	760									
	780									
	790									

POI cores										
Station	2-4 SL	4-5 SL	20-3 HYC	21-1 SL	25-1 HYC	37-1 SL	40-5 SL	41-5 SL	42-5 SL	43-5 SL
Latitude	48 22.73	51 08.12	54 26.430	54 26.751	54 00.844	53 59.796	51 20.045	51 36.908	51 42.701	51 53.757
Longitude	146 02.217	145 16.21	144 04.120	144 04.940	146 18.648	146 17.830	147 10.831	149 03.203	150 58.879	152 16.052
Water depth (m)	1265	870	685	702	1491	1497	1312	1114	1045	839
Depth	0	0	5	0	0	25	10	30	0	0
in core (m)	10	10	20	10	3	45	30	70	15	20
	25	40	40	30	5	60	50	95	40	130
	35	70	80	45	10	75	70	115	55	150
	55	110	80	75	20	85	90	125	75	170
	75	135	95	90	40	100	110	130	90	190
	95	160	110	110	80	115	120	135	110	220
	105	190	135	125	80	135	140	150	140	310
	125	210	170	140	100	155	160	190	170	340
	145	230	190	150	120	170	180	240	185	341
	150	253	220	165	140	190	195	242	195	360
	165	270	240	175	160	215	200	260	220	420
	180	290	260	185	145	232	220	290	250	440
	195	310	280	190	155	260	230	320	280	450
	210	385		200		270	245	330	310	480
	250	390		210		285	255	360	340	490
	257	415		220		300	270	420	370	520
	295	430				310	290	450	395	534
	205	455				330	300	510	405	543
	270	320				340	350	540	420	555
	285	345				342	380	570	440	580
	320	488				360	400	595	470	
	330	540				370	420	640	490	
	345	580				380	450	665	510	
	365	580				410	463	670	526	
	380	605				440	480	690	530	
	395	620				465	490		560	
	430	650				475	510		580	
	445	670				485	520		593	
	460	680				495	521		610	
	475	715				510	540		640	
	485	740				575	560		670	
	510	770				590	580		700	
	530	790					593			
	550	810					630			
	563						650			
	580						690			
							720			
							750			
							790			

Appendix 3.4

Sediment Physical Properties

Mechanical properties of sediments

Core number	Depth in core (cm)	Density of natural sediment D, g/cm^3	Density of dry sediment Dp, g/cm^3	Volume humidity (porosity) Wv, %	Weight humidity Ww, %
1	2	3	4	5	6
LV28-2-4	30	1.28	0.40	88.06	68.94
LV28-2-4	50	1.28	0.43	84.34	66.07
LV28-2-4	115	1.26	0.40	86.12	68.18
LV28-2-4	155	1.30	0.40	90.16	69.19
LV28-2-4	210	1.36	0.53	82.98	61.05
LV28-2-4	240	1.38	0.56	82.16	59.56
LV28-2-4	290	1.41	0.62	78.40	55.77
LV28-2-4	330	1.46	0.71	74.86	51.25
LV28-2-4	350	1.48	0.74	74.40	50.22
LV28-2-4	380	1.48	0.75	73.36	49.41
LV28-2-4	415	1.46	0.73	73.60	50.27
LV28-2-4	450	1.46	0.71	75.10	51.40
LV28-2-4	485	1.46	0.70	76.00	52.23
LV28-2-4	515	1.47	0.72	74.60	50.72
LV28-2-4	555	1.45	0.70	75.30	51.80
LV28-2-4	590	1.46	0.71	74.76	51.31
LV28-2-4	625	1.47	0.71	75.72	51.67
LV28-4-5	40	1.27	0.36	90.56	71.36
LV28-4-5	100	1.29	0.41	87.88	68.15
LV28-4-5	140	1.29	0.41	87.48	68.06
LV28-4-5	190	1.29	0.40	88.40	68.72
LV28-4-5	230	1.32	0.42	90.22	68.39
LV28-4-5	260	1.29	0.41	88.22	68.22
LV28-4-5	305	1.32	0.46	86.30	65.32
LV28-4-5	340	1.28	0.43	85.56	66.76
LV28-4-5	380	1.26	0.44	82.76	65.47
LV28-4-5	410	1.29	0.42	86.60	67.10
LV28-4-5	425	1.30	0.43	87.16	66.96
LV28-4-5	470	1.29	0.42	87.10	67.38
LV28-4-5	510	1.31	0.44	86.60	66.08
LV28-4-5	540	1.29	0.44	85.04	65.93
LV28-4-5	580	1.32	0.46	85.56	64.85
LV28-4-5	610	1.30	0.45	85.54	65.75
LV28-4-5	640	1.31	0.47	84.10	64.28
LV28-4-5	670	1.27	0.45	82.30	64.88
LV28-4-5	710	1.32	0.47	85.26	64.41
LV28-4-5	740	1.28	0.47	81.68	63.70

1	2	3	4	5	6
LV28-4-5	770	1.30	0.47	83.50	64.15
LV28-4-5	800	1.28	0.47	81.00	63.27
LV28-40-5	20	1.18	0.25	92.50	78.60
LV28-40-5	60	1.18	0.26	92.40	78.15
LV28-40-5	100	1.19	0.26	93.38	78.44
LV28-40-5	130	1.21	0.26	94.60	78.34
LV28-40-5	155	1.18	0.24	93.90	79.90
LV28-40-5	200	1.24	0.34	89.54	72.41
LV28-40-5	230	1.29	0.44	85.40	66.25
LV28-40-5	260	1.48	0.72	76.60	51.67
LV28-40-5	290	1.41	0.65	75.60	53.81
LV28-40-5	320	1.40	0.61	78.50	56.26
LV28-40-5	360	1.41	0.62	78.68	55.85
LV28-40-5	390	1.40	0.59	80.34	57.51
LV28-40-5	420	1.40	0.56	83.70	59.98
LV28-40-5	455	1.37	0.60	77.10	56.31
LV28-40-5	495	1.30	0.47	83.40	64.08
LV28-40-5	515	1.33	0.48	85.30	64.09
LV28-40-5	545	1.33	0.49	84.10	63.21
LV28-40-5	580	1.31	0.48	82.70	63.21
LV28-40-5	620	1.33	0.50	82.34	62.14
LV28-40-5	660	1.35	0.54	81.84	60.44
LV28-40-5	690	1.36	0.59	76.50	56.31
LV28-40-5	715	1.46	0.70	76.10	52.21
LV28-40-5	750	1.44	0.70	74.26	51.53
LV28-40-5	790	1.37	0.60	76.94	56.07
LV28-41-5	30	1.16	0.22	94.10	81.19
LV28-41-5	60	1.23	0.27	95.40	77.70
LV28-41-5	90	1.31	0.44	86.74	66.37
LV28-41-5	115	1.35	0.56	78.80	58.59
LV28-41-5	150	1.46	0.70	75.10	51.60
LV28-41-5	190	1.41	0.65	76.30	54.07
LV28-41-5	210	1.47	0.71	76.60	52.02
LV28-41-5	270	1.37	0.54	82.60	60.32
LV28-41-5	310	1.29	0.46	83.70	64.77
LV28-41-5	350	1.44	0.66	78.44	54.49
LV28-41-5	380	1.48	0.71	76.30	51.69
LV28-41-5	420	1.32	0.52	80.34	60.64
LV28-41-5	445	1.28	0.37	91.30	71.24
LV28-41-5	485	1.28	0.43	84.70	66.22
LV28-41-5	510	1.25	0.37	87.54	70.26
LV28-41-5	545	1.31	0.47	83.90	64.15
LV28-41-5	580	1.36	0.55	81.40	59.64

1	2	3	4	5	6
LV28-41-5	615	1.25	0.35	89.20	71.60
LV28-41-5	640	1.24	0.38	86.14	69.42
LV28-41-5	660	1.48	0.74	74.30	50.11
LV28-42-5	30	1.23	0.29	93.94	76.37
LV28-42-5	60	1.32	0.44	88.30	66.94
LV28-42-5	90	1.38	0.58	80.00	57.84
LV28-42-5	120	1.39	0.59	79.50	57.28
LV28-42-5	150	1.34	0.51	82.30	61.55
LV28-42-5	180	1.38	0.57	81.20	58.88
LV28-42-5	220	1.33	0.51	81.90	61.55
LV28-42-5	250	1.44	0.66	77.60	53.91
LV28-42-5	280	1.32	0.49	82.80	62.77
LV28-42-5	310	1.34	0.42	92.00	68.54
LV28-42-5	340	1.30	0.44	85.74	65.96
LV28-42-5	380	1.27	0.45	81.50	64.25
LV28-42-5	415	1.25	0.35	90.54	72.15
LV28-42-5	450	1.31	0.44	87.10	66.65
LV28-42-5	480	1.33	0.52	80.80	60.83
LV28-42-5	515	1.41	0.60	80.20	57.01
LV28-42-5	545	1.43	0.66	77.50	54.13
LV28-42-5	585	1.44	0.68	76.20	52.92
LV28-42-5	605	1.43	0.66	76.78	53.81
LV28-42-5	635	1.42	0.63	78.50	55.34
LV28-42-5	660	1.39	0.62	77.80	55.79
LV28-42-5	700	1.36	0.55	80.80	59.51
LV28-43-5	20	1.22	0.29	93.50	76.50
LV28-43-5	50	1.20	0.27	93.30	77.75
LV28-43-5	85	1.14	0.26	87.90	76.85
LV28-43-5	110	1.25	0.28	96.50	77.39
LV28-43-5	145	1.18	0.27	90.70	76.75
LV28-43-5	180	1.23	0.29	94.20	76.49
LV28-43-5	210	1.20	0.32	88.36	73.67
LV28-43-5	240	1.24	0.30	94.00	76.08
LV28-43-5	270	1.21	0.30	91.10	75.49
LV28-43-5	305	1.23	0.38	85.70	69.54
LV28-43-5	340	1.38	0.55	82.40	59.82
LV28-43-5	375	1.28	0.42	85.50	67.03
LV28-43-5	395	1.32	0.48	84.08	63.88
LV28-43-5	420	1.34	0.51	83.00	62.00
LV28-43-5	450	1.40	0.59	81.20	57.98
LV28-43-5	475	1.30	0.52	77.90	59.76
LV28-43-5	490	1.37	0.56	81.64	59.43
LV28-43-5	525	1.39	0.61	77.90	55.95

1	2	3	4	5	6
LV28-43-5	570	1.35	0.56	79.40	58.77
LV28-43-5	590	1.34	0.53	81.60	60.76
LV28-43-5	620	1.24	0.38	85.60	69.11
LV28-44-5	30	1.25	0.29	95.20	76.40
LV28-44-5	60	1.25	0.33	92.30	73.78
LV28-44-5	90	1.22	0.31	91.20	74.90
LV28-44-5	100	1.29	0.34	95.20	73.60
LV28-44-5	140	1.29	0.39	90.10	70.05
LV28-44-5	180	1.32	0.44	87.70	66.53
LV28-44-5	210	1.40	0.53	87.10	62.33
LV28-44-5	240	1.36	0.51	84.70	62.38
LV28-44-5	270	1.35	0.53	81.90	60.87
LV28-44-5	295	1.41	0.61	79.90	56.83
LV28-44-5	330	1.44	0.63	81.30	56.50
LV28-44-5	380	1.42	0.63	79.80	56.01
LV28-44-5	395	1.42	0.64	77.62	54.67
LV28-44-5	440	1.40	0.61	78.04	55.94
LV28-44-5	480	1.39	0.60	78.90	56.89
LV28-44-5	495	1.38	0.57	81.00	58.75
LV28-44-5	535	1.38	0.58	79.60	57.78
LV28-44-5	580	1.39	0.60	79.50	57.08
LV28-44-5	610	1.45	0.69	76.20	52.39
LV28-44-5	640	1.36	0.56	80.72	59.24
LV28-44-5	670	1.30	0.46	83.40	64.33
LV28-44-5	690	1.31	0.44	86.40	66.18
LV28-44-5	730	1.33	0.49	83.70	63.01
LV28-44-5	775	1.35	0.51	83.18	61.84
LV28-44-5	810	1.34	0.49	85.10	63.43
LV28-64-5	20	1.27	0.39	88.42	69.47
LV28-64-5	50	1.27	0.41	86.06	67.97
LV28-64-5	80	1.27	0.40	86.80	68.43
LV28-64-5	115	1.28	0.42	86.36	67.31
LV28-64-5	150	1.27	0.41	85.56	67.36
LV28-64-5	180	1.30	0.46	84.40	64.71
LV28-64-5	220	1.30	0.46	83.94	64.78
LV28-64-5	250	1.34	0.52	82.20	61.32
LV28-64-5	280	1.33	0.50	83.04	62.58
LV28-64-5	315	1.40	0.62	77.56	55.58
LV28-64-5	355	1.38	0.60	78.04	56.43
LV28-64-5	380	1.41	0.64	77.00	54.45
LV28-64-5	415	1.42	0.67	75.30	52.87
LV28-64-5	450	1.42	0.64	77.76	54.87
LV28-64-5	480	1.49	0.76	72.60	48.72

1	2	3	4	5	6
LV28-64-5	520	1.42	0.65	76.54	54.01
LV28-64-5	550	1.39	0.62	77.36	55.48
LV28-64-5	585	1.37	0.57	80.04	58.46
LV28-64-5	620	1.36	0.56	80.20	58.94
LV28-64-5	650	1.41	0.63	77.66	55.06
LV28-64-5	690	1.39	0.61	77.40	55.84
LV28-64-5	725	1.38	0.58	80.10	57.98
LV28-64-5	760	1.40	0.62	78.16	55.96
LV28-64-5	795	1.44	0.68	75.40	52.44
LV28-64-5	830	1.48	0.74	73.70	49.88
LV28-64-5	860	1.51	0.80	71.24	47.20
LV28-64-5	895	1.51	0.80	70.70	46.92
LV28-64-5	930	1.48	0.74	73.44	49.70
LV28-64-5	960	1.45	0.66	78.50	54.31
LV28-64-5	990	1.42	0.66	76.44	53.71
LV28-64-5	1020	1.41	0.64	77.32	54.71
LV28-64-5	1050	1.37	0.58	79.26	57.73
LV28-64-5	1080	1.40	0.61	78.20	56.04
LV28-64-5	1115	1.42	0.66	76.10	53.54

Appendix 4

Water Column Data

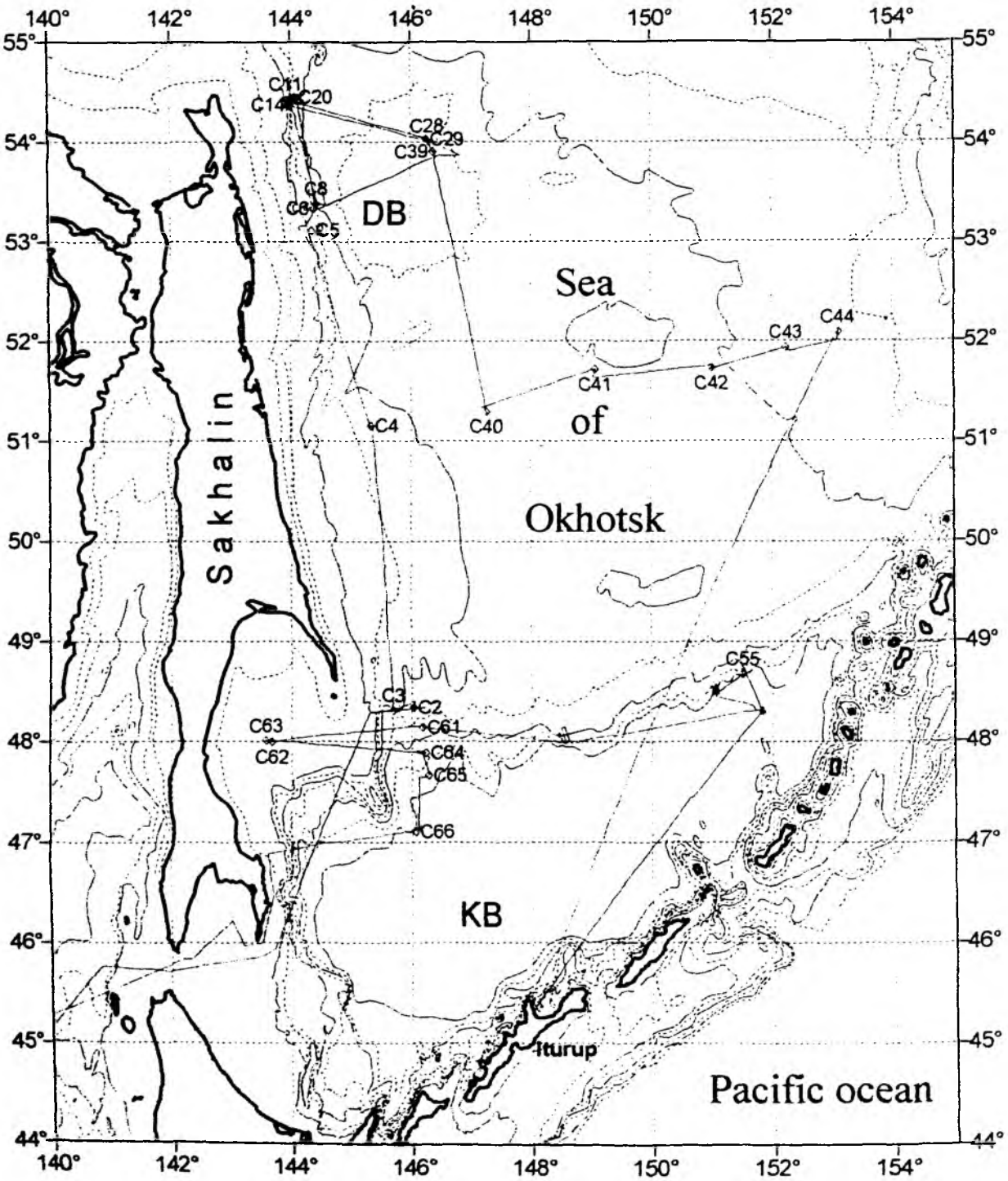

Fig. A4.1: Map of CTD stations carried out duringthe 28th cruise of RV 'Akademik M.A. Lavrentyev', August - September 1998

KOMEX II LV 28: Water column analysis

Station	Depth m	Si µM/l	PO_4 µM/l	NO_3 µM/l	NO_2 µM/l	NH_4 µM/l	CH_4 nl/l	C_2H_6 nl/l	CO_2 ml/l	GC O_2 µM/l	N_2 ml/l	Winkler O_2 µM/l	TA mM/kg	pH_{sws} (25)	Salinity	pot. Temp.	Depth m
CTD 2-1	6	5.7	0.04	0	0	0	67	4	0.13	250.1	11.4	285.4	2.225	7.888	34.468	14.238	6
	24	13.0	0.82	6.93	0	0	-	-	-	-	-	387.7	2.232	7.771	34.415	4.302	24
	55	30.7	1.71	19.93	0	0	200	6	0.3	245.6	11.2	327.9	2.241	7.598	34.346	0.201	55
	106	43.7	2.09	25.00	0	0	113	1	0.34	263.5	12.8	323.7	2.250	7.579	34.147	-0.909	106
	143	49.4	2.31	26.33	0	0	-	-	-	-	-	295.6	2.254	7.525	33.819	-0.729	143
	174	53.1	2.25	27.53	0	0	60	3	0.45	196.5	11	269.2	2.260	7.492	33.431	0.212	174
	252	74.4	3.09	35.55	0	0	-	-	-	-	-	185.4	2.286	7.362	33.259	1.074	252
	502	113.9	2.61	39.05	0	0	52	2	0.78	102.7	10.6	110.6	2.312	7.303	33.158	1.858	502
	752	153.4	3.15	42.86	0	0	-	-	-	-	-	56.0	2.353	7.285	33.088	2.289	752
	1001	164.9	3.12	43.63	0	0	14	1	0.71	62.5	11.1	43.9	2.380	7.315	32.972	2.348	1001
	1151	167.0	3.08	43.71	0	0	18	2	0.71	67.0	11	47.7	2.389	7.339	32.655	2.268	1151
	1296	174.8	2.93	42.76	0	0	17	1	0.7	67.0	10.6	51.1	2.396	7.352	32.444	2.165	1296
BW MUC 2-2	1308	187.6	2.89	42.19	0	0	-	-	-	-	-	55.3	-	-	-	-	1308

Station	Depth m	Si µM/l	PO_4 µM/l	NO_3 µM/l	NO_2 µM/l	NH_4 µM/l	CH_4 nl/l	C_2H_6 nl/l	CO_2 ml/l	GC O_2 µM/l	N_2 ml/l	Winkler O_2 µM/l	TA mM/kg	pH_{sws} (25)	Salinity	pot. Temp.	Depth m
CTD 3-2	10	1.5	0.24	0.21	0	0	-	-	-	-	-	295.9	-	-	32.4693	14.3178	10
	50	25.2	2.03	20.37	0	0	281	0.5	0.21	343.9	16.3	342.0	-	-	32.7822	-0.0770	50
	73	37.6	1.98	23.41	0	0	207	1.0	0.3	245.6	11.8	340.4	-	-	32.9558	-1.1658	73
	200	69.5	2.82	34.36	0	0	112	1.0	0.77	201.0	14.2	199.9	-	-	33.3822	0.0902	200
	501	111.6	3.1	38.19	0	0	61	1.0	0.86	156.3	16	111.3	-	-	33.8197	1.8524	501
	1000	165.7	3.26	42.71	0	0	-	-	-	-	-	42.6	-	-	34.3362	2.3270	1000
	1221	167.2	3.22	42.66	0	0	-	-	-	-	-	48.9	-	-	34.4481	2.2128	1221
	1250	169.3	3.12	42.11	0	0	17	0.5	0.74	89.3	15.1	49.7	-	-	34.4533	2.1870	1250
	1281	170.8	3.19	42.83	0	0	12	0	-	-	--	49.5	-	-	34.4590	2.1783	1281
	1311	170.8	3.12	42.33	0	0	16	0	0.78	-	12.9	49.7	-	-	34.4630	2.1709	1311
	1341	165.1	3.05	42.63	0	0	12	1.0	-	-	--	50.0	-	-	34.4654	2.1671	1341
	1375	173.4	3.03	42.34	0	0	26	1.0	0.77	89.3	13.6	51.6	-	-	34.4739	2.1513	1375

Station	Depth m	Si µM/l	PO_4 µM/l	NO_3 µM/l	NO_2 µM/l	NH_4 µM/l	CH_4 nl/l	C_2H_6 nl/l	CO_2 ml/l	GC O_2 µM/l	N_2 ml/l	Winkler O_2 µM/l	TA mM/kg	pH_{sws} (25)	Salinity	pot. Temp.	Depth m
CTD 4-2	5	0	0.15	0.8	0	0.12	244	1.0	-	-	-	307.5	-	-	31.5883	13.9617	5
	11	0	0.61	7.26	0	0.98	147	0	0.3	330.5	16.1	448.6	-	-	32.4279	5.0145	11
	26	27.8	1.73	19.33	0	2.62	-	-	-	-	-	431.2	-	-	32.7127	0.9323	26
	51	37.06	1.8	23.27	0	0.12	217	0.5	0.34	294.8	15.8	353.1	-	-	32.9276	-0.4078	51
	77	47.38	1.99	26.81	0	0	-	-	-	-	-	342.2	-	-	33.0045	-1.0327	77
	99	71.55	1.77	26.96	0	0.18	305	0.5	0.42	205.4	13.7	305.0	-	-	33.1077	-0.4388	99
	251	78.76	2.68	37.24	0	0	1166	0.5	0.58	178.6	12.5	213.8	-	-	33.3718	0.4416	251
	346	79.79	2.63	35.76	0	0	240	0	0.57	151.8	12.4	168.9	-	-	33.4952	1.0515	346
	401	103.47	2.92	40.63	0	0	290	0.5	0.62	151.8	12.1	179.1	-	-	33.5330	0.8028	401
	502	131.78	2.96	43.09	0	0	143	0	0.68	111.7	12.2	116.4	-	-	33.7545	1.7691	502
	601	143.1	3.07	42.79	0	0	-	-	-	-	-	75.4	-	-	33.9915	2.1565	601
	653	123.54	3.15	41.87	0	0.37	113	0	-	80.4	11.7	67.3	-	-	34.0428	2.1880	653
BW MUC 4-3	665	145.16	-	-	0	0	-	-	-	-	-	73.0	-	-	-	-	665

Station	Depth m	Si µM/l	PO_4 µM/l	NO_3 µM/l	NO_2 µM/l	NH_4 µM/l	CH_4 nl/l	C_2H_6 nl/l	CO_2 ml/l	GC O_2 µM/l	N_2 ml/l	Winkler O_2 µM/l	TA mM/kg	pH_{sws} (25)	Salinity	pot. Temp.	Depth m
CTD 5-1	3	3.6	0	0	0	0.44	60	1.0	0.09	214.4	8.9	279.4	-	-	27.5000	17.1219	3
	5	3.1	0	0	0	0.4	62	0.5	0.08	209.9	8.8	282.1	-	-	27.4991	17.1280	5
	11	2.6	0.17	0.33	0	0.36	69	0.5	0.09	241.2	9.8	305.9	-	-	28.7652	15.5375	11
	25	4.1	0.64	5.97	0	2.22	104	0.5	0.1	281.4	10.9	380.2	-	-	31.6024	5.9803	25
	50	7.2	1.35	14.20	0	3.49	128	0	0.15	281.4	11.4	382.1	-	-	32.7664	0.4809	50
	100	44.4	2.04	26.88	0	0.64	68	0	0.27	-	-	314.4	-	-	33.0751	-0.1047	100
	202	66.7	2.52	32.25	0	0.48	607	0.5	0.35	183.1	11.3	243.3	-	-	33.2630	0.0145	202
	302	66.1	2.48	30.71	0	0.43	-	-	-	-	-	234.0	-	-	33.3350	-0.2365	302
	402	71.3	2.58	31.77	0	0.39	556	0	0.48	174.2	11.9	216.4	-	-	33.3927	0.0318	402
	431	72.3	2.58	32.55	0	0.34	-	-	-	-	-	214.6	-	-	33.4020	0.0351	431
	472	86.8	2.73	33.75	0	0.36	446	0	0.62	165.2	13.1	178.8	-	-	33.5371	0.7348	472

KOMEX II LV 28: Water column analysis

Station	Depth m	Si µM/l	PO_4 µM/l	NO_3 µM/l	NO_2 µM/l	NH_4 µM/l	CH_4 nl/l	C_2H_6 nl/l	CO_2 ml/l	O_2 µM/l	N_2 ml/l	O_2 µM/l	TA mM/kg	pH_{sws} (25)	Salinity	pot. Temp.	Depth m
CTD 8-1	1	3.62	0	0	0	0	61	1	0.1	232.2	10.2	279.7	-	-	27.5199	17.0917	1
	4	3.10	0.08	0	0	0	57	1	0.09	236.7	10.2	288.1	-	-	27.5511	16.9566	4
	11	2.58	0.2	0.84	0	0	65	0.5	0.1	250.1	10.4	308.4	-	-	29.0613	15.2065	11
	28	4.13	0.63	4.22	0	2.08	80	0.5	0.08	299.2	12.1	375.5	-	-	31.9125	7.1757	28
	52	11.37	1.49	11.92	0	4.05	67	0.5	0.17	285.8	12.5	368.5	-	-	32.6871	1.3764	52
	102	33.58	1.92	19.54	0	2.01	60	0.5	0.23	268.0	12.2	343.2	-	-	32.9875	-0.0969	102
	204	66.13	2.57	30.24	0	0	269	0	0.46	201.0	12.7	231.4	-	-	33.2967	0.5789	204
	303	75.96	3.04	33.99	0	0	-	-	-	-	-	176.9	-	-	33.4438	1.0115	303
	399	88.35	3.07	34.99	0	0	261	0.5	0.64	138.4	12.6	141.9	-	-	33.5782	1.3700	399
	501	105.40	3.09	35.34	0	0	-	-	-	-	-	128.0	-	-	33.7197	1.5386	501
	543	110.56	3.16	35.07	0	0	516	0	0.72	366.2	12.9	120.9	-	-	33.7613	1.6062	543

Station	Depth m	Si µM/l	PO_4 µM/l	NO_3 µM/l	NO_2 µM/l	NH_4 µM/l	CH_4 nl/l	C_2H_6 nl/l	CO_2 ml/l	GC O_2 µM/l	N_2 ml/l	Winkler O_2 µM/l	TA mM/kg	pH_{sws} (25)	Salinity	pot. Temp.	Depth m
CTD 9-1	50	12.9	1.31	13.79	0	3.70	74	0.5	0.23	326.0	13	367.1	-	-	32.6978	1.1851	50
	151	60.5	2.31	30.35	0	0.18	51	0.5	0.36	232.2	12.8	261.2	-	-	33.2223	0.3119	151
	251	76.0	2.55	35.04	0	0.08	90	0.0	0.46	169.7	12.5	201.5	-	-	33.3993	0.8915	251
	300	79.1	2.63	34.95	0	0.41	360	0.5	0.58	174.2	12.8	187.2	-	-	33.4446	0.6878	300
	339	86.3	2.91	37.49	0	0	52	0.0	0.67	142.9	12.2	151.1	-	-	33.5378	1.2414	339
	402	95.1	2.31	37.83	0	0.42	47	0.0	0.75	129.5	12.4	136.0	-	-	33.6340	1.5023	402
	437	103.9	2.79	38.95	0	0	158	0.5	0.74	125.0	12.9	124.3	-	-	33.7241	1.7480	437
	470	113.2	2.56	40.89	0	0.03	318	0.5	0.78	116.1	12.5	114.2	-	-	33.7840	1.7647	470
	503	125.6	2.93	41.86	0	0	424	0.0	0.81	102.7	12.7	97.7	-	-	33.8864	1.9588	503
	553	134.3	3.02	42.1	0	0	714	0.5	-	-	-	87.9	-	-	33.9536	2.0228	553
	605	137.4	2.99	41.02	0	0	927	0.0	0.85	93.8	12.9	75.4	-	-	34.0338	2.1267	605

Station	Depth m	Si µM/l	PO_4 µM/l	NO_3 µM/l	NO_2 µM/l	NH_4 µM/l	CH_4 nl/l	C_2H_6 nl/l	CO_2 ml/l	GC O_2 µM/l	N_2 ml/l	Winkler O_2 µM/l	TA mM/kg	pH_{sws} (25)	Salinity	pot. Temp.	Depth m
CTD 11-1	4	4.7	0.05	0.12	0	0.05	-	-	-	-	-	294.6	-	-	26.2520	16.6342	4
	10	8.8	0.63	6.16	0	1.77	175	2	0.25	299.2	12.6	340.8	2.096	7.853	29.4512	9.201	10
	25	15.5	1.26	15.04	0	2.84	-	-	-	-	-	-	-	-	32.5151	0.8648	25
	51	26.4	1.61	19.75	0	2.40	74	1	0.43	303.7	13.4	348.1	2.238	7.633	32.9004	0.098	51
	76	41.9	1.9	24.64	0	0.89	-	-	-	-	-	321.9	-	-	33.0454	-0.2932	76
	100	58.4	-	-	-	-	75	0	0.58	254.6	13.9	267.0	2.251	7.520	33.1484	-0.293	100
	126	66.1	2.36	31.62	0	0.01	-	-	-	-	-	240.9	2.259	7.467	33.2422	0.206	126
	152	68.2	2.39	32.52	0	0	101	0	0.67	227.8	13.8	233.4	2.260	7.457	33.2716	0.303	152
	174	71.3	2.41	33.03	0	0	-	-	-	-	-	221.1	2.263	7.440	33.2992	0.325	174
	201	72.3	2.42	32.49	0	0	237	0	0.73	218.8	13.3	220.4	2.263	7.437	33.3090	0.308	201
	225	70.8	2.33	32.21	0	0	1728	0	0.64	223.3	13.6	193.4	2.266	7.442	33.3106	0.226	225
	248	66.7	2.23	32.09	0	0	1812	2	0.7	196.5	13.1	223.3	2.266	7.452	33.3099	0.221	248

Station	Depth m	Si µM/l	PO_4 µM/l	NO_3 µM/l	NO_2 µM/l	NH_4 µM/l	CH_4 nl/l	C_2H_6 nl/l	CO_2 ml/l	GC O_2 µM/l	N_2 ml/l	Winkler O_2 µM/l	TA mM/kg	pH_{sws} (25)	Salinity	pot. Temp.	Depth m
CTD 14-1	6	4.2	0.14	0.50	0	0.03	-	-	-	-	-	309.4	-	-	26.4602	15.9433	6
	26	12.6	1.34	14.22	0	2.65	-	-	-	-	-	370.4	-	-	32.4278	1.2639	26
	53	12.3	1.73	20.21	0	2.43	77	0	0.37	326.0	15.6	350.5	-	-	32.9495	0.1601	53
	105	50.2	2.26	28.90	0	0.86	73	0	0.44	276.9	15.1	290.5	-	-	33.1482	-0.1191	105
	154	68.5	2.62	34.05	0	0.42	95	0	0.61	223.3	14.9	224.3	-	-	33.2974	0.4137	154
	203	72.2	2.65	34.08	0	0.30	208	0	0.51	201.0	13.9	219.8	-	-	33.3193	0.2702	203
	233	70.6	2.58	33.87	0	0.65	-	-	-	-	-	219.0	-	-	33.3220	0.2598	233
	270	73.8	2.60	34.18	0	0.69	139	0	0.67	205.4	14.9	212.9	-	-	33.3382	0.2703	270
	300	74.3	2.63	33.86	0	0.76	208	0	0.69	214.4	15.2	209.1	-	-	33.3426	0.2933	300
	324	76.4	2.64	33.82	0	0.61	208	0	0.67	205.4	14.7	203.5	-	-	33.3811	0.3532	324
	352	73.2	2.60	32.95	0	0.59	-	-	-	-	-	205.2	-	-	33.3911	0.1927	352
	374	87.9	2.68	35.20	0	0.41	119	0	0.74	183.1	14.4	176.2	-	-	33.4709	0.8365	374

KOMEX II LV 28: Water column analysis

Station	Depth m	Si µM/l	PO_4 µM/l	NO_3 µM/l	NO_2 µM/l	NH_4 µM/l	CH_4 nl/l	C_2H_6 nl/l	CO_2 ml/l	O_2 µM/l	N_2 ml/l	O_2 µM/l	TA mM/kg	pH_{sws} (25)	Salinity	pot. Temp.	Depth m
CTD 20-1	8	3.1	0.31	2.25	0	0.87	309	0	0.16	241.2	10.7	320.8	1.993	7.976	26.7697	14.8306	8
	50	12.5	1.56	16.53	0	3.04	95	0	0.28	308.2	13.8	361.9	2.234	7.736	32.8365	0.4508	50
	150	51.9	2.12	28.24	0	0.17	84	0	0.39	236.7	13	285.0	2.257	7.579	33.1522	0.0952	150
	300	79.0	2.58	34.97	0	0.10	62	0	0.55	169.7	12.2	188.1	2.270	7.457	33.4208	0.9969	300
	452	103.9	2.85	38.05	0	0.35	118	0	0.78	134.0	12.6	128.9	2.300	7.388	33.6979	1.6035	452
	493	111.2	2.86	39.37	0	0.41	105	0	0.77	116.1	12.1	116.1	2.309	7.366	33.7860	1.7630	493
	522	121.6	2.92	40.07	0	0.25	562	0	0.84	116.1	12.5	96.5	2.329	7.371	33.8745	1.8988	522
	553	126.7	2.97	40.67	0	0.07	242	0	0.89	111.7	12.8	90.8	2.326	7.371	33.9107	1.9406	553
	578	130.4	2.88	40.53	0	0.15	78	0	0.97	93.8	11.1	84.4	2.327	7.364	33.9516	1.9992	578
	612	133.0	2.99	40.63	0	0.00	85	0	0.94	102.7	12.3	81.7	2.332	7.369	33.9811	2.0369	612
	641	145.4	2.90	40.45	0	0.00	67	0	0.84	93.8	12	72.5	2.339	7.367	34.0424	2.0937	641
	670	153.8	2.94	41.01	0	0.00	11076	0	1.02	n.a.	12.6	65.9	2.342	7.367	34.0919	2.1426	670

Station	Depth m	Si µM/l	PO_4 µM/l	NO_3 µM/l	NO_2 µM/l	NH_4 µM/l	CH_4 nl/l	C_2H_6 nl/l	CO_2 ml/l	GC O_2 µM/l	N_2 ml/l	Winkler O_2 µM/l	TA mM/kg	pH_{sws} (25)	Salinity	pot. Temp.	Depth m
CTD 28-1	78	29.3	1.69	22.85	0	0.09	267	4.0	0.24	272.4	12.8	338.05	2.233	7.628	32.9850	-1.4839	78
	503	118.6	2.85	39.72	0	0	128	0.0	0.68	102.7	11.3	97.83	2.311	7.347	33.8680	2.0106	503
	1000	165.1	3.09	43.40	0	0	78	1.0	0.66	58.1	10.1	37.61	2.375	7.332	34.3365	2.3172	1000
	1201	183.7	3.11	43.33	0	0	-	-	-	-	-	36.22	2.387	7.345	34.4107	2.2590	1201
	1251	185.8	3.09	43.88	0	0.04	66	1.0	0.75	62.5	10.8	36.31	2.388	7.349	34.4185	2.2510	1251
	1301	196.9	3.15	42.40	0	0.11	-	-	-	-	-	34.66	2.391	7.347	34.4256	2.2436	1301
	1335	198.4	3.12	43.40	0	0.11	72	0.5	0.76	53.6	10.6	33.35	2.394	7.344	34.4289	2.2388	1335
	1371	208.0	3.19	42.90	0	0.02	-	-	-	-	-	33.83	2.396	7.345	34.4325	2.2393	1371
	1401	211.0	3.14	43.06	0	0.06	728	0.5	0.76	53.6	10.5	-	2.397	7.356	34.4346	2.2387	1401
	1437	214.0	3.12	42.99	0	0.21	979	0.5	0.81	62.5	11.5	30.47	2.398	7.340	34.4354	2.2386	1437
	1467	215.0	3.28	42.69	0	0.14	1151	0.5	0.81	62.5	11.5	31.67	2.399	7.344	34.4363	2.2390	1467
	1493	214.5	3.17	42.41	0	0.21	2429	1.0	0.72	58.1	10.6	28.78	2.400	7.344	34.4368	2.2380	1493

Station	Depth m	Si µM/l	PO_4 µM/l	NO_3 µM/l	NO_2 µM/l	NH_4 µM/l	CH_4 nl/l	C_2H_6 nl/l	CO_2 ml/l	GC O_2 µM/l	N_2 ml/l	Winkler O_2 µM/l	TA mM/kg	pH_{sws} (25)	Salinity	pot. Temp.	Depth m
CTD 29-1	54	0	1.52	14.45	0	3.59	124	0	0.27	290.3	12.7	362.26	-	-	32.7445	-0.5168	54
	503	113.1	3.49	39.97	0	0	65	0.5	0.6	84.9	10.5	93.32	-	-	33.8919	2.0436	503
	1253	192.8	3.07	41.39	0	0	40	0.5	0.58	53.6	10.6	36.95	-	-	34.4201	2.2499	1253
	1333	197.9	3.18	42.89	0	0	-	-	-	-	-	33.42	-	-	43.4272	2.2423	1333
	1373	200.9	3.19	42.73	0	0	-	-	-	-	-	32.38	-	-	34.4299	2.2406	1373
	1412	201.4	3.18	42.40	0	0	-	-	-	-	-	31.84	-	-	34.4305	2.2377	1412
	1451	205.4	3.16	42.67	0	0	40	0	0.58	53.6	10.6	-	-	-	34.4311	2.2361	1451
	1492	204.9	3.15	42.83	0	0	-	-	-	-	-	31.60	-	-	34.4324	2.2355	1492
	1532	206.5	3.16	42.42	0	0	-	-	-	-	-	32.25	-	-	34.4333	2.2361	1532
	1568	210.5	3.20	42.52	0	0	-	-	-	-	-	30.80	-	-	34.4359	2.2369	1568
	1601	218.6	3.23	42.83	0	0	1135	0	0.68	53.6	11.3	30.69	-	-	34.4359	2.2389	1601
	1616	209.0	3.25	42.47	0	0	1780	0.5	0.88	67.0	13.6	30.89	-	-	34.4358	2.2391	1616

Station	Depth m	Si µM/l	PO_4 µM/l	NO_3 µM/l	NO_2 µM/l	NH_4 µM/l	CH_4 nl/l	C_2H_6 nl/l	CO_2 ml/l	GC O_2 µM/l	N_2 ml/l	Winkler O_2 µM/l	TA mM/kg	pH_{sws} (25)	Salinity	pot. Temp.	Depth m
CTD 39-1	50	0.5	1.38	14.10	0	3.95	110	2.0	0.27	303.7	13.0	373.3	-	-	32.7551	0.1132	50
	501	128.1	3.13	41.26	0	0.09	30	2.0	0.76	111.7	13.0	87.9	-	-	33.9360	2.0959	501
	1251	197.2	3.25	43.89	0	0.15	15	2.0	0.77	58.1	12.2	37.2	-	-	34.4013	2.2543	1251
	1294	196.2	3.26	42.81	0	0.07	15	1.0	0.79	62.5	12.8	36.8	-	-	34.4060	2.2501	1294
	1352	197.7	3.36	42.27	0	0.16	18	0.5	0.94	71.5	13.7	38.3	-	-	34.4102	2.2435	1352
	1393	201.8	3.28	42.70	0	0.28	18	1.0	0.99	71.5	13.7	38.9	-	-	34.4125	2.2403	1393
	1432	209.0	3.4	41.74	0	0.0	17	0	0.91	58.1	11.8	36.5	-	-	34.4148	2.2387	1432
	1467	210.5	3.42	43.00	0	0.0	26	0	0.90	58.1	12.1	35.6	2.399	7.356	34.4133	2.2356	1467
	1504	212.6	3.45	43.20	0	0.0	20	0	1.00	58.1	12.7	34.0	2.401	7.354	34.4123	2.2385	1504
	1537	219.7	3.48	43.28	0	0.0	11	0	0.95	58.1	12.7	31.3	2.401	7.340	34.4103	2.2364	1537
	1573	233.3	3.42	43.55	0	0.45	22	0	-	-	-	30.2	2.403	7.340	34.4111	2.2359	1573
	1596	232.5	3.49	43.39	0	0	23	0	1.01	80.4	14.1	31.0	2.404	7.332	34.4113	2.2355	1596

KOMEX II LV 28: Water column analysis

Station	Depth m	Si µM/l	PO_4 µM/l	NO_3 µM/l	NO_2 µM/l	NH_4 µM/l	CH_4 nl/l	C_2H_6 nl/l	CO_2 ml/l	CC O_2 µM/l	N_2 ml/l	Winkler O_2 µM/l	TA mM/kg	pH_{sws} (25)	Salinity	pot. Temp	Depth m
CTD 40-1	2	2 6	0	0	0	0	-	-	-	-	-	283 8	2 217	7 983	32 3810	14 1902	2
	2	2 1	0	0	0	0	88	3	0 19	232 2	10 2	284 6	2 221	7 983	32 2878	14 1848	2
	25	6 2	0 25	6 45	0	0 53	125	3	0 17	370 7	13 9	414 1	2 232	8 003	28 6834	7 2183	25
	52	18 4	1 64	18 57	0	7 18	113	1	0 38	312 8	13 8	380 3	2 234	7 985	33 9562	0 0795	52
	88	40 0	1 92	24 36	0	0	113	1	0 4	268 0	13	332 7	2 241	7 906	35 4082	-0 8231	88
	150	59 4	2 46	32 24	0	0	80	0 5	0 66	209 8	12 8	241 6	2 255	7 472	35 0711	0 3341	150
	251	75 8	2 90	36 02	0	0	78	0 5	0 91	185 2	12 3	176 5	2 269	7 383	34 8750	1 1053	251
	502	117 3	3 17	40 58	0	0	-	-	-	-	-	88 0	2 314	7 342	34 4021	2 0551	502
	753	156 6	3 34	43 1	0	0	-	-	-	-	-	51 5	2 358	7 327	34 3328	2 3789	753
	1003	179 3	3 37	43 24	0	0	12	1	0 6	71 5	12 4	38 8	2 385	7 332	34 3600	2 3152	1003
	1251	186 9	3 27	43 24	0	0	-	-	-	-	-	41 1	2 383	7 381	34 4447	2 2343	1251
	1275	186 3	3 21	42 85	0	0	21	1	0 68	75 8	12 6	42 0	2 394	7 362	34 4448	2 2341	1275
BW MUC 40-3	1287	149 6	3 11	39 29	0	0	-	-	-	-	-	43 0	-	-	-	-	1287

Station	Depth m	Si µM/l	PO_4 µM/l	NO_3 µM/l	NO_2 µM/l	NH_4 µM/l	CH_4 nl/l	C_2H_6 nl/l	CO_2 ml/l	CC O_2 µM/l	N_2 ml/l	Winkler O_2 µM/l	TA mM/kg	pH_{sws} (25)	Salinity	pot. Temp	Depth m
CTD 41-1	2	1 58	0	0 12	0	0	-	-	-	-	-	281 9	2 233	7 979	32 6877	13 9483	2
	11	2 08	0	0 21	0 2	0	68	1	0 14	283 5	-	283 2	2 237	7 976	32 6623	13 9310	11
	25	1 04	0 44	5 97	0 27	0 75	-	-	-	-	-	394 9	2 236	7 924	32 6868	3 3693	25
	50	7 18	1 35	14 14	0 32	3 91	100	0 5	0 33	312 6	-	373 8	2 237	7 724	32 7802	0 4015	50
	100	41 17	1 8	22 64	0 18	0 05	80	0 5	0 38	290 3	-	347 5	2 241	7 636	32 9984	-0 3208	100
	150	48 66	1 99	25 05	0 09	0	-	-	-	-	-	294 9	2 252	7 569	33 1392	-0 0914	150
	250	89 83	2 49	31 54	0 08	0	34	1	0 71	176 6	-	200 7	2 267	7 428	33 3868	1 0490	250
	501	105 78	3 01	35 77	0 09	0	36	1	0 88	116 1	-	113 0	2 306	7 357	33 7780	1 9178	501
	750	143 83	3 27	38 88	0 09	0	-	-	-	-	-	58 9	2 350	7 335	34 1174	2 3287	750
	802	193 83	3 38	39 77	0 18	0	28	0 5	0 93	71 5	-	37 6	2 382	7 335	34 2826	2 4392	902
	1002	183 43	3 17	39 2	0 05	0	-	-	-	-	-	33 8	2 383	7 349	34 3549	2 3904	1002
	1042	184 99	3 01	38 71	0 05	0 06	30	0 5	0 88	71 5	-	35 5	2 387	7 352	34 3734	2 3807	1042
BW MUC 41-1	1054	172 49	2 29	36 11	0	0	-	-	-	-	-	-	-	-	-	-	1054

Station	Depth m	Si µM/l	PO_4 µM/l	NO_3 µM/l	NO_2 µM/l	NH_4 µM/l	CH_4 nl/l	C_2H_6 nl/l	CO_2 ml/l	CC O_2 µM/l	N_2 ml/l	Winkler O_2 µM/l	TA mM/kg	pH_{sws} (25)	Salinity	pot. Temp	Depth m
CTD 42-2	2	1 0	0 28	0	0	0	-	-	-	-	-	288 7	2 216	8 020	32 5255	13 3703	2
	10	1 5	0 02	0	0	0	81	1	0 15	232 2	9 9	291 8	2 223	8 018	32 5202	13 3795	10
	26	4 6	0 46	6 13	0 14	1 29	-	-	-	-	-	398 4	2 226	7 917	32 6497	4 4760	26
	50	16 4	1 5	16 22	0 35	3 08	101	-	0 31	303 7	13 4	359 4	2 233	7 719	32 8204	0 7028	50
	76	38 0	1 86	21 53	0 15	1 1	-	-	-	-	-	343 4	2 239	7 658	32 9600	0 2223	76
	101	44 8	1 86	23 98	0 06	0	75	-	0 4	276 9	13 5	326 0	2 248	7 626	33 0610	0 1031	101
	152	54 9	2 29	27 45	0 08	0	-	-	-	-	-	278 2	2 254	7 562	33 2162	0 7273	152
	253	67 7	2 68	30 69	0 07	0	31	0	0 63	178 6	12	208 2	2 267	7 472	33 3919	1 2978	253
	503	103 1	3 79	38 31	0 05	0	41	0	0 84	111 7	11 4	116 2	2 307	7 386	33 7867	2 1403	503
	752	137 5	3 52	36 72	0 1	0	-	-	-	-	-	54 7	2 348	7 340	34 1200	2 4316	752
	951	152 4	3 69	40 52	0	0	45	1	0 9	71 5	12 5	38 1	2 372	7 357	34 3102	2 5759	951
	1009	186 3	3 69	39 9	0	0	43	0 5	0 94	71 5	12 6	37 1	2 381	7 366	34 3551	2 5028	1009
BW Muc 42-3	1021	166 6	3 66	39 71	0	0 02	-	-	-	-	-	38 5	-	-	-	-	1021

Station	Depth m	Si µM/l	PO_4 µM/l	NO_3 µM/l	NO_2 µM/l	NH_4 µM/l	CH_4 nl/l	C_2H_6 nl/l	CO_2 ml/l	CC O_2 µM/l	N_2 ml/l	Winkler O_2 µM/l	TA mM/kg	pH_{sws} (25)	Salinity	pot. Temp.	Depth m
CTD 43-1	2	1 1	0	0	0	0 14	-	-	-	-	-	289 4	2 222	8 032	32 6664	13 1691	2
	10	1 1	0	0	0	0 11	63	2	0 14	245 6	10 6	290 4	2 231	8 035	32 6609	13 1648	10
	25	4 8	0 50	6 58	0 07	0 81	-	-	-	-	-	422 3	2 235	7 918	32 7785	3 5697	25
	50	13 3	1 57	16 47	0 20	3 77	80	0 5	0 34	294 8	12 8	363 8	2 239	7 704	32 8777	0 5210	50
	75	37 9	1 79	20 89	0 05	0	-	-	-	-	-	352 2	2 240	7 665	32 9584	-0 0363	75
	100	45 4	1 96	23 75	0	0	69	1	0 39	276 9	12 6	348 9	2 242	7 648	33 0389	-0 0589	100
	151	51 2	2 23	26 40	0	0	48	1	0 49	245 6	13	291 1	2 253	7 577	33 1821	0 6684	151
	251	68 3	2 71	30 40	0	0	27	1	0 6	169 7	10 8	213 7	2 267	7 479	33 3832	1 4141	251
	500	96 1	2 93	35 26	0	0	36	1 5	0 84	125 0	12	123 9	2 303	7 379	33 7437	2 0557	500
	750	144 1	3 41	39 72	0 01	0	36	-	-	-	-	46 0	2 371	7 340	34 1794	2 6379	750
	800	162 2	3 43	39 77	0	0	48	1 5	0 89	75 9	12 1	36 9	2 370	7 324	34 2469	2 6273	800
	819	163 3	3 35	40 02	0 07	0	47	0 5	1 02	71 5	11 4	36 8	2 371	7 335	34 2483	2 6237	819
BW MUC 43-3	831	139 3	2 61	35 39	0 07	0	-	-	-	-	-	46 29	-	-	-	-	831

KOMEX II LV 28: Water column analysis

Station	Depth m	Si µM/l	PO_4 µM/l	NO_3 µM/l	NO_2 µM/l	NH_4 µM/l	CH_4 nl/l	C_2H_6 nl/l	CO_2 ml/l	O_2 µM/l	N_2 ml/l	O_2 µM/l	TA mM/kg	pH_{SWS} (25)	Salinity	pot. Temp.	Depth m
CTD 64-1	11	4.69	0.09	0	0	0.18	-	-	0.2	227.8	10.6	287.0	2.206	2.206	32.2667	14.5932	11
	54	32.86	1.95	17.22	0	1.99	-	-	0.26	250.1	12.5	349.1	2.238	2.238	32.8728	-0.8338	54
	128	51.63	2.17	21.74	0	0.26	-	-	0.56	232.2	13	290.8	2.253	2.253	33.1689	-0.4391	128
	256	76.14	3.84	27.49	0	0.17	-	-	0.98	169.7	12.4	196.1	2.27	2.270	33.3900	0.6755	256
	378	82.4	2.79	27.2	0	0.32	-	-	-	-	-	182.4	2.281	2.281	33.5163	0.7843	378
	505	112.12	3.14	31.32	0	0	-	-	1.15	107.2	11.9	108.2	2.318	2.318	33.8081	1.8956	505
	755	149.15	3.5	33.41	0	0.2	-	-	-	-	-	58.6	2.348	2.348	34.1320	2.2468	755
	1002	161.67	3.28	34.75	0	0.01	-	-	1.1	67.0	12.7	52.2	2.379	7.343	34.3408	2.3795	1002
	1249	168.97	3.23	34.31	0	0.01	-	-	-	-	-	50.8	2.39	7.375	34.4461	2.1588	1249
	1495	171.06	3.2	34.44	0	0.17	-	-	-	-	-	59.6	2.401	7.399	34.5044	2.0205	1495
	1746	174.18	3.19	34.15	0	0.21	-	-	-	-	-	71.5	2.405	7.414	34.5396	1.9021	1746
	1914	175.75	3.13	34.11	0	0.28	-	-	1.02	93.8	13	73.7	2.41	7.429	34.5586	1.8455	1914
BW MUC 64-3	1926	188.18	2.93	32.02	0	0.25	-	-	-	-	-	89.1	-	-	-	-	1926

Station	Depth m	Si µM/l	PO_4 µM/l	NO_3 µM/l	NO_2 µM/l	NH_4 µM/l	CH_4 nl/l	C_2H_6 nl/l	CO_2 ml/l	GC O_2 µM/l	N_2 ml/l	Winkler O_2 µM/l	TA mM/kg	pH_{SWS} (25)	Salinity	pot. Temp.	Depth m
CTD 65-1	11	7.76	0.06	0	0	0	-	-	0.17	205.4	9.1	279.9	-	-	32.3449	15.2396	11
	49	28.95	1.48	12.56	0	0	-	-	-	-	-	308.0	-	-	32.9188	0.9024	49
	64	36.19	1.8	16.18	0	0	-	-	0.65	272.4	13.6	333.4	-	-	32.9542	-0.4797	64
	77	38.77	1.62	15.59	0	0	-	-	-	-	-	310.9	-	-	33.0746	0.4869	77
	99	41.36	1.57	15.62	0	0	-	-	0.43	227.8	12.4	281.1	-	-	33.3138	2.3753	99
	123	47.05	1.89	18.24	0	0	-	-	-	-	-	290.2	-	-	33.1924	0.4174	123
	139	47.58	1.92	19.09	0	0	-	-	-	-	-	294.8	-	-	33.1588	-0.3535	139
	160	49.63	1.96	19.55	0	0	-	-	0.57	223.3	12.7	276.1	-	-	33.2482	0.5571	160
	503	80.13	2.25	23.69	0	0	-	-	0.74	160.8	12.1	182.8	-	-	33.7437	1.9197	503
	749	144.76	3.15	33.32	0	0	-	-	-	-	-	68.2	-	-	34.0768	2.1937	749
	1000	161.82	3.14	34.26	0	0	-	-	1.08	67.0	12.1	45.9	-	-	34.2858	2.3187	1000
	1167	168.02	3.08	33.91	0	0	-	-	-	-	-	48.1	-	-	34.3920	2.2217	1167

Station	Depth m	Si µM/l	PO_4 µM/l	NO_3 µM/l	NO_2 µM/l	NH_4 µM/l	CH_4 nl/l	C_2H_6 nl/l	CO_2 ml/l	GC O_2 µM/l	N_2 ml/l	Winkler O_2 µM/l	TA mM/kg	pH_{SWS} (25)	Salinity	pot. Temp.	Depth m
CTD 66-2	9	8.27	0.11	0	0	0	-	-	0.1	232.2	10.1	297.0	-	-	32.4311	14.2158	9
	54	24.82	1.74	15.01	0	0	-	-	0.35	285.8	13.5	337.9	-	-	32.8598	0.5207	54
	178	57.39	2.33	22.29	0	0	-	-	0.49	223.3	12.9	268.8	-	-	33.2397	0.1257	178
	254	69.28	2.66	25.2	0	0	-	-	0.59	192.0	13.2	219.5	-	-	33.3704	0.6611	254
	502	91.51	2.66	26.12	0	0	-	-	0.68	147.4	13	107.8	-	-	33.7756	1.9767	502
	749	141.86	3.3	32.72	0	0	-	-	-	-	-	71.6	-	-	34.0606	2.1757	749
	1000	164.4	3.32	34.52	0	0	-	-	0.9	62.5	12.2	50.2	-	-	34.2872	2.2765	1000
	1251	171.12	3.51	34.26	0	0	-	-	-	-	-	51.5	-	-	34.4392	2.1566	1251
	1500	173.71	3.4	34.03	0	0	-	-	0.84	71.5	11.8	63.6	-	-	34.5058	2.006	1500
	1750	176.81	3.42	33.9	0	0	-	-	-	-	-	70.9	-	-	34.5431	1.8881	1750
	1998	177.84	3.44	33.17	0	0	-	-	-	-	-	78.6	-	-	34.5694	1.7977	1998
	2248	177.84	3.44	32.63	0	0	-	-	0.76	84.9	12.1	84.9	-	-	34.5909	1.7202	2248

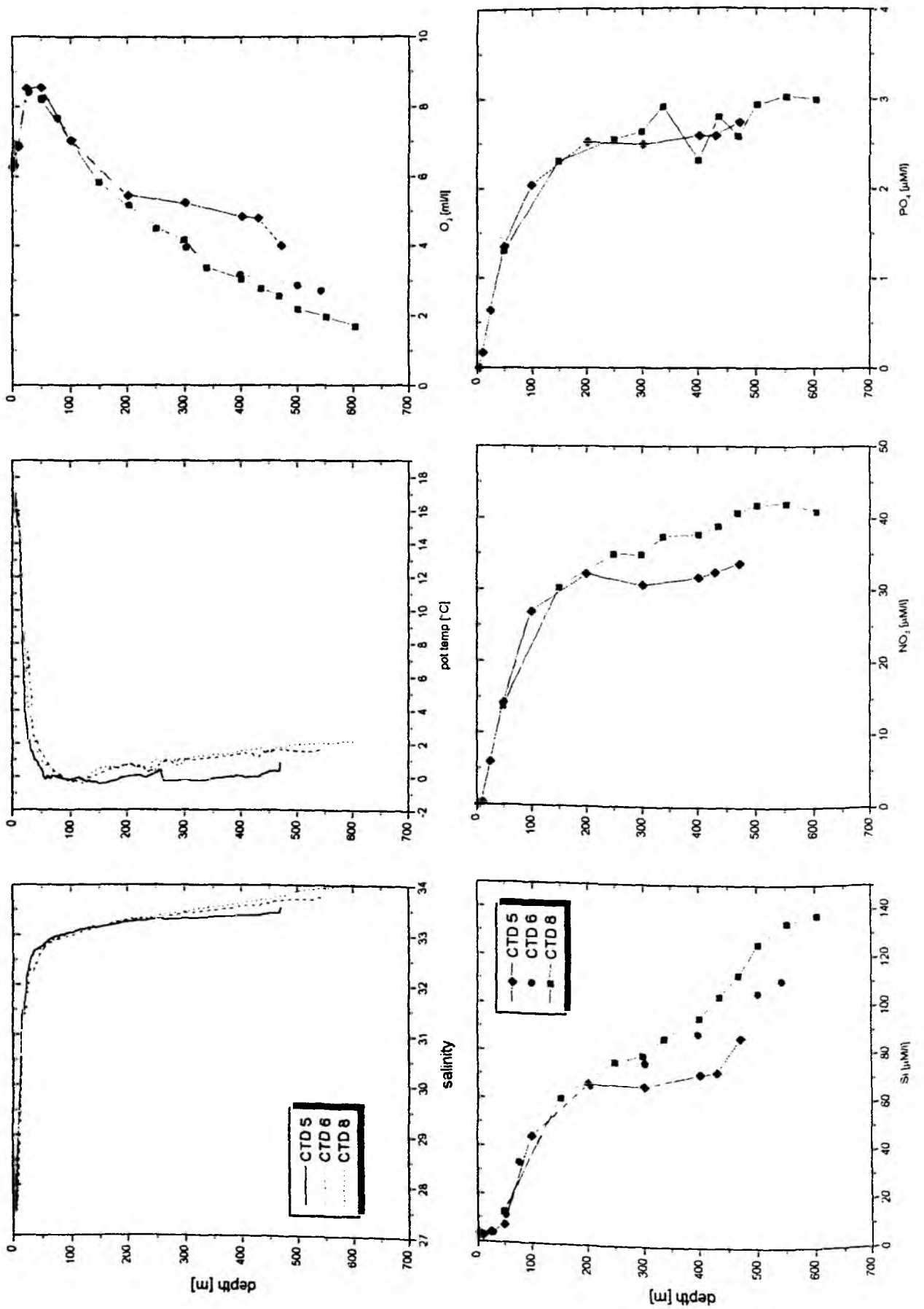

***Fig. A4.2**: Hydrographic and geochemical data for CTD stations 5-1, 6-1 and 8-1*

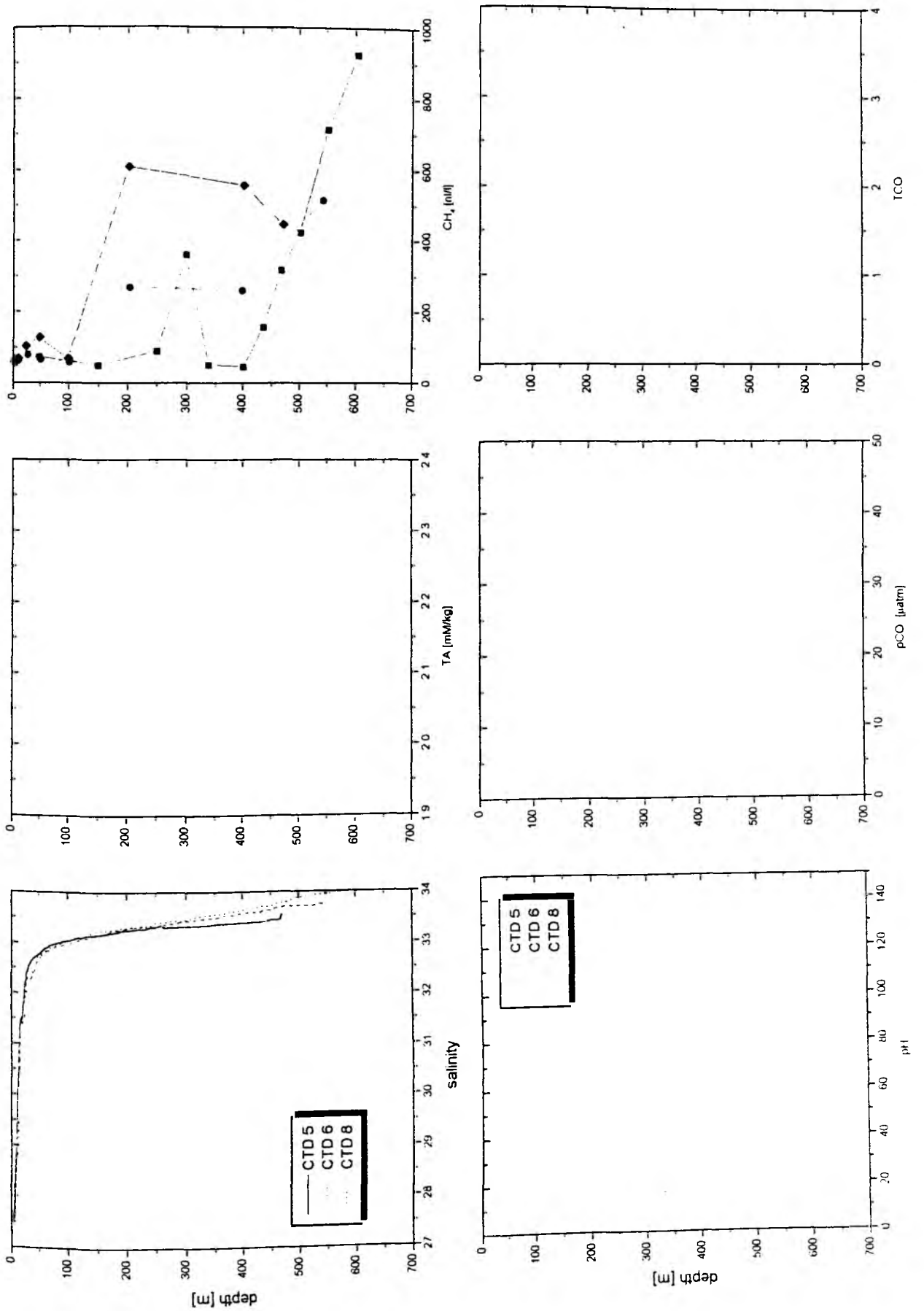

***Fig. A4.3**: Hydrographic and geochemical data for CTD stations 5-1, 6-1 and 8-1*

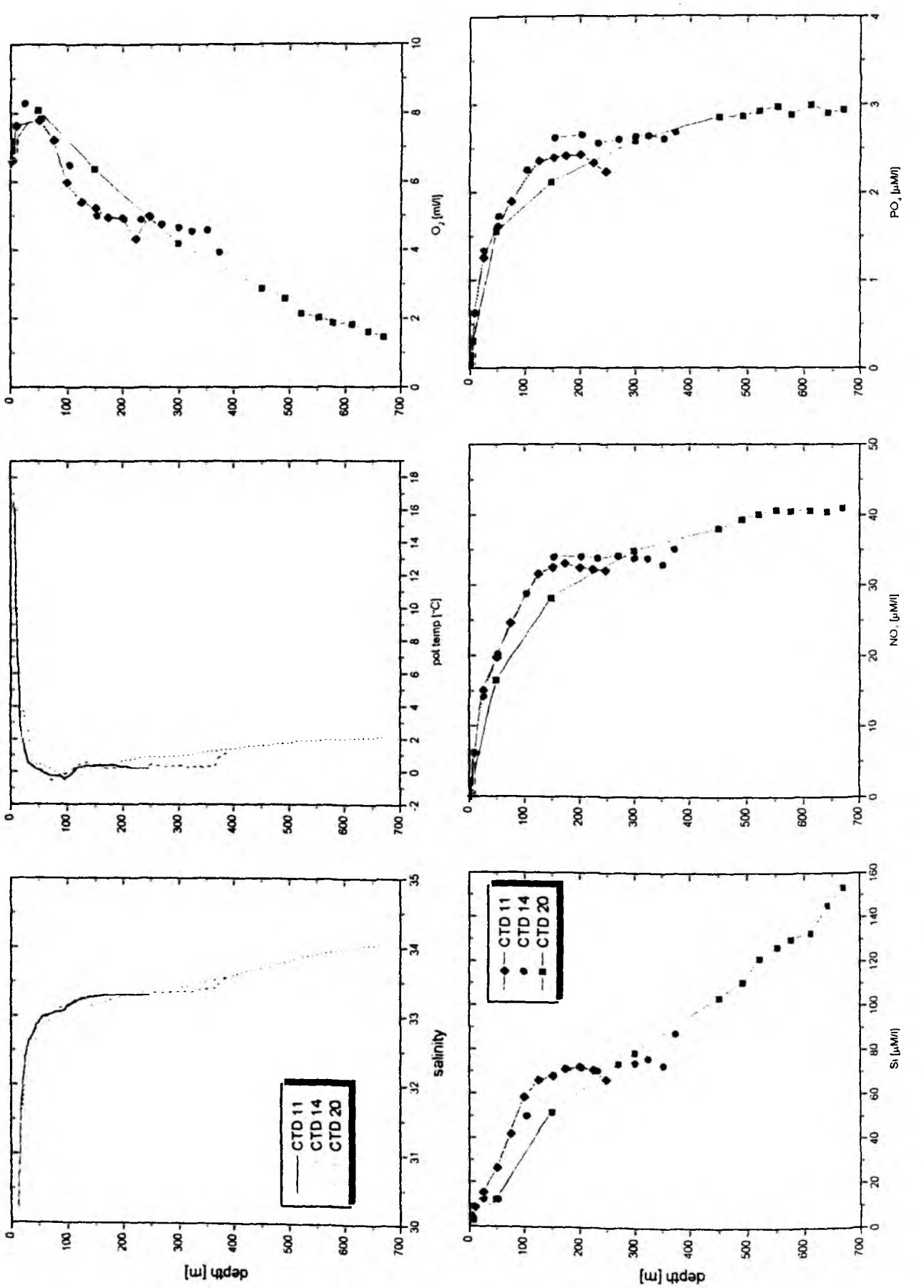

***Fig. A4.4**: Hydrographic and geochemical data for CTD stations 11-1, 14-1 and 20-1*

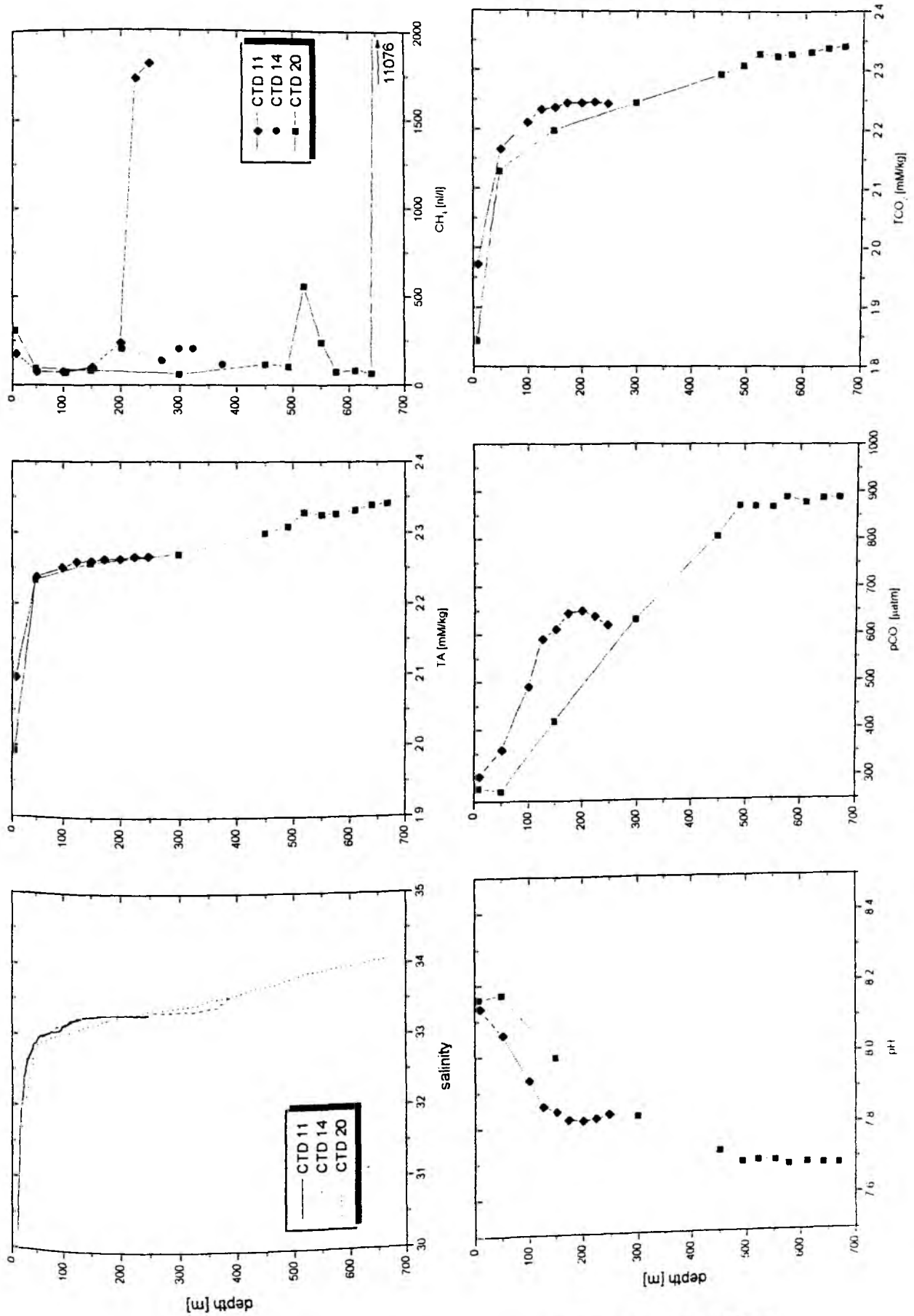

***Fig. A4.5**: Hydrographic and geochemical data for CTD stations 11-1, 14-1 and 20-1*

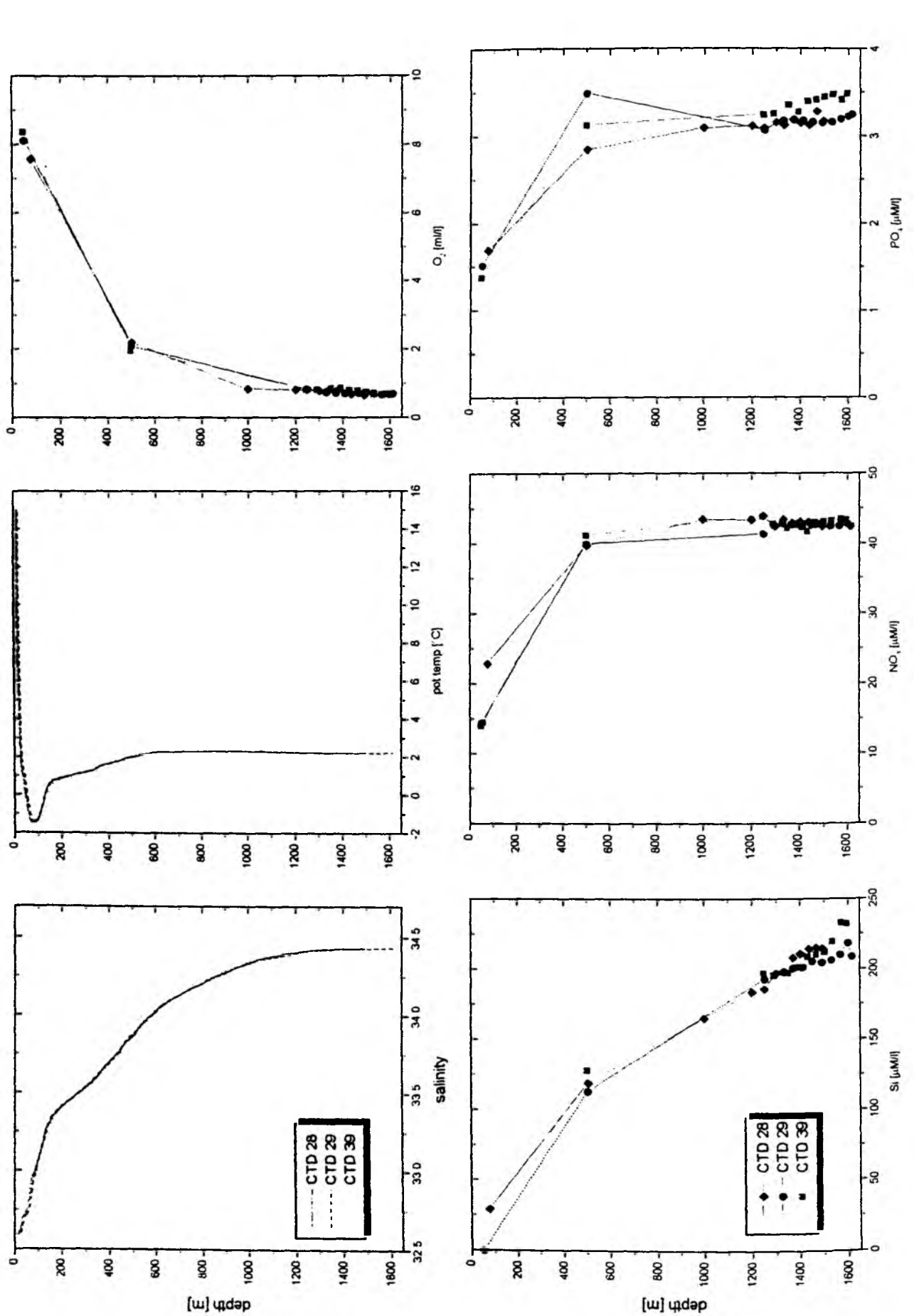

Fig. A4.6: Hydrographic and geochemical data for CTD stations 28-1, 29-1 and 39-1

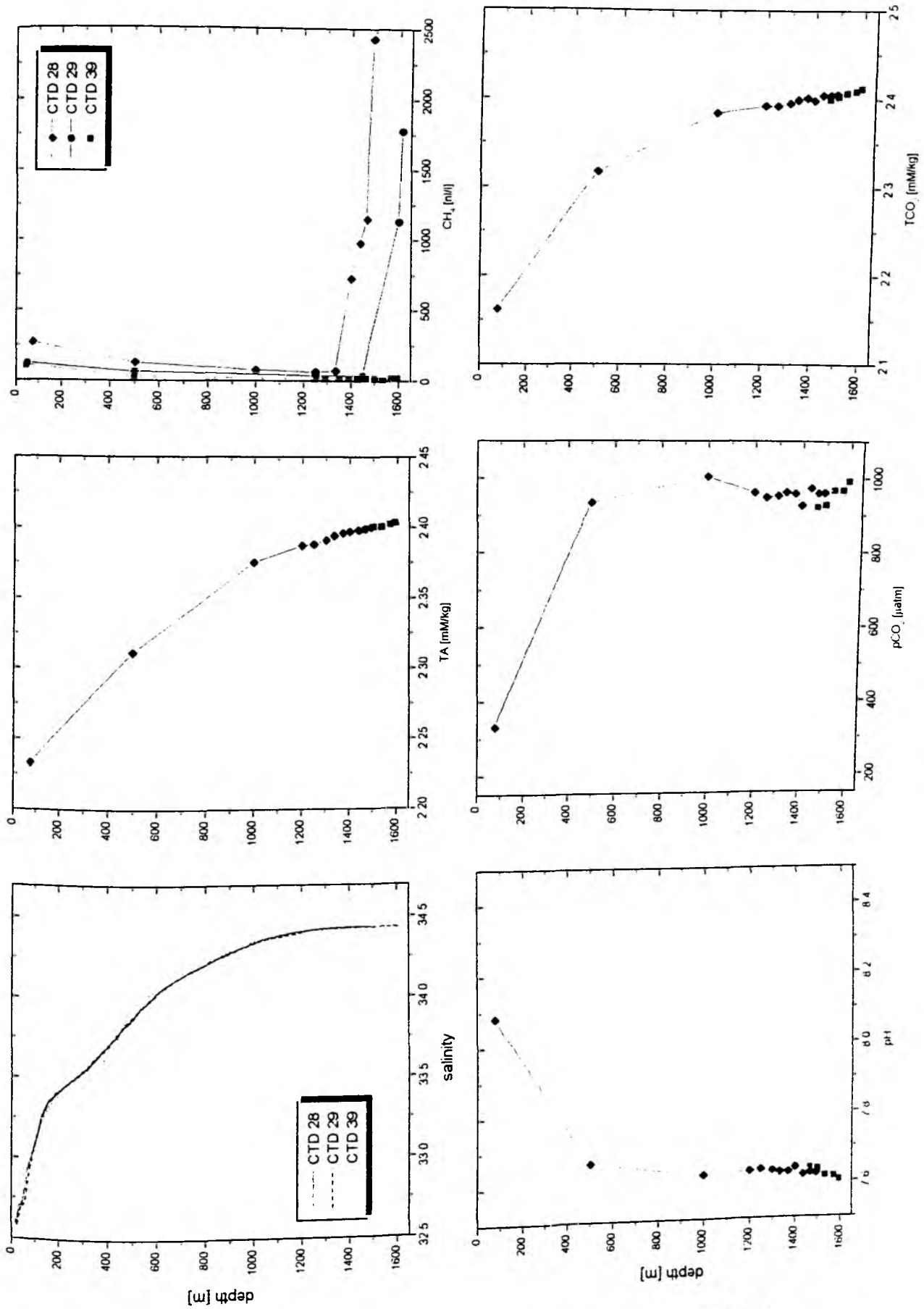

Fig. A4.7: Hydrographic and geochemical data for CTD stations 28-1, 29-1 and 39-1

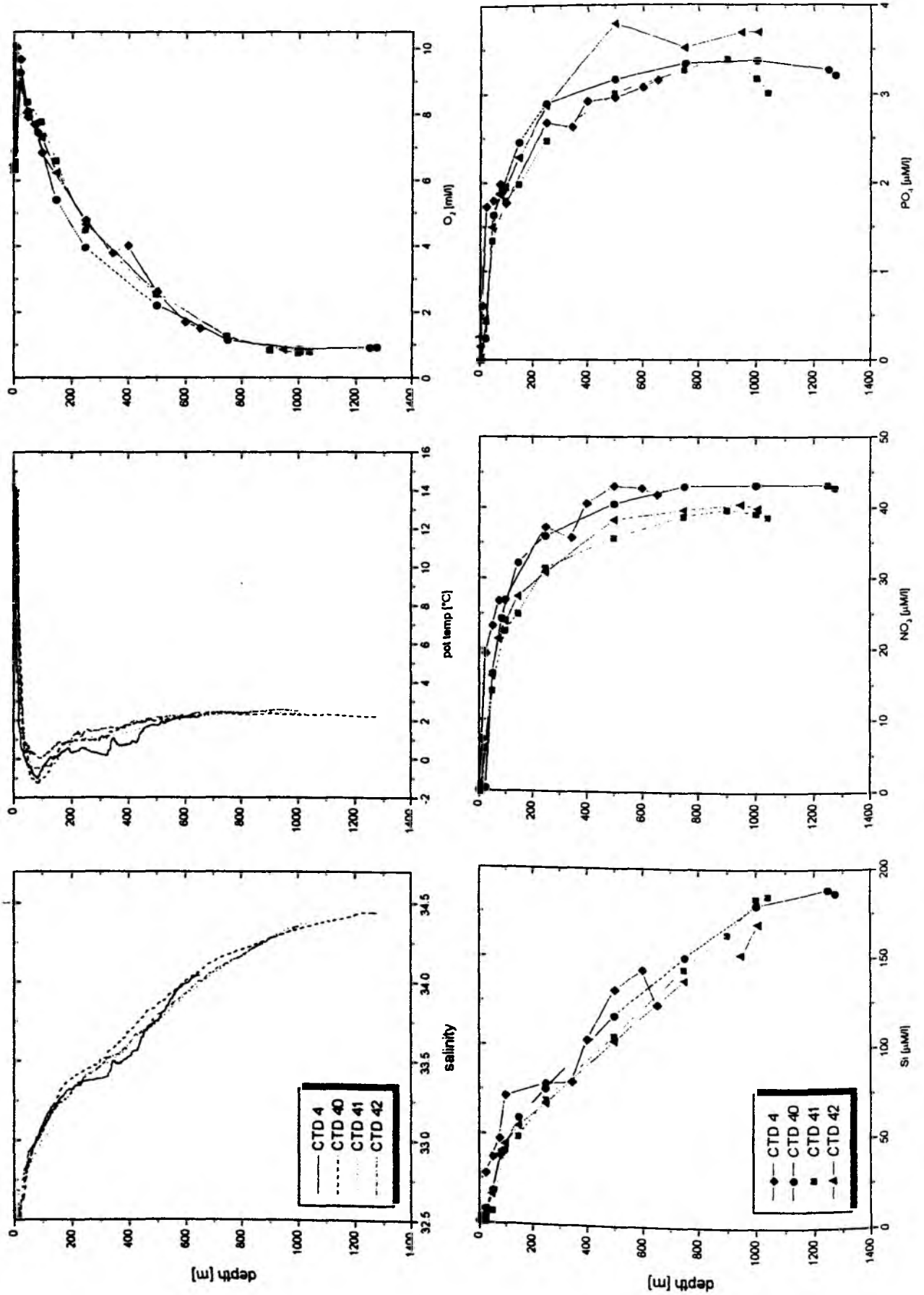

Fig. A4.8: Hydrographic and geochemical data for CTD stations 4-1, 40-1, 41-1 and 42-1

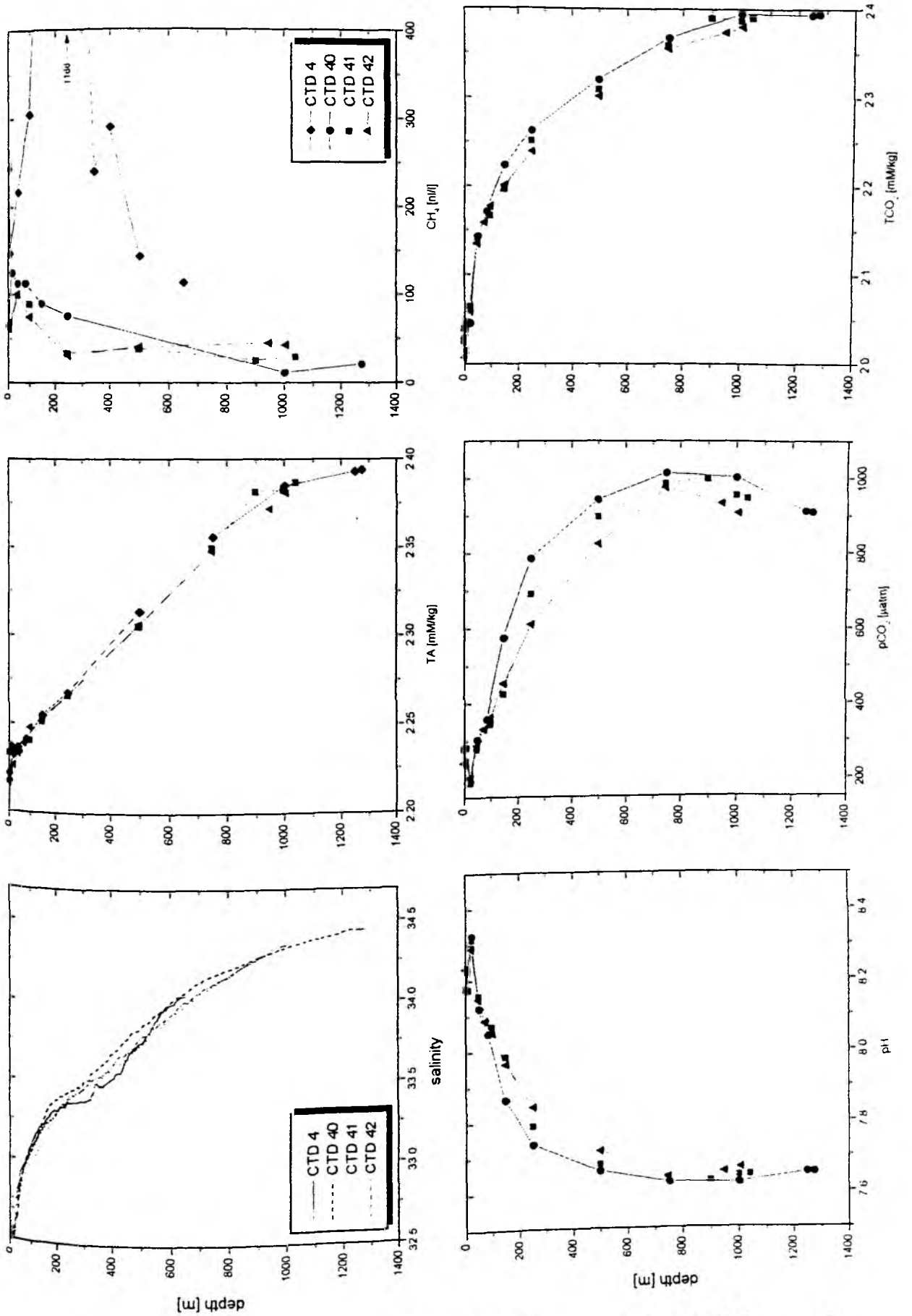

***Fig. A4.9**: Hydrographic and geochemical data for CTD stations 4-1, 40-1, 41-1 and 42-1*

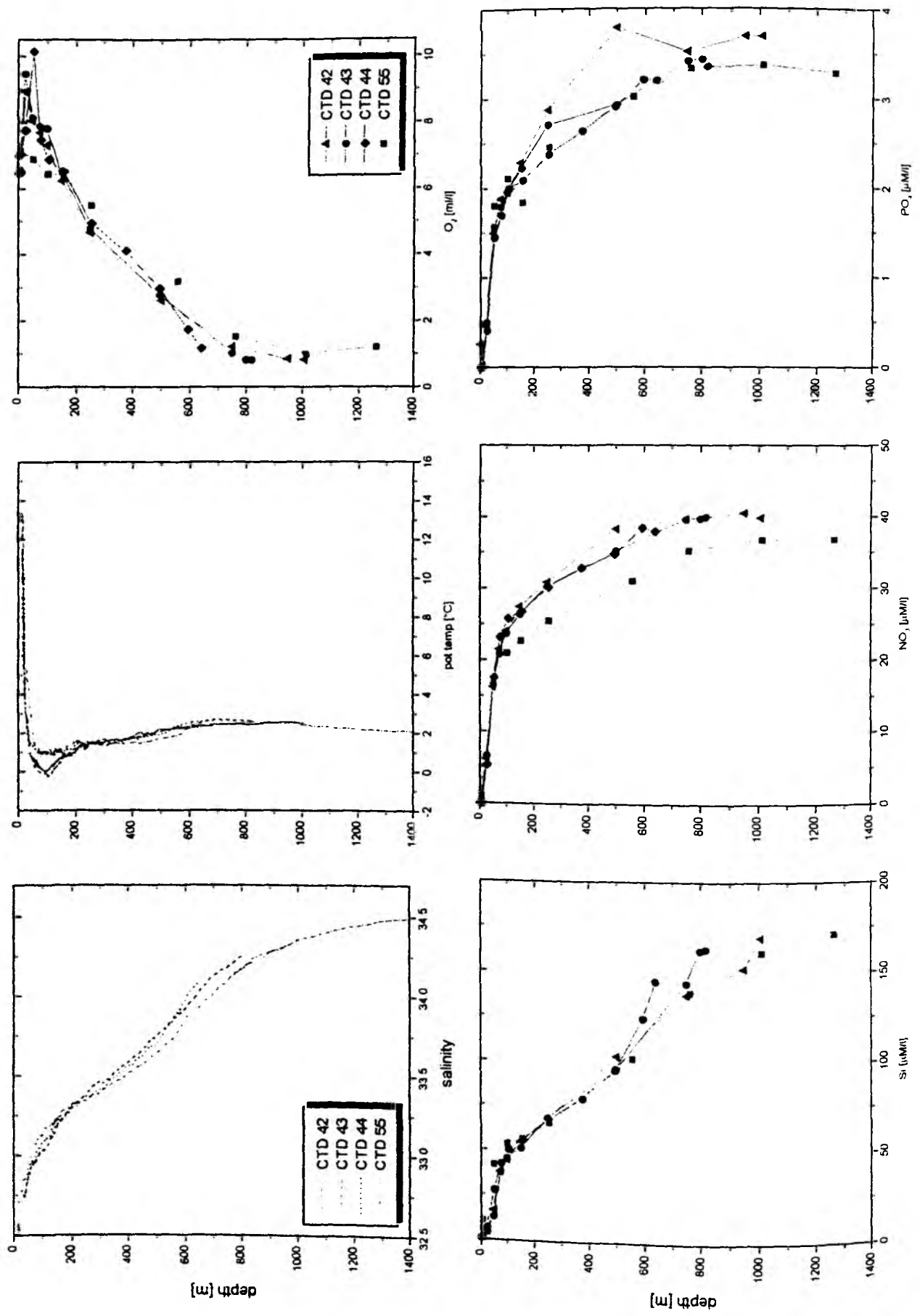

***Fig. A4.10**: Hydrographic and geochemical data for CTD stations 42-1, 43-1, 44-1 and 55-1*

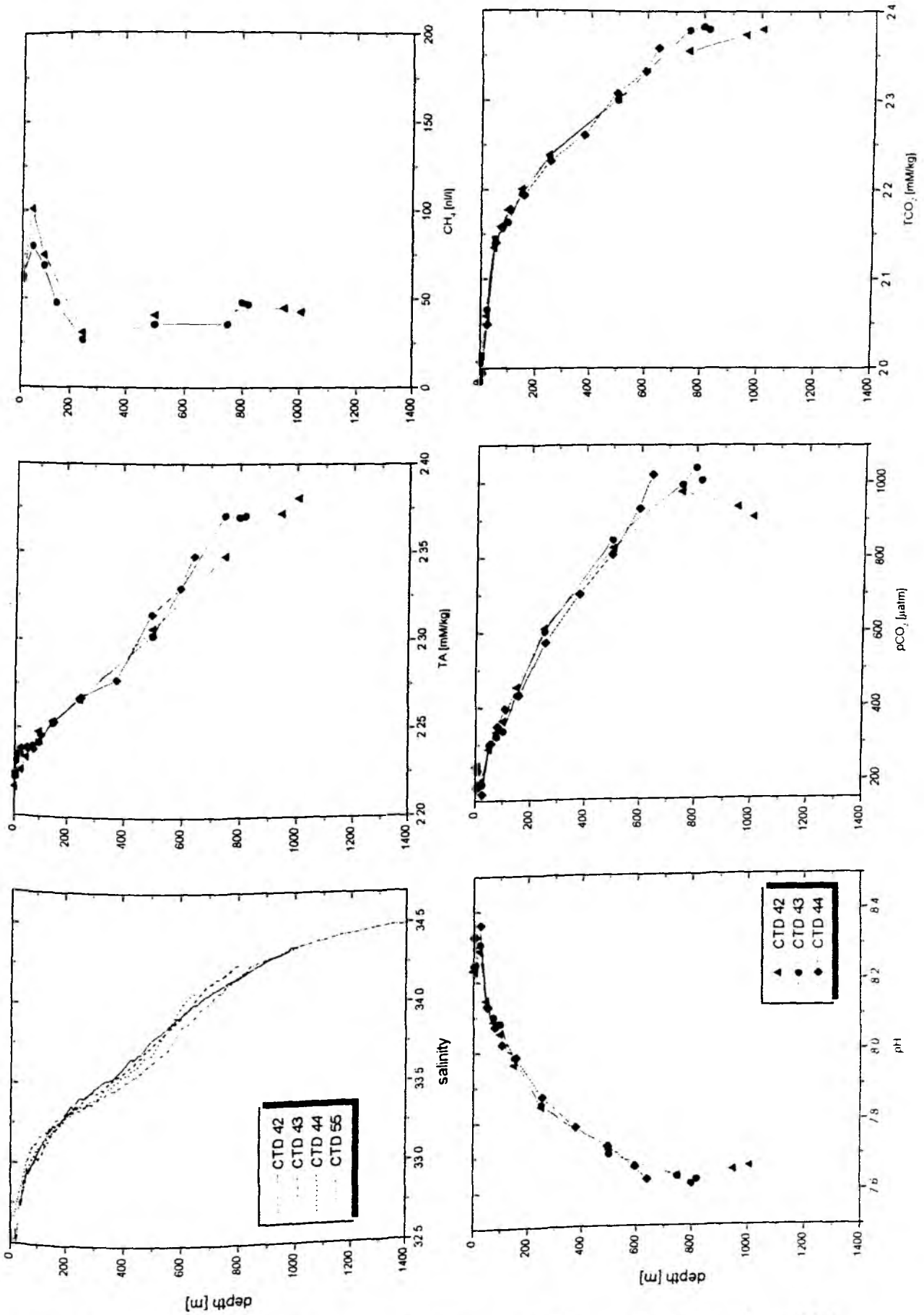

***Fig. A4.11**: Hydrographic and geochemical data for CTD stations 42-1, 43-1, 44-1 and 55-1*

Appendix 5

Pore Water Data and Sediment pH and Eh

KOMEX II LV 28: Porewater analysis

MUC 2-2

Depth cm	Si µM/l	PO_4 µM/l	NO_3 µM/l	NO_2 µM/l	NH_4 µM/l	H_2S µM/l	Cl mM/l	S psu	Temp. C	pH	pH (25)	TA mM/kg	CA mM/kg	Depth cm
0	187.63	2.89	42.19	0.00	0.00	0	550.62	34.42	7.2	7.88	-	2.417	10.106	0
0.25	436.70	3.44	41.69	0.27	0.38	0	553.89	34.63	5.0	7.71	-	2.203	10.025	0.25
0.75	506.15	5.56	27.96	0.43	6.79	0	552.25	34.52	4.8	7.52	-	2.261	9.976	0.75
1.5	578.25	5.61	13.63	0.25	3.69	0	549.80	34.37	4.4	7.50	-	2.319	9.815	1.5
2.5	*642.35*	*7.01*	*2.4*	*0.23*	*4.74*	*0*	-	-	*4.3*	*7.52*	-	-	-	2.5
3.5	679.75	8.41	0.42	0	10.83	0	-	-	4.5	7.52	-	-	-	3.5
4.5	634.35	7.74	0.26	0	13.47	0	-	-	4.4	7.52	-	-	-	4.5
5.5	639.68	7.44	0.16	0	15.96	0	553.24	34.58	4.3	7.58	-	2.452	9.836	5.5
6.5	638.35	6.61	0.45	0	18.05	0	-	-	4.2	7.59	-	-	-	6.5
7.5	634.35	9.47	1.04	0	7.58	0	-	-	4.2	7.59	-	-	-	7.5
8.5	641.03	6.13	0.16	0	24.40	0	-	-	4.3	7.61	-	-	-	8.5
9.5	638.35	5.24	0.06	0	30.49	0	-	-	4.1	7.59	-	-	-	9.5
11.5	649.03	4.92	0	0	36.33	0	554.55	34.66	4.1	7.59	-	2.452	9.836	11.5
14.5	679.75	5.58	0	0	45.57	0	-	-	4.1	7.65	-	-	-	14.5
17.5	683.75	6.45	0	0	52.50	0	-	-	4.0	7.67	-	-	-	17.5
20.5	677.08	8.52	0	0	53.37	0	551.27	34.46	4.1	7.67	-	2.796	9.704	20.5
23.5	683.75	9.54	0	0	68.46	*0*	-	-	4.0	7.65	-	-	-	23.5
26.5	686.43	13.8	0	0	63.90	0	-	-	4.0	7.61	-	-	-	26.5
29.5	685.10	10.8	0	0	71.43	0	-	-	4.1	7.61	-	-	-	29.5
32.5	-	-	-	-	0.18	-	-	-	4.3	7.56	-	-	-	32.5
34.5	691.78	0.75	0	0	166.20	0	554.55	34.66	4.5	7.56	-	3.085	9.905	34.5

SL(R) 2-4

Depth cm	Si µM/l	PO_4 µM/l	NO_3 µM/l	NO_2 µM/l	NH_4 µM/l	H_2S µM/l	Cl mM/l	S psu	Temp. C	pH	pH (25)	TA mM/kg	CA mM/kg	Depth cm
10	709.1	9.8	0	0	65.8	0	-	-	6.8	7.79	-	-	-	10
40	758.6	11.9	0	0	128.0	0	-	-	4.6	7.44	-	-	-	40
70	765.2	21.3	0	0	187.6	0	-	-	5.4	7.39	-	-	-	70
100	747.9	*28.4*	0	0	427.6	0	553.6	-	4.6	7.41	-	5.497	9.858	100
130	718.5	36.0	0	0	306.2	0	-	-	5.2	7.39	-	-	-	130
160	678.4	40.0	0	0	526.7	0	-	-	4.8	7.35	-	-	-	160
190	646.4	45.8	0	0	388.5	0	551.3	-	7.0	7.44	-	7.682	9.448	190
220	623.7	50.6	0	0	442.5	0	-	-	5.4	7.37	-	-	-	220
250	579.6	52.9	0	0	492.0	0	-	-	*6.6*	7.30	-	-	-	250
280	558.2	56.7	0	0	540.8	0	-	-	6.9	7.44	-	-	-	280
310	554.2	*66.0*	0	0	560.9	0	552.9	-	6.8	7.42	-	10.708	9.189	310
340	532.9	63.2	0	0	722.5	0	-	-	8.4	7.37	-	-	-	340
370	542.2	72.3	0	0	678.4	0	-	-	7.8	7.42	-	-	-	370
400	512.8	74.0	0	0	763.8	0	553.2	-	8.2	7.39	-	12.833	9.19	400
430	528.9	82.7	0	0	693.5	0	-	-	8.3	7.30	-	-	-	430
460	550.2	86.6	0	0	*712.0*	0	-	-	7.5	7.37	-	-	-	460
490	555.6	90.7	0	0	735.5	0	-	-	8.0	7.35	-	-	-	490
520	563.6	99.7	0	0	941.2	0	551.8	-	7.4	7.35	-	15.589	9.088	520
550	579.6	102.8	0	0	700.7	0	-	-	7.6	7.32	-	-	-	550
580	601.0	105.1	0	0	812.3	0	552.9	-	8.4	7.30	-	16.680	9.05	580
610	621.0	73.8	0	0	523.0	0	-	-	7.5	7.28	-	-	-	610

IBUC 15-2 A

Depth cm	Si µM/l	PO_4 µM/l	NO_3 µM/l	NO_2 µM/l	NH_4 µM/l	H_2S µM/l	Cl mM/l	S psu	Temp C	pH	pH (25)	TA mM/kg	CA mM/kg	Depth cm
0	66.3	2.5	31.02	0	2.28	3.62392	530.64	.	.	.	.	.	.	0
0.25	353.5	.	0	0	113.5	.	.	.	5.4	7.77	.	.	.	0.25
0.75	*477.5	.	0	0	29.1	15.18684	530.14	.	5.1	7.49	.	.	.	0.75
2	*311.5	.	0	0	122.3	341.844	535.55	.	5.3	7.59	.	.	.	2
3	*518.9	.	0	0	102.6	2708.6	536.53	.	5.5	7.77	.	.	.	3
4	*637.6	.	0	0	8.3	6468.884	539.48	.	5.3	7.86	.	.	.	4
5	*653.6	.	0	0	7.2	6515.584	546.85	.	5.2	7.68	.	.	.	5
6	*604.3	.	0	0	76.7	5760.912	536.53	.	5.2	7.89	.	.	.	6

* interference with H2S

IBUC 15-2 B

Depth cm	Si µM/l	PO_4 µM/l	NO_3 µM/l	NO_2 µM/l	NH_4 µM/l	H_2S µM/l	Cl mM/l	S psu	Temp C	pH	pH (25)	TA mM/kg	CA mM/kg	Depth cm
top	122.19	21.2	0	0	19.0	78.3626	529.16	.	6.4	7.86				top
bottom	161.14	25.7	0	0	34.4	1910.964	533.09	.	6.3	7.84				bottom

SL(G) 17-2

Depth cm	Si µM/l	PO_4 µM/l	NO_3 µM/l	NO_2 µM/l	NH_4 µM/l	H_2S µM/l	Cl mM/l	S psu	Temp C	pH	pH (25)	TA mM/kg	CA mM/kg	Depth cm
0	326.6	3.6	0	0	8.2	0.7	535.8	.	5.6	6.86				0
2	404.5	13.7	0	0	217.5	113.9	538.5	33.68	9.0	7.35		4.103	9.429	2
5	.	.	.	.	.	.	.	33.63			7.329			5
7	237.8	6	0	0	3	22.3	537.5	.	8.8	7.21				7
10	.	4.2	0	0	7.2	1.8	.	33.63	8.1	7.31		3.182	9.473	10
14	328.0	17.9	0	0	62.1	1.1	533.9	.	7.3	7.50		.	.	14
18	356.7	63.8	0	0	86.4	52.3	535.8	.	7.0	7.48				18
21	464.6	79.9	0	0	100.2	496.0	535.6	33.51	7.2	7.53		8.609	9.230	21
25	322.5	30.2	0	0	62.2	2204.2	543.4	.	6.6	7.56				25
28	387.8	44.9	0	0	66.4	3849.9	541.0	.	6.7	7.58				28
32	.	.	.	.	.	.	.	.	7.1	7.55				32
35	348.5	26.2	0	0	49.8	7113.3	542.4	33.92	8.8	7.50	7.604	27.986	7.882	35
38	304.7	50.6	0	0	60.6	5437.7	545.4	.	8.9	7.63				38
43	351.2	40.2	0	0	63.9	7718.7	544.4	34.04	7.5	7.38		34.316	7.881	43
48	369.0	55.9	0	0	84.3	8759.1	544.4	.	8.6	7.38				48
53	344.4	52.3	0	0	64.4	9364.3	546.9	34.20	9.2	7.41		36.979	8.049	53
58	359.4	63.7	0	0	72.3	8344.4	542.9	.	8.7	7.40				58
63	364.9	67.8	0	0	75.2	8481.7	542.9	33.96	9.6	7.40		37.333	8.360	63
67	.	.	.	.	.	.	.	34.08			7.595			67
68	355.3	81.8	0	0	83.4	9187.8	544.9	.	9.7	7.28		24.49		68
72	303.4	81.4	0	0	85.3	2454.6	545.9	.				25.67		72
78	282.9	113.9	0	0	87.4	2400.4	546.4	.	8.2	7.48		23.16		78
82	336.2	68.5	0	0	93.5	658.5	534.9	.	13.7	7.48		26.25		82

HYC 20-3

Depth cm	Si µM/l	PO_4 µM/l	NO_3 µM/l	NO_2 µM/l	NH_4 µM/l	H_2S µM/l	Cl mM/l	S psu	Temp. C	pH	pH (25)	TA mM/kg	CA mM/kg	Depth cm
1	623.7	8.9	0	0	0.1	1.9	533.1	-	8.2	7.19	-	-	-	1
3	-	-	-	-	-	-	-	33.36	-	-	7.449	-	-	3
6	669.3	8.6	0	0	1.5	0	542.4	33.92	5.8	7.25	-	2.521	9.723	6
11	622.2	12.4	0	0	33.4	0.7	536.5	33.56	4.1	7.30	7.535	2.522	9.792	11
16	558.3	7.4	0	0	26.7	0	548.0	-	3.9	7.30	-	-	-	16
21	547.8	7.0	0	0	28.2	0	-	-	3.6	7.31	-	-	-	21
26	556.7	8.8	0	0	41.5	0	-	-	3.7	7.31	-	-	-	26
31	567.4	2.4	0	0	0.5	0	-	-	4.7	7.28	-	-	-	31
36	584.4	7.4	0	0	40.3	0	-	-	6.5	7.23	-	-	-	36
41	593.3	6.8	0	0	29.7	0	-	-	5.3	7.27	-	-	-	41
46	572.0	13.0	0	0	43.9	0	-	-	4.2	7.30	-	-	-	46
51	596.3	9.1	0	0	45.5	0	538.0	31.65	4.7	7.26	7.650	2.540	9.758	51
56	622.2	10.5	0	0	69.7	0	-	-	4.4	7.29	-	-	-	56
61	594.8	5.4	0	0	71.8	3.5	-	-	5.4	7.26	-	-	-	61
66	640.4	7.2	0	0	139.4	24.4	-	-	4.5	7.29	-	-	-	66
71	649.5	10.4	0	0	207.8	25.0	-	-	4.6	7.28	-	-	-	71
76	572.0	15.6	0	0	302.5	125	-	-	4.7	7.28	-	-	-	76
81	663.2	24	0	0	444.2	263	-	-	5.9	7.25	-	-	-	81
86	663.2	23.4	0	0	438.5	279	-	-	6.4	7.24	-	-	-	86
91	731.7	43.5	0	0	669.4	473	-	-	6.2	7.24	-	-	-	91
96	724.1	50.7	0	0	766.6	444	-	-	6.2	7.24	-	-	-	96
101	742.3	55.4	0	0	849.2	849	545.4	34.11	6.1	7.19	-	12.198	9.091	101
111	786.7	70.2	0	0	1079.4	1079	-	-	8.1	7.19	-	-	-	111
121	740.8	86.4	0	0	1310.2	1310	-	-	8.3	7.19	-	-	-	121
131	721.0	100.2	0	0	1573.4	1573	-	-	8.5	7.18	-	-	-	131
141	783.4	110.2	0	0	1766.6	1767	-	-	8.9	7.17	-	-	-	141
151	758.0	124.6	0	0	2022.8	2023	544.4	34.04	8.2	7.19	-	23.622	7.910	151

HYC 21-1

Depth cm	Si µM/l	PO_4 µM/l	NO_3 µM/l	NO_2 µM/l	NH_4 µM/l	H_2S µM/l	Cl mM/l	S psu	Temp. C	pH	pH (25)	TA mM/kg	CA mM/kg	Depth cm
5	526.075	1.6	0	0	37.5	33.1	539.2	33.72	8.0	7.57	-	2.435	9.957	5
30	497.375	2.0	0	0	27.3	243	544.4	34.04	3.1	7.50	-	2.414	9.673	30
60	490.275	1.9	0	0	69.7	252	540.5	33.80	6.2	7.50	-	3.527	9.522	60
90	612.175	13.2	0	0	218.3	304	-	34.40	6.0	7.53	-	11.668	9.232	90
120	*759.75	95.8	0	0	376.7	7131	552.8	34.56	4.3	7.53	-	32.343	7.936	120
150	*1102.725	112.4	0	0	500.4	7895	556.2	34.89	3.8	7.48	-	42.853	7.165	150
175	*746.075	90.9	0	0	556.3	7369	553.2	34.58	7.5	7.39	-	40.970	6.958	175
177	*720.125	99.2	0	0	592.8	7001	542.9	-	7.2	7.88	-	-	-	177
182	685.95	46.6	0	0	383.4	6052	561.6	-	8.1	7.41	-	-	-	182
187	685.95	43.4	0	0	804.4	2440	551.8	-	11.5	7.71	-	-	-	187
192	720.125	47.0	0	0	599.2	3287	565.9	-	8.1	7.36	-	-	-	192
197	705.075	50.2	0	0	619.2	2850	552.8	34.56	9.0	7.39	-	36.028	6.616	197
203	603.975	49.2	0	0	645.0	3083	551.3	-	11.0	7.58	-	-	-	203
208	589.425	51.4	0	0	656.4	3275	558.2	34.89	-	-	-	35.173	6.768	208

*interference with H_2S

KOMEX II LV 28: Porewater analysis

SL(G) 20-2

Depth cm	Si µM/l	PO_4 µM/l	NO_3 µM/l	NO_2 µM/l	NH_4 µM/l	H_2S µM/l	Cl mM/l	S psu	Temp. C	pH	pH (25)	TA mM/kg	CA mM/kg	Depth cm
3	564.4	28.9	0	0	495	174	544.4	34.04	9.0	7.84	7.621	6.838	9.918	3
8	662.7	41.3	0	0	883	118	-	-	10.0	7.53	-	-	-	8
13	590.3	47.2	0	0	728	253	546.7	34.18	9.0	7.53	-	9.443	9.133	13
18	556.2	56.9	0	0	815	389	-	-	7.8	7.58	-	-	-	18
23	601.2	61.6	0	0	930	531	-	-	8.4	7.58	-	-	-	23
28	731.1	63.6	0	0	981	76	-	-	8.1	7.62	-	-	-	28
33	665.5	70.8	0	0	1094	719	-	-	8.1	7.57	-	-	-	33
38	672.3	72.6	0	0	1107	800	-	-	8.4	7.55	-	-	-	38
43	441.4	83.6	0	0	1293	840	-	-	8.8	7.60	-	-	-	43
48	669.6	84.8	0	0	1395	1078	-	-	18.1	7.57	-	-	-	48
53	604.0	89.6	0	0	1465	1191	549.6	34.37	17.7	7.62	7.655	19.364	8.599	53
58	572.6	92.8	0	0	1566	1542	-	-	17.5	7.53	-	-	-	58
63	576.7	98.2	0	0	1622	1317	-	-	17.4	7.55	-	-	-	63
68	702.4	109.6	0	0	1685	1967	-	-	17.3	7.53	-	-	-	68
73	732.4	111.6	0	0	1700	2112	550.6	34.43	18.2	7.53	-	23.141	7.990	73
76	717.4	120.2	0	0	1782	2091	-	-	19.2	7.57	-	-	-	76
86	711.9	116.4	0	0	1867	1591	-	-	17.5	7.53	-	-	-	86
96	716.0	120	0	0	1965	1623	-	-	17.6	7.51	-	-	-	96
106	711.9	122.5	0	0	2149	1644	550.0	34.39	17.1	7.55	7.612	28.981	7.233	106
116	728.3	123.5	0	0	2247	1010	-	-	16.9	7.50	-	-	-	116
126	664.1	125	0	0	2356	2504	-	-	17.5	7.51	-	-	-	126
136	679.1	131.5	0	0	2428	2379	545.6	34.11	17.4	7.60	-	34.262	6.562	136
146	686.0	134.5	0	0	2681	2767	-	-	17.2	7.51	-	-	-	146
156	677.8	128	0	0	2682	2656	-	-	17.4	7.51	-	-	-	156
166	680.5	116	0	0	2764	3095	-	-	18.1	7.46	-	-	5.712	166
176	636.8	115	0	0	2854	3555	-	-	15.2	7.51	-	-	-	176
186	773.4	126	0	0	3003	3493	-	-	13.6	7.53	-	-	-	186
206	722.9	127	0	0	3182	3913	550.6	34.42	13.3	7.53	7.569	45.644	5.175	206
226	736.5	130	0	0	3377	3985	-	-	13.1	7.51	-	-	-	226
246	722.9	135	0	0	3550	3078	-	-	13.1	7.46	-	-	-	246
266	669.6	142	0	0	3680	3116	-	-	14.3	7.43	-	-	-	266
280	709.2	144	0	0	3808	3590	-	-	14.4	7.50	-	-	-	280
300	651.8	154	0	0	3977	3109	552.3	34.52	15.1	7.48	7.552	51.038	4.629	300
320	690.1	159	0	0	4130	3296	-	-	15.2	7.45	-	-	-	320
340	673.7	160	0	0	4272	2665	-	-	14.9	7.43	-	-	-	340
360	677.8	161	0	0	4358	2635	-	-	15.2	7.41	-	-	-	360
380	769.3	172	0	0	4575	2425	-	-	16.1	7.39	-	-	-	380
400	677.8	178	0	0	4685	2653	546.0	34.15	14.1	7.39	7.490	52.628	4.315	400
420	721.5	240	0	0	4825	2971	-	-	14.5	7.39	-	-	-	420
440	647.7	197	0	0	5031	1952	-	-	14.6	7.38	-	-	-	440
460	681.9	208	0	0	5149	1246	-	-	14.5	7.41	-	-	-	460
480	702.4	210	0	0	5214	1293	-	-	16.6	7.41	-	-	-	480
500	643.6	226	0	0	5385	2828	548.3	34.28	15.6	7.41	7.655	62.429	3.852	500
520	522.0	232	0	0	5575	1988	-	-	16.0	7.41	-	-	-	520
540	623.1	240	0	0	5617	1624	-	-	16.1	7.39	-	-	-	540
560	610.8	251	0	0	5729	1582	-	-	15.8	7.41	-	-	-	560
572.5	658.6	237	0	0	5831	4	548.3	34.28	-	-	-	63.256	3.604	572.5

KOMEX II LV 28: Porewater analysis

SL(G) 24-1

Depth cm	Si µM/l	PO_4 µM/l	NO_3 µM/l	NO_2 µM/l	NH_4 µM/l	H_2S µM/l	Cl mM/l	S psu	Temp. C	pH	pH (25)	TA mM/kg	CA m m/kg	Depth cm
whole		23.6	0.00	0.00	722.4	3552	-	-	-	-	-	-	-	-

HYC 25-1

Depth cm	Si µM/l	PO_4 µM/l	NO_3 µM/l	NO_2 µM/l	NH_4 µM/l	H_2S µM/l	Cl mM/l	S psu	Temp. C	pH	pH (25)	TA mM/kg	CA m m/kg	Depth cm
1.0	397.4	1.72	17.32	7.24	5.2	0	547.3	-	13.4	7.57	-	-	-	1.0
4.5	397.4	1.84	14.72	2.92	5.4	0	548.3	34.28	9.9	7.58	7.597	2.301	9.838	4.5
7.5	401.8	1.88	4.40	1.44	3.9	0	550.3	-	9.1	7.62	-	-	-	7.5
10.5	388.8	2.36	0.52	0.20	8.6	0	544.7	34.06	10.0	7.57	7.695	2.513	9.721	10.5
13.5	369.6	3.32	0.12	0.04	12.1	0	544.9	-	9.7	7.57	-	-	-	13.5
17.5	368.4	2.80	0.36	0	12.5	0	549.3	-	9.8	7.60	-	-	-	17.5
22.5	385.6	2.48	4.12	0	19.7	0	549.3	34.34	10.2	7.62	-	2.608	9.761	22.5
27.5	393.2	2.44	2.64	0	19.2	0	553.2	-	9.0	7.71	-	-	-	27.5
32.5	408.2	2.48	2.20	0	18.1	0	550.0	-	9.6	7.69	-	-	-	32.5
37.5	419.0	2.28	0.24	0	17.2	0	545.4	-	9.2	7.71	-	-	-	37.5
42.5	416.8	1.80	0.00	0	19.0	0	547.3	-	9.5	7.69	-	-	-	42.5
47.5	399.6	2.52	0.60	0	23.3	0	550.0	-	10.0	7.67	-	-	-	47.5
52.5	425.4	4.04	0	0	38.9	0	546.4	34.60	10.0	7.71	7.912	2.705	9.764	52.5
57.5	439.4	4.00	0	0	34.3	0	550.6	-	10.2	7.65	-	-	-	57.5
68.0	435.0	3.76	0	0	35.2	0	550.9	-	12.0	7.58	-	-	-	68.0
73.0	435.0	7.00	0	0	68.9	0.7	549.0	34.32	12.1	7.62	-	2.724	9.763	73.0
78.0	442.4	3.88	0	0	44.6	0.7	550.6	-	11.3	7.58	-	-	-	78.0
88.0	416.0	3.24	0	0	50.0	1.5	552.5	-	11.2	7.58	-	-	-	88.0
98.0	429.6	3.76	0	0	60.1	6.7	543.2	-	11.4	7.53	-	-	-	98.0
108.0	428.0	3.88	0	0	73.0	11.6	545.6	34.11	11.6	7.57	7.775	2.667	9.787	108.0
118.0	460.8	3.52	0	0	67.3	12.0	551.9	-	11.7	7.51	-	-	-	118.0
128.0	481.2	3.56	0	0	75.2	30.3	547.7	34.25	12.3	7.48	-	2.667	9.800	128.0
138.0	503.8	3.92	0	0	81.5	20.2	547.0	-	12.4	7.46	-	-	-	138.0
148.0	556.4	3.76	0	0	91.9	32.1	552.3	34.52	13.5	7.46	7.706	2.762	9.751	148.0

MUC 30-3 A

Depth cm	Si µM/l	PO_4 µM/l	NO_3 µM/l	NO_2 µM/l	NH_4 µM/l	H_2S µM/l	Cl mM/l	S psu	Temp. C	pH	pH (25)	TA mM/kg	CA mM/kg	Depth cm
0	-	3.24	38.36	0	0.61	0	-	-	-	-	-	-	-	0
0.25	-	-	-	-	-	0	-	-	3.80	7.01	-	-	-	0.25
0.75	-	-	-	-	-	0	-	-	3.90	7.01	-	-	-	0.75
1.5	-	-	-	-	-	0	-	-	3.70	7.24	-	-	-	1.5
2.5	-	-	-	-	-	0	-	-	3.70	7.22	-	-	-	2.5
3.5	-	-	-	-	-	0	-	-	3.90	7.18	-	-	-	3.5
4.5	-	-	-	-	-	0	-	-	3.80	7.10	-	-	-	4.5
5.5	-	-	-	-	-	0	-	-	3.90	7.14	-	-	-	5.5
6.5	-	-	-	-	-	0	-	-	4.10	7.12	-	-	-	6.5
7.5	-	-	-	-	-	0	-	-	4.10	7.12	-	-	-	7.5
8.5	-	-	-	-	-	0	-	-	4.10	7.14	-	-	-	8.5
9.5	-	-	-	-	-	0	-	-	7.00	7.90	-	-	-	9.5
11.5	-	-	-	-	-	0	-	-	5.70	7.74	-	-	-	11.5
14.5	-	-	-	-	-	0	-	-	5.40	7.58	-	-	-	14.5
17.5	-	-	-	-	-	0	-	-	6.00	7.53	-	-	-	17.5
20.5	-	-	-	-	-	0	-	-	5.90	7.37	-	-	-	20.5
22.5	-	-	-	-	-	2.19	-	-	5.90	7.37	-	-	-	22.5

MUC 30-3 B

Depth cm	Si µM/l	PO_4 µM/l	NO_3 µM/l	NO_2 µM/l	NH_4 µM/l	H_2S µM/l	Cl mM/l	S psu	Temp. C	pH	pH (25)	TA mM/kg	CA mM/kg	Depth cm
0	-	-	-	-	-	0	-	-	-	-	-	-	-	0
1.5	-	-	-	-	-	0	-	-	4.3	7.14	-	-	-	1.5
4.5	-	-	-	-	-	0	-	-	4.4	7.32	-	-	-	4.5
7.5	-	-	-	-	-	0	-	-	4.6	7.37	-	-	-	7.5
10.5	-	-	-	-	-	0	-	-	4.2	7.41	-	-	-	10.5
13.5	-	-	-	-	-	0	-	-	4.2	7.28	-	-	-	13.5
16.5	-	-	-	-	-	0	-	-	4.4	7.3	-	-	-	16.5
19.5	-	-	-	-	-	0	-	-	4.2	7.26	-	-	-	19.5

MUC 30-3 D

Depth cm	Si µM/l	PO_4 µM/l	NO_3 µM/l	NO_2 µM/l	NH_4 µM/l	H_2S µM/l	Cl mM/l	S psu	Temp. C	pH	pH (25)	TA mM/kg	CA m m/kg	Depth cm
0	121.4	3.22	30.84	0.20	1.92	0	541.4	-	-	-	-	2.36	9.97	0
0.25	335.3	2.16	0	0	38.62	0	-	-	4.1	7.48	-	2.17	10.23	0.25
0.75	461.3	1.28	0	0	22.56	0	-	-	4.1	6.99	-	2.09	9.90	0.75
1.5	507.8	8.18	0	0	50.04	0	-	-	4.4	7.24	7.17	2.19	9.86	1.5
2.5	545.5	3.38	0	0	46.32	0	-	-	4.1	7.44	-	-	-	2.5
3.5	579.8	1.86	0	0	6.00	0	-	-	4.1	7.5	-	2.32	9.96	3.5
4.5	616.0	1.68	0	0	14.61	0	-	-	4.3	7.42	-	-	-	4.5
5.5	669.8	1.70	0	0	46.90	0	-	-	4.4	7.42	-	-	-	5.5
6.5	636.3	1.42	0	0	69.40	0	-	-	4.4	7.42	-	2.63	9.87	6.5
7.5	631.3	1.26	0	0	98.31	0	-	-	4.3	7.42	-	2.46	9.60	7.5
8.5	-	-	-	-	-	4.30	-	-	4.3	7.42	-	2.44	-	8.5
9.5	-	-	-	-	-	0	547.3	-	4.5	7.29	7.57	2.61	-	9.5
11.5	557.9	-	-	-	-	0	-	-	4.3	7.27	-	-	-	11.5
14.5	-	-	-	-	-	0	-	-	4.5	7.29	-	-	-	14.5
17.5	-	-	-	-	-	0	-	-	4.8	7.24	-	-	-	17.5
20	-	-	-	-	-	0	-	-	4.8	7.22	7.52	-	-	20

MUC 30-4 B

Depth cm	Si µM/l	PO_4 µM/l	NO_3 µM/l	NO_2 µM/l	NH_4 µM/l	H_2S µM/l	Cl mM/l	S psu	Temp. C	pH	pH (25)	TA mM/kg	CA mM/kg	Depth cm
0	-	2.54	37.7	0	0.15	-	539.5	-	-	-	-	-	-	0

KOMEX II LV 28: Porewater analysis

: 30-4 C

pth cm	Si µM/l	PO_4 µM/l	NO_2 µM/l	NO_3 µM/l	NH_4 µM/l	H_2S µM/l	Cl mM/l	S psu	Temp. C	pH	pH (25)	TA mM/kg	CA mM/kg	Depth cm
0	107 40	2 81	37 55	0	0 12	0	539 3	-	-	-	-	2.360	9.677	0
0 25	358 00	3 96	0	1 46	36 8	0	-	-	4 6	7 49	-	-	-	0.25
0 75	453 25	2 16	4 82	1 12	0 2	0	-	-	4 7	7 33	-	2.208	9.821	0.75
1 5	468 50	4 30	4 86	1 00	10 8	0	531 3	-	4 9	7 23	7.088	1.843	8.247	1.5
2 5	422 75	6 72	3 86	3 48	47 3	0	-	-	4 9	7 20	-	2.112	9.192	2.5
3 5	-	-	-	-	-	-	-	-	4 8	7 27	-	-	-	3.5
4 5	390 75	3 84	7 24	2 38	90 7	0	-	-	5 2	7 13	-	-	-	4.5
5 5	-	1 60	4 04	1 24	217 9	0	-	-	5 3	7 02	-	2.268	9.654	5.5
6 5	428 80	2 04	0	0	201 4	0	-	-	5 4	6 95	-	-	-	6.5
7 5	455 25	1 56	0	0	249 2	0	-	-	5 4	6 98	-	2.784	9.774	7.5
8 5	470 75	0	0	0	6 2	0	-	-	4 9	6 87	-	-	-	8.5
9 5	495 50	5 60	0	0	51 2	0	-	-	5 2	6 87	7.188	3.437	9.566	9.5
11 5	507 75	12 40	0	0	72 3	80 51	536 5	-	4 8	7 38	-	5.069	9.657	11.5
14 5	503 50	17 40	0	0	38 5	237 80	-	-	4 8	7 54	-	7.084	9.671	14.5
17 5	493 00	39 30	0	0	46 4	249 10	-	-	5 0	7 60	-	11 996	9.273	17.5
19 5	432 75	39 80	0	0	122 8	119 37	537 8	-	6 0	7 81	7.317	12.513	9.259	19.5

30-4 D

pth cm	Si µM/l	PO_4 µM/l	NO_2 µM/l	NO_3 µM/l	NH_4 µM/l	H_2S µM/l	Cl mM/l	S psu	Temp. C	pH	pH (25)	TA mM/kg	CA mM/kg	Depth cm
0	-	2 79	37 43	0 0	0 15	-	537 5	-	-	-	-	-	-	0
1 25	-	-	-	-	-	-	-	-	4 7	7 40	-	-	-	0.25
1 75	-	-	-	-	-	-	-	-	4 9	7 31	-	-	-	0.75
1 5	-	-	-	-	-	-	-	-	4 5	7 33	-	-	-	1.5
2 5	-	-	-	-	-	1 2	-	-	5 0	7 29	-	-	-	2.5
3 5	-	-	-	-	-	10 8	-	-	4 3	7 25	-	-	-	3.5
4 5	-	-	-	-	-	-	-	-	4 8	7 11	-	-	-	4.5
5 5	-	-	-	-	-	-	-	-	4 6	7 23	-	-	-	5.5
6 5	-	-	-	-	-	12	-	-	4 6	7 16	-	-	-	6.5
7 5	-	-	-	-	-	-	-	-	4 5	7 09	-	-	-	7.5
8 5	-	-	-	-	-	-	-	-	4 6	7 04	-	-	-	8.5
9 5	-	-	-	-	-	-	-	-	4 6	6 98	-	-	-	9.5
11 5	-	-	-	-	-	-	-	-	4 7	6 98	-	-	-	11.5
11 5	-	-	-	-	-	20 6	-	-	5 0	6 84	-	-	-	11.5
14 5	-	-	-	-	-	-	-	-	4 9	7 43	-	-	-	14.5
17 5	-	-	-	-	-	445 9	-	-	5 0	7 54	-	-	-	17.5
19 5	-	-	-	-	-	384 4	-	-	4 9	7 78	-	-	-	19.5

34-1

th cm	Si µM/l	PO_4 µM/l	NO_2 µM/l	NO_3 µM/l	NH_4 µM/l	H_2S µM/l	Cl mM/l	S psu	Temp. C	pH	pH (25)	TA mM/kg	CA mM/kg	Depth cm
0	236 5	3 29	42 25	0 10	0 86	0	549 06	34 34	-	-	-	2.396	10.065	0
25	529 8	0 05	0 35	0	0 19	0	549 31	34 34	4 7	7 55	-	2.304	10.043	0.25
75	562 0	1 34	0 36	0 35	0 79	0	-	-	4 6	7 58	-	-	-	0.75
5	606 8	1 83	0 58	0 45	1 11	0	-	-	4 7	7 60	-	-	-	1.5
2 5	646 0	0 00	0 00	0	0 12	0	-	-	4 6	7 70	-	-	-	2.5
3 5	666 3	4 92	14 20	0 52	6 55	0	-	-	4 6	7 79	-	-	-	3.5
4 5	678 3	3 14	0 18	0 30	0 15	0	-	-	4 6	7 79	-	-	-	4.5
5 5	674 5	5 05	5 80	0 57	0 61	0	-	-	4 5	7 77	-	-	-	5.5
6 5	660 3	6 15	4 77	0 27	6 71	0	-	-	4 5	7 79	-	-	-	6.5
7 5	684 8	6 54	2 17	0 12	6 47	0	-	-	4 4	7 83	-	-	-	7.5
8 5	690 0	5 75	0 00	0	0 03	0	-	-	4 4	7 87	-	-	-	8.5
9 5	674 3	6 17	0 48	0 20	0 18	0	548 85	34 20	4 4	7 83	-	2.568	10.01	9.5
10 5	651 3	7 40	0 41	0 05	8 11	0	-	-	4 3	7 81	-	-	-	10.5
11 5	673 3	7 78	1 10	0 03	9 97	0	-	-	4 3	7 81	-	-	-	11.5
12 5	680 8	7 23	2 25	0 34	0 13	0	-	-	4 3	7 79	-	-	-	12.5
13 5	697 8	7 32	1 21	0 39	0 19	0	-	-	4 3	7 81	-	-	-	13.5
14 5	693 8	7 22	0	0	5 58	0	-	-	4 3	7 81	-	-	-	14.5
15 5	680 8	9 16	0	0	13 10	0	-	-	4 4	7 79	-	-	-	15.5
16 5	646 0	4 14	0	0	7 38	0	-	-	4 4	7 77	-	-	-	16.5
18 5	647 3	8 90	0	0	0 00	0	545 87	34 13	4 3	7 79	-	2.722	9 962	18.5
21 5	642 0	9 98	0	0	25 32	0	-	-	4 3	7 83	-	-	-	21.5
24 5	630 5	11 56	0	0	32 18	0	-	-	4 5	7 79	-	-	-	24.5
27 5	607 3	11 10	0	0	35 64	0	-	-	4 4	7 81	-	-	-	27.5
30 5	611 0	8 58	0	0	10 94	0	540 46	33 80	4 4	7 87	-	2 972	9 909	30.5
33 5	580 0	7 46	0	0	0 00	0	-	-	4 4	7 85	-	-	-	33.5
36	590 3	8 06	0	0	0 00	0	-	-	5 8	7 97	-	-	-	36
38	576 3	11 68	0	0	53 12	0	-	-	5 6	7 91	-	-	-	38
40	542 5	9 82	0	0	58 98	0	545 87	34 13	6 0	8 37	-	3.374	9 844	40
42	549 0	11 26	0	0	57 14	0	-	-	6 0	7 87	-	-	-	42
44	536 3	11 26	0	0	68 20	0	546 36	34 16	5 6	7 95	-	3.317	9 859	44
45 5	540 0	11 12	0	0	66 44	0	547 34	34 22	5 6	7 97	-	3 241	9 915	45.5

KOMEX II LV 28: Porewater analysis

SL(R) 37-1

Depth cm	Si µM/l	PO_4 µM/l	NO_3 µM/l	NO_2 µM/l	NH_4 µM/l	H_2S µM/l	Cl mM/l	S psu	Temp. C	pH	pH (25)	TA mM/kg	CA mM/kg	Depth cm
3	-	-	-	-	-	-	-	-	-	-	7.699	-	-	3
7	373.5	-	-	-	-	-	542.4	33.92	4.8	7.49	7.895	2.491	9.982	7
20	483.3	2.9	0	0	17.0	0.0	547.0	34.20	3.8	7.65	-	2.741	9.994	20
30	465.0	4.1	0	0	24.6	0.0	544.4	34.04	4.6	7.68	8.187	3.335	9.892	30
40	479.3	7.3	0	0	32.3	0.0	548.4	-	4.4	7.73	-	-	-	40
50	443.3	7.2	0	0	29.2	0.0	547.7	34.25	5.1	7.78	8.084	3.345	9.892	50
60	447.0	8.7	0	0	34.1	2.4	550.8	-	6.6	7.77	-	-	-	60
70	447.0	10.4	0	0	36.2	6.9	541.4	-	5.0	7.75	-	-	-	70
80	431.5	12.0	0	0	37.6	5.0	551.8	-	5.4	7.70	-	-	-	80
90	429.0	12.4	0	0	40.8	7.5	548.3	-	6.5	7.70	-	-	-	90
100	451.0	13.4	0	0	40.6	10.6	549.0	34.32	7.5	7.66	7.895	3.202	9.199	100
110	451.0	13.4	0	0	50.0	13.9	550.8	-	7.8	7.70	-	-	-	110
120	452.3	13.4	0	0	48.5	8.8	551.8	-	7.1	7.63	-	-	-	120
130	444.5	13.0	0	0	50.7	11.3	550.8	-	7.9	7.59	-	-	-	130
150	438.1	12.0	0	0	56.4	18.9	550.8	34.44	8.0	7.58	7.809	3.680	9.340	150
170	444.5	10.0	0	0	61.9	4.2	548.3	-	9.2	7.58	-	-	-	170
190	456.0	12.1	0	0	74.3	32.9	548.7	-	8.7	7.58	-	-	-	190
210	470.3	11.0	0	0	82.6	16.4	549.0	34.32	9.1	7.54	8.015	3.911	9.377	210
230	471.5	11.5	0	0	86.5	-	551.8	-	9.4	7.54	-	-	-	230
250	463.8	12.4	0	0	116.3	48.3	550.3	34.40	9.1	7.52	7.827	4.158	9.193	250
270	476.0	11.1	0	0	97.7	68.8	549.3	-	9.1	7.47	-	-	-	270
290	470.3	13.2	0	0	96.8	138.6	551.8	-	9.4	7.51	-	-	-	290
310	461.3	12.9	0	0	98.5	80.8	549.6	34.37	9.3	7.47	7.818	4.255	9.894	310
330	452.3	11.1	0	0	102.1	58.4	553.2	-	9.4	7.45	-	-	-	330
350	449.5	11.4	0	0	102.6	80.3	551.3	34.46	9.4	7.45	7.964	4.332	9.971	350
370	430.3	10.1	0	0	103.4	138.8	551.3	-	9.5	7.49	-	-	-	370
390	431.5	8.7	0	0	100.7	46.7	552.8	-	10.3	7.47	-	-	-	390
410	441.8	9.1	0	0	100.4	105.0	546.4	34.16	10.1	7.47	7.981	4.352	9.742	410
430	412.3	7.3	0	0	93.5	-	553.2	-	10.2	7.61	-	-	-	430
440	374.8	7.6	0	0	96.9	-	539.0	-	10.8	7.92	-	-	-	440
450	400.5	8.7	0	0	96.6	6.6	548.3	34.28	10.1	7.78	7.904	4.409	9.854	450
460	394.0	8.6	0	0	101.4	9.7	547.0	-	10.3	7.61	-	-	-	460
465	434.0	-	0	0	-	8.3	548.0	-	10.6	7.47	-	-	-	465
470	438.0	9.3	0	0	97.2	62.0	551.9	-	10.7	7.44	-	-	-	470
475	431.5	9.2	0	0	97.8	52.1	548.0	-	10.8	7.44	-	-	-	475
480	439.3	9.1	0	0	99.4	67.8	548.3	34.28	10.8	7.44	7.988	4.198	9.777	480
485	468.5	9.9	0	0	93.7	64.1	544.1	-	10.1	7.44	-	-	-	485
490	416.0	8.5	0	0	94.8	33.6	542.4	-	11.1	7.40	-	-	-	490
495	418.5	8.3	0	0	94.7	31.0	541.4	-	11.3	7.40	-	-	-	495
500	343.8	8.5	0	0	92.6	27.3	541.4	-	11.3	8.34	-	-	-	500
510	413.5	9.7	0	0	92.3	28.7	538.2	33.67	11.3	7.47	7.775	3.952	9.691	510
600	-	-	-	-	-	-	-	-	-	-	7.912	-	-	600

MUC 44-2

Depth cm	Si µM/l	PO_4 µM/l	NO_3 µM/l	NO_2 µM/l	NH_4 µM/l	H_2S µM/l	Cl mM/l	S psu	Temp C	pH	pH (25)	TA mM/kg	CA mM/kg	Depth cm
0	186.5	-	-	-	-	-	-	-	-	-	-	-	-	0
0.25	410.3	3.01	25.35	6.4	25.48	-	538.5	33.68	-	-	-	2.11	9.946	0.25
0.75	470.5	2.14	0.69	0.53	0.38	-	-	-	-	-	-	-	-	0.75
1.5	552.5	6.55	2.99	0.31	0.11	-	536.04	33.53	-	-	-	2.339	10.075	1.5
2.5	614.1	0.29	3	0.11	11.67	-	-	-	-	-	-	-	-	2.5
3.5	653.7	0.23	1.9	0.34	18.88	-	540.79	33.82	-	-	-	2.339	9.944	3.5
4.5	674.3	0.33	1.39	0.26	21.19	-	-	-	-	-	-	-	-	4.5
5.5	677.0	14.90	0	0	20.2	-	540.95	33.84	-	-	-	2.474	10.047	5.5
6.5	678.3	7.20	0	0	24.4	-	-	-	-	-	-	-	-	6.5
7.5	677.0	5.80	0	0	16.2	-	540.95	33.84	-	-	-	2.512	10.081	7.5
8.5	675.6	11.00	0	0	91.7	-	-	-	-	-	-	-	-	8.5
9.5	693.4	5.90	0	0	39.4	-	536.04	33.53	-	-	-	2.493	9.964	9.5
11.5	727.6	10.30	0	0	48.4	-	537.02	33.6	-	-	-	2.609	10.145	11.5
14.5	705.7	10.80	0	0	42.7	-	-	-	-	-	-	-	-	14.5
17.5	715.3	10.10	0	0	46.8	-	540.95	33.84	-	-	-	2.628	10.06	17.5
20.5	705.7	10.80	0	0	42.3	-	-	-	-	-	-	-	-	20.5
23.5	704.3	10.10	0	0	46	-	541.94	33.89	-	-	-	2.704	10.074	23.5
26.5	718.0	10.00	0	0	48	-	543.41	33.99	-	-	-	2.685	10.387	26.5

SL(R) 44-4

Depth cm	Si µM/l	PO_4 µM/l	NO_3 µM/l	NO_2 µM/l	NH_4 µM/l	H_2S µM/l	Cl mM/l	S psu	Temp C	pH	pH (25)	TA mM/kg	CA mM/kg	Depth cm
75	734.4	13.43	0	0	80.70	-	545.1	-	3.7	7.63	7.848	2.953	10.048	75
110	734.4	13.43	0	0	135.10	-	-	-	3.2	7.69	7.792	3.185	9.981	110
140	738.5	14.00	0	0	114.60	-	542.4	-	3.7	7.71	7.854	3.338	9.975	140
175	728.9	13.10	0	0	153.20	-	-	-	4.4	7.71	-	-	-	175
200	711.2	14.33	0	0	169.60	-	543.1	-	5.4	7.71	8.015	3.569	9.967	200
225	697.5	16.56	0	0	185.70	-	-	-	5.2	7.73	-	-	-	225
250	677.0	17.79	0	0	227.50	-	545.4	-	4.2	7.71	7.754	3.990	9.910	250
275	653.7	18.95	0	0	253.70	-	-	-	4.9	7.67	-	-	-	275
310	604.5	18.37	0	0	155.80	-	544.4	-	6.1	7.67	7.802	4.586	9.890	310
340	596.3	19.93	0	0	312.80	-	544.9	-	6.1	7.67	7.878	4.873	9.863	340
375	603.1	20.43	0	0	341.00	-	-	-	5.2	7.63	-	-	-	375
405	616.8	23.15	0	0	371.50	-	545.4	-	5.8	7.63	7.844	5.238	9.894	405
445	631.8	22.32	0	0	405.70	-	544.9	-	5.5	7.62	7.857	5.527	9.867	445
475	634.6	3.13	0	0	111.80	-	-	-	5.8	7.63	-	-	-	475
505	649.6	24.22	0	0	450.50	-	543.9	-	5.8	7.63	7.694	5.682	9.842	505
540	657.8	25.29	0	0	481.90	-	537.5	-	6.1	7.58	7.433	5.699	9.864	540
575	629.1	24.80	0	0	515.80	-	-	-	6.1	7.6	-	-	-	575
605	619.5	26.28	0	0	462.90	-	546.4	-	6.7	7.6	7.621	6.160	9.770	605
640	620.9	27.10	0	0	525.40	-	541.0	-	6.7	7.54	7.700	6.294	9.769	640
675	651.0	32.37	0	0	589.30	-	-	-	6.6	7.54	-	-	-	675
715	651.0	29.00	0	0	597.40	-	543.9	-	6.9	7.54	7.270	6.430	9.755	715
770	667.3	34.76	0	0	669.70	-	542.9	-	7.0	7.54	-	6.699	9.705	770
810	675.6	32.13	0	0	656.20	-	544.7	-	7.1	7.54	7.841	6.795	9.705	810

Table A5: *Oxidation-reduction potential (Eh), pH(25) and oxidation volume (β) in sediments from the Sea of Okhotsk.*

St. No	Depth,cm	Eh(25), mv			$pH_{sws}(25)$	β, g-eqv/l·1000
		Pt-electrode	Ti-electrode	Fe-electrode		
1	2	3	4	5	6	7
LV28-17-2	5	-104	-245	-243	7.329	
	35	-287	-379	-382	7.604	3.000
	67	-294	-375	-374	7.595	3.000
LV28-20-2	3	-90	-120	-130	7.621	2.826
	50	-92	-162	-165	7.655	2.928
	100	-205	-302	-300	7.612	2.888
	200	-235	-343	-342	7.569	2.898
	300	-140	-250	-245	7.552	2.911
	400	-170	-317	-320	7.490	2.918
	500	-135	-330	-326	7.655	2.921
LV28-20-3	3	-80	-234	-230	7.449	2.829
	10	-78	-230	-220	7.535	2.784
	50	-60	-200	-190	7.650	2.888
LV28-25-1	3	200	140	150	7.579	0.556
	10	-85	-120	-124	7.895	2.641
	50	-118	-210	-205	7.912	2.976
	100	-109	-190	-183	7.775	2.999
	150	-106	-180	-180	7.706	3.000
LV28-30-3B	1.5	200	205	195	7.174	0.298
	10.5	-52	-50	-55	7.569	0.709
	19.5	-72	-125	-130	7.519	0.725
LV28-30-4B	1.5	100	94	98	7.088	0.210
	10.5	-104	-135	-140	7.188	0.750
	19	-135	-177	-185	7.317	0.750
LV28-37-1	3	250	270	260	7.699	0.165
	10	190	170	170	7.895	0.899
	25	2	-65	-60	8.187	2.164
	50	-56	-90	-100	8.084	2.512
	100	-90	-120	-130	7.895	2.826
	150	-98	-138	-146	7.809	2.944
	200	-106	-156	-152	8.015	2.738
	250	-104	-158	-158	7.827	2.728
	300	-107	-154	-152	7.818	2.944
	350	-96	-150	-155	7.964	2.954
	400	-80	-130	-135	7.981	2.706
	450	-98	-155	-160	7.904	2.385
	480	-85	-130	-132	7.988	2.911
	510	-86	-140	-142	7.775	2.829
	600	-99	-145	-150	7.912	2.829

Table A5 cont.: *Oxidation-reduction potential (Eh), pH(25) and oxidation volume (β) in sediments from the Sea of Okhotsk.*

1	2	3	4	5	6	7
LV28-44-4	75	50	-58	-62	7.648	1.977
	110	28	-68	-70	7.792	2.385
	140	-55	-138	-145	7.854	2.689
	200	-80	-135	-140	8.015	2.712
	250	-95	-140	-145	7.754	2.839
	310	-96	-145	-150	7.802	2.987
	340	-90	-145	-150	7.878	2.984
	405	-135	-150	-160	7.844	2.977
	450	-135	-155	-160	7.857	2.957
	505	-150	-160	-165	7.694	2.764
	540	-135	-155	-160	7.533	2.954
	605	-125	-160	-165	7.621	2.994
	640	-120	-150	-155	7.700	2.967
	715	-145	-130	-135	7.627	2.803
	810	-125	-130	-135	7.641	2.764

Appendix 6

Carbonate Parameters in Seawater and Pore Water

Table A6.1: *Calculated carbonate parameters and AOU for CTD stations sampled during the 28th cruise of RV 'Akademik Lavrentyev', August - September 1998.*

St. No	H, m	T, °C	S, psu	pH(p,t)	TCO2 mM/kg	H2CO3 mM/kg	pCO2 µatm	CO3 mM/kg	Lc	La	NTA mM/kg	NTCO2 mM/kg	AOU µM/kg
LV28-2-1													
	6	14.24	32.444	8.082	2.018	0.0142	366	0.1693	4.09	2.61	2.400	2.177	-26
	24	4.30	32.655	8.138	2.075	0.0165	304	0.1313	3.15	1.98	2.392	2.224	-64
	55	0.20	32.972	8.019	2.150	0.0251	398	0.0875	2.09	1.31	2.379	2.282	29
	106	-0.91	33.088	8.016	2.165	0.026	394	0.0838	1.98	1.25	2.380	2.290	44
	143	-0.72	33.158	7.946	2.187	0.0306	469	0.0731	1.71	1.08	2.379	2.308	70
	174	0.22	33.258	7.888	2.204	0.0343	545	0.0677	1.57	1.00	2.378	2.319	88
	252	1.09	33.431	7.709	2.273	0.0517	849	0.0485	1.11	0.71	2.393	2.380	162
	502	1.89	33.819	7.614	2.318	0.0621	1055	0.0423	0.91	0.59	2.393	2.399	229
	752	2.33	34.147	7.577	2.365	0.0663	1147	0.0413	0.85	0.56	2.412	2.424	278
	1001	2.41	34.346	7.604	2.381	0.0608	1056	0.0455	0.88	0.59	2.425	2.426	290
	1151	2.34	34.415	7.630	2.382	0.0565	980	0.0488	0.92	0.62	2.430	2.422	288
	1296	2.25	34.467	7.642	2.384	0.0542	936	0.0507	0.93	0.63	2.433	2.421	286
LV28-11-1													
	10	9.20	29.451	8.134	1.929	0.014	302	0.1383	3.39	2.12	2.491	2.292	-42
	51	0.10	32.900	8.060	2.134	0.023	358	0.0949	2.27	1.42	2.381	2.270	14
	100	-0.29	33.148	7.931	2.186	0.032	490	0.0719	1.7	1.07	2.377	2.308	96
	126	0.21	33.242	7.858	2.212	0.037	589	0.0631	1.48	0.94	2.378	2.329	116
	152	0.31	33.272	7.843	2.216	0.038	610	0.0615	1.44	0.91	2.377	2.331	123
	174	0.33	33.299	7.820	2.224	0.040	644	0.0588	1.37	0.86	2.379	2.338	134
	201	0.32	33.309	7.816	2.225	0.041	649	0.0583	1.35	0.85	2.378	2.338	135
	225	0.23	33.311	7.822	2.227	0.040	637	0.0591	1.36	0.86	2.381	2.340	162
	248	0.23	33.310	7.833	2.223	0.039	619	0.0606	1.39	0.88	2.381	2.336	133
LV28-20-1													
	8	14.83	26.770	8.161	1.797	0.011	278	0.1601	4.00	2.51	2.606	2.349	-52
	50	0.45	32.836	8.172	2.091	0.0169	271	0.121	2.89	1.82	2.381	2.229	-3
	150	0.10	33.152	7.996	2.171	0.0265	418	0.0844	1.97	1.25	2.383	2.292	74
	300	1.01	33.421	7.827	2.225	0.0385	630	0.0624	1.41	0.90	2.377	2.330	160
	452	1.63	33.698	7.726	2.277	0.048	806	0.0529	1.16	0.75	2.389	2.365	212
	493	1.79	33.786	7.694	2.294	0.0515	870	0.0501	1.08	0.70	2.392	2.376	223
	522	1.93	33.875	7.698	2.312	0.051	868	0.0514	1.11	0.72	2.406	2.389	240
	553	1.97	33.911	7.697	2.309	0.0509	867	0.0515	1.10	0.71	2.401	2.383	246
	578	2.03	33.952	7.685	2.312	0.052	889	0.0505	1.07	0.70	2.399	2.383	251
	612	2.07	33.981	7.690	2.315	0.0512	877	0.0514	1.09	0.71	2.402	2.384	253
	642	2.13	34.042	7.686	2.323	0.0517	887	0.0514	1.08	0.70	2.405	2.388	262
	670	2.18	34.092	7.685	2.326	0.0516	888	0.0515	1.07	0.70	2.404	2.388	268
LV28-28-1													
	78	-1.48	32.985	8.083	2.131	0.0223	331	0.0931	2.21	1.39	2.369	2.261	38
	503	2.04	33.868	7.666	2.302	0.0546	933	0.0478	1.03	0.67	2.388	2.379	238
	1000	2.38	34.336	7.625	2.370	0.0578	1003	0.0475	0.92	0.62	2.421	2.416	293
	1201	2.34	34.411	7.635	2.378	0.0555	961	0.0494	0.92	0.62	2.428	2.419	295
	1251	2.33	34.418	7.638	2.377	0.0547	949	0.05	0.92	0.63	2.428	2.417	295
	1301	2.33	34.426	7.634	2.381	0.055	953	0.0498	0.91	0.62	2.431	2.421	298
	1335	2.33	34.429	7.629	2.385	0.0556	963	0.0494	0.90	0.61	2.434	2.425	298
	1371	2.33	34.432	7.629	2.386	0.0553	959	0.0496	0.89	0.61	2.436	2.425	297
	1401	2.33	34.435	7.642	2.384	0.0535	927	0.0512	0.92	0.63	2.436	2.423	
	1437	2.33	34.435	7.620	2.390	0.0562	974	0.0489	0.87	0.60	2.437	2.429	300
	1467	2.34	34.436	7.625	2.390	0.0554	960	0.0495	0.87	0.60	2.438	2.429	299
	1493	2.34	34.437	7.623	2.391	0.0555	961	0.0495	0.87	0.60	2.439	2.430	302

Table A6.1 cont.: *Calculated carbonate parameters and AOU for CTD stations sampled during the 28th cruise of RV 'Akademik Lavrentyev', August - September 1998.*

t. No	H, m	T, °C	S, psu	pH(p,t)	TCO2 mM/kg	H2CO3 mM/kg	pCO2 µatm	CO3 mM/kg	Lc	La	NTA mM/kg	NTCO2 mM/kg	AOU µM/kg
V28-43-1													
	2	13.17	32.666	8.248	1.939	0.009	232	0.2244	5.41	3.45	2.381	2.078	-21
	10	13.17	32.661	8.251	1.946	0.009	231	0.2265	5.46	3.48	2.391	2.085	-22
	25	3.57	32.778	8.308	2.011	0.011	194	0.1795	4.31	2.71	2.387	2.147	-88
	50	0.52	32.878	8.134	2.108	0.019	298	0.1127	2.69	1.69	2.384	2.244	-6
	75	-0.03	32.958	8.101	2.124	0.021	322	0.1031	2.45	1.54	2.379	2.256	11
	100	-0.06	33.039	8.082	2.132	0.022	337	0.0994	2.35	1.48	2.375	2.259	14
	151	0.67	33.182	7.983	2.166	0.027	433	0.0842	1.97	1.24	2.376	2.285	63
	251	1.43	33.383	7.849	2.215	0.036	602	0.0663	1.51	0.96	2.377	2.322	132
	500	2.08	33.744	7.706	2.283	0.050	847	0.0519	1.12	0.73	2.389	2.368	213
	750	2.69	34.179	7.641	2.364	0.057	995	0.0488	1.00	0.66	2.428	2.421	283
	800	2.68	34.247	7.619	2.368	0.059	1041	0.0467	0.95	0.63	2.422	2.420	291
	819	2.68	34.248	7.632	2.365	0.057	1007	0.0481	0.97	0.64	2.423	2.417	292
V28-44-5													
	3	11.49	32.677	8.329	1.913	0.008	185	0.246	5.93	3.77	2.382	2.049	-34
	10	11.48	32.676	8.329	1.922	0.008	186	0.2471	5.95	3.78	2.393	2.059	-35
	27	3.49	32.815	8.362	1.988	0.009	168	0.1987	4.77	3.00	2.387	2.120	-13
	54	1.50	32.917	8.130	2.102	0.018	303	0.1165	2.78	1.75	2.380	2.235	-101
	79	0.92	33.013	8.072	2.126	0.021	349	0.101	2.40	1.51	2.373	2.254	20
	107	1.06	33.112	8.021	2.148	0.024	396	0.092	2.17	1.37	2.374	2.270	44
	157	1.13	33.212	7.985	2.166	0.026	433	0.0863	2.01	1.27	2.375	2.283	59
	256	1.52	33.366	7.871	2.210	0.034	572	0.0698	1.59	1.02	2.379	2.318	124
	378	1.66	33.523	7.783	2.241	0.042	701	0.059	1.31	0.84	2.378	2.340	159
	497	1.95	33.693	7.727	2.291	0.047	807	0.0543	1.18	0.76	2.405	2.380	206
	596	2.54	33.962	7.669	2.318	0.053	930	0.0499	1.06	0.69	2.401	2.389	254
	642	2.65	34.070	7.632	2.345	0.058	1020	0.0468	0.98	0.64	2.412	2.409	277
V28-62-1													
	1	15.47	32.328	8.211	1.992	0.010	255	0.2234	5.41	3.46	2.388	2.157	-22
	10	15.46	32.323	8.209	1.999	0.010	258	0.2233	5.40	3.46	2.396	2.165	-21
	20	9.35	32.557	8.238	2.050	0.011	239	0.1934	4.65	2.94	2.401	2.204	-86
	30	2.67	32.717	8.196	2.122	0.015	260	0.1396	3.35	2.10	2.404	2.270	-10
	51	-1.03	33.032	7.881	2.238	0.037	556	0.0624	1.49	0.94	2.399	2.371	94
	66	-1.07	33.035	7.856	2.244	0.039	590	0.059	1.41	0.88	2.399	2.377	101
	74	-1.07	33.034	7.853	2.246	0.039	594	0.0587	1.40	0.88	2.400	2.380	101
V28-63-1													
	61	-1.09	33.037	7.841	2.245	0.041	611	0.0569	1.36	0.85	2.395	2.378	106
	66	-1.09	33.037	7.836	2.249	0.041	619	0.0564	1.34	0.84	2.399	2.383	106
	71	-1.09	33.037	7.835	2.250	0.041	620	0.0564	1.34	0.84	2.400	2.384	106
	75	-1.09	33.036	7.835	2.250	0.041	620	0.0564	1.34	0.84	2.400	2.384	106
28-64-1													
	11	14.59	32.267	8.184	2.010	0.011	275	0.2062	4.98	3.18	2.393	2.180	-26
	54	-0.83	32.873	8.045	2.174	0.024	368	0.0882	2.11	1.32	2.383	2.315	21
	128	-0.44	33.169	7.949	2.209	0.030	468	0.0743	1.75	1.10	2.377	2.331	74
	256	0.69	33.390	7.745	2.266	0.048	770	0.0512	1.17	0.74	2.379	2.375	155
	378	0.80	33.516	7.734	2.278	0.048	785	0.051	1.13	0.73	2.382	2.379	167
	505	1.92	33.808	7.646	2.330	0.058	981	0.0455	0.98	0.64	2.400	2.412	229
	755	2.29	34.132	7.609	2.365	0.061	1057	0.0443	0.91	0.60	2.408	2.425	274
	1002	2.44	34.341	7.619	2.391	0.059	1019	0.0471	0.92	0.61	2.425	2.437	278
	1249	2.24	34.446	7.653	2.392	0.053	916	0.0515	0.95	0.65	2.428	2.430	281
	1495	2.12	34.504	7.676	2.395	0.049	845	0.0551	0.97	0.67	2.436	2.429	274
	1746	2.02	34.540	7.687	2.394	0.047	800	0.0573	0.95	0.67	2.437	2.426	263
	1914	1.98	34.559	7.700	2.395	0.045	761	0.0598	0.96	0.68	2.441	2.426	261

Table A6.1 cont.: *Calculated carbonate parameters and AOU for CTD stations sampled during the 28th cruise of RV 'Akademik Lavrentyev', August - September 1998.*

St. No	H, m	T, °C	S, psu	pH(p,t)	TCO2 mM/kg	H2CO3 mM/kg	pCO2 µatm	CO3 mM/kg	Lc	La	NTA mM/kg	NTCO2 mM/kg	AOU µM/kg
LV28-39-1													
	1467	2.33	34.413	7.641	2.386	0.053	924	0.0513	0.91	0.62	2.440	2.427	295
	1504	2.34	34.412	7.637	2.388	0.054	930	0.051	0.89	0.62	2.442	2.429	297
	1537	2.34	34.410	7.618	2.393	0.056	970	0.049	0.85	0.59	2.442	2.434	300
	1573	2.34	34.411	7.616	2.395	0.056	970	0.049	0.85	0.59	2.444	2.436	301
	1596	2.34	34.411	7.605	2.399	0.057	994	0.0479	0.82	0.57	2.445	2.440	300
LV28-40-1													
	2	14.19	32.391	8.179	1.963	0.011	280	0.2029	4.91	3.13	2.396	2.121	-21
	2	14.19	32.298	8.179	1.968	0.011	281	0.2029	4.91	3.13	2.407	2.133	-22
	25	7.22	28.663	8.326	1.993	0.010	193	0.1957	4.79	2.99	2.725	2.434	-99
	52	0.08	33.956	8.123	2.106	0.019	304	0.1101	2.62	1.65	2.303	2.171	-1
	86	-0.92	35.408	8.051	2.138	0.023	359	0.0937	2.20	1.39	2.215	2.113	32
	150	0.34	35.071	7.864	2.200	0.036	576	0.0667	1.54	0.98	2.250	2.196	110
	251	1.12	34.675	7.737	2.244	0.048	787	0.0525	1.19	0.76	2.289	2.265	167
	502	2.08	34.492	7.661	2.305	0.055	944	0.048	1.03	0.67	2.348	2.339	236
	753	2.43	34.333	7.628	2.353	0.058	1015	0.0468	0.96	0.63	2.402	2.399	279
	1003	2.38	34.360	7.626	2.380	0.058	1003	0.0479	0.93	0.62	2.429	2.424	292
	1251	2.32	34.445	7.655	2.378	0.053	913	0.052	0.96	0.65	2.432	2.416	290
	1275	2.32	34.445	7.655	2.378	0.053	911	0.0521	0.96	0.65	2.433	2.416	289
LV28-41-1													
	2	13.95	32.688	8.179	1.978	0.011	282	0.2039	4.92	3.14	2.391	2.118	-18
	11	13.93	32.682	8.176	1.983	0.011	284	0.203	4.89	3.12	2.396	2.124	-19
	25	3.39	32.689	8.317	2.009	0.011	189	0.1813	4.35	2.74	2.394	2.151	-60
	50	0.40	32.780	8.158	2.099	0.018	281	0.1174	2.81	1.76	2.388	2.241	-14
	100	-0.32	32.996	8.071	2.136	0.022	345	0.096	2.27	1.43	2.377	2.266	18
	150	-0.09	33.139	7.986	2.170	0.027	427	0.0818	1.91	1.21	2.378	2.292	67
	250	1.06	33.387	7.790	2.232	0.042	692	0.0574	1.31	0.83	2.377	2.340	147
	501	1.95	33.778	7.680	2.294	0.053	899	0.0489	1.06	0.68	2.389	2.377	224
	750	2.37	34.117	7.639	2.345	0.057	988	0.0474	0.97	0.64	2.411	2.406	275
	902	2.50	34.283	7.632	2.376	0.058	1002	0.0482	0.96	0.64	2.432	2.426	292
	1002	2.45	34.355	7.646	2.372	0.055	956	0.0502	0.97	0.65	2.428	2.417	296
	1042	2.45	34.373	7.648	2.375	0.055	949	0.0506	0.97	0.65	2.431	2.418	295
LV28-42-2													
	2	13.37	32.526	8.233	1.942	0.010	242	0.2184	5.28	3.36	2.385	2.090	-21
	10	13.38	32.520	8.230	1.949	0.010	244	0.218	5.26	3.35	2.393	2.098	-24
	26	4.48	32.650	8.289	2.004	0.011	204	0.1781	4.28	2.69	2.386	2.148	-72
	50	0.70	32.820	8.148	2.097	0.018	288	0.1163	2.78	1.75	2.381	2.236	-3
	76	0.22	32.960	8.088	2.126	0.021	333	0.1015	2.41	1.52	2.378	2.258	17
	101	0.11	33.061	8.053	2.146	0.023	364	0.0944	2.23	1.41	2.380	2.272	35
	152	0.73	33.216	7.965	2.174	0.028	454	0.0812	1.90	1.20	2.375	2.291	75
	253	1.31	33.392	7.843	2.217	0.037	610	0.0651	1.49	0.95	2.376	2.324	138
	503	2.17	33.787	7.717	2.285	0.048	826	0.0535	1.16	0.75	2.390	2.367	219
	752	2.48	34.120	7.644	2.341	0.056	975	0.0482	0.99	0.65	2.409	2.401	276
	951	2.64	34.310	7.657	2.359	0.053	935	0.0513	1.01	0.67	2.420	2.406	290
	1009	2.57	34.355	7.668	2.364	0.052	908	0.0528	1.03	0.69	2.426	2.408	292

Table A6.2: *Calculated carbonate parameter for pore water stations (MUC, SL) sampled during the 28th cruise of RV 'Akademik Lavrentyev', August - September 1998.*

ST. No	H, cm	T, °C	S, psu	TA mM/kg	pH(p,t)	TCO2 mM/kg	CO3 mM/kg	Lc	La
LV28-20-2	3	2.18	34.04	6.838	8.034	6.583	0.319	6.63	4.35
	53	2.18	34.37	19.364	8.068	18.554	0.9757	20.24	13.27
	106	2.18	34.39	28.981	8.014	27.96	1.3049	27.06	17.75
	206	2.18	34.42	45.644	7.948	44.378	1.7919	37.15	24.37
	300	2.18	34.52	51.038	7.931	49.716	1.9353	40.09	26.3
	400	2.18	34.15	52.628	7.86	51.68	1.703	35.34	23.17
	500	2.18	34.28	62.429	8.058	59.903	3.0743	63.74	41.81
LV28-20-3	6	2.18	33.92	2.521	7.832	2.484	0.0763	1.59	1.04
	11	2.18	33.56	2.522	7.954	2.453	0.0984	2.05	1.34
	50	2.18	33.65	2.54	8.079	2.432	0.1292	2.69	1.76
LV28-25-1	4.5	2.34	34.28	2.301	7.952	2.229	0.0963	1.69	1.17
	10.5	2.34	34.06	2.513	8.292	2.316	0.2083	3.67	2.52
	52.5	2.34	34.16	2.705	8.315	2.481	0.2351	4.13	2.85
	108	2.34	34.11	2.667	8.167	2.51	0.1734	3.05	2.1
	148	2.34	34.52	2.762	8.095	2.626	0.1562	2.74	1.89
LV28-30-4c	1.5	0.85	33.25	1.843	7.381	1.914	0.0187	0.41	0.27
	9.5	0.85	33.56	3.437	7.495	3.52	0.0454	1	0.64
	19.5	0.85	33.65	12.513	7.664	12.583	0.2413	5.33	3.43
LV28-37-1	7	2.34	33.92	2.491	8.293	2.295	0.2066	3.63	2.5
	30	2.34	34.04	3.335	8.6	2.861	0.48	8.44	5.81
	50	2.34	34.25	3.354	8.494	2.957	0.4048	7.11	4.9
	100	2.34	34.32	3.202	8.308	2.94	0.2753	4.83	3.33
	150	2.34	34.44	3.68	8.206	3.44	0.2599	4.56	3.14
	210	2.34	34.32	3.911	8.424	3.505	0.4173	7.32	5.05
	250	2.34	34.4	4.158	8.224	3.875	0.3042	5.34	3.68
	310	2.34	34.37	4.255	8.214	3.973	0.3045	5.39	3.71
	350	2.34	34.46	4.332	8.368	3.931	0.4165	7.38	5.07
	410	2.34	34.16	4.352	8.382	3.939	0.4277	7.58	5.21
	450	2.34	34.28	4.409	8.297	4.058	0.37	6.56	4.51
	480	2.34	34.28	4.198	8.391	3.792	0.4201	7.44	5.12
	510	2.34	33.67	3.952	8.163	3.724	0.252	4.48	3.07
V28-44-4	75	2.65	34.08	2.953	8.077	2.823	0.1541	3.17	2.09
	110	2.65	33.92	3.165	8.236	2.955	0.2273	4.68	3.08
	140	2.65	33.96	3.338	8.3	3.082	0.2715	5.59	3.68
	200	2.65	34.11	3.569	8.469	3.18	0.3989	8.21	5.4
	250	2.65	34.04	3.99	8.188	3.754	0.2607	5.37	3.53
	310	2.65	34.08	4.586	8.226	4.288	0.3237	6.66	4.38
	340	2.65	34.11	4.873	8.313	4.487	0.4072	8.38	5.51
	405	2.65	34.08	5.238	8.278	4.854	0.4096	8.43	5.54
	445	2.65	34.01	5.527	8.29	5.112	0.4413	9.08	5.97
	505	2.65	33.63	5.682	8.114	5.408	0.3172	6.54	4.3
	540	2.65	34.16	5.699	7.928	5.549	0.2181	4.49	2.95
	605	2.65	33.84	6.16	8.027	5.929	0.2888	5.95	3.91
	640	2.65	34.01	6.294	8.119	5.983	0.3576	7.36	4.84
	715	2.65	33.96	6.43	8.039	6.178	0.3098	6.37	4.19
	810	2.65	34.08	6.795	8.057	6.513	0.3407	7.01	4.61

Table A6.2 cont.: *Calculated carbonate parameter for pore water stations (MUC, SL) sampled during the 28th cruise of RV 'Akademik Lavrentyev', August - September 1998.*

LV28-17-2	2	0.85	33.68	4.103	7.891	4.027	0.1327	2.76	1.81
	10	0.85	33.63	3.182	7.827	3.144	0.0895	1.86	1.22
	21	0.85	33.51	8.609	8.15	8.193	0.4784	9.96	6.51
	35	0.85	33.92	27.986	8.028	27.048	1.2151	25.24	15.62
	43	0.85	34.04	34.316	7.898	33.651	1.133	23.52	15.4
	53	0.85	34.2	36.979	7.937	36.105	1.331	27.61	18.08
	63	0.85	33.96	37.333	7.904	36.588	1.2466	25.89	16.95

Appendix 7

Multinet Samples and Flow Through Volumes

Table A7: Samples and water volume flown through each net of the plankton sampler.

station	netnumber	depth in m	volume in cbm	F	S
LV 28-3-2	5	0-50	9,5	317	191
	4	50-130	6,3	218	134
	3	130-200	11,5	292	139
	2	200-500	21,1	410	129
	1	500-1000	30,2	529	126
LV 28-4-1	5	0-50	11,4	470	318
	4	50-130	5,0	287	220
	3	130-200	13,2	469	293
	2	200-300	8,5	525	412
	1	300-500	25,7	873	530
LV 28-7-1	5	0-50	1,4	492	473
	4	50-130	15,4	494	289
	3	130-200	9,4	595	470
	2	200-300	22,1	819	525
	1	300-500	52,4	1573	874
LV 28-14-2	5	0-50	28,3	859	482
	4	50-100	19,2	752	496
	3	100-150	2,0	622	595
	2	150-200	36,2	1304	821
	1	200-400	94,4	2832	1574
LV 28-29-1	5	0-50	34,4	1321	862
	4	50-130	21,5	1042	755
	3	130-200	36,7	1112	623
	2	200-500	131,6	3059	1305
	1	500-1000	160,4	4976	2837
LV 28-40-2	5	0-50	8,7	1439	1323
	4	50-130	6,7	1132	1043
	3	130-200	9,5	1239	1112
	2	200-500	21,6	3349	3061
	1	500-1000	44,0	5563	4977
LV 28-41-2	5	0-50	17,0	1666	1440
	4	50-130	10,8	1277	1133
	3	130-200	16,5	1461	1241
	2	200-500	38,5	3864	3351
	1	500-1000	56,8	6321	5564
LV 28-42-1	5	0-50	19,4	1926	1668
	4	50-130	16,2	1494	1278
	3	130-200	26,6	1816	1462
	2	200-500	95,3	5135	3865
	1	500-900	137,9	8159	6321
LV 28-43-2	5	0-50	13,9	2113	1928
	4	50-130	14,3	1686	1495
	3	130-200	16,9	2041	1816
	2	200-300	21,5	5424	5137
	1	300-500	44,0	8748	8161

Table A7 cont.: *Samples and water volume flown through each net of the plankton sampler.*

LV 28-44-1	5	0-50	12,6	2281	2113
	4	50-130	11,9	1846	1687
	3	130-200	16,1	2257	2042
	2	200-300	24,5	5750	5424
	1	300-500	49,3	9405	8748
LV 28-55-2	5	0-50	48,4	2932	2287
	4	50-130	71,0	2792	1846
	3	130-200	73,8	3241	2257
	2	200-500	158,6	7864	5750
	1	500-1000	238,7	12589	9407
LV 28-61-2	5	0-50	15,0	3134	2934
	4	50-130	9,0	2913	2793
	3	130-200	13,5	3422	3242
	2	200-500	27,1	8226	7865
	1	500-1000	61,9	13415	12590
LV 28-64-2	5	0-50	42,5	3703	3137
	4	50-130	39,3	3440	2916
	3	130-200	41,0	3969	3423
	2	200-500	127,7	9930	8227
	1	500-1000	267,8	16987	13417
LV 28-65-2	5	0-50	14,9	3905	3706
	4	50-130	12,5	3610	3443
	3	130-200	15,2	4173	3970
	2	200-500	59,3	10721	9931
	1	500-1000	142,7	18893	16991
LV 28-66-1	5	0-50	22,4	4205	3906
	4	50-130	23,8	3927	3610
	3	130-200	27,4	4538	4173
	2	200-500	89,2	11912	10723
	1	500-1000	127,5	20593	18893

Appendix 8

List of Participants

LIST OF PARTICIPANTS

Scientists

Kulinich Ruslan	chief of expedition
Obzhirov Anatoliy	deputy of chief
Lelikov Yevgeniy	deputy of chief
Botsul Anatoliy	deputy of chief
Sudakova Nadezhda	secretary
Gorbarenko Sergey	head of group
Tararin Igor'	head of group
Derkachev Aleksandr	head of group
Pavlova Galina	head of group
Nikolayeva Natal'ya	scientist
Yemel'yanova Tat'yana	scientist
Svarichevskiy Aleksandr	scientist
Terekhov Yevgeniy	scientist
Li Boris	scientist
Shul'ga Yuriy	engineer
Sosnin Valeriy	scientist
Galkin Sergey	scientist
Salyuk Anatoly	engineer
Zasko Darya	scientist
Suess Erwin	co-chief of cruise
Biebow Nicole	scientist
Nuernberg Dirk	scientist
Greinert Jens	scientist
Tiedemann Ralf	scientist
Werner Reinhard Andreas	scientist
Winckler Gisela	scientist
Geldmacher Joerg	scientist
Sahling Jens Heiko	scientist
Kaiser Andre	scientist
Nimmergut Anja Pia	scientist
Huetten Edna Patrizia	for. lang. assist.
Domeyer Bettina	technician
Oehmke Holger	technician
Kulescha Friedhelm	technician

Ship's crew

Osinny Vladimir	master
Dakus Aleksandr	ch.mate
Chekannikov Vladimir	2 nd mate
Miryanov Dmitriy	3 rd mate
Oblakov Sergey	radio-operator
Khrapko Yevgeniy	ch. Eng.
Khlynin Vitaliy	2 nd eng.
Dragunov Sergey	3 rd eng.
Dvornikov Sergey	4 th eng.
Badyuk Aleksandr	el. eng.
Pozyuban Vladimir	el. eng.
Golublev Vladimir	engineer
Zhuravkov Viktor	doctor
Burlakova Angelina	technician
Terent'yev Anatoliy	boats.
Artemenko Aleksandr	sailor
Koval' Valeriy	sailor
Obedin Sergey	sailor
Andrianov Yevgeniy	sailor
Khalitov Sergey	sailor
Nikishev Vadim	sailor
Plaum Oleg	sailor
Goncharuk Valeriy	turner
Luk'yanov Sergey	motorman
Moskalenko Mikhail	motorman
Sokolov Yevgeniy	motorman
Vinogradov Aleksandr	motorman
Andrianov Boris	electrician
Vanin Mikhail	electric welder
Konovalov Aleksandr	cook
Balayeva Ol'ga	cook
Korsunova Tat'yana	cook
Kushch Lyudmila	stewardess
Chumakova Marina	stewardess
Ovechkina Marina	stewardess
Varfolomeyeva Vera	stewardess
Timoshenko Natal'ya	stewardess